Biochemical mechanisms towards understanding Alzheimer's disease

A thesis submitted in fulfillment of the requirement for the degree of

DOCTOR OF PHILOSOPHY

of

RHODES UNIVERSITY

by

EDEN REBECCA PADAYACHEE

February 2013

Abstract

The start of the amyloidogenic pathway in Alzheimer's disease (AD) begins with the deposition of the $A\beta_{1-42}$ peptide surrounded by astrocytes. High levels of arginine and low amounts of neuronal nitric oxide synthase (nNOS) are associated with AD. These astrocytes store reserve arginine that is eventually metabolized by nNOS, within the vicinity of the $A\beta_{1-42}$ peptide. We propose the existence of an association vs. dissociation equilibrium between Aβ and nNOS such that nNOS is an amyloidogenic catalyst for fibrils. When Aβ binds to nNOS, it inhibits the activity of the enzyme (association phase). However when the amyloid peptide dissociates into a form that can no longer bind, later deduced as a fibril, the activity is restored. Thus, the interaction of Aβ with nNOS could serve to regulate the interaction between nNOS and arginine by restoring activity of the enzyme but at the same time promoting fibrillogenesis. Given this event occurring with the neuron, both nNOS and amyloid can serve as a biomarker for the early onset of AD. The enzyme nNOS catalyzed the formation of fibrils in the presence of Aβ peptides, while Ag nps were shown to reverse the fibril formation from Aβ peptides more so than Au and curcumin either through electrostatic or π-π stacking (aromatic) influences. Our studies have shown that the fragments of $A\beta_{1-42}$ i.e. the pentapeptide ($A\beta_{17-21}$) and the three glycine zipper peptides ($A\beta_{25-29}$, $A\beta_{29-33}$, $A\beta_{33-37}$) and the full length glycine zipper stretch ($A\beta_{25-37}$) all inhibited nNOS activity to varying degrees. The peptides $A\beta_{17-21}$ and $A\beta_{29-33}$ with their respective K_i values of 5.1 μM and 7.5 μM inhibited the enzyme the most. The K_i values for reversed sequenced peptides ($A\beta_{17-21r}$ and $A\beta_{29-33r}$) were two fold greater than that of the original peptides while the K_i values for the polar forms ($A\beta_{17-21p}$ and $A\beta_{29-33p}$) were between 3-4 fold greater than that of the original peptides. It was also found that Ag nps (K_i = 0.12 μM) inhibited the activity of nNOS the most compared to Au nps; (K_i = 0.15 μM) and curcumin (K_i = 0.25 μM). At 298K, all the ligands bound at a single site on the enzyme (n=1) and a single Trp residue (θ =1), (later identified as Trp678) was made available on the enzyme surface for quenching by the ligands. Increasing the temperature from 298K-313K, increased the value of K_{sv} and pointed to a dynamic quenching mechanism for Aβ peptides, nps and curcumin interaction with nNOS. The positive signs for entropy and enthalpy for all Aβ peptides nps and curcumin pointed to hydrophobic–hydrophobic interaction with the enzyme. The fact that K_d increased with temperature emphasized the endothermic nature of the binding reaction and the requirement of

thermal energy to aid in diffusion of the ligand to the active site. It was concluded that the binding reaction between the ligands and nNOS was non-spontaneous and endothermic at low temperatures (+ΔG) but spontaneous at high temperatures (-ΔG). The two amino acids Tyr706 and Trp678 moved from their original positions, subject to ligand binding. Trp678 moved a minimum distance of 5 Å toward the heme while Tyr706 moved a maximum distance of 14 Å away from the heme. AutoDock 4.2 was a valuable tool in monitoring the distance of Trp678 within the enzyme interior and fluorescence resonance energy transfer (FRET) was efficient in monitoring the distance moved by Trp residues on the enzyme surface.

Declaration

I declare that this thesis is my own, unaided work. It is being submitted for the degree of Doctor of Philosophy at Rhodes University. It has not been submitted before for any degree or examination in any other university.

_____

Signed on the 20th February 2013

Dedication

This thesis is dedicated to

My siblings, **Sandra Angini Padayachee** and **Lionel Manivel Padayachee**

Thank you for always being patient with me, believing in me and supporting me throughout my long journey and years of study and research at Rhodes University (2004-2012)

Acknowledgements

I would like to express my sincere gratitude and appreciation to the following people:

- To **Jehovah God**, in you I have trusted and through your holy spirit you have guided me to the ultimate success and completion of this thesis. Despite the odds and perils I have encountered, I have come off victorious. All the praise and honour must go to YOU, for you have endowed me with intellectual ability and reason. May your name, O **Jehovah** be glorified for all eternity.
- To my supervisor and mentor, Professor Chris Whiteley, your passion and dedication to research is a legacy that will continue to inspire me. Your patience, consistent guidance and vibrant nature has allowed me to accomplish this amazing feat. Thank you allowing me the opportunity to be your student and mentee in the name of scientific research.
- To Dr Earl Prinsloo, thank you for your invaluable advice and suggestions regarding the surface plasmon resonance study.
- To Dr Kevin Lobb, Department of Chemistry, Rhodes University, for assistance with molecular docking.
- To my beloved sister and brother, Sandra and Lionel Padayachee. Thank you for your patience and support. Thank you dearest sister for standing by me during the hard knocks of life and cheering me on to the finish line. You supported me down to the end. I couldn't have done it without you. There is no better friend than a brother or sister and there is no better friend than you both.
- To my team mates of Lab 129 C (2010-2012). In particular Phila Madlala, thank you for your warm smiles and much welcomed laughter during the rocky times. Your words of encouragement always inspired me.
- To Dr Afolake Sennuga, Dr Jacqui Marwijk and Dr Oluyomi Adeyemi, thank you all for proofreading certain chapters of this thesis.
- The financial assistance from the National Research Foundation (NRF) and Medical Research Council (MRC) toward this research is hereby acknowledged. Opinions expressed and conclusions arrived at, are those of the author and are not necessarily attributed to the NRF or MRC.

Table of Contents

Abstract ii
Declaration iv
Dedication v
Acknowledgements vi
Table of contents vii
List of Figures xii
List of Tables xix
List of Equations xxi
List of symbols and abbreviations xxii
Research outputs xxiv

1 Literature review 1

1.1 Alzheimers disease: an overview 1
1.2 AD: the burden 2
1.3 Hallmarks of AD 4
1.4 An overview of hypotheses related to AD 6
1.5 Amyloidogenesis 8
1.6 Properties of Aβ 10
1.7 Drug development 11
1.7.1 Immunization 12
1.7.2 Cholinergic drugs and non-steroidal anti-inflammatory drugs (NSAIDs) 13
1.7.3 Antioxidants 13
1.7.4 Polyphenols e.g. curcumin 13
1.7.5 Statins 15
1.7.6 Inhibition of β-and γ-secretase 15
1.7.7 Nanotechnology 16
1.7.8 New treatment directions in 2012 18
1.7.9 Peptide inhibitors 18
1.8 Nitric oxide synthases (NOSs) 19
1.8.1 Properties of nNOS 20
1.8.2 Catalysis 21

1.9 Involvement of nNOS and small β-peptide sequences in AD 22
1.10 Research focus 26
1.10.1 Hypothesis.....26
1.10.2 Aim 26
1.10.3 Objectives 26

2 Interaction of aβ peptides, nanoparticles (Ag/Au) and curcumin with nNOS: Inhibition studies 28

2.1 Introduction.....28
2.2 Theory of techniques utilized.....32
2.2.1 Ultraviolet-visible(UV-vis) absorbance spectroscopy.....32
2.3 Materials and Methods.....35
2.3.1 Materials 35
2.3.2 Methods.....36
2.3.2.1 Purification of nNOS 36
2.3.2.2 Characterization of nNOS.....36
2.3.2.3 Protein determination.....37
2.3.2.4 nNOS assay.....37
2.3.2.5 Isolation of curcuminoids from turmeric 38
2.3.2.6 Synthesis and characterization of Ag/Au nanoparticles 38
2.3.2.7 Time dependent inhibition of nNOS by Aβ,nanoparticles and curcumin.....39
2.3.2.8 Substrate dependent inhibition of nNOS by Aβ,nanoparticles and curcumin 40
2.3.2.9 Percentage inhibition of enzyme activity.....40
2.3.2.10 Statisitical analyses 40
2.4 Results and discussion 41
2.4.1 Time dependent inhibition of nNOS by incubation with original Aβ peptides 41
2.4.2 Substrate dependent inhibition of nNOS by incubation with original Aβ 42
2.4.3 Percent enzyme activity of nNOS by incubation with original Aβ peptides 43
2.4.4 Time dependent inhibition of nNOS by interaction with Aβ peptides (reversed and polar) 45
2.4.5 Substrate dependent inhibition of nNOS by interaction with Aβ peptides (reversed and polar) 46
2.4.6 Percent enzyme activity of nNOS by interaction with Aβ peptides (reversed and polar) ... 49
2.4.7 Time dependent inhibition of nNOS by Au, Ag nps and curcumin.....52
2.4.8 Substrate dependent inhibition of nNOS by Au, Ag nps and curcumin 53

2.4.9 Percent enzyme activity of nNOS by Au, Ag nps and curcumin.....54
2.5 Conclusions.....56

3 Interaction of Aβ peptides, nanoparticles(Ag/Au) and curcumin with nNOS: Fibrillogenesis studies 58

3.1 Introduction.....58
3.2 Theory of techniques utilized.....65
3.2.1 Thioflavin T (ThT) nucleation assay 65
3.3 Materials and Methods.....67
3.3.1 Materials 67
3.3.2 Methods.....67
3.3.2.1 Isolation of curcumin from turmeric.....67
3.3.2.2 Synthesis and characterization of Ag/Au nanoparticles 67
3.3.2.3 Co-incubation of nNOS and Aβ: Effect of nanoparticles 67
3.3.2.4 Co-incubation of nNOS and Aβ: Effect of curcumin 68
3.3.2.5 Co-incubation of nNOS and nanoparticles: Effect of Aβ peptides.....68
3.3.2.6 Co-incubation of nNOS and curcumin: Effect of Aβ peptides.....69
3.3.2.7 Co-incubation of Aβ and nanoparticles: Effect of nNOS 69
3.3.2.8 Co-incubation of Aβ and curcumin: Effect of nNOS 70
3.3.2.9 Statistical analysis.....70
3.4 Results and discussion 70
3.4.1 Co-incubation of nNOS and original Aβ peptides: Effect of nanoparticles 70
3.4.2 Co-incubation of nNOS and reversed and polar Aβ peptides: Effect of nanoparticles 73
3.4.3 Co-incubation of nNOS and nanoparticles: Effect of original Aβ peptides 75
3.4.4 Co-incubation of nNOS and nanoparticles: Effect of reversed and polar Aβ.....
.....77
3.4.5 Co-incubation of original Aβ peptides and nanoparticles: Effect of nNOS 77
3.4.6 Co-incubation of reversed and polar Aβ peptides and nanoparticles: Effect of nNOS 78
3.5 Conclusions.....83

4 Interaction of Aβ peptides, nanoparticles (Ag/Au) and curcumin with nNOS: Spectrofluorimetry,thermodynamics and surface plasmon resonance 85

4.1 Introduction....85
4.2 Theory of techniques utilized....90
4.2.1 Stern Volmer model....90
4.2.2 Thermodynamics....91
4.2.3 Surface plasmon resonance (SPR) spectroscopy....93
4.3 Materials and Methods....95
4.3.1 Materials....95
4.3.2 Methods....96
4.3.2.1 Isolation of curcumin from turmeric....96
4.3.2.2 Synthesis and characterization of Ag/Au nanoparticles....96
4.3.2.3 Fluoresence quenching and thermodynamic analysis at different temperatures....96
4.3.2.4 Surface plasmon resonance (SPR)....96
4.3.2.5 Statistical analyses....97
4.4 Results and discussion....97
4.4.1 Spectrofluorimetry and thermodynamics....97
4.4.2 Surface plasmon resonance....119
4.5 Conclusions....121

5 Interaction of Aβ peptides,nanoparticles (Ag/Au) and curcumin with nNOS:Molecular docking and fluoresence energy transfer (FRET).....123

5.1 Introduction....123
5.1.1 Molecular docking....123
5.1.2 FRET....125
5.2 Theory of techniques utilized....127
5.2.1 Molecular docking....127
5.2.2 Fluoresence energy transfer (FRET)....128
5.3 Materials and Methods....131
5.3.1 Materials....131
5.3.2 Methods....131
5.3.2.1 Isolation of curcumin from turmeric....131
5.3.2.2 Synthesis and characterization of Ag/Au nanoparticles....131
5.3.2.3 In silico analysis: AutoDock....131
5.3.2.4 FRET....133

5.4 Results and discussion 134
5.4.1 In silico analysis: AutoDock 134
5.4.1.1 Distance that Trp678 and Tyr706 shift when the original Aβ peptides and curcumin bind to the heme 136
5.4.1.2 Distance that Trp678 and Tyr706 shift when the reversed and polar Aβ peptides bind to the heme 139
5.4.1.3 Suggested 3-D models of modifed Ag and Au nps binding to heme 147
5.4.2 FRET 148
5.5 Conclusions 151

6 General discussions and future perspectives 153

6.1 General discussions 153
6.2 Future perspectives 156

References 160
Appendix: K_i statistical analysis.pzf:1way ANOVA of K_i: Tabular results.....183
Appendix: K_{sv} statistical analysis.pzf:1way ANOVA of K_{sv}: Tabular results.....186
Appendix: K_d statistical analysis.pzf:1way ANOVA of K_d : Tabular results.....208
Appendix: K_i statistical analysis.pzf:1way ANOVA of K_i: Tabular results.....229

List of Figures

Figure 1.1: PET scan using the tracer drug, florbetaben to visualize amyloid plaques during life. A healthy brain (A) vs. aging brain (B). Red patches on scan denote neurons. Aging brain (B) shows the characteristic shrinking of neurons (red patches) associated with the onset of AD (Taken from Cruz, 2012) *2*

Figure 1.2: Increasing percent of the population with dementia from age 60-85+ (Taken from Cummings, 2003) *3*

Figure 1.3: Recent statistics on the prevalence of AD every ten years from 1980 to 2050 (A) Projected numbers of people aged 65 and over in the U.S. population with Alzheimer's disease (in millions) using the U.S. census bureau estimates of population growth (B) (Taken from Alzheimer's Association, 2012 ..... *3*

Figure 1.4: The presence of plaques and tangles in the brain of AD patient (Taken from American Health Assistance Foundation, 2012) *5*

Figure 1.5: Two major hypotheses of AD postulated to explain its pathogenesis (Adapted from Parihar and Hemnani, 2004) *7*

Figure 1.6: Diagram illustrating the location of APP embedded in the cell membrane (A) and subsequent formation of Aβ plaques (B) (Taken from Anderson et al., 2013) *8*

Figure 1.7: Schematic diagram of processing of amyloid precursor protein (APP) and production of Aβ (Parihar and Hemnani, 2004) *9*

Figure 1.8: Schematic representation showing prevention strategies for AD (Adapted from Parihar and Hemnani, 2004) *12*

Figure 1.9: Isolation, extraction and structure of curcumin (Taken from Goel et al., 2008) *14*

Figure 1.10: The four major curcuminoids present in turmeric (Taken from Aggarwal et al., 2006) *14*

Figure 1.11: Artistic rendering of Aβ fibrillation in the presence of nps. (A) Nanoparticles (blue) and monomers of Aβ (green) (B) The association of Aβ fibrils with the surface of nanoparticles (Taken from Colvin and Kulinowski, 2007) *17*

Figure 1.12: Ribbon structure of homodimeric nNOS, illustrating the active site. Image was generated using Rasmol (Raswin molecular graphics [V 2.7.2.1] (Sayle and Bernstein, 1998-2001) (PDB: 1zvi) *20*

Figure 1.13 Domain structure of human nNOS, depicting two parts: oxygenase and reductase domain (Taken from Stuehr, 1997) *21*

Figure 1.14 Catalytic mechanism of neuronal nitric oxide synthase (Taken from Padayachee and Whiteley, 2011, 2013) *22*

Figure 1.15 An illustration describing the role of nNOS in the amyloidogenic pathway *23*

Figure 1.16: Schematic model of glycine-mediated interaction showing possible packing arrangement between residues 24-39 of neighboring Aβ molecules. The glycine zipper interface is represented by the jagged line, residue G37 is highlighted in red (Fonte et al., 2011) *24*

Figure 1.17: The amino acid sequence of $A\beta_{1-42}$ in symbol form, showing the hydrophobic pentapeptide, $A\beta_{17-21}$ and 3 'G-X-X-X-G' motifs called glycine zippers ($A\beta_{25-29}$ and $A\beta_{29-33}$ and $A\beta_{33-37}$) within the glycine zipper stretch ($A\beta_{25-37}$) *25*

Figure 1.18: The significance of short peptide sequences, nps and curcumin in amyloidogenesis..... 25

Figure 2.1: Michealis-Menten graph where enzyme activity depends on substrate concentration (A). Hanes-Woolf graph where V_{max} is determined from the reciprocal of the slope and K_m is the derived from the y intercept (B) (Taken from Gilbert, 2000)..... 33

Figure 2.2: Hanes-Woolf plot indicating V_{max} and K_m (in absence of inhibitor) and V_{max}^{app} and K_m^{app}(in presence of inhibitor). Types of inhibition are reflected: competitive inhibition (A); non-competitive inhibition (B) uncompetitive inhibition (C) and mixed inhibition (D) (Adapted from Gilbert, 2000) 34

Figure 2.3: TEM micrographs and size distribution of Au nps (A) and Ag nps (B) made from varying molar ratios of metal salts to HSAF. Scale bar = 100 nm. 200 particles were analyzed in each group. (i) 250:1; (ii) 500:1 ;(iii) 1000:1; (iv) 2000:1 and (v) 4000:1 (Sennuga et al., 2012) 39

Figure 2.4: Percent enzyme activity of nNOS (32 nM) by $A\beta_{17-21}$ ■; $A\beta_{25-29}$ ■; $A\beta_{29-33}$ ■; $A\beta_{33-37}$ ■ and $A\beta_{25-37}$ ■ in Tris-HCl buffer (50 mM, pH 7.6)(8 µM), in the presence of the substrate BAEE (8 µM) for a duration of 5 min. Enzyme activity at time (0 min) = 9 U/ml; values represents the mean (± S.E.M) of three trials..... 41

Figure 2.5: Hanes-Woolf plot of nNOS activity in the absence and presence of Aβ peptides. Concentrations of peptide: 0 nM (×); 2 µM (■); 4 µM (○); 6 µM (●); 8 µM (□). $A\beta_{17-21}$ [A] $A\beta_{25-29}$[B] $A\beta_{29-33}$ [C] $A\beta_{33-37}$ [D] $A\beta_{25-37}$[E]..... 42

*Figure 2.6: Percent enzyme activity of nNOS by interaction with $A\beta_{17-21}$ **[A]** $A\beta_{25-29}$ **[B]** $A\beta_{29-33}$ **[C]** $A\beta_{33-37}$ **[D]** and $A\beta_{25-37}$ **[E]** at [Aβ]= 2 µM ■ [S]= 4 µM ■; [S]= 6 µM ■; [S]= 8 µM■, in the presence of benzoyl arginine ethyl ester substrate[S] (0-8µM). Enzyme activity at 0 µM Aβ peptide = 9 U/ml.*

..... 44

Figure 2.7: Percent enzyme activity of nNOS (32 nM) by $A\beta_{17-21r}$ ■; $A\beta_{17-21p}$ ■; $A\beta_{29-33r}$ ■; $A\beta_{29-33p}$ ■ in Tris-HCl buffer (50 mM, pH 7.6) (8µM), in the presence of the substrate BAEE (8 µM) for a duration of 5 min. Enzyme activity at time (0 min) = 9 U/ml; values represents the mean (± S.E.M) of three trials

.. .. 46

Figure 2.8: Hanes-Woolf plot of nNOS activity in the absence and presence of Aβ peptides. Concentrations of peptide: 0 nM (×); 2 µM (■); 4 µM (○); 6 µM (●); 8 µM (□).$A\beta_{17-21r}$ [A] $A\beta_{17-21p}$ [B] $A\beta_{29-33r}$ [C] $A\beta_{29-33p}$ [D]..... 47

*Figure 2.9: Percent enzyme activity of nNOS by interaction with $A\beta_{17-21r}$ **[A]** $A\beta_{17-21p}$ **[B]** $A\beta_{29-33r}$ **[C]** $A\beta_{29-33p}$ **[D]** at [Aβ]= 2 µM ■ [S]= 4 µM ■; [S]= 6 µM ■; [S]= 8 µM■, in the presence of benzoyl arginine ethyl ester substrate[S] (0-8µM). Enzyme activity at 0 µM Aβ peptide = 9 U/ml.*

..... 49

Figure 2.10: 3-D structures of $A\beta_{17-21}$ (A) $A\beta_{17-21r}$ (B) $A\beta_{29-33}$ (C) $A\beta_{29-33r}$ (D) Structures built by Vega ZZ (v.2.4.0) 50

Figure 2.11: The enzyme nNOS (E) and Aβ fragment before association (A); association of nNOS and Aβ whereby peptide binds to enzyme active site, decreasing enzyme activity and thus no or limited fibril formation occurs (B); dissociation of Aβ in the form of fibrils (C1 and C2) 51

Figure 2.12: Percent enzyme activity of nNOS (32 nM) by Au ■, Ag ■ and curcumin ■ in Tris-HCl buffer (50 mM, pH 7.6) (0.09 µM), in the presence of the substrate BAEE (8 µM) for a duration of 5 min. Enzyme activity at time (0 min) = 9 U/ml, values represents the mean (± S.E.M) of three trial 52

Figure 2.13: Hanes-Woolf plot of nNOS activity in the absence and presence of nps and curcumin. Concentrations of nps and curcumin: 0 μM (✕); 0.03 μM (■); 0.06 μM (○); 0.09μM (●), Au [A] Ag [B] and curcumin[C]. *53*

*Figure 2.14: Percent enzyme activity of nNOS by interaction with Au [**A**] Ag [**B**] curcumin [**C**] at concentrations = 2 μM ■ [S]= 4 μM ■; [S]= 6 μM ■; [S]= 8 μM ■, in the presence of benzoyl arginine ethyl ester substrate[S] (0-8μM). Enzyme activity at 0 μM Aβ peptide = 9 U/ml.*

..... *55*

Figure 2.15: The enzyme nNOS (E), Aβ fragment and np/curcumin before association (A); association of nNOS with np/curcumin whereby either ligand binds, decrease enzyme activity and displace Aβ (B); dissociation of Aβ and np/curcumin with suppressed or no fibril formation by the action of nps/curcumin (C1 and C2) *56*

Figure 3.1: Electron micrograph of short, straight amyloid fibrils formed in water from $Aβ_{1-40}$ (70-80 Å in diameter), Bar = 1000 Å (A). Diagram showing an anti-parallel β-sheet arrangement with hydrogen bond distances of 4.8 Å, a sheet spacing of 10-11 Å and a repeat distance along the polypeptide chain of 6.9 Å (B) (Taken from Serpell., 2000) *58*

Figure 3.2: Schematic showing aggregation intermediates critical to amyloid-β-aggregation (Taken from DaSilva et al., 2010) *60*

Figure 3.3: Representation of the kinetic model for Aβ fibrillogenesis. Fibrillization of Aβ protein is nucleation dependent and two pathways are proposed. One is fibril nucleation on seeds. The second is nucleation within micelles (Taken from Lomakin et al., 1997) *61*

Figure 3.4: Illustration showing the "nucleation-polymerization" kinetics for amyloid fibril formation (Adapted from Nilsson, 2004) *61*

Figure 3.5: Diagram of $Aβ_{1-40}$ sequence suggesting regions with a high propensity for β-sheet structure (encircled in red). Clusters of hydrophobic residues are shown in red (Adapted from Serpell, 2000) ... *62*

Figure 3.6: Chemical structure of ThT, depicting the carbon-carbon bond (in red) between benzothiazol and aniline rings that becomes restricted in rotation upon binding to amyloid fibrils (Adapted from Reinke and Gestwicki., 2011)..... *66*

Figure 3.7: Plots of ThT fluorescence by nNOS catalyzed fibrillogenesis of Aβ treated with nps and/or curcumin in a final volume (200μL) in Tris HCl buffer (pH 7.6, 100 mM) at 25 °C. $Aβ_{17-21}$ (25 μM); Au,Ag,curcumin (0.15 μM)[A]; $Aβ_{17-21}$ (50 μM); Au,Ag,curcumin (0.30 μM)[B]; $Aβ_{25-29}$ (25 μM); Au,Ag,curcumin (0.15 μM)[C]; $Aβ_{25-29}$ (50 μM); Au,Ag,curcumin (0.30 μM)[D]; $Aβ_{29-33}$ (25 μM); Au, Ag, curcumin (0.15 μM)[E];$Aβ_{29-33}$ (50 μM); Au,Ag,curcumin (0.30μM)[F];A_{33-37}(25μM);Au,Ag,curcumin (0.15μM)[G];$Aβ_{33-37}$(50μM);Au,Ag,curcumin (0.30 μM)[H];A_{25-37} (25μM); Au, Ag, curcumin (0.15 μM) [I]; $Aβ_{25-37}$ (50μM); Au, Ag ,curcumin (0.30 μM) [J]. ■ — [Ag: 4 nm]; — ♦ [Au: 4 nm]; — ♦ [curcumin] *72*

Figure 3.8: Plots of ThT fluorescence induced by nNOS catalyzed fibrillogenesis of Aβ treated with nps and/or curcumin in a final volume (200μL) in Tris HCl buffer (pH 7.6, 100 mM) at 25 °C. $Aβ_{17-21r}$ (25 μM); Au,Ag, curcumin (0.15 μM) [A]; $Aβ_{17-21r}$ (50 μM); Au,Ag, curcumin (0.30 μM) [B]; $Aβ_{17-21p}$ (25 μM); Au, Ag, curcumin (0.15 μM) [C]; $Aβ_{17-21p}$ (50 μM); Au,Ag, curcumin (0.30 μM) [D]; $Aβ_{29-33r}$ (25 μM); Au,Ag, curcumin (0.15 μM) [E]; $Aβ_{29-33r}$ (50 μM); Au,Ag, curcumin (0.30 μM) [F] ; $Aβ_{29-33p}$ (25 μM); Au,Ag,curcumin (0.15 μM) [G]; $Aβ_{29-33p}$ (50 μM); Au,Ag, curcumin (0.30 μM) [H]. ■ — [Ag: 4 nm]; — ♦ [Au: 4 nm]; — ♦ [curcumin] *74*

Figure 3.9: Plots of ThT fluorescence of nps and/or curcumin (0.30 μM) co-incubated with nNOS (32 nM) treated with Aβ [50 μM] in a final volume (200μL) in Tris HCl buffer (pH 7.6, 100 mM) at 25 °C.

Addition of: $A\beta_{17\text{-}21}$ [A]; $A\beta_{25\text{-}29}$ [B]; $A\beta_{29\text{-}33}$[C]; $A_{33\text{-}37}$ [D]; $A\beta_{25\text{-}37}$[E]. — ■ [co-incubation of nNOS–np/curcumin]; — ● effect of Aβ on [nNOS-np]; — ● effect of Aβ on [nNOS-curcumin] 76

Figure 3.10: Plots of ThT fluorescence of nps and/or curcumin (0.30 μM) co-incubated with nNOS (32 nM) treated with Aβ [50 μM] in a final volume (200μL) in Tris HCl buffer (pH 7.6, 100 mM) at 25 °C. Addition of : $A\beta_{17\text{-}21r}$ [A]; $A\beta_{17\text{-}21p}$ [B]; $A\beta_{29\text{-}33r}$ [C]; $A\beta_{29\text{-}33p}$ [D]. — ■ [co-incubation of nNOS–np/curcumin]; — ● effect of Aβ on [nNOS-np]; — ● effect of Aβ on [nNOS-curcumin]. 77

Figure 3.11: Plots of ThT fluorescence of nps and/or curcumin (0.30 μM) co-incubated with Aβ (50 μM) treated with nNOS [32 nM] in a final volume (200μL) in Tris HCl buffer (pH 7.6, 100 mM) at 25 °C. In co-incubated solution: $A\beta_{17\text{-}21}$; Au,Ag,curcumin [A]; $A\beta_{25\text{-}29}$; Au,Ag,curcumin [B]; $A\beta_{29\text{-}33}$; Au,Ag,curcumin [C]; $A\beta_{33\text{-}37}$; Au,Ag,curcumin [D]; $A\beta_{25\text{-}37}$; Au, Ag, curcumin [E] — ■ [co-incubation of Aβ –np/curcumin]; — ● effect of nNOS on [Aβ-np]; — ● effect of nNOS on [Aβ-curcumin]. 78

Figure 3.12: Plots of ThT fluorescence of nps and/or curcumin (0.30 μM) co-incubated with Aβ (50 μM) treated with nNOS [32 nM] in a final volume (200μL) in Tris HCl buffer (pH 7.6, 100 mM) at 25 °C. In co-incubated solution: $A\beta_{17\text{-}21r}$; Au,Ag,curcumin [A]; $A\beta_{17\text{-}21p}$; Au,Ag,curcumin [B]; $A\beta_{29\text{-}33r}$; Au,Ag,curcumin [C]; $A\beta_{29\text{-}33p}$; Au,Ag,curcumin [D]; — ■ [co-incubation of Aβ –np/curcumin]; — ● effect of nNOS on [Aβ-np]; — ● effect of nNOS on [Aβ-curcumin]. 79

Figure 3.13: The behavior of nNOS as an amyloidogenic catalyst in driving nucleation and formation of seeds, leading to the elongation effect in fibrillogenesis. 80

Figure 3.14: Diagram illustrating monomer peptides in solution (A) getting trapped by a nanoparticle (B) which depletes amount of free monomer in solution (C) and prevents the fibril pathway from occurring (D) 81

Figure 3.15: Illustration depicting the "disrupting effect" of nps and/or curcumin on binary adducts nNOS (A_1) and Aβ (B) (1.) Binary adduct/complex (A_1B) (2.) the addition of np and/or curcumin (A_2) and its "disrupting effect" on the binary adduct/complex (3.) 82

Figure 4.1: Jablonski diagram illustrating the processes of absorption (excitation) and fluorescence (emission) (Adapted from Behlke et al., 2005) 85

Figure 4.2: Secondary structure of an arbitrary protein depicted in cartoon and coloured structure (Taken from Lesk, 2001) 87

Figure 4.3: Diagram of a free energy funnel describing the folding of a protein to a stable 3-D structure, the width of the folding funnel represents entropy and the depth represents enthalpy (taken from Kavraki, 2006) 88

Figure 4.4: Biological thermodynamics of a reaction include ΔG: ligand-enzyme interactions (A); ΔH: solvent-ligand and solvent-enzyme interactions (B); -TΔS: ligand and solvent entropy(C) 92

Figure 4.5: Schematic representation of a BIACORE flow cell and detection, illustrating the incidence angle (θ) which changes during a binding process (A); A sensorgram characterized by three phases: baseline, association and dissociation (B)(Adapted from Aguilar and Small, 2005) 94

Figure 4.6: Diagram of SPR sensor chip surface depicting 6 vertical ligand channels (L1-L6) and 6 horizontal analyte channels (A1-A6). L1-L5 contained nNOS immobilized at concentrations (5 μg/ml, 10 μg/ml, 25 μg/ml, 50 μg/ml and 100 μg/ml). L6 was the blank channel. A1-A4 contained $A\beta_{25\text{-}37}$, $A\beta_{33\text{-}37}$, $A\beta_{29\text{-}33}$ and $A\beta_{1\text{-}40}$ (100 μM). Each analyte (Aβ) passed through a unique detection point (x) at each intersection point. 97

Figure 4.7: Stern–Volmer plot [A]; modified Stern –Volmer plot [B]; Hill plot of log [(F_0-F)/F] versus log [q] [C]; Van't Hoff plot [D] for fluorescence quenching of nNOS (5μl) in triethanolamine HCl buffer (pH 7.4, 10mM) treated with $A\beta_{17\text{-}21}$ (5-40 μM) in a final volume (200μL) at different

temperatures – – – ○ [298K]; —□ [303K]; ... Δ [308K]; —■ [313K] .λ_{ex} = 290 nm and λ_{em} = 338 nm 98

Figure 4.8: Stern–Volmer plot [A]; modified Stern –Volmer plot [B]; Hill plot of log [(F_0-F)/F] versus log [q] [C]; Van't Hoff plot [D] for fluorescence quenching of nNOS (5µl) in triethanolamine HCl buffer (pH 7.4, 10mM) treated with $A\beta_{25-29}$ (5-40 µM) in a final volume (200µL) at different temperatures – – – ○ [298K]; —□ [303K]; ... Δ [308K]; —■ [313K] .λ_{ex} = 290 nm and λ_{em} = 338 nm 99

Figure 4.9: Stern–Volmer plot [A]; modified Stern –Volmer plot [B]; Hill plot of log [(F_0-F)/F] versus log [q] [C]; Van't Hoff plot [D] for fluorescence quenching of nNOS (5µl) in triethanolamine HCl buffer (pH 7.4, 10mM) treated with $A\beta_{29-33}$ (5-40 µM) in a final volume (200µL) at different temperatures – – – ○ [298K]; —□ [303K]; ... Δ [308K]; —■ [313K] .λ_{ex} = 290 nm and λ_{em} = 338 nm 100

Figure 4.10: Stern–Volmer plot [A]; modified Stern –Volmer plot [B]; Hill plot of log [(F_0-F)/F] versus log [q] [C]; Van't Hoff plot [D] for fluorescence quenching of nNOS (5µl) in triethanolamine HCl buffer (pH 7.4, 10mM) treated with $A\beta_{33-37}$ (5-40 µM) in a final volume (200µL) at different temperatures – – – ○ [298K]; —□ [303K]; ... Δ [308K]; —■ [313K] .λ_{ex} = 290 nm and λ_{em} = 338 nm 101

Figure 4.11: Stern–Volmer plot [A]; modified Stern –Volmer plot [B]; Hill plot of log [(F_0-F)/F] versus log [q] [C]; Van't Hoff plot [D] for fluorescence quenching of nNOS (5µl) in triethanolamine HCl buffer (pH 7.4, 10mM) treated with $A\beta_{25-37}$ (5-40 µM) in a final volume (200µL) at different temperatures – – – ○ [298K]; —□ [303K]; ... Δ [308K]; —■ [313K] .λ_{ex} = 290 nm and λ_{em} = 338 nm 102

Figure 4.12: Stern–Volmer plot [A]; modified Stern –Volmer plot [B]; Hill plot of log [(F_0-F)/F] versus log [q] [C]; Van't Hoff plot [D] for fluorescence quenching of nNOS (5µl) in triethanolamine HCl buffer (pH 7.4, 10mM) treated with $A\beta_{17-21r}$ (5-40 µM) in a final volume (200µL) at different temperatures – – – ○ [298K]; —□ [303K]; ... Δ [308K]; —■ [313K] .λ_{ex} = 290 nm and λ_{em} = 338 nm 103

Figure 4.13: Stern–Volmer plot [A]; modified Stern –Volmer plot [B]; Hill plot of log [(F_0-F)/F] versus log [q] [C]; Van't Hoff plot [D] for fluorescence quenching of nNOS (5µl) in triethanolamine HCl buffer (pH 7.4, 10mM) treated with $A\beta_{17-21p}$ (5-40 µM) in a final volume (200µL) at different temperatures – – – ○ [298K]; —□ [303K]; ... Δ [308K]; —■ [313K] .λ_{ex} = 290 nm and λ_{em} = 338 nm 104

Figure 4.14: Stern–Volmer plot [A]; modified Stern –Volmer plot [B]; Hill plot of log [(F_0-F)/F] versus log [q] [C]; Van't Hoff plot [D] for fluorescence quenching of nNOS (5µl) in triethanolamine HCl buffer (pH 7.4, 10mM) treated with $A\beta_{29-33r}$ (5-40 µM) in a final volume (200µL) at different temperatures – – – ○ [298K]; —□ [303K]; ... Δ [308K]; —■ [313K] .λ_{ex} = 290 nm and λ_{em} = 338 nm 105

Figure 4.15: Stern–Volmer plot [A]; modified Stern –Volmer plot [B]; Hill plot of log [(F_0-F)/F] versus log [q] [C]; Van't Hoff plot [D] for fluorescence quenching of nNOS (5µl) in triethanolamine HCl buffer (pH 7.4, 10mM) treated with $A\beta_{29-33p}$ (5-40 µM) in a final volume (200µL) at different temperatures – – – ○ [298K]; —□ [303K]; ... Δ [308K]; —■ [313K] .λ_{ex} = 290 nm and λ_{em} = 338 nm 106

Figure 4.16: Stern–Volmer plot [A]; modified Stern –Volmer plot [B]; Hill plot of log [(F_0-F)/F] versus log [q] [C]; Van't Hoff plot [D] for fluorescence quenching of nNOS (5µl) in triethanolamine HCl buffer (pH 7.4, 10mM) treated with Ag (4 nm) (5-40 µM) in a final volume (200µL) at different temperatures – – – ○ [298K]; —□ [303K]; ... Δ [308K]; —■ [313K] .λ_{ex} = 290 nm and λ_{em} = 338 nm 107

Figure 4.17: Stern–Volmer plot [A]; modified Stern –Volmer plot [B]; Hill plot of log [(F_0-F)/F] versus log [q] [C]; Van't Hoff plot [D] for fluorescence quenching of nNOS (5µl) in triethanolamine HCl buffer (pH 7.4, 10mM) treated with Au (4 nm) (5-40 µM) in a final volume (200µL) at different temperatures – – – ○ [298K]; —□ [303K]; ... Δ [308K]; —■ [313K] .λ_{ex} = 290 nm and λ_{em} = 338 nm 108

Figure 4.18: Stern–Volmer plot [A]; modified Stern –Volmer plot [B]; Hill plot of log [(F_0-F)/F] versus log [q] [C]; Van't Hoff plot [D] for fluorescence quenching of nNOS (5µl) in triethanolamine HCl buffer (pH 7.4, 10mM) treated with curcumin (5-40 µM) in a final volume (200µL) at different temperatures – – – ○ [298K]; —□ [303K]; ... Δ [308K]; —■ [313K] .λ_{ex} = 290 nm and λ_{em} = 338 nm 109

Figure 4.19: The mechanism of fibrillogenesis on the basis of the principle regarding association vs. dissociation between Aβ peptide and nNOS 117

Figure 4.20: Sensogram describing the immobilization of nNOS at a single channel (L1) (5µg/ml) [A] sensogram showing preliminary binding of $Aβ_{1-40}$ to nNOS [B] 119

Figure 5.1: The methods which classify protein docking (taken from Huang and Zou, 2010) 124

Figure 5.2: Illustrative process of FRET involving the donor (fluor A) and the acceptor (fluor B) (adapted from Takahashi et al., 2004) 129

Figure 5.3 : Empty binding site on nNOS in molecular surface colored atom by AutoDock 4.2 (A) and docked Aβ peptides in " hydrophobic pocket" of nNOS : $Aβ_{17-21}$ (B); $Aβ_{25-29}$ (C); $Aβ_{29-33}$ (D); $Aβ_{33-37}$ (E);$Aβ_{25-37}$ (F) $Aβ_{17-21r}$ (G); $Aβ_{17-21p}$ (H); $Aβ_{29-33r}$ (I) $Aβ_{29-33p}$ (J) [(PDB: 1zvi) (Aβ peptides: built by Vega ZZ) 135

Figure 5.4: The active site of nNOS depicting the heme and H_4B co-factors, illustrating the 4 amino nitrogen of the heme (NA) and the delta oxygen (O2D) [encircled in red] [(PDB: 1zvi; built by Vega ZZ)] (A), Distance of Trp678 from the rigid heme (NA) [encircled in red] (B), Distance of Tyr706 from the rigid heme (O2D) [encircled in red] (C). Performed by AutoDock 4.2 136

Figure 5.5: The active site of nNOS, showing $Aβ_{17-21}$ (A); $Aβ_{25-29}$ (B); $Aβ_{29-33}$ (C); $Aβ_{33-37}$ (D); $Aβ_{25-37}$ (E) and curcumin (F) docked in molecular surface coloured by CPK, depicting the distance of flexible Trp678 (encircled in red) from the rigid heme (NA) [(PDB: 1zvi) (Aβ peptides: built by Vega ZZ) (curcumin: accession number (HMDBO2269). Performed by AutoDock 4.2 137

Figure 5.6: The active site of nNOS, showing $Aβ_{17-21}$ (A); $Aβ_{25-29}$ (B); $Aβ_{29-33}$(C); $Aβ_{33-37}$ (D); $Aβ_{25-37}$ (E) and curcumin (F), depicting the distance of flexible Tyr706 (encircled in red) from the rigid heme (O2D). All Aβ peptides are docked in molecular surface (except $Aβ_{25-37}$); coloured by CPK, using AutoDock 4.2. Also $Aβ_{33-37}$ is docked by Accelrys Visualizer/Material Studios (version 2.0). Residues are displayed in stick solid and coloured by atom displaying hydrogen bonds (green dotted lines) [(PDB: 1zvi) (Aβ peptides: built by Vega ZZ) [curcumin: accession number (HMDBO2269)] 138

Figure 5.7: The active site of nNOS, showing $Aβ_{17-21r}$ (A); $Aβ_{17-21p}$ (B); $Aβ_{29-33r}$ (C); $Aβ_{29-33p}$ (D) docked in molecular surface coloured by CPK, depicting the distance of flexible Trp678 (encircled in red) from the rigid heme (NA) [(PDB: 1zvi) (Aβ peptides: built by Vega ZZ). Performed by AutoDock 4.2 139

Figure 5.8: The active site of nNOS, showing $A\beta_{17\text{-}21r}$ (A); $A\beta_{17\text{-}21p}$ (B); $A\beta_{29\text{-}33r}$ (C); $A\beta_{29\text{-}33p}$ (D) docked in molecular surface coloured by CPK, depicting the distance of flexible Tyr 706 (encircled in red) from the rigid heme (O2D) [(PDB: 1zvi) (Aβ peptides: built by Vega ZZ). Performed by AutoDock 4.2..... 140

Figure 5.9: Docking of curcumin (visualized by Accelrys Visualizer/Material Studios (version 2.0), depicting the two phenolic rings critical in interaction with nNOS. Residues are displayed in stick solid and coloured by atom displaying hydrogen bonds (green dotted lines) [(PDB: 1zvi) (curcumin: accession number (HMDBO2269)] 144

Figure 5.10: 2-D visualization of heme active site, showing heme propionyl groups and critical amino acids surrounding the heme co-factor within the active site of nNOS [visualized using Accelrys Visualizer/Material Studios (version 2.0)] 144

Figure 5.11: Diagram depicting a Ag np (1172) conjugated to Met170, modified from the x-ray structure of ferritin from Pyrococcus furiosus (PDB: 2x17) (A). The ferric ion (Fe) of the heme center may be crucial in electrostatically attracting the Ag np (A). Au np (3205) conjugated to Met96, modified from the x-ray structure of apoferritin with gold ions (PDB: 3H7G) (B). The diagram depicts the rear side of the heme coloured red) with Cys415 conjugated to the Fe^{+3} ion. The Cys415 possesses a sulphur atom (yellow) that maybe crucial to the attracting of the Au np (B). The heme was "fitted" to the nps using Deepview (V.4.1.) 147

Figure 5.12: Proposed mechanism of FRET in binding studies of BAEE, $A\beta$, nps and curcumin (acceptor) and nNOS (donor) 150

List of Tables

Table 1.1: Nanosystems designed for treatment of AD (Nazem and Mansoori, 2011) 17

Table 2.1 Values of V_{max} ($\mu mol.ml^{-1}.min^{-1}$) and) K_m (μM) and K_i (μM) for original Aβ peptides (μM) after interaction with nNOS. K_i values were estimated from Eq [5], pg 34 43

Table 2.2 Values of V_{max} ($\mu mol.ml^{-1}.min^{-1}$) and) K_m (μM) and K_i (μM) for reversed and polar Aβ peptides (μM) after interaction with nNOS. K_i values were estimated from Eq [5], pg 34..... 48

Table 2.3 Values of V_{max} ($\mu mol.ml^{-1}.min^{-1}$) and) K_m (μM) and K_i (μM) for [L = Au/Ag nps or curcumin] (μM), after interaction with nNOS. K_i values were estimated from Eq [5], pg 34..... 54

Table 4.1: Values for fluorescent parameters (K_{sv} [μM^{-1}], K_a [μM^{-1}],K_d [μM],θ and n) and thermodynamic parameters ΔH [$kJ.mol^{-1}.K^{-1}$]; ΔS [$J.mol^{-1}.K^{-1}$ and ΔG [$kJ.mol^{-1}.K^{-1}$] for the interaction of $A\beta_{17-21}$ with nNOS at various temperatures 98

Table 4.2: Values for fluorescent parameters (K_{sv} [μM^{-1}], K_a [μM^{-1}],K_d [μM],θ and n) and thermodynamic parameters ΔH [$kJ.mol^{-1}.K^{-1}$]; ΔS [$J.mol^{-1}.K^{-1}$] and ΔG [$kJ.mol^{-1}.K^{-1}$] for the interaction of $A\beta_{25-29}$ with nNOS at various temperatures 99

Table 4.3: Values for fluorescent parameters (K_{sv} [μM^{-1}], K_a [μM^{-1}],K_d [μM],θ and n) and thermodynamic parameters ΔH [$kJ.mol^{-1}.K^{-1}$]; ΔS [$J.mol^{-1}.K^{-1}$] and ΔG [$kJ.mol^{-1}.K^{-1}$] for the interaction of $A\beta_{29-33}$ with nNOS at various temperatures 100

Table 4.4: Values for fluorescent parameters (K_{sv} [μM^{-1}], K_a [μM^{-1}],K_d [μM],θ and n) and thermodynamic parameters ΔH [$kJ.mol^{-1}.K^{-1}$]; ΔS [$J.mol^{-1}.K^{-1}$] and ΔG [$kJ.mol^{-1}.K^{-1}$] for the interaction of $A\beta_{33-37}$ with nNOS at various temperatures 101

Table 4.5: Values for fluorescent parameters (K_{sv} [μM^{-1}], K_a [μM^{-1}],K_d [μM],θ and n) and thermodynamic parameters ΔH [$kJ.mol^{-1}.K^{-1}$]; ΔS [$J.mol^{-1}.K^{-1}$] and ΔG [$kJ.mol^{-1}.K^{-1}$] for the interaction of $A\beta_{25-37}$ with nNOS at various temperatures 102

Table 4.6: Values for fluorescent parameters (K_{sv} [μM^{-1}], K_a [μM^{-1}],K_d [μM],θ and n) and thermodynamic parameters ΔH [$kJ.mol^{-1}.K^{-1}$]; ΔS [$J.mol^{-1}.K^{-1}$] and ΔG [$kJ.mol^{-1}.K^{-1}$] for the interaction of $A\beta_{17-21r}$ with nNOS at various temperatures 103

Table 4.7: Values for fluorescent parameters (K_{sv} [μM^{-1}], K_a [μM^{-1}],K_d [μM],θ and n) and thermodynamic parameters ΔH [$kJ.mol^{-1}.K^{-1}$]; ΔS [$J.mol^{-1}.K^{-1}$] and ΔG [$kJ.mol^{-1}.K^{-1}$] for the interaction of $A\beta_{17-21p}$ with nNOS at various temperatures 104

Table 4.8: Values for fluorescent parameters (K_{sv} [μM^{-1}], K_a [μM^{-1}],K_d [μM],θ and n) and thermodynamic parameters ΔH [$kJ.mol^{-1}.K^{-1}$]; ΔS [$J.mol^{-1}.K^{-1}$] and ΔG [$kJ.mol^{-1}.K^{-1}$] for the interaction of $A\beta_{29-33r}$ with nNOS at various temperatures 105

Table 4.9: Values for fluorescent parameters (K_{sv} [μM^{-1}], K_a [μM^{-1}],K_d [μM],θ and n) and thermodynamic parameters ΔH [$kJ.mol^{-1}.K^{-1}$]; ΔS [$J.mol^{-1}.K^{-1}$] and ΔG [$kJ.mol^{-1}.K^{-1}$] for the interaction of $A\beta_{29-33p}$ with nNOS at various temperatures 106

Table 4.10: Values for fluorescent parameters (K_{sv} [μM^{-1}], K_a [μM^{-1}],K_d [μM],θ and n) and thermodynamic parameters ΔH [$kJ.mol^{-1}.K^{-1}$]; ΔS [$J.mol^{-1}.K^{-1}$] and ΔG [$kJ.mol^{-1}.K^{-1}$] for the interaction of Ag with nNOS at various temperatures..... 107

Table 4.11: Values for fluorescent parameters (K_{sv}[μM^{-1}], K_a [μM^{-1}],K_d [μM],θ and n) and thermodynamic parameters ΔH [$kJ.mol^{-1}.K^{-1}$]; ΔS [$J.mol^{-1}.K^{-1}$] and ΔG [$kJ.mol^{-1}.K^{-1}$] for the interaction of Au with nNOS at various temperatures..... 108

Table 4.12: Values for fluorescent parameters (K_{sv}[μM^{-1}], K_a [μM^{-1}],K_d [μM],θ and n) and thermodynamic parameters ΔH [$kJ.mol^{-1}.K^{-1}$]; ΔS [$J.mol^{-1}.K^{-1}$] and ΔG [$kJ.mol^{-1}.K^{-1}$] for the interaction of curcumin with nNOS at various temperatures..... 109

Table 4.13: A qualitative description of a reaction based on the signs of ΔH [$kJ.mol^{-1}.K^{-1}$]; ΔS [$J.mol^{-1}.K^{-1}$ and ΔG [$kJ.mol^{-1}.K^{-1}$] for the interaction of Aβ, nanoparticles and curcumin with nNOS at various temperatures(T)in Kelvin (K)(Masterton and Hurley, 2009; Whitten et al., 2007) 115

Table 5.1: Values for the distance (Å) that flexible Trp678 and Tyr706 moved relative to the rigid heme upon binding of Aβ peptides and curcumin. The corresponding binding energy ($kcal.mol^{-1}$) and docking Ki (μM) for binding of the ligands was calculated by AutoDock 4.2. The original distance of the Trp678 and Tyr706 from heme was 10 Å. The values for the experimental K_i were obtained in chapter 2....…..141

Table 5.2 Distance of tryptophan residues from the rigid heme (NA) (≤ 10 Å), not shown on Fig.5.5-Fig.5.8 142

Table 5.3: FRET values for efficiency of energy transfer (E)(%) and distance (r [Å]) between donor (D)[nNOS] and acceptor (A)[original Aβ, polar and reversed Aβ, nps and curcumin] based on the fluorescence of both donor and acceptor($F^{D,A}$) and the fluorescence of donor (F^D) (R_0 = 44 Å) 149

Table 5.4 Distance of tryptophan residues from the rigid heme (NA) (> 10 Å) 149

List of Equations

$A = \varepsilon cl$ ….. Eq [1] 32

$E + S \rightleftharpoons ES \rightleftharpoons E + P$ ….. Eq [2] 32

$V = V_{max}[S]/(K_m + [S])$ ….. Eq [3] 32

$[S]/V = [S]/V_{max} + K_m/V_{max}$ ….. Eq [4] 34

$K_i = [L].V_{max}^{app}/V_{max} - V_{max}^{app}$ ….. Eq [5] 34

Enzyme activity = $\Delta A.V_T.D_f / \varepsilon.t.l.V_e$ = µmol/ml/min ….. Eq [6] 37

$100 – (V_i/V_o \times 100)$ ….. Eq [7] 40

$F_0/F = 1 + K_{sv}[q]$ ….. Eq [8] 90

$F_0/\Delta F = 1/\theta\ K_{sv}[q] + 1/\theta$ ….. Eq [9] 90

$\text{Log}\ [F_0\text{-}F]/F = \text{Log}\ K_a + n \log [q]$ ….. Eq [10] 90

$\Delta G = \Delta H - T\Delta S$ ….. Eq [11] 92

$\ln K = - \Delta H/RT + \Delta S/R$ ….. Eq [12] 93

$\Delta G = RT\ln (K_d)$ ….. Eq [13] 127

Efficiency of transfer (E) = $1 - F^{D,A}/F^D = R_0^6/R_0^6 - r^6$ ….. Eq [14] 130

$R_0 = 8.79 \times 10^{-5} (Q_D\, k^2\, n^{-4}\, J)$ ….. Eq [15] 130

$J = [\sum F(\lambda)\varepsilon(\lambda)\lambda^4\Delta\lambda]/[\sum F(\lambda)\Delta\lambda]$ ….. Eq [16] 130

List of Symbols and Abbreviations

α: alpha
β: beta
γ: gamma
η: refractive index
$\varphi_{D:}$ fluorescence quantum yield of fluorescein
θ: number of tryptophan's exposed on enzyme
ε: extinction coefficient
ΔG: Gibbs energy change
ΔH: Enthalpy change
ΔS: entropy change
ΔF: change in fluorescence
$\Delta S_{protein}$: entropic contributions of a structured protein to the binding of a ligand
ΔS_{conf}: proteins internal conformational entropy
ΔS_{RT}: proteins rotational and translational entropy
λ_{ex}: excitation wavelength
λ_{em}: emission wavelength
nM: nanomolar
μM: micromolar
mM: millimolar
nm: nanometer
Å: Angstroms
s: second
R.U: response units
kcal/mol: kilo calories per mole
a.u.: arbitrary units
Aβ: amyloid beta
$A\beta_{17\text{-}21p}$/ $A\beta_{29\text{-}33p}$: polar amyloid beta
$A\beta_{17\text{-}21r}$/$A\beta_{29\text{-}33r}$: reversed amyloid beta
A: acceptor
AchE: acetylcholinesterase
AD: Alzheimer's disease
Ag: silver
Ala(A): Alanine
Asp(D): Aspartate
Au: gold
BAEE: N^{α}-benzoyl-L-arginine ethyl ester
c: concentration
*c**: critical micelle concentration
ChAT: choline acetyltransferase
ChE-Is : cholinesterase inhibitors
ChT: chymotrypsin
CNS: central nervous system
CPU: central processing unit
Cu:copper
D:donor
D_f: dilution factor
DMSO: dimethyl sulfoxide
E: the efficiency of energy transfer
EDTA: ethylenediaminetetra-acetic acid
EDAC: 1-ethyl-3-(3-dimethylaminopropyl) carbodiimide hydrochloride
eNOS: endothelial nitric oxide synthase
F: fluorescence in presence of quencher
F_0: fluorescence in absence of quencher
F^D: fluorescence of the donor
$F^{D,A}$: fluorescence of the donor and acceptor
FAD: flavin adenine dinucleotide
Fe: iron
FMN: flavin mononucleotide
FRET: fluorescence resonance energy transfer
GFP: green fluorescent protein
GxxxG: glycine zipper motif
Glu(E): Glutamate
Gly(G): Glycine
Gln (Q): Glutamine
H_4B: tetrahydro-L-biopterin dichloride
HCl: hydrochloric acid
His (H): Histidine

Al: Aluminium
APP: amyloid precursor protein
apoE: apolipoprotein E
Arg (R): Arginine
Asn (N): Asparagine
Ile (I): Isoleucine
iNOS: inducible nitric oxide synthase
J: the overlap integral between the acceptor emission and donor excitation
K_2PtCl_4: potassium tetrachloroplatinate (II)
K_{sv} : stern volmer constant
K_a: the association constant
K_d: the dissociation constant
K_i: the inhibitor constant
K:Kelvin
K_m^{app}: apparent concentration of substrate that leads to half–maximal velocity in presence of inhibitor
K_m: concentration of substrate that leads to half–maximal velocity
k^2: relative orientation of the donor and acceptor
l:path length
L-NHA: N-hydroxy –L-arginine
Leu (L): Leucine
LEV: Levetiracetam
L: ligands (Aβ,nps and curcumin)
Lys (K): Lysine
Met (M): Methionine
MRI: magnetic resonance imaging
MMPCs: mixed monolayer protected clusters
NO: nitric oxide
NADPH: nicotinamide adenine dinucleotide phosphate
NFTs: neurofibrillary tangles
NSAIDs: non-steroidal anti-inflammatory drugs
nps: nanoparticles
nNOS: neuronal nitric oxide synthase
n: number of binding sites
NMR: nuclear magnetic resonance
NaCl: sodium chloride
NaOH: sodium hydroxide
$NaBH_4$: sodium borohydride
HSAF: horse spleen apoferritin
HEWL: hen egg white lysozyme
[I]= concentration of inhibitor in μM
PBS: phosphate buffer saline
PrP: prion protein
Phe (F): Phenylalanine
PET: positron emission tomography
PS1 and PS2: presenilin proteins 1 and 2
PEG: polyethylene glycol
Q_D: the quantum yield of the donor
Q: quantum yield
q: quencher
[q]: concentration of quencher
ROS: reactive oxygen species
R_0: Förster distance
r: distance between donor and acceptor
RMSD: root mean square deviation
R: gas constant (8.314 $J.mol^{-1}.K^{-1}$)
[S]: concentration of substrate in μM
Ser(S): Serine
SPR: Surface Plasmon Resonance
S.E.M.: standard error mean
S_0 : ground energy state
S_1: relaxed singlet state
sulfo-NHS: N-hydroxysulfosuccinimide
Tyr (Y): Tyrosine
Trp (W): Tryptophan
TLC: thin layer chromatography
TEM: transmission electron microscopy
ThT: Thioflavin T
t: time
UV-vis: ultraviolet visible
V_{max}: maximum initial velocity or rate of a reaction
V_{max}^{app}: apparent maximum velocity in presence of inhibitor.
Val(V): Valine
V: activity of the enzyme in μmol/min
V_i: initial rate/activity of enzyme
V_0: enzyme activity without ligand
V_T: total volume

O2D: second delta oxygen
$ONOO^-$: peroxynitrite
V_e : volume of enzyme
Zn: Zinc

Research outputs

Publications:

1. Padayachee E.R. and Whiteley C.G. (2013) Interaction of glycine zipper fragments of Aβ-peptides with neuronal nitric oxide synthase: Kinetic, thermodynamic and spectrofluorimetric analysis. *Neuropeptides*,**47**:171-178

2. Padayachee E.R. and Whiteley C.G. (2011) Spectrofluorimetric analysis of amyloid peptides with neuronal nitric oxide synthase: Implications in Alzheimer's disease. *Biochimica et Biophysica Acta*, **1810**: 1136-1140

3. Padayachee E.R., Ngqwala N., Whiteley C.G. (2011) Association of β-amyloid peptide fragments with neuronal nitric oxide synthase: Implications in the etiology of Alzheimer's disease. *Journal of Enzyme Inhibition and Medicinal Chemistry*, **27**:356-64

N.B All 3 publications are attached as an amendment.

Conference outputs:

1. Presented: 'An understanding for the mechanism of Alzheimer's disease', Padayachee E.R and Whiteley C.G; work presented by myself at the Society for Neuroscience-42nd Annual Meeting, New Orleans, United States of America, October 2012.

2. Presented: 'A mechanistic understanding of the interaction between neuronal nitric oxide synthase (nNOS) and amyloid peptide (Aβ) motifs: an insight into the etiology of Alzheimer's disease', Padayachee E.R and Whiteley C.G; work presented by myself at the Academy of Science of South Africa (ASSAF): Changing lives through Chemistry, September 2011

3. Presented: 'Investigation into the affinity of amyloid peptide fragments with neuronal nitric oxide synthase: Implications in Alzheimer's disease', Padayachee E.R and Whiteley C.G; work presented by myself at South China University of Technology (SCUT) in Guangzhou Province (China), September 2010

4. Presented: '*Neuronal nitric oxide synthase and interaction with beta-amyloid peptides as a biomarker for Alzheimer's disease'*,Padayachee E.R and Whiteley C.G; work presented by myself at the International Society of Neurochemistry/Asian-Pacific Society of Neurochemistry (ISN/APSN) school at the Centre of Neuroscience, Mahidol University, Bangkok, Thailand, October 2010

Neuropeptides 47 (2013) 171–178

Contents lists available at SciVerse ScienceDirect

Neuropeptides

journal homepage: www.elsevier.com/locate/npep

Interaction of glycine zipper fragments of Aβ-peptides with neuronal nitric oxide synthase: Kinetic, thermodynamic and spectrofluorimetric analysis

E.R. Padayachee, C.G. Whiteley *

Department of Biochemistry, Microbiology and Biotechnology, Rhodes University, Grahamstown, South Africa

ARTICLE INFO

Article history:
Received 14 June 2012
Accepted 24 December 2012
Available online 31 January 2013

Keywords:
Amyloid peptides
Neuronal nitric oxide synthase
Alzheimer's disease
Kinetic
Thermodynamic
Spectrofluorimetric analysis
Dynamic quenching

ABSTRACT

Five peptide fragments [$A\beta_{17-21}$; $A\beta_{25-29}$; $A\beta_{29-33}$; $A\beta_{33-37}$; $A\beta_{25-37}$] of the toxic $A\beta_{1-40(42)}$ amyloid peptide were shown to bind with neuronal nitric oxide synthase by means of hydrophobic–hydrophobic forces. The enzyme has a single site for the amyloid peptide binding, which resulted in a quenching of the intrinsic fluorescence of the enzyme. Binding constants determined from Stern–Volmer analysis were between 9×10^{-3} and 1.8×10^{-2} μM^{-1}. As temperature increased these binding constants increased reflecting that the interaction of the amyloid peptides with nNOS was endothermic and the quenching was dynamic. Kinetic analysis revealed a non-competitive interaction of the amyloid peptides to the enzyme with inhibitor constants of 5.1 μM for $A\beta_{17-21}$ to about 8–12 μM for the other peptides. According to the van't Hoff relationship the thermodynamic parameters, ΔH, ΔS and ΔG for the interaction of the amyloid peptides were all positive and between 41.28 and 77.86 kJ mol^{-1} K^{-1}, 104.92 and 220.82 J mol^{-1} K^{-1} and 9.92 and 13.13 kJ mol^{-1} K^{-1}, respectively. This suggested that the transition state, created by the amyloid peptide-nNOS complex and generated during the initial stages of Aβ aggregation had to, initially, overcome an activation barrier. Since the ΔG values decreased as temperature increased it not only implied a non-spontaneous interaction but that hydrophobic forces were operative during the binding. By FRET analysis the distance between the donor enzyme and the acceptor amyloid peptide was between 2.7 and 2.8 nm. As the temperature increased from 298 K through 313 K (and higher) the fraction of these tryptophan residues that became exposed increased, to approach a value of 1. There was strong support for the initial interaction being through the glycine zipper regions of $A\beta_{25-37}$.

1. Introduction

The deposition of aggregated β-amyloid senile plaques and neurofibrillary tangles in the human brain are classic observations in the neuropathology of Alzheimer disease (AD) (Soto et al., 1994, 1995; Findeis 2007). An understanding of the mechanism of their formation, however, remains elusive. There are elevated levels of arginine in the cerebrospinal fluids of an Alzheimer's patient (Yi et al., 2009) and that the astrocytes, in a diseased brain, not only store arginine but are surrounded by these insoluble amyloid plaques (Poulos et al., 2002). It is uncertain whether the elevated level of arginine in the brains and cerebrospinal fluid of Alzheimer patients is as a result, or a cause, of the disorder (Yi et al., 2009). Since this accumulation of arginine may be as a result of inhibition of arginine-metabolising enzymes it would seem logical, therefore, in the etiology and pathogenesis of the disease, to investigate such enzymes and their intimate association with amyloid peptides (Padayachee et al., 2011; Padayachee and Whiteley, 2011). Alzheimer's disease (AD), a progressive and fatal neurodegenerative disorder supported by a variety of neuropsychiatric symptoms, behavioral disturbances (Soto et al., 1994), progressive impairment of activities of daily living and cognitive and memory deterioration can be manifested by considering both oxidative and nitrosative stress (Butterfield et al., 2007). It is not fully understood whether these levels of stress precede, contribute directly, or are as a result of AD pathogenesis (Butterfield et al., 2007).

A molecule that is responsible, not only for the increase of oxidative/nitrosative stress by *in vivo* formation of peroxynitrite but also in the modulation of different intracellular pathways associated with Alzheimer's disease, is nitric oxide (NO) and large amounts of NO are neurotoxic whereas smaller concentrations are neuroprotective (Calabrese et al., 2007). The production of NO in the brain is via neuronal nitric oxide synthase (nNOS) [EC. 1.14.13.39] that uses arginine as a substrate (Fig. 1). This reaction, localised within the astrocytes in the brain, induces proteins in the cellular environment to unfold and trigger the aggregation of susceptible peptides (Iwata et al., 2000) such as amyloid peptides into insoluble fibrils. An understanding of the function and action of

* Corresponding author. Address: Department of Biochemistry, Microbiology and Biotechnology, Rhodes University, P.O. Box 94, Grahamstown 6140, South Africa. Tel.: +27 46 6038085; fax: +27 46 6223984.
E-mail address: C.Whiteley@ru.ac.za (C.G. Whiteley).

0143-4179/$ - see front matter © 2013 Elsevier Ltd. All rights reserved.
http://dx.doi.org/10.1016/j.npep.2012.12.006

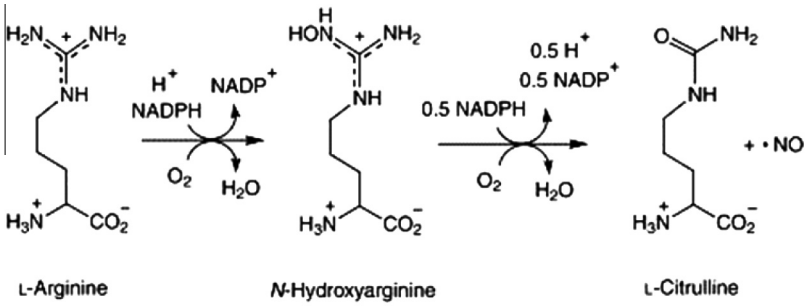

Fig. 1. Enzymatic reaction for neuronal nitric oxide synthase.

nNOS, with respect to amyloid peptide aggregation (fibrillogenesis) and subsequent formation of senile plaques, may facilitate an understanding of neurodegeneration in Alzheimer disease.

In a preliminary study (Padayachee et al., 2011; Padayachee and Whiteley, 2011) it was proposed that nNOS was first inhibited by the peptide fragments – $A\beta_{17-28}$, $A\beta_{25-35}$ and $A\beta_{32-35}$ – of the amyloid peptides $A\beta_{1-40(42)}$, and then was catalytic towards fibrillogenesis. Consequently it was essential to establish the critical amino acids within these fragments that were responsible, mechanistically, for their binding, inhibition and reasonable cause to fibril formation. Moreover it was of special interest to focus on several hydrophobic pentapeptide patches within the sequence Leu_{17}–Val_{18}–Phe_{19}–Phe_{20}–Ala_{21} and the glycine zipper regions [G-X-X-G] [Gly_{25}–Ser_{26}–Asn_{27}–Lys_{28}–Gly_{29}]; [Gly_{29}–Ala_{30}–Ile_{31}–Ile_{32}–Gly_{33}]; [Gly_{33}–Leu_{34}–Met_{35}–Val_{36}–Gly_{37}]. Zipper interactions have been identified and studied repeatedly with molecular dynamics simulations (Kim, 2009; Kim et al., 2005; Mikre et al., 2011; Berharnu and Hansmann, 2012).

We now present a kinetic, thermodynamic and a spectrofluorimetric analysis of the interaction of five amyloid peptide fragments [$A\beta_{17-21}$; $A\beta_{25-29}$; $A\beta_{29-33}$; $A\beta_{33-37}$ and $A\beta_{25-37}$] on neuronal nitric oxide synthase.

2. Materials and methods

2.1. Materials

Bovine brain was donated by Rosedale abattoir (Grahamstown, South Africa). The amyloid peptide fragments were synthesised by Biopep Peptide Research Group, Stellenbosch, South Africa. All reagents were of analytical grade and all solutions were prepared with deionised water obtained from a Milli-Q system. Ultra-violet and fluorimetric analyses were carried out on PowerWave microplate spectrophotometer and spectrofluorimeter (Bio-Tek Instruments) with 96 well plates, operated at 1 nm bandwidth using the KC Junior software program.

2.2. Purification of nNOS

Neuronal nitric oxide synthase was purified as previously described (Padayachee et al., 2011). In brief bovine brain (374 g) was homogenised by sonication (10 W, 30 s intervals, 4 min) in HEPES buffer (50 mM, pH 7.6, 600 ml) that contained ethylenediaminetetra-acetic acid [EDTA] (1.0 mM), NADPH (1.0 mM), dithiothreitol [DTT] (0.5 mM) and phenylmethylsulphonylfluoride [PMSF] (0.43 mM). The cell debris was removed by centrifugation (10,000*g*, 4 °C, 30 min) and the crude cell-free extract (20 ml), dialysed and then applied to a DEAE-Sepharose anion-exchanger resin, previously equilibrated with Tris–HCl buffer (50 mM, pH 7.6). Active fractions of nNOS were eluted with 0.75 M NaCl in the same buffer at a flow rate of 2 ml min^{-1}.

2.3. Characterisation of nNOS

The purity of the enzyme was confirmed by SDS–PAGE analysis and its optimum temperature, pH, thermal stability and kinetic parameters (K_m and V_{max}) established as previously described (Padayachee et al., 2011).

2.4. Protein determination

The protein concentration for all experiments was routinely determined according to the method of Bradford (Bradford, 1976). The assay was performed in triplicate in a 96-well microplate. Enzyme extract (5 μl) was added to a single well, followed by Bradford reagent (245 μl). The mixture was incubated at 22 °C for 10 min and absorbance of the solution measured at 595 nm and the concentration of the unknown samples was determined using a bovine serum albumin standard curve.

2.5. Neuronal nitric oxide synthase (nNOS) assay

This assay was conducted, with slight modification, according to the protocol previously described (Padayachee et al., 2011). In summary the reaction mixture contained benzoyl-L-arginine ethyl ester (5 mM, 10 μl), $CaCl_2$ (5 mM, 10 μl), dithiothreitol (2 mM, 10 μl) in Tris–HCl buffer (50 mM, pH 7.6, 940 μl). The reaction was started by the addition of enzyme extract (10 μl) in NADPH (1.0 mM, 10 μl) and allowed to incubate at 40 °C for 2 min, before being stopped with perchloric acid (5 M, 10 μl). This mixture (250 μl) was treated with chromogenic reagent (250 μl) and cooled to 22 °C for 2 min. The reduction of benzoyl-L-arginine ethyl ester was then determined spectrophotometrically at 530 nm. Chromogenic reagent was made from thiosemicarbazide (18 mM) in 2,3-butanedione monoxime solution (500 mg in 100 ml distilled water) and sulphuric:orthophosphoric acid (1:1) in the presence of ferric chloride (0.25 g). The citrulline extinction coefficient (ε_{530}) was 27.3 ml μmol^{-1} (Sakakibara and Yanagisawa, 2003). One unit of activity was defined as the amount of nNOS that produced 1 μmol of citrulline per min per ml reaction mixture.

2.6. Kinetic analysis

Partially purified nNOS (5 μl) in Tris HCl buffer (50 mM, pH 7.6) was treated with amyloid peptides $A\beta_{17-21}$, $A\beta_{25-29}$, $A\beta_{29-33}$, $A\beta_{33-37}$ and $A\beta_{25-37}$ (0–8 μM) in a total volume of 500 μl and in the presence of benzoyl arginine ethyl ester (0–8 μM). The nNOS activity was assayed, over a 5 min period, at each substrate concentration.

2.7. Fluorimetric analysis

2.7.1. Fluorescence resonance energy transfer (FRET)

The FRET assay procedure was based on a method previously described but with slight modifications (Prostak et al., 2005). Amy-

loid peptides ($A\beta_{17-21}$; $A\beta_{25-29}$; $A\beta_{29-33}$; $A\beta_{33-37}$ and $A\beta_{25-37}$) were dissolved in DMSO to a concentration of 1 mM. Three separate reactions, each with a final volume of 200 μl, were performed: reaction 1 between the acceptor chromophore (BAEE) and fluorescein (donor chromophore) [$F^{D,A}$]: fluorescein (3 μl; 1 mM), nNOS (5 μl), BAEE (5 μl; 1 mM) and triethanolamine buffer [10 mM/0.1 M NaCl; pH 7.4]. Reaction 2 was between the acceptor chromophore ($A\beta_{17-21}$; $A\beta_{25-29}$; $A\beta_{29-33}$; $A\beta_{33-37}$ and $A\beta_{25-37}$) and fluorescein (donor chromophore) [$F^{D,A}$]: fluorescein (3 μl; 1 mM); nNOS (5 μl); $A\beta_{17-21}$; $A\beta_{25-29}$; $A\beta_{29-33}$; $A\beta_{33-37}$ and $A\beta_{25-37}$ in DMSO (5 μl; 1 mM) and triethanolamine buffer [10 mM/0.1 M NaCl; pH 7.4]. Reaction 3 included determining the fluorescence of the donor (nNOS) [F^{D}] which was prepared by monitoring the fluorescence of nNOS alone with the omission of accepter chromophores. All three reactions were left to incubate at 25 °C for 15 min to allow sufficient interaction between the acceptor and fluorescein such that the fluorescence was an indication of the fluorescein-acceptor complex and not fluorescein alone. Fluorescence was read at 488 nm (excitation) and 518 nm (emission) (fluorescein dependent excitation and emission wavelength).

2.7.2. Quenching

Spectrofluorimetry was used to determine structural changes induced in nNOS by the interaction of the amyloid peptides with the purified enzyme. The excitation wavelength was fixed at 295 nm, the wavelength at which tryptophan absorbs, and the emission wavelength was at 482 nm. The change in fluorescence of a solution was monitored, over 10 min, as increasing concentrations of [$A\beta_{17-21}$; $A\beta_{25-29}$; $A\beta_{29-33}$; $A\beta_{33-37}$ and $A\beta_{25-37}$] (0–8 μl, 0–40 μM) were added to a reaction mixture of nNOS (5 μl) in triethanolamine buffer (pH 7.4, 10 mM) containing NaCl (100 mM) in a final volume of 200 μl. All fluorescence quenching experiments were performed at four different temperatures (25 °C [298 K]; 30 °C [303 K]; 35 °C [308 K]; 40 °C [313 K]).

2.8. Statistical analyses

All experiments were carried out in triplicate. Mean and standard deviation calculations and comparison of data using analysis of variance (ANOVA) was performed to 5% level of significance ($p < 0.05$) using Statistica for Windows, version 8 (Statsoft Inc.) and Microsoft Excel 2010.

3. Results and discussion

3.1. Binding site for amyloid peptides on nNOS

$$\log[F_o - F/F] = \log K_a + n \log[Q] \quad (1)$$

where F_o and F are the fluorescent intensities of nNOS in the absence and presence of amyloid peptide respectively; Q is the concentration of amyloid peptide; 'n' is the number of binding sites (on the purified enzyme available for the amyloid peptides K_a is the association constant [and its reciprocal dissociation constant (K_d)]. Both K_a and 'n' were estimated, respectively, from the slope of the linear regressions and the intercept on the log[(Fo−F)/F] axis (Fig. 2) (Xie et al., 2005) (Eq. (1)). In all of the cases it was clear that only one binding site was available (Table 1). The values obtained for the binding constants (K_d) at 298 K (Table 1) indicated a reasonable affinity between nNOS and the amyloid peptides. Furthermore if the plot log[(Fo−F)/F] vs log[Q] is performed at increasing temperatures the binding constants increased as temperature increased reflecting that the interaction of the amyloid peptides with nNOS was endothermic (Table 2). It should be mentioned that at each of the different temperatures $A\beta_{29-33}$ had approximately twice the affinity for the enzyme then all of the other peptides.

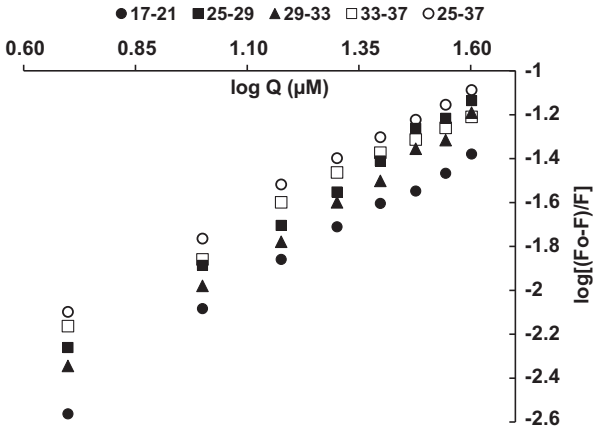

Fig. 2. Hill plots of log[(Fo−F)/F] versus log[Q] for the binding of $A\beta_{17-21}$; $A\beta_{25-29}$; $A\beta_{29-33}$; $A\beta_{33-37}$; $A\beta_{25-37}$ (0–40 μM) with nNOS (5 μl) in triethanolamine buffer (pH 7.4, 10 mM) containing NaCl (100 mM) in a final volume of 200 μl. Excitation wavelength (295 nm); emission wavelength (482 nm). Temperature 25 °C [298 K].

Table 1
Stern–Volmer quenching constants and inhibitor constants (K_i) from the interaction of nNOS (5 μl) in triethanolamine buffer (pH 7.4, 10 mM) containing NaCl (100 mM) in a final volume of 200 μl when treated with amyloid peptides $A\beta_{17-21}$; $A\beta_{25-29}$; $A\beta_{29-33}$; $A\beta_{33-37}$ and $A\beta_{25-37}$ (0–40 μM). Temperature 25 °C [298 K].

	$A\beta_{17-21}$	$A\beta_{25-29}$	$A\beta_{29-33}$	$A\beta_{33-37}$	$A\beta_{25-37}$
K_a $(\mu M)^{-1}$	0.17	0.14	0.37	0.19	0.18
K_d (μM)	6.06	6.99	2.67	5.37	5.49
K_{SV} $(\mu M)^{-1}$	0.015	0.018	0.009	0.11	0.014
n	1.16	1.15	1.13	1.08	1.12
θ	0.47	0.5	0.41	0.39	0.45
Ki (μM)	5.1	9.15	9.12	8.4	11.6

3.2. Kinetic analysis

A study into the effect of substrate concentration on the kinetic activity of nNOS was investigated by measuring enzyme activity over a range of benzoyl arginine ethyl ester concentrations (0–8 μM). A typical increase in substrate concentration resulted in a proportional increase in activity as shown by the Michaelis–Menten and Hanes–Woolf plots (Fig. 3; $A\beta_{17-21}$ shown) and for benzoyl arginine hydrolysis, the V_{max} and K_m were 10.88 μmol ml^{-1} min^{-1} and 2.54 μM, respectively. The turnover number (k_{cat}) and the catalytic efficiency, calculated using Eqs. (2) and (3) and were found to be 0.28 s^{-1} and 0.11 s^{-1} μM^{-1}, respectively. The total amount of enzyme [E_t] was 32.5 nmol.

$$k_{cat} = V_{max}/E_t \quad (2)$$

$$\text{Catalytic efficiency} = k_{cat}/K_m \quad (3)$$

The affinity of the nitric oxide synthase for amyloid peptides was determined by including the peptides to a concentration of between 0–8 μM with the substrate benzoyl arginine ethyl ester also between the same values (0–8 μM). The results indicated that for each peptide the V_{max} decreased accordingly (Fig. 3; $A\beta_{17-21}$ shown) while the K_m value remained unchanged at 2.54 μM. The inhibitor constant (K_i) calculated from equation 4 indicated the binding affinity of enzyme for inhibitor (Table 1).

$$K_i = [A\beta.V^{app}_{max.}]/[V_{max} - V^{app}_{max}] \quad (4)$$

where Aβ = concentration of amyloid peptide; $V^{app}_{max.}$ = apparent maximum velocity in the presence of amyloid peptides. Results showed that $A\beta_{17-21}$ inhibited nNOS the most as reflected by its rel-

Table 2
Stern–Volmer quenching constants from the interaction of nNOS (5 μl) in triethanolamine buffer (pH 7.4, 10 mM) containing NaCl (100 mM) in a final volume of 200 μl when treated with amyloid peptides $A\beta_{17-21}$; $A\beta_{25-29}$; $A\beta_{29-33}$; $A\beta_{33-37}$; $A\beta_{25-37}$ (0–40 μM). Temperature 25 °C [298 K]; 30 °C [303 K]; 35 °C [308 K]; 40 °C [313 K]; 45 °C [318 K] and 55 °C [328 K].

	$A\beta_{17-21}$			$A\beta_{25-29}$			$A\beta_{29-33}$			$A\beta_{33-37}$			$A\beta_{25-37}$		
K	K_{SV} $(\mu M)^{-1}$	K_d (μM)	θ	K_{SV} $(\mu M)^{-1}$	K_d (μM)	θ	K_{SV} $(\mu M)^{-1}$	K_d (μM)	θ	K_{SV} $(\mu M)^{-1}$	K_d (μM)	θ	K_{SV} $(\mu M)^{-1}$	K_d (μM)	θ
298	0.015	6.06	0.47	0.018	6.99	0.50	0.009	2.67	0.41	0.011	5.37	0.39	0.014	5.49	0.45
303	0.019	6.21	0.52	0.023	7.80	0.56	0.011	2.79	0.46	0.015	5.62	0.47	0.019	6.21	0.52
308	0.031	7.46	0.65	0.028	8.26	0.59	0.018	3.01	0.52	0.019	6.05	0.52	0.031	7.44	0.65
313	0.051	9.81	0.74	0.041	9.43	0.71	0.041	3.32	0.66	0.036	7.70	0.69	0.041	8.72	0.69
318	0.062	12.94	0.81	0.045	9.07	0.88	0.044	3.47	0.73	0.039	8.28	0.77	0.051	10.58	0.80
328	0.071	15.72	0.87	0.047	10.91	0.91	0.054	3.44	0.88	0.053	9.89	0.86	0.081	15.78	0.92

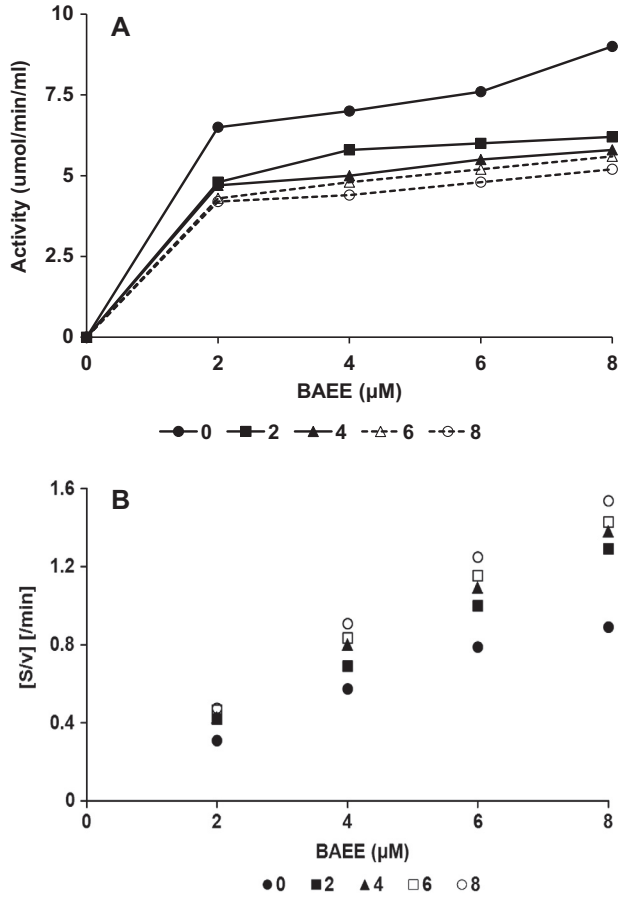

Fig. 3. (A) Michealis–Menten and (B) Hanes–Woolf plots of the interaction of $A\beta_{17-21}$ (0–8 μM) with nNOS (5 μl) in Tris HCl buffer (50 mM, pH 7.6) in the presence of benzoyl arginine ethyl ester [BAEE] (0–8 μM) in a total volume of 500 μl. The nNOS activity was assayed, over a 5 min period, at each substrate concentration.

atively low K_i value of 5.1 μM. K_i values for other peptides are noted (Table 1).

3.3. Fluorimetric analysis

3.3.1. Fluorescence energy resonance transfer (FRET)

Insight into molecular recognition of the binding of amyloid peptides with nNOS involves an investigation of hydrogen bonds, van der Waals forces as well as electrostatic and hydrophobic interactions. Neuronal nitric oxide synthase, with its 26 tryptophan, 32 tyrosine and 38 phenylalanine residues [PDB ID: 1OM4], is a most likely candidate for studying the actual binding pocket for the amyloid peptides through fluorescence spectroscopy involving FRET. Tryptophan fluor molecules within nNOS, behave as intrinsic quenchers decreasing the quantum yield of fluorescence (Q) and measuring the fluorophore accessibility to quenching allows for an estimation of the relative position of a fluorophore within the protein. The excitation energy of the donor molecule is transferred to an acceptor molecule without the emission of a photon. Absorption spectrum of the acceptor (fluor B) must overlap with the fluorescence emission spectrum of the donor (fluor A) which results in a decrease in donor emission along with an increase in acceptor emission intensity. If these fluors (fluor A and B) have unique locations in the protein, it is possible to measure distances or changes in distances within proteins (Ishii et al., 1999). The efficiency of energy transfer (E) is a quantitative measure of the number of quanta that are transferred from donor (D) to acceptor (A) and may be determined from the fluorescence intensity of a sample that contained only the donor D (i.e. F^D) and from a corresponding sample that contained acceptor (A) and a donor (D) (i.e. $F^{D,A}$) (Clegg, 1995). The use of FRET results from the strong dependence of the rate and efficiency of energy transfer on the sixth power of the distance r between D and A (Eq. (5)) (Sklar et al., 1977).

$$E = 1 - F^{D,A}/F^{D} = R_o^6/(R_o^6 + r^6) \quad (5)$$

where E is the efficiency of transfer between the donor and acceptor; r = distance between the donor and the acceptor; R_o = Förster distance when efficiency of transfer is 50%.

$$R_o^6 = 8.79 \times 10^{-25} \kappa^2 \eta^{-4} \varphi_D J \quad (6)$$

$$J = [\sum F(\lambda)\epsilon(\lambda)\lambda^4 \Delta\lambda]/[\sum F(\lambda)\Delta\lambda] \quad (7)$$

Ro depends on the relative orientation of the donor and acceptor (κ^2), the refractive index (η), the quantum yield of the donor (φ_D) in the absence of acceptor, and the overlap integral between the acceptor emission and donor excitation (J). $F(\lambda)$ is the fluorescence intensity of the fluorescent donor at wavelength (λ) and (λ) is the molar absorption coefficient of the acceptor at wavelength (λ).

The binding of the amyloid peptides caused a change in tryptophan fluorescence of nNOS and consequently the efficiency (E) of FRET can be represented by the actual distance between the donor (fluorescein) and acceptor (amyloid peptides) (Eq. (5)) (Ilichev et al., 2002). In the present study the values of κ^2, the average refractive index (η) and the fluorescence quantum yield of fluorescein (φ_D) are 0.667, 1.36 and 0.93 (Sjöback et al., 1995), respectively and from Eqs. ()()()(5)–(7) it would give respective values for J, E, Ro and r for $A\beta_{17-21}$; $A\beta_{25-29}$; $A\beta_{29-33}$; $A\beta_{33-37}$; $A\beta_{25-37}$ and BAEE [Table 3]. Any value for the distance between donor and acceptor (r) that is less than 10 nm and falls between 0.5 and 1.5 of the Ro value indicates a high probability that fluorescence transfer is taking place (Chen et al., 1990).

For each of the amyloid peptides the only intrinsic fluorophores present in any of the sequences are two phenyl rings (Phe_{19} and Phe_{20}) which have low quantum yield and so the possibility of

any internal quenching by these aromatic amino acids when $A\beta_{17-21}$ was bound to nNOS was negligible. Computational analysis of the active site of nNOS [PDB ID: 1OM4] showed that the arginine substrate binds within a distance of 2.98 nm [backbone chain nitrogen – heme oxygen] which is in good agreement to our fluorescent evaluation (2.36 nm). When each of the amyloid peptides became bound to nNOS these distances change to between 2.74 and 2.81 nm (Table 3). This means that the fraction of tryptophan residues depicted by θ (Eq. (8); Fig. 4) moves between 2.3 and 2.8 nm (about 23–28 Å) as either the substrate or the amyloid peptides bind. It is uncertain whether these tryptophan residues are the same in both cases. These differences in fluorescent intensities are due to the orientation relationship associated with their respective bindings that induced different conformational changes in nNOS. Consequently the position of the tryptophan residue(s) around the enzyme active site became positioned differently. The identity of this residue or residues, however, remains unknown at present and is a target for future research.

In view of the polarity of the active region of nNOS [Tyr_{588}, Glu_{592}, Asp_{597}, Gln_{478} and Tyr_{706}] it is unlikely that either the $A\beta_{17-21}$ peptide that contained the pentapeptide [Leu_{17}–Val_{18}–Phe_{19}–Phe_{20}–Ala_{21}] or the hydrophobic glycine zipper motifs $A\beta_{29-37}$ [Gly_{29}–Ala_{30}–Ile_{31}–Ile_{32}–Gly_{33}–Leu_{34}–Met_{35}–Val_{36}–Gly_{37}] would bind at this site in competition with normal substrate. Instead this argument supports our earlier finding from kinetic data that the amyloid peptides interact in a non-competitive manner with nNOS at a site remote to the active one. This does not rule out a possibility that the amyloid peptides may bind at the heme binding region. It should be pointed out, however, that the slightly more polar glycine zipper [Gly_{25}–Ser_{26}–Asn_{27}–Lys_{28}–Gly_{29}] was more suited to electrostatic interaction and hydrogen bonding with the enzymes active region.

In the absence of resonance energy transfer when nNOS and acceptor (BAEE or amyloid peptide) were not bound the donor signal of fluorescein was high and the emission of fluorescein-acceptor was low. When the enzyme-acceptor–donor complex formed, fluorescein, which was attached to the acceptor terminus, behaved as a 'fluorescence resonance gate' with a low donor signal (increased emission) while the acceptor signal was high (increased excitation) resulting in resonance energy transfer between donor and acceptor.

Since there was little significant difference in the binding parameters for all of the amyloid peptides it is tempting to suggest that any one of the 'glycine zipper motifs' was responsible for the initial interaction of the amyloid peptide with the enzyme. Support and evidence for this is forthcoming since 'glycine zipper' motifs can act as triggers in protein dimerisation, fibrillogenesis and proteolysis (Kim, 2009). Furthermore literature (Soto et al., 2007) indicates that $A\beta_{17-21}$ possesses a series of promising properties: it was able to cross the blood brain barrier, to inhibit (and disassemble) the formation of amyloid fibrils *in vitro* and *in vivo*, to prevent Aβ neurotoxicity in cell culture, to arrest amyloid deposition and to induce dissolution of preformed plaques in rat brain model of the amyloidogenic pathway. The use of $A\beta_{17-21}$ as a pseudoligand to block the process of fibrillogenesis showed promising future potential in the treatment of AD.

Table 3
Energy transfer parameters from FRET analysis for the interaction of amyloid peptides [$A\beta_{17-21}$; $A\beta_{25-29}$; $A\beta_{29-33}$; $A\beta_{33-37}$ and $A\beta_{25-37}$] and benzoyl arginine diethyl ester (BAEE) with nNOS as determined from Eqs. (5)–(7) [see text]. E is the efficiency of transfer between the donor (D) and acceptor (A); r = distance (nm) between the donor and the acceptor; Excitation wavelength (488 nm); emission wavelength (518 nm). $F^{D,A}$ = fluorescence intensity of a sample that contained both acceptor and a donor.

	$A\beta_{17-21}$	$A\beta_{25-29}$	$A\beta_{29-33}$	$A\beta_{33-37}$	$A\beta_{25-37}$	BAEE
$F^{D,A}$	130	108	169	124	109	46
E	0.935	0.946	0.915	0.938	0.945	0.977
r (nm)	2.83	2.74	2.97	2.81	2.74	2.36

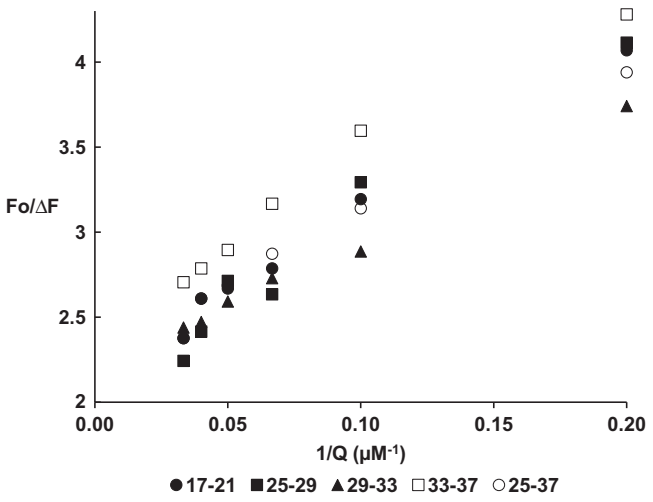

Fig. 4. Double reciprocal plots (modified Stern Volmer) for fluorescence quenching of nNOS (5 μl) in triethanolamine buffer (pH 7.4–10 mM) containing NaCl (100 mM) in a final volume of 200 μl when treated with amyloid peptides $A\beta_{17-21}$; $A\beta_{25-29}$; $A\beta_{29-33}$; $A\beta_{33-37}$; $A\beta_{25-37}$ (0–40 μM). Excitation wavelength (295 nm); emission wavelength (482 nm). Temperature 25 °C [298 K].

3.3.2. Quenching

As seen (Figs. 4 and 5) the addition of the amyloid peptides to nNOS resulted in a quenching in fluorescence with linearity in the Stern–Volmer plots implying that one, or more, tryptophan residues are close to the binding site. The possible quenching mechanism can be interpreted from the fluorescence analysis data and analysed according to the Stern–Volmer equations (Eqs. (8) and (9)) leading to a confirmation of binding constants, the Stern–Volmer constant (K_{SV}), estimated from the slope of the linear regression (Eq. (9)), as well as θ, the fractional maximum fluorescence

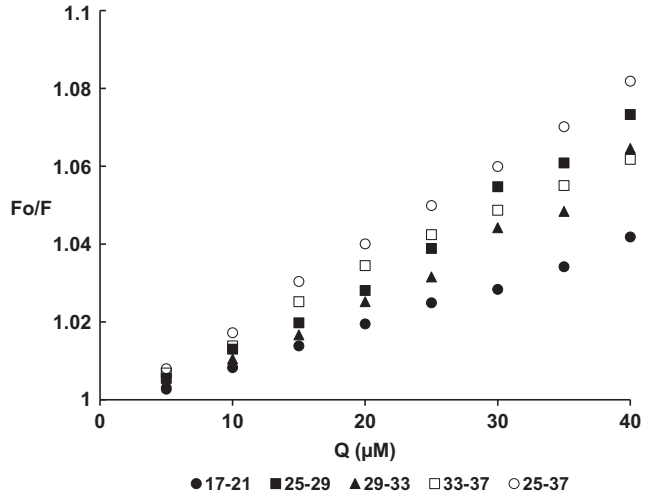

Fig. 5. Stern Volmer plots for fluorescence quenching of nNOS (5 μl) in triethanolamine buffer (pH 7.4, 10 mM) containing NaCl (100 mM) in a final volume of 200 μl when treated with amyloid peptides $A\beta_{17-21}$; $A\beta_{25-29}$; $A\beta_{29-33}$; $A\beta_{33-37}$ and $A\beta_{25-37}$ (0–40 μM). Excitation wavelength (295 nm); emission wavelength (482 nm). Temperature 25 °C [298 K].

intensity or number of available surface tryptophan residues (Table 1).

$$F_o/\Delta F = 1/(\theta K_{sv} Q) + 1/\theta \quad (8)$$

$$F_o/F = 1 + K_{sv} Q \quad (9)$$

where F_o, F = fluorescence in the absence and presence of amyloid peptide respectively; Q = concentration of amyloid peptide; K_{sv} = - Stern–Volmer constant; $\Delta F = F_o - F$; θ = fraction of accessible tryptophan residues.

It has been reported in recent literature (Amaral et al., 2010; Hao et al., 2010; Sambasivam et al., 2011) that a Stern–Volmer model is dependent on temperature and may be used in determining dynamic quenching constants. The differentiation, therefore, between a static and dynamic quenching mechanism is their dependence towards temperature and viscosity. A static mechanism is indicated by the formation of a non-fluorescent fluorophore-quencher complex while a dynamic one is characterised by a diffusion of the quencher, during the lifetime of the excited state, towards the fluorophore which, upon contact, returns to the ground state. Since FRET is dynamic in nature it must provide some proof, though perhaps speculative, of the probability that some of the quenching is dynamic in character. The Stern–Volmer constant, on the other hand, is a general term that can refer to either a dynamic or a static quenching process. Any upward-curving Stern–Volmer plot is indicative of a static quenching mechanism (Al-Kady et al., 2011; Schlamadinger et al., 2010) and since there was no evidence of this from our findings it supported a probable dynamic quenching. Since both static and dynamic quenching can afford linear Stern–Volmer plots differentiation between the two can only be achieved in a temperature dependent manner.

The binding data from both Stern–Volmer plots (cf: Figs. 4 and 5) of the nNOS tryptophan residues quenched by each of the amyloid peptides at different temperatures (25 °C [298 K]; 30 °C [303 K]; 35 °C [308 K]; 40 °C [313 K]) are shown [Tables 1 and 2] reflecting a probable dynamic rather than a static quenching because the K_{SV} increased with increasing temperature. Though there was possible enzyme denaturation at the higher temperatures of 45 °C [318 K] and 55 °C [328 K] it was pleasing to note that, not only did the K_{SV} values still increase with increasing temperature but that the fraction of accessible tryptophan residues also increased to approach a value of 1 (Table 2). Dynamic or FRET quenching arises from complex formation between the amyloid peptide and the enzyme for a short period of time. Upon binding of amyloid to nNOS, a process of collisions occurred whereby the excited energy of the fraction of tryptophan residue (θ) (Eq. (8); Fig. 4) was quenched by amyloid peptide and the resultant peptide-enzyme complex that formed was transient. As temperature increased from 298 K to 313 K (and higher) (Table 2), the larger thermal energy actually facilitated the diffusion of the amyloid peptide toward the enzymes binding site so that the fraction of tryptophan residues increased as they became more accessible and moved a distance of between 2.7 and 2.8 nm (Table 3).

The 'y intercept' in the respective Stern–Volmer plots (Fig. 5) was equivalent to 1, thereby indicating that fluorescence was only due to internal quenching by amino acids within the amyloid peptide and not the interplay of other fluors in solution which may result in external quenching.

3.4. Thermodynamic analysis

The thermodynamic parameters which are dependent on temperature were calculated according to the van't Hoff equation (Eq. (10)) in order to elucidate the interaction forces between the amyloid peptides and nNOS; ΔG is estimated (Eq. (11)) (Table 2).

$$\ln K_{sv} = -(\Delta H/RT) + (\Delta S/R) \quad (10)$$

$$\Delta G = \Delta H - T\Delta S \quad (11)$$

where R = gas constant (8.314 J mol^{-1} K^{-1}; ΔH = enthalpy change, ΔS = entropy change, ΔG = free energy change and K_{SV} = Stern Volmer binding constant at the corresponding temperature. Values of $\Delta H > 0$ and $\Delta S > 0$ indicates a hydrophobic interaction; $\Delta H < 0$ and $\Delta S < 0$ is indicative of hydrogen bonds and when $\Delta H = 0$ and $\Delta S > 0$ an electrostatic force prevails (Ross and Subramanian, 1981). A plot of ln$K$ vs $1/T$ (Fig. 6) would enable the determination of ΔH (slope) and ΔS (intercept) (Table 4). The positive ΔH and ΔS values (Table 4) implied hydrophobic forces are operative during the binding while the positive sign for ΔG (Table 4) indicates the interaction between the peptides and nNOS is non-spontaneous. This is indeed surprising since normal ligand–protein binding should be spontaneous with a negative ΔG. An explanation for this arises from earlier studies from our group (Padayachee et al., 2011; Padayachee and Whiteley, 2011) when it was established that as Aβ associates or binds to the nNOS it induces a conformational change in the enzyme – driven by hydrophobic interaction! The Aβ-nNOS complex is an amyloidogenic catalyst – initiating fibrillogenesis – changing the bound amyloid peptide into a form that can no longer bind (later deduced as a fibril). This process of fibrillogenesis is non-spontaneous and unfavourable. This argument is supported from other work in that fibrillogenesis requires the partial unfolding of the proteins or the partial folding of disordered proteins (Lansbury and Rochet, 2000). The initiation of fibrillogenesis is controlled by a large thermodynamically favourable entropy (large + ΔS). The fact that K_d increases with temperature reflects that the affinity of Aβ decreases at higher temperature (>313 K) until the peptide completely dissociates from the enzyme as a fibril. After the process of dissociation, the enzyme folds/refolds into a favourable native conformation which is a spontaneous process (and a negative ΔG). Consequently, in summary, the interaction of Aβ with nNOS (unfolding which initiates fibrillogenesis) is a thermodynamically unfavourable process at low temperatures (positive ΔG) but is coupled to a very spontaneous (folding) process at high temperatures with a negative ΔG.

It was noted that the more polar glycine zipper [Gly_{25}–Ser_{26}–Asn_{27}–Lys_{28}–Gly_{29}] which had the greatest association with the enzyme had the lowest value for ΔH (41.28 kJ mol^{-1} K^{-1}) and ΔS (104.92 J mol^{-1} K^{-1}) could be slightly more suited to electrostatic interaction and hydrogen bonding with the enzymes active region.

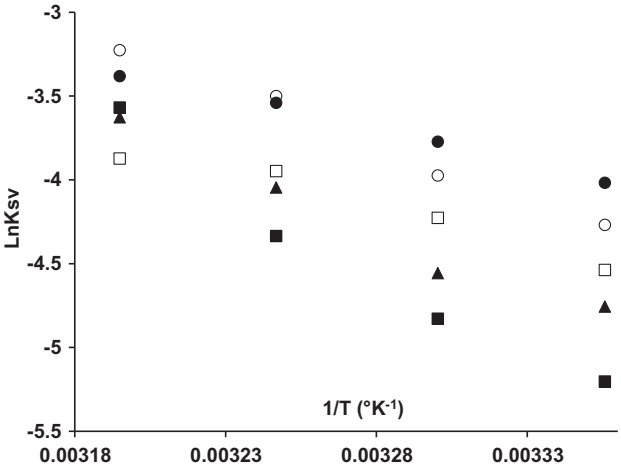

Fig. 6. van't Hoff plots for the determination of thermodynamic data [ΔH and ΔS] for the interaction of amyloid peptides (● ; $A\beta_{17-21}$; ■ ; $A\beta_{25-29}$; ▲ $A\beta_{29-33}$; □ $A\beta_{33-37}$ and ○ $A\beta_{25-37}$) with nNOS.

Table 4
Thermodynamic parameters ΔH [kJ mol^{-1} K^{-1}]; ΔS [J mol^{-1} K^{-1} and ΔG [kJ mol^{-1} K^{-1}] for the interaction of amyloid peptides [$A\beta_{17-21}$; $A\beta_{25-29}$; $A\beta_{29-33}$; $A\beta_{33-37}$ and $A\beta_{25-37}$]with nNOS. Temperature 25 °C [298 K]; 30 °C [303 K]; 35 °C [308 K] and 40 °C [313 K].

	$A\beta_{17-21}$			$A\beta_{25-29}$			$A\beta_{29-33}$			$A\beta_{33-37}$			$A\beta_{25-37}$		
K	ΔH	ΔS	ΔG	ΔH	ΔS	ΔG	ΔH	ΔS	ΔG	ΔH	ΔS	ΔG	ΔH	ΔS	ΔG
298	57.59	157.63	9.92	41.28	104.92	13.13	77.86	220.82	11.98	58.66	158.82	11.14	57.59	157.63	10.63
303			9.53			11.95			11.17			10.73			9.88
308			9.14			10.77			10.36			10.33			9.12
313			8.75			9.59			9.54			9.92			8.36

In view of all of the data presented the three glycine zipper motifs [G-X-X-X-G] [Gly_{25}–Ser_{26}–Asn_{27}–Lys_{28}–Gly_{29}]; [Gly_{29}–Ala_{30}–Ile_{31}–Ile_{32}–Gly_{33}]; [Gly_{33}–Leu_{34}–Met_{35}–Val_{36}–Gly_{37}], either individually or in tandem with each other, were critical in the initial interaction of the amyloid peptide with the enzyme.

The analysis of the primary structure and active site of each subunit of nNOS [PDB ID: 1OM4] reveals 13 tryptophan residues of which four [Trp_{409}, Trp_{561}, Trp_{587} and Trp_{678}] are within the active site, seven are near the enzyme surface and two others are buried elsewhere in the enzyme interior; Tyr_{588}, Glu_{592}, Asp_{597}, Gln_{478} and Tyr_{706} are also present within this active region and are capable of hydrogen bonding to the substrate. Quenching studies have demonstrated that binding of the amyloid peptides and/or the substrate decreases solvent exposure of a tryptophan residue implying that the local environment is altered with a decreased access to these Aβ. Since the parameter Θ is generally dependent on the polarity of the solvent it is the hydrophobic nature of the all of the amyloid peptides ($A\beta_{25-29}$ included) that induced conformational change in nNOS, allowing the tryptophan residue(s) to become more accessible (Tables 1 and 2). Aβ peptides interact with hydrophobic environments (Kanski et al., 2002; Soreghan et al., 1994) and so it was more than likely that nNOS-Aβ complexes were hydrophobic–hydrophobic associations once again endorsing that the hydrophobicity of the glycine zipper motifs was a trigger for the initial interaction of the amyloid peptide with the enzyme. These characteristic glycine zipper motifs have been identified in many proteins and, in the case of Aβ, were completely conserved suggesting that such motifs played an important role in their normal function that could have serious implications in the etiology and pathophysiology for Alzheimer's disease (Fonte et al., 2011; Kim et al., 2005; Mikre et al., 2011; Berharnu and Hansmann, 2012).

An in-depth molecular modelling and docking study of the interaction and binding of all of the amyloid peptide fragments to nNOS is on going and will be reported elsewhere.

4. Conclusions

The interaction between five short chained amyloid peptide fragments [$A\beta_{17-21}$; $A\beta_{25-29}$; $A\beta_{29-33}$; $A\beta_{33-37}$ and $A\beta_{25-37}$] and nNOS has been thoroughly investigated using, kinetic, thermodynamic and spectrofluorimetric analyses. Values for binding distances, binding modes and binding constants were obtained that was consistent with a non-spontaneous. dynamic quenching mechanism. The positive ΔG values implied that, during the initial stages of Aβ aggregation, an activation barrier of the Aβ-nNOS complex had to be overcome. Since the ΔG values decreased as temperature increased it not only implied a non-spontaneous interaction but that hydrophobic forces were operative during the binding.

As temperature increased from 298 K to 313 K (and higher) the larger thermal energy assisted in the diffusion of the amyloid peptide toward the enzymes binding site so that the fraction of tryptophan residues (θ) increased as they became more accessible moving a distance of between 2.7 and 2.8 nm. Not only did θ increase towards a value of 1 with increasing temperature but the K_{SV} values also increased supporting a dynamic quenching mechanism.

Kinetic analysis revealed that the K_m remained constant with the binding of the amyloid peptides to the enzyme reflecting that the peptides did not bind at the substrate binding site. It cannot be ruled out, however, that they may bind at the heme binding site of nNOS and a thorough molecular docking study is underway. The interactions were predominantly hydrophobic-hydrophobic supporting the involvement of the pentapeptide patch $A\beta_{17-21}$ and the glycine zipper regions of the amyloid peptides [$A\beta_{25-37}$].

Acknowledgments

The authors thank the Medical Research Council (South Africa) and Rhodes University Research Council for financial assistance.

References

Al-Kady, A.S., Geber, M., Hussein, M.M., Ebeida, E.M., 2011. Structural and fluorescence quenching characterization of hematite nanoparticles. Spectrochimica Acta 83, 398–405.
Amaral, A.F., Lemos, M.R.T., Dong, K.E., Bittencourt, M.F., Caetano, A.L., Pesquero, J.B., Viel, T.A., Buck, H.S., 2010. Participation of kinin receptors on memory impairment after chronic infusion of human amyloid β-1,40 peptide in mice. Neuropeptides 44, 93–97.
Berharnu, W.M., Hansmann, U.H.E., 2012. Structure and dynamics of amyloid-β-segment polymorphism. PLoS One 7 (7), 10.137/journal.pone 0041479.
Bradford, M.M., 1976. A rapid and sensitive method for quantitation of microgram quantities of protein utilizing the principle of protein-dye-binding. Analytical Biochemistry 72, 248–254.
Butterfield, D.A., Reed, T.T., Perluigi, M., De Marco, C., Coccia, R., Keller, J.N., Markesbery, W.R., Sultana, R., 2007. Elevated levels of 3-nitrotyrosine in brain from subjects with amnestic mild cognitive impairment: implications for the role of nitration in the progression of Alzheimer's disease. Brain Research 1148, 243–248.
Calabrese, V., Mancuso, C., Calvani, M., Rizzarelli, E., Butterfield, D.A., Stella, A.M.G., 2007. Nitric oxide in the central nervous system: neuroprotection versus neurotoxicity. Nature Reviews (Neuroscience) 8, 766–775.
Chen, G.Z., Huang, X.Z., Xu, J.G., Wang, Z.B., Zheng, Z.Z., 1990. Method of Fluorescent Analysis, 2nd ed. Science Press, Beijing, pp. 123–126.
Clegg, R.M., 1995. Fluorescence resonance energy transfer. Current Opinion in Biotechnology 6, 103–110.
Findeis, M.A., 2007. The role of amyloid β-peptide 1–42 in Alzheimer's disease. Pharmacology & Therapeutics 116, 266–286.
Fonte, V., Dostal, V., Roberts, C.M., Gonzales, P., Lacor, P., Magrane, J., Dingwell, N., Fan, E., Silverman, M.A., Stein, G.H., Link, C.D., 2011. A glycine zipper motif mediates the formation of toxic β-amyloid oligomers *in vitro* and *in vivo*. Molecular Neurodegeneration 6. http://dx.doi.org/10.1186/1750-1326-6-61.
Hao, J., Zhang, W., Zhang, P., Liu, R., 2010. Aβ (20–29) peptide blocking apoE/Aβ interaction reduces full length Aβ (42/40) fibril formation and cytotoxicity *in vitro*. Neuropeptides 44, 305–313.
Ilichev, Y.V., Perry, J.L., Simon, J.D., 2002. Interaction of ochratoxin A with human serum albumin: preferential binding of the dianion and pH effects. The Journal of Physical Chemistry B 106, 452–459.
Ishii, Y., Yoshida, T., Funatsu, T., Wazawa, T., Yanagida, T., 1999. Fluorescence resonance energy transfer between single fluorophores attached to a coiled-coil protein in aqueous solution. Chemical Physics 247, 163–173.
Iwata, N., Tsubuki, S., Takaki, Y., Watanabe, K., Sekiguchi, M., Hosoki, E., Kawashima-Morishima, M., Lee, H.J., Hama, E., Sekine-Aizawa, Y., Saido, T.C., 2000. Identification of the major $A\beta_{1-42}$ degrading catabolic pathway in brain parenchyma: suppression leads to biochemical and pathological deposition. Nature (Medicine) 6, 143–150.
Kanski, J., Aksenova, M., Butterfield, D.A., 2002. The hydrophobic environment of Met35 of Alzheimer's Aβ(1–42) is important for the neurotoxic and oxidative properties of the peptide. Neurotoxicity Research 4 (3), 219–223.

Kim, J., 2009. The role of GXXXG motif and – secretase components in APP processing. International Biological Central, 101–107.
Kim, S., Jeon, T.-J., Oberai, A., Yang, D., Schmidt, J.J., Bowie, J.U., 2005. Transmembrane glycine zippers: physiological and pathological roles in membrane proteins. Proceedings of the National Academy of Sciences 102 (40), 14278–14283.
Lansbury, P., Jr., Rochet, J., 2000, Amyloid fibrillogenesis: themes and variations, Current Opinion: Structural Biology 10(1), 60–68.
Mikre, W., Masunov, A.E., Berharnu, W.M., 2011. Can molecular dynamics simulations assist in design of specific inhibitors and imaging agents of amyloid aggregation? Structure, stability and free energy predictions for amyloid oligomers of VQIVYK, MVGGVV and LYQLEN Steric zipper. Journal of Molecular Modeling 17, 2423–2442.
Padayachee, E.R., Ngqwala, N.P., Whiteley, C.G., 2011. Association of β-amyloid peptide fragments with neuronal nitric oxide synthase: implications in the etiology of Alzheimer's disease. Journal of Enzyme Inhibition and Medicinal Chemistry. http://dx.doi.org/10(3109/14756366), 2011, 590805.
Padayachee, E.R., Whiteley, C.G., 2011. Spectrofluorimetric analysis for the interaction of amyloid peptides with neuronal nitric oxide synthase: Implications in Alzheimer's disease. Biochimica et Biophysica Acta 1810 (12), 1136–1140.
Poulos, T.L., Li, H., Shimizu, H., Flinspach, M., Jamal, J., Yang, W., Xian, M., Cai, T., Zhong, W.E., Jia, Q., Wang, P.G., 2002. The novel binding mode of *N*-Alkyl-*N*′-hydroxyguanidine to neuronal nitric oxide synthase provides mechanistic insights into NO biosynthesis. Biochemistry 41, 13868–13875.
Prostak, L., Barnea, E., Yaish, P., Zharhary, D., 2005. The Sigma-Aldrich BACE1 activity assay kit- a FRET based assay designed for BACE1 inhibitor screening. Sigma-Aldrich Inc., St. Louis, MO, USA.
Ross, P.D., Subramanian, S., 1981. Thermodynamics of protein association reactions: forces contributing to stability. Biochemistry 20, 3096–3102.
Sakakibara, Y., Yanagisawa, H., 2003. Agmatine deiminase from cucumber seedlings is a mono-specific enzyme: purification and characteristics. Protein Expression and Purification 30, 88–93.
Sambasivam, D., Sivanesan, S., Ashok, B.S., 2011. Structural preferences of Aβ fragments in different micellar environments. Neuropeptides 45, 369–373.
Schlamadinger, D.E., Kats, D.I., Kim, J.E., 2010. Quenching of tryptophan fluorescence in unfolded cytochrome C: biophysics experiment for physical chemistry students. Journal of Chemical Education 87 (9), 961–964.
Sjöback, R., Nygren, J., Kubista, M., 1995. Absorption and fluorescence properties of fluorescein. Spectrochimica Acta (A) 51, L7–L21.
Sklar, L.A., Hudson, B.S., Simoni, R.D., 1977. Conjugated polyene fatty acids as fluorescent probes: binding to bovine serum albumin. Biochemistry 16, 5100–5108.
Soreghan, B., Kosmoski, J., Glabe, C., 1994. Surfactant properties of Alzheimer's Aβ-peptides and the mechanism of amyloid aggregation. Journal of Biological Chemistry 269 (46), 28551–28554.
Soto, C., Branes, M.C., Alvarez, J., Inestrosa, N.C., 1994. Structural determinants of the Alzheimer's amyloid β-peptide. Journal of Neurochemistry 63, 1191–1198.
Soto, C., Castano, E., Frangione, B., Inestrosa, N.C., 1995. The α-helical to β-strand transition in the N-terminal fragment of the amyloid β-peptide modulates amyloid formation. Journal of Biological Chemistry 266, 4025–4028.
Soto, P., Griffin, M.A., Shea, J., 2007. New insights into the mechanism of Alzheimer's amyloid-β fibrillogenesis inhibition by *N*-methylated peptides. Biophysical Journal 93, 3015–3025.
Xie, M.X., Xu, X.Y., Wang, Y.D., 2005. Interaction between hesperetin and human serum albumin revealed by spectroscopic methods. Biochimica et Biophysica Acta 1724, 215–224.
Yi, J., Horky, L.H., Friedlich, A.L., Shi, Y., Rogers, J.T., Huang, Y., 2009. L-Arginine and Alzheimer's disease. International Journal of Clinical Pathology 3, 211–238.

Biochimica et Biophysica Acta 1810 (2011) 1136–1140

Contents lists available at SciVerse ScienceDirect

Biochimica et Biophysica Acta

journal homepage: www.elsevier.com/locate/bbagen

Spectrofluorimetric analysis of the interaction of amyloid peptides with neuronal nitric oxide synthase: Implications in Alzheimer's disease

Eden R. Padayachee, Chris G. Whiteley *

Department of Biochemistry, Microbiology and Biotechnology, Rhodes University, Grahamstown, South Africa

ARTICLE INFO

Article history:
Received 29 March 2011
Received in revised form 30 August 2011
Accepted 1 September 2011
Available online 10 September 2011

Keywords:
Neuronal nitric oxide synthase
Alzheimer's disease
Amyloid peptide
Fluorescence resonance energy transfer
Fluorescence quenching

ABSTRACT

Background: The deposition of aggregated β-amyloid peptide senile plaques and the accumulation of arginine within the astrocytes in the brain of an Alzheimer's patient are classic observations in the neuropathology of the disease. It would be logical, in the aetiology and pathogenesis, to investigate arginine-metabolising enzymes and their intimate association with amyloid peptides.
Methods: Neuronal nitric oxide synthase (nNOS) was isolated, purified and shown, through fluorescence quenching spectroscopy and fluorescence resonance energy transfer (FRET), to interact with structural fragments of $A\beta_{1-40}$ and be catalytic towards amyloid fibril formation.
Results: Only one binding site on the enzyme was available for binding. Two amyloid peptide fragments of $A\beta_{1-40}$ ($A\beta_{17-28}$ and $A\beta_{25-35}$) had Stern–Volmer values (K_{SV}) of 0.111 μM^{-1} and 0.135 μM^{-1} indicating tight binding affinity to nNOS and easier accessibility to fluor molecules during binding. The polarity of this active site precludes binding of the predominantly hydrophobic amyloid peptide fragments contained within $A\beta_{17-28}$ and within two glycine zipper motifs [G-X-X-X-G-X-X-X-G] [$A\beta_{29-37}$] and bind to the enzyme at a site remote to the active region.
Conclusions: The interaction and binding of $A\beta_{17-28}$ and $A\beta_{25-35}$ to nNOS causes the movement of two critical tryptophan residues of 0.77 nm and 0.57 nm respectively towards the surface of the enzyme.
General significance: The binding of Aβ-peptide fragments with nNOS has been studied by spectrofluorimetry. The information and data presented should contribute towards understanding the mechanism for deposition of aggregated Aβ-peptides and fibrillogenesis in senile plaques in an AD brain.

1. Introduction

Alzheimer's disease (AD) is defined as a progressive and fatal neurodegenerative disorder manifested by cognitive and memory deterioration, progressive impairment of activities of daily living, and a variety of neuropsychiatric symptoms and behavioural disturbances [1]. In view of this and in order to develop an early diagnostic marker for the disease, it is necessary to elucidate the mechanisms of AD-related degenerative pathways within the brain to provide a medical and scientific based understanding of the disease.

The deposition of aggregated β-amyloid (Aβ) senile plaques in the human brain is a classic observation in the neuropathology of Alzheimer's disease [2–4] and an understanding of the mechanism of their formation remains elusive. The astrocytes in the diseased brain not only function to store arginine but are surrounded by the insoluble amyloid plaques [5] and so it would be logical, in the aetiology and pathogenesis of Alzheimer's disease, to investigate arginine-metabolising enzymes and their intimate association with amyloid peptides. It must also be mentioned that the pathogenesis of Alzheimer's disease can be manifested by considering both oxidative and nitrosative stress [6]. Whether these levels of stress precede, contribute directly or are as a result of AD pathogenesis is not fully understood [6].

Nitric oxide synthase (NOS) [EC. 1.14.13.39] is an enzyme that oxidises L-arginine to L-citrulline and nitric oxide (NO), an important signalling molecule in the brain (Fig. 1) and since there were elevated levels of arginine in the brain and cerebrospinal fluid of AD patients [7] it pointed towards a metabolic interference with this enzyme during the pathophysiology of the disease. Nitric oxide, however, can also be described as a 'janus' molecule in cell death or cell survival since it is responsible not only for the increase of oxidative/nitrosative stress by *in vivo* formation of peroxynitrite but also in the modulation of different intracellular pathways associated with Alzheimer's disease. Large amounts of NO are neurotoxic whereas smaller concentrations are neuroprotective [8]. Notwithstanding the importance of oxidative/nitrosative stress within the context of the pathogenicity of Alzheimer's disease it follows that such a study would fall under the umbrella of inducible nitric oxide synthase (iNOS). Since we were predominantly interested in arginine metabolising enzymes associated with neuronal functions following our study on the affect of amyloid peptides on brain peptidylarginine-deiminase our attention was to focus on neuronal nitric oxide synthase (nNOS). The fact that iNOS levels also increased in AD patients [9] and

* Corresponding author at: Department of Biochemistry, Microbiology and Biotechnology, Rhodes University, P.O. Box 94, Grahamstown, 6140, South Africa. Tel.: +27 46 6038085; fax: +27 46 6223984.
E-mail address: C.Whiteley@ru.ac.za (C.G. Whiteley).

0304-4165/$ – see front matter © 2011 Elsevier B.V. All rights reserved.
doi:10.1016/j.bbagen.2011.09.002

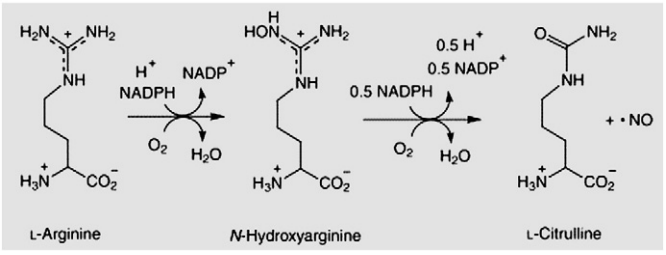

Fig. 1. Schematic representation of enzyme reaction for neuronal nitric oxide synthase.

consequently may induce fibrillogenesis will be a target for future research.

The possibility that nNOS may act as an enzymatic biomarker for AD may be understood by considering its role in the amyloidogenic pathway (amyloid fibril formation). Agents that prevent the initial stages of Aβ formation (Aβ nucleation) could be more effective than those that merely block the final stages (Aβ deposition) [10].

Little is known about the removal of amyloid peptides *in vivo* and it is thought that a decrease in Aβ catabolism was directly responsible for the accumulation of these peptides in the brain and their subsequent aggregation and plaque formation [11]. The higher the concentration of Aβ *in vivo*, the more likely they were to aggregate and form insoluble plaques. Amyloid fibrils are generally formed through a process of assembly of amyloid peptides either self-induced or by a proteolytic mechanism and it is well known that $A\beta_{1-40/42}$ and the neurotoxic $A\beta_{25-35}$ fragment were capable of generating amyloid fibrils [12,13].

The amyloid peptide precursors to these aggregated fibril deposits originate by means of a series of secretase enzymes that act upon a membrane bound amyloid precursor protein (APP). β- and γ-secretase cut APP to release a 40 (42) residue amyloid peptide [$A\beta_{1-40/42}$] while α- and γ-secretase cut APP to release a 24 (26) residue amyloid peptide [$A\beta_{17-40/42}$] [14]. Earlier reports from our group [15–17] have shown that a five residue hydrophobic fragment $A\beta_{17-21}$ [Leu_{17}-Val_{18}-Phe_{19}-Phe_{20}-Ala_{21}] and three glycine zipper motifs [G-X-X-X-G] within $A\beta_{25-37}$ [Gly_{25}-Ser_{26}-Asn_{27}-Lys_{28}-Gly_{29}-Ala_{30}-Ile_{31}-Ile_{32}-Gly_{33}-Leu_{34}-Met_{35}-Val_{36}-Gly_{37}] (Fig. 2) not only initially inhibit the arginine metabolising enzymes – peptidylargininedeiminase (PAD) and neuronal nitric oxide synthase (nNOS) – but also act as catalysts in the enzyme-induced process of fibrillogenesis.

In the present paper we have used a spectrofluorimetric approach to investigate the role and binding of specific β-amyloid peptide fragments [$A\beta_{17-28}$ and $A\beta_{25-35}$] of $A\beta_{17-40}$ on neuronal nitric oxide synthase as an understanding towards the mechanism of catalysis for fibrillogenesis. In particular this investigation is centred on fluorescence quenching, binding constants, binding sites, energy transfer, binding distances and suggested conformational changes of nNOS by the binding of these amyloid peptide fragments.

2. Materials and methods

2.1. Materials

Bovine brain was kindly donated by Rosedale abattoir (Grahamstown, South Africa). All reagents were from commercial sources and dissolved in milli-Q water.

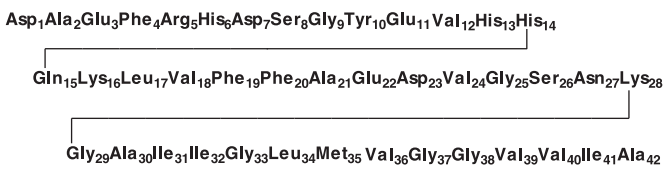

Fig. 2. Amino acid sequence for amyloid peptide $A\beta_{1-42}$.

2.2. Neuronal nitric oxide synthase (nNOS) assay

This assay was conducted, with slight modification, according to the protocol previously described [17,18]. In summary the reaction mixture contained benzoyl-L-arginine ethyl ester (5 mM, 10 μl), $CaCl_2$ (5 mM, 10 μl), dithiothreitol (2 mM, 10 μl) in Tris–HCl buffer (50 mM, pH 7.6, 940 μl). The reaction was started by the addition of enzyme extract (10 μl) in NADPH (1.0 mM, 10 μl) and allowed to incubate at 40 °C for 2 min, before being stopped with perchloric acid (5 M, 10 μl). This mixture (250 μl) was treated with chromogenic reagent (250 μl) and cooled to 22 °C for 2 min. The reduction of benzoyl-L-arginine ethyl ester was then determined spectrophotometrically at 530 nm. Chromogenic reagent was made from thiosemicarbazide (18 mM) in 2,3-butanedione monoxime solution (500 mg in 100 ml distilled water) and sulphuric: orthophosphoric acid (1:1) in the presence of ferric chloride (0.25 g). The citrulline extinction coefficient (ε_{530}) was 27.3 $ml \cdot \mu mol^{-1}$ [19]. One unit of activity was defined as the amount of nNOS that produced 1 μmol of citrulline per min per ml reaction mixture.

2.3. Protein determination

The protein concentration for all experiments was routinely determined according to the method of Bradford [20]. The assay was performed in triplicate in a 96-well microplate. Enzyme extract (5 μl) was added to a single well, followed by Bradford reagent (245 μl). The mixture was incubated at 22 °C for 10 min and absorbance of the solution measured at 595 nm and the concentration of the unknown samples was determined using a bovine serum albumen standard curve.

2.4. Purification of nNOS

Neuronal nitric oxide synthase was purified as previously described [17]. In brief bovine brain (374 g) was homogenised by sonication (10 W, 30 s intervals, 4 min) in HEPES buffer (50 mM, pH 7.6, 600 ml) that contained EDTA (1.0 mM), NADPH (1.0 mM), DTT (0.5 mM) and PMSF (0.43 mM). The cell debris was removed by centrifugation (10,000 ×*g*, 4 °C, 30 min) and the crude cell-free extract (20 ml), dialysed and then applied to a DEAE-Sepharose anion-exchanger resin, previously equilibrated with Tris–HCl buffer (50 mM, pH 7.6). Active fractions of nNOS were eluted with 0.75 M NaCl in the same buffer at a flow rate of 2 $ml \cdot min^{-1}$.

2.5. Characterisation of nNOS

The purity of the enzyme was confirmed by SDS-PAGE analysis and its optimum temperature, pH, thermal stability and kinetic parameters (K_m and V_{max}) established as previously described [17].

2.6. Fluorimetric analysis

2.6.1. Quenching

Spectrofluorimetry was used to determine structural changes induced in nNOS by the interaction of the amyloid peptides with the purified enzyme. The excitation wavelength was fixed at 295 nm, the wavelength at which tryptophan absorbs, and the emission wavelength was at 482 nm. The change in fluorescence of a solution was monitored as increasing concentrations of $A\beta_{17-28}$, $A\beta_{25-35}$ and $A\beta_{32-35}$ (0–2 μM) were added to a reaction mixture of nNOS (5 μl) in Tris–HCl buffer (pH 7.6, 100 mM) in a final volume of 1.0 ml.

2.6.2. Fluorescence resonance energy transfer (FRET)

The FRET assay procedure was based on a method previously described but with slight modification [21]. Reactions were performed with substrate (BAEE) and either $A\beta_{17-28}$ or $A\beta_{25-35}$ (2 μM) as the acceptor chromophores and fluorescein (100 μM; 200 μl) as the donor chromophore with purified nNOS (50 μl) in fluorescent buffer (NaCl,

250 mM, HEPES 5 mM, pH 7.6) in a final volume of 500 µl. Fluorescence was read at an excitation wavelength of 488 nm and an emission wavelength of 518 nm (fluorescein dependent excitation and emission wavelength).

2.7. Statistical analyses

All experiments were carried out in triplicate. Mean and standard deviation calculations and comparison of data using analysis of variance (ANOVA) was performed to 5% level of significance ($p<0.05$) using Statistica for Windows, version 8 (Statsoft Inc.) and Microsoft Excel 2007.

3. Results and discussion

3.1. Binding site for amyloid peptides on nNOS

$$\log[(Fo–F)/F] = \log Ka + n\log[Q] \quad (1)$$

The number of binding sites (n) on the purified enzyme, which were available for the amyloid peptides, and the association constant (Ka) [and its reciprocal dissociation constant (Kd)] were estimated, respectively, from the slope of the linear regressions and the intercept on the log [(Fo − F)/F] axis (Fig. 3) [22] [Eq. (1)]. In all of the cases it was clear that only one binding site was available (Table 1).

3.2. Fluorimetric analysis

3.2.1. Quenching

Tryptophan fluorescence is a well established principle in order to study the micro-environment for ligand binding to biological macromolecules. Any insight into molecular recognition of the binding of amyloid peptides with nNOS involves an investigation of hydrogen bonds, van der Waals forces as well as electrostatic and hydrophobic interactions. Consequently fluorescence quenching was used to identify the actual binding pocket for amyloid peptides in the nNOS enzyme. As seen (Fig. 4) the addition of the amyloid peptides resulted in a static quenching in fluorescence with linearity in the Stern–Volmer plots. The Stern–Volmer quenching constant (K_{SV}) was estimated from the slope of the linear regression of the Stern–Volmer relationship [Eq. (2)] and the greater the K_{SV} the greater the quenching and ease of accessibility to fluor molecules.

It was noted that the K_{SV} of $A\beta_{17–28}$ and $A\beta_{25–35}$ (0.111 μM^{-1} and 0.135 μM^{-1} respectively) indicated that these two peptides showed the substantial quenching ability with comparable easy access to fluor molecules (surface tryptophans) compared to the K_{SV} of $A\beta_{32–35}$ (0.071 μM^{-1}). The 'y intercept' in the respective Stern–Volmer plots (Fig. 4) was equivalent to 1, thereby indicating that fluorescence was only due to internal quenching by amino acids within the amyloid peptide and not the interplay of other fluors in solution which may result in external quenching. It was tempting to consider that, in view of these K_{SV} values of the two peptides $A\beta_{17–28}$ and $A\beta_{25–35}$ that the three glycine zipper motifs [G-X-X-X-G] [Gly_{25}-Ser_{26}-Asn_{27}-Lys_{28}-Gly_{29}]; [Gly_{29}-Ala_{30}-Ile_{31}-Ile_{32}-Gly_{33}]; and [Gly_{33}-Leu_{34}-Met_{35}-Val_{36}-Gly_{37}] were critical in the initial interaction of the amyloid peptide with the enzyme.

Quenching data from the fluorescence analysis were then analysed according to the modified Stern–Volmer equation (Eq. (3)) leading to a confirmation of binding constants as well as θ, the fractional maximum fluorescence intensity or number of available surface tryptophan residues (Table 1).

$$Fo/F = 1 + KsvQ \quad (2)$$

$$Fo/\Delta F = 1/(\theta KsvQ) + 1/\theta \quad (3)$$

where Fo, and F = fluorescence in the absence and presence of amyloid peptide respectively; Q = concentration of amyloid peptide; K_{SV} = Stern–Volmer constant; ΔF = Fo − F; and θ = fraction of accessible tryptophan residues.

The analysis of the primary structure and active site of each subunit of nNOS [PDB ID: 1OM4] reveals 13 tryptophan residues of which four [Trp_{409}, Trp_{561}, Trp_{587} and Trp_{678}] are within the active site, seven are near the enzyme surface and two others are buried elsewhere in the enzyme interior; Tyr_{588}, Glu_{592}, Asp_{597}, Gln_{478} and Tyr_{706} are also present within this active region and are capable of hydrogen bonding to the substrate. Quenching studies have demonstrated that $A\beta_{17–28}$ and $A\beta_{25–35}$ binding decreases solvent exposure of Trp residues (Fig. 5)

Table 1
Stern–Volmer quenching constants from the interaction of nNOS (5 µl) in Tris–HCl buffer (pH 7.6, 100 mM) treated with amyloid peptides $A\beta_{17–28}$, $A\beta_{32–35}$ and $A\beta_{25–35}$ (0–2 µM) in a final volume (1.0 ml).

Parameter	$A\beta_{17–28}$	$A\beta_{25–35}$	$A\beta_{32–35}$
n	1.13	0.99	1.12
Ka $(\mu M)^{-1}$	8.8	6.7	16.6
Kd (µM)	0.113	0.149	0.06
K_{SV} $(\mu M)^{-1}$	0.111	0.135	0.071
θ	2	2	0

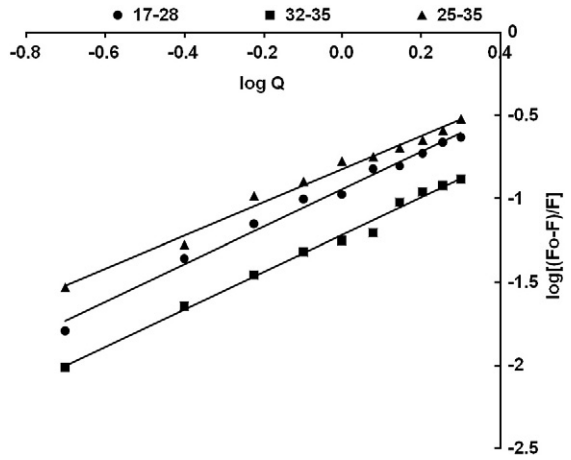

Fig. 3. Hill plots of log [(Fo − F)/F] *versus* log [Q] for the binding $A\beta_{17–28}$ (•), $A\beta_{32–35}$ (■) and $A\beta_{25–35}$ (▲) (0–2 µM) with nNOS (5 µl) in Tris–HCl buffer (pH 7.6, 100 mM) in a final volume (1.0 ml).

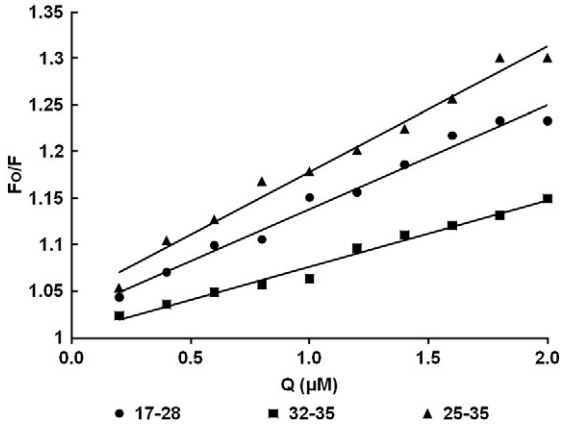

Fig. 4. Stern–Volmer plots for fluorescence quenching of nNOS (5 µl) in Tris–HCl buffer (pH 7.6, 100 mM) treated with amyloid peptides $A\beta_{17–28}$ (•), $A\beta_{32–35}$ (■) and $A\beta_{25–35}$ (▲) (0–2 µM) in a final volume (1.0 ml). Excitation wavelength was fixed at 295 nm and emission wavelength was at 482 nm.

implying that the local environment near these Trp residues is altered with a decreased access to these Aβ. The fraction of Trp near the enzyme surface ( ) was determined as the reciprocal of the y-intercept (Fig. 5). Since the parameter is generally dependent on the polarity of the solvent it is the hydrophobic nature of the $A\beta_{17-28}$ and $A\beta_{25-35}$ sequence that induced conformational change in nNOS, bringing two Trp residues to the surface of the enzyme (=2) (Table 1). Once again this endorses a speculation that the hydrophobicity of the glycine zipper motif [Gly_{29}-Ala_{30}-Ile_{31}-Ile_{32}-Gly_{33}] was a trigger for the initial interaction of the amyloid peptide with the enzyme. No tryptophan residue was exposed on the enzyme surface during the binding of $A\beta_{32-35}$ [θ = 0]. Moreover the low K_{SV} values for $A\beta_{32-35}$ (0.071 μM^{-1}), confirmed that accessibility of this peptide to the TRP residues was negligible. An in-depth molecular modelling and docking study of the interaction and binding of all of the amyloid peptide fragments to nNOS is currently on going and will be reported elsewhere.

3.2.2. Fluorescence energy resonance transfer (FRET)

Fluorescence spectroscopy involving FRET was used as an additional tool to examine protein/enzyme structure, conformational changes and an exact position of an amyloid peptide within the active site when the amyloid peptide was bound to nNOS. Tryptophan fluor molecules within nNOS, behave as intrinsic quenchers decreasing the quantum yield of fluorescence (Q) and measuring the fluorophore accessibility to quenching allows for an estimation of the relative position of a fluorophore within the protein. The excitation energy of the donor molecule is transferred to an acceptor molecule without the emission of a photon. Absorption spectrum of the acceptor (fluor B) must overlap with the fluorescence emission spectrum of the donor (fluor A) which results in a decrease in donor emission along with an increase in acceptor emission intensity. If these fluors (fluor A and B) have unique locations in the protein, it is possible to measure distances or changes in distances within proteins [23]. The efficiency of energy transfer (E) is a quantitative measure of the number of quanta that are transferred from donor (D) to acceptor (A) and may be determined from the fluorescence intensity of a sample that contained only the donor D (*i.e.* F^D) and from a corresponding sample that contained acceptor (A) and a donor (D) (*i.e.* $F^{D,A}$) [Eq. (4)] [24]. Moreover, the use of FRET results from the strong dependence of the rate and efficiency of energy transfer on the sixth power of the distance R between D and A [Eq. (4)] [25].

$$E = 1 - F^{D.A}/F^{D} = Ro^6/\left(Ro^6 + r^6\right) \quad (4)$$

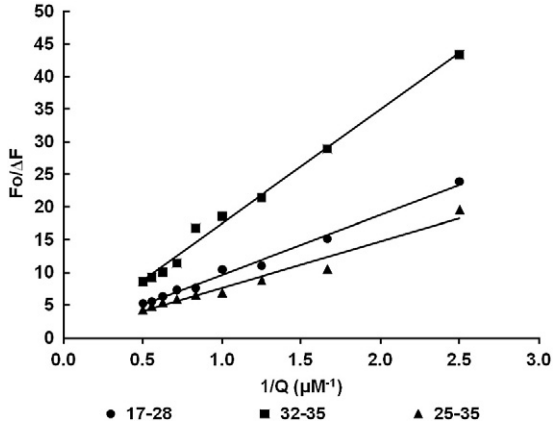

Fig. 5. Double reciprocal plots (modified Stern–Volmer) for fluorescence quenching of nNOS (5 μl) in Tris–HCl buffer (pH 7.6, 100 mM) treated with amyloid peptides $A\beta_{17-28}$ (•), $A\beta_{32-35}$ (■) and $A\beta_{25-35}$ (▲) (0–2 μM) in a final volume (1.0 ml). Excitation wavelength was 295 nm and emission wavelength was 482 nm.

where E is the efficiency of transfer between the donor and acceptor; r = distance between the donor and the acceptor; Ro = Förster distance when efficiency of transfer is 50%.

$$Ro^6 = 8.79 \times 10^{-252} \eta^{-4} \varphi_D J \quad (5)$$

$$J = \left[\sum F(\lambda)\varepsilon(\lambda)\lambda^4 \Delta\lambda\right] \Big/ \left[\sum F(\lambda)\Delta\lambda\right] \quad (6)$$

Ro depends on the relative orientation of the donor and acceptor (k^2), the refractive index (η), the quantum yield of the donor (φ_D) in the absence of acceptor, and the overlap integral between the acceptor emission and donor excitation (J). F(λ) is the fluorescence intensity of the fluorescent donor at wavelength (λ) and ε(λ) is the molar absorption coefficient of the acceptor at wavelength (λ).

From Figs. 4 and 5 it was established that the binding of the amyloid peptides caused a change in tryptophan fluorescence of purified nNOS. It followed that the efficiency (E) of FRET can be represented by the actual distance between the donor (fluorescein) and acceptor (amyloid peptides) (Eq. (4)) [26]. In the present study the values of κ^2, the average refractive index (η) and the fluorescence quantum yield of fluorescein (φ_D) are 0.667, 1.36 and 0.93 [27] respectively and from Eqs. (4), (5) and (6) it would give respective values for J, E, Ro and r for $A\beta_{17-28}$, $A\beta_{25-35}$ and BAEE (Table 2). According to literature [28] any value for the distance between donor and acceptor (r) that is less than 10 nm and falls between 0.5 and 1.5 of the Ro value indicates a high probability that fluorescence transfer is taking place.

For $A\beta_{17-28}$, the only intrinsic fluorophores present in the sequence were two phenyl rings (Phe_{19} and Phe_{20}) which have low quantum yield and the possibility of any internal quenching by these aromatic amino acids when $A\beta_{17-28}$ was bound to nNOS was negligible. Furthermore it was interesting to note that the fluorescence intensity between BAEE and fluorescein was 27.03 compared to 12.96 and 14.19 between $A\beta_{17-28}$ and $A\beta_{25-35}$ and fluorescein (Table 2). These differences in fluorescent intensities were due to the orientation relationship associated with their respective bindings that induced different conformational changes in nNOS. Consequently the position of the tryptophan residues around the enzyme active site became positioned differently.

Once again computational analysis of the active site of nNOS [PDB ID: 1OM4] shows that the substrate [BAEE] binds within a distance of 2.46 nm which is in good agreement to our fluorescent evaluation (2.35 nm). When $A\beta_{17-28}$ and $A\beta_{25-35}$ became bound to nNOS these distances changed to 1.58 and 1.78 nm respectively. We were confident that this difference in binding distances was directly due to the movement of the two tryptophan residues indicated above (Fig. 5). The identity of these two residues, however, remains unknown at present and is a target for future research.

In the absence of resonance energy transfer when nNOS and acceptor (BAEE or amyloid peptide) were not bound the donor signal of fluorescein was high and the emission of fluorescein-acceptor was low. When the enzyme-acceptor–donor complex formed, fluorescein, which was

Table 2
Fluorescent energy transfer parameters from the interaction of nNOS (50 μl) in buffer (HEPES, 5 mM, pH 7.6; NaCl 250 mM) in a final volume (500 μ) with substrate (BAEE) or $A\beta_{17-28}$ or $A\beta_{25-35}$ (2 μM) as acceptor and fluorescein (100 μM, 200 μl) as donor chromophore. Fluorescence was read at an excitation wavelength of 488 nm and an emission wavelength of 518 nm. F^D, $F^{D,A}$ = fluorescence of donor and donor–acceptor respectively, E = efficiency of energy transfer, J = overlap integral of the fluorescence emission spectrum of the donor and the absorption spectrum of the acceptor, Ro = critical distance between acceptor and donor when the transfer efficiency = 50%, r = distance between acceptor and donor.

Acceptor	F^D	$F^{D,A}$	Ro (nm)	J (10^{-14}) l·M^{-1}	E	r (nm)
$A\beta_{17-28}$	46.42	12.96	1.85	0.25	0.72	1.58
$A\beta_{25-35}$	46.42	14.19	2.04	0.275	0.69	1.78
BAEE	46.42	27.03	2.22	0.3	0.42	2.35

attached to the acceptor terminus, behaved as a 'fluorescence resonance gate' with a low donor signal (increased emission) while the acceptor signal was high (increased excitation) resulting in resonance energy transfer between donor and acceptor.

Earlier [17] we established that the incubation of these amyloid peptides with nNOS for an extended period (30 min–96 h) afforded amyloid fibril deposits and though it may be speculation that a 'glycine zipper motif' is involved it is still tempting to suggest that these motifs were responsible for the initial interaction of the amyloid peptide with the enzyme. Further study is continuing along these lines and will be reported elsewhere. Support and evidence for this is forthcoming since 'glycine zipper' motifs can act as triggers in protein dimerisation, fibrillogenesis and proteolysis [29]. Furthermore literature [30] indicates that $A\beta_{17-21}$ possesses a series of promising properties: it was able to cross the blood brain barrier, to inhibit (and disassemble) the formation of amyloid fibrils *in vitro* and *in vivo*, to prevent Aβ neurotoxicity in cell culture, to arrest amyloid deposition and to induce dissolution of preformed plaques in rat brain model of the amyloidogenic pathway. The use of $A\beta_{17-21}$ as a pseudoligand to block the process of fibrillogenesis showed promising future potential in the treatment of AD.

Thus, the distance values were reflective of important structural modifications within nNOS active site when either the peptides or substrate was bound. In view of the polarity of the active region of nNOS [Tyr_{588}, Glu_{592}, Asp_{597}, Gln_{478} and Tyr_{706}] it is unlikely that either the $A\beta_{17-28}$ peptide that contained the pentapeptide patch [Leu_{17}-Val_{18}-Phe_{19}-Phe_{20}-Ala_{21}] or the hydrophobic glycine zipper motifs $A\beta_{29-37}$ [Gly_{29}-Ala_{30}-Ile_{31}-Ile_{32}-Gly_{33}-Leu_{34}-Met_{35}-Val_{36}-Gly_{37}] would bind at this site in competition with normal substrate. Instead this argument supports our earlier finding from kinetic data [17] that the amyloid peptides interact in a non-competitive manner with nNOS at a site remote to the active one. It should be pointed out, however, that the more polar glycine zipper [Gly_{25}-Ser_{26}-Asn_{27}-Lys_{28}-Gly_{29}] was more suited to electrostatic interaction and hydrogen bonding with the enzymes active region.

4. Conclusions

The interaction between nNOS and $A\beta_{17-28}$ and $A\beta_{25-35}$ has been studied by fluorescent techniques. The data revealed that nNOS has only one binding site and that its fluorescence was statically quenched by the amyloid peptide supporting the formation of a nNOS-$A\beta_{17-28}$ and/or nNOS-$A\beta_{25-35}$ complex. Furthermore two tryptophan residues became more accessible as the fluorophores and moved by approximately 0.77 and 0.57 nm during binding of the amyloid peptides. By FRET analysis the distance between the substrate (BAEE) and these tryptophans was estimated at 2.35 nm while the distance between $A\beta_{17-28}$ (or $A\beta_{25-35}$) and these same tryptophans was 1.58 (or 1.78 nm) respectively. These values were well within the limit for probability of binding. A molecular modelling study to identify these two tryptophan residues and to consider a probable mechanism for the interaction and binding of other amyloid peptide fragments to nNOS is currently on going and will be reported elsewhere.

Acknowledgements

The authors thank the National Research Foundation (South Africa) and Rhodes University Research Council for financial assistance.

References

[1] G.R.Y. de Meyer, W. Martinet, T.J.L. van De Parre, A.G. Herman, H. Bult, M.M. Kock, D.M. Jans, Processing of amyloid precursor protein as a biochemical link between atherosclerosis and Alzheimer's disease, Cardiovasc. Hematol. Disord. Drug Targets 6 (2006) 21–34.
[2] C. Soto, M.C. Branes, J. Alvarez, N.C. Inestrosa, Structural determinants of the Alzheimer's amyloid β-peptide, J. Neurochem. 63 (1994) 1191–1198.
[3] M.A. Findeis, The role of amyloid β-peptide 1–42 in Alzheimer's disease, Pharmacol. Ther. 116 (2007) 266–286.
[4] C. Soto, E. Castano, B. Frangione, N.C. Inestrosa, The α-helical to β-strand transition in the N-terminal fragment of the amyloid β-peptide modulates amyloid formation, J. Biol. Chem. 266 (1995) 4025–4028.
[5] T.L. Poulos, H. Li, H. Shimizu, M. Flinspach, J. Jamal, W. Yang, M. Xian, T. Cai, W.E. Zhong, Q. Jia, P.G. Wang, The novel binding mode of *N*-Alkyl-*N*′-hydroxyguanidine to neuronal nitric oxide synthase provides mechanistic insights into NO biosynthesis, Biochemistry 41 (2002) 13868–13875.
[6] D.A. Butterfield, T.T. Reed, M. Perluigi, C. De Marco, R. Coccia, J.N. Keller, W.R. Markesbery, R. Sultana, Elevated levels of 3-nitrotyrosine in brain from subjects with amnestic mild cognitive impairment: implications for the role of nitration in the progression of Alzheimer's disease, Brain Res. 1148 (2007) 243–248.
[7] J. Yi, L.H. Horky, A.L. Friedlich, Y. Shi, J.T. Rogers, Y. Huang, L-arginine and Alzheimer's disease, Int. J. Clin. Pathol. 3 (2009) 211–238.
[8] V. Calabrese, C. Mancuso, M. Calvani, E. Rizzarelli, D.A. Butterfield, A.M.G. Stella, Nitric oxide in the central nervous system: neuroprotection versus neurotoxicity, Nat. Rev. Neurosci. 8 (2007) 766–775.
[9] E. Barone, F. Di Domenico, G. Cenini, R. Sultana, R. Coccia, P. Preziosi, M. Perluigi, C. Mancuso, D.A. Butterfield, Oxidative and nitrosative modifications of biliverdin reductase-A in the brain of subjects with Alzheimer's disease and amnestic mild cognitive impairment, J Alzheimer's Dis 25 (4), 2011.
[10] J.L. Cummings, The Neuropsychiatry of Alzheimer's Disease and Related Dementias, Taylor and Francis, London and New York, 2003.
[11] N. Iwata, S. Tsubuki, Y. Takaki, K. Watanabe, M. Sekiguchi, E. Hosoki, M. Kawashima-Morishima, H.J. Lee, E. Hama, Y. Sekine-Aizawa, T.C. Saido, Identification of the major $A\beta_{1-42}$ degrading catabolic pathway in brain parenchyma: suppression leads to biochemical and pathological deposition, Nat. Med. 6 (2000) 143–150.
[12] P.D. Gorevic, E.M. Castano, R. Sarma, B. Frangione, Ten to fourteen residue peptides of Alzheimer's disease protein are sufficient for amyloid fibril formation and its characteristic X-ray diffraction pattern, Biochem. Biophys. Res. Comm. 147 (1987) 854–862.
[13] C.J. Pike, A.J. Walencewicz-Wasserman, J. Kosmoski, D.H. Cribbs, C.G. Glabe, C.W. Cotman, Structure-activity analyses of β-amyloid peptides: contribution of the $A\beta_{25-35}$ region to aggregation and neurotoxicity, J. Neurochem. 64 (1995) 253–265.
[14] W. Ha-Na, B. Sang-Ha, P. Jong-Sung, G. A-Ryeong, Y. Sunghee, Y. Young-Kwang, J. Dong-Gyu, Secretases as therapeutic targets for Alzheimer's disease, Biochem. Biophys. Res. Comm. 404 (2011) 10–15.
[15] C.A. Louw, A. Gordon, N. Johnston, C. Mollatt, G. Bradley, C.G. Whiteley, Arginine deiminases: therapeutic tools in the etiology and pathogenesis of Alzheimer's disease, J. Enz. Inhib. Med. Chem. 22 (1) (2007) 121–126.
[16] P. Mohlake, C.G. Whiteley, Arginine metabolising enzymes as therapeutic tools for Alzheimer's disease: peptidyl arginine deiminase catalyses fibrillogenesis of β-amyloid peptides, Mol. Neurobiol. 41 (2–3) (2010) 149–158.
[17] E. Padayachee, N. Ngqwala, C.G. Whiteley, Enzyme Inhib. Med. Chem. (2011), doi: 10.3109/14756366.2011.590805.
[18] T.R.C. Boyde, M. Rahmatullah, Optimization of conditions for the colorimetric determination of citrulline using diacetyl monoxime, Anal. Biochem. 107 (1980) 424–431.
[19] Y. Sakakibara, H. Yanagisawa, Agmatine deiminase from cucumber seedlings is a mono-specific enzyme: purification and characteristics, Prot. Expr. Purif. 30 (2003) 88–93.
[20] M.M. Bradford, A rapid and sensitive method for quantitation of microgram quantities of protein utilizing the principle of protein-dye-binding, Anal. Biochem. 72 (1976) 248–254.
[21] L. Prostak, E. Barnea, P. Yaish, D. Zharhary, L. Prostak, E. Barnea, P. Yaish, D. Zharhary, The Sigma-Aldrich BACE1 Activity Assay Kit — A FRET Based Assay Designed for BACE1 Inhibitor Screening, Sigma-Aldrich Inc, St.Louis, MO, USA, 2005.
[22] M.X. Xie, X.Y. Xu, Y.D. Wang, Interaction between hesperetin and human serum albumin revealed by spectroscopic methods, Biochim. Biophys. Acta 1724 (2005) 215–224.
[23] Y. Ishii, T. Yoshida, T. Funatsu, T. Wazawa, T. Yanagida, Fluorescence resonance energy transfer between single fluorophores attached to a coiled-coil protein in aqueous solution, Chem. Phys. 247 (1999) 163–173.
[24] R.M. Clegg, Fluorescence resonance energy transfer, Curr. Opin. Biotech. 6 (1995) 103–110.
[25] L.A. Sklar, B.S. Hudson, R.D. Simoni, Conjugated polyene fatty acids as fluorescent probes: binding to bovine serum albumin, Biochemistry 16 (1977) 5100–5108.
[26] Y.V. Ilichev, J.L. Perry, J.D. Simon, Interaction of ochratoxin A with human serum albumin: preferential binding of the dianion and pH effects, J. Phys. Chem. B 106 (2002) 452–459.
[27] R. Sjöback, J. Nygren, M. Kubista, Absorption and fluorescence properties of fluorescein, Spectrochim. Acta (A) 51 (1995) L7–L21.
[28] G.Z. Chen, X.Z. Huang, J.G. Xu, Z.B. Wang, Z.Z. Zheng, Method of Fluorescent Analysis, 2nd ed Science Press, Beijing, 1990 123–126.
[29] J. Kim, The role of GXXXG motif and γ-secretase components in APP processing, Int. Bio. Cent. 1 (2009) 1–7.
[30] P. Soto, M.A. Griffin, J. Shea, New insights into the mechanism of Alzheimer's amyloid-β fibrillogenesis inhibition by *N*-methylated peptides, Biophys. J. 93 (2007) 3015–3025.

Journal of Enzyme Inhibition and Medicinal Chemistry, 2011, 1–9, Early Online

ISSN 1475-6366 print/ISSN 1475-6374 online
DOI: 10.3109/14756366.2011.590805

informa
healthcare

RESEARCH ARTICLE

Association of β-amyloid peptide fragments with neuronal nitric oxide synthase: Implications in the etiology of Alzheimers disease

Eden Padayachee, Nosiphiwe Ngqwala, and Chris G Whiteley

Department of Biochemistry, Microbiology and Biotechnology, Rhodes University, Grahamstown, South Africa

Abstract

Neuronal nitric oxide synthase (nNOS) was purified on DEAE-Sepharose anion-exchange in a 38% yield, with 3-fold recovery and specific activity of 5 μmol.min^{-1}.mg^{-1}. The enzyme was a heterogeneous dimer of molecular mass 225 kDa having a temperature and pH optima of 40°C and 6.5, K_m and V_{max} of 2.6 μM and 996 nmol.min^{-1}.ml^{-1}, respectively and was relatively stable at the optimum conditions ($t_{½}$ = 3 h). β-Amyloid peptide fragments $A\beta_{17-28}$ was the better inhibitor for nNOS (K_i = 0.81 μM). After extended incubation of nNOS (96 h) with each of the peptide fragments, Congo Red, turbidity and thioflavin-T assays detected the presence of soluble and insoluble fibrils that had formed at a rate of 5 nM.min^{-1}. A hydrophobic fragment $A\beta_{17-21}$ [Leu_{17}– Val_{18} – Phe_{19}– Phe_{20}– Ala_{21}] and glycine zipper motifs within the peptide fragment $A\beta_{17-35}$ were critical in binding and in fibrillogenesis confirming that nNOS was amyloidogenic catalyst.

Keywords: Neural nitric oxide synthase, Alzheimer disease; inhibition, amyloid peptides

Introduction

Though the deposition of aggregated β-amyloid senile plaques and neurofibrillary tangles in the human brain are classic observations in the neuropathology of Alzheimer disease[1–3] an understanding of the mechanism of their formation remains elusive. Furthermore it also remains uncertain whether the elevated level of arginine in the brains and cerebrospinal fluid of Alzheimer patients is as a result, or a cause, of the disorder[3]. Any drug and/or metabolite that can inhibit the progression of the neurological disorder requires an understanding of the molecular causes underlying the neurodegenerative processes.

Since it has been reported[4] that the astrocytes in the diseased brain not only function to store arginine but are surrounded by the insoluble amyloid plaques it would be logical, in the etiology and pathogenesis of Alzheimers disease, to investigate arginine-metabolising enzymes and their intimate association with amyloid peptides. Neuronal nitric oxide synthase (nNOS) [EC. 1.14.13.39] uses arginine as a substrate producing citrulline and nitric oxide (NO) (Scheme 1). This reaction, localized within the astrocytes in the brain, induces proteins in the cellular environment to unfold and trigger the aggregation of susceptible peptides[5] such as amyloid peptides. An understanding of the function and action of nNOS, with respect to amyloid peptide aggregation and subsequent formation of senile plaques, may facilitate an understanding of neurodegeneration in Alzheimer disease.

Earlier reports from our group[6,7] have shown that certain amyloid peptide fragments, not only initially inhibit the arginine-metabolising enzyme—peptidylarginine deiminase—but also act as catalysts in the enzyme induced process of fibrillogenesis. It is thought that a decrease in Aβ catabolism is directly responsible for the accumulation of this peptide in the brain and its subsequent aggregation and plaque formation[8]. The higher the concentration of Aβ *in vivo*, the more likely they are to aggregate and form insoluble plaques. Amyloid fibrils are generally formed through a process of assembly of

Address for Correspondence: C.G.Whiteley, Department of Biochemistry, Microbiology and Biotechnology, Rhodes University, P.O.Box 94, Grahamstown, 6140, South Africa. Tel.: +27–46-6038085, Fax: +27–46-6223984. E-Mail: C.Whiteley@ru.ac.za

(Received 10 March 2011; revised 12 May 2011; accepted 19 May 2011)

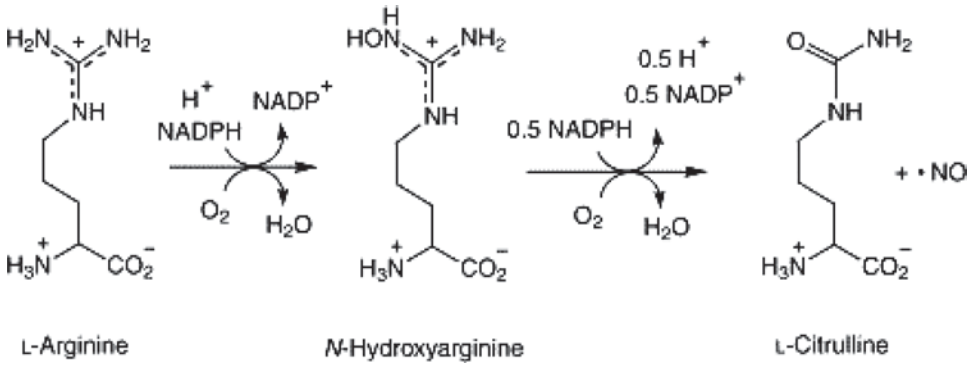

Scheme 1. Schematic representation of enzyme reaction for neuronal nitric oxide synthase.

amyloid proteins either self-induced or by a proteolytic mechanism. It is relatively well known[8,9] that there are a number of amyloidogenic proteins and short peptide fragments, including the $A\beta_{25-35}$ fragment itself, that are capable of producing amyloid fibrils[10] and neurotoxic oligomers[11].

This present study uses a series of readily available different sized Aβ peptides [$A\beta_{17-28}$, $A\beta_{22-35}$ and $A\beta_{32-3}5$] along with the neurotoxic elements $A\beta_{25-35}$ and $A\beta_{1-40}$, in order to investigate which sequence would, primarily, be involved in inhibition of nNOS and which sequence would be involved in the formation of amyloid fibrils induced by nNOS. Kinetic analysis was used to measure the kinetic parameters (V_{max}, K_m] and affinity constants (K_i) while turbidity at 400 nm[12], Congo Red assay[13] and Thioflavin-T (Th-T) staining fluorescence[14–16] were used to investigate the formation of insoluble fibrils and aggregation kinetics of nNOS induced fibril formation.

Materials and methods

Materials

Bovine brain was kindly donated by Rosedale abattoir (Grahamstown, South Africa). All amyloid peptides [$A\beta_{17-28}$, $A\beta_{22-35}$, $A\beta_{32-35}$, $A\beta_{25-35}$ and $A\beta_{1-40}$], acrylamide; bis-acrylamide, bromophenol blue, *N, N, N′, N′*- tetramethylethylenediamine, ammonium persulphate, β-mercaptoethanol, Coomassie Blue commercial stain, Nα-benzoyl-L-arginine ethyl ester hydrochloride, DL-citrulline, calcium chloride, tetrahydro-L-biopterin dichloride, β-nicotinamide adenine dinucleotide phosphate reduced tetrasodium salt, thiosemicarbazide, 2,3 butanedione monoxime, DEAE-Sepharose®, bovine serum albumin, Bradford reagent, ethylenediaminetetracetic acid and 4-(2-hydroxyethyl) piperazine-*N*′-(2-ethane-sulphonic acid monosodium salt [Hepes] were obtained from Sigma-Aldrich (Johannesburg, South Africa). Commercial nNOS obtained from rat brain, dithiothreitol (DTT), sodium dodecyl sulphate (SDS), glycerol (50%), Tris (hydroxymethyl) aminomethane, phenylmethylsulphonylfluoride (PMSF), ferric chloride hexahydrate ($FeCl_3$), sodium chloride (NaCl), perchloric acid, sulphuric acid, ortho-phosphoric acid, glacial acetic acid and hydrochloric acid were obtained from Merck Chemicals (Statsoft Inc., Sandton, South Africa). Molecular weight markers were obtained from PEQGOLD (Erlangen, Germany). In all the experiments, reagents were dissolved in milli-Q water and all the experimental conditions throughout the purification were performed at 0–4°C except where indicated. Snake skin dialysis tubing was obtained from Pierce (Rockford, IL). UV analyses were performed on a PowerWave XTM microplate reader (Bio-Tek Instruments, Winooski, VT).

nNOS assay

This assay was conducted, with slight modifications, according to the protocol previously described[17]. The reaction mixture contained benzoyl-L-arginine ethyl ester (5 mM, 10 µl), $CaCl_2$ (5 mM, 10 µl), DTT (2 mM, 10 µl) in Tris-HCl buffer (50 mM, pH 7.6, 940 µl). The reaction was started by the addition of brain extract (10 µl) in NADPH (1.0 mM, 10 µl) and allowed to incubate at 40°C for 2 min, before being stopped with perchloric acid (5 M, 10 µl). This mixture (250 µl) was treated with chromogenic reagent (250 µl) and cooled to 22°C for 2 min. The reduction of benzoyl-L-arginine ethyl ester was then determined spectrophotometrically at 530 nm. Chromogenic reagent was made from thiosemicarbazide (18 mM) in 2.3 butanedione monoxime solution (500 mg in 100 ml distilled water) and sulphuric:orthophosphoric acid (1:1) in the presence of $FeCl_3$ (0.25 g). The citrulline extinction coefficient (ε_{530}) was 27.3 ml.µmol^{-1}[18]. One unit of activity was that amount of nNOS that produced 1 µmol of citrulline per min per ml reaction mixture.

Protein determination

The protein concentration for all experiments was routinely determined according to the method of Bradford[19]. The assay was performed in triplicate in a 96-well microplate. Enzyme extract (5 µl) was incubated (22°C, 10 min) with Bradford reagent (245 µl), the absorbance measured at 595 nm and the concentration determined from a BSA standard curve.

Purification of nNOS

Isolation

Fresh bovine brain (374 g) was homogenized by sonication (10W, 30 s intervals, 4 min) in Hepes buffer (50 mM,

pH 7.6, 600 ml) that contained EDTA (1.0 mM), NADPH (1.0 mM), DTT (0.5 mM) and PMSF (0.43 mM). The cell debris was removed by centrifugation (10,000*g*, 4°C, 30 min) and the crude cell-free extract assayed for nNOS activity and protein concentration then stored as 20 ml aliquots at–70°C until required.

Anion- exchange on DEAE-Sepharose

The crude extract (20 ml), obtained after centrifugation and sonication was applied to a DEAE-Sepharose anion-exchange resin, previously equilibrated with Tris-HCl buffer (50 mM, pH 7.6) and washed with the same buffer until A_{280} was at the baseline. The adsorbed proteins were then eluted with NaCl (0–1 M) in the same buffer at a flow rate of 2 ml.min^{-1} and fractions (5 ml) collected, assayed for nNOS and protein and active fractions pooled and dialysed overnight against Tris-HCl buffer (50 mM, pH 7.6).

Characterisation of nNOS

pH, temperature, stability and kinetic profiles

To determine the pH optimum, the enzyme extract (10 µl) was assayed in different buffers [sodium acetate (pH 3–5.5, 50 mM); Hepes (pH 6–7, 50 mM); Tris-HCl buffer (pH 7.5–9, 50 mM)] under the standard assay conditions. The temperature optimum of the partially purified enzyme was determined in Tris-HCl buffer (pH 7.6, 50 mM) over a range of 20–70°C. The reaction was started by addition of enzyme suspension (10 µl) at the different temperatures. The temperature stability of nNOS was determined at the optimum temperature and pH. nNOS activity at time zero was considered to be 100% relative activity and aliquots (10 µl) were removed at 1 h intervals and analyzed for nNOS activity for a maximum period of 12 h. The kinetic properties (K_m and V_{max}) were determined by varying the substrate (benzoyl-L-arginine ethyl ester, 3 ml) between 0 and 10 µM. nNOS activity was determined at each substrate concentration.

SDS and native PAGE analyses

The effectiveness of the purification process was determined by SDS-polyacrylamide gel electrophoresis (PAGE) after the method of Laemmli[20] on samples exhibiting synthase activity. Samples from each purification step (20 µl) and a standard molecular weight marker (10–170 kDa), were electrophoresed on 12% SDS-PAGE at 200 V. The gels were stained with Coomassie Brilliant Blue R-250, then destained in methanol: acetic acid: water (1:1:8 v/v/v). The molecular weight of the partially purified nNOS was determined using a standard curve of log molecular weight versus distance migrated. The procedure for native PAGE was performed with 12% separating gel at the same constant voltage of 200 V. After electrophoresis, the protein band was sliced out, re-suspended in Tris-HCl buffer (20 mM, pH 6.5, 1.0 ml) and incubated with benzoyl-L-arginine ester (0.1 g). The activity was assayed as previously described.

Interaction of nNOS with amyloid peptides

Kinetic analysis

Partially purified nNOS (5 µl) in Tris HCl buffer (50 mM, pH 7.6) was treated with amyloid peptides $A\beta_{1-40}$, $A\beta_{22-35}$, $A\beta_{17-28}$, $A\beta_{32-35}$ and $A\beta_{25-35}$ at 2 µM in a total volume of 1.0 ml and in the presence of benzoyl arginine ethyl ester (0–10 µM). The nNOS activity was assayed, at each substrate concentration.

Congo Red assay

Congo Red assay was performed according to that reported in the literature[13] with slight modifications. Partially purified nNOS (5 µl) in Tris HCl buffer (100 mM, pH 7.6) was mixed with amyloid peptides $A\beta_{1-40}$, $A\beta_{22-35}$, $A\beta_{17-28}$, $A\beta_{25-35}$ and $A\beta_{32-35}$ (10 nM). Aliquots (20 µl) were periodically removed over 96 h and incubated (30 min) with a Congo Red solution (12.5 µM), prepared in Tris-HCl buffer (pH 7.6, 100 mM) containing NaCl (150 mM) in a final volume of 1.0 ml. Absorbance was read at 480 and 540 nm at 24 h intervals and the degree of fibrillogenesis estimated from the amount of Congo Red bound to the fibrils (equation 1) where the values 25.955 and 46.306 are the extinction coefficients of Congo Red-fibril complex and Congo Red, in units of ml.µmol^{-1}, respectively.

$$\text{Bound Congo Red } (\mu M) = [A^{540}/25.955] - [A^{480}/46.306]\ [12] \qquad (1)$$

Th-T assay

Th-T was used to indicate the presence of Aβ fibrils using a modified version of that previously reported[14–16]. nNOS solution (5 µl) was added to a reaction mixture containing Th-T (2 µl, 3.14 mM) and NaOH (200 µl, 10 mM) in Tris HCl buffer (pH 7.6, 100 mM) and NaCl (150 mM) in a final volume of 1.0 ml. Increasing concentrations of each Aβ peptide were added and incubated (22°C, 30 min) and the shift in fluorescence monitored at an excitation wavelength of 440 nm and an emission wavelength of 482 nm.

Turbidity assay

The turbidity assay was performed as previously described[12] with a slight modification. Aliquots (5 µl) of each Aβ peptide dissolved in dimethylsulphoxide were added to Tris-HCl buffer (10 mM, pH 7.6) and partially purified nNOS (5 µl) to give a final concentration of 5 nM. Aggregation of fibrils was measured as turbidity at 400 nm.

Transmission electron microscopy (TEM)

A 10 µl sample of either amyloid peptide alone or those that had been challenged with nNOS was placed onto a carbon-coated copper grid, excess liquid removed by carefully blotting with filter paper and then the sample negatively stained with uranyl acetate (2%, 30 s), washed twice in deionised water, blotted dry with filter paper and viewed using a JEOL JEM-1210 TEM at an acceleration voltage of 100 kV.

Statistical analyses

All experiments were carried out in triplicate. Mean and standard deviation calculations and comparison of data using analysis of variance was performed to 5% level of significance ($p < 0.05$) using Statistica for Windows, version 8 (Statsoft Inc.) and Microsoft Excel 2007.

Results and discussion

The enzyme proved difficult to obtain in a pure form and so a partially purified product was used. Preliminary attempts to purify nNOS by ammonium sulphate fractionation and/or polyethylene glycol led to about 80–85% loss in activity and so were abandoned in favour of ion-exchange chromatography on DEAE-Sepharose. Eight active fractions (39–46) were eluted with ~0.75 M NaCl in Tris-HCl buffer (50 mM, pH 7.6) (Figure 1) to afford partially purified nNOS in 38% yield, 3-fold recovery and a specific activity of 5 μmol.min^{-1}.mg^{-1}. SDS-PAGE analysis revealed that the partially purified nNOS from the DEAE-Sepharose column appeared to be a dimer of ~75 kDa and 150 kDa (Supplementary material, Figure 1A). This indicated an overall molecular weight of the total enzyme of 225 kDa which was similar to values of 230 kDa reported[21,22]. The source of the commercial sample of nNOS (Supplementary material, Figure 1A; Lane C) was not from the bovine brain but from the rat brain and under the conditions of the SDS-PAGE did not show any dimers whatsoever. Native-PAGE revealed a single band for the partially purified enzyme estimated at 225 kDa (Supplementary material, Figure 1B).

The enzyme indicated a pH optimum at pH 6.5 as there was a 40% decrease in activity between pH 4.5 and 6.5 and 6.5 and 8 but rapidly lost its activity beyond these extremes (Supplementary material, Figure 2A). Similar values of 6.8 were reported by Riveros-Moreno et al.[23] Based on the temperature profile (Supplementary material, Figure 2B), the enzyme showed an optimum of 40°C as there was a 40% decrease in activity between 25 and 40°C and 80% decrease between 40 and 60°C. This optimum temperature was comparable to a reported value of 37°C for nNOS[24]. The nNOS had a half life of ~3 h (Supplementary material, Figure 2C) when incubated under optimal conditions of temperature and pH.

A study into the effect of substrate concentration on the kinetic activity of nNOS was investigated by measuring enzyme activity over a range of benzoyl arginine ethyl ester concentrations (0–10 μM). A typical increase in substrate concentration resulted in a proportional increase in activity as shown by the Michaelis–Menten and Hanes–Woolf plots (Figure 2) and for benzoyl arginine hydrolysis, the V_{max} and K_m were 996 nmol.min^{-1} and 2.6 μM, respectively. The turnover number (k_{cat}) and the catalytic efficiency, calculated using equations 2 and 3 and were found to be 50.8 min^{-1} and 19.54 min^{-1}.μM^{-1}, respectively. The total amount of enzyme [Et] was 19.6 nmol.

$$k_{cat} = V_{max}/E_t \quad (2)$$

$$\text{Catalytic efficiency} = k_{cat}/K_m \quad (3)$$

The kinetic constant K_m (2.6 μM) indicated a similar affinity for benzoyl arginine compared with other reported values (11 μM; 2 μM; 3.2 μM; 1.5 μM) for nNOS[22–25] and the V_{max} of 996 nmol.min^{-1} was only slightly lower than that of 1 μmol.min^{-1} reported elsewhere[25].

The affinity of the nitric oxide synthase for amyloid peptides was determined by including the peptides to a final concentration of 2 μM with the substrate benzyl arginine ethyl ester (0–10 μM, 1 ml). The results indicated that with $A\beta_{17-28}$ the V_{max} decreased from 996 to 286

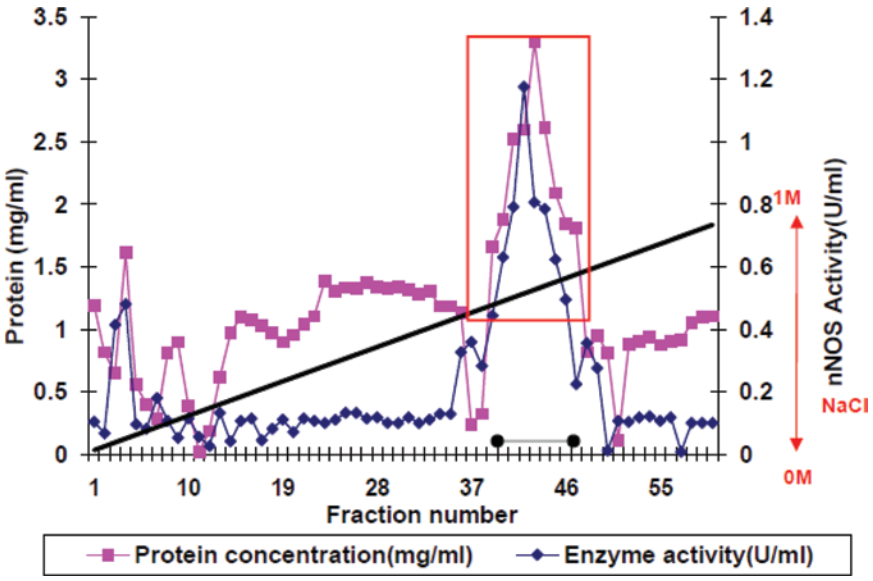

Figure 1. Elution profile of DEAE-Sepharose ion-exchange chromatography. Proteins eluted with linear NaCl gradient (0–1 M) in Tris-HCl buffer (50 mM, pH 7.6); Flow rate, 2 ml/min (5 ml per tube). (See colour version of this figure online at www.informahealthcare.com/enz)

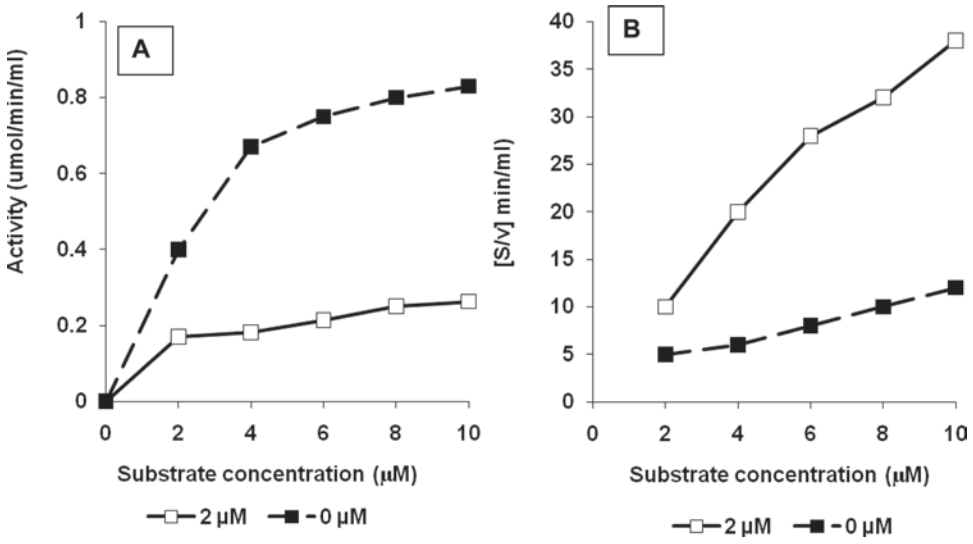

Figure 2. A: Michaelis–Menten and B: Hanes–Woolf plots for $A\beta_{17-28}$ interaction with nNOS in the presence of different concentrations of benzoyl arginine ethyl ester.

$nmol.min^{-1}ml^{-1}$ (Figure 2) while the K_m value remained unchanged at 2.6 μM indicating that the nNOS was inhibited, in a non-competitive fashion, by the amyloid peptide. Furthermore each of the other amyloid peptides ($A\beta_{1-40}$, $A\beta_{22-35}$, $A\beta_{32-35}$ and $A\beta_{25-35}$) at a concentration of 2 μM, also inhibited nNOS. The inhibitor constant (K_i) calculated from equation 4, indicated the binding affinity of enzyme for inhibitor (Table 1).

$$K_i = [A\beta.V_{max}.^{app}]/[V_{max} - V_{max}^{app}] \quad (4)$$

where Aβ = concentration of amyloid peptide; V_{max}^{app} = apparent maximum velocity in the presence of amyloid peptides. Results showed that $A\beta_{17-28}$ inhibited nNOS the most as reflected by its low K_i value of 0.81 μM compared to the other K_i values for $A\beta_{1-40}$, $A\beta_{22-35}$, $A\beta_{25-35}$ and $A\beta_{32-35}$ (14.4 μM; 7.4 μM; 10 μM and 8.8 μM) (Table 1).

When each of the amyloid peptides (at 2 μM) was incubated with the enzyme for an extended period (20–30 min) interesting results were forthcoming in that full enzyme activity was restored (Table 2). This time-dependent observation suggested an association—dissociation between nNOS and the amyloid peptide fragment of which the strength and time of effect was dependent on the type and concentration of the fragment. Furthermore it pointed to the fact that the enzyme converted the amyloid peptide into a form that was no longer capable of binding. In our opinion (and as we will indicate later) there was a strong probability that, first soluble then insoluble, amyloid fibrils had been generated by a process called fibrillogenesis. Since the enzyme activity was restored to its original value after about 20 min it ruled out any possibility that the fibrils blocked the enzyme active site. Though the data in Table 2 does not infer any quantifying evaluation for the interaction of the amyloid peptides with the enzyme it does support the fact that $A\beta_{17-28}$ peptide caused rapid inhibition

Table 1. Inhibitor binding constants (K_i) for amyloid peptides on nNOS.

Aβ	1–40	22–35	17–28	32–35	25–35
Ki (μM)	14.4	7.4	0.81	8.8	10

(95% within 2 min). All of the other peptides had slightly less influence producing about 90% inhibition within 4–6 min.

For all β-amyloid peptides studied, the concentration of fibrils was quantified through the Congo Red assay according to equation 1. From the results (Table 3) about 80% soluble fibrils were formed from all of the peptides within 0.5 h of incubation with nNOS. Moreover, it was interesting to note that up to 96 h the percentage rate of decrease in soluble fibrils, as detected by the Congo Red assay, was mirrored by the rate of formation of insoluble fibrils detected by the turbidity assay (Table 3). All of the various Aβ-peptides, in the absence of nNOS, showed no change in absorbance over the 96 h aggregation period, thus concluding that the peptide themselves did not form fibrils. With $A\beta_{1-40}$ there was an ~10–15% decrease in soluble fibril every 24 h up to 96 h while with $A\beta_{22-35}$ the amount of soluble fibrils remained at about 69% up to 48 h and then decreased by a further 18% up to 72 h with only 9.3% soluble fibrils remaining after 96 h. $A\beta_{17-28}$ showed a similar trend with 56% soluble fibrils remaining after 48 h followed by a surprising increase to 76.7% at 72 h and then 14% remaining at 96 h. With respect to $A\beta_{25-35}$ and $A\beta_{32-35}$ a steady rate in the decrease of soluble fibrils every 24 h up to 96 h was observed with the former leaving 28% and the latter 52.3% soluble fibrils after 96 h.

The extent of aggregation of each peptide was determined with the formation of insoluble fibrils as determined by turbidity, at 400 nm, as a function of time (Table 3). All controls for the various Aβ peptides in the absence of nNOS showed little or no turbidity concluding that the amyloid peptides on their own did not produce

insoluble fibrils correlating with the control results from the Congo Red assay. From the turbidimetric results, the various Aβ peptides indicated an amount of 8–40% of insoluble fibrils during the initial 0.5 h incubation which increased gradually to 100% by 96 h, and this correlated with soluble fibril decrease as obtained from the Congo Red results.

Fluorescence of Th-T is used extensively for the identification, quantification and rate of formation of amyloid fibriuls; free Th-T showed weak, negligible fluorescence in solution. It is not the intention in this present manuscript to discuss the mechanism of the formation of the amyloid fibrils as this had been covered in detail elsewhere[26–28]. Nevertheless it was pertinent to mention that since there is stoichiometry and saturation binding between Th-T and the fibrils any increased change in fluorescence can be equated directly with their rate of formation. When each of the amyloid peptides [$A\beta_{1-40}$, $A\beta_{22-35}$, $A\beta_{17-28}$, $A\beta_{32-35}$ and $A\beta_{25-35}$] at increasing concentrations was incubated for 30 min with nNOS in the presence of Th-T there was a gradual change in fluorescence up to a saturation maximum (Figure 3). This supported our findings with the Congo Red and turbidity assays that nNOS was catalytic towards fibril formation. Furthermore all controls for the various Aβ peptides in the absence of nNOS showed little or no fluorescent change concluding that the amyloid peptides on their own did not undergo fibrillogenesis. It was also consistent with the possibility that amyloid peptides were converted into a form that could no longer bind to the enzyme.

All of the peptides produced fibrils at a rate of 5 nM. min^{-1} (Figure 3). However nNOS induced both $A\beta_{17-28}$ and $A\beta_{25-35}$ to afford fibrils with a yield 8-fold greater than from $A\beta_{32-35}$. The other peptides [$A\beta_{1-40}$ and $A\beta_{22-35}$] gave fibrils with only three to 4-fold yield more than $A\beta_{32-35}$ (Figure 3). The incubation time of nNOS with amyloid peptides and Th-T was 30 min and substantiated the results obtained for Congo Red and turbidity as fibrils began to form rapidly within 0.5 h, irrespective of whether the fibril was soluble or insoluble. From the data obtained by both Th-T staining fluorescence and Congo Red assay we were confident that the aggregates formed were in fact amyloid.

Aβ peptides interact with hydrophobic environments[29,30] and so it was more than likely that nNOS-Aβ complexes were hydrophobic-hydrophobic associations. Examining the amino acid sequence of the Aβ-peptides that were readily induced to form fibrils pointed us towards two hydrophobic patches with sequences Leu_{17}– Val_{18}– Phe_{19}– Phe_{20}– Ala_{21} and Gly_{25}– Ser_{26}– Asn_{27}– Lys_{28}– Gly_{29}– Ala_{30}– Ile_{31}– Ile_{32}– Gly_{33}. This latter sequence looked especially promising in view of the glycine zipper [G-X-X-X-G-X-X-X-G] recognition motif[31]. We were also very aware of a third hydrophobic peptide glycine zipper motif that existed with a sequence Gly_{33}– Leu_{34}– Met_{35}– Val_{36}– Gly_{37}. These characteristic glycine zipper motifs have been

Table 2. Influence of amyloid peptides on nNOS activity over time.

nNOS activity ($\mu mol.min^{-1}.ml^{-1}$

	Time (min)											
Aβ	0	2	4	6	8	10	12	14	16	18	20	30
1–40	5.00	2.58	4.73	1.44	3.65	1.54	2.58	1.61	4.08	4.51	5.00	5.00
17–28	5.00	0.35	3.00	0.52	2.35	3.63	2.67	2.00	2.98	4.02	5.00	5.00
22–35	5.00	3.00	2.25	0.22	3.57	4.44	0.52	3.13	2.49	3.44	5.00	5.00
25–35	5.00	3.57	0.41	2.55	1.38	3.19	0.63	1.39	3.56	4.65	5.00	5.00
32–35	5.00	4.00	2.28	0.49	2.52	1.35	0.35	2.25	3.88	4.72	5.00	5.00

Table 3. % Soluble and insoluble fibrils formed over time from incubation of amyloid peptides with nNOS.

% Soluble fibrils

	Time (h)					
Aβ	0	0.5	24	48	72	96
1–40	nd	81.2	69.7	53.1	37.4	24.7
17–28	nd	83.8	70.1	56.2	76.7	14.2
22–35	nd	69.4	69.2	70.2	51.6	9.3
25–35	nd	81.7	70.0	56.3	36.0	27.9
32–35	nd	79.6	60.0	41.8	75.9	52.3

% Insoluble fibrils

	Time (h)					
Aβ	0	0.5	24	48	72	96
1–40	0.00	28.6	39.1	61.4	90.0	100
17–28	0.00	29.7	40.2	60.7	89.9	100
22–35	0.00	40.0	60.0	79.4	90.2	100
25–35	0.00	19.8	39.2	60.0	94.1	100
32–35	0.00	8.4	39.9	55.7	92.7	100

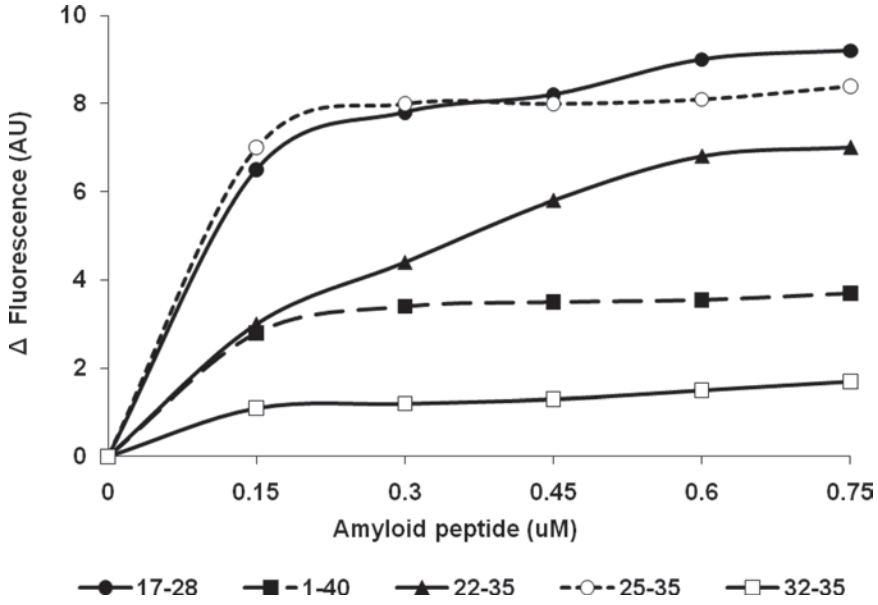

Figure 3. Change in fluorescence of Th-T as an indicator to the formation of amyloid fibrils catalysed by nNOS on amyloid peptide fragments.

identified in many proteins as a transmembrane helix-turn-helix and, in the case of Aβ, were completely conserved suggesting that such motifs played an important role in their normal function that could have serious implications in the etiology and pathophysiology for Alzheimers disease[32,33]. There was evidence[34–36] that fibrillogenesis of amyloid peptides may be catalysed by several biomacromolecules including enzymes and/or proteins though the actual specific mechanism remains elusive. By correlating our present kinetic analysis, Th-T fluorescence data and the Congo Red and turbidity assays it was tempting to suggest that the hydrophobic patches and/or glycine zippers between residues 17 and 35 mediated the process of fibrillogenesis of the amyloid peptides. Though we have no definitive proof whether the original peptide fragments were random coils or α-helices there was evidence of a rapid conversion of the peptide, initiated by the enzyme, into a soluble β-conformation rendering it no longer able to bind with the enzyme. Then after ~30 min there was a further change, also initiated by nNOS, and the formation of insoluble fibril aggregates.

The rapid fibril formation, detected by Th-T, could be explained via the nucleation effect which was accelerated by seeding. An ordered nucleus was formed only after a lag phase and in a 'supersaturated' solution of fibrils that had formed from 'seeds' (initially present) which eventually exceeded the critical concentration of amyloid peptide[37,38]. This effect was enhanced by micelles that were in equilibrium with soluble Aβ monomers that provided nuclei for new fibrils allowing further formation of fibrils with time. Based on this model, it was suggested that with increased amount of fibrils, there were more micelles that remained in solution until a point of saturation. It had been suggested that these soluble amyloid oligomers, rather than the mature aggregates represented the primary toxic mechanism of amyloid pathogenesis[39]. Once the aggregation process had begun and a critical nucleus had formed, the soluble fibrils, that had been detected by the Congo Red assay, now formed insoluble fibrils and precipitated out of solution (Table 3).

The structure of the insoluble amyloid fibrils generated from the proteolytic action of nNOS with $A\beta_{17-28}$ was examined under TEM to investigate aggregate morphology. They revealed extensive formation of fibrils compared to the enzyme (nNOS) and amyloid peptide before induction (Supplementary material, Figure 3A and B). Within the first 30 min, fibrils appeared mainly as short, rod-like structures (Supplementary material, Figure 3C) and after 24 h, fibrillization of amyloid peptides appeared to have progressed from these short discrete fibrils to a mass of much longer fibrils in a branched network (Supplementary material, Figure 3D). This supported the morphology pattern of fibrils as illustrated from literature[30–41]. These observations also substantiated Congo red, turbidity and Th-T results which showed that fibrils, initially formed within 30 min, remained soluble and then after 24 h aggregated to form a mass of slender, long fibrils in a typical branched network.

Conclusions

All Aβ peptides inhibited nNOS with $A\beta_{17-28}$ inhibiting the most (K_i = 0.81 μM) within 2 min. Extended incubation of the peptides with nNOS suggested the presence of an association—dissociation equilibrium and helped to explain the onset of fibrillogenesis and the role of nNOS as an amyloidogenic catalyst.

The Congo Red assay proved to be successful in the quantification of soluble fibrils while the turbidity assay and Th-T were simple and reliable methods in identifying and quantifying the process of aggregation driven by the formation of insoluble fibrils. Most importantly the

enzyme was inhibited when the Aβ peptide initially was bound to nNOS. Then after several minutes the peptide dissociated and was converted into a soluble fibril which remained attached to the enzyme but did not inhibit its activity. Eventually the nNOS-Fib(sol) complex reached a saturation point in solution resulting in a rapid dissociation of fibrils to account for the increase in soluble fibrils with time as revealed by the Congo Red assay. Subsequent decrease in soluble fibrils over 96 h was mirrored by an increase in concentration in insoluble fibril as detected by turbidity. The Th-T assay showed that the rate of formation of insoluble fibrils was 5 nM.min^{-1} with $A\beta_{17-28}$ and $A\beta_{25-35}$ the most prominent peptides in fibrillogenesis confirming that nNOS was an amyloidogenic catalyst. It also suggested that amyloid fibril formation required proteolysis and that different amyloid peptides produced different quantities of fibrils over a given time. We are confident that the hydrophobic pentapeptide patches and/or glycine zipper motifs between residues 17 and 37 were responsible for both initial binding and proteolytic catalysis into fibrils.

Acknowledgements

The financial assistance from The Medical Research Council (South Africa) toward this research is hereby acknowledged.

Declaration of interest

The authors report no conflict of interest. The authors alone are responsible for the content and writing of the paper.

References

1. Soto C, Brañes MC, Alvarez J, Inestrosa NC. Structural determinants of the Alzheimer's amyloid beta-peptide. J Neurochem 1994;63:1191–1198.
2. Findeis MA. The role of amyloid beta peptide 42 in Alzheimer's disease. Pharmacol Ther 2007;116:266–286.
3. Yi J, Horky LL, Friedlich AL, Shi Y, Rogers JT, Huang X. L-arginine and Alzheimer's disease. Int J Clin Exp Pathol 2009;2:211–238.
4. Arif M, Kato T. Increased expression of PAD2 after repeated intracerebroventricular infusions of soluble Abeta(25-35) in the Alzheimer's disease model rat brain: effect of memantine. Cell Mol Biol Lett 2009;14:703–714.
5. Soto C, Castano E, Frangione B, Inestrosa NC. The α-helical to β-strand transition in the N-terminal fragment of the amyloid β-peptide modulates amyloid formation. J Biol Chem 1995;266:4025–4028.
6. Louw C, Gordon A, Johnston N, Mollatt C, Bradley G, Whiteley CG. Arginine deiminases: therapeutic tools in the etiology and pathogenesis of Alzheimer's disease. J Enzyme Inhib Med Chem 2007;22:121–126.
7. Mohlake P, Whiteley CG. Arginine metabolising enzymes as therapeutic tools for Alzheimer's disease: peptidyl arginine deiminase catalyses fibrillogenesis of beta-amyloid peptides. Mol Neurobiol 2010;41:149–158.
8. Iwata N, Tsubuki S, Takaki Y, Watanabe K, Sekiguchi M, Hosoki E et al. Identification of the major Abeta1-42-degrading catabolic pathway in brain parenchyma: suppression leads to biochemical and pathological deposition. Nat Med 2000;6:143–150.
9. Gorevic PD, Castano EM, Sarma R, Frangione B. Ten to fourteen residue peptides of Alzheimer's disease protein are sufficient for amyloid fibril formation and its characteristic x-ray diffraction pattern. Biochem Biophys Res Commun 1987;147:854–862.
10. Pike CJ, Walencewicz-Wasserman AJ, Kosmoski J, Cribbs DH, Glabe CG, Cotman CW. Structure-activity analyses of beta-amyloid peptides: contributions of the beta 25-35 region to aggregation and neurotoxicity. J Neurochem 1995;64:253–265.
11. Gruden MA, Davidova TB, Malisauskas M, Sewell RD, Voskresenskaya NI, Wilhelm K et al. Differential neuroimmune markers to the onset of Alzheimer's disease neurodegeneration and dementia: autoantibodies to Abeta((25-35)) oligomers, S100b and neurotransmitters. J Neuroimmunol 2007;186:181–192.
12. Evans KC, Berger EP, Cho CG, Weisgraber KH, Lansbury PT Jr. Apolipoprotein E is a kinetic but not a thermodynamic inhibitor of amyloid formation: implications for the pathogenesis and treatment of Alzheimer disease. Proc Natl Acad Sci USA 1995;92:763–767.
13. Klunk WE, Pettegrew JW, Abraham DJ. Two simple methods for quantifying low-affinity dye-substrate binding. J Histochem Cytochem 1989;37:1293–1297.
14. Naiki H, Higuchi K, Nakakuki K, Takeda T. Kinetic analysis of amyloid fibril polymerization in vitro. Lab Invest 1991;65: 104–110.
15. Le Vine H. Thioflavin T interaction with synthetic Alzheimer's disease β-amyloid peptides: detection of amyloid aggregation in solution. Prot Sci 1993;2:404–410.
16. Le Vine H. Quantification of β-sheet amyloid fibril structures with Thioflavin-T. Methods Enzymol 1999;309:274–284.
17. Boyde TR, Rahmatullah M. Optimization of conditions for the colorimetric determination of citrulline, using diacetyl monoxime. Anal Biochem 1980;107:424–431.
18. Sakakibara Y, Yanagisawa H. Agmatine deiminase from cucumber seedlings is a mono-specific enzyme: purification and characteristics. Protein Expr Purif 2003;30:88–93.
19. Bradford MM. A rapid and sensitive method for the quantitation of microgram quantities of protein utilizing the principle of protein-dye binding. Anal Biochem 1976;72:248–254.
20. Laemmli UK. Cleavage of structural proteins during the assembly of the head of bacteriophage T4. Nature 1970;227:680–685.
21. Packer L. (1994). Methods in Enzymol: Oxygen radicals in biological systems: Part C. Academic Press Inc, USA. 233.
22. Rosazza JPN, Chen C. Purified nitric oxide synthase from rat brain. University of Iowa Research Foundation. 1996;675:821.
23. Riveros-Moreno V, Heffernan B, Torres B, Chubb A, Charles I, Moncada S. Purification to homogeneity and characterisation of rat brain recombinant nitric oxide synthase. Eur J Biochem 1995;230:52–57.
24. Hiki K, Hattori R, Kawai C, Yui Y. Purification of insoluble nitric oxide synthase from rat cerebellum. J Biochem 1992;111:556–558.
25. Bredt DS, Snyder SH. Isolation of nitric oxide synthetase, a calmodulin-requiring enzyme. Proc Natl Acad Sci USA 1990;87:682–685.
26. Hawe A, Sutter M, Jiskoot W. Extrinsic fluorescent dyes as tools for protein characterization. Pharm Res 2008;25:1487–1499.
27. Krebs MR, Bromley EH, Donald AM. The binding of thioflavin-T to amyloid fibrils: localisation and implications. J Struct Biol 2005;149:30–37.
28. Biancalana M, Makabe K, Koide A, Koide S. Molecular mechanism of thioflavin-T binding to the surface of beta-rich peptide self-assemblies. J Mol Biol 2009;385:1052–1063.
29. Choo-Smith LP, Garzon-Rodriguez W, Glabe CG, Surewicz WK. Acceleration of amyloid fibril formation by specific binding of Abeta-(1-40) peptide to ganglioside-containing membrane vesicles. J Biol Chem 1997;272:22987–22990.
30. McLaurin J, Franklin T, Fraser PE, Chakrabartty A. Structural transitions associated with the interaction of Alzheimer beta-amyloid peptides with gangliosides. J Biol Chem 1998;273:4506–4515.

31. KimS,JeonTJ,OberaiA,YangD,SchmidtJJ,BowieJU.Transmembrane glycine zippers: physiological and pathological roles in membrane proteins. Proc Natl Acad Sci USA 2005;102:14278–14283.
32. Munter LM, Voigt P, Harmeier A, Kaden D, Gottschalk KE, Weise C et al. GxxxG motifs within the amyloid precursor protein transmembrane sequence are critical for the etiology of Abeta42. Embo J 2007;26:1702–1712.
33. Yazawa H, Yu ZX, Takeda, Le Y, Gong W, Ferrans VJ et al. Beta amyloid peptide ($A\beta_{42}$) is internalized via the G-protein-coupled receptor FPRL1 and forms fibrillar aggregates in macrophages. Faseb J 2001;15:2454–2462.
34. Wetzel R. Characterisation of in vitro protein deposition Methods Enzymology 1999;309:189–476.
35. Esler WP, Stimson ER, Mantyh PW, Maggio JE. Deposition of soluble amyloid-beta onto amyloid templates: with application for the identification of amyloid fibril extension inhibitors. Meth Enzymol 1999;309:350–374.
36. Terzi E, Hölzemann G, Seelig J. Interaction of Alzheimer beta-amyloid peptide(1-40) with lipid membranes. Biochemistry 1997;36:14845–14852.
37. Lansbury P. Jnr, Rochet J. Amyloid fibrillogenesis: themes and variations. Curr Opin:Struct Biol 2000;10:60–68.
38. Caflisch A, Pellarin R. Interpreting the aggregation kinetics of amyloid peptides. J Mol Biol 2006;360:882–892.
39. Glabe CG. Common mechanisms of amyloid oligomer pathogenesis in degenerative disease. Neurobiol Aging 2006;27:570–575.
40. Fülop L, Zarándi M, Soos K, Penke B. Self-assembly of Alzheimer's disease-related amyloid peptides into highly ordered nanostructures. Nanopages 2006;1:69–83.
41. Chakrabartty A, Fraser PE, Yip CM, Go S, Plaskos NP, Yang D, Huang THJ. Structural studies of soluble oligomers of the Alzheimer β-amyloid peptide. J Molec Biol 2000;297: 73–87.

1 Literature review

1.1 Alzheimer's disease: an overview

Alzheimer's disease (AD) is a disorder of the brain which destroys areas of the brain critical in memory and cognitive function. This progressive disease is the most common form of dementia among the elderly (Lahiri *et al*., 2004). The presence of the characteristic histopathologic features called plaques and tangles was first found in non-elderly demented patients by Alois Alzheimer (Alzheimer, 1907). Shortly thereafter, Oscar Fisher recognized that brains of elderly demented individuals also contained plaques (Fischer, 1907). In subsequent years, based on these findings, the disease came to be diagnostically referred to as Alzheimer's disease (AD) (Kraepelin, 1910). The latter situation was considered a normal part of aging and for many decades was referred to as senile dementia (Boller and Forbes, 1998). Today, AD is the most commonly diagnosed as senile dementia. A hundred years of research have spurred on clinical and scientific advancements in understanding the etiology and pathogenesis of AD and subsequent insight into senile dementia.

One of the most important facts about AD is that its victims, often exhibit strange, irrational and emotionally upsetting behavior of which are merely symptoms of the disease. These symptoms, however offer no insight into the biochemical mechanism of AD. Hence it is necessary to establish a molecular mechanism for AD, which is crucial to the design of therapeutic agents against the disease that could possibly halt its progression. Besides the risk factors of age and the genetic and environmental factors associated with the disease (Huang and Mucke, 2012), the main cause of AD remains unknown, thus it is essential to attempt to unravel the biochemical mechanisms underlying AD. In actual fact, a definitive diagnosis of AD can only occur at post-mortem, after pathologic examination of brain tissue, or amyloid plaques can be visualized using magnetic resonance imaging (MRI) and positron emission tomography (PET) scans (Fig.1.1). There is a new method which uses the drug florbetaben as a tracer for amyloid plaques during a PET scan of the aged brain (Fig.1.1) (Cruz, 2012). In order to prove that the florbetaben PET scan could detect beta-amyloid in the brain, the global phase III study directly compared brain

regions in the PET scan to respective brain regions after death during autopsy (Fig.1.1). Based on these 246 brain regions, the study found florbetaben to detect beta-amyloid with a sensitivity of 77 % and a specificity of 94 %. However the research was performed on patients with late onset AD and future tests will need to establish its effectiveness as a diagnostic tool to detect very early signs of AD (Cruz, 2012).

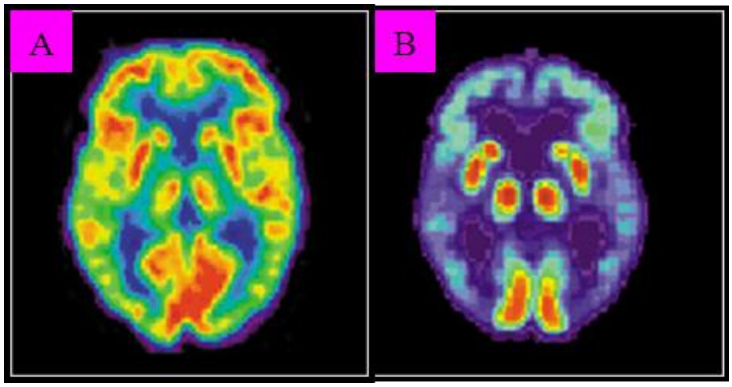

*Figure 1.1: PET scan using the tracer drug, florbetaben to visualize amyloid plaques during life. A healthy brain (**A**) vs. aging brain (**B**). Red patches on scan denote neurons. Aging brain (**B**) shows the characteristic shrinking of neurons (red patches) associated with the onset of AD (Taken from Cruz, 2012).*

1.2 AD: The burden

The future growth in the public-health impact of AD depends strongly on age distribution, specifically on the growth of the oldest age groups of the population (Cummings, 2003). The risk of senile dementia has been associated with aging and hence, increases the likelihood of AD (Mebane-Sims, 2009). In view of this fact, AD is set to grow at an alarming rate because the projected growth of citizens over the age of 65 is unprecedented and on a global scale (Cummings, 2003). The frequency of dementia is said to double in every five years in the population group with ages of 60-85+ (Fig.1.2, Cumming, 2003). These findings, however, do not include the smaller percentage of the population of the ages 40-50 who are also affected by AD. The prevalence of AD is in particular increasing in the United States (US), thus, the congress of the US has classified the treatment of this disease as a major national priority. In 2012, about 2.5 million Americans, aged 85 years and older were diagnosed with the disease and

by 2050, this number is expected quadruple to 21 million (Fig.1.3A). Furthermore, it is estimated that by 2030, the number of people aged 65+ years, who are suffering from AD, will reach 7.7 million (i.e. about a 50 % increase from what was observed in 2010 (Fig.1.3B, Alzheimer's Association, 2012).

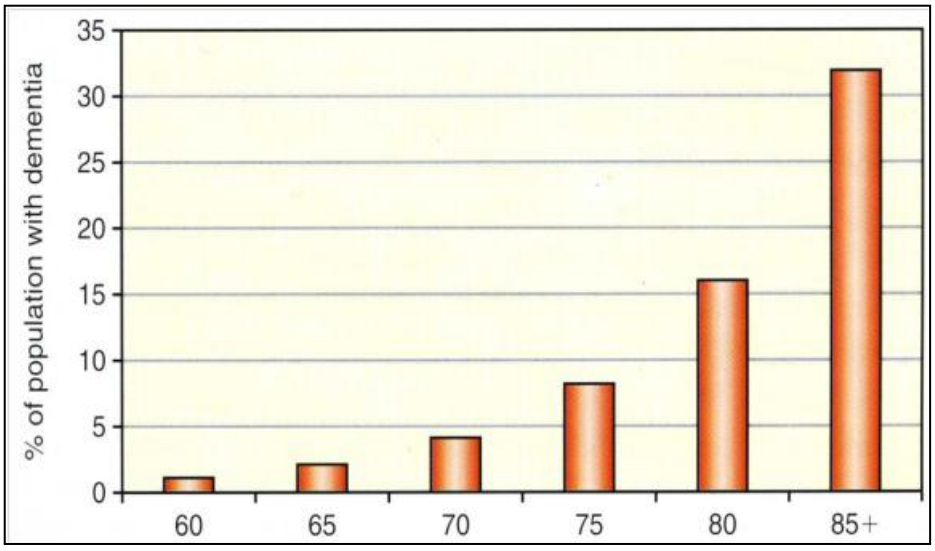

Figure 1.2: Increasing percent of the population with dementia from age 60-85+ (Taken from Cummings, 2003).

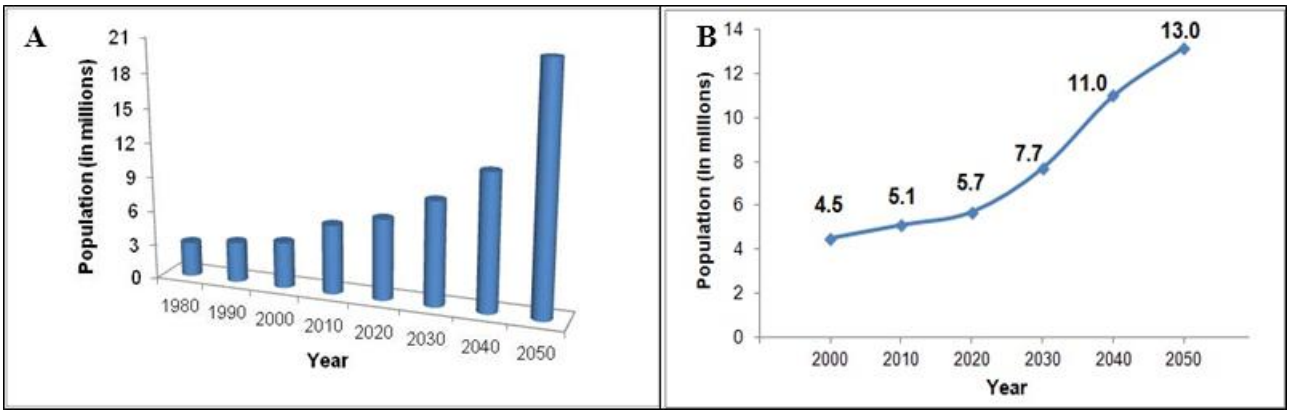

*Figure 1.3: Recent statistics on the prevalence of AD every ten years from 1980 to 2050 (**A**) Projected numbers of people aged 65 and over in the U.S. population with Alzheimer's disease (in millions) using the U.S. census bureau estimates of population growth (**B**) (Taken from Alzheimer's Association, 2012).*

The disease however is also common to Africa and parts of Asia. In Africa, it is expected that the number of individuals over the age of 65 will increase from 17.7 million to 37.9 million

between 1997 and 2025. Presently in South Africa, more than 140 000 aged suffer from dementia (Cummings, 2003). The payments for the care of patients with AD for 2012 were estimated to be $200 billion and the projected cost of care are estimated to be $1.1 trillion by 2050 (Alzheimer's Association, 2012). These costs are staggering, particularly in light of predictions that the worldwide number of AD cases (currently estimated at 36 million) will triple by 2050 (Wimo and Prince, 2010). The socio-economic impact is however more drastic for developing countries like South Africa because these countries have developing economies with limited healthcare budgets and health care facilities. It is clear from these shocking statistics that AD places an enormous emotional and financial burden on patients, their families, and the society (Huang and Mucke, 2012). In light of this, research on anti-AD treatment is done in the hope that drug therapies will decrease overall costs associated with this illness and more importantly improve the quality of life for the patient, their family and the caregiver.

1.3 Hallmarks of AD

AD can be classified into familial and/or sporadic forms, depending on gene mutations or deposition of amyloid beta (Aβ) peptide. It has been reported that 5 % of all cases of AD are associated with gene mutations and are classified as familial AD (Perry *et al*., 2005). The most influential genetic risk factor for sporadic AD is allelic variation in the apolipoprotein E (apoE) gene (Huang and Mucke, 2012). Three isoforms of apoE occur in the human population and they differ by single amino acid changes. ApoE3 is the most common allele; this is followed by apoE4 and then apoE2. These variants of apoE may affect the rate of amyloidogenesis to different extents. The apoE4 allele correlates with an early onset of AD and an increased amount of cerebral plaque (Cramer *et al*., 2012; Huang and Mucke, 2012). The majority of AD cases are sporadic, typified by the deposition of Aβ within the brain. The formation of Aβ is preceded by mutations in the amyloid precursor protein (APP). The mutations in this protein create the hallmarks of AD pathogenesis; namely, the formation of Aβ-aggregates (amyloid plaques) and the subsequent formation of neurofibrillary tangles (NFTs). These hallmarks are thought to drive a pathologic cascade in AD and ultimately lead to neuronal death (De Meyer *et al.,* 2006) (Fig.1.4).

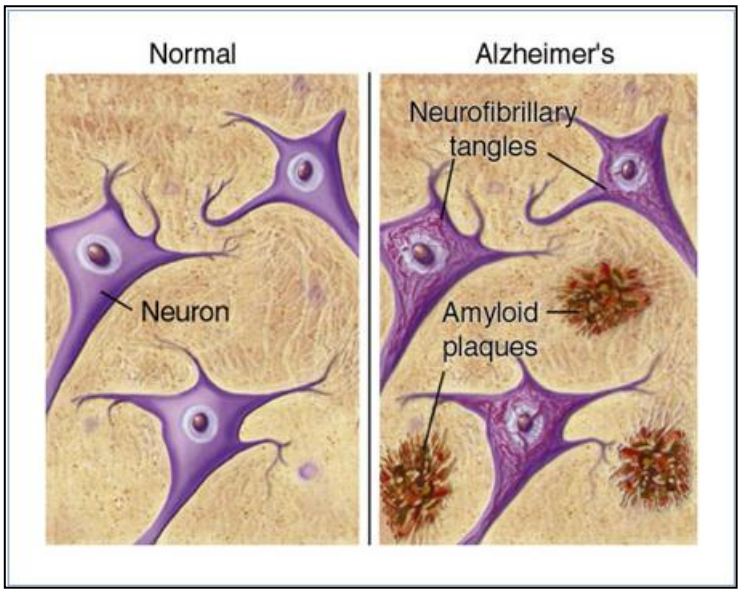

Figure 1.4: The presence of plaques and tangles in the brain of an AD patient (Taken from American Health Assistance Foundation, 2012)

Tau proteins are microtubule associated proteins found in neurons. Microtubules are rod like structures that help maintain cell structure and serve to transport nutrients and organelles within the cell (Huang and Jiang, 2009). When tau proteins become defective i.e. hyperphophorylated, the microtubules collapse to form insoluble twisted fibers called NFT's (Fig.1.4) (Parihar and Hemnani, 2004). Hyperphosphorylation of the tau protein occurs when Aβ aggregates outside a neuron alters the tau proteins inside the cell, ultimately altering the activities of enzymes such as the kinases. The affected kinases add many phosphates to the tau, changing the chemical properties of tau proteins, and thus, causing them to form insoluble filaments (Woo *et al.*, 2011). Recent studies have suggested that altered neural network activity, dysfunction and loss of synapses and degeneration of neurons lead to cognitive decline in AD (Huang and Mucke, 2012). Hence, it is likely that these abnormalities are caused by copathogenic interactions among diverse factors and pathways within the AD brain, resulting in the multifactorial nature of the disease (Palop and Mucke, 2010; Huang and Mucke, 2012).

1.4 An overview of hypotheses related to AD

The cholinergic hypothesis and the amyloid cascade hypothesis are two major hypotheses postulated to explain the molecular mechanism of AD (Fig. 1.5; Parihar and Hemnani, 2004). Recently a novel hypothesis has been proposed, that leads to a reduction in AD, called the "the sink hypothesis." This hypothesis revealed that reduced levels of Aβ in the central nervous system (CNS) could result in lower levels Aβ oligomers and senile plaques and consequently reduce the progression of AD (Zhang and Lee, 2011). The apoE4 proteolysis hypothesis proposes that, apoE4 is more susceptible to proteolytic cleavage than apoE3, resulting in the formation of neurotoxic fragments which accelerate the impairment of neuronal and tau protein function. Hence, there is a need for the development of specific protease inhibitors that could cleave apoE in neurons and thus reduce the production of neurotoxic apoE fragments (Huang and Mucke, 2012). The cholinergic theory describes the loss of cholinergic markers to impairment of cognitive and memory functions (Fig.1.5). These markers include choline acetyltransferase (ChAT), acetyl cholinesterase (AchE) and the acetylcholine neurotransmitter (Parihar and Hemnani, 2004). This lead to the development of AchE inhibitors which helped restore the reduced amounts of acetylcholine found in AD patients (Selkoe, 2004). The available cholinergic therapies, however, only improve the symptoms temporarily, but cannot block the disease progression or cognitive decline. Thus, it is evident that the augmentation of cholinergic and amyloid cascade hypothesis could be a successful treatment strategy. Despite this, the amyloid cascade hypothesis remains a dominant theory in the AD. The amyloid cascade hypothesis (Hardy and Higgins, 1992), suggested that the pathogenesis of AD is initiated by the overproduction and extracellular deposition of Aβ and the intracellular deposition of NFT's. These depositions in turn initiate multiple neurotoxic pathways (Fig.1.5.) The basis for this hypothesis comes from numerous studies demonstrating the toxicity of Aβ in neurons and amyloid plaques in transgenic mice (Lahiri *et al*., 2004; Tayeb *et al*., 2012). The amyloid cascade hypothesis is, however open to criticism, since Aβ is normally found in the cerebrospinal fluid of healthy patients as well as Alzheimer patients. In fact it has been shown that up to 30 % of normal individuals aged 70 + can have amyloid plaques without any cognitive dysfunction (Tayeb *et al*., 2012).

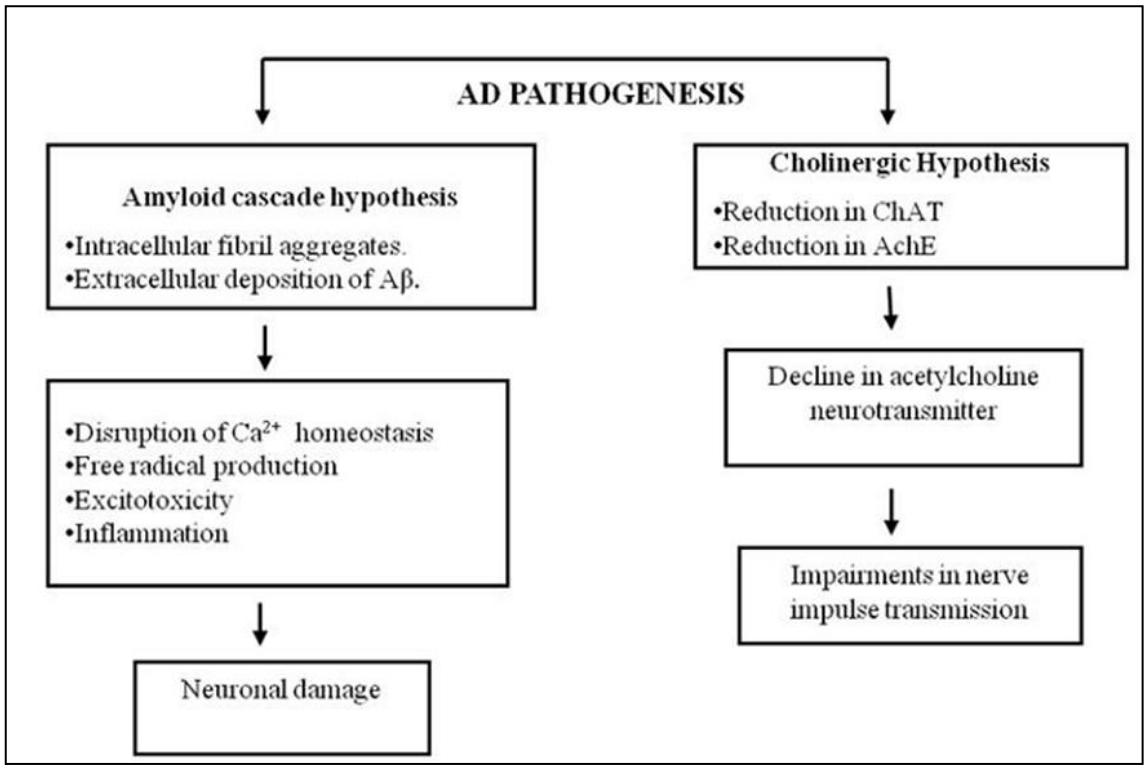

Figure 1.5: Two major hypotheses of AD postulated to explain its pathogenesis (Adapted from Parihar and Hemnani, 2004).

In addition, mechanisms have emerged, in which amyloid deposits do not act as a primary causative agent of neurodegeneration (Drouet *et al*., 2000). For example, it has been shown that an increase in the synthesis of APP and Aβ is an attempt by neurons to detoxify elevated levels of redox active metals such as copper (Cu) iron (Fe) (Maynard *et al*.,2005). In view of such evidence, the protective role afforded by Aβ in the initial stages of AD should not be underestimated (Perry *et al*., 2005). This is interesting since the complete removal of this form of peptide, may upset the homeostatic balance within the nervous system. Despite ongoing critique, the amyloid cascade hypothesis is still supported by molecular genetic studies and continues to be a favored hypothesis in the understanding of the pathogenesis of AD. As the Aβ hypothesis evolves, more and more attention has been paid to intracellular Aβ toxicity because a thousand molecules of intracellular Aβ are potent enough to induce cell death compared with the micromolar toxicity range of extracellular Aβ (Zhang and Lee, 2011). Mechanisms of Aβ toxicity include reactive oxygen species (ROS), nitric oxide productions, decreased membrane

fluidity and inflammatory processes that contribute to the pro-oxidant nature of Aβ (Parihar and Hemnani, 2004). Moreover, the presence of transition metals such as Cu, Fe, zinc (Zn), aluminum (Al) and their interaction with Aβ is also known to generate ROS and lead to toxicity levels of Aβ (Perry *et al*., 2005). Thus, Aβ related toxicity makes it crucial to understand the process of amyloidogenesis (i.e. the origin of Aβ and its formation) and thus forms the basis for the design of therapeutics to alleviate the associated toxic effects.

1.5 Amyloidogenesis

The amyloid cascade hypothesis is driven by the genetic mutation in the APP protein which is the precursor to amyloid formation. APP is a transmembrane cell surface glycoprotein, encoded by a gene which is located on chromosome 21. APP is involved in viability, growth, morphological and functional plasticity of nerve cells and also plays a role in learning or memory processes. Thus a mutation in the protein blocks these processes and leads to eventual neuron death (Parihar and Hemnani, 2004). The protein has a large hydrophilic amino terminal extracellular domain, a single hydrophobic putative transmembrane domain and a small carboxy-terminal cytoplasmic domain (Parihar and Hemnani, 2004). More significantly, the abnormal processing of the APP triggers the aggregation of Aβ via secretase cleavage at the extracellular domain of the protein (Parihar and Hemnani, 2004).

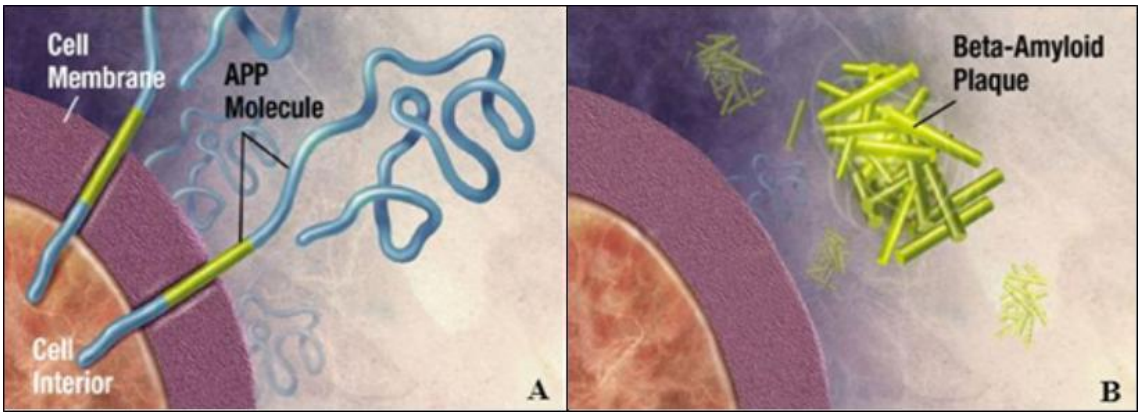

*Figure 1.6: Diagram illustrating the location of APP embedded in the cell membrane (**A**) and subsequent formation of Aβ plaques (**B**) (Taken from Anderson, 2013)*

The APP molecule sticks partly inside and partly outside the cell (Fig.1.6A). The Aβ fragments aggregate to form clumps outside the cell and subsequently join other molecules and nerve cells to produce insoluble plaques (Fig.1.6B).

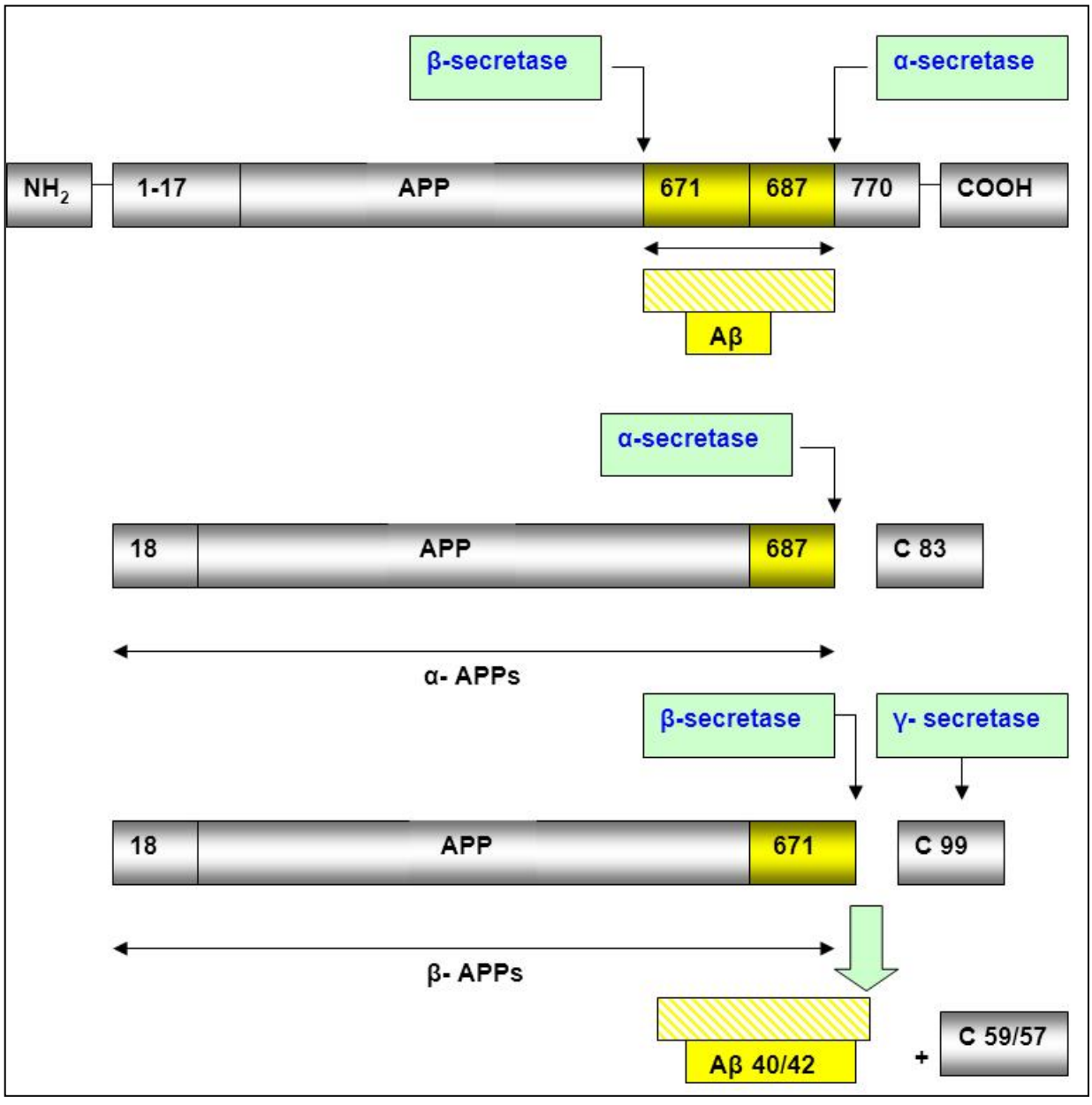

Figure 1.7: Schematic diagram of processing of amyloid precursor protein (APP) and production of Aβ (Parihar and Hemnani, 2004).

Since the APP was confirmed to be the protein of origin for Aβ, it is important to understand the underlying mechanisms involved in this protein mutation (Parihar and Hemnani, 2004; Anderson, 2013). Two secretase enzymes; namely, β-secretase and γ-secretase are involved in amyloidogenesis while the third secretase namely α-secretase plays a partial role in this process. Though the precise molecular identity of γ-secretase remains unresolved, recent evidence suggests that membrane-associated presenilin proteins 1 and 2 (PS1 and PS2), which act in association with another protein called nicastrin, may constitute the γ-secretase complex (De Felice *et al*., 2002). β-secretase (also known as BACE or memapsin), however, has recently been identified as an aspartic protease (De Felice *et al*., 2002). The process of Aβ production starts when α- and β-secretase cleave the APP molecule at different positions leading to the release of large soluble N-terminal fragments; namely, α-APPs and β-APPs, respectively (Fig.1.7). APP is cleaved by α-secretase at residue 687 to produce α-APPs and the C-terminal fragment C83. The cleavage by α-secretase, however, does not contribute to Aβ formation. In contrast, β-secretase cleavage generates the free N-terminus of Aβ and is, therefore, considered the first critical step in amyloid formation. The aspartyl protease cleaves at residue 671 to produce β-APPs and the C-terminal fragment C99. The C99 fragment is further cleaved by γ –secretase within the APP transmembrane domain to release Aβ, which is critical in the pathogenesis and etiology of AD (Fig.1.7) (Parihar and Hemnani, 2004). It is now accepted that the presence of amyloid peptides is crucial in the underlying mechanism of AD. Hence, it is necessary to understand their nature, function and potential mechanisms within the brain.

1.6 Properties of Aβ

The term ‘amyloid’ was coined by Virchow on the basis of its histological staining by iodine (Virchow, 1854). The term is derived from amylose or amylon and means ‘starch like’ and the nature of carbohydrate was termed glycosaminoglycans (Parihar and Hemnani, 2004). It was recognized, however, that the amyloid deposits consisted mainly of protein (Fraser *et al*., 1993). Thus the extracellular accumulation of fibrillar protein deposits with unique structural properties is generically referred to as amyloid (Parihar and Hemnani, 2004). To be more specific, in AD, the term ‘amyloid’ is equated to Aβ (Mathis *et al*., 2007). More recently, the term ‘amyloid’

generally refers to many types of β-pleated sheet proteins found in the central nervous system (Mathis *et al*., 2007).

Aβ protein contains 42 amino acids in its peptide sequence and is associated with lipoprotein particles which make Aβ highly hydrophobic such that it is partially inserted into lipids by its hydrophobic C-terminal tail (Kontush, 2001). Neuronal cells are more active than other cells (e.g. astrocytes, neuroblastoma, hepatoma) in producing Aβ and seem to be the major source of Aβ in the brain (Kontush, 2001). Once Aβ is formed it can pursue several possible pathways. It can be released as a soluble form by adopting mainly a random coil conformation, and then either be removed or aggregated at higher concentrations to form a fibril (β-sheet) in the process called fibrillogenesis (Bokvist *et al*., 2003). An interesting question that remains unresolved is whether the *in vivo* pathogenicity of these amyloid proteins depend on specific conformations (e.g. β-pleated sheet structures) or these proteins require self-aggregation or binding to other proteins to assume these conformational states.

Nevertheless, there is substantial evidence to indicate that Aβ aggregation leads to fibrillogenesis and understanding the mechanism of fibrillogenesis is critical to understanding the etiology and pathogenesis of AD. It has been proposed that during the process of fibrillogenesis, once protein unfolding begins, there is a lag phase during which no protein fibrils are observed, this is then followed by a rapid production of protein fibrils (Colvin and Kulinowski, 2007). During the lag phase, many non-fibrous short peptide sequences known as oligomers form and act as seeds for fibril formation (Colvin and Kulinowski, 2007). Developing drug treatment strategies to halt the onset and progression of fibrillogenesis are key factors to be considered in managing, not only the symptoms of the disease but also the designing of specific inhibitors, enzymes or peptides which can target the underlying mechanism of AD.

1.7 Drug development

To date, no treatment has been clinically proven to modify the disease process in a way that significantly slows or prevents the progression of AD (Hampel *et al*., 2013; Alzheimer's Association, 2012). There are several different pharmacological agents, however, that may

temporarily suppress certain debilitating symptoms as well as possible agents that may target the underlying cause of AD (Fig.1.8).

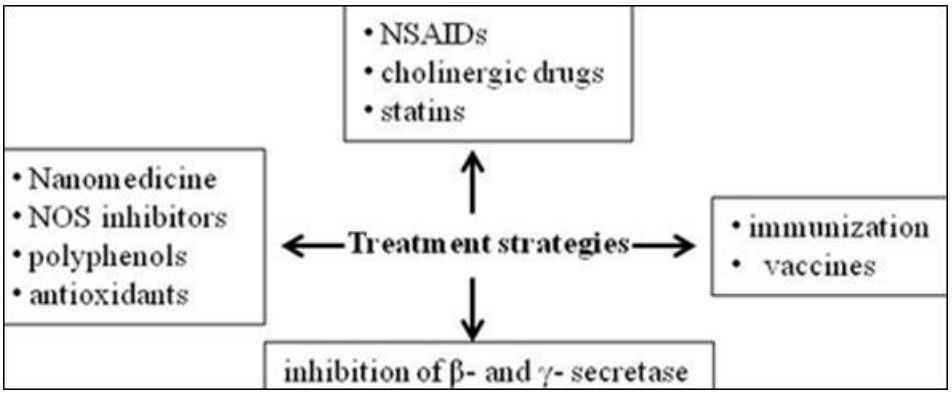

Figure 1.8: Schematic representation showing prevention strategies for AD (Adapted from Parihar and Hemnani, 2004)

1.7.1 Immunization

Immunotherapy is a new and promising approach to the treatment of AD through either active Aβ-peptide vaccination or passive infusion of anti-Aβ monoclonal antibodies (Haass and Selkoe, 2007). CAD-106 is a vaccine that comprises $A\beta_{1–6}$ coupled to a virus-like particle. This vaccine can induce Aβ-specific antibodies and reduce amyloid accumulation in animals, without stimulating T cells and causing microhaemorrhages (Haass and Selkoe, 2007). ACI-24 is a vaccine that contains $A\beta_{1–15}$ embedded within a liposomal surface, and reduces brain amyloid load and restores memory deficits in mice (Mangialasche *et al*., 2011). Another active immunization strategy is based on Affi topes, short peptides mimicking parts of native $A\beta_{1–42}$ without its sequence identity. AD-01 and AD-02 are the names of typical Affi topes, amongst others which have demonstrated AD modifying properties, when interacting with Aβ (Mangialasche *et al*., 2011). Immunization strategies have advantages and disadvantages. Active immunotherapy guarantees high concentrations of antibody at reduced costs. There exists, however the problem of rapidly reducing antibody concentrations when needed by the patient. On the other hand, with passive immunotherapy, concentrations of antibody can be controlled, even though their administration is time consuming and costly (Mangialasche *et al*., 2011).

1.7.2 Cholinergic drugs and non-steroidal anti-inflammatory drugs (NSAIDs)

Cholinergic drugs include cholinesterase inhibitors (ChE-Is) and acetylcholinesterase inhibitors such as donepezil, galantamine and rivastigmine (De Meyer *et al*., 2006). ChE-Is improve cholinergic function in AD by preventing the breakdown of intrasynaptic acetylcholine by acetylcholinesterase. As a result, acetylcholine can exist for a longer time period within the synapse and signal transmission within the cholinergic neuron is enhanced (Cummings, 2003). In addition, NSAIDs down regulate pro-inflammatory signals as well as the autoimmune response from microglia cells which produces free radicals within amyloid plaques (Parihar and Hemnani, 2004).

1.7.3 Antioxidants

Melatonin is known to improve cognitive function and play a role in anti-oxidative injury, inhibition of Aβ deposition and fibril formation (Smith *et al.*, 2007). Recently resveratrol, a polyphenol found mainly in grapes and red wine was demonstrated to attenuate Aβ -induced toxicity (Huang *et al*., 2011), promote Aβ clearance and reduce senile plaques through its antioxidant activity (Huang *et al*., 2011).

1.7.4 Polyphenols e.g. curcumin

Curcumin (diferuloylmethane) is extracted from the plant *Curcuma longa* (commonly known as turmeric) (Fig.1.9). The yellow-pigmented fraction of turmeric contains curcuminoids. There are four major curcuminoids present in turmeric; (1) curcumin (2) demethoxycurcumin (curcumin II), (3) bisdemethoxycurcumin (curcumin III) and (4) cyclocurcumin (Fig.1.10) (Goel *et al*., 2008). Curcumin has been demonstrated to have anti-oxidant, anti-inflammatory, and cholesterol-lowering properties, all three key processes involved in the pathogenesis of AD (Ishrat *et al*., 2009). Recent evidence indicates that curcumin is effective in preventing cognitive deficits, and might be beneficial for the treatment of sporadic dementia of associated with AD (Ishrat *et al*., 2009).

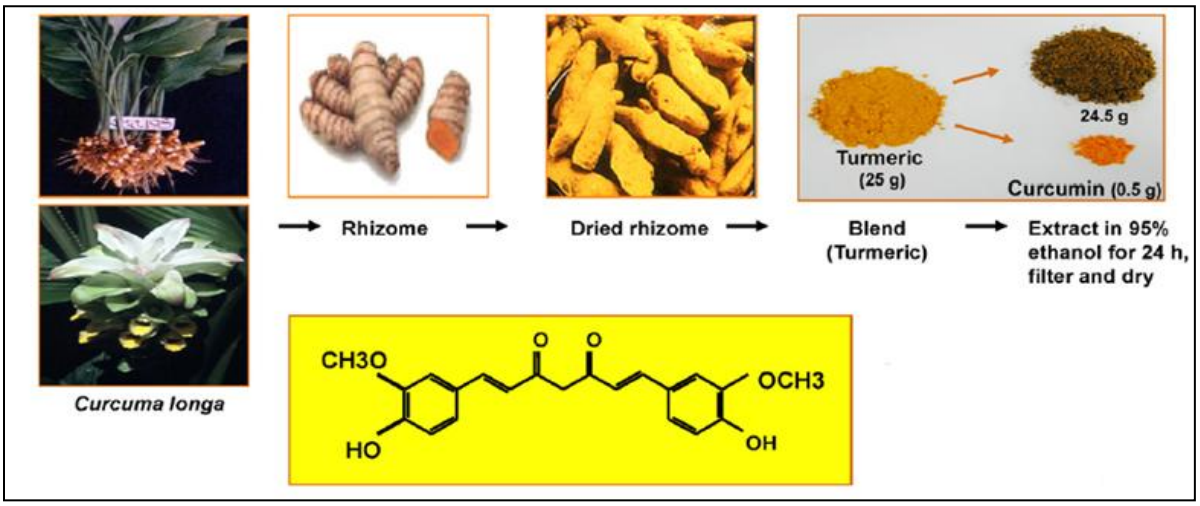

Figure 1.9: Isolation, extraction and structure of curcumin (Taken from Goel et al., 2008).

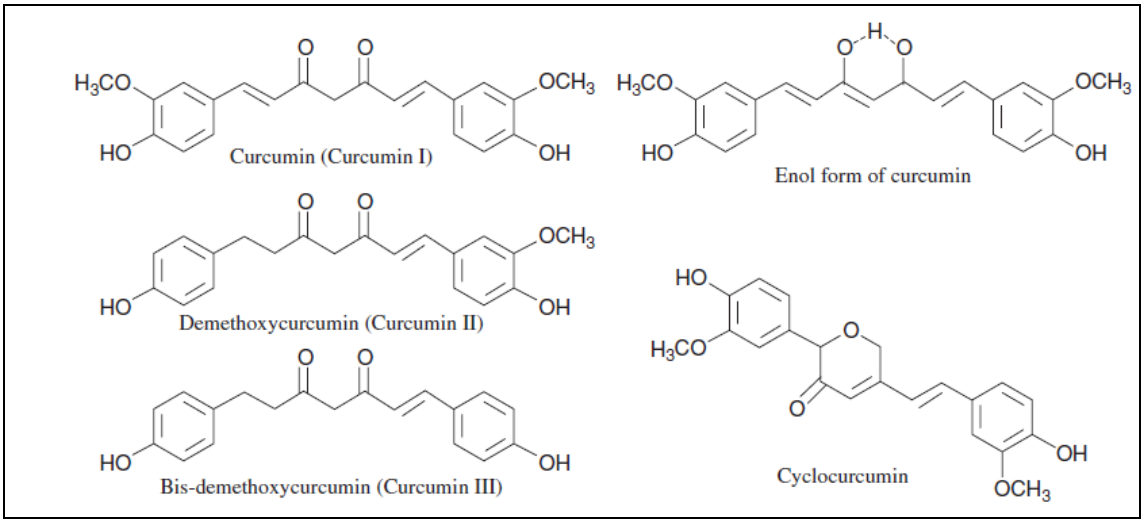

Figure 1.10: The four major curcuminoids present in turmeric (Taken from Aggarwal et al., 2006).

Curcumin also plays a significant role in anti-amyloid therapy. It was found that curcumin inhibited the formation and extension of Aβ fibrils and destabilized preformed fibrils from $A\beta_{1-40}$ in a dose-dependent fashion, at a concentration range of between 0.1 μM and 1 μM (Ono *et al.*, 2004). Curcumin is known to inhibit oligomer formation by binding to and solubilizing plaque formation (Yang *et al.*, 2005). In addition, the molecule lowers Aβ aggregation and toxicity by binding to redox-active metals in the brain such as Fe^{2+} and Cu^{2+}.

Despite its therapeutic properties, one of the most important limitations of curcumin is its low bioavailability. Curcumin seems to be metabolized through conjugation and reduction such that either no curcumin or only low levels of curcumin metabolites are detected in serum or tissue (Aggarwal and Sung, 2008). Different approaches have been undertaken to enhance the bioavailability of curcumin, one such approach is nanotechnology (i.e. the use of nanoparticles). Recently, curcumin has been encapsulated/conjugated with polymeric nanoparticles (nps) such as micelles or liposomes (Mimeault and Batra, 2011; Mathew *et al*., 2012; Ringman *et al*., 2012). This approach was shown to improve the bioavailability of curcumin, and thus provide a more effective inhibition for the formation of fibrils *in vitro* (Taylor *et al*., 2011).

1.7.5 Statins

Statins e.g. simvastatin are inhibitors of the cholesterol-synthesizing enzyme, HMG-CoA-reductase which influences Aβ production (Citron, 2002). A study has reported that in elderly patients with hypercholesterolemia the risk of developing dementia was reduced 60-70 % when they were treated with a statin (De Meyer *et al*., 2006). Although statins may slow the progression of the neurodegenerative process, however, they are not able to reverse neuronal degeneration once it has occurred (Castellani *et al*., 2008).

1.7.6 Inhibition of β- and γ- secretase

A further protective neuroprotective strategy is the inhibition of β-and γ-secretase and stimulation of α-secretase activity (Cummings, 2003). The generation of such inhibitors is currently a challenge since a drug that blocks the function of γ-secretase might not be effective in patients developing AD, due to the multifactorial nature of the disease. Therefore, agents that prevent the initial stages of Aβ formation (Aβ nucleation) could be more effective than those that merely block the final stages (Aβ deposition) (Cummings, 2003). Certain inhibitors of γ-secretase that prevents the production of Aβ include gelatinase A, bafilomicin A, calpain inhibitor and brefeldin (De Felice *et al*., 2002). Furthermore, recent studies have examined the protease inhibitor MG132 and calcium ionofore A23187 as potential inhibitors of β-secretase. It is important to note, however, that the human β-secretase can participate in the processing of

other physiological substrates in addition to APP, and may be involved in important biological functions that could be affected by the use of such inhibitors (De Felice *et al*., 2002).

1.7.7 Nanotechnology

Nanotechnology simply denotes the man-made use of nano-sized particles for industrial and medical purposes (Aitken *et al*., 2004). Nanoparticles (nps) are defined as solid particles within a size range of 1-1000 nm. Currently, the controllable production of nps (1-100 nm) has been achievable (Nazem and Mansoori, 2011). The targeting of nps to site-specific affected areas within the body can be achieved by attaching target ligands to the surface of the particles (Mohanraj and Chen, 2006). These ligands could be antibodies, carbohydrates, peptides or proteins and could interact with the np through covalent and hydrogen bonds. Such methods have been experimentally shown to extend the versatility and stability of nps (Vinogradov *et al*., 2002; Ishii *et al*., 2003). The drug is dissolved, entrapped, encapsulated or attached to a nanoparticle matrix and its properties are easily manipulated to achieve passive and active drug targeting (Vinogradov *et al*., 2002; Ishii *et al*., 2003). The major goals in designing nps as a delivery system is to control its properties, i.e. particle size, surface area, concentration and the release of pharmacologically active agents in order to achieve a high success rate of efficacy (Mohanraj and Chen, 2006). The uses of nps, however, have limitations. Apart from being toxic to the body their small size and large surface area can lead to particle aggregation, making physical handling of nps difficult in liquid and dry forms (Zhang *et al*.,2007; Schrand *et al*.,2010). In addition, their small size and large surface area could also result in limited drug loading and burst release (Mohanraj and Chen, 2006). These practical problems (Schrand *et al.*, 2010) have to be overcome before nps can be used clinically or made commercially available.

In recent years, significant amount of research was focused on finding “neuroprotective agents”, therapeutics that could stop the disease progression by targeting specific molecular mechanisms in AD. These approaches include using “regenerative agents” (neuroprotective and/or neuroregenerative) and are known as “disease-modifying approaches”. They are distinguished from symptomatic approaches by the fact that in addition to alleviating the symptoms, they are

aimed to stop the progression of the disease altogether. Table 1.1 describes potential nanosystems employed in anti-AD dug treatment and therapy (Nazem and Mansoori, 2011).

Table 1.1: Nanosystems designed for treatment of AD (Nazem and Mansoori, 2011)

Nanosystem	Function	Targeted mechanism
Nanogels	Aβ anti-assembly	oligomerization of Aβ
Fullerene	anti-oxidant	oxidative stress
Au nps	Aβ anti-assembly	Aβ cell membrane toxicity
Dendrimers	Aβ anti-assembly	Aβ cell membrane toxicity

Most nanoparticles have been reported to self-organize into structures similar to those of Aβ peptides. Thus, it would be of interest to investigate the effect of nps on amyloid fibrillogenesis since the assembly behavior of these nanoparticles is similar to that of biological species. Infact, the interaction of nps with fibrils has been shown to be a definite phenomenon and so points to their efficiency as therapeutic agents in AD (Fig.1.11, Colvin and Kulinowski, 2007).

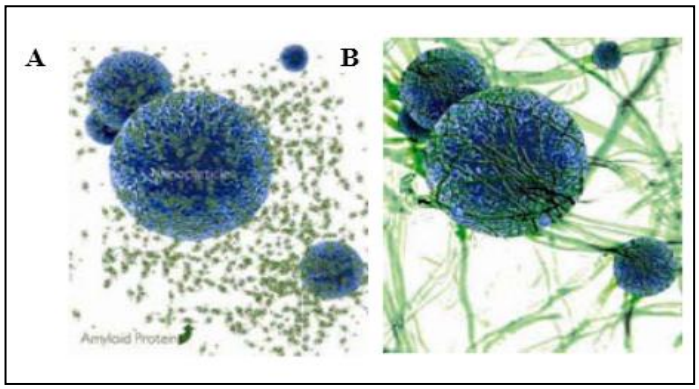

*Figure 1.11: Artistic rendering of Aβ fibrillation in the presence of nps. (**A**) Nanoparticles (blue) and monomers of Aβ (green) (**B**) The association of Aβ fibrils with the surface of nanoparticles (Taken from Colvin and Kulinowski, 2007).*

Nanoparticles have a dual effect on fibril formation, i.e. nps either promote aggregation or slow down aggregation. The size and surface concentration of nps play a role in accelerating fibrillogenesis. This have been demonstrated in an experiment which showed that the loss of α-helix content in adsorbed enzymes on nps was strongly dependent on particle size (Yan *et al*., 2009). Results showed that that greater loss of α-helicity in the enzyme was associated with larger np size. Larger nps tend to cause unfolding of the adsorbed protein/enzyme due to stronger

protein interactions, more unfolding and less enzymatic activity (Yan *et al*., 2009). N-acetyl-L-cysteine-capped quantum dots (3-5 nm) was also reported to inhibit the generation of fibrils which was attributed to the formation of hydrogen bonds (Kotov *et al*., 2011). The same bonds are involved in peptide-np systems which promote Aβ aggregation. TGA (thioglycolic acid)-stabilized cadmium tellurium nps were also found to inhibit the formation of fibrils and closely resembled proteins in terms of size, charge an association behavior (Kotov *et al*., 2011).

1.7.8 New treatment directions in 2012

Recently, a skin cancer drug called bexarotene has been considered for AD treatment (Cramer *et al*., 2012). After a dose of this drug was orally administered to demented younger mice, the levels of Aβ in the brain were "rapidly lowered" within six hours and a 25 % reduction was sustained for 70 hours. In older mice with established amyloid plaques, seven days of treatment reduced the number of plaques in the brain by 50 % (Cramer *et al*., 2012). Similarly, another drug called Levetiracetam (LEV) has been discovered to suppress neuronal network dysfunction and reverse synaptic and cognitive deficits in AD (Sanchez *et al*., 2012). In order to maximize its therapeutic impact, however, LEV treatment regimens will have to be optimized further with respect to dosage. The onset or length of treatment may also have to be combined with other drugs which complement LEV's mode of action (Sanchez *et al*., 2012). It is thus clear that in light of the recent ongoing trials for drugs against AD, a single cure is unlikely to be found. This might mean gaining insight into the networks of interactions between enzymes and peptides crucial in the AD pathway, rather than focusing on a single potential drug target. Thus, it is desirable to understand a mechanism underlying the disease pathways by identifying potent small molecule inhibitors. One such group of protein inhibitors are the peptide inhibitors.

1.7.9 Peptide inhibitors

In general, peptide inhibitors have a hydrophobic core which binds to the hydrophobic core of the Aβ. Certain residues of the peptide behave as an anchor for the inhibitor to bind. The peptide inhibitors function by competing for hydrophobic and electrostatic interactions that form hydrogen bonded β-sheet structures. The weakening of hydrogen bonds among β-sheets of the

amyloid fibril lead to the dissolution of β-amyloid fibrils and point to the potency of such inhibitors in the fibrillogenesis pathway (Chen *et al*., 2005).

Currently, the role of short peptide fragments derived from the $A\beta_{1-40}$ sequence on amyloid aggregation has sparked interest in AD research (Padayachee and Whiteley, 2011, Padayachee and Whiteley, 2012). In this regard, fibril formation can be impaired by the substitution of hydrophilic for hydrophobic residues in the hydrophobic region of the $A\beta_{1-40}$ sequence (Giordano *et al*., 2009). Pseudopeptides have also been designed with the aim of disrupting hydrogen bonding that stabilizes the β-sheet structure. The five residue β-sheet breaker peptide, (Ac-Leu-Pro-Phe-Phe-Asp (OH)-NH_2) capped with *N*- and *C*- terminal protection, and having a proline and aspartic residue substituted for valine and alanine was synthesized and it has been shown that the proline residue in this peptide inhibited β-sheet formation (Soto,1999; Soto *et al*., 1998).

To date, research into amyloid peptide inhibition has been limited. Thus, another relatively new strategy in preventing Alzheimer's is the potential of nitric oxide synthase (NOS) enzyme inhibitors. In particular, the interaction of neuronal nitric oxide synthase (nNOS) and its interaction with Aβ are significant because previous research (Padayachee and Whiteley, 2011, Padayachee and Whiteley, 2012) has hypothesized that nNOS is a catalyst in the formation of fibrils from Aβ. Infact, the entire amyloidogenic pathway involving nNOS and Aβ occurs within a neuron in the brain. Thus the close proximity of the Aβ to nNOS makes it a good starting point at attempting to selectively inhibit nNOS. The inhibition of nNOS by Aβ will thereby prevent the fibrillogenesis of amyloid peptides, thereby suppressing fibrilization-dependant neurotoxicity and thus slowing the progression of AD. It is therefore significant to establish a mechanism of nNOS-Aβ interaction, in order to gain insight into a possible model for fibrillogenesis.

1.8 Nitric oxide synthases (NOSs)

NOSs are a class of enzymes found in mammals and other species that utilize L-arginine to generate nitric oxide (NO), an important signaling molecule in the brain (Poulos *et al*., 2002). Like many enzymes, these NOSs are designed to function as active dimers comprised of

identical subunits. There are three isoforms of NOS: neuronal NOS (nNOS) (Fig.1.12), endothelial NOS (eNOS) and inducible NOS (iNOS) (Zhang and Snyder, 1995). This research is mainly focused on the interaction of nNOS (Fig.1.12) with Aβ in relation to regulating the substrate arginine since high concentrations of arginine are found in the brain of AD patients (Yi *et al.,* 2009).

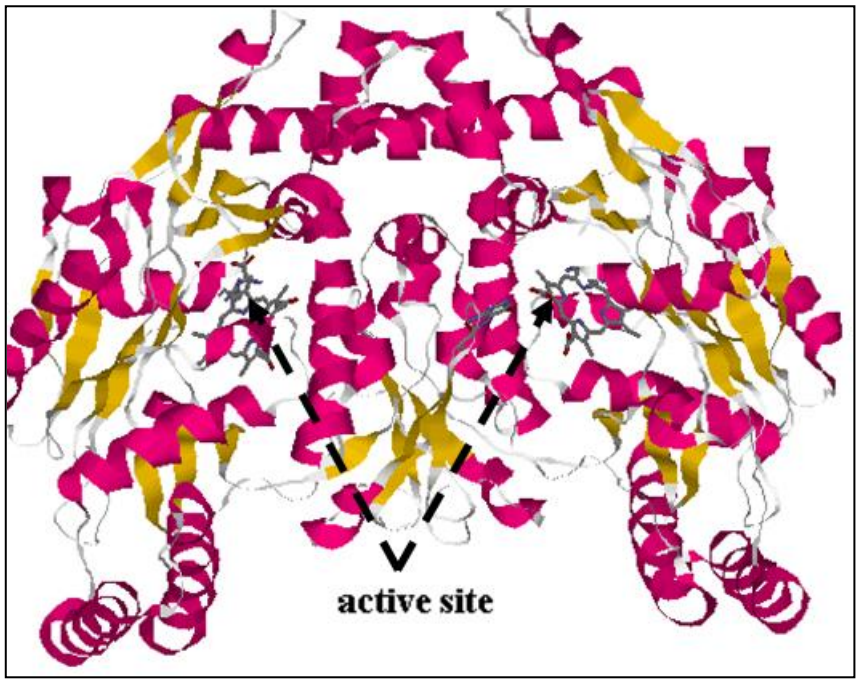

Figure 1.12: Ribbon structure of homodimeric nNOS, illustrating the active site. Image was generated using Rasmol (Raswin molecular graphics [V 2.7.2.1] (Sayle and Bernstein, 1998-2001) (PDB: 1zvi).

1.8.1 Properties of nNOS

The enzyme nNOS consists of two parts: an oxygenase domain and a reductase domain aligned in a head to head manner (Fig.1.13) with a short calmodulin (CaM) linker. The *N*-terminal oxygenase domain contains binding sites for L-arginine (ARG); tetrahydro-L-biopterin dichloride (H_4B) and heme (Fe). The C-terminal domain of the enzyme represents the reductase domain which binds the flavin co-factors, FMN and FAD and NADPH; a calmodulin–binding sequence (CaM) is present between FMN and FAD (Fig.1.13). Active NOS may assemble in two sequential post-translational steps that each involves a separate domain of the enzyme. The protein first acquires a functional reductase domain by binding FAD or FMN and CaM (Stuehr,

1997). This generates a folded NOS monomer that is capable of catalyzing electron transfer from NADPH but is inactive regarding NO synthesis. The monomers then assemble into a dimer in a reaction that requires sufficient heme to be present and may be promoted by the presence of L-arginine and tetrahydro-L-biopterin dichloride to activate NO synthesis (Stuehr, 1997).

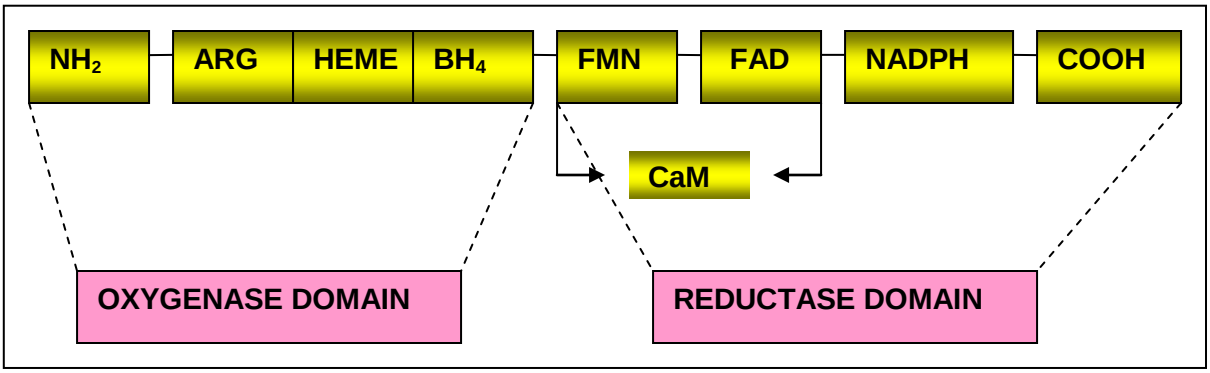

Figure 1.13: Domain structure of human nNOS, depicting two parts: oxygenase and reductase domain (Taken from Stuehr, 1997).

1.8.2 Catalysis

It can be expected that the isoforms of an enzyme exhibit different isoform-specific activities. This, however, may not be the case with NOS due to the fact that all isoforms have the same cofactors and the same co-substrate requirements (Marletta *et al*., 1998). The nNOS-catalyzed conversion of L-arginine to L-citrulline and nitric oxide is known to be the sum of two partial reactions namely; oxygenation of arginine to *N*-hydroxyarginine, followed by oxygenation of *N*-hydroxyarginine to citrulline and nitric oxide (Campos *et al*., 1995).

The first step in the reaction is the *N*-hydroxylation of L-arginine, yielding *N*-hydroxy –L-arginine (L-NHA) as an intermediate. L-NHA is further oxidized to L-citrulline and NO in an NADPH–and O_2-dependent step (Fig. 1.14) (Marletta *et al*., 1998). L-NHA functions effectively as a substrate for nNOS and requires not only a guanidinium moiety but also an amino acid head group for catalysis to occur (Fig. 1.14) (Poulos *et al*., 2002). Moreover, NO synthesis requires a sequential transfer of three electrons between the reductase and oxygenase domains to convert L-arginine to citrulline and NO. The nitrogen of NO is derived from the

guanidino nitrogen atoms of L-arginine while the oxygen is derived from molecular oxygen (O_2) (Bruckdorfer, 2005).

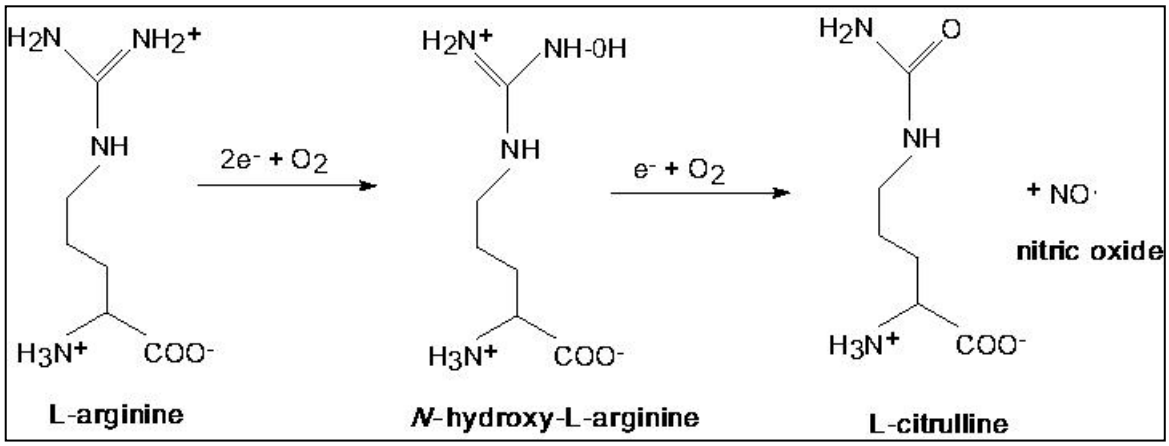

Figure 1.14: Catalytic mechanism of nNOS (Taken from Padayachee and Whiteley, 2011, 2013).

The reductase domain converts NADPH into $NADP^+$ and feeds electrons via FAD or FMN (either one of the flavin cofactors are necessary for catalysis) to an iron protoporphyrin IX (Fe site) in the oxygenase domain. The heme (Fe) center and H_4B in the oxygenase domain converts arginine and oxygen into citrulline and NO. It must be noted that electron flow through the reductase domain requires the presence of bound calcium ion or calmodulin (Ca^{2+}/CaM) (Knowles *et al*., 2001). Moreover, the nNOS isoform contains a 250-amino acid N-terminal leader sequence not present in the other two NOS isoforms. The leader sequence is involved in binding proteins that target nNOS to discrete regions in the cell. In addition, the presence of a protein–interaction domain called a PDZ domain also sets nNOS apart from other isoforms and targets the enzyme to sites in the nerve synapses (Marletta *et al*., 1998).

1.9 Involvement of nNOS and small β-peptide sequences in AD

The schematic diagram (Fig.1.15) illustrates the amyloidogenic pathway incorporating the catalysis of nNOS and its subsequent effect on the pathway. Previous studies (Padayachee and Whiteley, 2011) on the interaction of nNOS with $A\beta_{1-40}$ have shown that the Aβ peptide does inhibit nNOS. The fact that there is a low level of citrulline and a high level of arginine in the cerebrospinal fluid of AD patients could mean that there is a decrease in the enzyme that

metabolizes this amino acid i.e. nNOS, and thus reflects the possible use of nNOS as a biomarker in AD (Yi *et al*., 2009). On the other hand when arginine levels are low and nNOS catalytic activity is high, there is excess production of NO and formation of superoxide radicals which generate reactive oxygen species (ROS) and peroxynitrite ($ONOO^-$) which are far more neurotoxic than NO (Fig.1.15).

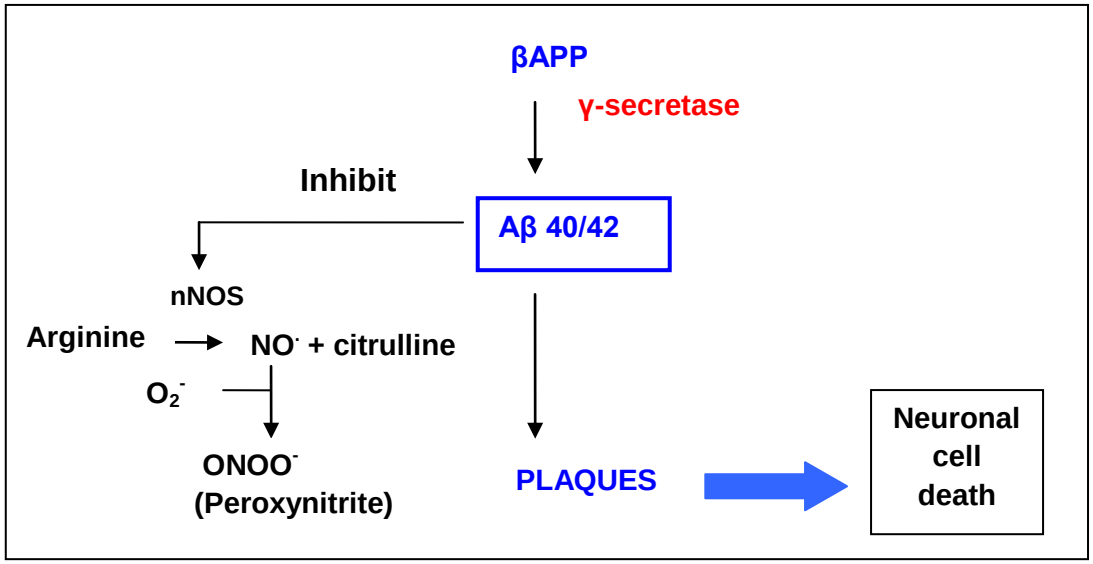

Figure 1.15: An illustration describing the role of nNOS in the amyloidogenic pathway

Thus, since amyloid peptides are in effect composed of a specific 1-42 amino acid stretch and are surrounded by astrocytes, which also function to store reserve arginine in brain tissue which is eventually metabolized by nNOS, it would be interesting to investigate which segment(s) within the $A\beta_{1\text{-}40}$ peptide would inhibit nNOS such that levels of arginine in the brain can be regulated. Currently, the aggregation of secreted soluble Aβ into oligomers and large Aβ fibrils is considered to be a crucial event in AD onset and the effect of specific Aβ sequences on the ability to form fibrils has been studied (Carlo, 2010, Padayachee and Whiteley, 2011; Padayachee and Whiteley, 2012; 2013). These small peptide motifs could also bind to Aβ monomers and prevent their assembly into fibrils (Woo *et al*., 2011; Padayachee and Whiteley, 2011; Padayachee and Whiteley, 2012; 2013). Thus as a starting point, great effort must be made to understand the mechanism of fibrillogenesis using short peptide motifs within $A\beta_{1\text{-}40}$. The term motif refers to a particular amino acid sequence that is characteristic of a specific

biochemical function. Interestingly, the hydrophobic C-terminal region of Aβ contains a Gly-XXX-Gly-XXX-Gly motif, termed a "glycine zipper" (Kim *et al*., 2005). The glycine zipper motif has been shown to drive the packing of transmembrane α-helices (Fig.1.16) (Fonte *et al*., 2011).

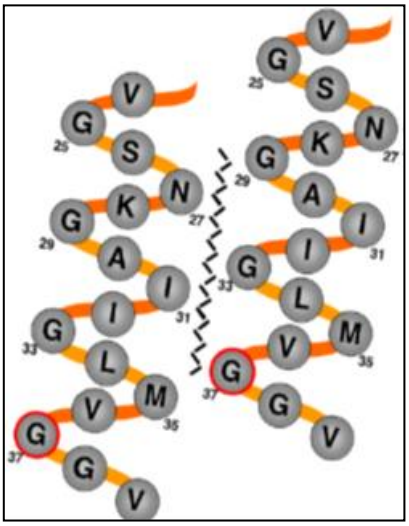

Figure 1.16: Schematic model of glycine-mediated interaction showing possible packing arrangement between residues 24-39 of neighboring Aβ molecules. The glycine zipper interface is represented by the jagged line, residue G37 is highlighted in red (Fonte et al., 2011).

Therefore it could be that aggregation inhibitors targeting the GxxxG motif may be able to block the amyloidogenic pathway in AD. The peptide motif, $A\beta_{17-28}$ has been discovered to have anti-aggregating potential and is able to cross the blood brain barrier (Woo *et al*., 2011). In addition, $A\beta_{17-21}$ within $A\beta_{1-40}$ has been identified (Carlo, 2010, Padayachee and Whiteley, 2011; Padayachee and Whiteley, 2012) and shown to cross the blood brain barrier, to inhibit or disassemble the formation of fibrils *in vitro* and *in vivo* and to prevent Aβ neurotoxicity in cell culture (Giordano *et al*., 2009). Also, the blood brain barrier-permeable synthetic peptide, $A\beta_{12-28P}$ which is homologous to the binding site of apoE on Aβ but bears a strategic single amino acid substitution was found to reduce Aβ toxicity in cell culture and amyloid deposition in transgenic mice (Yang *et al*., 2011).The interaction of these short peptide motifs: the pentapeptide motif ($A\beta_{17-21}$) (Fig.1.17) and three glycine zipper motifs: $A\beta_{25-29;}$ $A\beta_{29-33;}$ $A\beta_{33-37}$ and the complete glycine zipper stretch: $A\beta_{25-37}$ (Fig.1.17) with nNOS will hint towards a mechanistic

understanding of fibrillogenesis and determine the relative affinities of interaction between enzyme and peptide.

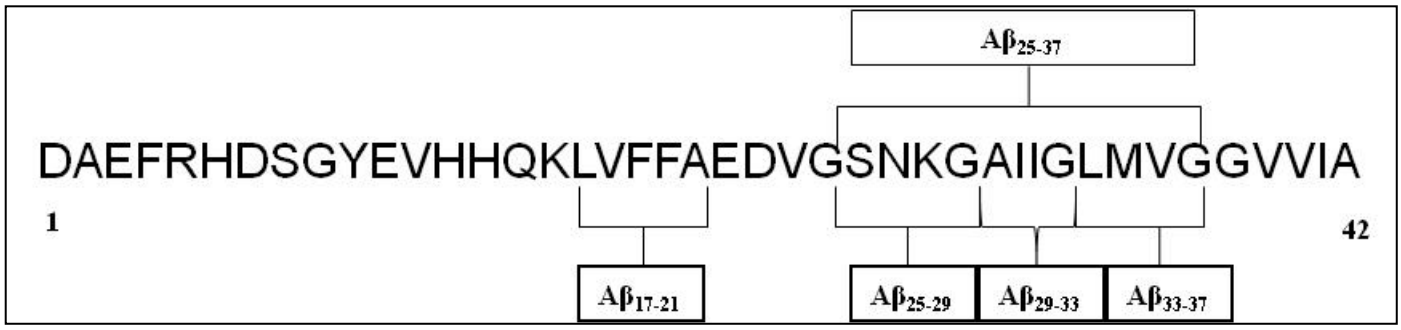

Figure 1.17: The amino acid sequence of $A\beta_{1-42}$ in symbol form, showing the hydrophobic pentapeptide, $A\beta_{17-21}$ and 3 'G-X-X-X-G' motifs called glycine zippers ($A\beta_{25-29}$ and $A\beta_{29-33}$ and $A\beta_{33-37}$) within the glycine zipper stretch ($A\beta_{25-37}$).

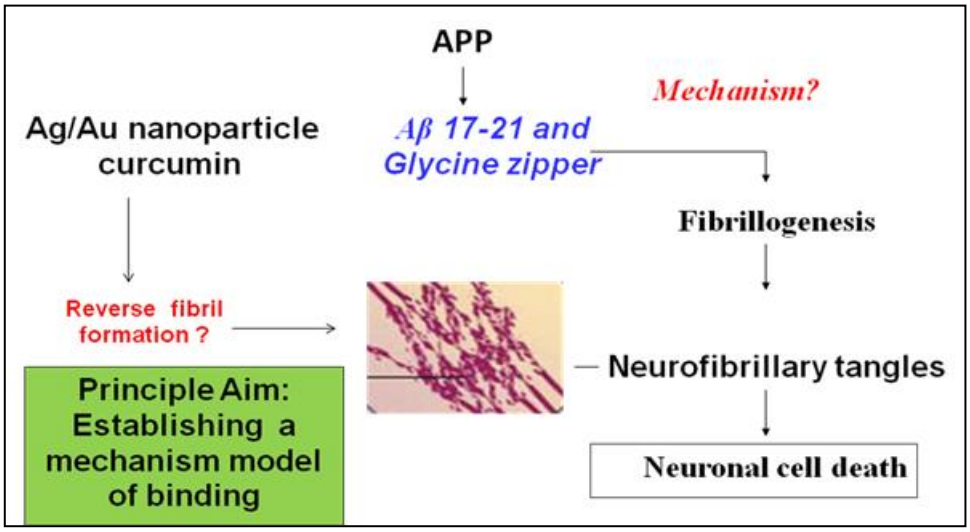

Figure 1.18: The significance of short peptide sequences, nps and curcumin in amyloidogenesis

This is significant as an ever increasing number of cellular pathways in neurons, astrocytes and microglia have been implicated in Aβ toxicity but the mechanism by which Aβ causes cell death and cognitive decline remain unclear (Aguilar and Small, 2005). For example, research has also shown that the total number of glycine residues (glycine zipper regions) in the C-terminal region of Aβ is the key determinant of toxicity, but it is difficult to develop a molecular model that would account for this explanation (Fonte *et al.*, 2011). Research has also shown that Gly33

maybe a possible site for free radical propagation processes that are initiated on Met35 of $A\beta_{1-42}$ that contributes the peptides toxicity in the Alzheimer's disease brain (Kanski *et al*., 2001). Moreover, the reversal/inhibition of Aβ fibrils by curcumin and nps may be used as a way to support the interaction between nNOS and Aβ and the resultant fibrillar product, providing a mechanism of binding and model for fibrillogenesis (Fig.1.18).

1.10 Research focus

1.10.1 Hypothesis

The binding of: the hydrophobic pentapeptide ($A\beta_{17-21}$), glycine zipper motifs ($A\beta_{25-29}$, $A\beta_{29-33}$, $A\beta_{33-37}$) and $A\beta_{25-37}$; the reversed sequences ($A\beta_{17-21r;}$ $A\beta_{29-33r}$) as well as polar sequences ($A\beta_{17-21p}$; $A\beta_{29-33p}$), silver/gold nanoparticles and curcumin to nNOS will establish a mechanism of interaction crucial to providing insight into fibrillogenesis and understanding the biochemical mechanism of AD.

1.10.2 Aim

To compare and contrast the mechanism of binding between Aβ peptides, gold, silver nps and curcumin with nNOS in order to establish a mechanistic model of fibrillogenesis.

1.10.3 Objectives

1. To evaluate the inhibition constant (K_i) for $A\beta_{17-21}$, $A\beta_{25-29}$, $A\beta_{29-33}$, $A\beta_{33-37}$, $A\beta_{25-37}$, the reversed sequences ($A\beta_{17-21r;}$ $A\beta_{29-33r}$) as well as polar sequences ($A\beta_{17-21p}$; $A\beta_{29-33p}$); Au, Ag nps and curcumin to nNOS and determining % enzyme activity in a substrate and time dependent manner in the presence of these ligands.

2. To determine whether nNOS, Aβ, nps and/or curcumin, individually or in tandem with each other, can potentially inhibit, delay onset, prevent or even reverse aggregation of amyloid fibril formation, using ThT fibrillogenesis assays.

3. To utilize the Stern Volmer model to calculate the quenching constant (K_{sv}), number of binding sites (n), number of tryptophan's exposed on enzyme surface (θ), the association

constant(K_a), the dissociation constant (K_d). To also differentiate between static and dynamic quenching for the interaction of $A\beta_{17-21}$, $A\beta_{25-29}$, $A\beta_{29-33}$, $A\beta_{33-37}$ and $A\beta_{25-37}$, the reversed sequences ($A\beta_{17-21r;}$ $A\beta_{29-33r}$) as well as polar sequences ($A\beta_{17-21p}$; $A\beta_{29-33p}$), and Au, Ag nps and curcumin with nNOS.

4. To determine free Gibbs energy (ΔG), enthalpy (ΔH) and entropy (ΔS) for interaction of $A\beta_{17-21}$, $A\beta_{25-29}$, $A\beta_{29-33}$, $A\beta_{33-37}$ and $A\beta_{25-37}$, the reversed sequences ($A\beta_{17-21r;}$ $A\beta_{29-33r}$) as well as polar sequences ($A\beta_{17-21p}$; $A\beta_{29-33p}$) as well as for Au, Ag nps and curcumin with nNOS at different temperatures (298 K, 303 K, 308 K and 313 K).

5. Monitoring the real-time binding of $A\beta_{1-40}$, $A\beta_{29-33}$, $A\beta_{33-37}$ and $A\beta_{25-37}$ to nNOS, using Surface Plasmon Resonance (SPR).

6. To utilize computational molecular docking using AutoDock 4.2 software to study conformational changes in the enzyme, upon binding of $A\beta_{17-21}$, $A\beta_{25-29}$, $A\beta_{29-33}$, $A\beta_{33-37}$ and $A\beta_{25-37}$ the reversed sequences ($A\beta_{17-21r;}$ $A\beta_{29-33r}$) as well as polar sequences ($A\beta_{17-21p}$; $A\beta_{29-33p}$) to nNOS. To use fluorescence resonance energy transfer (FRET) studies to monitor the movement of the Trp residues on nNOS subject to the binding of $A\beta_{17-21}$, $A\beta_{25-29}$, $A\beta_{29-33}$, $A\beta_{33-37}$ and $A\beta_{25-37}$, the reversed sequences ($A\beta_{17-21r;}$ $A\beta_{29-33r}$) as well as polar sequences ($A\beta_{17-21p}$; $A\beta_{29-33p}$); Au, Ag nps and curcumin to the enzyme.

2 Interaction of Aβ peptides, nanoparticles (Ag/Au) and curcumin with nNOS: Inhibition studies

2.1 Introduction

Inhibitors are substances which decrease the rate of an enzyme-catalyzed reaction when combined directly to the enzyme. There are two main groups of inhibitors, namely reversible and irreversible. Reversible inhibitors are involved in a non-covalent interaction with the enzyme and can be removed by dialysis to restore full enzyme activity, while the covalent inhibition of the irreversible form cannot be restored (Palmer, 1995). Moreover, reversible inhibition includes competitive inhibition, uncompetitive inhibition, noncompetitive inhibition and mixed inhibition. The competitive inhibitors specifically bind at the enzyme's catalytic site, where it competes with substrate for binding in a dynamic equilibrium–like process (Fersht, 1999; Silverman, 2000). The uncompetitive inhibitors bind only to the enzyme-substrate complex at locations other than the catalytic site. Substrate binding modifies the enzyme structure, making the inhibitor-binding site available (Fersht, 1999; Silverman, 2000). The non-competitive inhibitor binds only to the enzyme-substrate complex other than at the enzymes catalytic site. Substrate binding is unaltered but the enzyme-substrate-inhibitor (ESI) complex cannot form products (Palmer, 1995). Mixed inhibition is a mixture of partial competitive and pure non-competitive inhibition (Silverman, 2000). In mixed inhibition, the inhibitor binds to an allosteric site on the enzyme irrespective of whether it is bound to the substrate or not, and at the same time tends to have greater affinity for one state or the other (Fersht, 1999; Silverman, 2000).

Reports in literature have demonstrated that the binding of Aβ to other proteins or enzymes induce conformational change in the binding partner and if the binding partner is an enzyme, the conformational change is usually followed by either activation or inhibition of enzyme activity. For example, the enzyme acetylcholinesterase (AChE) was found to bind to the monomeric form of Aβ and induce conformational change through a peripheral anionic site on the enzyme (De

Ferrari *et al*., 2001; Bartolini *et al*., 2003). Another study demonstrated that after the administration of Aβ-related peptides into the rat brain, nNOS activity increased (O'Mahony *et al*., 1998; Stepanichev *et al*., 2000), while a recent study reported that $A\beta_{1-40}$ and $A\beta_{25-35}$ strongly inhibited the activity of nNOS (Padayachee and Whiteley, 2011). Furthermore, as was established in previous studies (Padayachee *et al*., 2011; Padayachee and Whiteley, 2011; 2013), enzyme inhibition of nNOS is preceded by binding of Aβ which is an early event in the process of fibrillogenesis.

In addition the assembly of protein fibrils relies on the interaction between proteins of specific motifs. Glycine zipper motifs have been recently found to drive the packing of transmembrane of α-helices (Fonte *et al*., 2011). This is significant as it was proposed that the formation of an α-helical structure by membrane-associated Aβ drives the formation of oligomers and a local increase in concentration of Aβ in turn catalyses β-sheet formation (Abedini *et al*., 2009). Also $A\beta_{16-20}$ (a hydrophobic core region within Aβ), is also thought to be a critical element in aggregation. The model arose from experiments, in which the binding of Aβ peptides to the full length $A\beta_{1-40}$ was tested and found that only three truncations ($A\beta_{10-19}$, $A\beta_{11-20}$ or $A\beta_{12-21}$) were capable of significant binding (Tjernberg *et al*., 1996). Further studies showed that the systematic substitution of the hydrophobic residues $A\beta_{17-20}$ in $A\beta_{10-42}$ for hydrophilic amino acids reduced fibril formation (Hilbich *et al*., 1992). Moreover short fragments and fragment analogues of $A\beta_{1-42}$ such as $A\beta_{4-8}$, $A\beta_{30-34}$ and $A\beta_{38-42}$, displayed a protective effect against Aβ-mediated neurotoxicity, suggesting the strong potential of Aβ recognition sequences as lead compounds in AD research (Szgedi *et al*., 2005). It is clear from these findings that shortened peptide fragments derived from the original Aβ structure can often be inhibitory and be used to investigate binding events. These peptides have nearly identical sequences to those involved with β-sheet alignment of the fibril.

Moreover, depending on the secondary structure adopted by the *N*-terminal domain of Aβ, the peptide can adopt two different conformational states in solution; (1) anti-parallel β-sheet structure (highly amyloidogenic) and (2) random coil or an α-helix structures (poorly

amyloidogenic) (Soto *et al*., 1995; Hang *et al*., 1997). Either form was found to predominate during *in vitro* studies. In this regard, it has also been demonstrated that protein misfolding or unfolding precedes the conformational change of the peptide from α-helix to β-sheet which drives the aggregation of Aβ into fibrils (Soto, 2001; De Felice and Ferreira, 2002). In view of this important finding, it might be possible to use molecules such as polyphenols and nanoparticles (nps) to selectively inhibit protein folding (Veselovsky *et al*., 2002; Jones and Mezzenga, 2012). Curcumin is a natural polyphenol composed of more than one aromatic ring which has been suggested to play a major role in amyloid fibrillation through aromatic stacking and π-π interactions (Gazit *et al*., 2002; Tartaglia *et al*., 2004). With the involvement of aromatic phenol rings, it is reasonable to suspect that curcumin may induce an inhibitory effect toward fibril formation. The inhibitory affect of curcumin has been seen in two research cases. Firstly curcumin was found to inhibit the conversion of prion protein (PrP) *in vitro* (Breydo *et al*., 2005) and secondly the polyphenol was found to disaggregate the fibrils formed from of hen egg-white lysozyme (HEWL) (Wang *et al*., 2009). No studies up to date (2013), however have been conducted on the effect of curcumin on nNOS activity. Since the inhibition of nNOS activity was found to be associated with fibrillogenesis (Padayachee and Whiteley, 2011), the binding of curcumin to nNOS will serve to clarify the role of curcumin in preventing nNOS catalyzed fibrillogenesis. Curcumin can also be used as a known model of inhibition and can be compared to the potential inhibitory effects by metallic nps.

There are numerous studies (Wu *et al*., 2009; Fei and Perrett, 2009) which have shown that the structure and function of an enzyme can be altered by nps, suggesting the role of these particles in influencing enzyme activity. The interaction between enzyme and np is governed by structure, size, surface chemistry, charge and surface shape which in turn regulate enzyme activity (Albanese *et al*., 2012). For example, a study by Fischer *et al*., 2003, demonstrated that mixed monolayer protected gold clusters (MMPCs) exhibited different inhibitory effects upon binding to the protein chymotrypsin (ChT). The activity assay indicated that inhibition was a fast reversible mechanism, followed by a slower irreversible process (Fischer *et al*., 2003). The

addition of cationic surfactants on the anionic gold surface reversed the "irreversible" inhibition of ChT through electrostatic interactions (Fischer *et al*., 2003). Proteins, by virtue of having cysteine and lysine residues, represent a unique ligand for the binding of metallic nps (Bhattacharya and Mukherjee, 2008). This is due to the attraction of gold (Au) and silver (Ag) nps to the thiol and amine functional groups of a protein. The most unique property of Ag nanoparticles is their anti-microbial properties attributed to Ag^{+} ions released into solution. Also, in minute concentrations Ag is not toxic to cells as it is known to bind to structural proteins and enzymes (Bhattacharya and Mukherjee, 2008). The fact that the active site of nNOS contains a binding site, (among other binding sites) for Fe^{+3} (heme), ligated to a cysteine residue (Siddhanta *et al*., 1996) makes this enzyme an ideal target for np binding.

It would be important to investigate what the effect of nps on nNOS structure would be and whether the enzyme becomes activated or deactivated in the presence of Au and Ag nps. The interaction mechanism of Aβ peptides, nps and curcumin with nNOS has not been previously studied. Nevertheless, a study has shown that Aβ and excess arginine accumulation occurs within neurons found in the brain of an AD patient (Cantoni *et al.*, 2002). Thus, it is clear that high levels of arginine can be attributed to low nNOS catalytic activity within the neuron, which is also the site for Aβ production and the formation of fibrils. Hence, it is significant to investigate whether these Aβ peptides, nanoparticles and curcumin have the potential to inhibit nNOS and thus maintain homeostatic levels of both enzyme and substrate in the neuron. This further implies then that Aβ, nps and curcumin are influential in altering the levels of nNOS found in the brain which may result in the enzyme being a potential biomarker in AD.

The objectives of this chapter will be to use steady state enzyme kinetics to determine the binding affinities of Aβ peptides, gold nanoparticles (Au nps), silver nanoparticles (Ag nps) and curcumin to nNOS by the calculation of the inhibition constant (K_i).

2.2 Theory of techniques utilized

2.2.1 Ultraviolet-visible (UV-vis) absorbance spectroscopy

UV-vis absorption spectroscopy is a technique that can be used to explore the structural changes of a protein and to investigate protein-ligand complex formation (Chi *et al*., 2011). This is important because the formation of pathological protein complexes may be responsible for the development of some components of AD (Selkoe, 1998). Spectrophotometry describes the absorption of light by substances in the ultraviolet or visible regions of the spectrum (Fersht, 1999). The absorbance (A) usually follows Beer's law, (Eq [1]):

$$A = \varepsilon cl \qquad \text{..... Eq [1]}$$

where (ε) is the extinction coefficient, (c) is its concentration (units usually in molarity) and (l) is the path length (in cm) of the light through the solution. A compound may be assayed by measuring (A) if ε is known (Fersht, 1999). Spectrophotometry is particularly useful with naturally occurring chromophores and the sensitivity of the technique depends on the extinction coefficient involved. Absorbance spectroscopy is the technique used to study conventional enzyme kinetic methods, which provides insight into biochemical mechanisms. A general mechanism (Eq [2]): provides a description of individual chemical steps that make up the overall reaction, where enzyme (E) converts substrate (S) to product(s) (P) and accelerates the rate of the reaction. How fast a reaction occurs is governed by the rate constant for the reaction (Gilbert, 2000).

$$E + S \rightleftharpoons ES \rightleftharpoons E + P \qquad \text{..... Eq [2]}$$

Many complex mechanisms often follow the simple Michaelis-Menten equation (Eq [3]), when only one substrate is varied at a time and the others are held constant (Gilbert, 2000).

$$V = V_{max}[S]/ (K_m + [S]) \qquad \text{..... Eq [3]}$$

where (V) is the activity of the enzyme in μmol/min, (V_{max}) is the activity of the enzyme approached at saturating concentrations of substrate ([S]) in μmol/min, (K_m) is the concentration of substrate required to produce a velocity that is 50 % of V_{max} (Gilbert, 2000). A typical Michaelis-Menten graph (Fig.2.1A) describes this relationship.

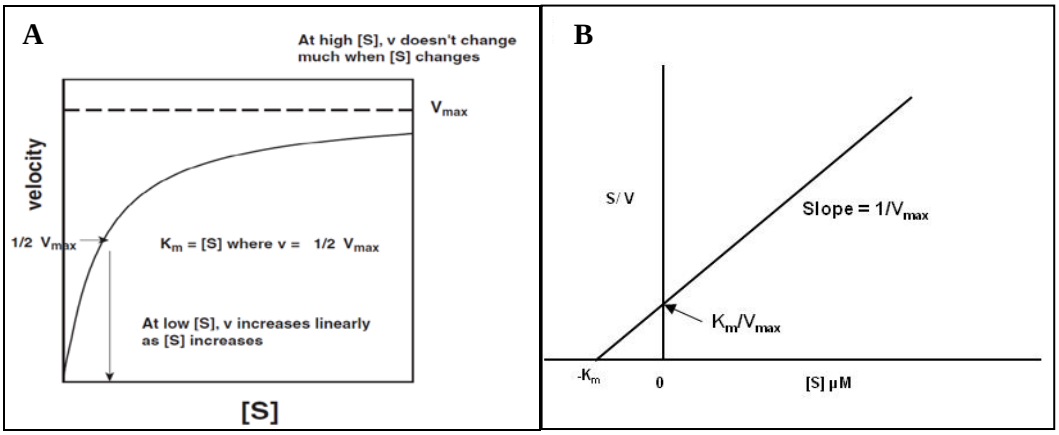

*Figure 2.1: Michealis-Menten graph where enzyme activity depends on substrate concentration (**A**). Hanes-Woolf graph where V_{max} is determined from the reciprocal of the slope and K_m is the derived from the y intercept (**B**) (Taken from Gilbert, 2000).*

At low concentrations of substrate, increasing the substrate concentration increases the activity of the reaction, but at high substrate concentrations, increasing the initial substrate concentration does not have much of an effect on the activity. Almost all enzyme-catalyzed reactions show saturation behavior. At a high enough substrate concentration, the reaction just won't go any faster than V_{max} (Gilbert, 2000).

There are three transformations of the Michealis-Menten equation (Eq [3]), which are represented by different graphical plots: Lineweaver-Burk, Eadie-Hofstee and the Hanes-Woolf plot (Fersht, 1999; Fersht and Requena, 1971a, b; Schimdt and Westheimer, 1971). For the purposes of the present research, the Hanes-Woolf plot and equation (Fig.2.1B, Eq [4]) will be used to determine not only the parameters K_m and V_{max} but also the inhibition constant (K_i), by repeating the experiment at several different concentrations of inhibitor. The concentration of inhibitor needed to inhibit the enzyme depends on how tightly the inhibitor binds to the enzyme. The inhibition

constant (K_i), calculated from (Eq [5]), will be used to describe how tightly an inhibitor binds to the enzyme and will offer insight into the mechanism of protein-ligand interactions (Gilbert, 2000).

$$[S]/V = [S]/V_{max} + K_m/V_{max} \quad \text{..... Eq [4]}$$

$$K_i = [L].V_{max}^{app}/V_{max} - V_{max}^{app} \quad \text{..... Eq [5]}$$

where [L] = concentration of Aβ, np or curcumin; (V_{max}^{app}) = V_{max}/1+ [I]/K_i and reflects the maximum velocity of the enzyme, in the presence of Aβ, np or curcumin; and (V_{max}) = maximum velocity of nNOS alone.

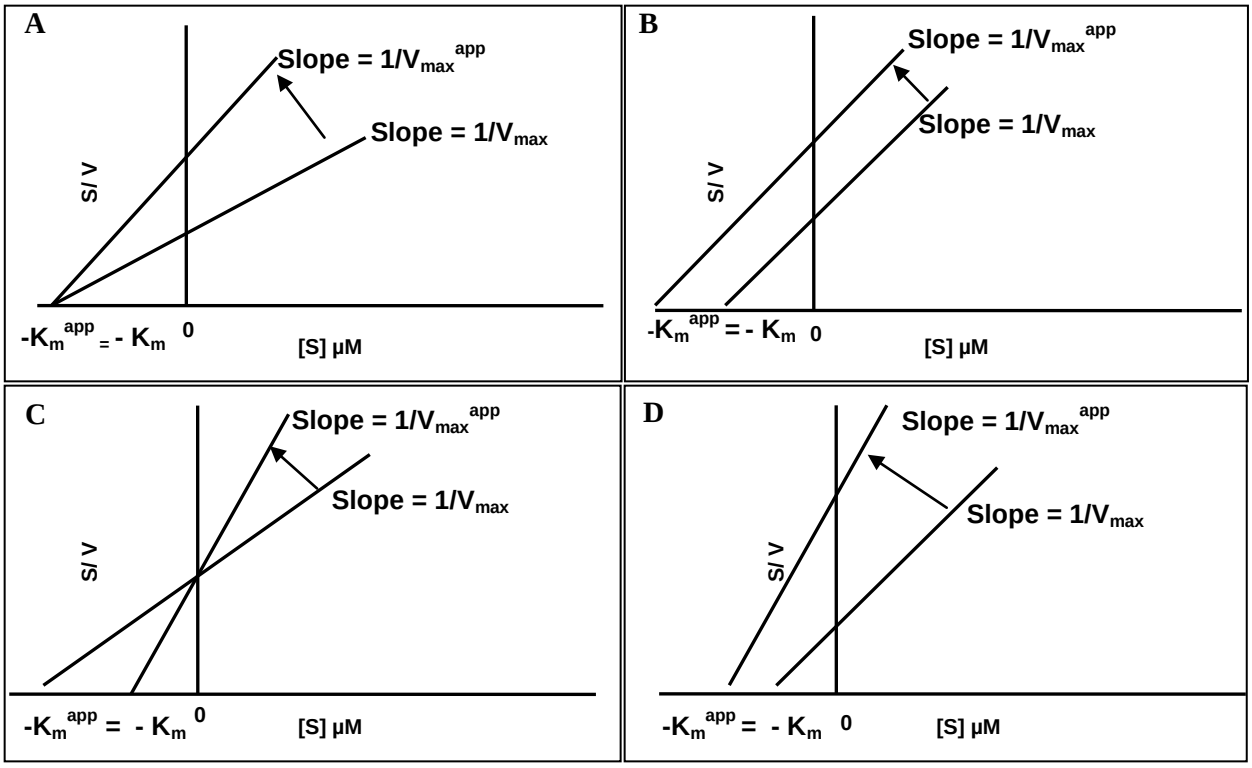

*Figure 2.2: Hanes-Woolf plot indicating V_{max} and K_m (in absence of inhibitor) and V_{max}^{app} and K_m^{app}(in presence of inhibitor). Types of inhibition are reflected: competitive inhibition (**A**); non-competitive inhibition (**B**) uncompetitive inhibition (**C**) and mixed inhibition (**D**) (Adapted from Gilbert, 2000)*

According to Eq [5] and Fig.2.2, the unique pattern of lines on the Hanes-Woolf plot is associated with a characteristic type of inhibition. The type of inhibition depends on the magnitude and trend that K_m and V_{max} values follow at each inhibitor concentration (Eq [5]). In competitive inhibition (Fig.2.2A), V_{max}^{app} is unchanged while K_m^{app} is increased; in non-competitive inhibition (Fig.2.2B), K_m^{app} appears unaltered while V_{max}^{app} decreases proportionately to inhibitor concentration. In uncompetitive inhibition (Fig.2.2C), both V_{max}^{app} and K_m^{app} are decreased. Mixed inhibition (Fig.2.2D), may result in an increase in K_m^{app} when the enzyme affinity decreases and a decrease in K_m^{app} when the enzyme affinity increases for either substrate or inhibitor. In either case for mixed inhibition, V_{max}^{app} decreases with increasing inhibitor and substrate concentration (Silverman, 2000; Gilbert, 2000).

2.3 Materials and Methods

2.3.1 Materials

Bovine brain was donated by Rosedale abattoir (Grahamstown, South Africa). All Aβ peptides were synthesized by Biopep Peptide Research Group, Stellenbosch, South Africa. All Aβ peptides were further dissolved in 100 % DMSO in order to retain their monomeric conformation. The Aβ fragments which were synthesized included the original sequences ($A\beta_{17-21}$; $A\beta_{25-29}$; $A\beta_{29-33}$; $A\beta_{33-37}$ and $A\beta_{25-37}$), the reversed sequences ($A\beta_{17-21r;}$ $A\beta_{29-33r}$) as well as polar sequences ($A\beta_{17-21p}$; $A\beta_{29-33p}$). The synthesis of the polar sequences involved the substitution of the two phenyl rings in $A\beta_{17-21}$ and the two isoleucine residues in $A\beta_{29-33}$ with two glutamic acid residues. The reason for synthesizing the reversed and polar sequences for just $A\beta_{17-21}$ and $A\beta_{29-33}$ was due to their ability to inhibit nNOS activity the most when compared to other Aβ peptides. This will be discussed in section 2.4 (results and discussion).

The metallic nps [Au/Ag (4 nm)] were synthesized and characterized in our laboratories (Sennuga *et al*, 2012 a, b). The gold and silver nanoparticle dilutions were made with distilled water while curcumin was dissolved in 100% DMSO, due to its poor solubility in water. Ground turmeric was obtained from an oriental spice shop in Durban, Kwa-zulu Natal. Horse spleen apoferritin

(HSAF, 48 mg/ml), preparative TLC aluminum plates coated with silica gel (2000 micron in thickness), ethylenediaminetetra-acetic acid [EDTA], N^{α}-benzoyl-L-arginine ethyl ester hydrochloride (BAEE); DL-citrulline; calcium chloride; 2,3-butanedione monoxime, thiosemicarbazide, DEAE-Sepharose anion-exchanger resin and commercial nNOS (rat brain) were purchased from Sigma Aldrich (South Africa). Dithiothreitol (DTT); Thioflavin T (ThT); Tris (hydroxymethyl) aminomethane; HEPES, DMSO, perchloric acid; sulphuric acid; ortho-phosphoric acid; glacial acetic acid; hydrochloric acid; phenylmethylsulphonyl fluoride (PMSF), $FeCl_3$ and snake skin dialysis tubing were obtained from Merck Chemicals (South Africa). All reagents were of analytical grade and all solutions were prepared with deionized water obtained from a Milli-Q system. A self-regulated temperature water bath (Model 130); dry heating mantle; pH meter (Ionolab) was purchased from Sigma Aldrich (South Africa). Absorbance spectroscopy was carried out on PowerWave microplate spectrophotometer (Bio-Tek Instruments) with 96 well plates, operated at 1 nm bandwidth using the KC Junior software program.

2.3.2 Methods

2.3.2.1 Purification of nNOS

nNOS was purified as previously described (Padayachee *et al.*, 2011). In brief, bovine brain (374 g) was homogenized by sonication (10 W, 30 s intervals, 4 min) in HEPES buffer (50 mM, pH 7.6, 600 ml) that contained ethylenediaminetetra-acetic acid [EDTA] (1.0 mM), NADPH (1.0 mM), DTT (0.5 mM) and PMSF (0.43 mM). The cell debris was removed by centrifugation (10000 x g, 4 ºC, 30 min) and the crude cell-free extract (20 ml), dialyzed and then applied to a DEAE-Sepharose anion-exchanger resin, previously equilibrated with Tris-HCl buffer (50 mM, pH 7.6). Active fractions of nNOS were eluted with 0.75 M NaCl in the same buffer at a flow rate of 2 $ml.min^{-1}$.

2.3.2.2 Characterization of nNOS

The purity of the enzyme was confirmed by SDS-PAGE analysis and its optimum temperature, pH, thermal stability and kinetic parameters (K_m and V_{max}) established as previously described (Padayachee *et al.*, 2011).

2.3.2.3 Protein determination

The protein concentration for all experiments was routinely determined according to the method of Bradford (Bradford, 1976). The assay was performed in triplicate in a 96-well microplate. Enzyme extract (5 µl) was added to a single well, followed by Bradford reagent (245 µl). The mixture was incubated at 22 ºC for 10 min and absorbance of the solution measured at 595 nm and the concentration of the unknown samples was determined using a bovine serum albumin standard curve.

2.3.2.4 nNOS assay

This assay was conducted, with slight modification, according to the protocol previously described (Boyde and Rahmatullah, 1980; Padayachee *et al.*, 2011). In summary the reaction mixture contained BAEE (5 mM, 10 µl), $CaCl_2$ (5 mM, 10 µl), DTT (2 mM, 10 µl) in Tris-HCl buffer (50 mM, pH 7.6, 940 µl). The reaction was started by the addition of enzyme extract (10 µl) in NADPH (1.0 mM, 10 µl) and allowed to incubate at 40 ºC for 2 min, before being stopped with perchloric acid (5 M, 10 µl). This mixture (250 µl) was treated with chromogenic reagent (250 µl) and cooled to 22 ºC for 2 min. The reduction of benzoyl-L-arginine ethyl ester was then determined spectrophotometrically at 530 nm. Chromogenic reagent was made from thiosemicarbazide (18 mM) in 2, 3-butanedione monoxime solution (500 mg in 100 ml distilled water) and sulphuric: orthophosphoric acid (1:1) in the presence of ferric chloride (0.25 g). The citrulline extinction coefficient (ε_{530}) was 27.3 ml.µmol^{-1} (Sakakibara and Yanagisawa, 2003). The activity of nNOS was determined according to Eq [6]. One unit of activity was defined as the amount of nNOS that produced 1 µmol of citrulline per min per ml reaction mixture.

$$\textbf{Enzyme activity} = \Delta A.V_T.D_f / \varepsilon.t.l.V_e = \textbf{µmol/ml/min} \qquad \text{….. Eq [6]}$$

where (ΔA) is change in absorbance, (V_T) = total volume, (D_f) = dilution factor, (ε) = extinction coefficient, (t) = time, (l) = path length and (V_e) = volume of enzyme.

2.3.2.5 Isolation of curcuminoids from turmeric

The isolation and extraction of curcuminoids from ground turmeric was performed using the procedure by Anderson *et al*, 2000, with slight modifications. Ground turmeric (10 g) was added to dichloromethane (25 ml) and was magnetically stirred and heated at reflux for 1 h. The mixture was suction filtered and the filtrate was concentrated in a hot-water bath maintained at 50 °C. The reddish-yellow oily residue was triturated with hexane (10 ml) and the resulting solid (0.409 g) was collected by suction filtration. Crude solid (200 mg) obtained after trituration with hexane was dissolved in 99 % dichloromethane-1 % methanol (v/v) and the crude mixture was collected and spotted on thin-layer chromatography (TLC) aluminum sheets coated with silica gel. The plate was developed three times using 99 % dichloromethane-1 % methanol (v/v) at which three colorful distinct bands were observed at R_f values: 0.40, 0.18, and 0.079. These R_f values were close to that obtained in literature, namely, 0.49, 0.22, 0.085 (Anderson *et al.*, 2000) indicating the possible presence of the three major curcuminoids: curcumin, demethoxycurcumin (curcumin II) and bisdemethoxycurcumin (curcumin III). Fractions on TLC that showed similar R_f values to those in literature were then pooled and the organic solvent was removed to obtain the powder form of the curcumin mixture (40 mg). It would be have been ideal to isolate each individual curcuminoid and study its effect, however for the purposes of this study a curcumin mixture was preferred as a preliminary study on the effect that curcumin has on fibrillogenesis. More in-depth studies regarding the effect of individual curcuminoids on fibrillogenesis will be the subject of future work.

2.3.2.6 Synthesis and characterization of Ag/Au nanoparticles

Au and Ag nps were biologically synthesized in the presence of Horse spleen apoferritin (HSAF), as described by Gálvez *et al*., 2008 and Sennuga *et al*., 2012 a, b. To summarise, HSAF was incubated with varying concentrations of K_2PtCl_4 to give a theoretical loading of 250-4000 metal atoms per HSAF. The pH was maintained at pH 8 with a few drops NaOH (0.1 M) and the

mixture was allowed to react by stirring (1 h, 4 °C) after which $NaBH_4$ (20-fold of metal salt concentration) was added. The solution was stirred further for 1 h until full reduction was achieved as determined by visual change in color. After dialysis, and size-exclusion chromatography the presence, purity and stability of the M-nps-HSA samples were assessed by native polyacrylamide gel electrophoresis. The particles were then characterized and size distribution was visualized using transmission electron microscopy (TEM) (Fig.2.3). The molar ratio of Au and Ag to HSAF was 500:1 and it was this solution [Fig.2.3A, B (ii)] that was used in subsequent experiments. On average, the size of Au and Ag nps was ≈ 4 nm, based on the size distribution of particles [Fig.2.3A, B (ii)]. Since nps were encased in HSAF, controls containing just HSAF (0.3-0.12 μM) were prepared.

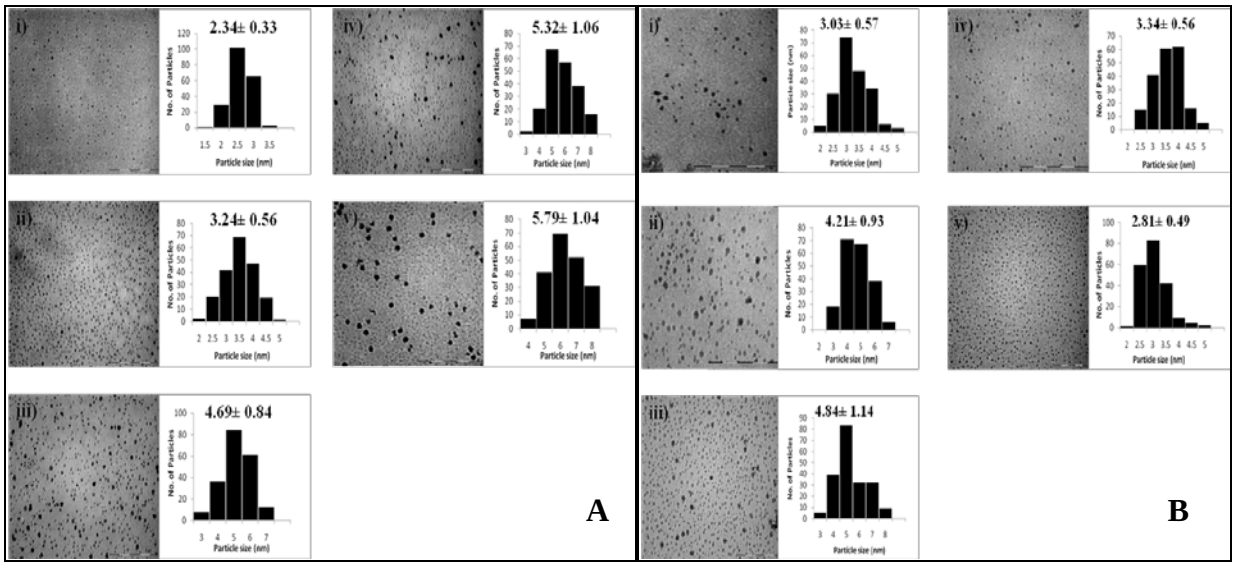

*Figure 2.3: TEM micrographs and size distribution of Au nps (**A**) and Ag nps (**B**) made from varying molar ratios of metal salts to HSAF. Scale bar = 100 nm. 200 particles were analyzed in each group. (i) 250:1; (ii) 500:1 ;(iii) 1000:1; (iv) 2000:1 and (v) 4000:1 (Sennuga et al., 2012)*

2.3.2.7 Time dependent inhibition of nNOS by Aβ, nanoparticles and curcumin

To further investigate their role in time dependent inhibition, the original sequences [$A\beta_{17-21,}$ $A\beta_{25-29,}$ $A\beta_{29-33,}$ $A\beta_{33-37}$ and $A\beta_{25-37}$] ; the reversed and polar sequences [$A\beta_{17-21r}$,$A\beta_{29-33r}$, $A\beta_{17-21p}$ and $A\beta_{29-33p}$] (8 μM); Au and Ag nps (≈ 4 nm) (0.09 μM) were incubated with nNOS (32

nM) in Tris-HCl buffer (50 mM, pH 7.6) in the presence of substrate BAEE (8 µM). The nNOS assay was performed as described previously (2.3.2.4, pg 37). Controls used for each interaction were: HSAF, Aβ, np and curcumin alone; nNOS/Aβ, nNOS/np nNOS/curcumin; BAEE/Aβ, BAEE/np BAEE/curcumin. Absorbance was read at 530 nm in intervals of 1 min for 5 min and values represented the mean (± S.E.M.) of three trials.

2.3.2.8 Substrate dependent inhibition of nNOS by Aβ, nanoparticles and curcumin

To investigate their role in substrate dependent inhibition, the original sequences [$A\beta_{17-21}$, $A\beta_{25-29}$, $A\beta_{29-33}$, $A\beta_{33-37}$ and $A\beta_{25-37}$] ; the reversed and polar sequences [$A\beta_{17-21r}$,$A\beta_{29-33r}$, $A\beta_{17-21p}$, $A\beta_{29-33\,p}$] (2- 8 µM); Au and Ag nps (≈ 4 nm) (0.03-0.09 µM), in a total volume of 500 µl and in the presence of BAEE (0-8 µM) were incubated with nNOS (32 nM) in Tris HCl buffer (50 mM, pH 7.6) for 5 min. The nNOS activity was assayed at 530 nm, over a 5 min period at each substrate concentration. Controls used for each interaction were: HSAF, Aβ, np and curcumin alone; nNOS/Aβ, nNOS/np nNOS/curcumin; BAEE/Aβ, BAEE/np BAEE/curcumin. The value of K_i (inhibitor constant) was calculated using Eq [5], pg 34 and values represented the mean (± S.E.M.) of three trials.

2.3.2.9 Percentage inhibition of enzyme activity

The percent inhibition of the enzyme activity due to the presence of increasing concentrations of ligand (Aβ, nps or curcumin was calculated by Eq [7] (Bartolini *et al.*, 2003) :

$$100 - (V_i / V_o \times 100) \qquad \text{..... Eq [7]}$$

Where (V_i) is the initial rate of nNOS, calculated in the presence of ligand (amyloid peptide, nanoparticles and/or curcumin) and (V_0) is the enzyme activity without ligand.

2.3.2.10 Statistical analyses

All experiments were carried out in triplicate. Mean and standard deviation calculations and comparison of data using analysis of variance (ANOVA) was performed to 5 % level of

significance ($p < 0.05$) using Statistica for Windows, version 8 (Statsoft Inc.) and Microsoft Excel 2010.

2.4 Results and discussion

2.4.1 Time dependent inhibition of nNOS by incubation with original Aβ peptides

Results (Fig.2.4) for time dependent inhibition, in the absence of Aβ peptides, showed 100 % nNOS activity at time 0 min. Activity of nNOS then decreased, in the presence of Aβ peptides within the first minute. This suggests the rapid association/binding of Aβ peptide to nNOS, also indicating that the initial event of binding was an instantaneous process. $A\beta_{17-21}$, $A\beta_{25-29}$ and $A\beta_{29-33}$ showed the most decrease in activity to about 80 % within the 1 min and then activity decreased to about 40-60 % within 2-5 min, whilst $A\beta_{33-37}$ and $A\beta_{25-37}$ showed an approximate 40 % drop in activity within 1 min and 20-35 % drop within 2-5 min. This reveals that $A\beta_{17-21}$, $A\beta_{25-29}$ and $A\beta_{29-33}$ may have a tighter binding affinity to nNOS than $A\beta_{33-37}$ and $A\beta_{25-37}$, and this will be confirmed by calculating the inhibition constants of the respective peptides.

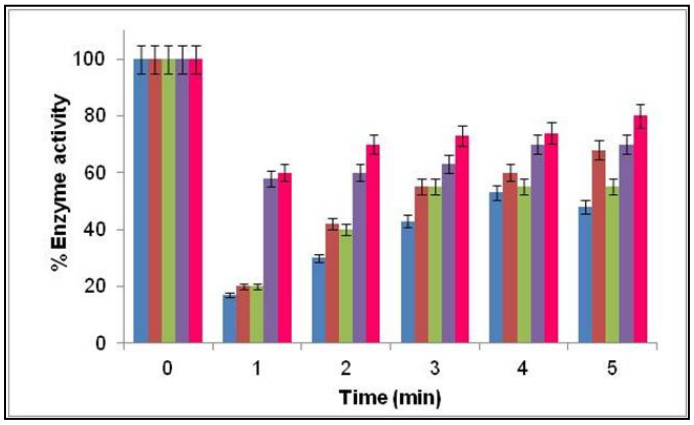

Figure 2.4: Percent enzyme activity of nNOS (32 nM) by $A\beta_{17-21}$ ■; $A\beta_{25-29}$ ■; $A\beta_{29-33}$ ■; $A\beta_{33-37}$ ■ and $A\beta_{25-37}$ ■ in Tris-HCl buffer (50 mM, pH 7.6) (8 µM), in the presence of the substrate BAEE (8 µM) for a duration of 5 min. Enzyme activity at time (0 min) = 9 U/ml; values represents the mean (± S.E.M) of three trials.

Hanes-Woolf plots (Fig.2.5, Table 2.1) for the interaction of nNOS with each peptide motif were constructed. The results showed that for all Aβ peptides, V_{max} and K_m (ONE WAY ANOVA- p

> 0.05) decreased proportionately to Aβ concentration. Though this pointed to the Aβ peptides behaving most probably as mixed inhibitors, it cannot be conclusive evidence and further studies will need to be done.

2.4.2 Substrate dependent inhibition of nNOS by incubation with original Aβ

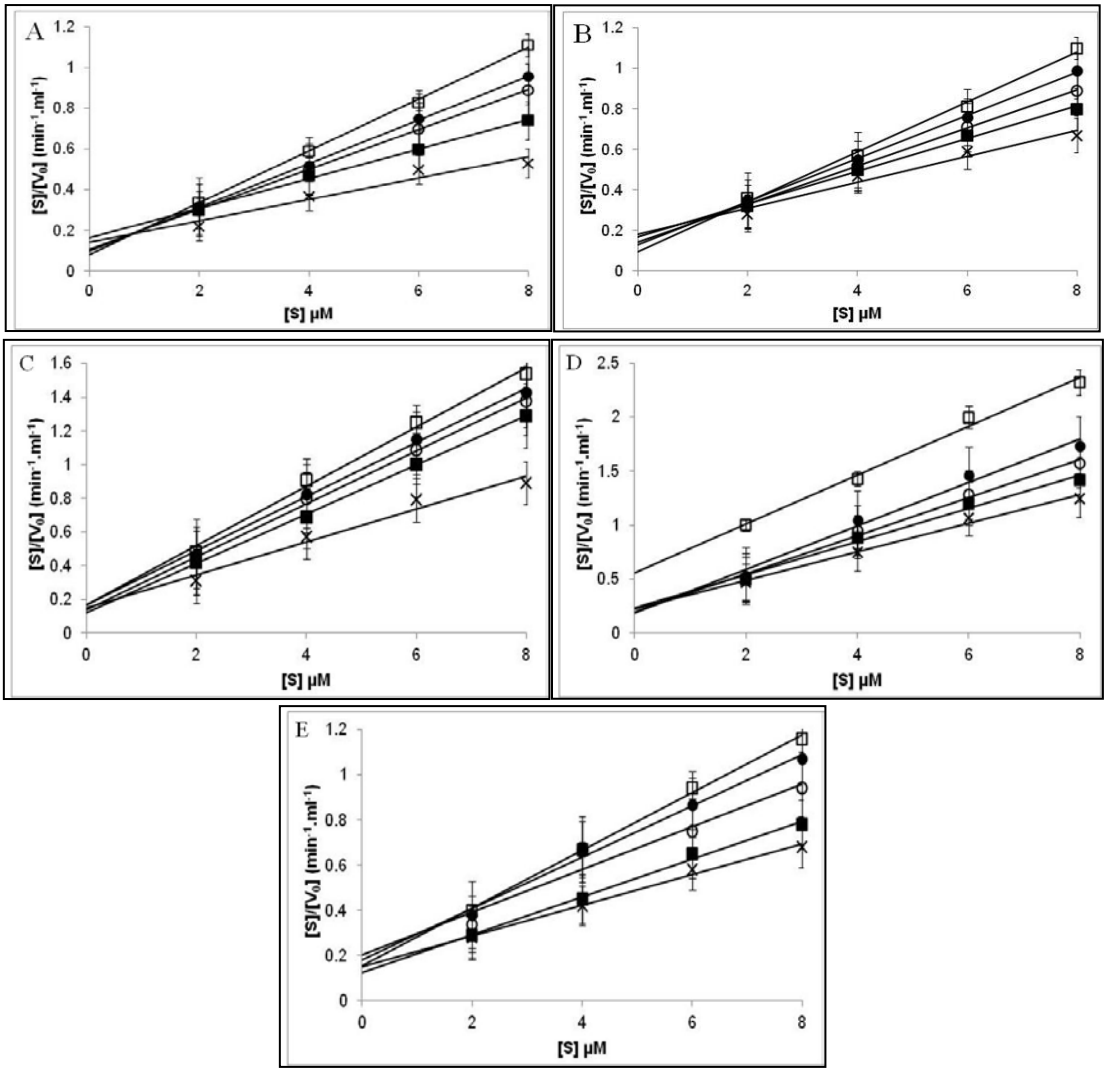

*Figure 2.5: Hanes-Woolf plot of nNOS activity in the absence and presence of Aβ peptides. Concentrations of peptide: 0 nM (×); 2 µM (■); 4 µM (○); 6 µM (●); 8 µM (□). $Aβ_{17-21}$ **[A]** $Aβ_{25-29}$**[B]** $Aβ_{29-33}$ **[C]** $Aβ_{33-37}$ **[D]** $Aβ_{25-37}$**[E]***

The inhibitor constant (K_i) (from [Eq.5], pg.34) indicated the binding affinity of the enzyme for inhibitor (Table 2.1). It was shown that the original amyloid peptides ($A\beta_{17-21}$, $A\beta_{25-29}$, $A\beta_{29-33}$, $A\beta_{33-37}$ and $A\beta_{25-37}$) inhibited nNOS at concentrations between 2 and 8 μM, respectively. Results (Table 2.1) also showed that $A\beta_{17-21}$ inhibited nNOS to a greater degree as reflected by its low K_i (5.1 μM) (ONE WAY ANOVA- $p > 0.05$) compared to the higher K_i values of $A\beta_{25-29}$, $A\beta_{29-33}$, $A\beta_{33-37}$ and $A\beta_{25-37}$ (9.1 μM; 7.5 μM; 8.4 μM and 11 μM) (ONE WAY ANOVA- $p > 0.05$). The differences in K_i values between the original Aβ peptides are not significant but comparable. Statistical analyses on the various peptides attached, pg 183-185. These K_i values fall within range of the previous K_i values calculated for $A\beta_{17-28}$, $A\beta_{22-35}$, $A\beta_{32-35}$ and $A\beta_{25-35}$ (1.92 μM, 7.4 μM; 8.8 μM and 10 μM) (Padayachee and Whiteley, 2011).

Table 2.1 Values of V_{max} (μmol.ml^{-1}.min^{-1}) and) K_m (μM) and K_i (μM) for original Aβ peptides (μM) after interaction with nNOS. K_i values were estimated from Eq [5], pg 34

	V_{max} (μmol.ml^{-1}.min^{-1})					K_m (μM)					K_i (μM)				
[Aβ]	**17-21**	**25-29**	**29-33**	**33-37**	**25-37**	**17-21**	**25-29**	**29-33**	**33-37**	**25-37**	**17-21**	**25-29**	**29-33**	**33-37**	**25-37**
0	18	15	10	7.5	14	2.6	2.7	1.5	1.6	2.2	0	0	0	0	0
2	13	12	6.8	6.5	11	2.2	2.1	0.82	1.5	2.1	5.1	9.1	7.5	8.4	11
4	10	10	6.4	5.6	10	1.0	1.5	0.89	1.1	1.4					
6	9.3	9.3	6.2	4.9	8.8	0.93	1.2	1.0	0.92	1.5					
8	7.8	8.1	5.6	4.4	7.8	0.63	1.0	0.94	0.82	1.2					

2.4.3 Percent enzyme activity of nNOS by incubation with original Aβ peptides

According to results (Fig.2.6), the general trend showed that all Aβ peptides in the presence of BAEE inhibited the enzyme activity the most at a lowest concentration (2 μM). All values represented the mean (± S.E.M) of three trials. The values for % inhibition at 2 μM of inhibitor and substrate (Fig.2.6) were calculated approximately as: $A\beta_{17-21}$ (88 %); $A\beta_{25-29}$ (80 %); $A\beta_{29-33}$ (83 %); $A\beta_{33-37}$ (76%); $A\beta_{25-37}$ (65 %). These results confirmed time dependent inhibition studies (Fig.2.4) which revealed that $A\beta_{17-21}$ and $A\beta_{29-33}$ displayed the greatest inhibition (≈ 80 %) inhibition at 1 min. The potent inhibition potential of $A\beta_{17-21}$ and $A\beta_{29-33}$ on nNOS further correlates with their lowest K_i values (5.1 μM and 7.5 μM), respectively. These two peptides had the tightest binding affinity to the enzyme or enzyme-substrate complex, and thus were able to

inhibit the activity of the enzyme to a greater degree within the first minute as compared to $A\beta_{25-29}$, $A\beta_{33-37}$ and $A\beta_{25-37}$. Moreover, activity was seen to be restored at a highest concentration (8 μM) of Aβ peptides in the presence of BAEE (Fig.2.6).

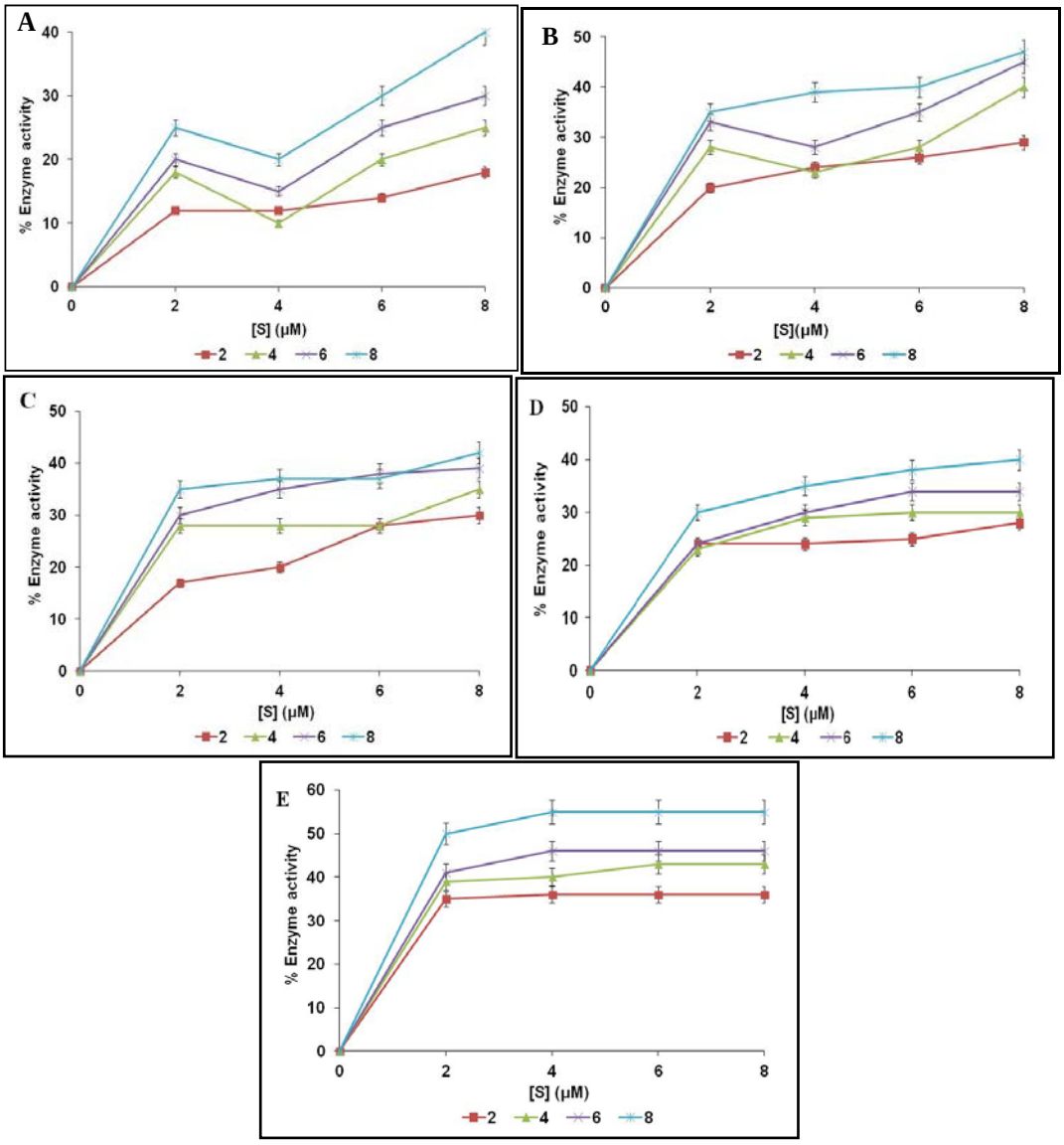

*Figure 2.6: Percent enzyme activity of nNOS by interaction with $A\beta_{17-21}$ [**A**] $A\beta_{25-29}$ [**B**] $A\beta_{29-33}$ [**C**] $A\beta_{33-37}$ [**D**] and $A\beta_{25-37}$ [**E**] at [Aβ]= 2 μM ■ [S]= 4 μM ■; [S]= 6 μM ■; [S]= 8 μM■, in the presence of benzoyl arginine ethyl ester substrate[S] (0-8μM). Enzyme activity at 0 μM Aβ peptide = 9 U/ml.*

Amongst the Aβ peptides studied, $A\beta_{25-29}$ is hydrophilic in nature, possibly accounting for its relatively high K_i value (9.1 μM), in comparison to $A\beta_{17-21}$ and $A\beta_{29-33}$. For $A\beta_{25-29}$ the effect of the hydrophobic side chain of the lysine residue (Lys28), with four methylene groups, is counter-balanced by an ionized hydrophilic ε-amino group (Voet and Voet, 2011), which would have a positive charge in an aqueous environment thereby decreasing any contributing inhibitory effect from this amino acid residue. The amide side chains of asparagines (Asn27) are also polar and can serve as hydrogen-bond donors and acceptors. Support of this argument of levels in hydrophobicity and inhibitory potency is not, unfortunately, supported with $A\beta_{33-37}$ (K_i = 8.4 μM) having valine, methionine and leucine residues. In defence of this feature, however, it is pointed out that $A\beta_{33-37}$ is reported to be a toxic glycine zipper fragment due to the presence of Met35 (Kanski *et al*., 2001; Harmeier *et al*., 2009) which facilitates the generation of ROS. The sulphur containing methionine donates electrons, leading to the formation of methionine sulfoxide and hydrogen peroxide. Research has also shown that the Gly33 is critical to the oxidative and neurotoxic properties of $A\beta_{1-42}$, as it is a possible site for the generation of free radicals (Kanski *et al*., 2001; Harmeier *et al*., 2009; Fonte *et al*., 2011). In fact the substitution of G33 or G37 with leucines prevented $A\beta_{1-40}$ fibrillogenesis and destabilized the fibril structure by disrupting the glycine-zipper-packing interface (Kim *et al*., 2005). Molecular simulations by accelrys visualizer (version 2.0) software have shown the secondary structure of $A\beta_{25-37}$ to be α-helical. Although, we cannot be certain that $A\beta_{25-37}$ has the same secondary structure in its isolated form as in the whole $A\beta_{1-40}$ peptide, the amphipathic nature of it alpha-helical structure would favour hydrophobic association and possibly drive inhibition effects. The length and bulky nature of $A\beta_{25-37}$, however, may have somewhat hindered its association to the enzyme, resulting in reduced affinity to the binding site and resulting in the highest K_i value (11 μM).

2.4.4 Time dependent inhibition of nNOS by interaction with Aβ peptides (reversed and polar)

Since previous results (Fig.2.4-Fig.2.6), showed that $A\beta_{17-21}$ and $A\beta_{29-33}$ had the lowest K_i values of 5.1 μM and 7.5 μM, respectively, it was significant to examine whether their powerful

inhibition effect would be reduced or enhanced in any way when the enzyme was incubated with Aβ peptides having a modified structure. This was investigated either by reversing the peptide sequence of these two motifs and/or by introducing polar glutamic acid residues to replace the two phenyl rings and two isoleucine residues in $A\beta_{17\text{-}21}$ and $A\beta_{29\text{-}33}$.

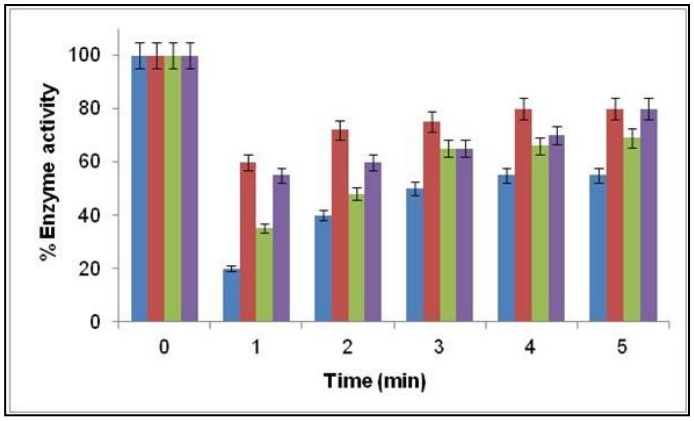

Figure 2.7: Percent enzyme activity of nNOS (32 nM) by $A\beta_{17\text{-}21r}$ ■; $A\beta_{17\text{-}21p}$ ■; $A\beta_{29\text{-}33r}$ ■; $A\beta_{29\text{-}33p}$ ■ in Tris-HCl buffer (50 mM, pH 7.6)(8 µM), in the presence of the substrate BAEE (8 µM) for a duration of 5 min. Enzyme activity at time (0 min) = 9 U/ml; values represents the mean (± S.E.M) of three trials.

The approximate % drop in activity within 1 min (Fig.2.7) was as follows: $A\beta_{17\text{-}21r}$ (80 %), $A\beta_{29\text{-}33r}$ (62 %), $A\beta_{17\text{-}21p}$ (40 %), $A\beta_{29\text{-}33p}$ (42 %). Thereafter within 2-5 min, the approximate drop in activity was as follows: $A\beta_{17\text{-}21r}$ (50-60 %), $A\beta_{29\text{-}33r}$ (40-50 %), $A\beta_{17\text{-}21p}$ (20-30 %), $A\beta_{29\text{-}33p}$ (20-40 %). These results indicated that within 1 min, the reversed sequences bound to the nNOS binding site with greater affinity than their polar counterparts. However, this would only be confirmed by the calculation of the relative K_i values. This also indicated that reversing the sequences of $A\beta_{17\text{-}21}$ and $A\beta_{29\text{-}33}$, did not alter their effect on activity, as both the original and reversed (Fig.2.8) sequences displayed approximately 62-80 % inhibition in a minute. The introducing of polar groups, however, to these sequences, reduced the inhibition effect to approximately 40 % within 1 min, indicating that the polar glutamic acid somehow weakened the interaction between enzyme and peptide.

2.4.5 Substrate dependent inhibition of nNOS by interaction with Aβ peptides (reversed and polar)

According to results (Fig. 2.8, Table 2.2), the values of V_{max} decreased with increasing inhibitor concentration from 0-8 μM ($p > 0.05$). The values for K_m, however, increased from 0-8 μM, indicating that that at 8 μM substrate, the enzyme affinity may have decreased for either the substrate or Aβ as is the rule for mixed inhibition. The kinetic behavior also pointed towards probable mixed inhibition, but, once again, is not conclusive. According to Table 2.2, the K_i values for $A\beta_{17\text{-}21r}$ (11 μM) and $A\beta_{29\text{-}33r}$ (13 μM) ($p > 0.05$) were twice as high as that of their respective original sequences (5.1 μM and 7.5 μM) ($p > 0.05$) supporting that their affinity to the enzyme binding site was less pronounced. This was surprising, considering that the reversed sequences of Aβ inhibited the enzyme (62-80 %) within a minute (Fig.2.7).

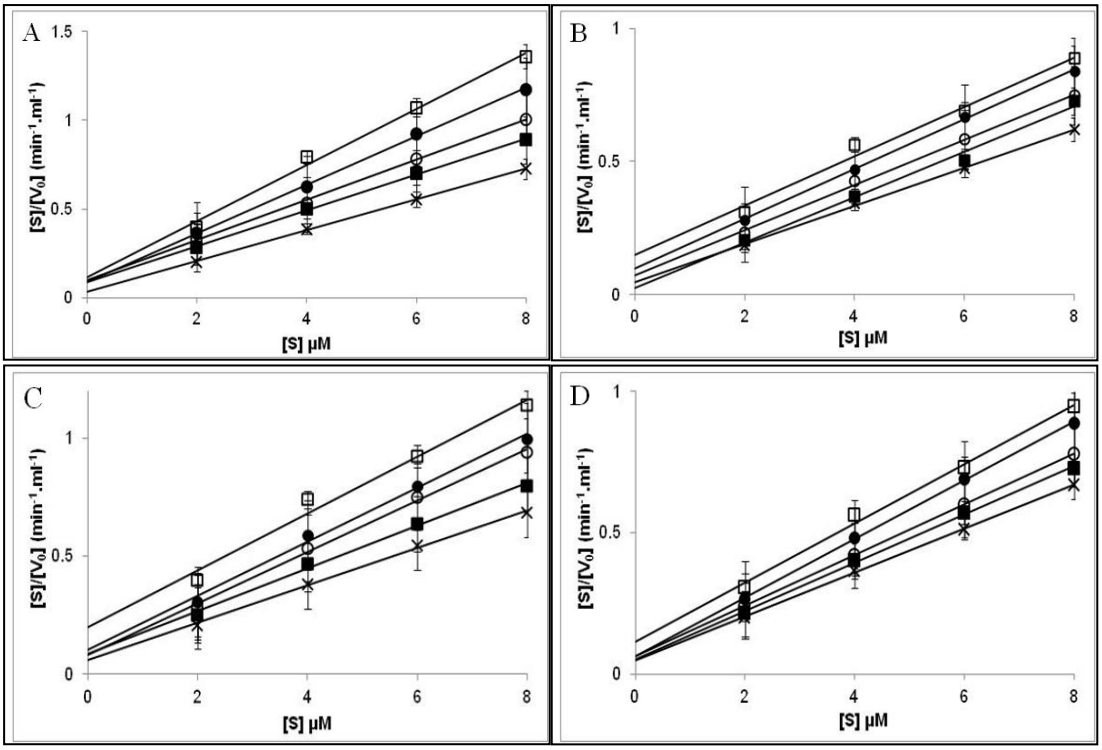

*Figure 2.8: Hanes-Woolf plot of nNOS activity in the absence and presence of Aβ peptides. Concentrations of peptide: 0 nM (×); 2 μM (■); 4 μM (○); 6 μM (●); 8 μM (□).$A\beta_{17\text{-}21r}$ **[A]** $A\beta_{17\text{-}21p}$ **[B]** $A\beta_{29\text{-}33r}$ **[C]** $A\beta_{29\text{-}33p}$ **[D]**.*

According the % activity results (Fig.2.9), the general trend, showed that both polar and reversed forms, in the presence of BAEE inhibited the enzyme activity the most at a lowest concentration

(2 μM). All values represented the mean (± S.E.M) of three trials. The values for % inhibition at 2 μM of inhibitor and substrate (Fig.2.9) were calculated as: $A\beta_{17\text{-}21r}$ (91 %); $A\beta_{17\text{-}21p}$ (72 %); $A\beta_{29\text{-}33r}$ (85 %); $A\beta_{29\text{-}33p}$ (75%).

Table 2.2 Values of V_{max} (μmol.ml^{-1}.min^{-1}) and) K_m (μM) and K_i (μM) for reversed and polar Aβ peptides (μM) after interaction with nNOS. K_i values were estimated from Eq [5], pg 34

	V_{max} (μmol.ml^{-1}.min^{-1})				**K_m (μM)**				**K_i (μM)**			
[Aβ]	**17-21r**	**17-21p**	**29-33r**	**29-33p**	**17-21r**	**17-21p**	**29-33r**	**29-33p**	**17-21r**	**17-21p**	**29-33r**	**29-33p**
0	11	13	12	12	2.4	2.6	2.7	2.6	0	0	0	0
2	9.8	11	11	11	2.8	2.3	2.9	2.6	11	19	13	21
4	8.8	11	9.1	11	2.8	2.8	2.7	2.7				
6	7.3	10	8.7	9.6	2.6	3.0	2.8	2.6				
8	6.3	10	8.2	9.5	2.7	3.6	3.6	3.1				

The results showed that the hydrophobicity of the reversed sequences Aβ-peptides [$A\beta_{17\text{-}21r;}$ $A\beta_{29\text{-}33r}$] had more influence on enzyme inhibition when compared with the substituted polar sequenced Aβ-peptides [$A\beta_{17\text{-}21p}$; $A\beta_{29\text{-}33p}$] (Table 2.2). Also, the K_i values of $A\beta_{17\text{-}21p}$ (19 μM) and $A\beta_{29\text{-}33p}$ (21 μM) were 3-4 times higher than those of the original sequences (5.1 μM and 7.5 μM) ($p < 0.001$). This suggests that the response in activity exhibited by the polar forms of peptide was very significant, when compared to the original and reversed forms (attached,pg 183-185). It can be inferred, too that the presence of the double phenylalanine and isoleucine residues in $A\beta_{17\text{-}21}$ and $A\beta_{29\text{-}33}$ are critical for inhibition to occur. This deduction is valid, since the presence of these residues significantly increased binding affinity to the enzyme in the original sequences. The enzyme-peptide association of the polar and reversed sequences is relatively weak compared to the original sequences, probably since the relative positions of the phenylalanine and isoleucine residues are reversed. This is illustrated in Fig.2.10, where the original and reversed sequences are compared regarding the relative positions of their amino acids. This further implies that the identity and relative positions of amino acids as well as the degree of polarity of a sequence are factors which influence the inhibitory effect.

2.4.6 Percent enzyme activity of nNOS by interaction with Aβ peptides (reversed and polar)

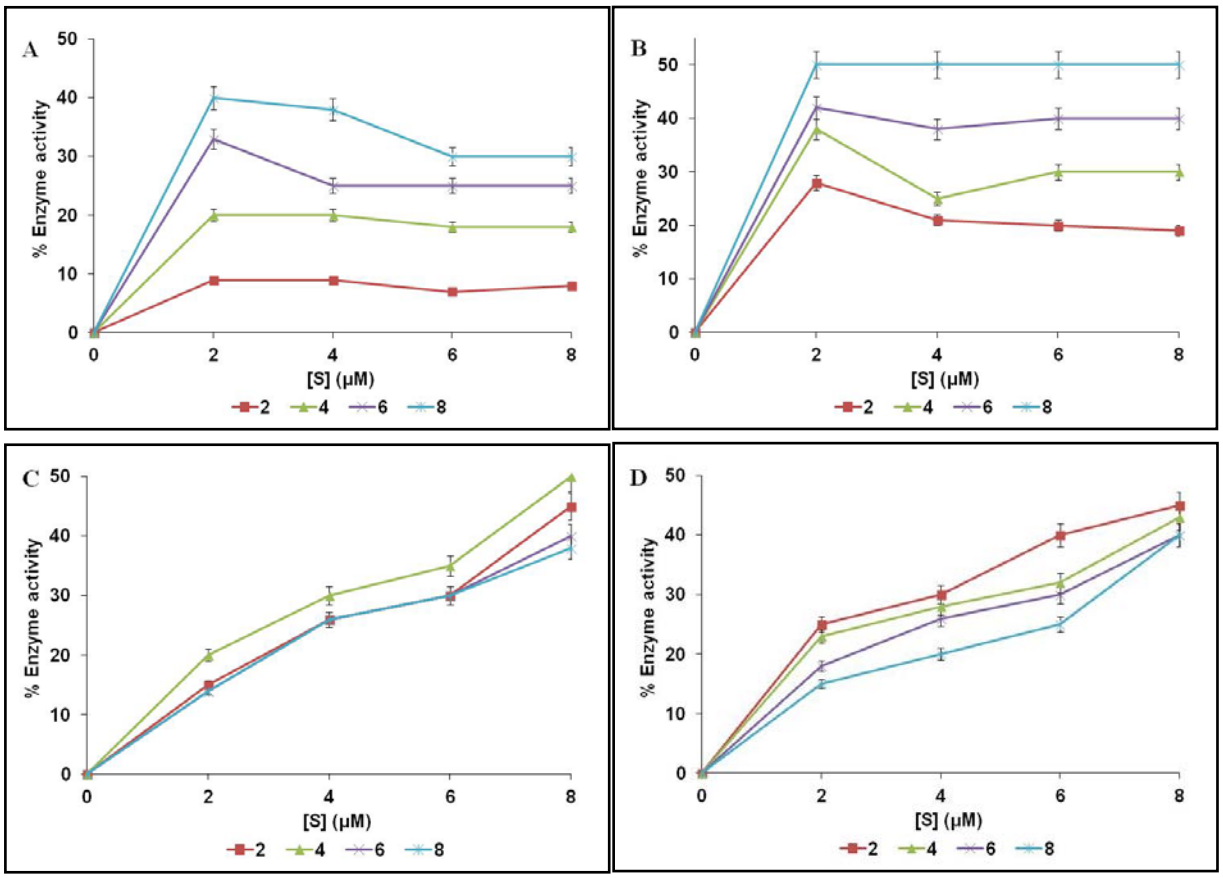

*Figure 2.9: Percent enzyme activity of nNOS by interaction with $Aβ_{17-21r}$ [**A**] $Aβ_{17-21p}$ [**B**] $Aβ_{29-33r}$ [**C**] $Aβ_{29-33p}$ [**D**] at [Aβ]= 2 μM ■ [S]= 4 μM ■; [S]= 6 μM ■; [S]= 8 μM■, in the presence of benzoyl arginine ethyl ester substrate[S] (0-8μM). Enzyme activity at 0 μM Aβ peptide = 9 U/ml.*

Moreover, it is known that hydrophobic-hydrophobic interactions are one of the important forces in protein-ligand interactions (De Meyer *et al*., 2006). According to this fact, it is expected that the non-polar amino acids: valine, leucine and alanine, present in the $Aβ_{17-21}$ (Fig.2.10A) would interact favourably with other non-polar amino acids via their methylene (-CH_2-) and methyl (-CH_3-) functional groups present in their side chains. These hydrophobic interactions between peptide and enzyme may have been responsible for the potent inhibition effect by $Aβ_{17-21}$. The change in position of these same non-polar amino acids, when reversing the $Aβ_{17-21}$ sequence

(Fig.2.10B) may have also altered the distance from one hydrophobic amino acid to the other as well as altered the distance between the hydrophobic amino acids of the peptide and the hydrophobic amino acids of nNOS, thus "disrupting" the hydrophobic interaction critical in mechanism of inhibition. If the potency for inhibition for Aβ peptides was controlled by the respective degree in hydrophobicity of the side chain, then the isoleucine and alanine residues of $A\beta_{29\text{-}33}$ were also critical in this regard, as well as the reversed positions of these amino acids within $A\beta_{29\text{-}33}$ (Fig.2.10C, D). Also, the introduction of the polar glutamic acid residues to both $A\beta_{17\text{-}21}$ and $A\beta_{29\text{-}33}$ may have weakened hydrophobic interaction between the enzyme and peptide compared to the original sequences and thus resulted in the highest K_i values (19 μM and 21 μM), respectively.

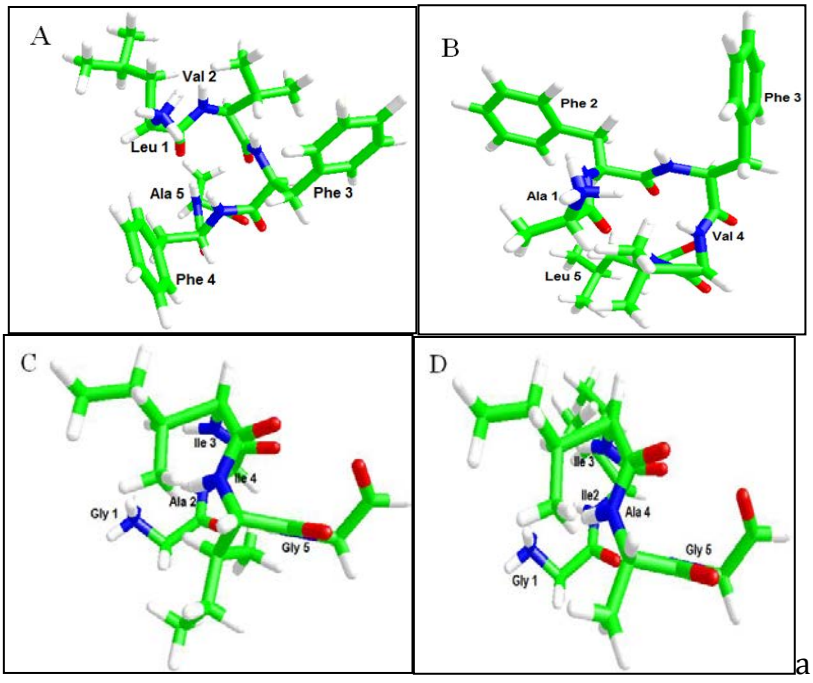

*Figure 2.10: 3-D structures of $A\beta_{17\text{-}21}$ (**A**) $A\beta_{17\text{-}21r}$ (**B**) $A\beta_{29\text{-}33}$ (**C**) $A\beta_{29\text{-}33r}$ (**D**) Structures built by Vega ZZ (v.2.4.0)*

A question arises: What would be the mechanism for the inhibition? According to results (Table 2.1 and Table 2.2), the interaction of nNOS with the original, reversed and polar Aβ was proposed to be mixed inhibition. This was due to the substantial decrease in V_{max} and changes in

K_m which decreased for the original peptides, while K_m increased for the reversed and polar peptides. If the substrate (BAEE) was not already bound, Aβ could be competitive with substrate in binding to the active site. Also, increasing the concentration of substrate and Aβ proportionately seemed to reverse the effect of inhibition by the Aβ peptides, also suggesting the possibility that the peptides could have been competing with substrate at the active site. In addition, Aβ could have also bound in a non-competitive manner, to the enzyme or enzyme-substrate complex at a site other than the active site. In fact non-competitive inhibition is a special case of mixed inhibition (Silverman, 2000). The results do not point to a specific type of inhibition but proves that all Aβ motifs (including polar and reversed) inhibit nNOS activity. The site on the enzyme at which binding occurs cannot be established, since nNOS has a variety of binding sites for Arg, Heme, H_4B, FMN and NADPH and more in-depth docking studies will need to be performed to clarify the exact site of binding.

According to time dependent inhibition studies, the association of nNOS to Aβ was very rapid within the first minute, suggesting that the formation of nNOS-Aβ complexes was an early event during the Aβ aggregation process. The formation of enzyme-Aβ complexes has been confirmed in literature (Alvarez *et al*., 1997, 1998). As compared with results from earlier studies in our group on the binding mechanism of amyloid peptides ($Aβ_{1-40}$, $Aβ_{22-35}$, $Aβ_{17-28}$, $Aβ_{32-35}$ and $Aβ_{25-35}$), the association of Aβ to the enzyme obeys the principle of association vs. dissociation (Padayachee and Whiteley, 2011) (Evans *et al*., 1995).

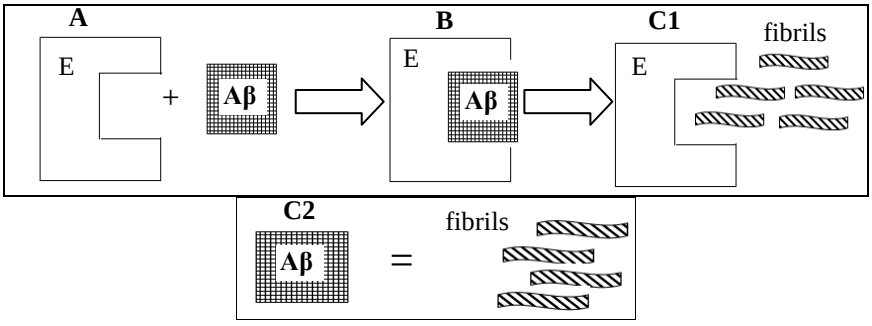

*Figure 2.11: The enzyme nNOS (E) and Aβ fragment before association (**A**); association of nNOS and Aβ whereby peptide binds to enzyme active site, decreasing enzyme activity and thus no or limited fibril formation occurs (**B**); dissociation of Aβ in the form of fibrils (**C1** and **C2**)*

According to Fig.2.11, the association of peptide with enzyme (E) did not immediately lead to the catalytic formation of fibrils (B). Once the peptide dissociated from the enzyme (C1) and activity was restored, so too did the catalytic formation of fibrils occur (C2). In this way, inhibition of activity is associated with a low amount or no fibril formation, while restoration of activity is associated with fibril formation. Such reasoning also supports the fact that some amyloidogenic proteins (referred to as fragments) are released from precursors by proteolysis. Mutations that enhance the proteolytic sensitivity of the precursor promote fibril formation by causing an increase in the steady-state level of the fibrillogenic fragment (Lansbury and Rochet, 2000), thus adding proof to the fact that nNOS is an amyloidogenic catalyst in fibril formation. So far, it has been shown that Aβ binds to nNOS and inhibits its activity, it is imperative to consider the binding mechanism of nanoparticles and curcumin to nNOS, since their interaction will provide further insight into inhibitory mechanisms.

2.4.7 Time dependant inhibition of nNOS by Au, Ag nps and curcumin

According to results (Fig.2.12), in the absence of nps and curcumin at 0 min, the activity of nNOS was 100 %. The presence of nps, however, resulted in a 60-62 % drop in activity compared to a 40 % drop in activity by curcumin within 1 min. Nanoparticles thus seemed to possess greater inhibition potential than curcumin.

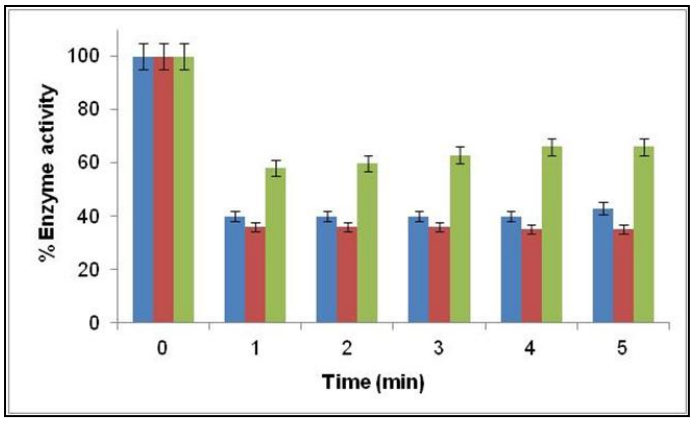

Figure 2.12: Percent enzyme activity of nNOS (32 nM) by Au ■, Ag ■ and curcumin ■ in Tris-HCl buffer (50 mM, pH 7.6) (0.09 µM), in the presence of the substrate BAEE (8 µM) for a duration of 5 min. Enzyme activity at time (0 min) = 9 U/ml; values represents the mean (± S.E.M) of three trials

2.4.8 Substrate dependant inhibition of nNOS by Au, Ag nps and curcumin

Absorbance wavelength was fixed at 530 nm; values represent the mean (± S.E.M.) of three trials. According to (Fig.2.13, Table 2.3), the values for V_{max} decreased while the values for K_m increased, with increasing concentration of inhibitor.

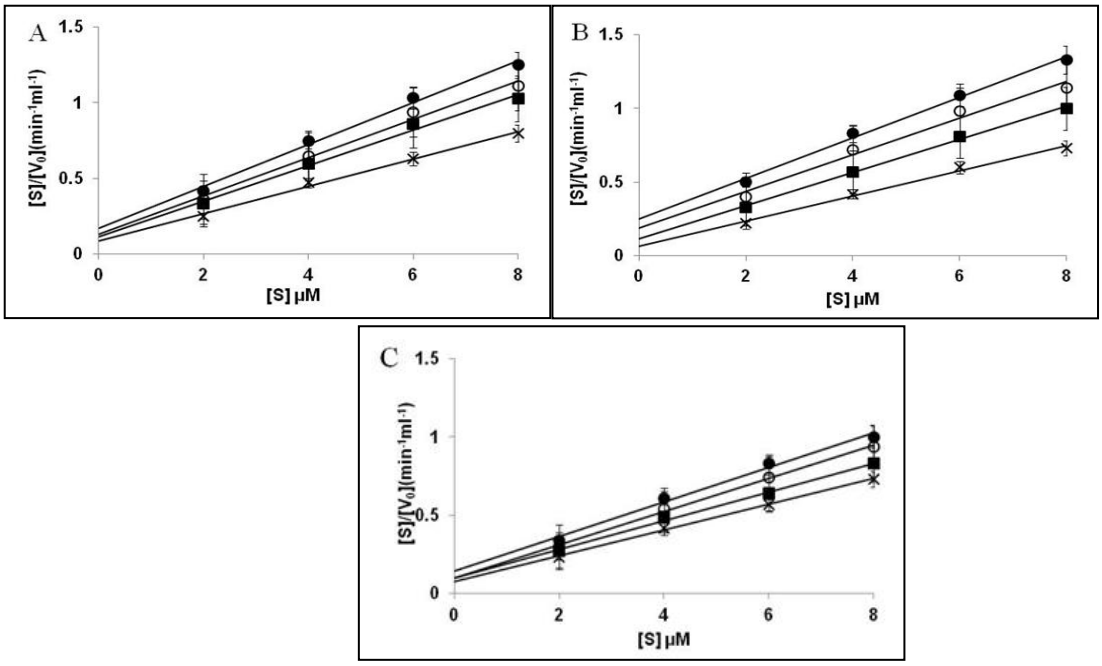

*Figure 2.13: Hanes-Woolf plot of nNOS activity in the absence and presence of nps and curcumin. Concentrations of nps and curcumin: 0 µM (×); 0.03 µM (■); 0.06 µM (○); 0.09µM (●), Au [**A**] Ag [**B**] and curcumin[**C**]*

This kinetic relationship is an unusual case of inhibition since the trends are deviant from competitive, non-competitive and uncompetitive inhibition. The trend values rather point towards mixed inhibition but this is not conclusive and will need to be confirmed by spectrofluorimetry and molecular docking studies. According to mixed inhibition, the trend shown by K_m may suggest that the enzyme has less affinity for either the substrate or the inhibitor. According to (Fig. 2.13, Table 2.3), the Ag np, has the tightest binding affinity to the enzyme because of its lowest K_i value (0.12 µM) ($p > 0.05$), compared to the K_i values for Au (0.15 µM) and curcumin (0.25 µM) ($p > 0.05$). The differences in K_i values between Au, Ag and

curcumin are not significant but comparable. Statistical analysis on the various Au, Ag and curcumin are attached, pg 183-185. These results correlated with time dependent studies (Fig.2.12) which showed that curcumin had a 40 % inhibition potential compared to nanoparticles which had a 60 % inhibition potential.

Table 2.3 Values of V_{max} ($\mu mol.ml^{-1}.min^{-1}$) and) K_m (μM) and K_i (μM) for [L = Au/Ag nps or curcumin] (μM), after interaction with nNOS. K_i values were estimated from Eq [5], pg 34

	V_{max} ($\mu mol.ml^{-1}.min^{-1}$)			K_m (μM)			K_i (μM)		
[L]	**Au**	**Ag**	**curcumin**	**Au**	**Ag**	**curcumin**	**Au**	**Ag**	**curcumin**
0	11	11	12	0.97	0.76	0.90	0	0	0
0.03	8.5	8.8	10	1.0	1.0	1.0	0.15	0.12	0.25
0.06	7.9	8.0	9.4	1.0	1.4	0.9			
0.09	7.2	7.2	9.0	1.2	1.8	1.3			

2.4.9 Percent enzyme activity of nNOS by Au, Ag nps and curcumin

Also, according to percent enzyme activity plots (Fig.2.14), metallic nps and curcumin showed inhibition potential at the lowest substrate (2 μM) and inhibitor concentrations (0.03 μM) as: Ag (85%), Au (79%) and curcumin (70 %), once again indicating the potent inhibition of Ag nps on activity. All values represented the mean (± S.E.M) of three trials.

The hydrophobic interaction, π-π stacking and electrostatic interactions have been attributed as the major mechanisms in np-protein interactions (Wu *et al*., 2009). A higher surface concentration of nps means more protein is adsorbed on the np surface and a crowded environment facilitates protein-protein interaction and greater loss of activity through perturbation of protein secondary structure. In contrast at low surface concentrations, interactions are readily formed between protein and the hydrophobic surface of the np, reducing the net energy barrier to unfolding (Fei and Perrett, 2009). Thus the surface concentration of both gold and silver nps could also have played a role in inhibition. In addition, protein-np interaction has recently been based on the idea of the "nanoparticle-protein corona" which is the biological identity of a nanoparticle, as it is the region on the protein that the nanoparticle interacts with (Lynch and Dawson, 2008). In our studies, the "np-protein corona" could be the Fe^{+3} (heme)

which is ligated to a cysteine residue constituting a sulphur functional group. These elements at the active site most probably attracted the nanoparticle and became its "biological identity. However, in depth molecular docking studies need to be performed in order to confirm this. Nevertheless, our results have established that nps do bind to nNOS and inhibits the enzymes activity.

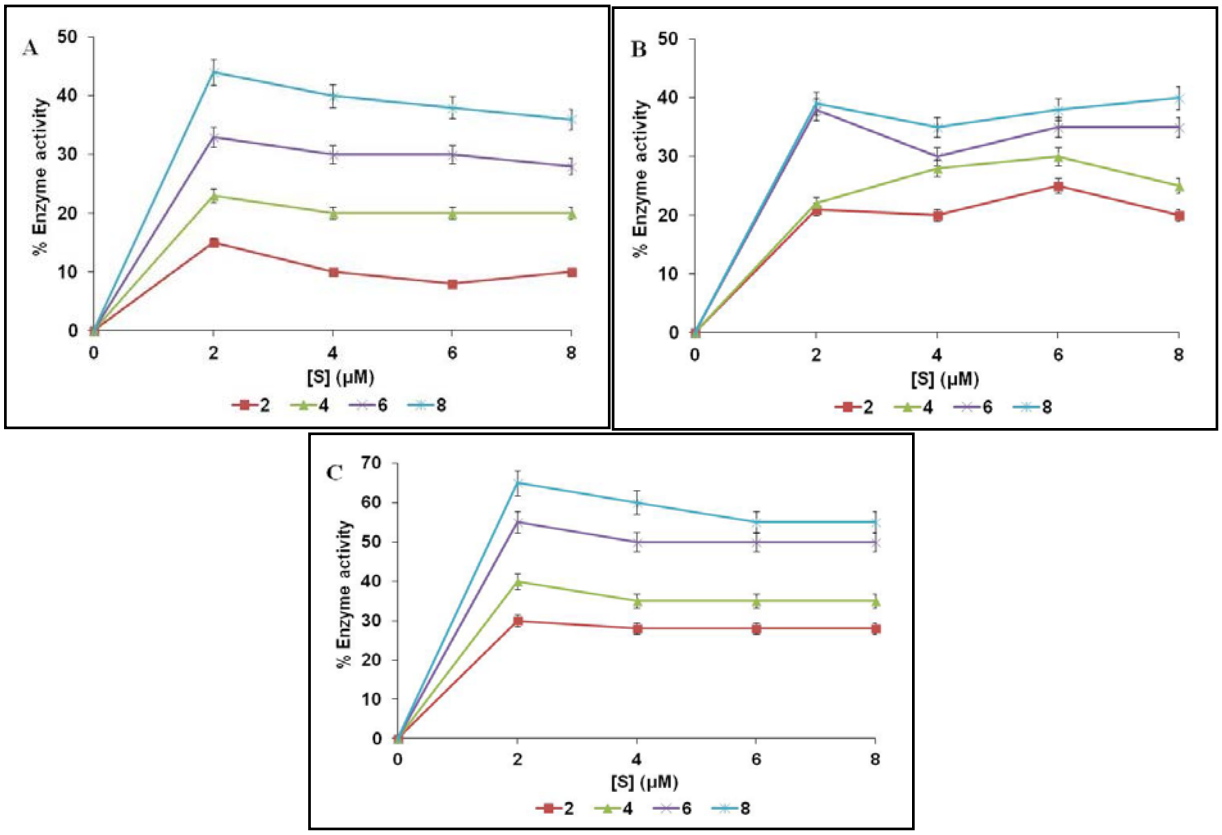

*Figure 2.14: Percent enzyme activity of nNOS by interaction with Au [**A**] Ag [**B**] curcumin [**C**] at concentrations = 2 μM ■ [S]= 4 μM ■; [S]= 6 μM ■; [S]= 8 μM ■, in the presence of benzoyl arginine ethyl ester substrate[S] (0-8μM). Enzyme activity at 0 μM Aβ peptide = 9 U/ml.*

Curcumin is another compound found to be an efficient *in vitro* inhibitor of fibril formation via its aromatic side chains (Porat *et al*., 2006). Hence, given that fibrillogenesis is a catalytic product of Aβ and nNOS interaction (Padayachee and Whiteley, 2011; 2013), it could be reasoned that the aromatic moieties within Aβ or curcumin could "disrupt" Aβ-nNOS complex formation (inhibit catalysis of nNOS) via aromatic interactions. This is yet to be confirmed in molecular

docking studies. Moreover, our results that curcumin inhibited nNOS activity support findings reported in the literature where oral curcumin treatment also reduced central nervous inducible nitric oxide synthase activity (Cole *et al*., 2003).

The likely mechanism of np and curcumin inhibition is reflected in Fig.2.15. The nps/curcumin could displace the peptide and bind to the enzyme's (E) active site (Fig.2.15B), inhibiting the activity of the enzyme and thus inhibiting the process of fibrillogenesis (Fig.2.15C2). In the process, nps or curcumin and/or Aβ become displaced (Fig.2.15C1). The enzyme binding site could be non-catalytic in the preliminary binding event but later the ligands could bind at the active site, such that the binding induces conformational change in the enzyme. Conformational changes in nNOS are yet to be confirmed in spectrofluorimetry and thermodynamic studies. Thus dissociation of Aβ or may not form a fibril as the enzyme has not catalyzed the peptide due to the inhibition by the np/curcumin (Fig.2.15C2).

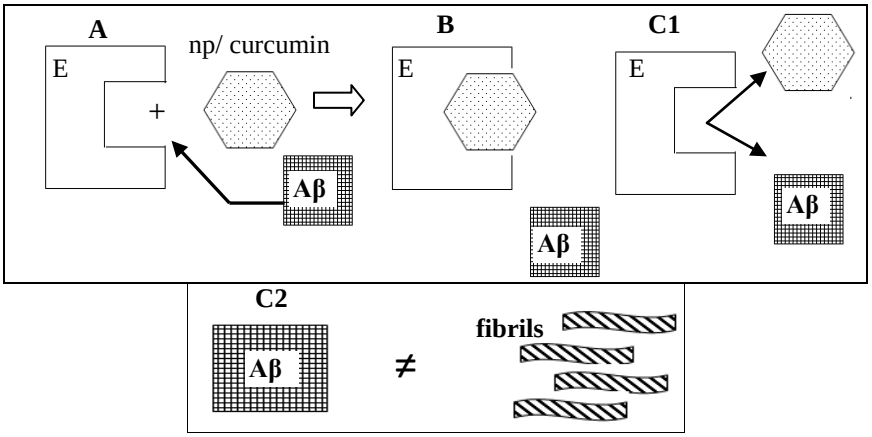

*Figure 2.15: The enzyme nNOS (E), Aβ fragment and np/curcumin before association (**A**); association of nNOS with np/curcumin whereby either ligand binds, decrease enzyme activity and displaces Aβ (**B**); dissociation of Aβ and np/curcumin with suppressed or no fibril formation by the action of nps/curcumin (**C1** and **C2**).*

2.5 Conclusions

All Aβ peptides: [$A\beta_{17-21}$, $A\beta_{25-29}$, $A\beta_{29-33}$, $A\beta_{33-37}$, $A\beta_{25-37}$], including the polar and reversed peptides, nps and curcumin inhibited nNOS successfully with the original $A\beta_{17-21}$ inhibiting the

activity of nNOS to a greater extent (K_i =5.1 μM). Also the Ag np was found to display greater inhibition ability (K_i =0.12 μM) compared to the Au np and curcumin. The Ag np and $A\beta_{17-21}$ exhibited > 80 % inhibition at low concentrations of substrate and inhibitor (2 μM). Results indicated that the initial binding event was an instantaneous process, occurring within the first minute. The reversed and polar sequences had higher K_i values than the original Aβ but the reversed sequences had lower K_i values: $A\beta_{17-21r}$ (11 μM) and $A\beta_{29-33r}$ (13 μM) in comparison to the polar sequences: K_i values of $A\beta_{17-21p}$ (19 μM) and $A\beta_{29-33p}$ (21 μM). The lower inhibitory effect of the reversed sequences was postulated due to the reversed positions of phenylalanine and isoleucine residues. The polar sequences confirmed the critical role of phenylalanine and isoleucine in inhibition as these residues were replaced with glutamic acid. The low ability of polar sequences to inhibit nNOS activity also pointed to the importance of hydrophobic interaction between the enzyme and peptide in driving inhibition. The type of inhibition could not be established but was proposed to be mixed, and the location of the actual site of binding on the enzyme needs to be established using docking models. The binding of Aβ peptides to nNOS influenced the process of fibrillogenesis through the principle of association (inhibition) and dissociation (restoration of enzyme activity). After activity was restored, the peptide could no longer bind to the enzyme and became dissociated from the enzyme in the form that could no longer bind, later deduced as a fibril (Padayachee and Whiteley, 2011; 2013). According to our results, it has been proposed that nanoparticles and curcumin displaced the binding of the Aβ peptide by binding at the active site so that fibrillogenesis was inhibited. The mechanism of fibrillogenesis between nNOS and Aβ and the subsequent inhibition or the reversal of the formation of fibrils by nanoparticles and curcumin requires a more in depth analysis and will be the subject of the next chapter.

3 Interaction of Aβ peptides, nanoparticles (Ag/Au) and curcumin with nNOS: Fibrillogenesis

3.1 Introduction

Amyloid-beta proteins are one of 16 proteins capable of forming amyloid-like fibrils which is a key pathological feature in AD (Goldschmidt *et al*., 2010). There are two major properties which qualify Aβ as a fibril forming protein: (1) the presence of self-complementary β-sheets that form the spine of an amyloid fibril and (2) sufficient 'conformational freedom' of the β-sheets to interact with other molecules through inter- and intra-molecular interactions (Goldschmidt *et al*., 2010). Electron microscopy (EM) studies have revealed that amyloid fibrils are typically long, straight, and unbranched, ranging from 0.1 to 10 μmeter in length (Fig.3.1A) (Serpell, 2000). Early studies using X-ray fiber diffraction revealed that all amyloid fibrils share a cross-β-structure, composed of β-strands which run perpendicular to the axis of the fibril, and backbone hydrogen bonds which run parallel to the fibril axis (Fig.3.1B).

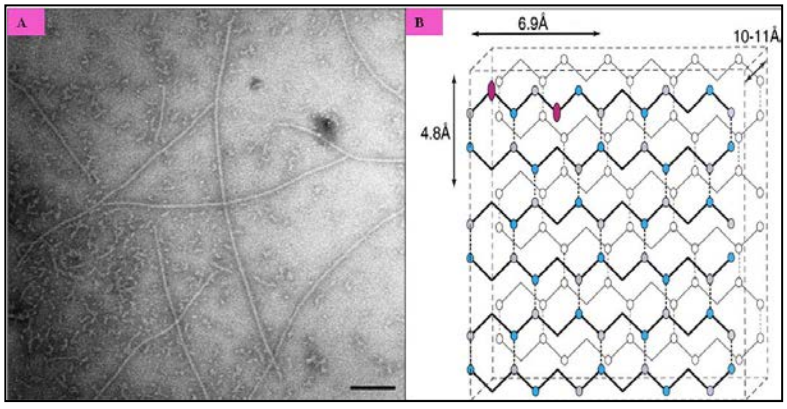

*Figure 3.1: Electron micrograph of short, straight amyloid fibrils formed in water from $A\beta_{1-40}$ (70-80 Å in diameter), Bar = 1000 Å (**A**). Diagram showing an anti-parallel β-sheet arrangement with hydrogen bond distances of 4.8 Å, a sheet spacing of 10-11 Å and a repeat distance along the polypeptide chain of 6.9 Å (**B**) (Taken from Serpell, 2000)*

In $A\beta_{1-40}$ fibrils, residues $A\beta_{1-10}$ are found to be unstructured, and residues $A\beta_{11-40}$ form a staggered β-turn-β unit stabilized by a salt bridge between Asp23 and Lys28. Phe19 is in contact

with Leu34 and Gln15 is in contact with Val36 while His13 is in contact with Val40 (Ahmed *et al*., 2010). More recently, the cross section of $A\beta_{1-40}$ fibrils has been shown to consist of either two or three β-turn-β units, depending on the morphology of the fibril. Fibrils with striated ribbon morphology have two-fold symmetry with intermolecular contacts between Met35 and Gly33 and between Ile31 and Gly37 (Ahmed *et al*., 2010). In contrast, fibrils with a twisted morphology have 3-fold symmetry with intermolecular contacts between Ile31 and Val39 (Ahmed *et al*., 2010). There are two aspects of amyloid fibril formation that can be characterized *in vitro* namely; the determination of the structure of the fibril and the process of fibril formation (i.e., mechanism and kinetics). Both processes begin with the characterization of the component peptide or protein by traditional techniques such as turbidity assays or assays containing Congo red or Thioflavin T dyes used to study protein structure (Nilsson, 2004).

Aβ can adopt two different conformational states in solution, depending on the secondary structure adopted by the *N*-terminal domain. One species is highly amyloidogenic and has pre-dominantly anti-parallel β-sheet structure, whilst the other is poorly amyloidogenic and contains mainly random coil or an α-helix structure (monomeric in nature) (Bartolini *et al*., 2003). Firstly, the peptide molecule is usually maintained in its monomeric form. Once information about the initial secondary structure is known, the protein is subjected to conditions to promote aggregation into amyloid fibrils. The exact conditions are highly variable and sample dependent. Secondly, once conditions that promote fibril formation are established, the kinetics of the process is examined by assaying the solution for fibrils at specific time intervals (Nilsson, 2004).

Regarding the process of fibrillogenesis, aggregation can occur through unfolding intermediates and unfolded states or through protein self-association (Wang *et al*., 2010). Intermediates are precursors of the aggregation process since they expose more hydrophobic patches and have a higher flexibility relative to the folded state. Interaction (attraction) of these intermediates leads to the formation of protein aggregates which are initially soluble but gradually become insoluble as they exceed certain size and solubility limits (forming precipitates) (Wang *et al*., 2010). Direct association into protein aggregates, without going through the intermediate state occurs simply

through electrostatic and hydrophobic interactions. Weaker van der Waals forces can also initiate the association process (Wang *et al*., 2010).

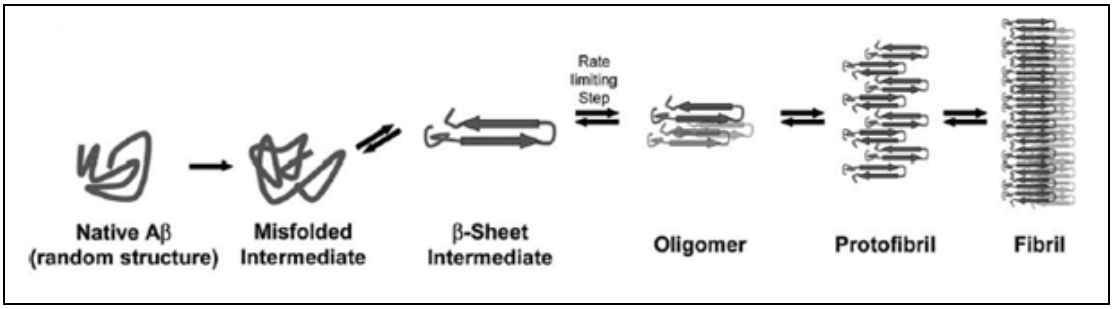

Figure 3.2: Schematic showing aggregation intermediates critical to amyloid-β-aggregation (Taken from DaSilva et al., 2010)

According to Fig.3.2, fibrillogenesis is initiated when Aβ undergoes a conformational change from a random structure to a β-sheet rich intermediate which forms high-order oligomers composed of multiple monomer units. Protofibrils result from the addition of existing monomers on fibril ends, which further assemble into insoluble fibrils (Fig.3.2). It has been suggested, however that soluble amyloid oligomers may represent the primary toxic mechanism of amyloid pathogenesis, rather than insoluble fibrils (Glabe, 2006). It appears that the majorities of protein aggregation events are initiated by the formation of an aggregation nucleus and hence is a nucleation-dependent aggregation. During this process, two pathways of fibril nucleation are proposed: (1) fibril nucleation on seeds; (2) nucleation within micelles, whose presence depends on the peptide concentration (C) exceeding the critical micelle concentration (*c**). Micelles are in fast equilibrium with free monomers at concentration (*c**) (Fig.3.3). Moreover, nuclei are spontaneously formed out of micelles and fibrils grow by binding monomers to fibril ends with the rate proportional to the concentration of free monomers (Lomakin *et al.*, 1997). There is a dynamic equilibrium which also exists between monomers and micelles which suggests that, despite their ordered arrangement, fibrils are dynamic assemblies.

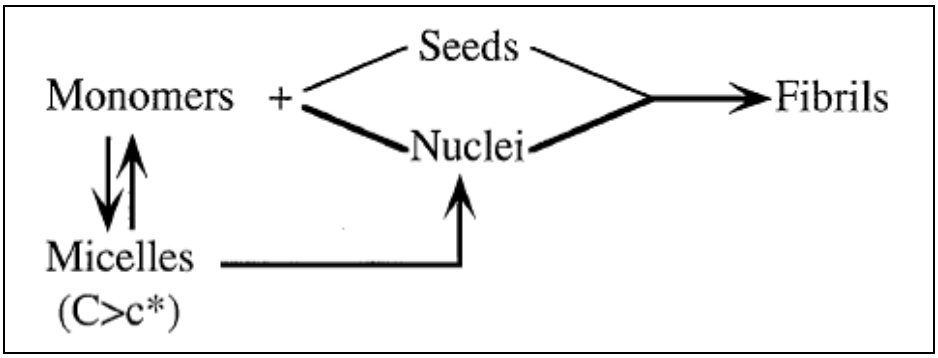

Figure 3.3: Representation of the kinetic model for Aβ fibrillogenesis. Fibrillization of Aβ protein is nucleation dependent and two pathways are proposed. One is fibril nucleation on seeds. The second is nucleation within micelles (Taken from Lomakin et al., 1997)

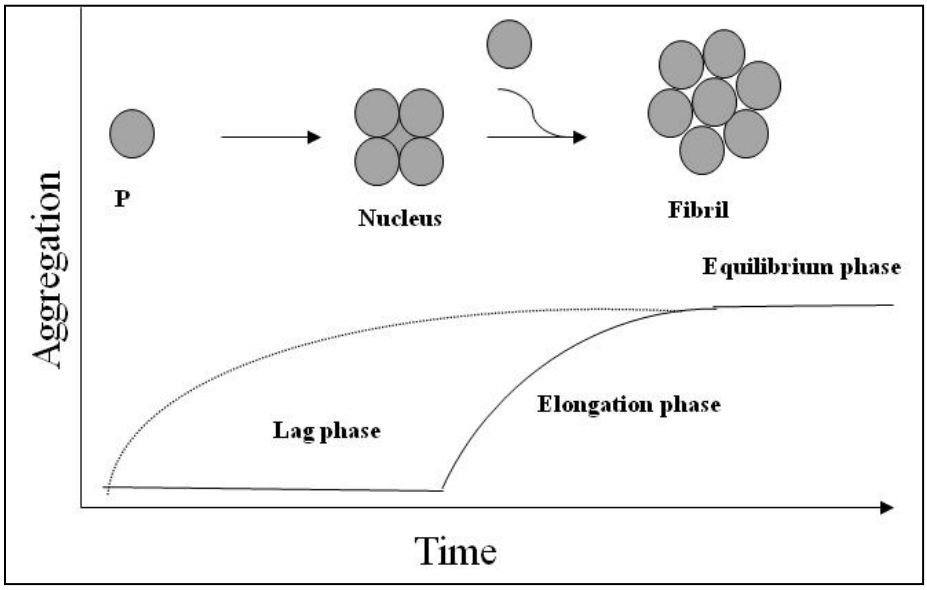

Figure 3.4: Illustration showing the "nucleation-polymerization" kinetics for amyloid fibril formation (Adapted from Nilsson, 2004)

During nucleation dependent polymerization, three different kinetic phases are evident: lag, elongation (or growth), and monomer-fibril equilibrium phase (Fig.3.4). The lag phase refers to the period of time where no aggregation is observed for protein (P). During this time the thermodynamically unfavorable process of initial association occurs. Once the aggregation process begins and a critical nucleus is formed, the aggregation proceeds rapidly into amyloid fibrils (elongation phase) (Fig.3.4). Hydrophobic interaction is the major driving force in the

nucleation step. The nucleus contains multiple sites for the addition of monomers, allowing for rapid, thermodynamically favorable growth of high order aggregates termed oligomers. The lag phase however can be overcome (dotted line) by the addition of a pre-formed nucleus (Fig.3.4) (Nilsson, 2004). The preformed nucleus which is the core of the amyloid deposit might be seeded with intracellular Aβ or derived from an insoluble pool of Aβ (Parihar and Hemnani, 2004). Elongation or growth phase refers to the addition of monomers on pre-existing fibrils, this occurs once the protein concentration exceeds the critical concentration (Caflisch and Pellarin, 2006) (Fig.3.4). The monomer-fibril equilibrium refers to the reversibility of monomers associating into fibrillar aggregates and fibrillar aggregates dissociating into monomers.

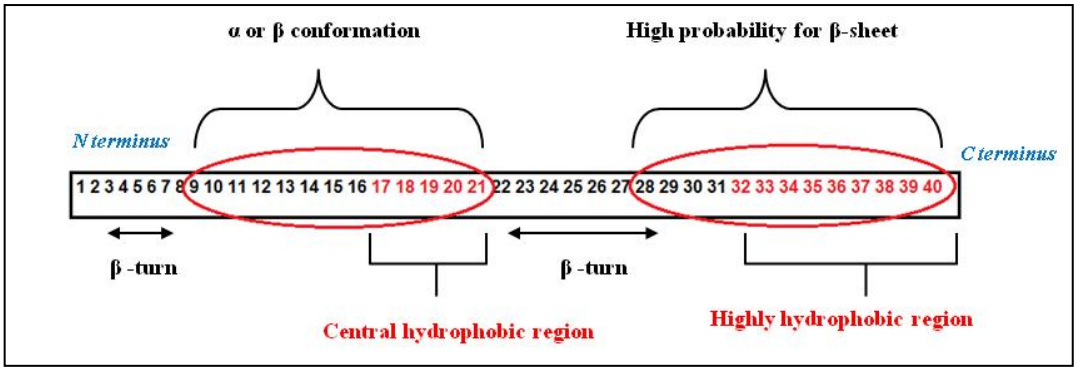

Figure 3.5: Diagram of $A\beta_{1\text{-}40}$ sequence suggesting regions with a high propensity for β-sheet structure (encircled in red). Clusters of hydrophobic residues are shown in red (Adapted from Serpell, 2000)

In nature, numerous polypeptide sequences have shown that specific residues play key roles in forming fibril assemblies by increasing the propensity for β-sheet formation (Hamada *et al*., 2009; Jones and Mezzenga, 2012). In addition, it has been observed that the ability of a protein to undergo an α to β conformational change is facilitated by amino acid regions that adopt an α-helical conformation within the native structure and at the same time as having a high propensity for the β-sheet structure (Fig.3.5) (Kallberg *et al*., 2001). The *N*-terminus is thought to be important for initiating α-β conformational switching. Residues 1-9 may be exposed on the surface of the fibers and may be involved in interaction between fibrils but are not necessary for fibril formation (Fig. 3.5) (Serpell, 2000). A mechanism for the α-helix (monomer) to β-sheet (oligomer) transition may involve the deprotonation of side chains: Asp7, Glu11, Glu22 and

Asp23 above pH 4 and the protonation of His6, 13 and 14, causing a destabilization of the α-helix (Serpell, 2000). The two β-turns at positions 3-8 and at positions 22 and 23-27 are also thought to contribute to malignant conformation in $A\beta_{1-40}$ fibrils (Serpell, 2000). The hydrophobic residues 17-21 and 32-40 are the major β-sheet regions and function as a key determinant in aggregation (Fig.3.5) (DaSilva *et al.*, 2010).

Strong evidence also supports the role of aromatic residues, particularly phenylalanine in the formation of fibrils by π-π stacking interactions along the β-sheet length (Gazit, 2007; Jones and Mezzenga, 2012). Intermediate helical states, hydrophobic interactions, and hydrogen bonding are also important amino acid properties to promote β-sheets (Kammerer *et al*., 2004). Moreover, baseline factors such as physical forces, ionic strength and pH also tend to promote formation of fibrils (Liu *et al*., 2000; Nichols *et al*., 2002; Akkermans *et al*., 2006). As the assembly of protein fibrils relies on the interaction between proteins of specific sequences, the insertion of shortened or slightly modified peptides can often be inhibitory (Padayachee *et al*., 2011; Padayachee and Whiteley, 2011; 2013, Jones and Mezzenga, 2012). These peptides have nearly identical sequences to those involved with β-sheet alignment of the fibril; however these fragments are critically shortened to prevent the appropriate β-sheet stacking for fibril formation (Jones and Mezzenga, 2012). If one assumes the targeted binding site on Aβ has β structure, then inhibitors based on Aβ-derived peptide sequences can be expected to have a propensity for β structure and the ability to form high-affinity complexes with Aβ (Padayachee *et al*., 2011; Padayachee and Whiteley, 2011; 2013; Findeis and Molineaux, 1999). In this way, different peptide fragments, derived from the original Aβ structure, were utilized to inhibit Aβ fibril formation. For example, the inhibition of fibril formation was found by $A\beta_{16-20}$ and $A\beta_{25-35}$ (Tjernberg *et al*., 1996; Ban *et al*., 2004). It was also suggested that the hydrophobic residues $A\beta_{17-21}$ formed core interactions between protofibrils (Serpell, 2000). Hence, due to their marked affinity for amyloid proteins, certain shorter peptide fragments can serve as self-recognition sequences to disrupt amyloid fibril formation. For example, the $A\beta_{17-21}$ (LVFFA) motif which contained two phenyl rings was found to inhibit amyloid formation from $A\beta_{1-40}$ (Gazit, 2005). Such inhibition was probably based on recognition between the aromatic moieties and electrostatic repulsion by the positively charged

lysine residues (Gazit, 2005; Härd and Lendel, 2012). Following early research conducted on the $A\beta_{16-20}$ (KLVFF) motif (Tjernberg *et al*., 1996; Soto *et al*., 1998), recent research has been conducted on similar, small peptide fragments (called the β-sheet breaker peptides) as lead sequences for Aβ inhibitors (Padayachee *et al*., 2011; Padayachee and Whiteley, 2011; 2013; Hard and Lendel, 2012). For example, it was shown that that the KLVFF recognition element when combined with disruptive elements such as cationic lysines in KLVFFKKKK can be effective at inhibition. It was furthermore possible to enhance the activity of peptide inhibitors of Aβ aggregation, such as LVFFA, through modification of the amino termini by organic reagents such as cholic acid (Härd and Lendel, 2012). A drawback, however of β-sheet breaker inhibitors is that they themselves form amyloid fibrils. An alternative strategy to block β-sheet extension in fibrils is through *N*-methylation which prevents hydrogen bond formation between amino acids. *N*-methylation achieves steric hindrance for amyloid formation and *N*-methylated peptides are soluble in water and are able to potentially penetrate the cell membrane (Härd and Lendel, 2012).

Nanoparticles (nps) play a dual role in promoting as well as inhibiting the formation of fibrils (Auer *et al*., 2009). For the purpose of this chapter, our focus is on the potential of nps to inhibit fibril formation which is a pathogenic feature of AD. A few articles have been published on the effect of nps on fibrillogenesis. For example, Xiao and coworkers have showed an inhibition effect of -*N*-acetyl cysteine-capped cadmium tellurium quantum dots of size of 3–5 nm on $A\beta_{1-40}$ fibrillogenesis (Xiao *et al*., 2010). In another case, dual effect of commercial polystyrene nps with amino modification was observed on $A\beta_{1-40}$ fibrillogenesis (Cabaleiro-Lago *et al*., 2010). The most recent literature on np interaction on fibrillogenesis, involved the inhibition of $A\beta_{1-40}$ fibrillogenesis by conjugated quantum dots (Thakur *et al*., 2011). In addition, literature (Kumar *et al*., 2012; Wang *et al*., 2009; Yang *et al*., 2005) have so far confirmed that curcumin does inhibit fibril formation. Since curcumin is a known inhibitor of fibril formation (Wang *et al*., 2009; Ono *et al*., 2004 and Yang *et al*., 2005), its mechanism of reversal or inhibition of fibrils may be used as a control and compared to the mechanism of fibril formation by metallic nps. No such studies, on whether nps and curcumin can both inhibit and/or reverse fibril formation catalyzed by nNOS have been undertaken. Hence, the objective of this chapter is to use the

Thioflavin T assay, which measures the concentration of fibrils to investigate whether nps and/or curcumin, individually or in tandem with nNOS and/or Aβ will inhibit, delay onset, or even reverse the formation of fibrils. This would have future clinical implications in a *de novo* synthesis of small molecule inhibitors for the treatment of amyloid-forming diseases such as AD.

3.2 Theory of techniques utilized

3.2.1 Thioflavin T (ThT) nucleation assay

In a typical nucleation assay (Jarret and Lansbury, 1993; Jarret *et al*., 1993), the formation of amyloid fibrils is observed over time. The amyloidogenic peptide is dissolved in an appropriate buffer under conditions, where it is initially in an unaggregated state. An initial period of time occurs where no aggregation is detected (e.g. as the ThT dye binds) but prefibrils are formed (Findeis and Molineaux, 1999). Once a particular quantity of prefibrils has accumulated in the sample, fibril formation is then rapid, continuing until the aggregated peptide is maximum, whereupon the reaction plateaus (Findeis and Molineaux, 1999). A compound that interferes with this nucleation will delay the onset of fibrillogenesis. Inhibitory potency of such a compound can then be expressed as the ratio of the time to the nucleation in the presence of the inhibitor over the time to nucleation in the absence of test compound (Findeis and Molineaux, 1999). An inhibitor of fibrillogenesis will thus have a ratio or lag greater than one and can also lower the quantity of fibrils by the end of the assay. Both lag and percentage inhibition is used to characterize compounds tested as inhibitors (Findeis and Molineaux, 1999). In the present study, Aβ was dissolved in dimethyl sulfoxide (DMSO) organic solvent to obtain a monomeric starting sample. Aβ in its monomeric form was thus used to selectively monitor nNOS interaction and its induced shift from α to random to β-sheets conformation, previous to fibril formation.

Thioflavin T (Fig.3.6) is a benzothiazole–based dye first noted to bind to amyloid in 1959 (Vassar and Culling, 1959). It was noted that the fluorescence of ThT was quenched in solution, but that its quantum yield greatly increased when bound to the β-sheet structure of amyloid fibrils (Reinke and Gestwicki, 2011). ThT was adapted by Levine (Levine III and Scholten,

1999) into a convenient, inexpensive assay for monitoring fibril formation *in vitro*. The protocol has been largely unchanged and is perhaps the most widely use method for monitoring Aβ aggregation. Thioflavin T has a three-ring structure (Fig.3.6); the conjugated benzothiazol and aniline rings which are arranged in an almost planar orientation (≈ 30 º) in a minimum energy conformation.

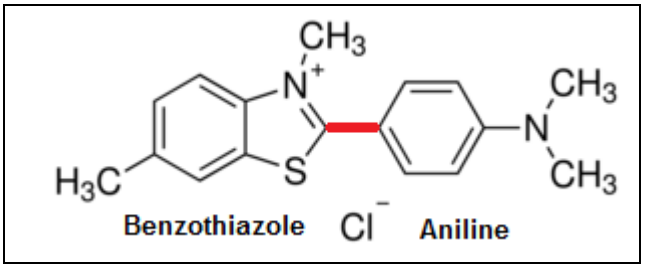

Figure 3.6: Chemical structure of ThT, depicting the carbon-carbon bond (in red) between benzothiazol and aniline rings that becomes restricted in rotation upon binding to amyloid fibrils (Adapted from Reinke and Gestwicki., 2011)

ThT fluorescence is thought to increase when bound to Aβ fibrils, due to the restriction of the rotational freedom of the carbon-carbon bond between the benzothiazol and aniline rings, such that the excited state is readily populated and the planar/flat geometry of the molecule allows it to be inserted within the channels or grooves associated with fibril formation (Fig. 3.6) (Reinke and Gestwicki., 2011). The binding to amyloid fibril probably stabilizes the planar form of the molecule and leads to a 10–500 fold increase in ThT fluorescence intensity (Fink and Munishkina, 2007). In an unbound state, the rings are in a twisted conformation, resulting in self-quenching and low fluorescence efficiency. Interestingly, ThT has two excitation wavelengths (~ 335 nm and ~ 430 nm) and two corresponding emission wavelengths (~ 425–455 nm and 483 nm) which correspond to two conformations of the ThT molecule (planar and twisted) (Fink and Munishkina, 2007). The advantage of the Thioflavin T assay is that it is rapid, high capacity, inexpensive and can be performed on fluorescence plate readers (LeVine III and Scholten, 1999).

3.3 Materials and Methods

3.3.1 Materials

Materials were used as described in Chapter 2, 2.3.1, pg. 35. Thioflavin T was purchased from Sigma Aldrich (South Africa). All reagents were of analytical grade and all solutions were prepared with deionized water obtained from a Milli-Q system. Fluorimetry analyses were carried out on PowerWave microplate spectrofluorimeter (Bio-Tek Instruments) with 96 well plates, operated at 1 nm bandwidth using the KC Junior software program.

3.3.2 Methods

3.3.2.1 Isolation of curcumin from turmeric

As described in Chapter 2, 2.3.2.5, pg. 38.

3.3.2.2 Synthesis and characterization of Ag/Au nanoparticles

As described in Chapter 2, 2.3.2.6, pg. 38. Since nps were encased in HSAF, 2 apoferritin controls (0.30 μM, 0.15 μM) were prepared to ensure that the effect on fibrillogenesis was not due to any effect from apoferritin.

3.3.2.3 Co-incubation of nNOS and Aβ: Effect of nanoparticles

In order to induce fibrils the original Aβ peptides [$A\beta_{17-21}$, $A\beta_{25-29}$, $A\beta_{29-33}$, $A\beta_{33-37}$ and $A\beta_{25-37}$] and the reversed and polar sequences [$A\beta_{17-21r}$,$A\beta_{29-33r}$, $A\beta_{17-21p}$, $A\beta_{29-33p}$] [25 μM, 50 μM] were incubated with nNOS (5 μl,32 nM) in a reaction mixture containing ThT (3 μl, 3.14 mM) in Tris HCl buffer (pH 7.6, 100 mM) in a final volume of 200 μl for 15 min at 25°C. Au nps and Ag nps (averaging 4 nm) (0.15 μM, 0.30 μM) were then added to the solution of induced fibrils and the ThT fluorescence was read at 10 s intervals for a total of 1 minute in order to investigate whether nps would reverse the fibril formation. A solution of ThT alone was monitored under the same conditions as above to establish the basal fluorescence. A solution of Aβ-Tris HCl buffer without ThT was used as a control. The fluorescence intensity above the control was indicative of fibril formation. The positive controls were Aβ-Au, Aβ-Ag, nNOS-Au and nNOS-Ag and

nNOS alone. The change in fluorescence was monitored at λ_{ex} = 440 nm and λ_{em} = 482 nm and values obtained represented the mean (± S.E.M) of three trials.

3.3.2.4 Co-incubation of nNOS and Aβ: Effect of curcumin

The fibrils were induced as described above (section 3.3.2.3). A solution of curcumin (0.15 μM, 0.30 μM) was then added to the induced solution of fibrils and the ThT fluorescence was read at 10 s intervals for a total of 1 minute in order to investigate whether curcumin would reverse the fibril formation. A solution of ThT alone was monitored under the same conditions as above to establish the basal fluorescence. A solution of Aβ-Tris HCl buffer without ThT was used as a control. The fluorescence intensity above the control was indicative of fibril formation. The positive controls were Aβ-curcumin and nNOS-curcumin and nNOS alone. The change in fluorescence was monitored at λ_{ex} = 440 nm and λ_{em} = 482 nm and values obtained represented the mean (± S.E.M) of three trials.

3.3.2.5 Co-incubation of nNOS and nanoparticles: Effect of Aβ peptides

In order to establish whether nps could influence the initial formation of fibrils by nNOS with Aβ, Au nps and Ag nps (averaging 4 nm) (0.30 μM) were incubated with nNOS (5 μl, 32 nM) in a reaction mixture containing ThT (3 μl, 3.14 mM) in Tris HCl buffer (pH 7.6, 100 mM) in a final volume of 200 μl for 15 min. The original sequences [$A\beta_{17\text{-}21}$, $A\beta_{25\text{-}29}$, $A\beta_{29\text{-}33}$, $A\beta_{33\text{-}37}$ and $A\beta_{25\text{-}37}$]; and the reversed and polar sequences [$A\beta_{17\text{-}21r}$, $A\beta_{29\text{-}33r}$, $A\beta_{17\text{-}21p}$, $A\beta_{29\text{-}33p}$] [50 μM] were then added to the co-incubated mixture of nNOS and np and the ThT fluorescence was read at 10 s intervals for a total of 1 minute in order to investigate whether nps would reverse the fibril formation or prevent its formation in the first place. A solution of ThT alone was monitored under the same conditions as above to establish the basal fluorescence. A solution of Aβ-Tris HCl buffer without ThT was used as a control. The fluorescence intensity above the control was indicative of fibril formation. The positive controls were Aβ-Au, Aβ-Ag, nNOS-Au and nNOS-Ag and nNOS alone. The change in fluorescence was monitored at λ_{ex} = 440 nm and λ_{em} = 482 nm and values obtained represented the mean (± S.E.M) of three trials.

3.3.2.6 Co-incubation of nNOS and curcumin: Effect of Aβ peptides

In order to establish whether curcumin could influence the initial formation of fibrils by nNOS with Aβ, a solution of curcumin (0.30 µM) was incubated with nNOS (5 µl, 32 nM) in a reaction mixture containing ThT (3 µl, 3.14 mM) in Tris HCl buffer (pH 7.6, 100 mM) in a final volume of 200 µl for 15 min. The original sequences [$A\beta_{17\text{-}21}$, $A\beta_{25\text{-}29}$, $A\beta_{29\text{-}33}$, $A\beta_{33\text{-}37}$ and $A\beta_{25\text{-}37}$]; and the reversed and polar sequences [$A\beta_{17\text{-}21r}$, $A\beta_{29\text{-}33r}$, $A\beta_{17\text{-}21p}$, $A\beta_{29\text{-}33p}$] [50 µM] were then added to the co-incubated mixture of nNOS and curcumin and the ThT fluorescence was read at 10 s intervals for a total of 1 minute. A solution of ThT alone was monitored under the same conditions as above to establish the basal fluorescence. A solution of Aβ-Tris HCl buffer without ThT was used as a control. The fluorescence intensity above the control was indicative of fibril formation. The positive controls were Aβ-curcumin, nNOS-curcumin, and nNOS alone. Change in fluorescence was monitored at λ_{ex} = 440 nm and λ_{em} = 482 nm and values obtained represented the mean (± S.E.M) of three trials.

3.3.2.7 Co-incubation of Aβ and nanoparticles: Effect of nNOS

In order to establish whether nps could influence the initial formation of fibrils by nNOS with Aβ, Au nps and Ag nps (averaging 4 nm) (0.30 µM) were incubated with original sequences [$A\beta_{17\text{-}21}$, $A\beta_{25\text{-}29}$, $A\beta_{29\text{-}33}$, $A\beta_{33\text{-}37}$ and $A\beta_{25\text{-}37}$] and the reversed and polar sequences [$A\beta_{17\text{-}21r}$, $A\beta_{29\text{-}33r}$, $A\beta_{17\text{-}21p}$, $A\beta_{29\text{-}33p}$] (50 µM) in a reaction mixture containing ThT (3 µl, 3.14 mM) in Tris HCl buffer (pH 7.6, 100 mM) in a final volume of 200 µl for 15 min. The nNOS (5µl, 32 nM) was then added to the Aβ-np solution and the ThT fluorescence was read at 10 s intervals for a total of 1 minute. A solution of ThT alone was monitored under the same conditions as above to establish the basal effect of ThT. A solution of Aβ-Tris HCl buffer without ThT was used as a control. The fluorescence intensity above the control was indicative of fibril formation. The positive controls were Aβ-Au, Aβ-Ag, nNOS-Au and nNOS-Ag, and nNOS alone. Change in fluorescence was monitored at λ_{ex} = 440 nm and λ_{em} = 482 nm and values obtained represented the mean (± S.E.M) of three trials.

3.3.2.8 Co-incubation of Aβ and curcumin: Effect of nNOS

In order to establish whether curcumin could influence the initial formation of fibrils by nNOS with Aβ, a solution of curcumin (0.30 μM) was incubated with original sequences [$A\beta_{17-21,}$ $A\beta_{25-29,}$ $A\beta_{29-33,}$ $A\beta_{33-37}$ and $A\beta_{25-37}$] and the reversed and polar sequences [$A\beta_{17-21r}$, $A\beta_{29-33r}$, $A\beta_{17-21p}$, $A\beta_{29-33p}$] (50 μM) in a reaction mixture containing ThT (3 μl, 3.14 mM) in Tris HCl buffer (pH 7.6, 100 mM) in a final volume of 200 μl for 15 min. The nNOS (5μl, 32 nM) was then added to the Aβ-curcumin solution and the ThT fluorescence was read at 10 s intervals for a total of 1 minute. A solution of ThT alone was monitored under the same conditions as above to establish the basal effect of ThT. A solution of Aβ-Tris HCl buffer without ThT was used as a control. The fluorescence intensity above the control was indicative of fibril formation. . The positive controls were Aβ-curcumin, nNOS-curcumin and nNOS alone. Change in fluorescence was monitored at λ_{ex} = 440 nm and λ_{em} = 482 nm and values obtained represented the mean (± S.E.M) of three trials.

3.3.2.9 Statistical analysis

All experiments were carried out in triplicate. Mean and standard deviation calculations and comparison of data using analysis of variance (ANOVA) was performed to 5 % level of significance ($p < 0.05$) using Statistica for Windows, version 8 (Statsoft Inc.) and Microsoft Excel 2010

3.4 Results and discussion

3.4.1 Co-incubation of nNOS and original Aβ peptides: Effect of nanoparticles

According to results (Fig.3.7 and Fig.3.8), all Aβ peptides formed fibrils instantaneously, as indicated by the peak in ThT fluorescence at 0 s (15-40 a.u). The production of fibrils in the presence of nNOS supports our previous findings that nNOS is an amyloidogenic catalyst for Aβ fibril formation (Padayachee *et al*., 2011; Padayachee and Whiteley, 2011; 2013). For the original peptides (Fig.3.7), the production of fibrils was concentration dependent as increasing the concentration of Aβ from 25 μM to 50 μM, subsequently increased ThT fluorescence from ≈

15 a.u to 20-40 a.u at 0 s. Also, fibril production at an Aβ concentration of 50 μM was most pronounced for $A\beta_{17-21}$ (Fig.3.7B) and $A\beta_{29-33}$ (Fig.3.7F).

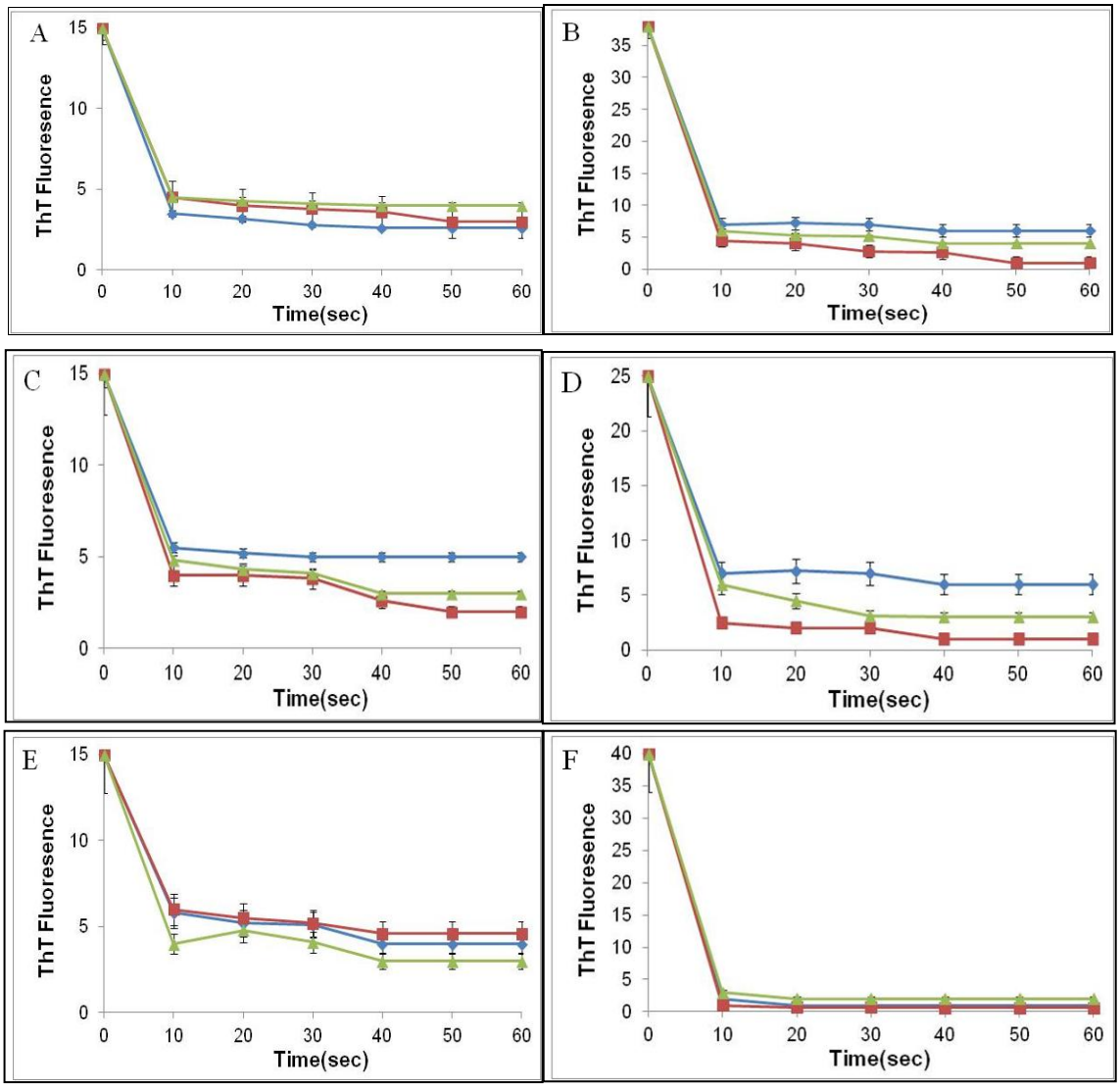

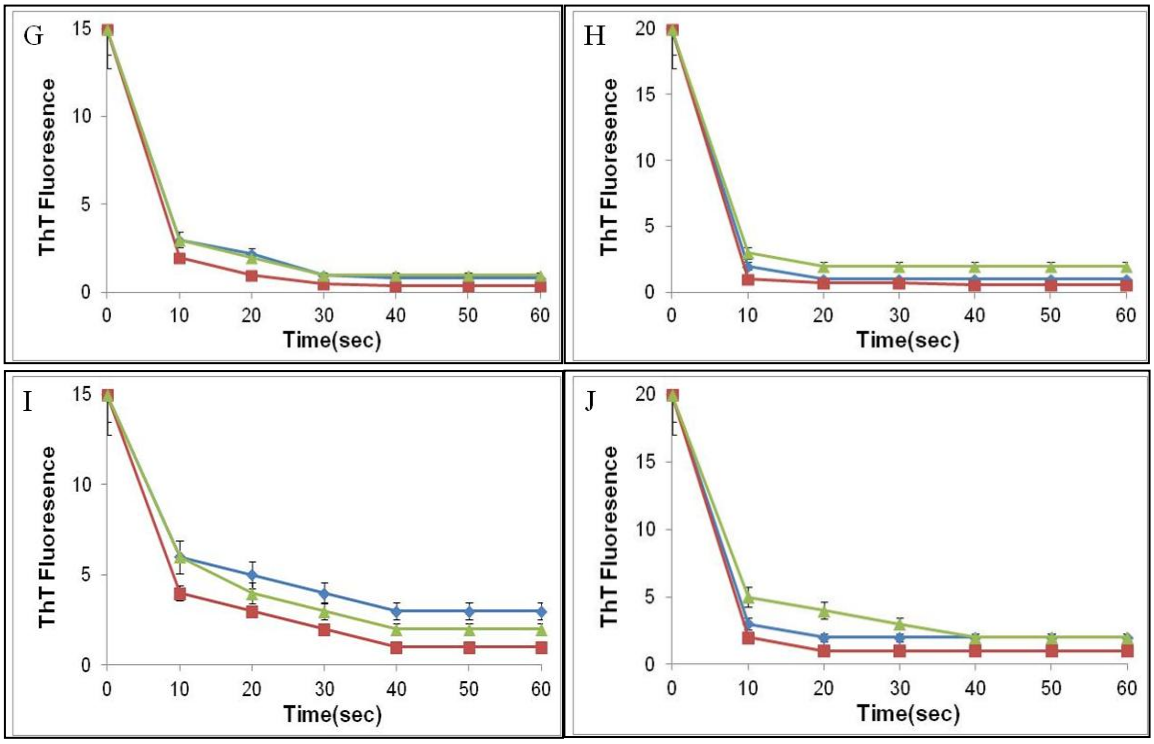

*Figure 3.7: Plots of ThT fluorescence by nNOS catalyzed fibrillogenesis of Aβ treated with nps and/or curcumin in a final volume (200µL) in Tris HCl buffer (pH 7.6, 100 mM) at 25 °C. $Aβ_{17-21}$ (25 µM); Au,Ag,curcumin (0.15 µM)[**A**]; $Aβ_{17-21}$ (50 µM); Au,Ag,curcumin (0.30 µM)[**B**]; $Aβ_{25-29}$ (25 µM); Au,Ag,curcumin (0.15 µM)[**C**]; $Aβ_{25-29}$ (50 µM); Au,Ag,curcumin (0.30 µM)[**D**]; $Aβ_{29-33}$ (25 µM); Au, Ag, curcumin (0.15 µM)[**E**];$Aβ_{29-33}$ (50 µM); Au,Ag,curcumin (0.30µM)[**F**];A_{33-37}(25µM);Au,Ag,curcumin (0.15µM)[**G**];$Aβ_{33-37}$(50µM);Au,Ag,curcumin (0.30 µM)[**H**];A_{25-37} (25µM); Au, Ag, curcumin (0.15 µM) [**I**]; $Aβ_{25-37}$ (50µM); Au, Ag ,curcumin (0.30 µM) [**J**]. ■ — [Ag: 4 nm]; —♦ [Au: 4 nm]; — ♦ [curcumin].*

The catalysis of more fibrils from $Aβ_{17-21}$ and $Aβ_{29-33}$ by nNOS, can be attributed to their tighter binding affinity to the enzyme compared to the affinity of the other Aβ peptides [$Aβ_{17-21}$ (K_i = 5.1 µM) and $Aβ_{29-33}$ (K_i = 7.5 µM) (chapter 2)]. However, the production of fibrils from the polar and reversed sequences, in the presence of nNOS (Fig.3.8) was not concentration dependent, and the quantity of fibrils formed (10-15 a.u) was the same for either concentration of 25 µM or 50 µM. This result can also be attributed to the weaker association of the polar and reversed sequences to the enzyme compared to that of the original peptides (K_i =11-21 µM, chapter 2).

3.4.2 Co-incubation of nNOS and reversed and polar Aβ peptides:Effect of nanoparticles

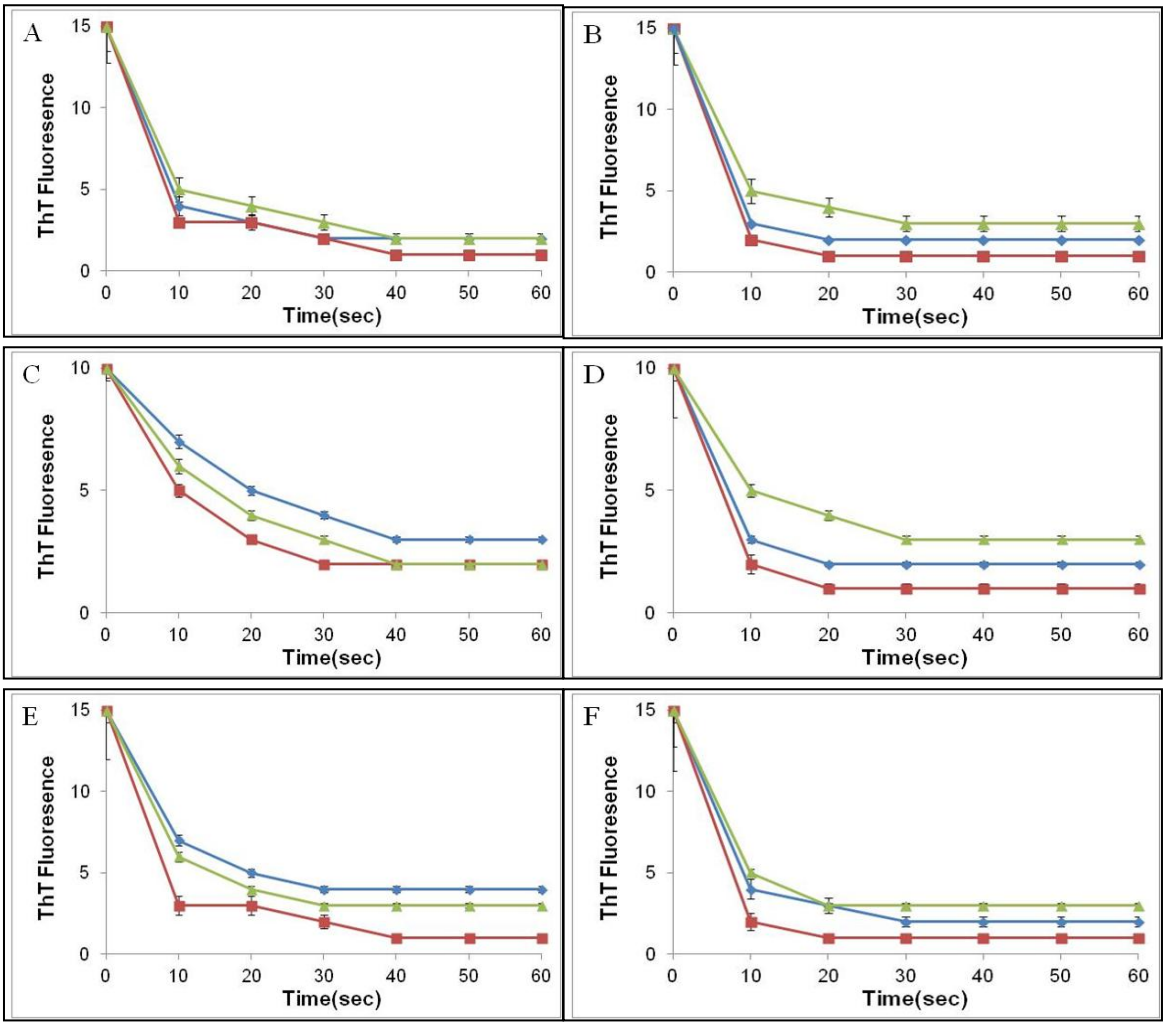

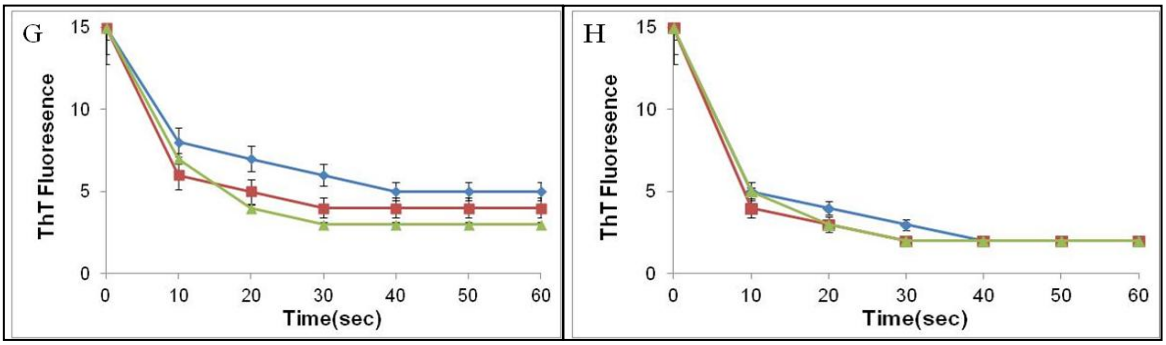

*Figure 3.8: Plots of ThT fluorescence induced by nNOS catalyzed fibrillogenesis of Aβ treated with nps and/or curcumin in a final volume (200μL) in Tris HCl buffer (pH 7.6, 100 mM) at 25 °C. $Aβ_{17-21r}$ (25 μM); Au,Ag, curcumin (0.15 μM) [**A**]; $Aβ_{17-21r}$ (50 μM); Au,Ag, curcumin (0.30 μM) [**B**]; $Aβ_{17-21p}$ (25 μM); Au, Ag, curcumin (0.15 μM) [**C**]; $Aβ_{17-21p}$ (50 μM); Au,Ag, curcumin (0.30 μM) [**D**]; $Aβ_{29-33r}$ (25 μM); Au,Ag, curcumin (0.15 μM) [**E**]; $Aβ_{29-33r}$ (50 μM); Au,Ag, curcumin (0.30 μM) [**F**] ; $Aβ_{29-33p}$ (25 μM); Au,Ag,curcumin (0.15 μM) [**G**]; $Aβ_{29-33p}$ (50 μM); Au,Ag, curcumin (0.30 μM) [**H**]. ■ — [Ag: 4 nm]; — ♦ [Au: 4 nm]; — ♦ [curcumin].*

Nevertheless, for all Aβ peptides (Fig.3.7 and Fig.3.8), the addition of nps and curcumin resulted in a significant drop in ThT fluorescence at 10 s. The low ThT fluorescence (≈ < 5 a.u) was indicative of a low concentration of fibrils formed, relative to the fibrils already induced in the absence of nps and/or curcumin at 0 s (15-40 a.u). The result indicated that fibril formation was reversed by nps and curcumin. Increasing the concentration of nps and curcumin from 0.15 to 0.30 μM had a similar effect on reversing fibril formation (≈ < 5 a.u), indicating that that reversal of fibrils was not as concentration dependent as was the formation of fibrils at 0 s. Interestingly, in the cases of $Aβ_{29-33}$ (Fig.3.7F) and $Aβ_{33-37}$ (Fig.3.7H), a higher concentration (0.30 μM) of nps and curcumin seemed to completely reverse fibril formation as ThT fluorescence was found to decrease to ≈ 0 a.u.

Also, in most instances, in the presence of Ag nps at a concentration of 0.30 μM, the fluorescence was found to decrease to ≈ 1 a.u at 10 s (Fig.3.7B-J and Fig.3.8B-F). These results suggest that Ag may have an enhanced ability to reverse fibrils, compared to gold and curcumin. Also, the inhibitory function of silver nps is further compounded by the fact that silver has antibacterial properties and exhibits increased chemical activity due to its large surface to

volume ratios and crystallographic surface structure (Galdiero *et al*., 2011). The reversal effect by nps and curcumin for all Aβ peptides was found to level off after 10 s (Fig.3.7 and Fig.3.8). The maximum ThT fluorescence (15-20 a.u), from original $A\beta_{25-37}$ and $A\beta_{33-37}$ (Fig.3.7G-J) indicated that at either concentration of 25 μM or 50 μM, these peptides were sufficient in inducing fibrils at 0 s. The polar $A\beta_{17-21}$ and $A\beta_{29-33}$ peptides also produced a ThT fluorescence of 10 and 15 a.u, respectively at concentrations of 25 μM and 50 μM at 0 s (Fig.3.8C, D, G, H). It is clear from these results that the hydrophobicity of a sequence affects the amount of fibrils formed. For $A\beta_{17-21}$ and $A\beta_{25-37}$, the individual glycine zipper motifs: $A\beta_{29-33}$ and $A\beta_{33-37}$ which constituted the entire stretch was critical in aggregating together via their hydrophobic residues compared to the polar sequences which produced fibrils but at a lower amount at 0 s. Also, $A\beta_{25-29}$, the more polar of the glycine zippers surprisingly, produced a similar amount of fibrils to $A\beta_{33-37}$ (15-20 a.u). At time 0 s, at 25 μM and 50 μM, polar $A\beta_{25-29}$ produced a ThT fluorescence of 15 and 25 a.u, respectively (Fig.3.7C-D). At the same time it was evident that nps and curcumin reversed the fibrils formed from both polar and non-polar sequences indicating that amino acid sequence is important in fibril formation but does not influence the reversing of fibril formation.

3.4.3 Co-incubation of nNOS and nanoparticles: Effect of original Aβ peptides

When nNOS was incubated with either nps or curcumin, ThT fluorescence was at baseline for 1 min indicating that no fibrils formed from the co-incubated mixture (Fig.3.9 and Fig.3.10). When the original, polar and reversed Aβ peptides were added to the incubated mixture, there was a peak in ThT fluorescence at 0 s (10-40 a.u.), indicating the instantaneous production of fibrils (Fig.3.9 and Fig.3.10). For $A\beta_{17-21}$ and $A\beta_{29-33}$, at 0 s, the fibrils formed peaked to 30 and 40 a.u, respectively compared to the other Aβ peptides (Fig.3.9A, C). Fibril formation was thus influenced by the tighter binding affinity of these peptides to the enzyme. The reversed and polar forms showed a peak in ThT fluorescence between 10-15 a.u at 0 s (Fig.3.10A-D). Within 30 s, the fibrils formed from all Aβ peptides began to decrease and began to plateau from 30 to 40 s (Fig.3.9 and Fig.3.10). Nanoparticles and curcumin were reversing the formation of fibrils but

not completely preventing their formation. In addition, curcumin (purple line, Fig.3.9 and Fig.3.10) was shown to have a greater ability in reversing fibrils than nps (green line, Fig.3.9 and Fig.3.10).

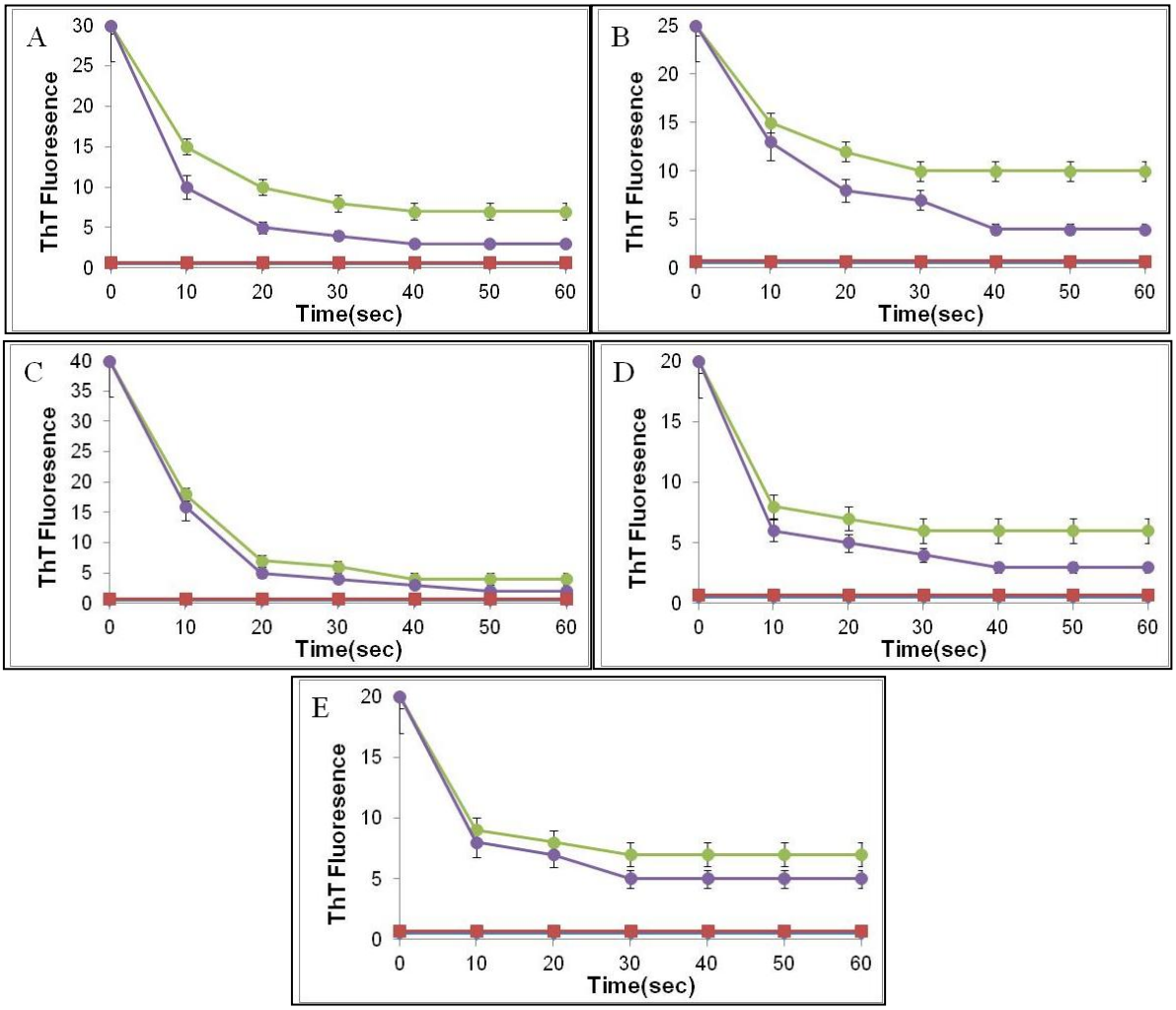

*Figure 3.9: Plots of ThT fluorescence of nps and/or curcumin (0.30 μM) co-incubated with nNOS (32 nM) treated with Aβ [50 μM] in a final volume (200μL) in Tris HCl buffer (pH 7.6, 100 mM) at 25 °C. Addition of: $Aβ_{17-21}$ [**A**]; $Aβ_{25-29}$ [**B**]; $Aβ_{29-33}$[**C**]; A_{33-37} [**D**]; $Aβ_{25-37}$[**E**]. — ■ [co-incubation of nNOS–np/curcumin]; — ● effect of Aβ on [nNOS-np]; — ● effect of Aβ on [nNOS-curcumin]*

3.4.4 Co-incubation of nNOS and nanoparticles: Effect of reversed and polar Aβ

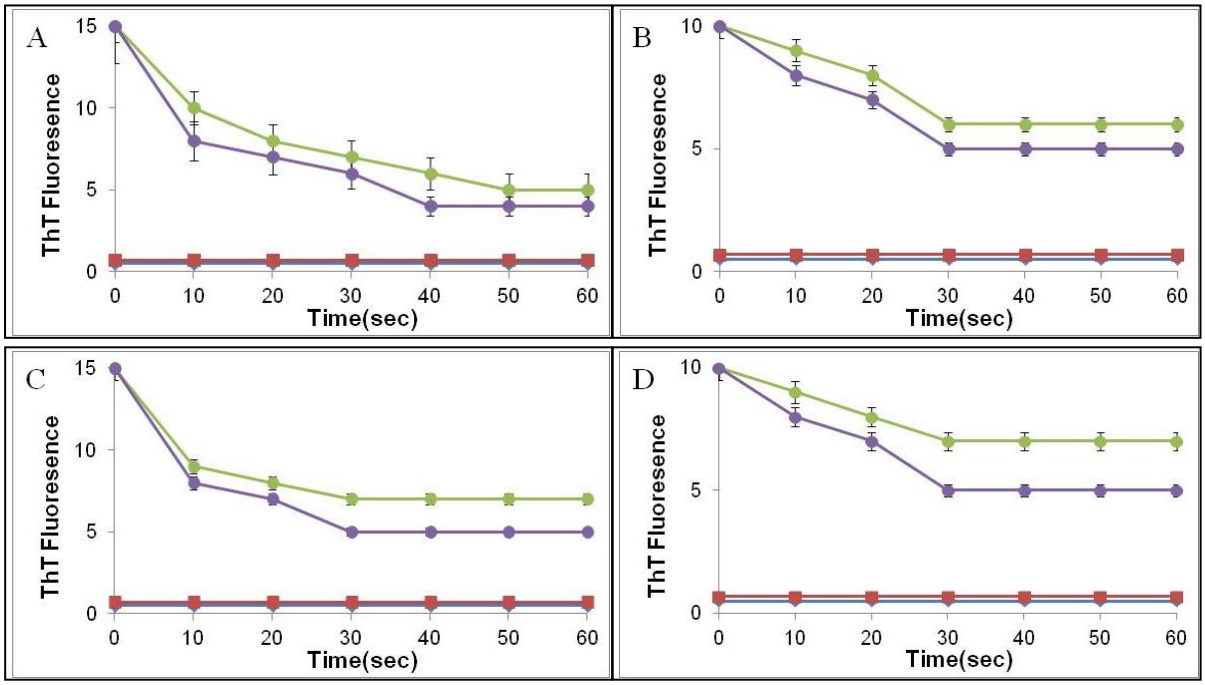

*Figure 3.10: Plots of ThT fluorescence of nps and/or curcumin (0.30 μM) co-incubated with nNOS (32 nM) treated with Aβ [50 μM] in a final volume (200μL) in Tris HCl buffer (pH 7.6, 100 mM) at 25 °C. Addition of: $Aβ_{17-21r}$ [**A**]; $Aβ_{17-21p}$ [**B**]; $Aβ_{29-33r}$ [**C**]; $Aβ_{29-33p}$ [**D**]. — ■ [co-incubation of nNOS–np/curcumin]; — ● effect of Aβ on [nNOS-np]; — ● effect of Aβ on [nNOS-curcumin]*

3.4.5 Co-incubation of original Aβ peptides and nanoparticles: Effect of nNOS

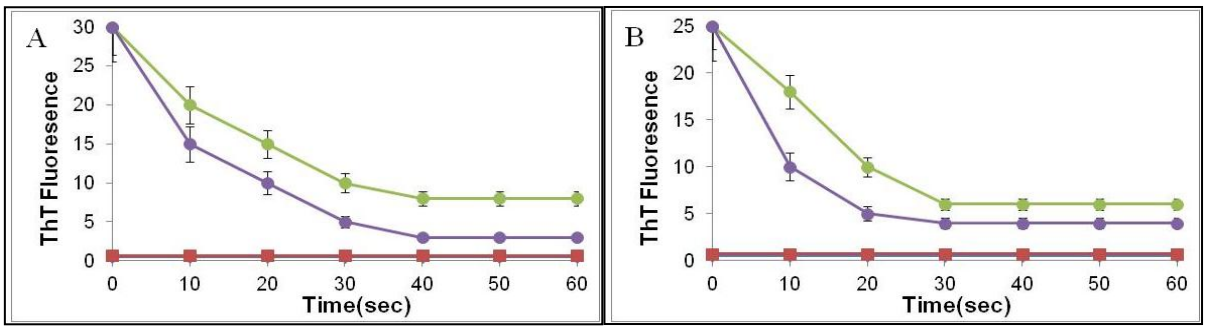

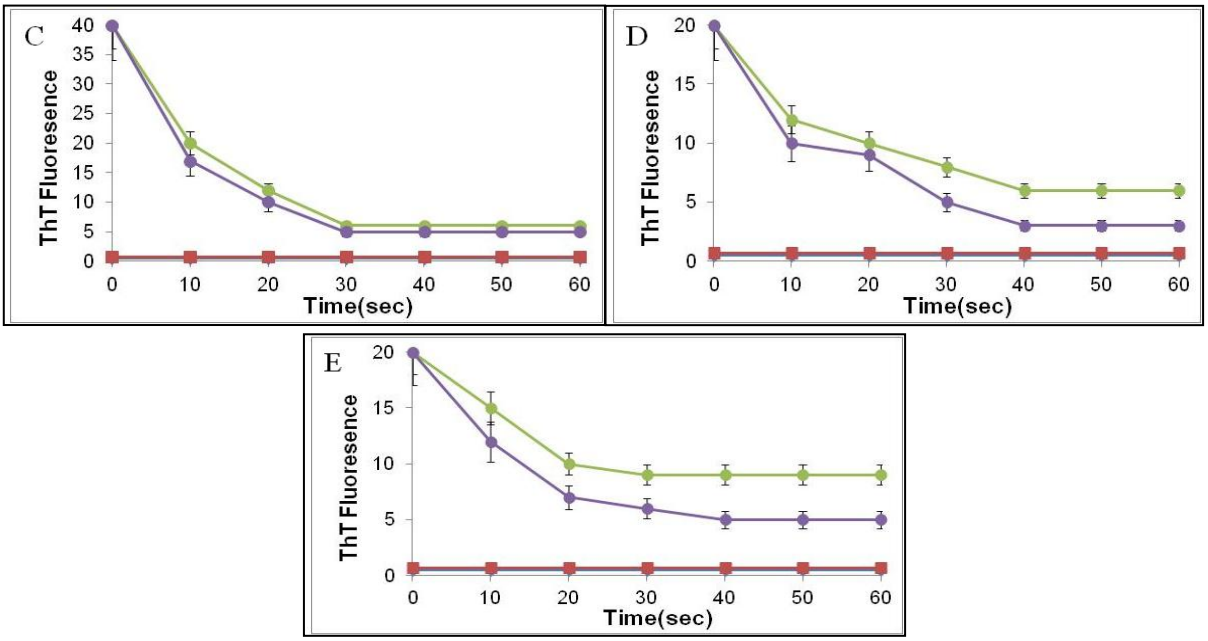

*Figure 3.11: Plots of ThT fluorescence of nps and/or curcumin (0.30 μM) co-incubated with Aβ (50 μM) treated with nNOS [32 nM] in a final volume (200μL) in Tris HCl buffer (pH 7.6, 100 mM) at 25 °C. In co-incubated solution: $Aβ_{17-21}$; Au,Ag,curcumin [**A**]; $Aβ_{25-29}$; Au,Ag,curcumin [**B**]; $Aβ_{29-33}$; Au,Ag,curcumin [**C**]; $Aβ_{33-37}$; Au,Ag,curcumin [**D**]; $Aβ_{25-37}$; Au, Ag, curcumin [**E**] — ■ [co-incubation of Aβ –np/curcumin]; — ● effect of nNOS on [Aβ-np]; —● effect of nNOS on [Aβ-curcumin]*

3.4.6 Co-incubation of reversed and polar Aβ peptides and nanoparticles: Effect of nNOS

The co-incubation of all Aβ peptides with either nps or curcumin also did not form fibrils as the ThT fluorescence was at baseline (Fig.3.11 and Fig.3.12). $Aβ_{17-21}$ and $Aβ_{29-33}$ once again formed a large amount of fibrils upon the addition of nNOS at 0 s, as ThT fluorescence peaked to 30 and 40 a.u, respectively (Fig.3.11A,C). Within 30 s, it was also evident that nps and curcumin reversed the formation fibrils but did not stop their formation, upon the addition of nNOS (Fig.3.11 and Fig 3.12). After 30 s, the formation of fibrils also reached a plateau like in previous results. Moreover, curcumin effectively dropped the ThT fluorescence for all Aβ peptides (purple line, Fig.3.11 and Fig.3.12) compared to nps (green line, Fig.3.11 and Fig.3.12). These results show that just like in the presence of Aβ, so too in the presence of nNOS, curcumin had a greater ability to reverse the formation of fibrils from these peptides than nps. More specifically,

curcumin had a far greater effect in reversing fibrils from $A\beta_{17-21}$, $A\beta_{29-33}$ and $A\beta_{33-37}$ (≤ 5.a.u) from 30 s to 60 s compared to its effect on the other peptides (Fig.3.11A, C, D). The pronounced effect of curcumin reversing fibrils (≤ 5.a.u) from 30 s to 60 s was also evident in the cases of the polar and reversed sequences (Fig.3.12A-D).

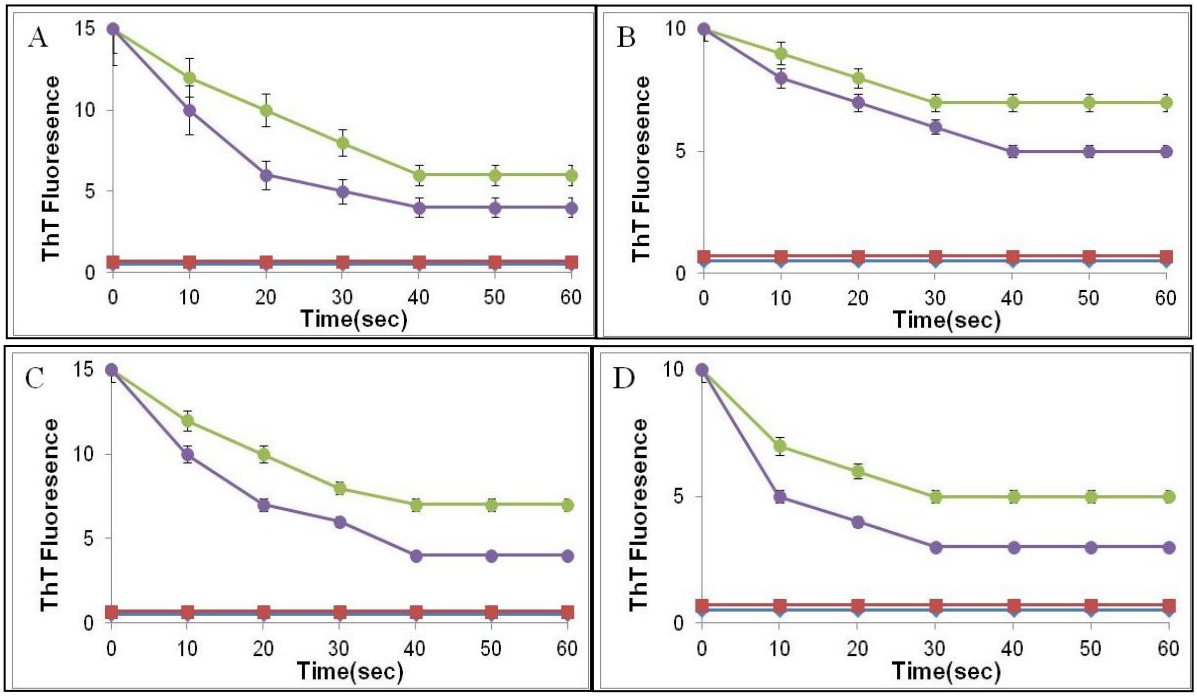

*Figure 3.12: Plots of ThT fluorescence of nps and/or curcumin (0.30 μM) co-incubated with Aβ (50 μM) treated with nNOS [32 nM] in a final volume (200μL) in Tris HCl buffer (pH 7.6, 100 mM) at 25 °C. In co-incubated solution: $A\beta_{17-21r}$; Au,Ag,curcumin [**A**]; $A\beta_{17-21p}$; Au,Ag,curcumin [**B**]; $A\beta_{29-33r}$; Au,Ag,curcumin [**C**]; $A\beta_{29-33p}$; Au,Ag,curcumin [**D**]; — ■ [co-incubation of Aβ –np/curcumin]; — ● effect of nNOS on [Aβ-np]; — ● effect of nNOS on [Aβ-curcumin]*

Our results, in the presence of either Aβ or nNOS have shown that curcumin had a far greater affinity to reverse fibrils formed from $A\beta_{17-21}$ peptide, compared to other Aβ peptides. Since Porat *et al*., 2006 has hypothesized that aromatic interactions may play a role in accelerating fibril formation, it is tempting to speculate that aromatic interaction between the two phenyl rings of $A\beta_{17-21}$ and the two polyphenol rings of curcumin is the mechanism by which fibrils are been reversed. This will be confirmed later in docking simulations (chapter 5). Also, the action of nps and curcumin in reversing fibrils from the hydrophobic $A\beta_{17-21}$, $A\beta_{29-33}$ and $A\beta_{33-37}$ point

to the hydrophobic interactions between np and/or curcumin with Aβ. This effect was minimal for the mixtures with polar sequences (Fig.3.12 B, D) as the decrease in ThT fluorescence was not as significant, especially for the polar $A\beta_{17-21}$ (Fig.3.12 B).

During the process of fibrillogenesis: three different kinetic phases are generally evident: lag, elongation (or growth), and the monomer-fibril equilibrium phase (Caflisch and Pellarin, 2006, Fig.3.4, pg.61). The existence of a rapid elongation/growth phase and an equilibrium phase in our fibrillogenesis graphs, pointed toward a nucleated-polymerization model for fibrillogenesis. The results (Fig.3.7 and Fig.3.8) have also shown that nNOS in the presence of Aβ catalyzed the formation of fibrils most probably through a nNOS-amyloid complex. The formation of such a complex is a valid phenomenon as there is evidence supporting the existence of enzyme-amyloid complexes in accelerating fibril formation. It was discovered for example, that acetylcholinesterase (AChE) was able to accelerate the assembly of Aβ into fibrils by decreasing the lag phase for aggregation and thus behaving as a chaperone for Aβ assembly into oligomers (Alvarez *et al*., 1998).

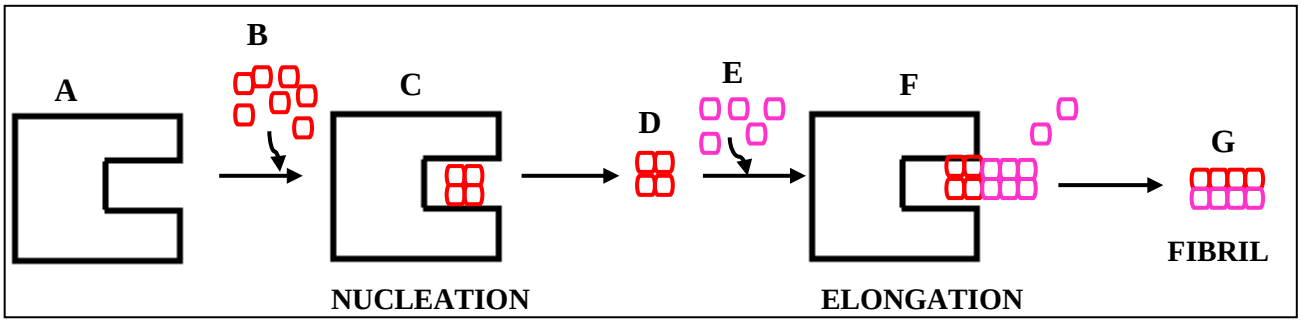

Figure 3.13: The behavior of nNOS as an amyloidogenic catalyst in driving nucleation and formation of seeds, leading to the elongation effect in fibrillogenesis

According to Fig.3.13, we propose a similar chaperone function for nNOS acting on Aβ assembly either by increasing the seeds necessary for the nucleation step or by stimulating fibril elongation. Firstly, free Aβ monomers (B) in solution bind to nNOS active site (A), resulting in nucleation leading to the aggregation of monomers (C). Thereafter, seed aggregates (E) derived from the existing pool of Aβ or when Aβ concentration exceeds the critical micelle concentration

(c*) becomes entrapped by nNOS (F) and added on to existing aggregated monomers, leading to the elongation effect and the subsequent formation of elongated fibrils (G).

In addition, according to results (Fig.3.7-Fig.3.12), just as fibrils were formed instantaneously so too did the effect of the nps and curcumin on the induced fibrils also occurred instantaneously within 30 s. According to Fig.3.14, the monomer was bound to the nanoparticle and thereby decreased the amount of monomer or oligomers in solution. Trapping of monomers or oligomers disturbed the monomer-oligomer equilibrium, affecting the nucleation step, eliminating the lag phase and reversing fibril formation. The absence of a lag phase as was shown by the ThT plots (Fig.3.7and Fig.3.8) could also be due to the existence of seed aggregates derived from the existing pool of soluble Aβ or when amyloid concentration exceeded the critical micelle concentration (c*). This is referred to as the seeding effect and is a phenomena which occurs when the rate of β-amyloid aggregation/ or Aβ fibril formation is elevated by the presence of prefibrillar species (Wetzel, 2006).

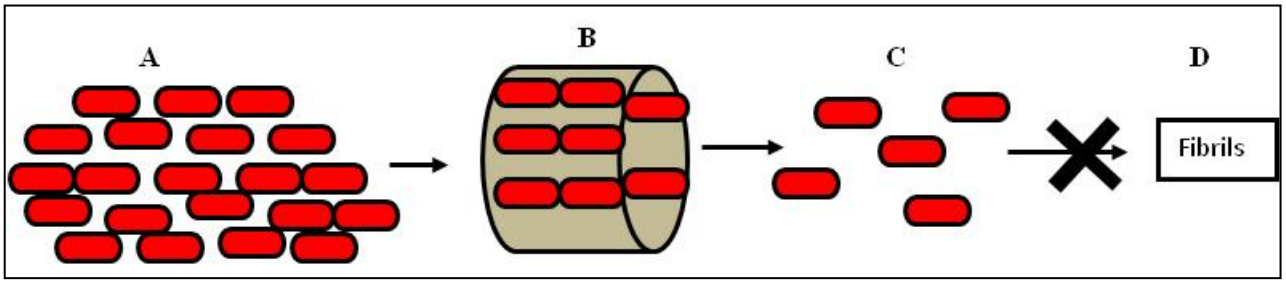

*Figure 3.14: Diagram illustrating monomer peptides in solution (**A**) getting trapped by a nanoparticle (**B**) which depletes amount of free monomer in solution (**C**) and prevents the fibril pathway from occurring (**D**)*

Remember too that nps are always covered by biological molecules *in vivo* according to the "corona effect" (Lynch and Dawson, 2008) creating a hydrophobic environment around the np such that the binding of peptides to np is stronger for a more hydrophobic surface. Infact it has been suggested that nps provide a more hydrophobic environment than water (Cabaleiro-Lago *et al*., 2008). As a result, increasing the hydrophobicity of the np reduced the lag time prior to aggregation. This could have occurred where the nps polarity was influenced by the hydrophobic

nature of the Aβ motifs surrounding them. Thus no lag time was observed as the depletion of monomeric peptide by the particles, prevented the formation of a critical nucleus in the initial association phase and hence prevented growth of fibril or elongation from occurring. In addition, binary adducts occur when the properties of the individual components of a system are largely conserved in the primary or intermediate crystalline phases of a two component (A and B) system (Herbstein, 1993). Based on this view, since fibril formation is based on a two component system, i.e. includes the interaction of nNOS and Aβ, it is interesting to consider the mechanism of how nps and curcumin reverse fibril formation based on the concept of binary adducts. According to Fig.3.15, a direct interaction between nNOS (A_1) and Aβ (B) (Fig. 3.15) could have lead to the formation of a binary adduct (A_1B), preceding the formation of the fibril. The addition of np and/or curcumin (A_2) (Fig. 3.15) to the binary adduct may have produced a "disrupting effect" as it broke apart the binary adduct such that it no longer existed in solution and was no longer reactive to ThT to fluorescence. Hence a decrease in ThT fluorescence was observed, in the presence of nps and/or curcumin.

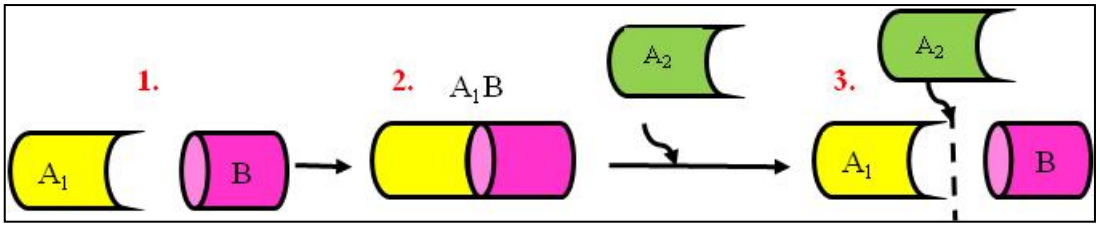

*Figure 3.15: Illustration depicting the "disrupting effect" of nps and/or curcumin on binary adducts nNOS (A_1) and Aβ (B) (**1**.) Binary adduct/complex (A_1B) (**2**.) the addition of np and/or curcumin (A_2) and its "disrupting effect" on the binary adduct/complex (**3**.)*

It has been documented that due to its radical termination nature, the generation of dimeric form of curcumin contributes to its antioxidant properties. Also the presence of dimeric species formed in aged curcumin solution enhanced inhibitory potency against fibril formation (Wang *et al*., 2009). In our studies, even though the effect of curcumin was still potent on reversing fibril formation, the reversal effect cannot be attributed to the presence of dimeric species, since the pre-incubation time was short (15 min). This proved that even in its non-dimer state, curcumin was still involved in a rapid, instantaneous reversal of fibril formation. It must also be noted that

the curcumin was included in a mixture of demethoxycurcumin and bis-demethoxycurcumin, also pointing to the potency of reversal on fibril formation by the combined effects of all three curcuminoids.

3.5 Conclusions

In general, the ThT fluorescent assay was successful in monitoring aggregation and disaggregation effects, which is crucial in gaining insight into the mechanism of fibrillogenesis. It was revealed that the function of nNOS to catalyze the formation of fibrils was dependent on the degree of binding affinity each peptide had for the enzyme. $A\beta_{17-21}$ and $A\beta_{29-33}$ were found to form the most fibrils due to their tightest binding affinity to nNOS (chapter 2). Also, it was evident that the hydrophobic nature of $A\beta_{17-21}$, the three glycine zipper peptides and $A\beta_{25-37}$ was a trigger in the formation of fibrils and thus was a force critical in the association of the peptides with the enzyme. It was also deduced that nNOS and Aβ are two species that are critical in the formation of fibrils, which is an instantaneous process. The role of nNOS was proposed to be a chaperone, involved in the entrapment of free monomers and seed aggregates to initiate the events of nucleation and elongation, critical for the formation of fibrils to occur. According to results, it was clear that nps and curcumin reversed fibril formation but did not inhibit or prevent their formation. The reversal of fibrils was not dependent on the amino acid sequence of the peptides as curcumin and nps reversed fibrils from both polar and non-polar forms of Aβ. Three mechanisms for the reversal effects by np and/or curcumin were proposed: (1) via depletion of free Aβ monomer in solution and blocking potential aggregation sites on the nNOS molecule due to large surface area of the np and aromatic interactions of the curcumin molecule, (2) via hydrophobic interaction between the Aβ peptide and np and/or curcumin (3) via the "disrupting effect" of nps and/or curcumin on the formation of binary adducts between Aβ and nNOS. These mechanisms, in light of reported findings (Wetzel *et al*., 2005, Cabaleiro-Lago *et al*., 2008, Wang *et al*.,2009, Lynch and Dawson, 2008) on the mechanism of fibrillogenesis from other proteins are valid deductions, but are yet to be proven as to which one is the favoured mechanism for nNOS catalyzed fibrillogenesis. Further insights into these mechanisms may be forthcoming

from a fluorimetric and thermodynamic analysis of the interaction between nNOS and Aβ, which is the subject of Chapter 4.

4 Interaction of Aβ peptides, nanoparticles (Ag/Au) and curcumin with nNOS: Spectrofluorimetry, thermodynamics and surface plasmon resonance

4.1 Introduction

The Ukrainian born physicist, Aleksander Jablonski described the history of a single fluorescence event by means of a Jablonski diagram (Fig.4.1) (Behlke *et al*., 2005).

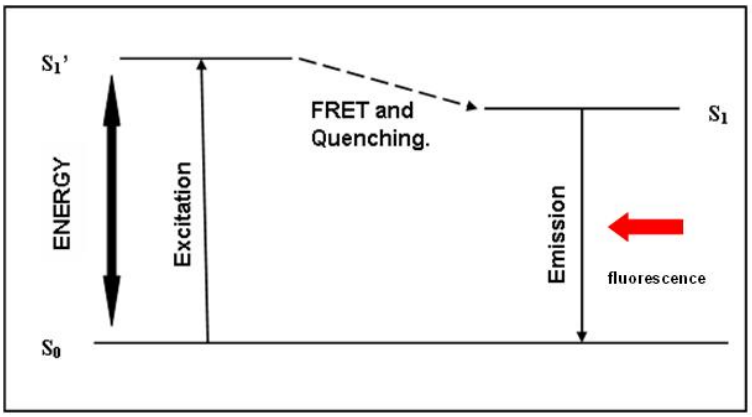

Figure 4.1: Jablonski diagram illustrating the processes of absorption (excitation) and fluorescence (emission) (Adapted from Behlke et al., 2005)

The fluorescent molecule begins in its ground energy state (S_0) and is converted to an excited singlet state (S_1') by absorbing energy of a specific wavelength. When the molecule releases the absorbed energy, it reverts to the relaxed singlet state (S_1). Thereafter, the molecule will return to its ground energy state by releasing the remaining energy. A single fluorescent event occurs within a few nanoseconds (Behlke *et al*., 2005). Fluorescence spectroscopy is a valuable and versatile method for studying the complex mechanisms of protein–small ligand interaction and a common fluorescent technique used is fluorescence quenching (Fink and Munishkina, 2007). The probability of fluorescence is described by the quantum yield (Q) which is the ratio of the number of photons emitted to the number of photons absorbed (unit of light) and a reduction in Q results in quenching (Freifelder, 1976). There are two types of quenchers, i.e. intrinsic

quenchers (usually aromatic rings within the protein itself) and extrinsic quenchers (added to the protein e.g., the quencher molecule fluorescein or Thioflavin T. For proteins, there are only three intrinsic quenchers, namely tryptophan, tyrosine and phenylalanine. Tryptophan (Trp) is commonly used in quenching as both phenylalanine and tyrosine have a very low Q (Freifelder, 1976). During the binding of a ligand, the sensitivity of the Trp fluorescence of a protein is either associated with a change in the absorption or emission spectrum. This change can be used as an observable in the determination of the association constants, binding modes and rate constants that describe the affinity of the ligand to the receptor (Fink and Munishkina, 2007). These constants provide insight into the conformational changes in either enzyme or ligand during binding which can assist in explaining the mechanism of AD in terms of protein folding and unfolding. More insight into these fluorescence constants associated with quenching will be discussed in the theory section of this chapter (section 4.2.1, pg. 90, 91). According to literature (Kang *et al*., 2011, Albanese *et al*., 2012), the fluorescence of a fluorophore can also be artificially altered by metal nanoparticles. In order to obtain a desired fluorescence, the metal type and size of the np as well as distance between the fluorophore and particle can be manipulated (Kang *et al*., 2011).

Fluorescence spectroscopy is a useful method for determining the interaction between a quencher, usually a small molecule and a protein. Stern-Volmer kinetics is used to calculate static and dynamic quenching constants as well as the number of binding sites available to the complex. These results provide insight into the structural changes and the microenvironment around the fluorophore in the protein (Crouse *et al*., 2011). In literature, the powerful tool of spectrofluorimetry has been used to investigate the binding of bovine serum albumin with various ligands like chloroamphenicol, flavanoids, antibiotic drugs and traditional Chinese medicine compounds such as berberine and puerarin (Liu 2010, 2012; Agudelo *et al*.,2012; Hu *et al*.,2010, He *et al*.,2008). Fluorescence quenching studies of curcumin by hydrogen peroxide has also been studied (Iwunze, 2004). Research within our group has also investigated the fluorescence quenching of nNOS by Aβ peptides (Padayachee and Whiteley, 2011; 2013).

Fluorescence quenching studies are, moreover significant as AD arises from conformational disorders involving the incorrect folding or clumping together of proteins (Soto, 2001). Literature has shown that protein misfolding is governed by forces that act on protein structure which influences its specific conformations (Soto, 2001; Ferreira and De Felice, 2001). One such force is the hydrophobic effect (Fig.4.2) which predicts the tendency of hydrophobic side chains to sequester themselves in the interior of a protein, away from contact with solvent, thus promoting aggregation affects significant to AD. Also, the folding of a protein is also dependent on the amino acid sequence laid out in the primary structure and the environment in which the folding occurs (Lynch and Dawson, 2008). The regions of interaction/binding in a protein are usually dominated by hydrophobic amino acids such as arginine, histidine, asparagine, tryptophan, tyrosine, serine and aromatic residues (Jones and Thornton, 1996; Stites, 1997).

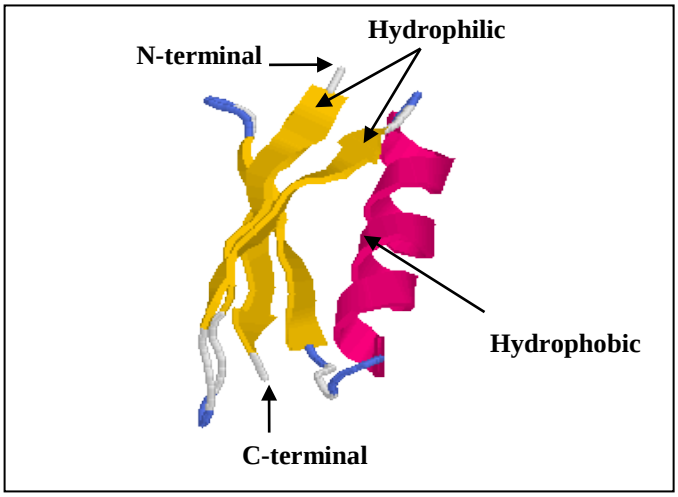

Figure 4.2: Secondary structure of an arbitrary protein depicted in cartoon and coloured structure (Taken from Lesk, 2001)

There are various theories that attempt to explain how exactly a protein undergoes folding. One such is the 'folding funnel theory', proposed by Wolynes *et al*., 1995 (Fig.4.3). As depicted (Fig.4.3), the width of the free energy funnel decreases as the protein molecule navigates, indicating a decrease in entropy. The entropy is minimum at the bottom of the funnel, thereby

reducing the number of conformations. The rate of folding is proportional to the slope of the folding funnel (Wolynes *et al*., 1995; Bryngelson *et al*., 1995).

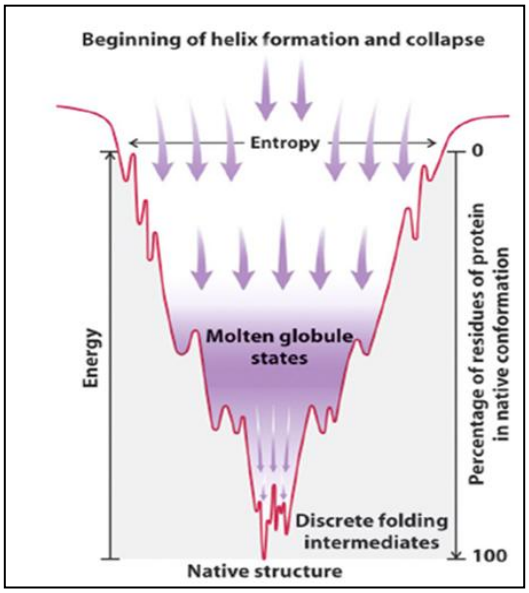

Figure 4.3: Diagram of a free energy funnel describing the folding of a protein to a stable 3-D structure, the width of the folding funnel represents entropy and the depth represents enthalpy (taken from Kavraki, 2006)

It is now widely accepted that that the 3-D structures of proteins are thermodynamically controlled and can be attained through the formation of intermediates (different configurations) which is kinetically governed (Yon, 1997). In view of this, thermodynamics of steady state and kinetic reactions can also be a further technique employed to understand the nature of bonds and the spontaneity of the reaction. Thermodynamics allows us to compare the stability of reactants and products and predict which compounds are favored by the equilibrium (Gummadi, 2003). Thermodynamic analysis is based on the magnitude and signs of the thermodynamic parameters, namely: enthalpy (ΔH), entropy (ΔS) and Gibbs energy (ΔG) and will be discussed in theory section of this chapter (section 4.2.2, pg.91) (Gummadi, 2003). These parameters provide insight into the mechanism of protein folding and unfolding. The enthalpies (ΔH) and entropies (ΔS) of unfolding are very temperature dependent because the heat capacity of the unfolded state is significantly greater than that of the folded state. The heat capacity difference probably results

from the temperature dependent ordering of water molecules around the non-polar portions of the protein molecules, more of which are solvent accessible in the unfolded state (Murphy *et al*.,1990). Literature has shown that temperatures at 300K-348K also induced unfolding characterized by a weakened protein core and loss of secondary structure (Gursky and Aleshkov, 2000; Kolinski *et al*., 1999; Ikeda *et al*., 2003).

There are two models of protein folding that are currently being confirmed. The first is the diffusion collision model, in which the formation of a nucleus precedes the formation of the secondary structure of the protein, and finally these secondary structures collide to form a tightly packed structure (Karplus and Weaver, 1976). The second is the nucleation-condensation model in which the secondary and tertiary structures of the protein are made at the same time (Fersht, 1995, 1997). Studies (Kiefhaber *et al*., 2011, Gianni *et al*., 2003) have shown that some proteins show characteristics of both of these folding models. Infact, three independent lines of evidence indicate that protein-folding rates and mechanisms are largely determined by a protein's topology rather than its inter-atomic interactions (Alm and Baker, 1999; Baker, 2000). The topology of a protein is influenced by the process of unfolding/folding and subsequent conformational changes. In view of this, four questions need to be answered (1) which conformation of the unfolded partner is recognized by the partner; (2) what is the role of the binding partner for folding and stability?; (3) do the interactions merely provide sufficient energy to shift the equilibrium towards the folded conformation or are interactions with the partner required to define the structure of the folded state?; (4) to what extent does the partner influence the folding process (Kiefhaber *et al*., 2011). Answers to these questions can provide insight in to the binding mechanism between ligands namely, Aβ peptides, nps and curcumin with the enzyme (nNOS). The objective of this chapter will be to determine the fluorescent and thermodynamic parameters namely; K_{sv}, K_a, K_d, n, ΔG, ΔH and ΔS for the ligand interaction (Aβ peptides, nps and curcumin) with nNOS at 298 K,303 K, 308 K and 313 K.

4.2 Theory of techniques utilized

4.2.1 Stern Volmer model

Fluorescence quenching is a process which decreases the intensity of the fluorescence emission (Eftink and Ghiron, 1981; Eftink, 1991). The quencher refers to the ligands which in our case represent Aβ or np or curcumin that interact with the fluorophore (e.g. Trp residues on nNOS) and which takes away or quenches the excited energy belonging to nNOS. The Stern Volmer relationship, named after Otto Stern and Max Volmer, (Stern and Volmer, 1919) allows an exploration of the kinetics of the fluorescent deactivation process. The first parameter studied is the Stern-Volmer constant (K_{sv}), also referred to as a quenching constant as it quantifies the efficiency of quenching and therefore the sensitivity of the quencher as well as provide information about the accessibility of the fluorophore (Eftink,1991). The classical Stern Volmer equation (Eq [8]) was used in the estimation of K_{sv}. Generally a greater K_{sv} means greater quenching and ease of accessibility to fluor molecules. In addition, the second parameter (θ) Eq [9] quantifies the number of fluorophores (e.g. Trp residues) near or on the surface of the enzyme and may be determined from Eq [9].

$$\mathbf{F_0/F = 1 + K_{sv}\,[q]} \qquad \textbf{….. Eq [8]}$$

where F_0 and F are, respectively, the fluorescence in the absence and presence of the quencher (q). [q] is the concentration of the quencher (Aβ, Au/Ag nps and/or curcumin) and K_{sv} is the Stern Volmer constant

$$\mathbf{F_0/\Delta F = 1/\theta\ K_{sv}[q] + 1/\theta} \qquad \textbf{….. Eq [9]}$$

where ΔF is change in fluorescence between quencher and fluorophore. The number of binding sites (n) on the purified enzyme, available for the binding of the ligands, and the association constant (K_a) and its reciprocal dissociation constant (K_d) were estimated from Eq [10]

$$\mathbf{Log\,[F_0\text{-}F]/F = Log\,K_a + n\ log\,[q]} \qquad \textbf{….. Eq [10]}$$

It has also been established that quenching can occur by different mechanisms like dynamic quenching and static quenching (Eftink and Ghiron, 1981; Eftink, 1991; Lakowicz, 2009). Dynamic quenching depends upon diffusion due to the collision between the excited state fluorophore and the quencher. The fluorophore loses energy and become de-excited (Eftink and Ghiron, 1981; Eftink, 1991; Lakowicz, 2009). In addition, higher temperatures results in larger diffusion coefficients so that the bimolecular quenching constants are expected to increase with increasing temperature (Xiao *et al*., 2008; Eftink, 1991; Eftink and Ghiron, 1981; Lakowicz, 2009). In contrast, in static quenching when K_{sv} is inversely correlated with temperature, the probable quenching mechanism is initiated by compound formation rather than dynamic collision i.e. K_{sv} decreases with an increase in temperature (Xiao *et al*., 2008; Eftink, 1991; Eftink and Ghiron, 1981; Lakowicz, 2009). Static quenching is due to the formation of a dark complex between the ground state fluorophore and the quencher, causing the fluorophore to behave as a non-fluorescent molecule (Eftink and Ghiron, 1981; Eftink, 1991; Lakowicz, 2009). The two mechanisms can be distinguished from each other, by the differing dependence on temperature on the Stern Volmer constant (K_{sv}) values (Xiao *et al*., 2008). Moreover a recent model, referred to as the Tachiya model (Xiao *et al*., 2008; Qin *et al*., 2010) was also used as an alternative to calculate the binding constants and parameters of Aβ, np and curcumin interaction with nNOS. Unfortunately the data obtained from the Tachiya model did not support the findings of the Stern Volmer model for reasons not established. Thus more insight and investigation into the use of this model for fluorescence quenching is required in order for it to validate the results obtained from the Stern Volmer model.

4.2.2 Thermodynamics

Immense research has been conducted on studying the free energy of association between ligands and receptors (Foloppe and Hubbard, 2006). The equilibrium constant depends exponentially on the free energy of change (ΔG) associated with the formation of complexes between ligand and receptor (Foloppe and Hubbard, 2006). Biological thermodynamics is defined by Eq [11] and the biological thermodynamics of a reaction is depicted in Fig.4.4. The

free energy change (ΔG) can be estimated from Eq [11], based on the binding constants (K_{sv}) at different temperatures.

$$\Delta G = \Delta H - T\Delta S \quad \text{..... Eq [11]}$$

Change in enthalpy (ΔH) during a chemical reaction is the heat absorbed or released in the breaking and formation of bonds and reflects changes in bonding (Masterton and Hurley, 2009; Whitten *et al*., 2007). These bonds include Van de Waals, hydrogen bonding and charge interactions. ΔH is also associated with the amount of heat evolved or consumed in the course of a reaction (Masterton and Hurley, 2009; Whitten *et al*., 2007). Negative values of ΔH are associated with exothermic reactions (energy release) while positive values are associated with an endothermic reaction (energy absorption). A negative ΔH leads to a negative ΔG and therefore, a spontaneous reaction while a positive ΔH is associated with a non-spontaneous reaction (Masterton and Hurley, 2009; Whitten *et al*., 2007).

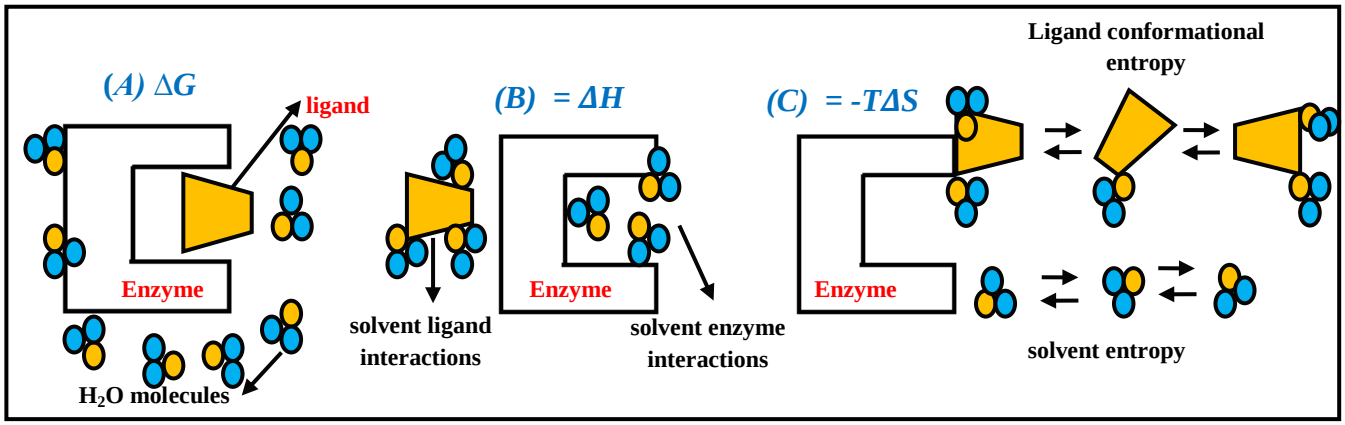

*Figure 4.4: Biological thermodynamics of a reaction include ΔG: ligand-enzyme interactions (**A**); ΔH: solvent-ligand and solvent-enzyme interactions (**B**); -TΔS: ligand and solvent entropy(**C**)*

According to the second law of thermodynamics, the total entropy of a system and its surroundings always increases for a spontaneous process and is associated with a tendency toward disorder (freedom of motion) in protein molecules (Marlow *et al*., 2010). The contributions by solvent entropy (ΔS) are usually framed in terms of the hydrophobic effect. In principle, the entropic contributions of a structured protein to the binding of a ligand ($\Delta S_{protein}$)

includes both changes in its internal conformational entropy (ΔS_{conf}) as well as changes in rotational and translational entropy (ΔS_{RT}) (Marlow *et al*.,2010). A positive ΔS occurs when products tend to have more freedom of motion than that of the reactants such that ΔG is negative and spontaneous. A negative ΔS occurs when products tend to have less freedom of motion than that of the reactants, such that ΔG is positive and non-spontaneous (Masterton and Hurley, 2009; Whitten *et al*., 2007). Reactions tend to favor products with the greatest entropy (Marlow *et al*., 2010). If the enthalpy change (ΔH) does not vary significantly in the temperature range studied, its value and that of entropy change (ΔS) can be calculated from the Van't Hoff Eq [12]:

$$\mathbf{\ln K_{sv} = - \Delta H/RT + \Delta S/R} \quad \textbf{….. Eq [12]}$$

where R is the gas constant (8.314 $J.mol^{-1}.K^{-1}$), T = 298 K, 303 K, 308 K and 313 K and K_{sv} is the Stern-Volmer constant.

4.2.3 Surface plasmon resonance (SPR) spectroscopy

The SPR method is used to measure real-time binding events between proteins and ligands and provides data for kinetic and thermodynamic characterization for protein-ligand interactions (Aguilar and Small, 2005; Myszka, 1997; Myszka *et al*., 1999). BIACORE is an example of a commercially available instrument which employs the method of SPR in analyzing many samples in a fast and convenient manner (Aguilar and Small, 2005). Recently, the ProteOn XPR 36 system was introduced as an alternative to the BIACORE instrumentation. The procedure allows for 6 x 6 injections in perpendicular directions providing reduced experimental time (Bronner *et al*., 2006). The principle of SPR is based on the immobilization of enzyme or peptide on the sensor surface. When the analyte is injected in a continuous flow, it adsorbs onto the immobilized ligand (Fig.4.5A). This leads to a change in adsorbed mass at the sensor surface which leads to a change in the incident angle (θ), and a consequent change in refractive index, which is recorded on the sensorgram (Fig.4.5B) (Cooper, 2002; Aguilar and Small., 2005). Nevertheless, before immobilization can occur, the chip is activated using amine coupling

reagents: of 1-ethyl-3-(3-dimethylaminopropyl) carbodiimide hydrochloride (EDAC) and N-hydroxysulfosuccinimide (sulfo-NHS).

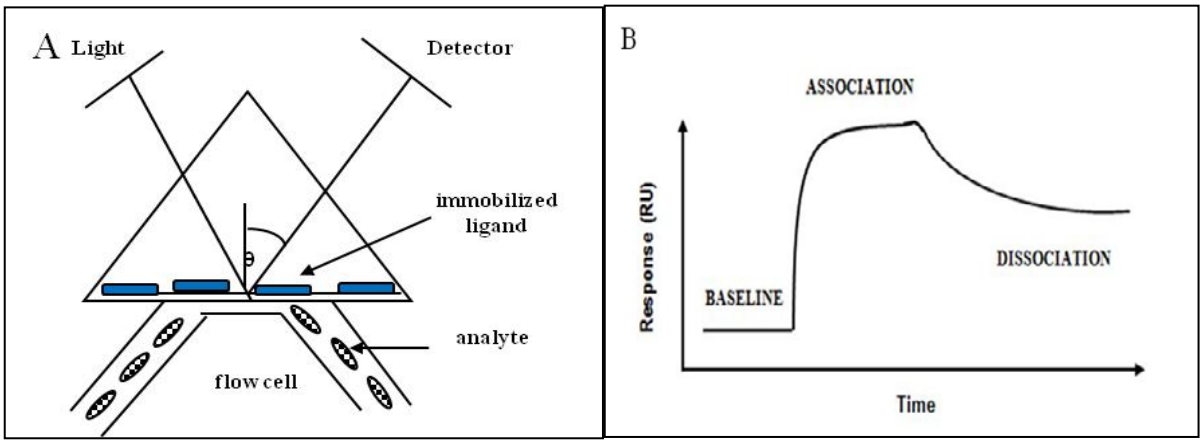

*Figure 4.5: Schematic representation of a BIACORE flow cell and detection, illustrating the incidence angle (θ) which changes during a binding process (**A**); A sensorgram characterized by three phases: baseline, association and dissociation (**B**)(Adapted from Aguilar and Small, 2005)*

These reagents form esters that interact with amine groups on the ligand to form stable, covalent amide bonds, ensuring that efficient coupling reactions occur (Bronner *et al*., 2006). Following immobilization of the ligand, any remaining activated carboxylic groups on the chip surface are deactivated with 1M ethanolamine hydrochloride which removes any remaining electrostatically bound proteins (Bronner *et al*., 2006). What makes SPR particularly advantageous is that, fibril growth can be monitored over a shorter time frame (3 s to 30 min) (Cannon *et al*., 2004). Also due to the biosensors continuous flow system, the concentration of Aβ monomer injected can be maintained at a constant rate and concentration so that fibrils can grow consistently (Cannon *et al*., 2004).

Within the past decade, there has been a wide variety of literature on the use of SPR in monitoring aggregation events involving amyloid peptides and usually the peptides tested were found to inhibit aggregation (Cairo *et al*., 2002; Hasegawa *et al*., 2002; Cannon *et al*., 2004). In these cases either Aβ fibrils were prepared and immobilized on the sensor chip and interacted with Aβ monomers. For example, it was found that $A\beta_{16\text{-}20}$ was the shortest Aβ fragment to bind

to $A\beta_{1-40}$ and SPR was used to confirm the nature of interaction between this peptide and Aβ (Tjernberg *et al*., 1996; Aguilar and Small, 2005). Myszka and colleagues further developed an SPR-based assay for fibril formation, with response data that fitted a three-step polymerization model (Cannon *et al*., 2004). In this regard, SPR was used to extract kinetic data from the association and dissociation phases of the peptide during fibril formation (Cannon *et al*., 2004).

In a recent study, SPR was used to monitor the conformational change of immobilized Aβ upon exposure to Cu^{2+} and Zn^{2+} ions contained in buffer solution. A difference in metal binding affinity between $A\beta_{1–28}$ and $A\beta_{1–42}$ was detected, suggesting that SPR is a novel method to characterize the interactions between Aβ and metal ions (Yao *et al*., 2012). In addition, two studies have been found in literature where SPR was used to measure enzyme-protein interactions. For example a study was conducted whereby the binding affinity of biotinylated peptide ligands (SERG and GEKD) to an enzyme called quinoprotein glucose dehydrogenase (PQQGDH) was measured (Yagi *et al*., 2007). A more recent study used the SPR biosensor to investigate the proteolytic action of trypsin against four proteins i.e. lactate dehyrogenase, gelatin, poly l lysine and bovine serum albumin (Syed *et al*., 2011). To date, there are no studies on nNOS-Aβ interaction or Aβ interaction with enzymes in general. Hence, for the purposes of this study, SPR was used as an alternative to fluorescence spectroscopy to provide insight into nNOS-Aβ interaction in real time.

4.3 Materials and Methods

4.3.1 Materials

Materials were used as described in Chapter 2, 2.3.1, pg. 35. Triethanolamine/HCl was purchased from Sigma Aldrich. All reagents were of analytical grade and all solutions were prepared with deionized water obtained from a Milli-Q system. Fluorimetry analyses were carried out on PowerWave microplate spectrofluorimeter (Bio-Tek Instruments) with 96 well plates, operated at 1 nm bandwidth using the KC Junior software program.

4.3.2 Methods

4.3.2.1 Isolation of curcuminoids from turmeric

As described in Chapter 2, 2.3.2.5, pg. 38.

4.3.2.2 Synthesis and characterization of Ag/Au nanoparticles

As described in Chapter 2, 2.3.2.6, pg. 38. Since nps were encased in HSAF, apoferritin controls (5-40 μM) were prepared.

4.3.2.3 Fluorescent quenching and thermodynamic analysis at different temperatures

Intrinsic protein fluorescence of nNOS was measured according to our published procedure (Padayachee *et al*., 2011; Padayachee and Whiteley, 2011; 2013). Excitation wavelength of 290 nm with an excitation slit of ± 1.5 nm and an emission of 338 nm with an emission slit of ± 5 nm was used. The peptides [$A\beta_{17\text{-}21}$, $A\beta_{25\text{-}29}$, $A\beta_{29\text{-}33}$, $A\beta_{33\text{-}37}$, $A\beta_{25\text{-}37}$, $A\beta_{17\text{-}21r}$, $A\beta_{29\text{-}33r}$, $A\beta_{17\text{-}21p}$ and $A\beta_{29\text{-}33p}$], Au/Ag nps (4 nm) and the curcuminoid solution (5-40 μM) were incubated with nNOS (5 μl) in triethanolamine/HCl buffer (10 mM, pH 7.4) containing NaCl (0.1 M) in a final volume of (200 μl) for 5 min to allow sufficient time for ligand-protein interaction. Each incubation was performed at four different temperatures: 25°C [298 K]; 30°C [303 K]; 35°C [308 K]; 40°C [313 K]. All values represented the mean (± S.E.M.) of three trials.

4.3.2.4 Surface plasmon resonance (SPR)

Surface plasmon spectroscopy was performed on a ProteOn XPR36 instrument (Bio-Rad) at 25°C using PBS (pH 7.4) as a running buffer. Briefly, a GLH sensor chip, ideal for protein-small molecule interactions (> 20 kRU) was preconditioned with successive 30 μl pulses of 0.5 % SDS, 50 mM NaOH, 100 mM HCl and 300 mM EDTA (pH 8.5) in both horizontal and vertical directions. Prior to ligand immobilization, the surface of the chip was activated by standard amine coupling procedure described in 4.2.3; pg.93, 94. Rat brain nNOS (Sigma Aldrich) was then immobilized at varying concentrations (5 μg/ml, 10 μg/ml, 25 μg/ml, 50 μg/ml and 100 μg/ml) in the vertical channels L1–L6 at 25 μl/min, and the chip was subsequently stabilized through injection of 30 μl of the running buffer at 100 μl/min (Fig.4.6). The amyloid peptides:

$A\beta_{25-37}$, $A\beta_{33-37}$, $A\beta_{29-33}$ and $A\beta_{1-40}$ (100 µM) were dissolved in PBS/5 % DMSO buffer and then injected, across ligand channels at 30 µl/min for 60 s association and 300 s dissociation periods (Fig.4.6). These were the only peptides which produced a less turbid solution in the above mentioned buffer system, compared to the other peptides. Buffer blanks without Aβ were used as controls and channel L6 contained blank buffer which was a negative control for nNOS. The chip was regenerated using 1 M NaCl (30 µl, 100 µl/min). Data was collected, analyzed and the interaction displayed in real-time by ProteOn Manager™.4.3

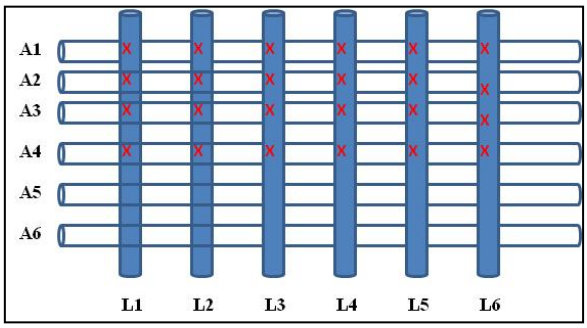

Figure 4.6: Diagram of SPR sensor chip surface depicting 6 vertical ligand channels (L1-L6) and 6 horizontal analyte channels (A1-A6). L1-L5 contained nNOS immobilized at concentrations (5 µg/ml, 10 µg/ml, 25 µg/ml, 50 µg/ml and 100 µg/ml). L6 was the blank channel. A1-A4 contained $A\beta_{25-37}$, $A\beta_{33-37}$, $A\beta_{29-33}$ and $A\beta_{1-40}$ (100 µM). Each analyte (Aβ) passed through a unique detection point (x) at each intersection point.

4.3.2.5 Statistical analyses

All experiments were carried out in triplicate. Mean and standard deviation calculations and comparison of data using analysis of variance (ANOVA) was performed to 5 % level of significance ($p < 0.05$) using Statistica for Windows, version 8 (Statsoft Inc.) and Microsoft Excel 2010.

4.4 Results and discussion

4.4.1 Spectrofluorimetry and thermodynamics

The quenching of nNOS fluorescence and thermodynamic analysis by the various Aβ-peptides, nps (Ag/Au) and curcumin with nNOS was analyzed by Stern Volmer and Van't Hoff plots.

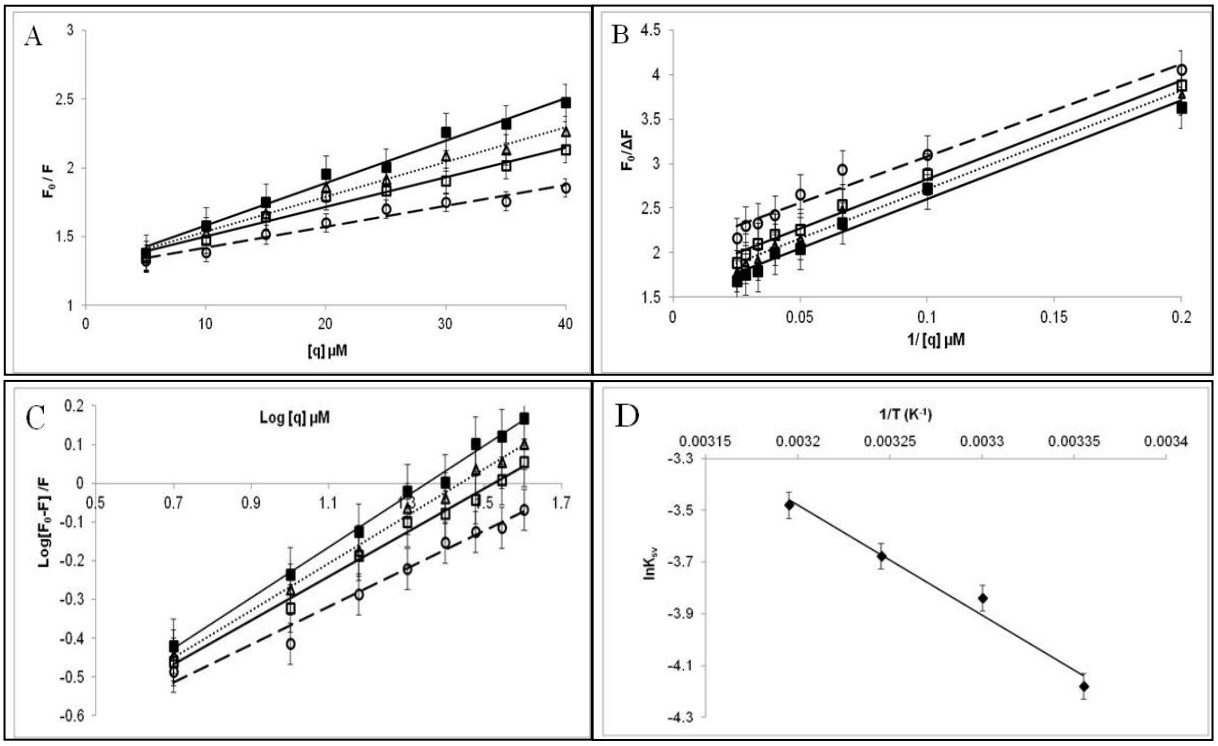

*Figure 4.7: Stern–Volmer plot [**A**]; modified Stern –Volmer plot [**B**]; Hill plot of log [(F_0-F)/F] versus log [q] [**C**]; Van't Hoff plot [**D**] for fluorescence quenching of nNOS (5µl) in triethanolamine HCl buffer (pH 7.4, 10mM) treated with* ***Aβ*** $_{17-21}$ *(5-40 µM) in a final volume (200µL) at different temperatures – – – ○ [298 K]; —□ [303 K]; ... Δ [308 K]; —■ [313 K] .λ_{ex} = 290 nm and λ_{em} = 338 nm*

Table 4.1: Values for fluorescent parameters (K_{sv} [μM^{-1}], K_a [μM^{-1}],K_d [µM],θ and n) and thermodynamic parameters ΔH [kJ.mol^{-1}.K^{-1}]; ΔS [J.mol^{-1}.K^{-1} and ΔG [kJ.mol^{-1}.K^{-1}] for the interaction of $Aβ_{17-21}$ with nNOS at various temperatures.

K	ΔH	ΔS	ΔG	K_{sv}	K_d	K_a	θ	n
298	58	158	9.9	1.5 x10^{-2}	6.0	0.17	0.5	1
303			9.5	1.9 x10-2	6.2	0.16	0.5	1
308			9.1	3.1 x10^{-2}	7.8	0.13	0.7	1
313			8.7	5.1 x10^{-2}	9.8	0.10	0.7	1

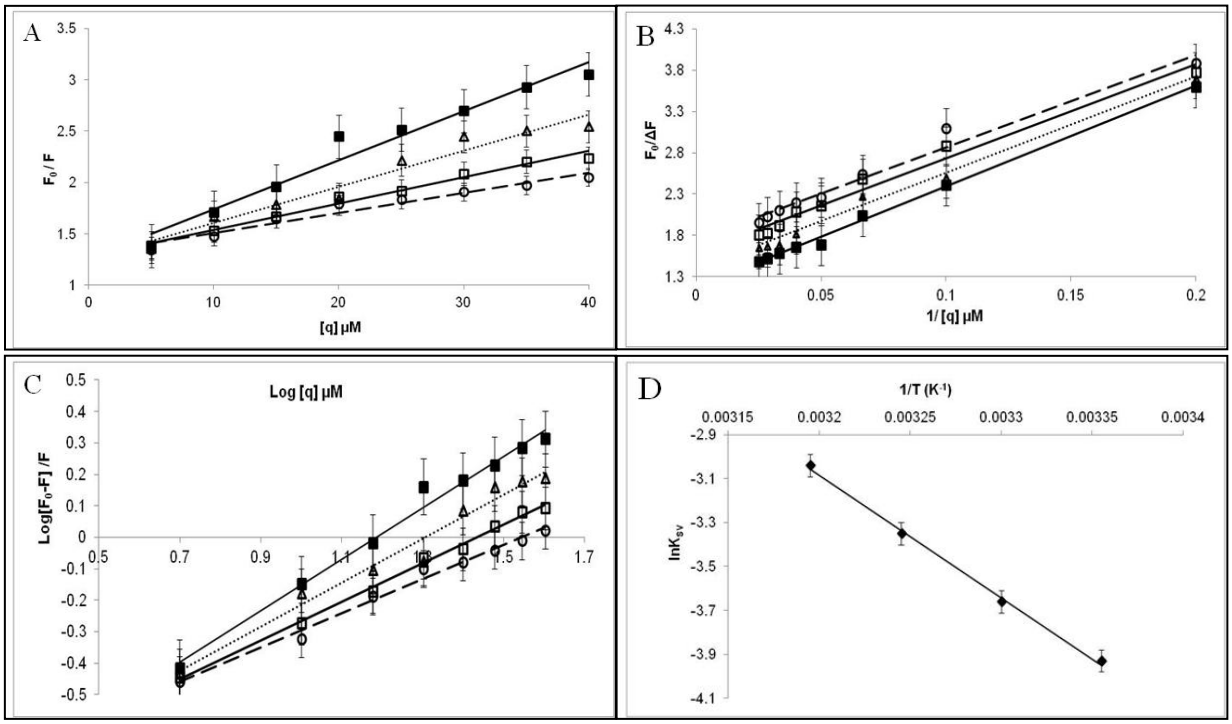

*Figure 4.8: Stern–Volmer plot [**A**]; modified Stern –Volmer plot [**B**]; Hill plot of log [(F_0-F)/F] versus log [q] [**C**]; Van't Hoff plot [**D**] for fluorescence quenching of nNOS (5µl) in triethanolamine HCl buffer (pH 7.4, 10mM) treated with **$A\beta_{25-29}$** (5-40 µM) in a final volume (200µL) at different temperatures – – – ○ [298 K]; —□ [303 K]; ... Δ [308 K]; —■ [313 K] .λ_{ex} = 290 nm and λ_{em} = 338 nm*

Table 4.2: Values for fluorescent parameters (K_{sv} [μM^{-1}], K_a [μM^{-1}],K_d [μM],θ and n) and thermodynamic parameters ΔH [kJ.mol^{-1}.K^{-1}]; ΔS [J.mol^{-1}.K^{-1}] and ΔG [kJ.mol^{-1}.K^{-1}] for the interaction of $A\beta_{25-29}$ with nNOS at various temperatures.

K	ΔH	ΔS	ΔG	K_{sv}	K_d	K_a	θ	n
298	41	105	13	1.8 x10^{-2}	6.9	0.14	0.5	1
303			12	2.3 x10^{-2}	7.8	0.13	0.6	1
308			11	2.8 x10^{-2}	8.3	0.12	0.6	1
313			9.5	4.1 x10^{-2}	9.4	0.11	0.7	1

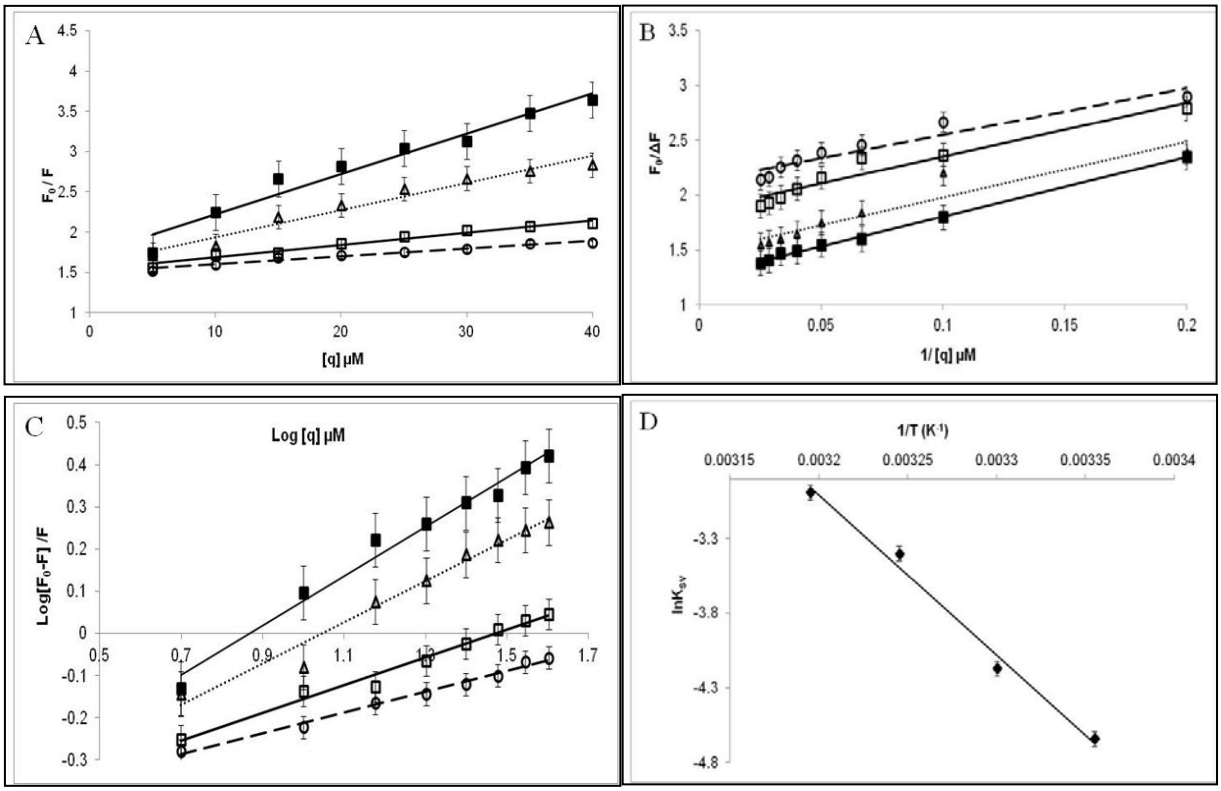

*Figure 4.9: Stern–Volmer plot [**A**]; modified Stern –Volmer plot [**B**]; Hill plot of log [(F_0-F)/F] versus log [q] [**C**]; Van't Hoff plot [**D**] for fluorescence quenching of nNOS (5µl) in triethanolamine HCl buffer (pH 7.4, 10mM) treated with **$A\beta_{29-33}$** (5-40 µM) in a final volume (200µL) at different temperatures – – – ○ [298 K]; —□ [303 K]; ... Δ [308 K]; —■ [313 K] .λ_{ex} = 290 nm and λ_{em} = 338 nm*

Table 4.3: Values for fluorescent parameters (K_{sv} [μM^{-1}], K_a [μM^{-1}],K_d [µM],θ and n) and thermodynamic parameters ΔH [kJ.mol^{-1}.K^{-1}]; ΔS [J.mol^{-1}.K^{-1}] and ΔG [kJ.mol^{-1}.K^{-1}] for the interaction of $A\beta_{29-33}$ with nNOS at various temperatures.

K	ΔH	ΔS	ΔG	K_{sv}	K_d	K_a	θ	n
298	78	220	12	9×10^{-3}	2.7	0.37	0.4	1
303			11	1.1×10^{-2}	2.8	0.36	0.4	1
308			10	1.8×10^{-2}	3.0	0.33	0.5	1
313			9.5	4.1×10^{-2}	3.3	0.30	0.6	1

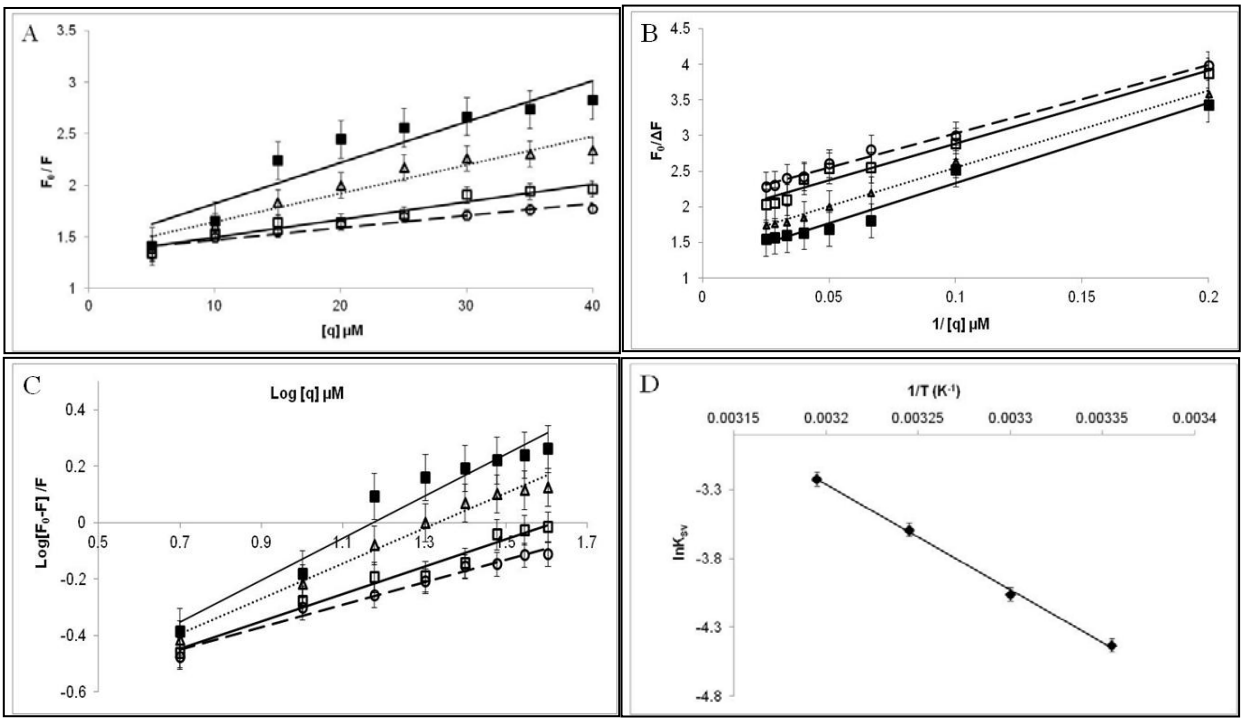

*Figure 4.10: Stern–Volmer plot [**A**]; modified Stern –Volmer plot [**B**]; Hill plot of log [(F_0-F)/F] versus log [q] [**C**]; Van't Hoff plot [**D**] for fluorescence quenching of nNOS (5µl) in triethanolamine HCl buffer (pH 7.4, 10mM) treated with **$Aβ_{33-37}$** (5-40 µM) in a final volume (200µL) at different temperatures – – – ○ [298 K]; —□ [303 K]; ... Δ [308 K]; —■ [313 K] .λ_{ex} = 290 nm and λ_{em} = 338 nm*

Table 4.4: Values for fluorescent parameters (K_{sv} [μM^{-1}], K_a [μM^{-1}],K_d [μM],θ and n) and thermodynamic parameters ΔH [kJ.mol^{-1}.K^{-1}]; ΔS [J.mol^{-1}.K^{-1}] and ΔG [kJ.mol^{-1}.K^{-1}] for the interaction of $Aβ_{33-37}$ with nNOS at various temperatures.

K	ΔH	ΔS	ΔG	K_{sv}	K_d	K_a	θ	n
298	59	158	11	1.1 x10^{-2}	5.4	0.19	0.4	1
303			11	1.5 x10^{-2}	5.6	0.18	0.4	1
308			10	1.9 x10^{-2}	6.1	0.16	0.5	1
313			9.9	3.6 x10^{-2}	7.7	0.13	0.6	1

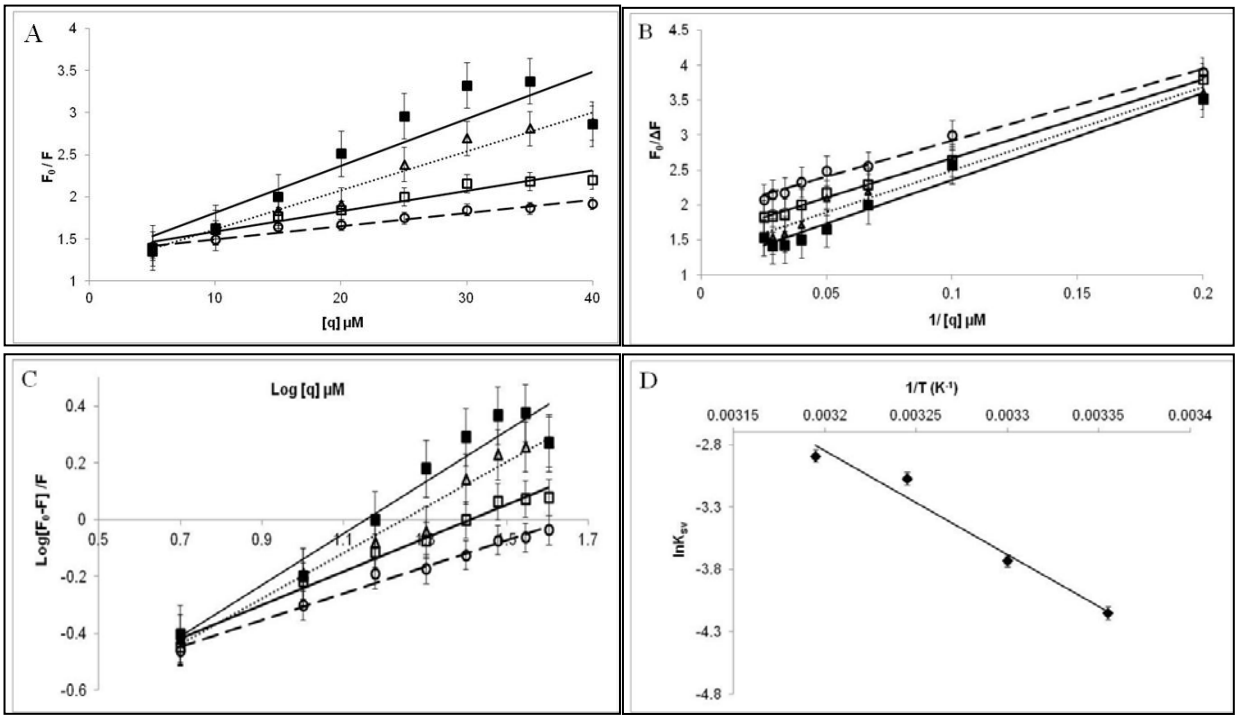

*Figure 4.11: Stern–Volmer plot [**A**]; modified Stern –Volmer plot [**B**]; Hill plot of log [(F_0-F)/F] versus log [q] [**C**]; Van't Hoff plot [**D**] for fluorescence quenching of nNOS (5µl) in triethanolamine HCl buffer (pH 7.4, 10mM) treated with **$Aβ_{25-37}$** (5-40 µM) in a final volume (200µL) at different temperatures – – – ○ [298 K]; —□ [303 K]; ... Δ [308 K]; —■ [313 K] .λ_{ex} = 290 nm and λ_{em} = 338 nm*

Table 4.5: Values for fluorescent parameters (K_{sv} [μM^{-1}], K_a [μM^{-1}],K_d [μM],θ and n) and thermodynamic parameters ΔH [kJ.mol^{-1}.K^{-1}]; ΔS [J.mol^{-1}.K^{-1}] and ΔG [kJ.mol^{-1}.K^{-1}] for the interaction of $Aβ_{25-37}$ with nNOS at various temperatures.

K	ΔH	ΔS	ΔG	K_{sv}	K_d	K_a	θ	n
298	58	158	11	1.4 x10^{-2}	5.5	0.18	0.4	1
303			9.9	1.9 x10^{-2}	6.2	0.16	0.5	1
308			9.1	3.1 x10^{-2}	7.4	0.14	0.7	1
313			8.4	4.1 x10^{-2}	8.7	0.11	0.7	1

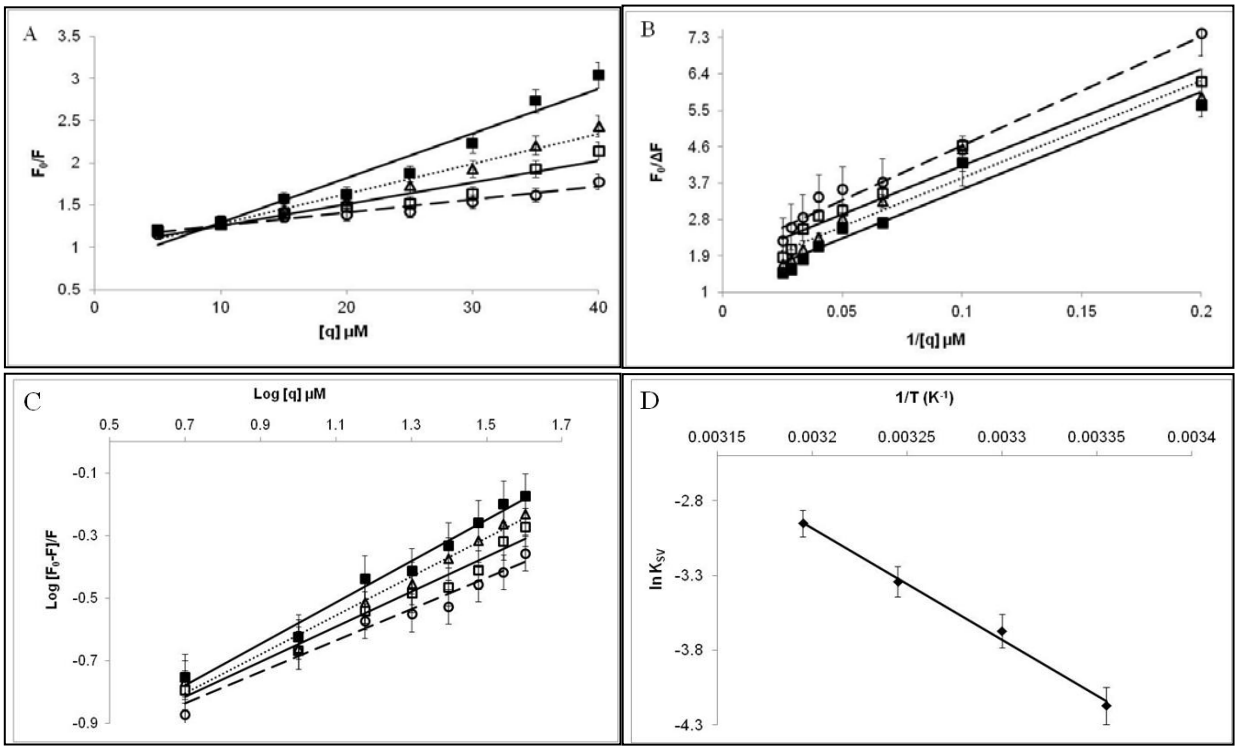

*Figure 4.12: Stern–Volmer plot [**A**]; modified Stern –Volmer plot [**B**]; Hill plot of log [$(F_0$-F)/F] versus log [q] [**C**]; Van't Hoff plot [**D**] for fluorescence quenching of nNOS (5μl) in triethanolamine HCl buffer (pH 7.4, 10mM) treated with **$A\beta_{17\text{-}21r}$** (5-40 μM) in a final volume (200μL) at different temperatures – – – ○ [298 K]; —□ [303 K]; … Δ [308 K]; —■ [313 K] .λ_{ex} = 290 nm and λ_{em} = 338 nm*

Table 4.6: Values for fluorescent parameters (K_{sv} [μM^{-1}], K_a [μM^{-1}],K_d [μM],θ and n) and thermodynamic parameters ΔH [kJ.mol^{-1}.K^{-1}]; ΔS [J.mol^{-1}.K^{-1}] and ΔG [kJ.mol^{-1}.K^{-1}] for the interaction of $A\beta_{17\text{-}21r}$ with nNOS at various temperatures.

K	ΔH	ΔS	ΔG	K_{sv}	K_d	K_a	θ	n
298	62	174	10	1.5 x10^{-2}	15	6.7 x10^{-2}	1	1
303			9.3	2.5 x10^{-2}	16	6.3 x10^{-2}	1	1
308			8.4	3.5 x10^{-2}	17	5.9 x10^{-2}	1	1
313			7.5	5.2 x10^{-2}	17	5.9 x10^{-2}	1	1

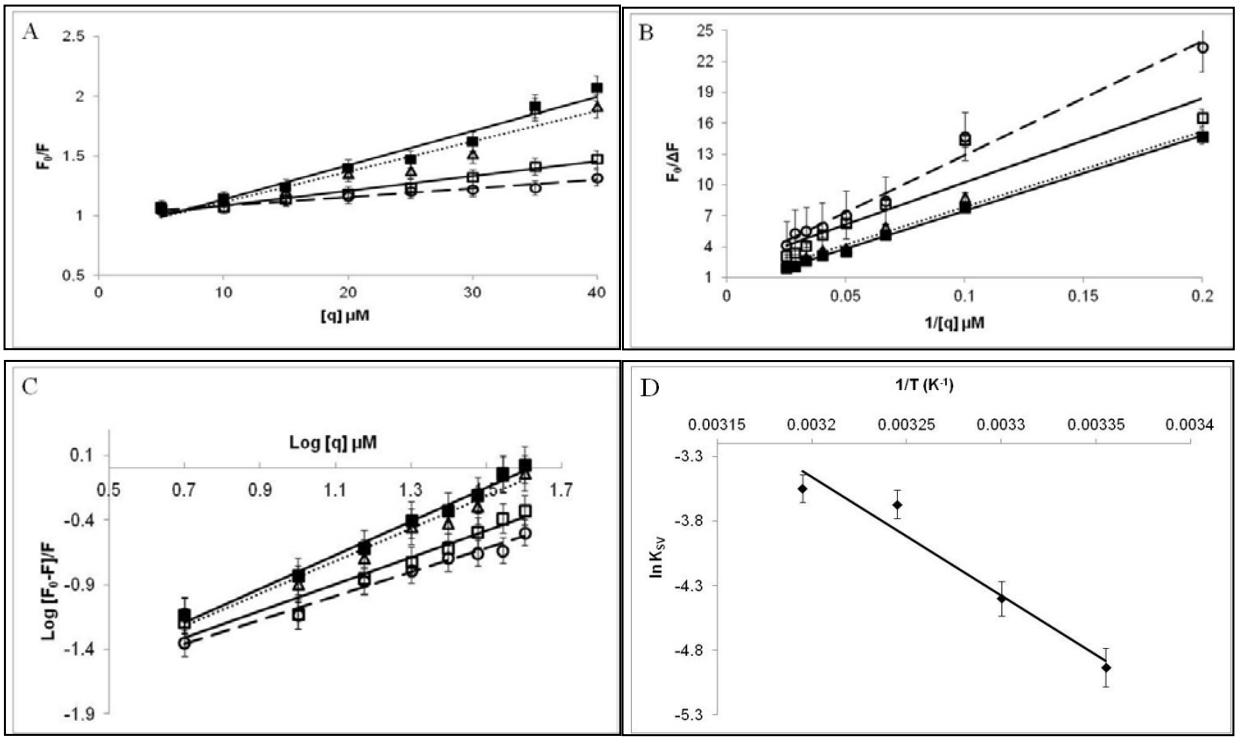

*Figure 4.13: Stern–Volmer plot [**A**]; modified Stern –Volmer plot [**B**]; Hill plot of log [(F_0-F)/F] versus log [q] [**C**]; Van't Hoff plot [**D**] for fluorescence quenching of nNOS (5µl) in triethanolamine HCl buffer (pH 7.4, 10mM) treated with **$Aβ_{17-21p}$** (5-40 µM) in a final volume (200µL) at different temperatures – – – ○ [298 K]; —□ [303 K]; … Δ [308 K]; —■ [313 K] .$λ_{ex}$ = 290 nm and $λ_{em}$ = 338 nm*

Table 4.7: Values for fluorescent parameters (K_{sv} [$µM^{-1}$], K_a [$µM^{-1}$],K_d [µM],θ and n) and thermodynamic parameters ΔH [$kJ.mol^{-1}.K^{-1}$]; ΔS [$J.mol^{-1}.K^{-1}$] and ΔG [$kJ.mol^{-1}.K^{-1}$] for the interaction of $Aβ_{17-21p}$ with nNOS at various temperatures.

K	ΔH	ΔS	ΔG	K_{sv}	K_d	K_a	θ	n
298	76	215	12	7.2×10^{-3}	101	9.9×10^{-3}	1	1
303			11	1.2×10^{-2}	108	9.3×10^{-3}	1	1
308			9.8	2.5×10^{-2}	125	8.0×10^{-3}	2	1
313			8.7	2.9×10^{-2}	126	7.9×10^{-3}	5	1

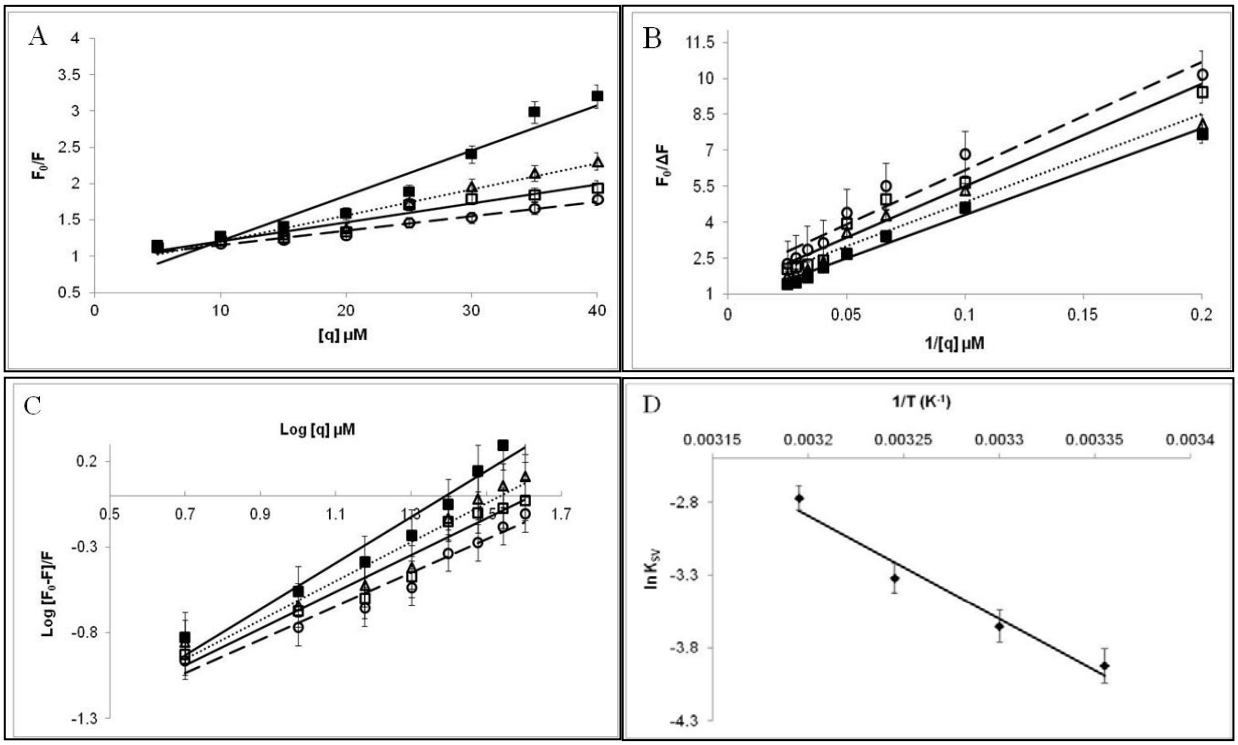

Figure 4.14: Stern–Volmer plot [A]; modified Stern –Volmer plot[B]; Hill plot of log [(F_0-F)/F] versus log [q] [C]; Van't Hoff plot [D] for fluorescence quenching of nNOS (5μl) in triethanolamine HCl buffer (pH 7.4, 10mM) treated with $Aβ_{29\text{-}33r}$ (5-40 μM) in a final volume (200μL) at different temperatures – – – ○ [298 K]; —□ [303 K]; ... Δ [308 K]; —■ [313 K] .λ_{ex} = 290 nm and λ_{em} = 338 nm

Table 4.8: Values for fluorescent parameters (K_{sv} [μM^{-1}], K_a [μM^{-1}],K_d [μM],θ and n) and thermodynamic parameters ΔH [$kJ.mol^{-1}.K^{-1}$]; ΔS [$J.mol^{-1}.K^{-1}$ and ΔG [$kJ.mol^{-1}.K^{-1}$] for the interaction of $Aβ_{29\text{-}33r}$ with nNOS at various temperatures.

K	ΔH	ΔS	ΔG	K_{sv}	K_d	K_a	θ	n
298	59	163	10	1.9×10^{-2}	52	1.9×10^{-2}	1	1
303			9.1	2.6×10^{-2}	55	1.8×10^{-2}	1	1
308			8.3	3.6×10^{-2}	56	1.8×10^{-2}	1	1
313			7.5	6.2×10^{-2}	74	1.4×10^{-2}	1	1

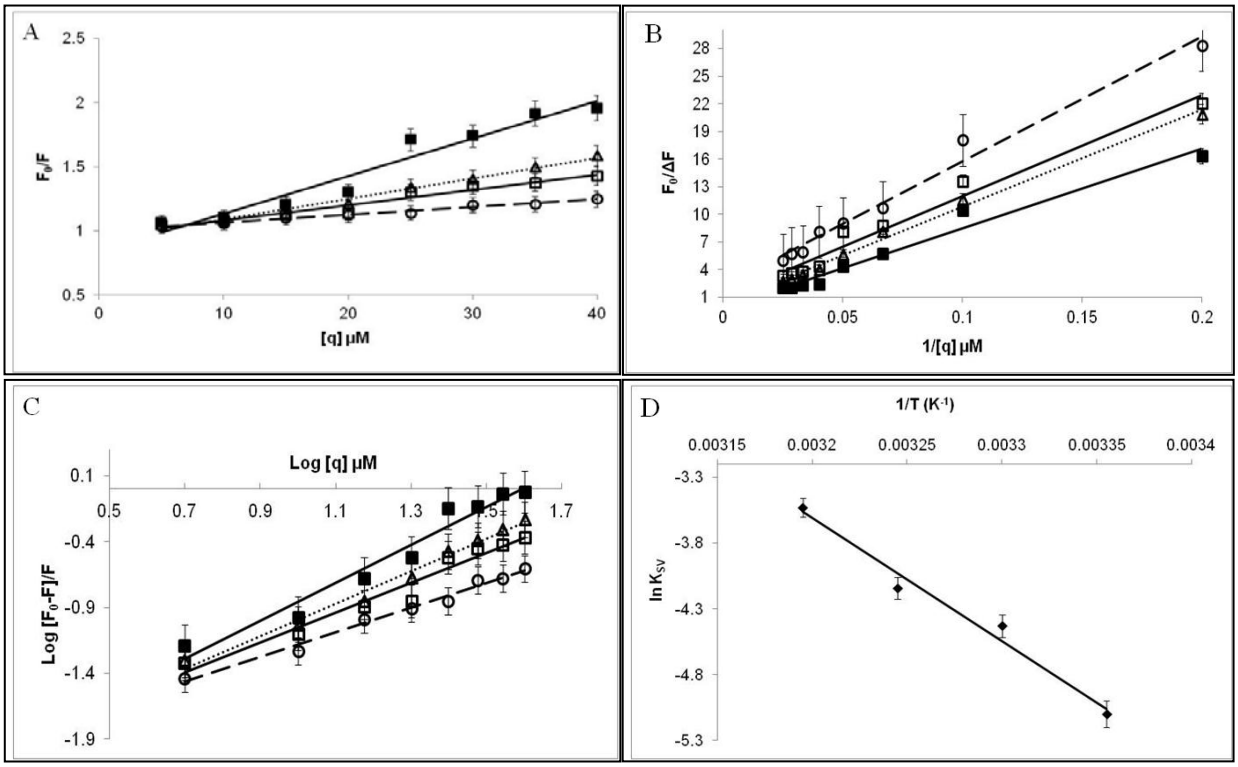

*Figure 4.15: Stern–Volmer plot [**A**]; modified Stern –Volmer plot [**B**]; Hill plot of log [$(F_0-F)/F$] versus log [q] [**C**]; Van't Hoff plot [**D**] for fluorescence quenching of nNOS (5µl) in triethanolamine HCl buffer (pH 7.4, 10mM) treated with **$A\beta_{29\text{-}33p}$** (5-40 µM) in a final volume (200µL) at different temperatures – – – ○ [298 K]; —□ [303 K]; ... Δ [308 K]; —■ [313 K] .λ_{ex} = 290 nm and λ_{em} = 338 nm*

Table 4.9: Values for fluorescent parameters (K_{sv} [μM^{-1}], K_a [μM^{-1}],K_d [µM],θ and n) and thermodynamic parameters ΔH [$kJ.mol^{-1}.K^{-1}$]; ΔS [$J.mol^{-1}.K^{-1}$ and ΔG [$kJ.mol^{-1}.K^{-1}$] for the interaction of $A\beta_{29\text{-}33p}$ with nNOS at various temperatures.

K	ΔH	ΔS	ΔG	K_{sv}	K_d	K_a	θ	n
298	78	218	13	6.1×10^{-3}	132	7.6×10^{-3}	1	1
303			12	1.2×10^{-2}	153	6.6×10^{-3}	1	1
308			11	1.6×10^{-2}	166	6.0×10^{-3}	4	1
313			10	2.9×10^{-2}	200	5.0×10^{-3}	5	1

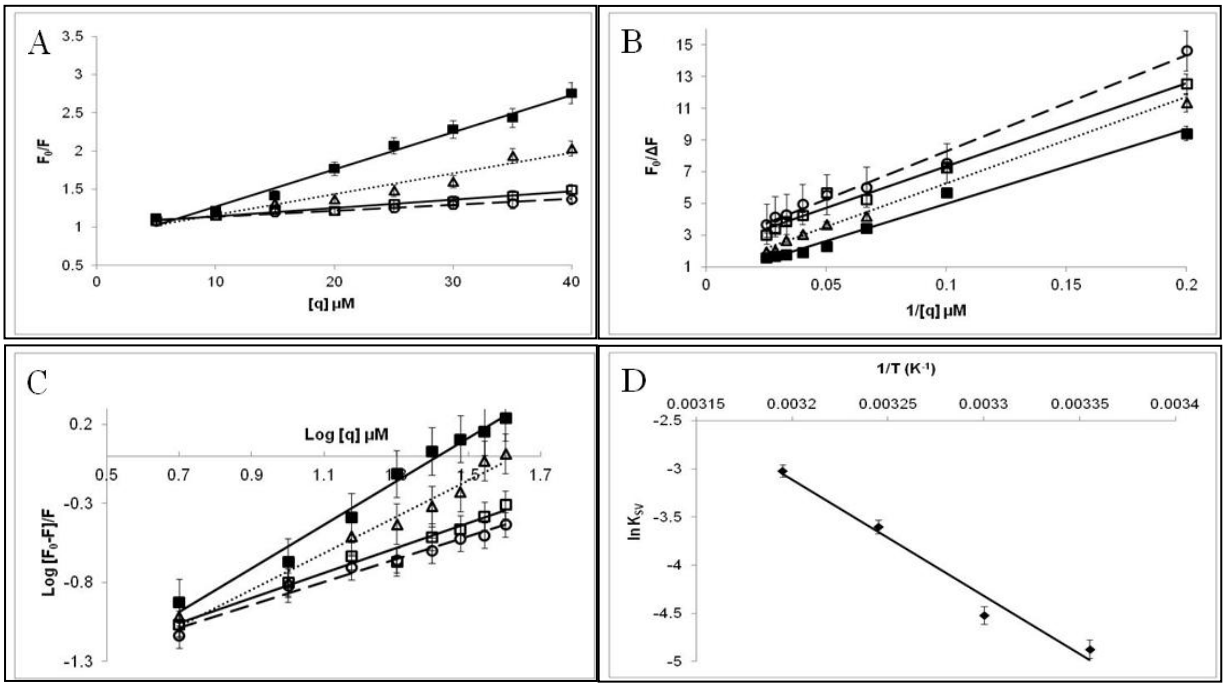

*Figure 4.16: Stern–Volmer plot [**A**]; modified Stern –Volmer plot [**B**]; Hill plot of log [$(F_0$-F)/F] versus log [q] [**C**]; Van't Hoff plot [**D**] for fluorescence quenching of nNOS (5µl) in triethanolamine HCl buffer (pH 7.4, 10mM) treated with **Ag (4 nm)** (5-40 µM) in a final volume (200µL) at different temperatures – – – ○ [298 K]; —□ [303 K]; ... Δ [308 K]; —■ [313 K] .λ_{ex} = 290 nm and λ_{em} = 338 nm*

Table 4.10: Values for fluorescent parameters (K_{sv}[μM^{-1}], K_a[μM^{-1}],K_d[μM],θ and n) and thermodynamic parameters ΔH [$kJ.mol^{-1}.K^{-1}$]; ΔS [$J.mol^{-1}.K^{-1}$] and ΔG [$kJ.mol^{-1}.K^{-1}$] for the interaction of Ag with nNOS at various temperatures.

K	ΔH	ΔS	ΔG	K_{sv}	K_d	K_a	θ	n
298	100	296	12	7.7 x10^{-3}	39	2.6 x10^{-2}	1	1
303			10	1.0 x10^{-2}	40	2.5 x10^{-2}	1	1
308			8	2.7 x10^{-2}	76	1.3 x10^{-2}	1	1
313			7	4.8 x10^{-2}	89	1.1 x10^{-2}	5	1

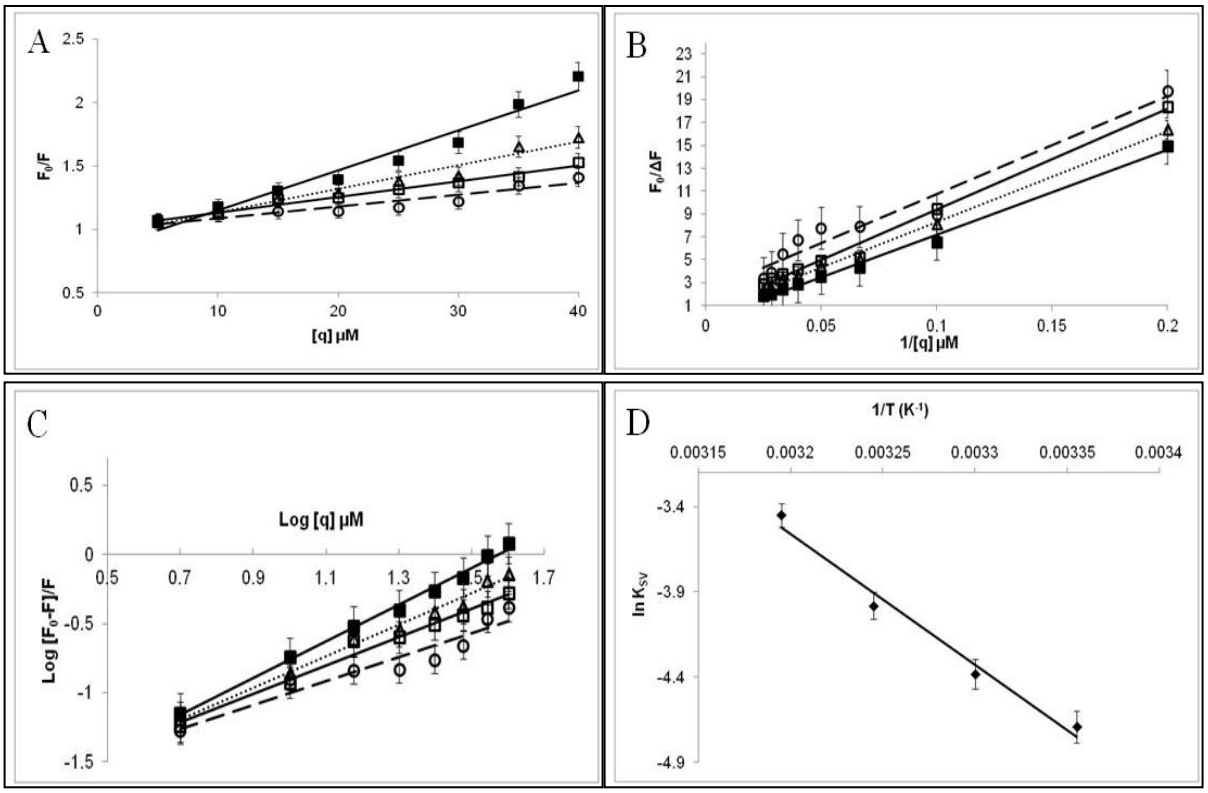

Figure 4.17: [A] Stern–Volmer plot; [B] modified Stern –Volmer plot; [C] Hill plot of log [(F_0-F)/F] versus log [q]; [D] Van't Hoff plot for fluorescence quenching of nNOS (5µl) in triethanolamine HCl buffer (pH 7.4, 10mM) treated with ***Au (4 nm)*** *(5-40 µM) in a final volume (200µL) at different temperatures – – – ○ [298 K]; —□ [303 K]; ... Δ [308 K]; —■ [313 K] .λ_{ex} = 290 nm and λ_{em} = 338 nm*

Table 4.11: Values for fluorescent parameters (K_{sv}[μM^{-1}],K_a [μM^{-1}],K_d [µM],θ and n) and thermodynamic parameters ΔH [kJ.mol^{-1}.K^{-1}]; ΔS [J.mol^{-1}.K^{-1} and ΔG [kJ.mol^{-1}.K^{-1}] for the interaction of Au with nNOS at various temperatures.

K	ΔH	ΔS	ΔG	K_{sv}	K_d	K_a	θ	n
298	64	175	12	9.2×10^{-3}	73	1.4×10^{-2}	1	1
303			11	1.2×10^{-2}	86	1.2×10^{-2}	2	1
308			9.9	1.8×10^{-2}	97	1.0×10^{-2}	3	1

313		9.0	3.2×10^{-2}	119	8.4×10^{-3}	5	1

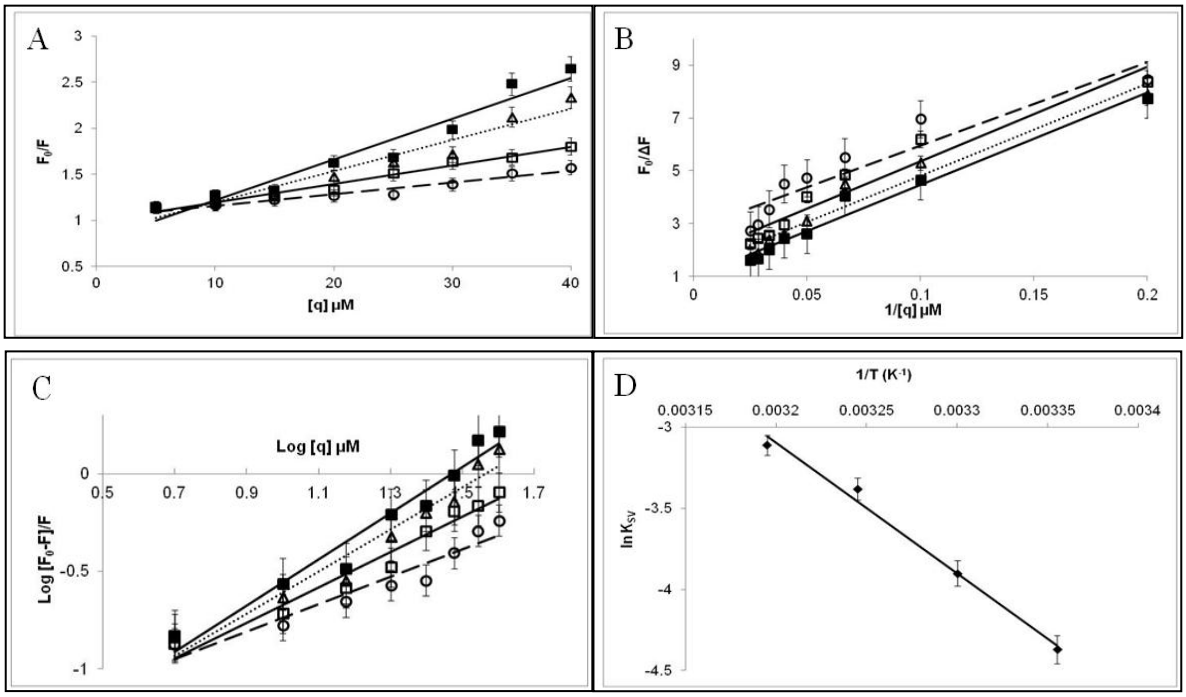

*Figure 4.18: Stern–Volmer plot [**A**]; modified Stern –Volmer plot [**B**]; Hill plot of log [(F_0-F)/F] versus log [q] [**C**]; Van't Hoff plot [**D**] for fluorescence quenching of nNOS (5µl) in triethanolamine HCl buffer (pH 7.4, 10mM) treated with curcumin (5-40 µM) in a final volume (200µL) at different temperatures – – – ○ [298 K]; —□ [303 K]; ... Δ [308 K]; —■ [313 K] .λ_{ex} = 290 nm and λ_{em} = 338 nm*

Table 4.12: Values for fluorescent parameters (K_{sv}[μM^{-1}], K_a[μM^{-1}],K_d[μM],θ and n) and thermodynamic parameters ΔH [kJ.mol^{-1}.K^{-1}]; ΔS [J.mol^{-1}.K^{-1} and ΔG [kJ.mol^{-1}.K^{-1}] for the interaction of curcumin with nNOS at various temperatures.

K	**ΔH**	**ΔS**	**ΔG**	**K_{sv}**	**K_d**	**K_a**	**θ**	**n**
298	67	189	11	1.2×10^{-2}	27	3.7×10^{-2}	1	1
303			10	2.0×10^{-2}	38	2.6×10^{-2}	1	1
308			8.6	3.3×10^{-2}	48	2.0×10^{-2}	1	1
313			7.7	4.4×10^{-2}	54	1.9×10^{-2}	1	1

The 'y intercept' in the respective Stern Volmer plots (Fig.4.7A-Fig.4.18A) were equivalent to 1, thereby indicating that fluorescence was only due to internal quenching by amino acids within the nNOS and not the interplay of external quenchers. The Stern Volmer constants (K_{sv}) were also calculated from the Stern Volmer plots (Fig.4.7A-Fig.4.18A) while the modified Stern Volmer plots (Fig.4.7B-Fig.4.18B) were used to calculate parameter θ. The number of binding sites (n) on the purified enzyme, which were available for the Aβ peptides and the respective association constant (K_a) [and their reciprocal dissociation constant (K_d)] were estimated from the slopes of the linear regressions and the intercept on the Hill plot axis (Fig.4.7C-Fig.4.18C).

N.B The results at 298 K for all Aβ peptides, nps and curcumin will be discussed first so as to give an indication of the mechanism of binding at standard temperature. Thereafter, the effect of increasing temperature will be discussed as an indication as to the type of quenching involved.

The analysis of the primary structure and active site of nNOS of each subunit of nNOS [PDB ID: 1zvi] revealed 13 tryptophan residues of which four [Trp409, Trp561, Trp587 and Trp678] are within the active site, seven are near the enzyme surface and two others are buried elsewhere in the enzyme interior (Padayachee and Whiteley, 2011; 2013). Fluorescence quenching could be attributed to these Trp residues, on the surface or within the active site of nNOS. At 298 K, according to Fig.4.7B-Fig.4.18B (Table 4.1-Table 4.12), the quenching effect of all Aβ peptides, including nps and curcumin was associated with the exposure of a single Trp residue ($\theta \approx 1$). The binding event between Aβ and nNOS was necessary to induce conformational change, which most probably lead to this amino acid been exposed for quenching. The identity and location of this single Trp amino acid will be confirmed by molecular modeling studies (chapter 5). Moreover, since the parameter θ is generally dependent on the polarity of the solvent, it could be suggested that it is the hydrophobic nature of the original Aβ peptides (reversed sequenced

peptides included) that induced conformational change in nNOS, bringing one Trp residue to the surface of the enzyme.

At 298 K (Table 4.3), it was shown that $A\beta_{29-33}$ had the lowest K_{sv} (9 $x10^{-3}$ μM^{-1}) compared to other original Aβ peptides [$A\beta_{17-21}$ (1.5 $x10^{-2}$ μM^{-1}); $A\beta_{25-29}$ (1.8 $x10^{-2}$ μM^{-1}); $A\beta_{33-37}$ (1.1 $x10^{-2}$ μM^{-1}); $A\beta_{25-37}$ (1.4 $x10^{-2}$ μM^{-1}) (Table 4.1,4.2,4.4 and 4.5). This indicated that the binding of $A\beta_{29-33}$ did not quench the fluorescence of the single Trp residue ($\theta \approx 1$) (Table 4.3) on nNOS since it was not easily accessible to the Trp, compared to the other peptides. Moreover the reversed form ($A\beta_{17-21r}$) displayed similar quenching ability to the original peptide ($A\beta_{17-21}$) due to a similar K_{sv} value of 1.5 $x10^{-2}$ μM^{-1} (Table 4.1 and Table 4.6) while $A\beta_{29-33r}$ was shown to exhibit a greater ability to quench than its original form due to its larger K_{sv} value of 1.9 $x10^{-2}$ μM^{-1} (Table 4.8). However the polar forms of the peptides ($A\beta_{17-21p}$ and $A\beta_{29-33p}$) displayed the lowest quenching abilities (K_{sv} =7.2 x 10^{-3} μM^{-1} and 6.1 $x10^{-3}$ μM^{-1}, respectively (Table 4.7 and Table 4.9), indicating that the polar glutamic acids quenched the fluorescence of the Trp residues to a lesser degree than the other peptide implying that polar amino acids induced a lesser degree of conformational change in nNOS. This could also be attributed to polar glutamic acid groups interfering with the "hydrophobic effect" that is so important in aggregation.

At 298 K, the similar K_{sv} values of Ag and Au nps of values 7.7 x 10^{-3} μM^{-1} and 9.2 x 10^{-3} μM^{-1}, respectively (Table 4.10-Table 4.11) also exhibited the lowest quenching effects compared to curcumin (1.2 $x10^{-2}$) (Table 4.12). These results indicated that the single Trp residue was more favourably quenched by the aromatic rings of curcumin than by the nps. The presences of the aromatic moieties belonging to curcumin may also have the potential to behave as intrinsic quenchers within the molecule. In addition, Aβ peptides, nps and curcumin were all associated with a single binding site on nNOS (n =1) (Table 4.1-Table 4.12).

In terms of binding affinity at 298 K, $A\beta_{29-33}$ had the tightest binding affinity as reflected by its lowest K_d (2.7 μM) (Table 4.3). This finding correlated well with its small K_i value of 7.5 μM compared to $A\beta_{25-29}$, $A\beta_{33-37}$ and $A\beta_{25-37}$ (chapter 2). The pentapeptide ($A\beta_{17-21}$) had a high K_d

value (6.9 μM) (Table 4.1) which meant that the pentapeptide was loosely associated with the enzyme. These findings indicated that for $A\beta_{17\text{-}21}$ and $A\beta_{29\text{-}33}$, it was not the tight binding affinity that determined stronger inhibition, but it was the nature of the amino acid sequence and the identity of the amino acids which influenced binding. All the other original peptides, namely, $A\beta_{25\text{-}29}$ (Table 4.2; K_d =6.9 μM); $A\beta_{33\text{-}37}$ (Table 4.4; K_d = 5.4 μM) and $A\beta_{25\text{-}37}$ (Table 4.5; K_d = 5.5 μM); displayed a similar binding affinity to nNOS, with $A\beta_{25\text{-}29}$ having a slightly higher K_d value due to its hydrophilic amino acids (Ser26, Asn27). According to Table 4.7 and Table 4.9, for $A\beta_{17\text{-}21p}$ and $A\beta_{29\text{-}33p}$ the high values for K_d (101 μM and 132 μM) compared to the K_d values of $A\beta_{17\text{-}21r}$ and $A\beta_{29\text{-}33r}$ (15 μM and 52 μM) (Table 4.6 and Table 4.8) revealed that polar glutamic acid residues could not interact favorably with the hydrophobic binding pocket of the enzyme. Moreover at 298 K, curcumin had a K_d value of 27 μM (Table 4.12), which was much lower than the K_d values of Ag and Au nps (39 μM and 73 μM), respectively (Table 4.10–Table 4.11). This indicated that curcumin had a tighter binding affinity to nNOS at 298 K than the nps.

Since results have shown that, at 298 K, all Aβ peptides, nps and curcumin were involved in quenching, it was necessary to identify the type of quenching involved by considering the change of fluorescence of nNOS by the Aβ peptides, nps and curcumin at increasing temperatures from 298 K to 303 K, 308 K and 313 K, respectively. Accordingly (Fig.4.7A-Fig.4.18A) (Table 4.1-Table 4.12), the value of K_{sv} increased with an increase in temperature pointing toward a dynamic quenching mechanism whereby high temperatures provided thermal energy to aid in the diffusion of ligands to the nNOS binding site. It was also shown that the quenching abilities of all Aβ peptides, nps and curcumin were more enhanced at higher temperatures (313 K) (Table 4.1-Table 4.12). This could mean that a greater conformation change in the enzyme occurred at 313K, thus exposing a single Trp residue of the enzyme to participate in quenching with Aβ. For the original and reversed Aβ peptides (Table 4.1- Table 4.5 and Table 4.6, 4.8), θ was equivalent to 1 at all temperatures, indicating that increasing the temperature during the binding of these sequences, did not increase the number of exposed Trp amino acids. It was interesting, however that for $A\beta_{17\text{-}21p}$ and $A\beta_{29\text{-}33p}$, increasing the temperature, influenced the number of exposed Trp residues. For $A\beta_{17\text{-}21p,}$ 2 Trp residues were exposed at 308 K and 5 at 313 K (Fig.4.13B, Table

4.7), while for $A\beta_{29\text{-}33p,}$ 4 Trp residues were exposed at 308 K and 5 at 313 K (Fig.4.14B, Table 4.9). According to the analysis of the primary structure of nNOS [PDB ID: 1zvi] (Padayachee and Whiteley, 2011; 2013), the 2-4 Trp residues exposed at 308 K, may be located at the active site while the 5 Trp's ,exposed at 313 K may be those near the enzyme surface. This will be confirmed by molecular docking studies (chapter 5). Nevertheless the results show that, contrary to findings at 298 K, the binding of $A\beta_{17\text{-}21p}$ and $A\beta_{29\text{-}33p}$ at higher temperatures (308 K-313 K) facilitated a greater conformational change in the enzyme, thus leading to the exposure of more than 1 Trp residue for quenching. Furthermore, despite increasing the temperature, the number of binding sites (n) still remained as one for all Aβ peptides, nps and curcumin (Table 4.1-Table 4.12).

For Ag (Fig.4.16B, Table 4.10), the number of exposed Trp residues (θ) increased from 1 (303 K) to 5 (313 K) and for Au (Fig.4.17 B, Table 4.11), they increased from 2 (308 K) to 5 (313 K). For curcumin, on the other hand, (Fig.4.18B, Table 4.12), the number of exposed Trp residues remained at 1 from 298 K-313 K. This indicated that the binding of nps at high temperatures accelerated the rate of unfolding and conformational change in the enzyme, thus exposing more surface Trp residues to participate in quenching, which was not the case with curcumin.

In general the reversed sequenced Aβ peptides, at 313 K had higher K_{sv} values: [$A\beta_{17\text{-}21r}$ (5.2 $x10^{-2}$ μM^{-1}) $A\beta_{29\text{-}33r}$ (6.2 $x10^{-2}$ μM^{-1})] (Table 4.6 and Table 4.8) compared to the original and polar sequenced Aβ peptides [$A\beta_{17\text{-}21}$ (5.1 $x10^{-2}$ μM^{-1}), $A\beta_{29\text{-}33}$ (4.1 $x10^{-2}$ μM^{-1}), $A\beta_{17\text{-}21p}$ (2.8 $x10^{-2}$ μM^{-1}) $A\beta_{29\text{-}33p}$ (2.9 $x10^{-2}$ μM^{-1})](Table 4.1-Table 4.5, Table 4.7 and Table 4.9). This highlights that the position of key amino acids, phenylalanine and isoleucine were important for interaction with the enzyme. In the reversed sequenced Aβ peptides, it is most probable that phenylalanine and isoleucine, in their altered positions from the original sequences were better orientated to participate in quenching with the enzyme. The lack of these key amino acids in the polar sequenced peptides, however, resulted in a subsequently lower quenching constant.

According to Table 4.10 and Table 4.12, at 313 K, the Ag np and curcumin had similar and higher K_{sv} values of 4.8 $x10^{-2}$ μM^{-1} and 4.4 $x10^{-2}$ μM^{-1}, respectively compared to the Au np (3.2

$x10^{-2}$ μM^{-1}) (Table 4.11). These findings suggested that Ag had a greater quenching effect than Au and that the aromatic moieties of curcumin favoured an even greater quenching at higher temperatures.

For all Aβ peptides, nps and curcumin, the values of K_d increased with increasing temperature reflecting that the binding reaction was endothermic (Table 4.1- Table 4.12). For all Aβ, nps and curcumin, the value of K_d was the highest at 313 K, a strong indication that higher temperatures the peptides became less and less associated with the enzyme. Inhibition studies (chapter 2) proposed that the dissociation of the peptide in a form that no longer binds was termed a fibril. Our studies are now hinting at the possibility that high temperatures may favour fibrillogenesis, by favouring dissociation of the peptide from the enzyme. This is reasonable to conclude as fibrils have been found to be stable and resistant to a wide range of external factors, including high temperatures (Mankar *et al*., 2011; Shammas *et al*., 2011). Compared to their original forms, the polar and reversed sequences of Aβ peptides had substantially higher K_d values (Table 4.6-Table 4.9). Within the temperature range of 298 K-313 K, the K_d values were: [$A\beta_{17-21r}$ (15-17 μM); $A\beta_{29-33r}$ (52-74 μM)], [$A\beta_{17-21p}$ (101-126 μM); $A\beta_{29-33p}$ (132-200 μM)] suggesting that these peptides had a greater tendency to become less associated to nNOS at high temperatures than the original sequenced Aβ peptides. Once again indicating that the identity, position and polarity of amino acids within these short chain fragments has a strong influence on their binding to nNOS.

According to Table 4.10-Table 4.12, at 313 K, curcumin was shown to be more tightly associated with the enzyme (K_d = 54 μM), compared to Ag (K_d = 89 μM) and Au (K_d = 119 μM). This indicates that aromatic interaction by the polyphenol rings of curcumin play a more prominent role in the binding event to nNOS than electrostatic charge effects from Ag and Au nps.

According to a two way Anova statistical analysis, the numerical differences in K_{sv} was only significant at 313 K ($p < 0.001$, $p < 0.01$ and $p < 0.05$) for the comparison between $A\beta_{17-21}$and $A\beta_{17-21p}$; $A\beta_{17-21r}$ and $A\beta_{17-21p;}$ $A\beta_{29-33}$ and $A\beta_{29-33r;}$ $A\beta_{29-33r}$ and $A\beta_{29-33p}$; Ag and Au. The rest of

the K_{sv} response values exhibited by peptides, nps and curcumin were non-significant ($p > 0.05$) and are described in the appendix, pg 186-207. In addition, the numerical differences in K_d were very significant at all temperatures ($p < 0.001$) for the comparison between $A\beta_{17-21}$ and $A\beta_{17-21p}$; $A\beta_{29-33}$ and $A\beta_{29-33r}$; $A\beta_{29-33}$ and $A\beta_{29-33p;}$ $A\beta_{17-21r}$ and $A\beta_{17-21p;}$ $A\beta_{29-33r}$ and $A\beta_{29-33p}$; Au and curcumin. For the comparison between Au and Ag, K_d was only significant ($p < 0.05$) at 303 K. The rest of the K_d response values exhibited by peptides, nps and curcumin were non-significant ($p > 0.05$) and is described in the appendix, pg 208-228.

According to enthalpy change (ΔH) and entropy change (ΔS), the model of interaction between proteins can be concluded as: (1) $\Delta H > 0$ and $\Delta S > 0$ are indicative of hydrophobic forces; (2) $\Delta H < 0$ and $\Delta S < 0$ are indicative of Van de Waals interactions and hydrogen bonds; (3) $\Delta H < 0$ and $\Delta S > 0$ are indicative of electrostatic interactions (Ross and Subramanian, 1981; Strazza *et al*., 1985). Table 4.13 describes the nature of a biological reaction and can be used to define what to expect in a reaction based on the signs of the thermodynamic parameters (Masterton and Hurley, 2009; Whitten *et al*., 2007).

Table 4.13: A qualitative description of a reaction based on the signs of ΔH [kJ.mol^{-1}.K^{-1}]; ΔS [J.mol^{-1}.K^{-1} and ΔG [kJ.mol^{-1}.K^{-1}] for the interaction of Aβ, nanoparticles and curcumin with nNOS at various temperatures (T) in Kelvin (K)(Masterton and Hurley, 2009; Whitten et al., 2007)

ΔH	ΔS	-TΔS	ΔG	Nature of reaction
-	+	-	-	spontaneous at all T
+	-	+	+	non-spontaneous at all T.
+	+	-	+ **or** -	spontaneous at high T, non-spontaneous at low T.
-	-	+	+ **or** -	spontaneous at low T, non-spontaneous at high T.

The thermodynamic parameters ΔH (slope) and ΔS (intercept) and subsequently the free energy change (ΔG) for the interaction of the Aβ peptides, nps and curcumin with nNOS were determined from the Van't Hoff plot (Fig.4.7D- Fig.4.18D). The positive ΔH and ΔS values for all Aβ peptides, nps and curcumin (Table 4.1-Table 4.12) implied hydrophobic forces were operative during the binding. The positive sign for ΔG for all Aβ peptides, nps and curcumin

(Table 4.1-Table 4.12) indicated that the interaction between the ligands and nNOS was non-spontaneous. According to a two way Anova statistical analysis, the numerical difference in ΔG was only significant at 298 K ($p < 0.001$ and $p < 0.05$) for the comparison between $Aβ_{17-21}$ and $Aβ_{25-29}$; $Aβ_{17-21}$ and $Aβ_{29-33;}$ $Aβ_{25-29}$ and $Aβ_{33-37;}$ $Aβ_{17-21r}$ and $Aβ_{17-21p}$ and $Aβ_{17-21}$ and $Aβ_{17-21p}$. The differences in ΔG values were significant ($p < 0.001$ and $p < 0.05$) at all temperatures for the comparison between $Aβ_{25-29}$ and $Aβ_{25-37}$; $Aβ_{29-33}$ and $Aβ_{29-33r;}$ $Aβ_{29-33r}$ and $Aβ_{29-33p}$. The differences in ΔG values between Au and Ag were only significant at 308 K and 313 K ($p < 0.05$). The differences in ΔG between all other peptides, nps and curcumin is described in the appendix, pg 229-248.

For original Aβ peptides, the highest ΔH (78 $kJ.mol^{-1}.K^{-1}$) and highest ΔS (220 $J.mol^{-1}.K^{-1}$) was shown for $Aβ_{29-33}$ (Table 4.3). This finding suggests that a large amount of heat was absorbed during the binding of this particular peptide and that this particular peptide was associated with the greatest conformational entropy with nNOS. This result validates the previous finding that $Aβ_{29-33}$ had a tight binding affinity to the enzyme due to its relative low K_d value of 2.7 μM (Table 4.3). Moreover, hydrophobic interaction was most probably predominant compared to the Van de Waal and hydrogen bonding interactions (to be confirmed in molecular modeling, chapter 5), due to the presence of highly hydrophobic isoleucine residues within $Aβ_{29-33}$. In addition, $Aβ_{17-21}$ had a ΔH (58 $kJ.mol^{-1}.K^{-1}$) and ΔS (158 $J.mol^{-1}.K^{-1}$) (Table 4.1), nearly identical to the ΔH and ΔS values of $Aβ_{33-37}$ [59 $kJ.mol^{-1}.K^{-1}$; 159 $J.mol^{-1}.K^{-1}$] and of $Aβ_{25-37}$[58 $kJ.mol^{-1}.K^{-1}$; 158 $J.mol^{-1}.K^{-1}$] (Table 4.4 and Table 4.5). These results indicate that the binding of these three peptides to the enzyme was influenced by a similar dependence on heat, hydrophobic forces as well as influencing similar conformational entropy within the enzyme. Also, the high K_d value for $Aβ_{17-21}$ i.e. 6.0 μM at 298 K (Table 4.1), confirmed that the nature and identity of the amino acids within the pentapeptide, played a more significant role in interaction than its affinity for the enzyme.

In addition, $Aβ_{25-29}$ was the most polar off all of the original peptides used and its less significant role in binding was confirmed by its low enthalpy and entropy values: ΔH (41 $kJ.mol^{-1}.K^{-1}$) and

ΔS (105 $J.mol^{-1}.K^{-1}$) and the highest K_d value of 6.9 μM (Table 4.2, Fig.4.7D). Unfortunately, this reasoning did not hold true for the polar peptides ($Aβ_{17-21p}$ and $Aβ_{29-33p}$) which had the highest ΔH (76 and 78 $kJ.mol^{-1}.K^{-1}$) and highest ΔS (215 and 218 $J.mol^{-1}.K^{-1}$) compared to $Aβ_{17-21r}$ and $Aβ_{29-33r}$ (Table 4.6-Table 4.9). These results indicated that in contrast to reversed sequenced Aβ peptides, the high rotational freedom (ΔS) of the polar glutamic acid side chain likely influenced greater ligand conformational entropy within the enzyme and high energy (ΔH) input in the binding reaction. This in turn induced greater conformational change in nNOS such that 5 Trp residues (Table 4.7 and Table 4.9) were exposed for quenching as temperature increased.

Compared to Au and curcumin, the Ag np had the highest ΔH (100 $kJ.mol^{-1}.K^{-1}$) and highest ΔS (296 $J.mol^{-1}.K^{-1}$) (Table 4.10-Table 4.12) which indicated that the Ag np induced greater conformational change in the enzyme which was temperature dependent, compared to Au and curcumin. Nevertheless a relatively high ΔS value of 189 $J.mol^{-1}.K^{-1}$ (Table 4.12) for curcumin still pointed to the existence of conformational entropy possibly associated with its polyphenol rings.

Thus the reaction between Aβ peptides, nps and curcumin with nNOS was entropy driven due to binding of ligands inducing conformational change in the enzyme. It appears that the first event in binding could be most appropriately described in terms of "a hydrophobically bound heme complex" (Atamna and Boyle, 2006). The binding studies of Aβ, nps and curcumin to nNOS at temperatures ≤ 313 K pointed to a non-spontaneous, endothermic process. Earlier studies (Padayachee *et al*., 2011; Padayachee and Whiteley, 2011; 2013) established that the Aβ-nNOS complex is an amyloidogenic catalyst, initiating fibrillogenesis which presumably changes the bound Aβ into a form that could longer bind (later deduced as a fibril). The process of fibrillogenesis is non-spontaneous. This was supported by other work that fibrillogenesis requires the partial unfolding of proteins or the partial folding of disordered proteins (Rochet and Lansbury, 2000). Also the unfolding process is governed by large thermodynamically favourable entropy which is confirmed by the large positive values of ΔS. The fact that K_d is increasing

with temperature reveals that the association or affinity of Aβ at higher temperatures (> 313 K) starts to decrease until the peptide completely dissociates from the enzyme as a fibril. The process of dissociation has been confirmed and has been consistent with experimental studies involving the dissociation $A\beta_{16-22}$ fibrils probed by molecular docking simulations (Takeda and Klimov, 2007).

Using these findings, it can be explained that the dissociation of Aβ fragments at this point involved two main stages: a probable locked and docked state (Fig.4.19).

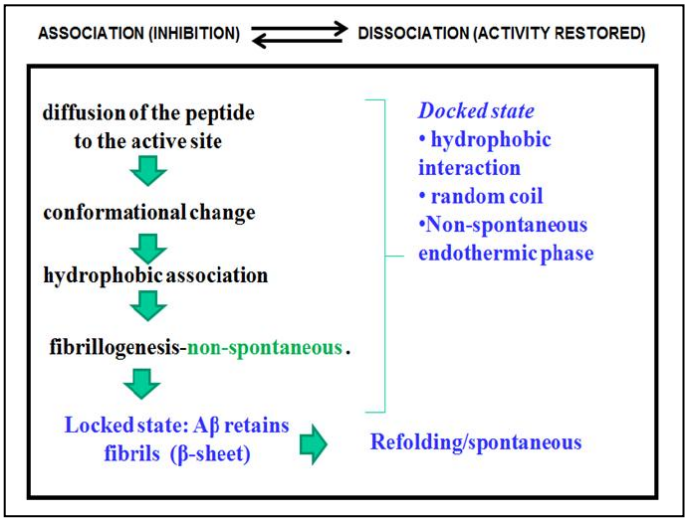

Figure 4.19: The mechanism of fibrillogenesis on the basis of the principle regarding association vs. dissociation between Aβ peptide and nNOS

First the Aβ motif docked into the nNOS active state and at this stage its structure gets elongated before reaching a fibril state in a locked phase. (Straub and Thirumalai, 2011) After the process of dissociation, the enzyme folds/refolds into a favourable native conformation which is a spontaneous process (-ΔG). Consequently, in summary the interaction of Aβ with nNOS was a thermodynamically unfavourable process at low temperatures (+ΔG) but was coupled to a very spontaneous (folding) process at high temperatures (-ΔG) (Fig.4.19). Our results have also established that the binding of Ag/Au nps and/or curcumin to nNOS led to an entropy gain, possibly releasing a water molecule belonging to the heme of the active site. It is also known that

there is a water molecule found between the heme propionyl groups of nNOS (Stuehr *et al*., 2009; Zhou and Zhu, 2009 and Groves and Wang, 2000). The inhibiting of fibrillogenesis by these small ligands was also an endothermic reaction with K_d increasing and ΔG decreasing. This pointed to an endothermic, non-spontaneous reaction and increasing the temperature from 298 K-313 K, provided thermal energy for the diffusion of these ligands to the heme active site, leading to the displacement of the Aβ by nps and curcumin and preventing its associated transition into a fibril (chapter 2). At temperatures > 313 K, the nps and curcumin assisted in the refolding event of nNOS and could possibly behave as chaperones of the enzyme. Thus, in a similar way to Aβ-nNOS interaction, the interaction of nps and curcumin with nNOS was also a thermodynamically unfavourable process at low temperatures but a spontaneous process at higher temperatures.

4.4.2 Surface plasmon resonance

The binding of the peptides, $A\beta_{1-40}$, $A\beta_{29-33}$, $A\beta_{33-37}$ and $A\beta_{25-37}$ were studied in real time but only $A\beta_{1-40}$ showed a partial result of ≈ 45 R.U (response units) (Fig.4.20 B). The reason as to why the analytes: $A\beta_{29-33}$, $A\beta_{33-37}$ and $A\beta_{25-37}$ showed no response or binding to immobilized nNOS (Fig.4.20A) might have probably been due to the peptides aggregating in solution. Even though turbidity was less pronounced for $A\beta_{1-40}$, $A\beta_{29-33}$, $A\beta_{33-37}$ and $A\beta_{25-37}$ than the other peptides, the solubility of these peptides in PBS/5 % DMSO still produced turbid solutions. This is surprising though; as literature (Broersen *et al*., 2011) has shown that organic solvents disrupt hydrophobic associations and help maintain the monomeric conformation of the peptide. In the current experiment, all analytes were dissolved in the organic solvent DMSO, and yet yielded turbid solutions. In trying to explain this phenomenon, it was important to consider the effect that varying concentrations of DMSO would have on Aβ solubility.

According to previous solvent aggregation studies (Jackson and Mantsch, 1991; Shen and Murphy; 1995), DMSO was found to be competitive for hydrogen bonding with the carbonyl groups of Aβ peptides to the amine groups on the peptide, thus destabilizing β-structure. This effect was found to be enhanced by solubilizing peptides in 100 % DMSO, such that a complete

loss of β-structure was observed in proteins with high β-sheet content. At a low percentage of DMSO (10 %), however, the hydrogen bond between DMSO and the amine groups of peptide were much weaker and hence were insufficient to disrupt β-sheet structure (Jackson and Mantsch, 1991).

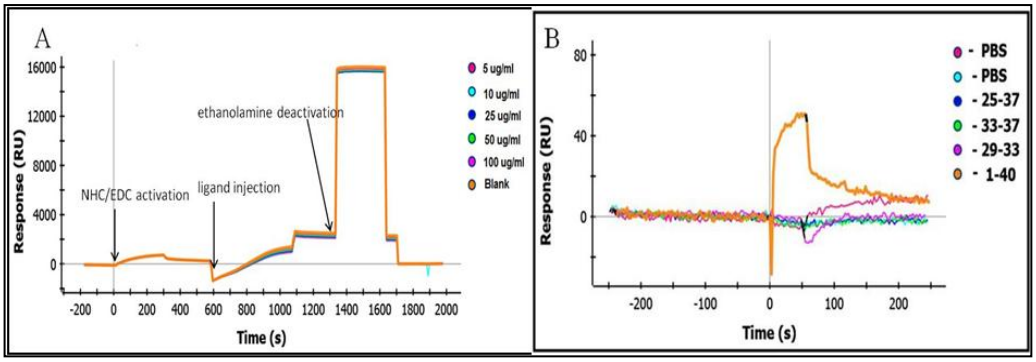

*Figure 4.20: Sensogram describing the immobilization of nNOS at a single channel (L1) (5µg/ml) [**A**] sensogram showing preliminary binding of $A\beta_{1-40}$ to nNOS [**B**]*

In our SPR experiment, the hydrophobic Aβ peptides: $A\beta_{29-33}$, $A\beta_{33-37}$ and $A\beta_{25-37}$ were dissolved in 5 % DMSO due to ProteOnXPR36 being unable to handle a high percentage of organic solvent. According to past experiments (Jackson and Mantsch, 1991), this percentage was too low to maintain a completely monomeric solution, hence the turbidity in solution was observed. In addition, $A\beta_{29-33}$, $A\beta_{33-37}$ and $A\beta_{25-37}$ contain methyl/methylene functional groups in their side chains. For $A\beta_{25-37}$ the bulkiness of these carbon-hydrogen chains were compounded by the presence of aromatic phenyl rings. As a result, these peptides are not linear peptides and their secondary structure effects may have affected interaction with immobilized nNOS.

According to modeling and simulation by Accelrys Visualizer/Material Studios (version 2.0), the secondary structure of $A\beta_{25-37}$ is alpha-helical in nature. This could have been its native state in PBS containing 5 % DMSO. Since alpha-helices are amphipathic, the resultant conformational change in solution could have resulted in the exposure and interaction of its hydrophobic glycine zipper constituents with each other, resulting in a turbid solution. Also, if the entire Aβ-peptide failed to bind to the sensor surface due to the aggregation effect, it would make sense that its

constituent glycine zippers would also fail to bind. It can also be reasoned that $A\beta_{25-37}$ is the hydrophobic core region of the entire $A\beta_{1-40}$ peptide, such that hydrophobic-hydrophobic interaction occurred more rapidly for the glycine zipper sequence and favoured more aggregation than the for the entire $A\beta_{1-40}$ peptide.

Nevertheless, the failure of the $A\beta_{29-33}$, $A\beta_{33-37}$ and $A\beta_{25-37}$ to elicit a response on SPR cannot be fully accounted for and opens up an area of research into trying to optimize analytes in their random coil conformation, thus approaching the study of peptide solubility from a new angle. Recently, Yu and Zheng, 2011, used molecular dynamic simulations to design a molecular structure called an Aβ globulomer, using monomer or dimer building blocks. The Aβ polymorphic structure has no β-sheet component and hence makes it difficult to aggregate (Yu and Zheng, 2011). Although this study is purely *in silico* based, it can be a start in understanding possible ways of synthesizing Aβ peptides in a form that will not tend to aggregate, but at the same time still have fibril forming potential which can be studied using biosensor technology. This will limit the use of harsh solvents used initially to solubilize Aβ peptides.

4.5 Conclusions

Fluorescence quenching indicated that all ligands (Aβ, nps and curcumin) bound to a single site on the enzyme (n=1). At 298 K, the binding of all ligands to nNOS resulted in conformational change, which exposed one surface Trp residue (θ =1) for quenching. As the temperature was increased to 313 K the number of Trp residues did not change, except in the case of the polar sequences and Au and Ag nps ($\theta > 1$ at 308-313 K). All ligands, moreover displayed a dynamic quenching mechanism as an increase in temperature resulted in greater K_{sv} values. This suggests that thermal energy was critical for diffusion of the ligand to the enzyme. At 313 K, however the reversed sequenced Aβ peptides had higher K_{sv} values: [$A\beta_{17-21r}$ (5.2×10^{-2} μM^{-1}) $A\beta_{29-33r}$ (6.2×10^{-2} μM^{-1})] compared to the original and polar sequenced peptides. It was proposed that phenylalanine and isoleucine residues in their altered positions allowed for more convenient access to Trp residues on or within nNOS, thus improving the efficiency of quenching by $A\beta_{17-21r}$ and $A\beta_{29-33r}$. This highlights that the position and presence of key amino acids, phenylalanine

and isoleucine were important in the Aβ peptides for interaction with the enzyme. In addition, the evaluation of K_d for $A\beta_{29\text{-}33}$ (K_d = 2.7 μM) showed that this peptide had the tightest binding affinity to nNOS compared to $A\beta_{17\text{-}21}$ (K_d= 6.0 μM) which supported the finding that the identity of the amino acids were crucial for binding. The peptides, $A\beta_{29\text{-}33p}$ (K_d = 132 μM) and $A\beta_{17\text{-}21p}$ (K_d =101 μM) had weaker affinity for the enzyme binding site; possibly due to the polar glutamic acid groups disrupting the hydrophobic interaction with the enzyme.

Ag has a greater quenching effect (K_{sv} = 4.8 $x10^{-2}$ μM^{-1}) than Au (K_{sv} = 3.2 $x10^{-2}$ μM^{-1}) and it was suggested that the aromatic moieties of curcumin favoured greater quenching at higher temperatures [313 K] (K_{sv} = 4.4 $x10^{-2}$ μM^{-1}).

Our results have further shown that the interaction of Aβ peptides, nps and curcumin with nNOS occurred via hydrophobic-hydrophobic interactions (+ΔH and +ΔS) and was entropy driven. The binding reaction was non-spontaneous and endothermic at low temperatures (+ΔG) but spontaneous at high temperatures (-ΔG). Molecular docking studies will be used to identify the Trp residues exposed and their location during the interaction of the Aβ-peptides, nps and curcumin with nNOS. In addition, fluorescence energy transfer (FRET) will confirm any conformational changes in the enzyme upon ligand binding and will be the subject of chapter 5.

5 Interaction of Aβ peptides, nanoparticles (Ag/Au) and curcumin with nNOS: Molecular docking and fluorescence resonance energy transfer(FRET)

5.1 Introduction

5.1.1 Molecular docking

Molecular docking is a technique whereby different conformations of ligands are computationally generated in protein receptor binding sites and given the atomic coordinates of the ligand and receptor, docking aims to predict the "best fit" for the complex formed (Mihasan, 2012; Sousa *et al*., 2006; Warren *et al*., 2006). Molecular docking has been spurred on by advances in x-ray crystallography, nuclear magnetic resonance (NMR) and molecular biology which have increased the number of available 3-D structures of biologically important proteins (Bohacek and McMartin, 1997; Szymczyna *et al*., 2009). The theoretical basis of molecular docking relies on four models, namely the (1) lock-and-key; (2) induced-fit, (3) symmetry and (4) "population shift" models (Gschwend *et al*., 1996). The lock-and-key model (Fischer, 1894) regards the ligand and receptor as rigid molecules, while the induced fit model, introduced by Koshland (Koshland, 1958) regards the ligand as flexible and responsible for inducing conformational change in the protein before a suitable fit occurs (Gschwend *et al*., 1996). The "symmetry model" proposes that proteins possess an axis of symmetry and when a ligand binds, the protein shifts from a low affinity T to the high affinity R state, where the T state is thermodynamically favourable (Nussinov and Ma, 2012). The "population shift" model (Nussinov and Ma, 2012) implies that instead of targeting a single pose of a given ligand on a single receptor, one should ideally look for the most populated alternatives from an ensemble of solutions comprising several different binding conformations (Nussinov and Ma, 2012; Sousa *et al*., 2006). The first docking programme was developed by the Kuntz group and named DOCK (Kuntz *et al*., 1982). DOCK was based on the lock-and-key model and was successfully applied in studies involving serine protease specificity (Ribeiro *et al*., 2010) and in DNA binding (Fanelli

and Ferrari, 2006). Literature has also supported the induced-fit model as been popular in defining structural changes in proteins (Sundberg and Mariuzza, 2000).

The classification of protein-ligand docking is based on the three aspects, namely (1) protein flexibility, (2) ligand sampling and (3) scoring function, as depicted in Fig.5.1.

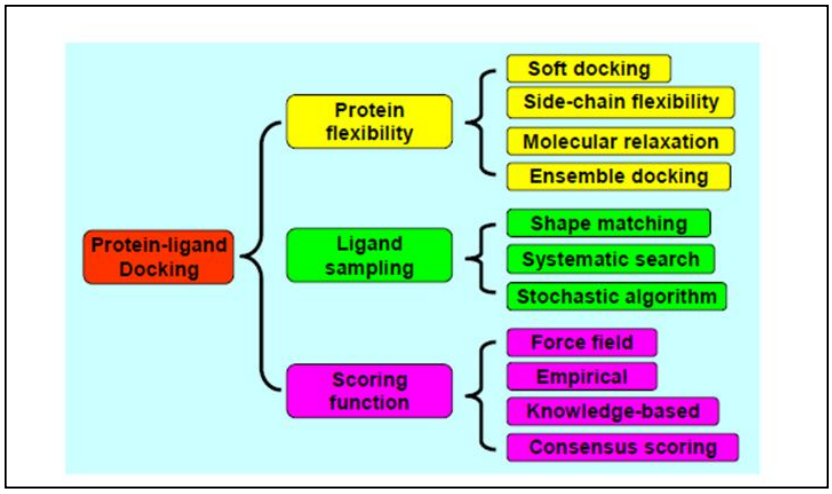

Figure 5.1: The methods which classify protein docking (taken from Huang and Zou, 2010)

The current challenge in docking is the issue of flexibility, since proteins have many degrees of freedom. To overcome this problem, various approaches described in Fig.5.1 have been used. One such method, incorporating ligand flexibility is "soft docking" which softens Van der Waals interactions in docking calculations (Ferrari *et al*., 2004). Another includes keeping the side chains flexible and the protein back-bone rigid (Nabuurs *et al*., 2007; Meiler and Baker, 2006). Monte Carlo and molecular dynamic simulations serve to relax the protein-backbone, while ensemble docking involves the docking of multiple protein structures to represent different conformational changes and is the most widely used method (Cozzini *et al*., 2008; Totrov *et al*., 2008). The second element of docking is sampling which is a performed using method of shape matching, systematic search and stochastic algorithms (Fig.5.1). These algorithms generate specific ligand orientations around the chosen binding site of the protein (Huang and Zou, 2010). Thirdly, the scoring function (Fig.5.1) directly determines the accuracy of the algorithm and the

lowest energy score is deemed as the "best fit" (Jain, 2006; Gohlke *et al*., 2001). Speed and accuracy determine whether a scoring function is both computationally efficient and reliable (Huang and Zou, 2010). Force-field, empirical, knowledge-based and consensus scoring are typical energy functions described in Fig.5.1. The validation of the final docking result is based upon existing experimental data e.g. binding constants (Mihasan, 2012). This highlights a challenge to protein docking as a fully automated method, without human intervention still does not exist (Mihasan, 2012). Receptor and backbone flexibility, as well as modeling co-factors and solvation effects still remain a major challenge to docking. Also, the docking algorithms need to be further improved based on these challenges to improve reliability of results (Mihasan, 2012). Nevertheless, the powerfulness of the docking technique cannot be underestimated in the light of its applications in small molecule docking, pharmacophore generation, nucleic acid and protein-protein interactions (Mihasan, 2012). Current docking programmes include AutoDock, Gold, FLexX, Fred, Dock, and CHARMM (Morris *et al*., 2009). AutoDock has been used to monitor the docking of ligands to various enzymes such as cytochrome c peroxidase, acetylcholine receptor, cytochrome P450 as well as in the modeling and design of protease inhibitors (Rosenfeld *et al*., 2003; Babakhani *et al*., 2009; Muralidhara *et al*., 2007, Jochim *et al*., 2009). Also, selective inhibitors have been docked with nNOS, using AutoDock 3.0 (Fang *et al*., 2009; Ji *et al*., 2008). Moreover AutoDock has applications in x-ray crystallography, structure-based drug design, virtual screening, combinatorial library design and protein-protein docking and chemical mechanism studies (Morris *et al*., 2009). In addition, it has been shown that the binding of ligands to proteins or enzymes alter the conformational flexibility of proteins by changing its surrounding microenvironment (Liu and Altman, 2011).

5.1.2 FRET

The technique of fluorescence energy transfer (FRET), developed by Theodor Förster in 1954, is a special type of fluorescence quenching whereby energy transfer occurs between fluorophores through dipole-dipole interaction (Clegg, 1995, 1996; Wu and Brand, 1994). FRET is unique in its ability to measure distances between defined sites in protein structures and to determine their

geometry. The spatial distances that are calculated between a ligand and receptor (10-100 Å) enable insight into the mechanism of interaction between ligand and receptor, and also enable researchers to identify and detect the enzyme-protein or protein-protein associations formed within biological systems (Clegg, 1995, 1996; Wu and Brand, 1994). For example FRET has monitored Ca^{2+} induced structural changes (Miki *et al*., 1998) and, FRET has analyzed the attachment and fusion of viruses (Orynbayeva *et al.*, 2007). Interactions of membrane proteins with each other and with the membrane itself can also be detected by FRET (Loura and Prieto, 2011). For example, FRET was used to detect lipid domains around a peptide fragment of the human immunodeficiency virus (HIV) glycoprotein envelope (Gawrisch *et al*., 1993). Moreover, the versatility of the technique is shown in real-time imaging, using autofluoresecent proteins e.g. the green fluorescent protein (GFP) (Truong and Ikura, 2001). A recent study took advantage of this imaging strategy, to monitor apoptosis by the human death receptor ligand TRAIL which binds to four distinct membrane receptors (TRAILR1- TRAILR4) (Scheurich, 2012).

In the present work two classes of inhibitors were identified: (1) the peptide inhibitors (the pentapeptide ($A\beta_{17-21}$), glycine zipper fragments ($A\beta_{25-29,}$ $A\beta_{29-33}$ and $A\beta_{33-37}$) and the entire glycine zipper stretch ($A\beta_{25-37}$) and (2) the non-peptide/small molecule inhibitors (Ag/Au nanoparticles and curcumin) (chapter 2). The first objective of our current study is to employ an *in silico* approach, using the docking programme AutoDock 4.2 to explore the inhibition mechanism of the above mentioned inhibitors with nNOS. The binding energies and K_i values for the inhibitor binding to nNOS will be calculated and compared to experimental K_i values, obtained earlier in chapter 2. The second objective will be to use the "spectroscopic ruler", FRET to help evaluate the distance between the Trp residues on the enzyme surface and the peptide or non-peptide inhibitor when either binds to the single site on nNOS. The identity of the single Trp residue (θ =1) which was involved in quenching with the ligands (chapter 4), will subsequently be revealed. Also, the nature of the single binding site (n=1) for these ligands on the enzyme (chapter 4) will be addressed. The information gained will assist in predicting the mechanism of binding and inhibition by peptide and non-peptide inhibitors with nNOS.

5.2 Theory of techniques utilized

5.2.1 Molecular docking

AutoDock 4.2 was the docking programme of choice; the version is faster than earlier versions and allows for the side chains of the molecule to be fully flexible, with high quality flexible docking occurring within one minute. Also, up to 40 000 rigid dockings can be performed within a day on a single central processing unit (Morris *et al*., 1998, 2009; Gromiha, 2011). Autodock 4 in general, consists of two main programmes. The first, AutoDock performs the docking of the ligand to a set of grids describing the target protein. Autodock has a free-energy scoring function that is based on a linear regression analysis, the AMBER force field and a large set of protein-ligand complexes with known inhibition constants. There is usually a good correlation between predicted K_i values and experimental data (Huey *et al*., 2007; Morris *et al*., 2009; Gromiha, 2011). The second, AutoGrid generates an electrostatic potential grid map and a desolvation map (Morris *et al*., 2009). AutoGrid is used to calculate the noncovalent energy of interaction between the rigid part of the receptor and a probe atom that is located at various points of the grid lattice (Gromihar, 2011). In AutoDock, $K_i = K_d$ (dissociation constant). Like K_d, the parameter K_i will be directly related to the free energy of binding (ΔG) according to [Eq13]. Tighter binding means a more negative ΔG and a smaller K_d/K_i, while lower affinity means a less negative ΔG and a larger K_d/K_i (Sargis, 2010; Morris *et al*., 2009).

$$\Delta G = RT\ln(K_d) \qquad \text{..... Eq [13]}$$

where R is the gas constant (8.314 $J.mol^{-1}.K^{-1}$), T = 298K.

Once a suitable protein structure has been chosen for the docking process, the region of interest for the docking procedure has to be determined. Usually, this is the active site of the enzyme or the binding site of a receptor. Identification of the binding region can be identified in three ways, namely, (1) existence of highly conserved amino acids (Yao *et al*., 2003; Caffrey *et al*., 2004), (2) recognition of a motif that shows core residues distinct from that of the surface (Neuvirth *et al*., 2004) (3) recognition of "hot-spot" residues or "anchor residues" which are a cluster of

tightly packed residues which contribute to low binding energies and stability of bound complexes (Rajamani *et al*., 2004). In addition, if the structure of the target receptor is known, then the proposed ligand can be designed based on electrostatic properties, hydrophobicity or surface complementarity (Deremble and Lavery, 2005; Bohacek and McMartin, 1997). The preparation of the ligand for docking involves pre-calculation of different conformers and assignment of rotatable bonds or a grid representation of the molecule. Other tasks may include evaluation of partial charges for the ligand atoms (Morris *et al*., 2009). In Autodock the ligand was treated as being flexible by assigning user-specified torsions as rotatable (Morris *et al*., 2009).

In AutoDock, the examination of the docking process uses the Lamarckian genetic algorithm which was found the most favourable for ligand binding orientations (Morris *et al*., 1998, 2009). The output files generated contained the final predicted conformations and root-mean square deviation (RMSD) values from the bound crystal structures, the docked energy and the estimated free energy of binding for each cluster. The free energy was computed as the sum of the docked energies, torsional energies and the intramolecular interaction energies for the ligand (Morris *et al*., 1998, 2009). Finally, AutoDock clusters by first sorting out all docked conformations from lowest energy (best docking) to the highest energy. The best overall docked conformation is used as a "seed" for the first cluster. Then the co-ordinates of the second best conformation are compared to those of the best to calculate the RMSD between the two conformations. If the calculated RMSD is smaller than the specified cutoff of 0.5 Å by default, this conformation is added to the bin containing the best conformation (Morris *et al*., 1998, 2009). In this way, resulting docked conformations were clustered together using an RMSD of 0.5 Å. Moreover a single conformational cluster indicates a single ligand binding event.

5.2.2 Fluorescence resonance energy transfer (FRET)

The process of FRET is based on the dipolar coupling between the emission dipole of a donor and the absorption dipole of an acceptor (Fig.5.2). As illustrated, the excitation energy of the donor molecule is transferred to an acceptor molecule without the emission of a photon.

Absorption spectrum of the acceptor (fluor B) must overlap with the fluorescence emission spectrum of the donor (fluor A). This results in a decrease in donor emission intensity accompanied by an increase in acceptor emission intensity. If these fluors (fluor A and B) have unique locations in the protein, it will be possible to measure distances or changes in distances within proteins (Ishii *et al*., 1999; Takahashi *et al*., 2004).

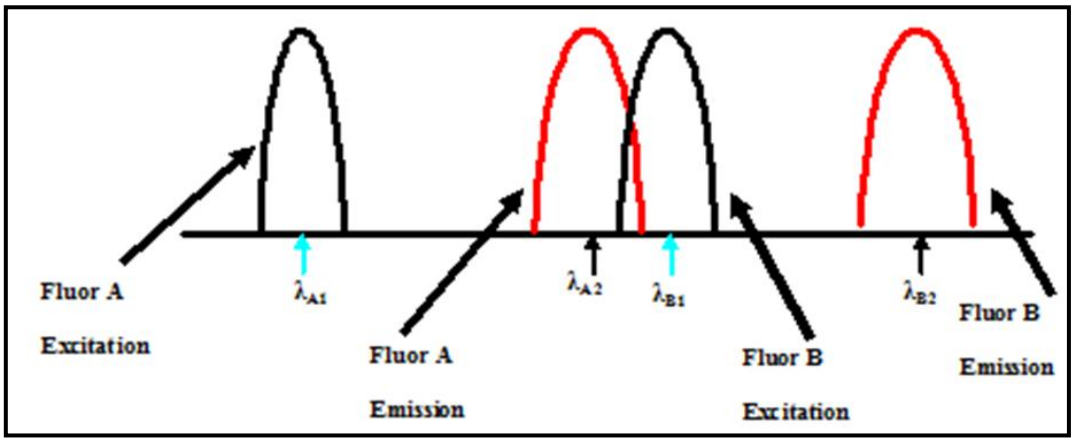

Figure 5.2: Illustrative process of FRET involving the donor (fluor A) and the acceptor (fluor B) (adapted from Takahashi et al., 2004)

In addition the rate of FRET depends on three factors: (1) the extent of spectral overlap of the donors emission spectrum and the acceptor absorption spectrum,(2) the appropriate orientation of the dipoles of the fluorophores (3) the distance (r) between the donor and acceptor (20-100 Å) (Clegg,1995,1996). According to literature, any value for the distance between donor and acceptor (r) that is less than 100 Å and falls between 0.5 and 1.5 of the R_0 (Förster distance) value indicates a high probability that fluorescence transfer is taking place (Chen *et al*., 2003). In addition, the efficiency of energy transfer (E) is a quantitative measure of the number of quanta that are transferred from donor (D) to acceptor (A). The efficiency of FRET can be determined either by time-dependent measurements, involving the fluorescence lifetimes of the donor (D) and the donor-acceptor pair (DA) or by steady state measurements, involving fluorescence measurements of the D (i.e., F^D) and DA pair (i.e., $F^{D,A}$) (Clegg,1995,1996; Chen *et al*, 2003). If

the values of F^D and $F^{D,A}$ are normalized to their respective concentrations of D, the efficiency for a single D-A pair can be calculated according to Eq [14].

$$\textbf{Efficiency of transfer (E)} = 1 - F^{D,A}/F^D = R_0^6/R_0^6 - r^6 \quad \text{..... Eq [14]}$$

where $F^{D,A}$ is fluorescence of donor (D) and acceptor (A); F^D is the fluorescence of donor (D); r is the distance between donor and acceptor molecules and R_0 is the Förster distance (44 Å).

The Förster critical distance (R_0) refers to the distance between the donor and acceptor where the energy transfer is 50 % of the maximum (Ishii *et al.*, 1999). R_0 depends on the relative orientation of the donor and acceptor (k^2), the refractive index (n), the quantum yield of the donor (Q_D), and the overlap integral between the acceptor emission and donor excitation (J) as shown by Eq [15]. The overlap integral can be calculated from Eq [16]. In the present study the values of κ^2, the average refractive index (η) and the fluorescence quantum yield of fluorescein (φ_D) are 0.667, 1.36 and 0.93 (Sjoback *et al*., 1995, Padayachee and Whiteley, 2011), respectively. From equations 14-16, it would give respective values for J, E, R_0 and r for $A\beta_{17-21}$; $A\beta_{25-29}$; $A\beta_{29-33}$; $A\beta_{33-37}$; $A\beta_{25-37}$ and BAEE (the substrate for nNOS) and curcumin.

$$R_0 = 8.79 \times 10^{-5} (Q_D\, k^2\, n^{-4}\, J) \quad \text{..... Eq [15]}$$

$$J = [\sum F(\lambda)\varepsilon(\lambda)\lambda^4 \Delta\lambda]/[\sum F(\lambda)\Delta\lambda] \quad \text{..... Eq [16]}$$

Also according to a report, intrinsic fluorophores like tryptophan can be labeled covalently with extrinsic probes (Clegg *et al*., 1995). Based on this principle, an extrinsic type of quencher called fluorescein was incubated with ligand molecules and the relative distance between the donor and acceptor molecules were calculated using the R_0 value of fluorescein, which was within the range of 49-55 Å (Lakowicz *et al*., 2003). An average R_0 value of fluorescein i.e. 44 Å was used for the purposes of our study. It must be noted that the calculation of the FRET parameters (including R_0) can also be performed using a computer program named Igor Pro (Wavemetrics

Inc), incorporated into Microsoft Excel spreadsheet (Hink *et al*., 2003; Visser and Rolinski, 2010).

5.3 Materials and Methods

5.3.1 Materials

Computerized molecular modeling and docking studies was performed using Autodock 4.2, molecular graphics laboratory, The Scripps research institute (Morris *et al*., 1998). The computer software Vega ZZ 2.4.0 (1996-2010) was used to perform energy minimization on nNOS and amyloid structures and curcumin. Protein-protein interactions were visualized using Accelrys Visualizer/Material Studios (version 2.0) (www.accelrys.com). Model images were rendered using Swiss–PDB viewer (V.4.1) (aka Deepview), Swiss Institute of Bioinformatics (Guex *et al*., 1997, 2012) (www.expasy.org). Triethanolamine/HCl was purchased from Sigma Aldrich. All reagents were of analytical grade and all solutions were prepared with deionized water obtained from a Milli-Q system. Fluorimetry analyses were carried out on PowerWave microplate spectrofluorimeter (Bio-Tek Instruments) with 96 well plates, operated at 1 nm bandwidth using the KC Junior software program.

5.3.2 Methods

5.3.2.1 Isolation of curcuminoids from turmeric

As described in Chapter 2, 2.3.2.5, pg.38.

5.3.2.2 Metal nanoparticle synthesis and characterization

As described in Chapter 2, 2.3.2.6, pg.38. Since nps were encased in HSAF, apoferritin controls (15 μM) were prepared.

5.3.2.3 In silico analysis: AutoDock

The crystal structure of rat nNOS (PDB: 1zvi) was used as a template for binding studies. Prior knowledge that the active site contained the heme and BH_4 co-factors resulted in the search for

these co-factors in the protein structure active site. This site was kept rigid while the rest of the protein was kept flexible. This site containing cofactors (i.e. the active site) was kept rigid while the rest of the protein was kept flexible. The structure (PDB: 1zvi) was desolvated, the heme and tetrahydrobiopterin (H_4B) cofactors were retained at the binding site and the crystal structure underwent energy minimizations using the computer software Vega ZZ 2.4.0. The rigid Heme co-factor/residue was taken as the reference point for measurements of distances that the Trp residues moved relative to their native position from the rigid Heme, upon binding of ligand (Aβ peptide). This 'movement' is better clarified as a change in distance of the Trp residue from its native position (before ligand binding). The original, polar, reversed amyloid sequences and curcumin (accession number: HMDBO2269) were designed built and minimized using Vega ZZ 2.4.0 and torsions of ligand were set at zero on AutoDock. Docking studies were performed on a Celeron (R) Dual-Core CPU 2 GB, 32-bit operating system. Using AutoDock 4.2 (Morris *et al*., 1998), the AutoDock tool set was used to merge non-polar hydrogen's such that all permitted torsions were allowed in docking studies. The active site of nNOS and the surrounding residues were mapped using the AutoGrid 4.2 algorithm, incorporating a grid box of dimensions 60 x 60 x 60 units along x, y and z axes, respectively. Atom maps were generated for all potential interactions between the ligand (amyloid and curcumin) and the amino acid Trp678 and Tyr706. Tyr706 is the only amino acid surrounding the active site that forms a hydrogen bond to the delta oxygen of the heme co-factor. Trp678 was one of the closest Trp residues to the active site and was significant to binding studies since Trp's are predominantly involved in quenching. In view of this, Trp678 and Tyr706 were kept flexible and heme and H_4B co-factors at the active site were kept rigid in order to monitor the interaction. Inhibition constants were calculated from AutoDock, Eq [13], pg. 126. The dockings were executed using a Lamarckian genetic algorithm to create populations containing 150 individuals and allowing for a maximum of 2.5×10^6 energy evaluations. For each ligand, "100 dockings" were generated with visual analysis and ligand scoring data was used to decide upon the optimal conformation for each docking run. At the end of a docking experiment with multiple runs, a cluster analysis was performed. Docking solutions with a ligand all atom RSMD values within 0.5 Å of each other were clustered together and ranked by the lowest

docking energy. The lowest energy clusters of all docking experiments were selected as representative binding modes. Protein-protein interactions were visualized using Accelrys Visualizer/Material Studios (version 2.0) and Deepview (V.4.1).

5.3.2.4 FRET

The FRET assay procedure was based on a method previously described but with slight modifications (Padayachee and Whiteley, 2011; 2013; Prostak *et al*., 2005). The use of fluorescein as a 'fluorescence resonance gate' in FRET is unique to the current protocol and was not previously described by Prostak *et al*., 2005. Reactions were performed with the original sequenced peptides [$A\beta_{17\text{-}21}$, $A\beta_{25\text{-}29}$, $A\beta_{29\text{-}33}$, $A\beta_{33\text{-}37}$ and $A\beta_{25\text{-}37}$]; the reversed and polar sequenced peptides [$A\beta_{17\text{-}21r}$; $A\beta_{29\text{-}33r}$, $A\beta_{17\text{-}21p}$ and $A\beta_{29\text{-}33p}$] (15 µM, 5 µl). Curcumin and Au/Ag-nps (4 nm), (15µM, 5µl) were also prepared. The Aβ peptides, nps and curcumin were the acceptor chromophores and where incubated with the donors: fluorescein (3 µl; 1mM) and nNOS (5 µl) in triethanolamine buffer [10 mM /0.1M NaCl; pH 7.4] in a final volume of 200 µl. The fluorescence of the donor (nNOS) [F^D] was determined by monitoring the fluorescence of nNOS alone without any accepter chromophores. The controls were nps alone, apoferritin alone, curcumin alone and fluorescein alone and were subjected to the same conditions as above. Reactions were left to incubate at 25 °C for 15 min to allow sufficient interaction between the acceptor or donor and fluorescein such that the fluorescence was an indication of the fluorescein-acceptor or fluorescein-donor complex and not fluorescein alone. It is not obvious on where fluorescein is located or what it is conjugated too in the experiment. Irrespective, the role of fluorescein was to behave as a 'fluorescence resonance gate' for transferring energy between the donor and acceptor and its exact location is not important in the current experiment. Fluorescein can behave as either a donor or an acceptor, depending on where it is located or conjugated too, during the co-incubation period of 15 min. Fluorescence was monitored at λ_{ex} = 448 nm and λ_{em} = 518 nm (fluorescein dependent excitation and emission wavelength). The rigid heme co-factor was taken as the reference point for measurements of distances that the Trp residues moved relative to their native position upon binding of ligand (Aβ peptide). This 'movement' is better understood as a change in distance of the Trp residue from its native position (before ligand

binding). This was deduced through careful computational analysis of the active site of nNOS, which showed the native positions of Trp625, Trp421, Trp676, Trp510, Trp306 and Trp716 as being > 2.5 nm relative to the Heme at the active site.

5.4 Results and discussion

5.4.1 In silico analysis: AutoDock

AutoDock has confirmed that all the ligands (Aβ peptides and curcumin) were docked to a single pocket/cavity within the enzyme (n=1) (Fig.5.3).The nature of the active site is hydrophobic due to the hydrophobic amino acids and aromatic nature of the ligands which bind at the site, facilitating hydrophobic interaction between ligand and receptor. Thus, the binding site of nNOS where Aβ interaction and curcumin occurred can be described as a 'hydrophobic binding pocket'.

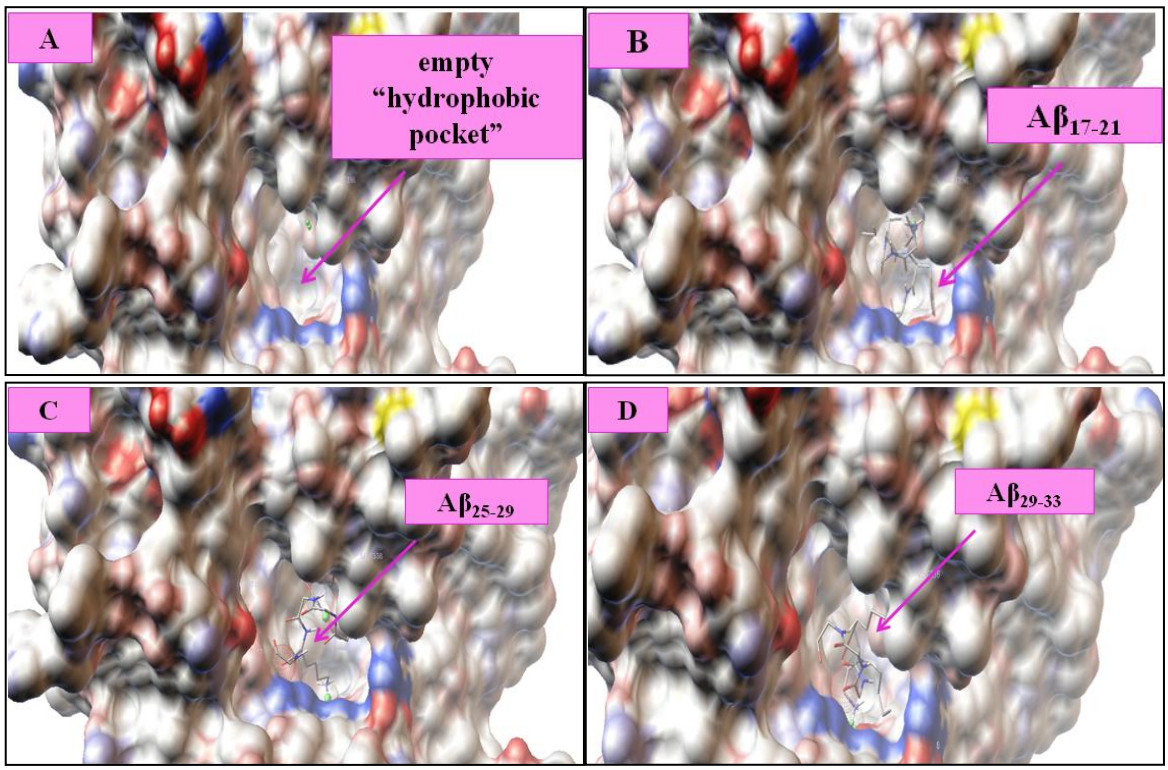

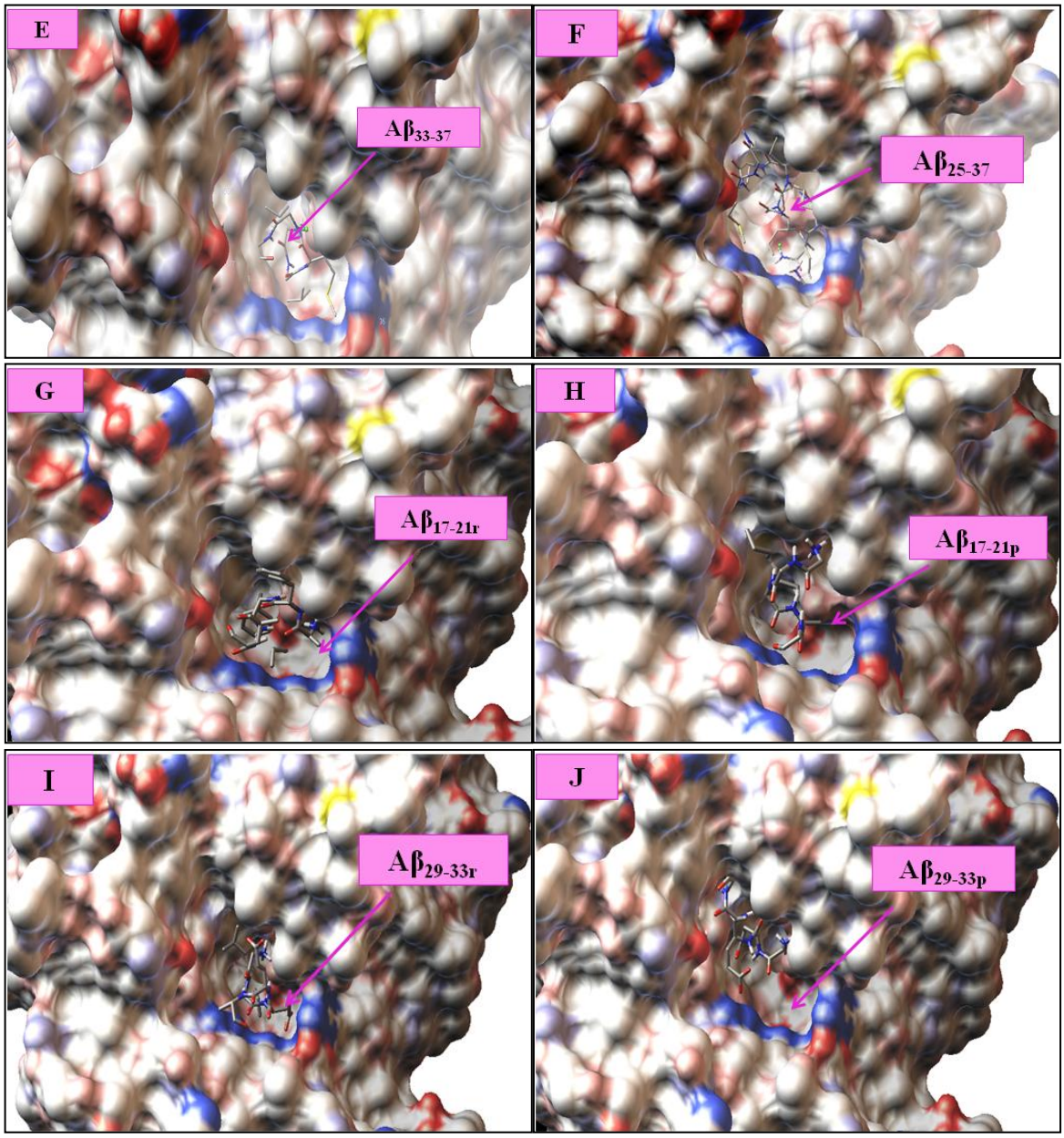

*Figure 5.3 : Empty binding site on nNOS in molecular surface colored atom by AutoDock 4.2 (**A**) and docked Aβ peptides in " hydrophobic pocket" of nNOS : $Aβ_{17-21}$ (**B**); $Aβ_{25-29}$ (**C**); $Aβ_{29-33}$ (**D**); $Aβ_{33-37}$ (**E**);$Aβ_{25-37}$ (**F**) $Aβ_{17-21r}$ (**G**); $Aβ_{17-21p}$ (**H**); $Aβ_{29-33r}$ (**I**) $Aβ_{29-33p}$ (**J**) [(PDB: 1zvi) (Aβ peptides: built by Vega ZZ)*

The pyrrole rings of the heme contain four nitrogen atoms (NA, NB, NC and ND) and four oxygen's (O2 A, B, C, D), referred to as the propionyl groups of the heme (Fig.5.4A). During

docking, the heme center was kept rigid and Trp678 and Tyr706 were kept flexible. Trp678 (Fig.5.4B) was closest to the active site and Tyr706 was the only amino acid to form a hydrogen bond to the delta oxygen on the heme (O2D) (Fig.5.4C). The movement of the flexible Trp678 was tracked relative to the nitrogen (NA) atom of the heme and the movement of Tyr706 was tracked relative to the O2D of the heme. In the unbound state of the enzyme, both Trp678 and Tyr706 maintained a distance of 10 Å from NA and O2D, respectively (Fig.5.4B, C).

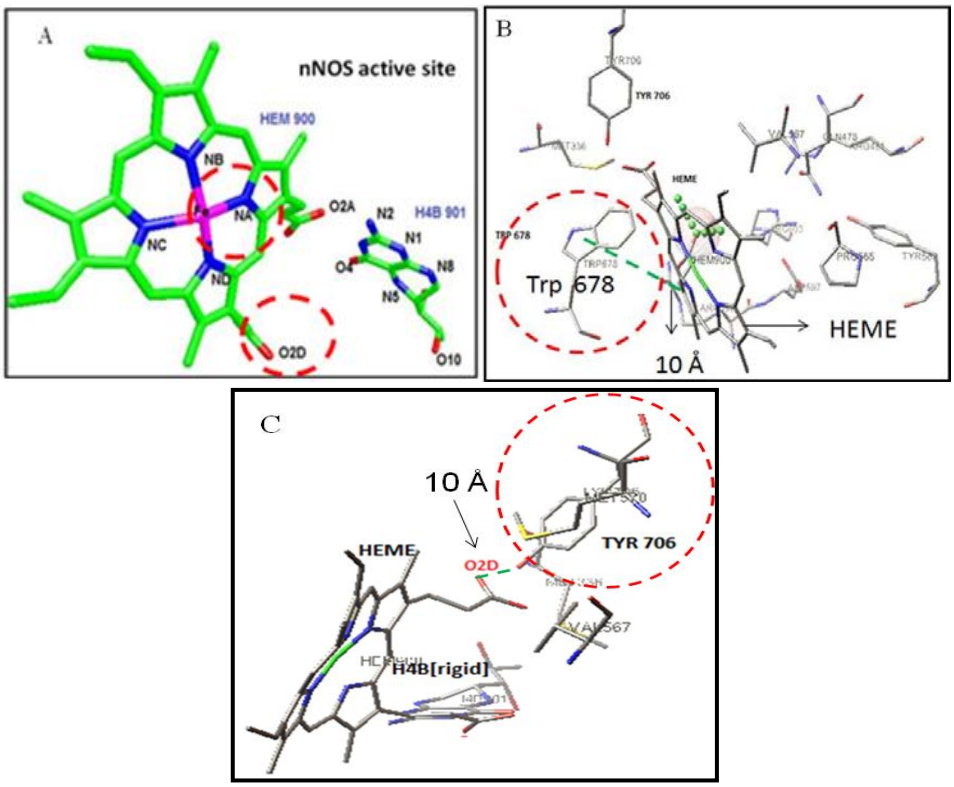

*Figure 5.4: The active site of nNOS depicting the heme and H_4B co-factors, illustrating the 4 amino nitrogen of the heme (NA) and the delta oxygen (O2D) [encircled in red] [(PDB: 1zvi; built by Vega ZZ)] (**A**), Distance of Trp678 from the rigid heme (NA) [encircled in red] (**B**), Distance of Tyr706 from the rigid heme (O2D) [encircled in red] (**C**). Performed by AutoDock 4.2*

5.4.1.1 Distance that Trp678 and Tyr706 shift when the original Aβ peptides and curcumin bind to the heme

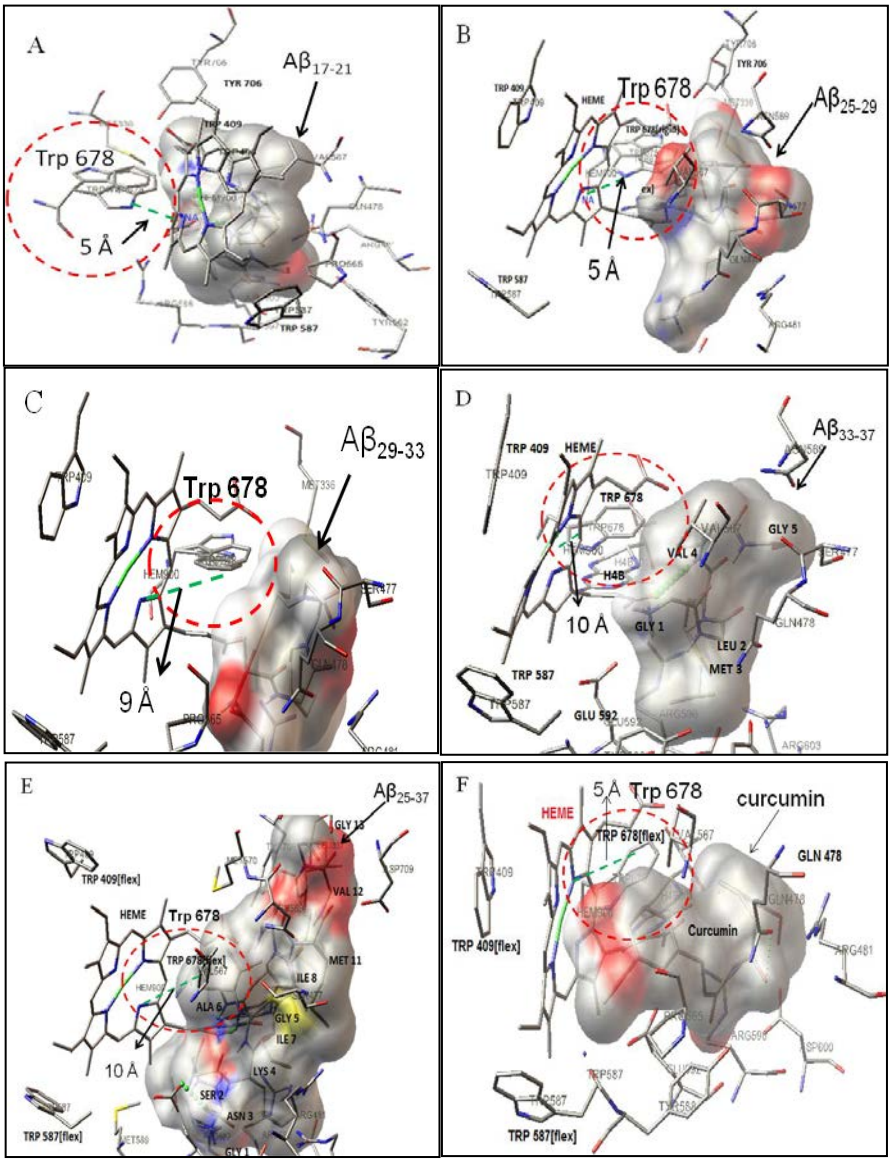

*Figure 5.5: The active site of nNOS, showing $A\beta_{17-21}$ (**A**); $A\beta_{25-29}$ (**B**); $A\beta_{29-33}$ (**C**); $A\beta_{33-37}$ (**D**); $A\beta_{25-37}$ (**E**) and curcumin (**F**) docked in molecular surface coloured by CPK, depicting the distance of flexible Trp678 (encircled in red) from the rigid heme (NA) [(PDB: 1zvi) (Aβ peptides: built by Vega ZZ) (curcumin: accession number (HMDBO2269). Performed by AutoDock 4.2.*

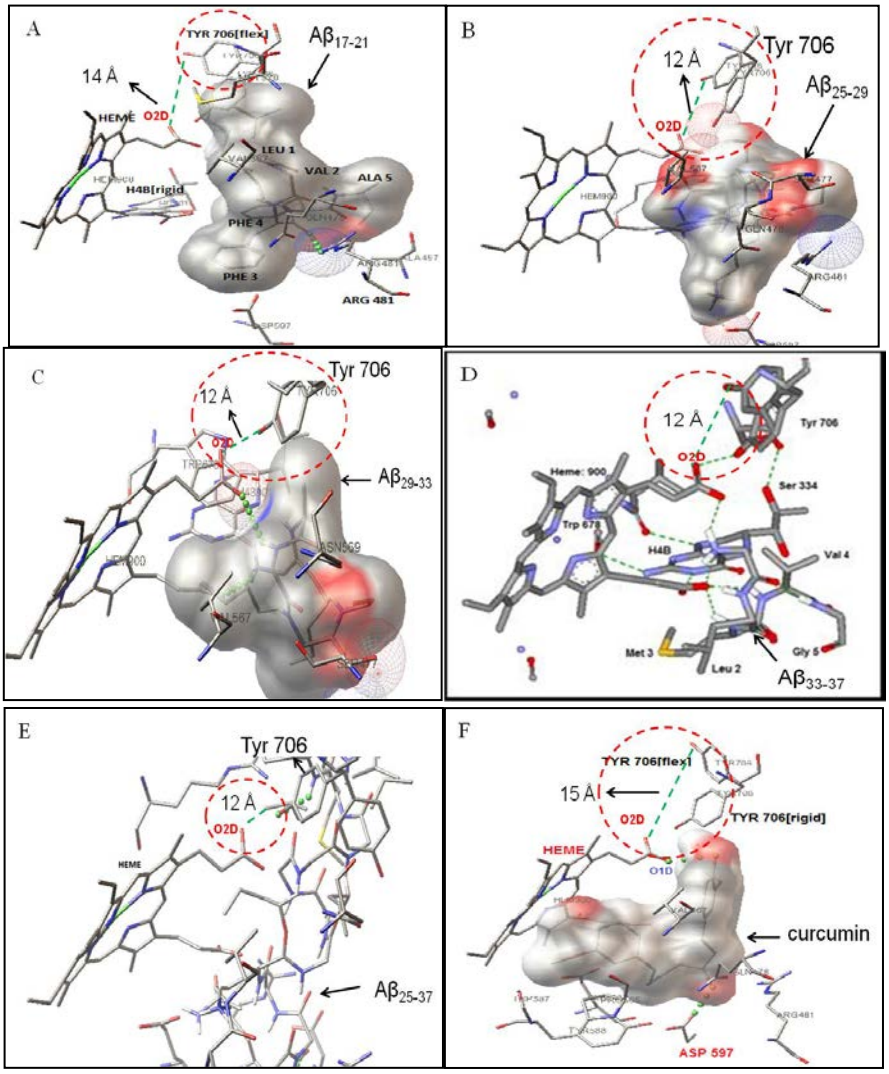

*Figure 5.6: The active site of nNOS, showing $Aβ_{17-21}$ (**A**); $Aβ_{25-29}$ (**B**); $Aβ_{29-33}$(**C**); $Aβ_{33-37}$ (**D**); $Aβ_{25-37}$ (**E**) and curcumin (**F**), depicting the distance of flexible Tyr706 (encircled in red) from the rigid heme (O2D). All Aβ peptides are docked in molecular surface (except $Aβ_{25-37}$); coloured by CPK, using AutoDock 4.2. Also $Aβ_{33-37}$ is docked by Accelrys Visualizer/Material Studios (version 2.0). Residues are displayed in stick solid and coloured by atom displaying hydrogen bonds (green dotted lines) [(PDB: 1zvi) (Aβ peptides: built by Vega ZZ) [curcumin: accession number (HMDBO2269)].*

According to results (Fig.5.5 A,B,F), the binding of $Aβ_{17-21,}$ $Aβ_{25-29}$ and curcumin to nNOS caused Trp678 to shift half the distance (5 Å) closer to the rigid heme (NA), while for $Aβ_{29-33}$ (Fig.5.5C), Trp 678 shifted a total of 9 Å towards the heme (NA). For $Aβ_{33-37}$ and $Aβ_{25-37}$ (Fig.5.5D, E), Trp678 remained at a distance of 10 Å from the heme (NA). According to the

results (Fig.5.6B, C, D, E), the binding of $A\beta_{25\text{-}29}$, $A\beta_{29\text{-}33}$, $A\beta_{33\text{-}37}$ and $A\beta_{25\text{-}37}$, resulted in the Tyr706 breaking its hydrogen bond and moving 12 Å away from the heme (O2D). When $A\beta_{17\text{-}21}$ and curcumin was bound to nNOS (Fig.5.6A, F), Tyr706 moved the greatest distance away from the heme (O2D), namely 14 Å and 15 Å, respectively.

5.4.1.2 Distance that Trp678 and Tyr706 shift when the reversed and polar Aβ peptides bind to the heme

According to the results, $A\beta_{17\text{-}21r}$ moved 5 Å closer to the heme (NA) and $A\beta_{29\text{-}33r}$ moved 10 Å closer to the heme (NA) (Fig.5.7 A, C). The binding of the $A\beta_{17\text{-}21p}$ (Fig.5.7 B), caused no change in the distance of Trp 678, while $A\beta_{29\text{-}33p}$ (Fig.5.7 D), caused Trp678 to shift 8.6 Å closer to the heme (NA). According to Fig.5.8A-D, the distance at which Tyr706 moved away from heme O2D was, namely, $A\beta_{17\text{-}21r}$ (13 Å); $A\beta_{17\text{-}21p}$ (14 Å); $A\beta_{29\text{-}33r}$ (12 Å) and $A\beta_{29\text{-}33p}$ (12.3 Å).

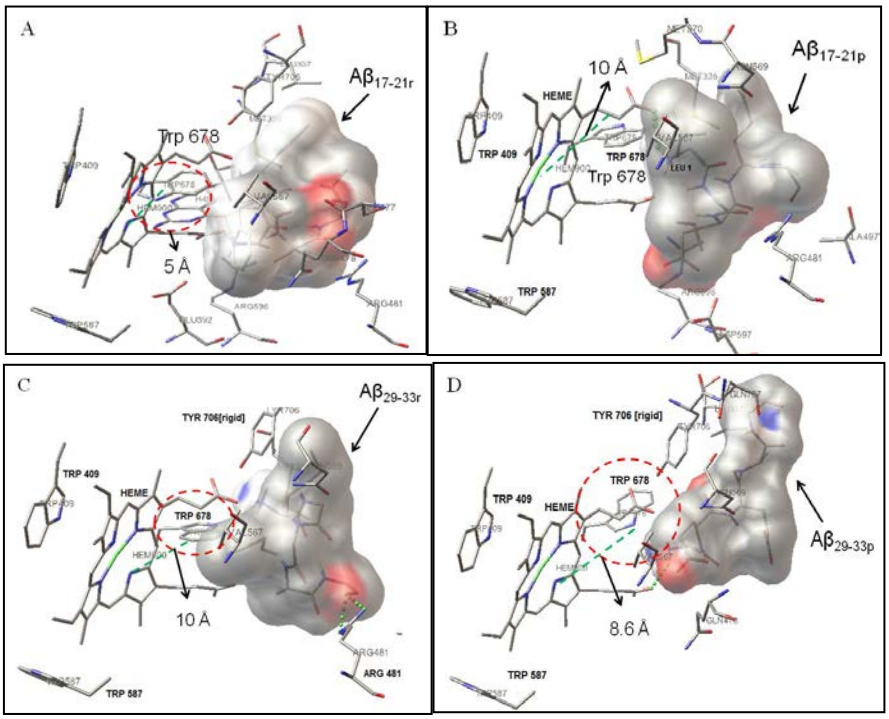

*Figure 5.7: The active site of nNOS, showing $A\beta_{17\text{-}21r}$ **(A)**; $A\beta_{17\text{-}21p}$ **(B)**; $A\beta_{29\text{-}33r}$ **(C)**; $A\beta_{29\text{-}33p}$ **(D)** docked in molecular surface coloured by CPK, depicting the distance of flexible Trp678 (encircled in red) from the rigid heme (NA) [(PDB: 1zvi) (Aβ peptides: built by Vega ZZ). Performed by AutoDock 4.2*

It seemed that the binding of the polar and reversed forms for each sequence of $A\beta_{17-21}$ and $A\beta_{29-33}$ to nNOS caused Tyr706 to shift approximately the same distance from the O2D of the heme. In general, the lower the free energy of binding the greater the interaction between nNOS and Aβ and the binding energies calculated by AutoDock were sufficient driving forces to unfold nNOS.

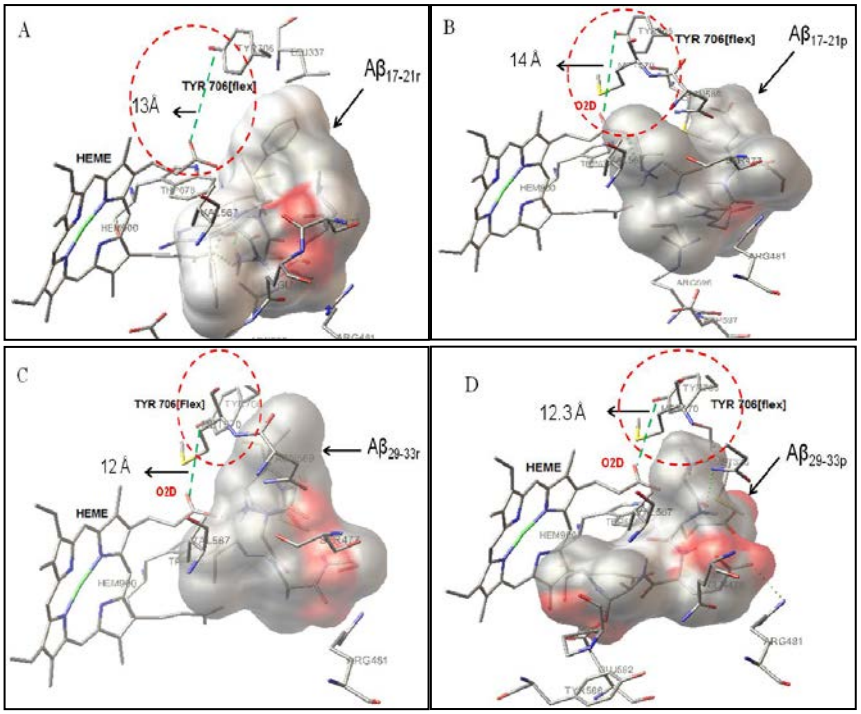

*Figure 5.8: The active site of nNOS, showing $A\beta_{17-21r}$ **(A)**; $A\beta_{17-21p}$ **(B)**; $A\beta_{29-33r}$ **(C)**; $A\beta_{29-33p}$ **(D)** docked in molecular surface coloured by CPK, depicting the distance of flexible Tyr706 (encircled in red) from the rigid heme (O2D) [(PDB: 1zvi) (Aβ peptides: built by Vega ZZ). Performed by AutoDock 4.2*

The cluster analysis of each docking run (results not shown) clearly showed that 90 % of docked conformations were within a single dominant cluster. According to Table 5.1, when Trp678 was kept flexible, the lowest free energy of binding (kcal.mol^{-1}) was for the original Aβ peptides, namely, $A\beta_{17-21}$ (-6.0), $A\beta_{29-33}$ (-7.1), $A\beta_{25-29}$ (-6.4) and $A\beta_{33-37}$ (-5.0). When Tyr706 was kept flexible, the lowest binding energies (kcal.mol^{-1}) were similarly attributed to the original sequences, namely $A\beta_{17-21}$ (-7.2), $A\beta_{29-33}$ (-7.1), $A\beta_{25-29}$ (-6.8) and $A\beta_{33-37}$ (-6.1) (Table 5.1). The low binding energies by these peptides also indicated the crucial role of the pentapeptide and glycine zipper peptides in interaction with nNOS.

Due to its length and bulky nature, $A\beta_{25-37}$ had the highest free energy of binding (-0.8 kcal.mol^{-1}), when Trp678 was kept flexible, indicating that it's binding affinity to nNOS was weaker than the other peptides (Table 5.1). This correlated with its high K_i value of 11 μM (chapter 2). This was however, not the case when Tyr706 was kept flexible because the binding energy was significantly reduced to -5.8 kcal.mol^{-1}(Table 5.1). A possible explanation for this is that the flexibility of Tyr706 afforded greater ease of binding for $A\beta_{25-37}$ to nNOS, than that afforded by the flexible Trp678. Also, $A\beta_{17-21p}$ and $A\beta_{29-33p}$ had the highest binding energies (-2.9 kcal.mol^{-1} and -3.1 kcal.mol^{-1}) compared to the binding energies of the reversed sequenced peptides ($A\beta_{17-21r}$ and $A\beta_{29-33r}$) (- 4.5 kcal.mol^{-1} and -5.0 kcal.mol^{-1}) (Table 5.1).

Table 5.1: Values for the distance (Å) that flexible Trp678 and Tyr706 moved relative to the rigid heme upon binding of Aβ peptides and curcumin. The corresponding binding energy (kcal.mol^{-1}) and docking Ki (μM) for binding of the ligands was calculated by AutoDock 4.2. The original distance of the Trp678 and Tyr706 from heme was 10 Å. The values for the experimental K_i were obtained in chapter 2.

		Trp678			Tyr706		
Aβ	**Experiment K_i**	**Distance shifted**	**Binding energy**	**Docking K_i**	**Distance shifted**	**Binding energy**	**Docking K_i**
17-21	5.1	5	- 6.0	6.2	14	- 7.2	5
17-21r	11	5	-4.5	207	13	-5.0	212
17-21p	19	10	-2.9	672	14	-2.8	785
29-33	7.5	9	-7.1	9.5	12	-7.1	6.1
29-33r	13	10	-5.0	450	12	-4.9	236
29-33p	21	8.6	-3.1	478	12.3	-3.0	592
25-29	9.1	5	-6.4	8.5	12	-6.8	9.6
33-37	8.4	10	-5.0	10	12	-6.1	10.6
25-37	11	10	-0.8	20	14	-5.8	52
curcumin	0.25	5	-6.6	1	15	-6.6	1

These results indicated that the polar glutamic acid weakened the binding affinity of the polar sequences to the enzyme. On the other hand the hydrophobic nature of the reversed sequenced peptides enhanced their binding affinity to the enzyme. A similar result was found when Tyr706 was kept flexible. The polar peptides ($A\beta_{17-21p}$ and $A\beta_{29-33p}$) had similar high binding energies (-2.8 kcal.mol^{-1} and -3.0 kcal.mol^{-1}) compared to the reversed sequenced peptides (-5.0 kcal.mol^{-1} and -4.9 kcal.mol^{-1}) (Table 5.1). Curcumin had the same binding energy (-6.6 kcal.mol^{-1}), when either Trp678 or Tyr706 were kept flexible (Table 5.1).

According to Table 5.1, the K_i (experimental and Autodock) were comparable only for $A\beta_{17-21}$, $A\beta_{29-33}$, $A\beta_{25-29}$ and $A\beta_{33-37}$. However $A\beta_{25-37}$ had higher docking K_i (20 μM and 52 μM) (Table 5.1) compared to K_i (experimental) of 11 μM. The same was true for docked curcumin (K_i = 1 μM) compared to K_i (experimental) of 0.25 μM (Table 5.1). Also, the docked polar and reversed sequenced peptides had K_i values which were considerably higher in magnitude than their K_i (experimental). The reason for the unusual lack in correlation of the K_i values for curcumin and the $A\beta_{25-37}$ and the polar and reversed peptides remain unknown. In AutoDock, since $K_d = K_i$ and is related to free energy Eq [13], high K_i values (Table 5.1) meant that the polar and reversed sequenced peptides had a lower affinity and a more positive binding energy, which supported thermodynamic findings (chapter 4). It must also be noted that computerized docking took into account steric hindrance of the bulky side chains of $A\beta_{25-37}$ (a factor excluded in bench work experiments), thus increasing the K_i from 20-52 μM (Table 5.1). In the laboratory, curcumin was extracted as a mixture, along with its three sister curcuminoids. The apparent favourable inhibitory effect by all four curcuminoids was supported by a low experimental K_i of 0.25 μM, compared to the actual single form of curcumin docked within nNOS (K_i =1 μM). Irrespective, it is clear that both K_i values (experimental and AutoDock) reflected that curcumin had a tight binding affinity to the enzyme active site and formed a stable complex with the enzyme. The results also suggested that the inhibition potential of curcumin was maximized in the presence of curcumin I, curcumin II and cyclocurcumin but more studies into curcuminoids would need to be conducted and forms the basis of future work.

Table 5.2 Distance of tryptophan residues from the rigid heme (NA) (≤ 10 Å), not shown on Fig.5.5-Fig.5.8

TRP	**W_{561}**	**W_{409}**	**W_{587}**	**W_{678}**	**W_{711}**
Å	**9**	**10**	**10**	**10**	**10**

According to Table 5.2, the structure of nNOS (PDB: 1zvi) consists of 5 Trp amino acids located within ≈10 Å of the heme binding region (Padayachee and Whiteley, 2011; 2013) and any one of them could potentially be identified as the single Trp residue (θ =1) involved in quenching with all ligands found in chapter 4. Since these Trp amino acids are all within the active site, it is

reasonable to conclude that inhibition by all of these ligands occurred at the active site of the enzyme. Only in the case of the polar Aβ peptides ($A\beta_{17\text{-}21p}$ and $A\beta_{29\text{-}33p}$), did the number of Trp amino acids increase to 5 at 313 K (chapter 4). These were identified as Trp561, Trp409, Trp587, Trp678 or Trp711 and remained around 10 Å from the heme (Fig.5.5-Fig.5.8). For the current study, only one of these five amino acids (Trp678) was chosen to monitor changes in distance upon ligand binding to nNOS. The reason why the Trp678 remained at approximately 10 Å from heme (Table 5.2) for the interaction of $A\beta_{17\text{-}21p}$ and $A\beta_{29\text{-}33p}$ could be due to their weaker binding affinity to nNOS (chapter 2) decreasing the degree of conformational change in nNOS. Trp678 moved a distance of 5 Å from the heme when both the original and reversed forms of $A\beta_{17\text{-}21}$ were bound to the enzyme. This could be due to the fact that $A\beta_{17\text{-}21}$ had greater inhibition of the enzyme (K_i=5.1 μM) resulting in considerable structural changes. The fact that the binding of the reversed form of $A\beta_{29\text{-}33}$ caused Trp678 to remain in its original position (10 Å) while the binding of the reversed form of $A\beta_{17\text{-}21}$ induced a change in distance (5 Å) confirmed that it is the identity of the amino acids, rather than their order which influenced their binding to nNOS. Surprisingly, the binding of the hydrophilic $A\beta_{25\text{-}29}$ to nNOS induced greater conformational change in the enzyme as Trp678 moved 5 Å, compared to the binding of $A\beta_{33\text{-}37}$ and $A\beta_{25\text{-}37}$ (Table 5.1). This suggested that in the case of $A\beta_{25\text{-}29}$, electrostatic interaction by the positively charged amino group of Lys28, rather than hydrophobic interaction, was predominant.

The binding of curcumin to nNOS resulted in Trp678 of the active site shifting a distance of 5 Å closer to the rigid heme (NA) and Tyr706 moved 15 Å away from the rigid heme (O2D) (Table 5.1), indicating that the binding of curcumin induced conformational change in the enzyme. Also, according to inhibition studies (chapter 2) and fibrillogenesis studies (chapter 3), it was speculated that the two phenolic rings of curcumin were critical in inhibiting nNOS activity and reversing fibril formation. According to Fig.5.9, phenolic rings 1 and 2 of curcumin were shown to form hydrogen bonds (green dashed lines) with the nitrogen atoms of the heme (NA and NB) and the oxygen of H_4B (O4) of the active site. The interactions are encircled in red dashed circles (Fig.5.9), validating the crucial role of aromatic interactions in the curcumin molecule. Also the interactions of curcumin with nNOS was not amino acid sequence dependent as

compared to the Aβ peptides, but rather its binding to enzyme or to fibril forming protein is conformation-dependent so that its aromatic rings are easily accessible for hydrogen bonding or Van de Waal interactions. Our findings agree with a previous study which found that the interaction and inhibition ability of curcumin is linked to the possession of 2 aromatic rings spaced 16-19 Å apart and at least 1 polar aprotic functional group per a ring (Jones and Mezzenga, 2012).

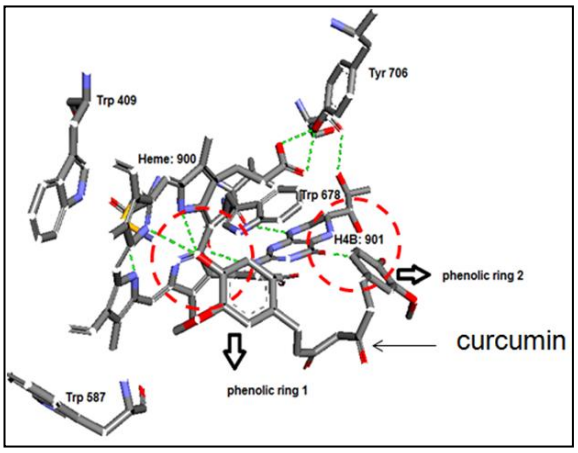

Figure 5.9: Docking of curcumin (visualized by Accelrys Visualizer/Material Studios (version 2.0), depicting the two phenolic rings critical in interaction with nNOS. Residues are displayed in stick solid and coloured by atom displaying hydrogen bonds (green dotted lines) [(PDB: 1zvi) (curcumin: accession number (HMDBO2269)]

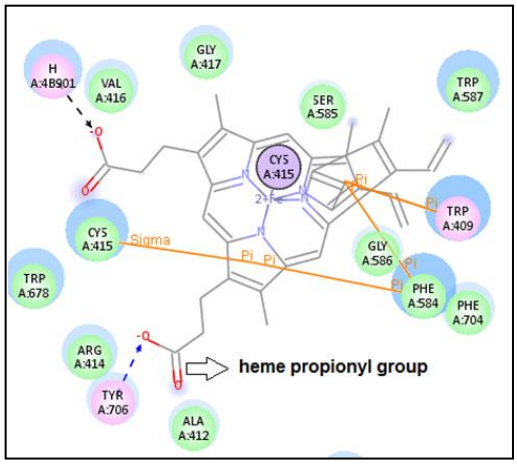

Figure 5.10: 2-D visualization of heme active site, showing heme propionyl groups and critical amino acids surrounding the heme co-factor within the active site of nNOS [visualized using Accelrys Visualizer/Material Studios (version 2.0)]

According to Fig.5.10, it can be seen that there are a variety of redox co-factors and amino acids in the catalytic assembly of nNOS which influences its activity. Tyr706 and H_4B901 (in the circles which are shaded pink) are shown to be interacting with the propionyl groups on the heme. Trp409 (also shaded pink) is shown to be interacting with one of the pyrrole rings of the heme. Trp409, Trp678 and Trp587 (shaded green) are three amino acids shown to be closest to the active site. Cys415, Phe584 and Trp409 are also depicted as been involved in pi-pi and sigma interactions. Also, the hydrophobic amino acids (Arg414, Ala412,Cys415, Ser585, Val416, Trp409, Trp678, Trp587, Phe584) are some of the critical amino acids surrounding the active site which may be involved in binding interactions with the inhibitors (Aβ peptides and curcumin) (Fig.5.10). Ser585 and Tyr706 both contain an 'OH' group which protects the hydrophobic pocket. The side chains of Tyr, Phe and Trp provide an "aromatic box" which provides both edge-to-face and stacking interactions. Also, strong gains in binding affinity could be obtained by filling this pocket (Zacharias and Dougherty, 2002). Due to the delocalization of electrons on aromatic rings, the face of the rings has a partial net negative charge, whereas the hydrogen atoms on the edge of the rings have a corresponding partial positive charge. Electrostatic interactions between these partial charges facilitate aromatic interaction with the enzyme (Veselovsky *et al*., 2002).

In view of this, Tyr706 is a crucial amino acid because by exposing its aromatic side chain to the binding site and given its set of electronic properties, this amino acid possesses a set of preferred interaction geometries with nNOS. Also, Ala412 and Val416 are hydrophobic amino acids of the active site which point to a hydrophobic binding pocket for the inhibitor. Accelrys Visualizer/Material Studios (version 2.0), was used to depict the Aβ hydrophobic amino acids interacting with Ala412 and Val416 of the enzyme active site in all instances of binding to nNOS (results not shown). Thus, confirming that hydrophobic interactions were responsible for the formation of the bound Aβ-nNOS complex.

Research has shown that a common feature of high potency inhibitors is the presence of an amino group in the side chain (Litzinger *et al*., 2006). In our studies, Arg481 and Arg414 provided electrostatic stabilization. Also, the two negatively charged amino acids: Asp597 and Glu592 and the positively charged Arg481 were also critical in electrostatic interaction between Aβ motifs and nNOS. These amino acids surrounded the bound Aβ-nNOS complex and formed hydrogen bonds with the complex (Fig.5.5 D; Fig.5.6 B, A, F and Fig. 5.8 C, D).

Visualization by Accelrys Visualizer/Material Studios (version 2.0) (results not shown) depicted Aβ peptides and curcumin forming hydrogen bonds with the heme propionyl groups [(Heme 900:O1D and O2D)] and with the nitrogen and oxygen atoms of H_4B (N2,N3,N8, O10,O4). Such interactions between Aβ and nNOS point to the role of the heme and H_4B cofactors in explaining the mechanism of inhibition. According to literature, dimerization increases nNOS activity by creating high affinity binding sites for L-arginine and H_4B, thus facilitating electron flow from one monomer to the other (Siddhanta *et al*., 1996; Groves and Wang, 2000; Alderton *et al*., 2001). Dimerization is also known to shift the heme iron spin equilibrium back toward high spin thus increasing the reduction potential of the heme and enabling electron transfer by the H_4B co-factor (Siddhanta *et al*., 1996). In view of these findings and our results (Fig.5.5-Fig.5.8), it could be that the inhibitors prevented H_4B from reducing the heme group and this destabilized the dimer of nNOS, leading to the inhibition of nNOS activity.

The observation that binding can result in significant conformational changes of partner molecules led to the induced-fit concept (Koshland, 1958). The binding of Aβ peptides and curcumin to nNOS clearly induced conformational change in the enzyme as was evident by the change in distance and orientation of Tyr706 and Trp678. Thus it could be postulated that the type of binding mechanism between Aβ peptides and curcumin with nNOS was induced fit. This will, however, need to be confirmed by a more in-depth analysis of the "induced-fit" model and "symmetry model". The interaction of the ligands with nNOS can further be explained in phases. During the initial diffusive approach, guided by hydrogen bonding, hydrophobic forces and electrostatic interaction, the ligands encounter each other many times before the heme complex

forms (Fig.5.5-Fig.5.8). This is referred to as the association phase, proposed in chapter 2. Also, Aβ peptides in their native or monomeric state favour an α-helix structure (Kelly, 1998; Takano, 2008). In view of this during the association phase, the Aβ peptides in their native state bind as monomers to nNOS and interact with the "hydrophobic pocket" of nNOS. This drives the enzyme to a structural intermediate in which the environment of the active site residues, especially Trp678 and Tyr706 becomes altered, thus affecting the catalytic characteristics of nNOS and initiating conformational change to a β-structure termed a fibril, after which a period of dissociation occurred (Padayachee *et al*.,2011; Padayachee and Whiteley, 2011; 2013).

5.4.1.3 Suggested 3-D models of modified Ag and Au nps binding to heme

Metallic nps cannot be docked because the scoring function of the binding of a protein to a metal needs to be addressed and a specific metal binding term needs to be developed in order to generate suitable metal parameter files and the relevant atom maps for AutoDock. This opens up new avenues of research concerning nanoparticle crystallography which can facilitate enhanced and in-depth insights into protein-np interactions in the field of bioinformatics (Farrow *et al*., 2010).

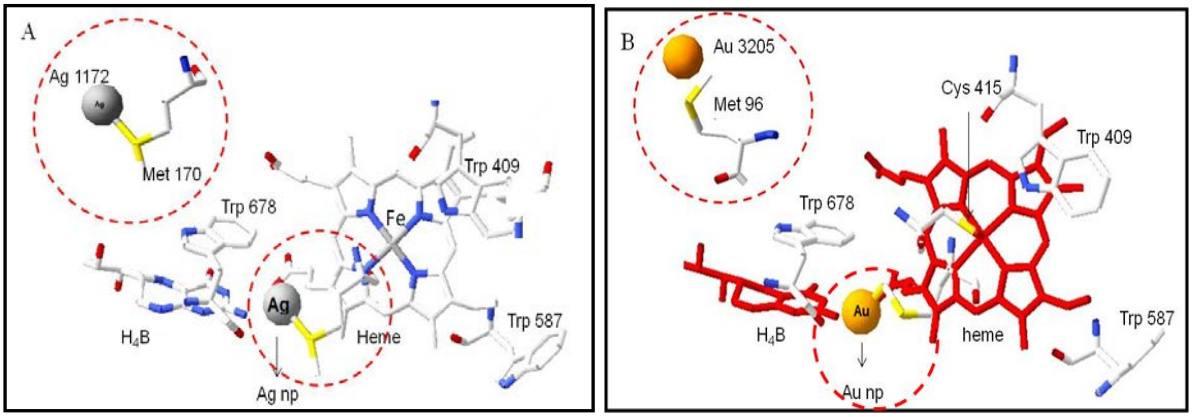

*Figure 5.11: Diagram depicting a Ag np (1172) conjugated to Met170, modified from the x-ray structure of ferritin from Pyrococcus furiosus (PDB: 2x17) (**A**). The ferric ion (Fe) of the heme center may be crucial in electrostatically attracting the Ag np (**A**). Au np (3205) conjugated to Met96, modified from the x-ray structure of apoferritin with gold ions (PDB: 3H7G) (**B**). The diagram depicts the rear side of the heme coloured red) with Cys415 conjugated to the Fe^{+3} ion. The Cys415 possesses a sulphur atom*

*(yellow) that maybe crucial to the attracting of the Au np (**B**). The heme was "fitted" to the nps using Deepview (V.4.1.)*

The Au and Ag nps were thus modified from existing ferritin (PDB: 2x17) and appoferritin (PDB: 3H7G) structures and fitted to the heme of nNOS, using Deepview (V.4.1) (Fig.5.11A, B). To suggest that electrostatic attraction was possibly the predominant force in the binding of nps to nNOS, the Ag np (grey) was attracted to the Fe^{+3} center (shaded grey) of the heme cofactor (Fig.5.11A). For this to occur, the charge on the Ag atom would have to be negative. Also the Au np was attracted to the sulphur atom of Cys415 attached to the heme (Fig.5.11B). Since this was only a model, further studies would have to be conducted to verify these findings using bioinformatics.

5.4.2 FRET

FRET studies confirmed that Trp residues do indeed change their distance in the presence of ligand bound to nNOS. According to Table 5.3, the distance that a Trp residue moved in the presence of bound Aβ was: 28 Å ($A\beta_{17\text{-}21}$); 27 Å ($A\beta_{25\text{-}29}$); 29 Å ($A\beta_{29\text{-}33}$); 28 Å ($A\beta_{33\text{-}37}$); 27 Å ($A\beta_{25\text{-}37}$). The distance that a Trp residue moved in the presence of bound polar and reversed sequenced Aβ was: 31 Å ($A\beta_{17\text{-}21r}$); 30 Å ($A\beta_{29\text{-}33r}$); 34 Å ($A\beta_{17\text{-}21p}$); 37 Å ($A\beta_{29\text{-}33p}$). In the presence of bound nps and curcumin, a Trp residue moved 20 Å (Ag); 18 Å (Au) and 20 Å (curcumin).

In the presence of bound BAEE, a Trp moved a distance of 23 Å. According to Table 5.4, the identity of this Trp residue could either be Trp625, Trp510 or Trp716, all three of which lay > 20 Å from the heme. Regardless, the distance moved by Trp upon BAEE binding (23 Å) (Table 5.3) was in agreement with computational analysis of the active site of nNOS [PDB ID: 1zvi] which showed that the arginine substrate binds within a distance of 24.6 Å [backbone chain nitrogen - heme oxygen] (Padayachee and Whiteley, 2011; 2013). The FRET values (Table 5.3), clearly showed that the Trp residues moved a far greater distance away from the heme (on average between 18-37 Å) in the presence of bound ligand, compared to the relatively short distance (≤ 10 Å) when the Trp residues moved toward the heme (Fig.5.5-Fig.5.8). These

distances (18-37Å), calculated from the FRET analysis is the new distances that the Trp residues move from their native position. The difference of the FRET distance from the native distance is taken into account as a reflection of how far the Trp residue has shifted, relative to its native distance from the rigid Heme. A case in point is that Trp_{625} is in its native position from the rigid Heme at 28 Å (Table 5.4) and then $Aβ_{29\text{-}33p}$ binds to the enzyme, such that the FRET distance (new distance) of Trp_{625} from the heme was measured as 37 Å (Table 5.3). This means that the Trp_{625} moved a difference of 9 Å (0.9 nm) from its original/native position. This reasoning can be applied to FRET distance measurements for all Aβ peptides, nps and curcumin.

According to Table 5.4, Trp625, Trp421, Trp676, Trp510, Trp306 and Trp716 are found within the same range of distances from the heme as the results shown for FRET analysis (on average between 18-37 Å). In view of this finding, it is reasonable to conclude that the identity of the Trp monitored by FRET could be either one of these 6 Trp residues shown in Table 5.4.

Table 5.3: FRET values for efficiency of energy transfer (E)(%) and distance (r [Å]) between donor (D)[nNOS] and acceptor (A)[original Aβ, polar and reversed Aβ, nps and curcumin] based on the fluorescence of both donor and acceptor($F^{D,A}$) and the fluorescence of donor (F^{D}) (R_0 = 44 Å)

Acceptor	F^{D}	$F^{D,A}$	E	r (Å)
$Aβ_{17\text{-}21}$	1992	130	94	28
$Aβ_{25\text{-}29}$	1992	108	95	27
$Aβ_{29\text{-}33}$	1992	169	92	29
$Aβ_{33\text{-}37}$	1992	124	94	28
$Aβ_{25\text{-}37}$	1992	109	95	27
BAEE	1992	46	98	23
$Aβ_{17\text{-}21r}$	1992	154	92	31
$Aβ_{29\text{-}33r}$	1992	150	92	30
$Aβ_{17\text{-}21p}$	1992	215	89	34
$Aβ_{29\text{-}33p}$	1992	215	89	37
Ag (4 nm)	1992	18	99	20
Au (4 nm)	1992	10	99	18
Curcumin	1992	22	98	20

Table 5.4 Distance of tryptophan residues from the rigid heme (NA) (> 10 Å)

TRP	W_{625}	W_{421}	W_{676}	W_{510}	W_{306}	W_{716}
Å	**28**	**15**	**19**	**23**	**19**	**29**

Also, these 6 Trp residues are located on the surface of nNOS. Thus, it can be concluded that FRET analysis monitored the distance of any of the 6 Trp residues on the enzyme surface, while AutoDock studies monitored the movement of any of the 5 Trp residues buried within the active site of nNOS. Also the energy transfer between nNOS (donor) and ligand (acceptor) was highly efficient (E = ≥ 89 %) for all ligands (Table 5.3). Moreover, the mechanism of FRET in understanding binding studies of BAEE, Aβ peptides, nps and curcumin (acceptors) with nNOS (donor) is illustrated in Fig.5.12.

The acceptors were incubated in the presence of fluorescein. It must be noted that nNOS and/or fluorescein have the potential to behave as donor molecules. In the absence of resonance energy transfer, the donor (fluorescein or nNOS) (1) and the acceptor (2) remained unbound such that the signal of fluorescein (F) was high and the emission of fluorescein acceptor (A) was low. However, when the enzyme-acceptor–donor (E-A-D) complex formed (3), fluorescein (D) which was attached to the acceptor terminus (2) behaved as a 'fluorescence resonance gate' for transferring excited energy from the donor (nNOS in this case) to the acceptor. Acceptors (ligands) thus experienced an increase in excitation energy after the emission by fluorescein (Fig.5.12).

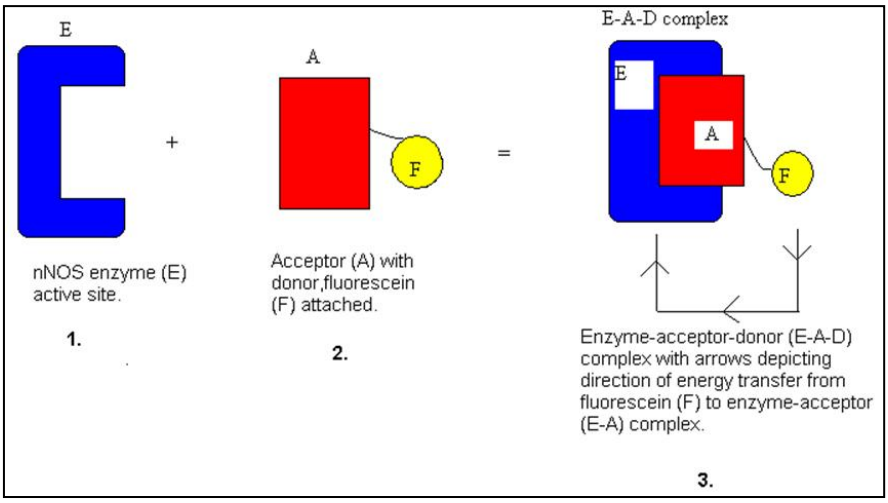

Figure 5.12: Proposed mechanism of FRET in binding studies of BAEE, Aβ, nps and curcumin (acceptor) and nNOS (donor).

5.5 Conclusions

AutoDock and FRET were efficient molecular docking and fluorimetric tools to account for the change in distance of 11 of a total of 13 Trp amino acids found in nNOS. On the one hand, AutoDock monitored the distance moved by only one Trp amino acid, namely Trp678 which was one of the 5 potential Trp amino acids (Trp561, Trp409, Trp587, Trp678 and Trp711) located in the interior of the enzyme. On the other hand, FRET monitored the distance moved by any of the 6 Trp amino acids found on the surface of the enzyme, namely, Trp625, Trp421, Trp676, Trp510, Trp306 and Trp716. Trp678 was identified as the single Trp residue involved in quenching by ligands and its location was confirmed to be within the active site of the enzyme. The single site of binding on nNOS was thus clarified to be the active site containing the heme and H_4B cofactors. The specific shift in distance and change in orientation of Trp678 and Tyr706 upon binding of Aβ (including polar and reversed sequences) and curcumin suggests that these amino acids belonging to nNOS were crucial in facilitating the binding of ligands to the active site. Also the original and reversed sequences had the lowest binding energies compared to the polar sequences, indicating that hydrophobic interaction was crucial in maintaining a stable complex with nNOS, while polar glutamic acid interfered with complex formation between ligand and enzyme. Also, the K_i (experimental) values of the original sequenced peptides were approximately the same as those K_i (AutoDock) values which was the not the case for $A\beta_{25-37}$, curcumin, and the polar and reversed sequenced peptides. It is clear that in general, the high K_i values obtained from AutoDock and those obtained experimentally, although not comparable, still exemplified the inability of $A\beta_{25-37}$, and polar and reversed sequenced peptides to bind favourably to the active site of nNOS and form a stable complex with the enzyme. Docking for curcumin (K_i = 1 μM), excluded the role of the other two curcuminoids which played a role in lowering the experimental K_i value to 0.25 μM, suggesting that curcuminoids in the presence of curcumin may enhance inhibition of nNOS more than curcumin on its own.

In addition, 3-D models of np-nNOS interaction proposed that electrostatic interaction with the Fe^{+3} heme center and the sulphur functional groups in Cys415 attached to the heme could be a

likely mechanism by which nps inhibited nNOS activity. Docking also confirmed that the binding of curcumin to the enzyme, induces conformational change in the enzyme and the aromatic interactions were crucial in inhibition of enzyme activity and reversing fibril formation. Also it was established that it is the preferred conformation of the curcumin molecule, rather than its amino acid sequence which determines its inhibitory and anti-amyloid function. Also, it was depicted via AutoDock that Aβ peptides and curcumin interacted with the BH_4 co-factor, resulting in an inactive monomeric form of nNOS and was another likely explanation as to how the ligands inhibited the activity of the enzyme.

6 General discussions and future perspectives

6.1 General discussions

Fibrillogenesis is central to the pathogenesis of AD (Dong *et al*., 2012). Hence mechanisms into how fibrils form is an essential step to gaining insight into the disease and to assist in designing compounds which may inhibit, prevent or suppress fibril formation. Experimental findings have supported the hypothesis that interaction of the hydrophobic pentapeptide ($A\beta_{17-21}$), the glycine zipper motifs ($A\beta_{25-29}$, $A\beta_{29-33}$, $A\beta_{33-37}$ and $A\beta_{25-37}$); the reversed sequences ($A\beta_{17-21r;}$ $A\beta_{29-33r}$) as well as polar sequences ($A\beta_{17-21p}$; $A\beta_{29-33p}$), silver/gold nanoparticles and curcumin with nNOS has provided insight into a mechanistic understanding of fibrillogenesis (Padayachee *et al*, 2011, Padayachee and Whiteley, 2011; 2013).This chapter will summarize all experimental results obtained in support of the hypothesis. The enzyme nNOS and its metabolic substrate arginine along with the accumulation of amyloid peptides are all located in the astrocytes of an Alzheimer's patient's brain. Thus, it was significant that $A\beta_{17-21,}$ $A\beta_{25-29,}$ $A\beta_{29-33}$; $A\beta_{33-37}$ and $A\beta_{25-37}$ bound to nNOS and inhibited the enzyme to varying degrees with respective K_i values of 5.1 µM; 9.1 µM; 7.5 µM, 8.4 µM and 11 µM. The K_i value for $A\beta_{17-21}$ was the lowest; namely, 5.1 µM, indicating that this fragment inhibited the activity of nNOS the most, while the K_i value for $A\beta_{29-33}$ (7.5 µM) was the second peptide at displaying potent inhibitory potential.

Reversing the sequences of $A\beta_{17-21}$ and $A\beta_{29-33}$ increased the K_i values to twice their original value to 11 µM and 13 µM, respectively. These findings revealed that the original positions of the hydrophobic amino acids, i.e. phenylalanine and isoleucine (Phe19 and Phe20; Ile31 and Ile 32) were critical in inhibiting nNOS activity. However the substitution of the Phe and Ile residues of $A\beta_{29-33}$ and $A\beta_{17-21}$ with polar glutamic acid residues increased the K_i value to between 3 and 4 fold that of their original values. These findings indicated that association between enzyme and peptide was driven by hydrophobic interaction. Moreover the K_i values which were obtained from AutoDock 4.2 correlated with the K_i values of the original sequences. It was also found that Ag nps had a slight tighter association to the enzyme (K_i = 0.12 µM) compared to Au (K_i = 0.15 µM) and curcumin (K_i = 0.25 µM). The inhibition of nNOS activity, subject to the binding of Aβ peptides, nps and curcumin supported our previous findings that the

mechanism of interaction was based on the principle of association-dissociation. Dissociation of the Aβ from the enzyme into a form that could no longer bind was termed a fibril (Padayachee *et al*., 2011, Padayachee and Whiteley, 2011; 2013).

In addition, ThT fibrillogenesis assays successfully reported two major findings, i.e. (1) nNOS is an amyloidogenic catalyst for the formation of fibrils from glycine zippers and pentapeptides and (2) curcumin and nps hinder the catalytic ability of nNOS to form fibrils from these Aβ peptides by reversing the formation of fibrils. Ag nps had a greater ability to reverse fibrils than Au and curcumin. Spectrofluorimetry successfully confirmed binding and thermodynamic parameters and AutoDock revealed that conformational change of nNOS occurred, subject to ligand binding. All ligands bound at a single site, the active site and formed a complex with the heme co-factor. The binding of all ligands to nNOS, induced conformational change in the enzyme such that ≈ 1 Trp residue was exposed for quenching at 298K. The identity of this single Trp residue was Trp678 from molecular docking studies. The increase in temperature from 298K-313K pointed to a dynamic quenching mechanism whereby thermal energy aided in diffusion of all ligands to the active site. With the binding of polar Aβ peptides and nps, more than 1 Trp residue was exposed at the surface of the enzyme. Also, the value for the Stern-Volmer constant (K_{sv}) at 313K was greater for the reversed sequenced peptides [$A\beta_{17\text{-}21r}$ (5.2×10^{-2} μM^{-1}); $A\beta_{29\text{-}33r}$ (6.2×10^{-2} μM^{-1})] than the polar and original sequenced ones. These findings have shown that even though the original positions of isoleucine and phenylalanine contributed to greater inhibition, the reversed positions of these same amino acids played a prominent role in quenching.

Ag nps were found to be equally potent in inhibition and quenching of nNOS. The ΔH and ΔS of Ag nps i.e. 100 $kJ.mol^{-1}.K^{-1}$ and 296 $J.mol^{-1}.K^{-1}$ was also higher in value than that of Au and curcumin indicating that Ag displayed the strongest interaction with nNOS. The increase in K_d values with temperature supported the fact that thermal input was a requirement in interaction of ligands with the enzyme. With increasing temperature, the dissociation of ligand from enzyme was favoured. In the case of Aβ, it could be suggested that dissociation of the peptide from the enzyme into a fibril was most favoured at high temperatures. Also, at 298K, $A\beta_{29\text{-}33}$ had the lowest K_d (2.7 μM) compared to the K_d of $A\beta_{17\text{-}21}$ (6.0 μM) , indicating that it was the identity

of the hydrophobic amino acids and not so much their affinity to the enzyme which played a role in the mechanism of binding of Aβ to the enzyme. It was conclusive that hydrophobic interaction dominated the interaction between the ligands and nNOS due to the positive signs for enthalpy and entropy. This finding was further compounded by the fact the more polar $A\beta_{25-29}$ had the lowest ΔH and ΔS (41 $kJ.mol^{-1}.K^{-1}$ and 105 $J.mol^{-1}.K^{-1}$) compared to other Aβ peptides. Also the polar peptides had the highest K_d values (≥ 100 μM) within the temperature range of 298K-313K. It was concluded that the binding reaction between the ligands and nNOS was non-spontaneous and endothermic at low temperatures (+ΔG) but spontaneous at high temperatures (-ΔG).

It was clear that the Trp678 and Tyr706 were two crucial amino acids in the mechanism of inhibition, with reference to their altered distance from the active site upon ligand binding. Moreover the original and reversed peptides formed more energetically favourable complexes with nNOS as indicated by their lower binding energies compared to their polar forms. AutoDock 4.2 was a valuable tool in monitoring the distance of one of five amino acids located within the enzyme, i.e. Trp678. On the other hand FRET was efficient in monitoring the distance moved by either one of six Trp amino acids located on the enzyme surface, i.e. Trp625, Trp421, Trp676, Trp510, Trp306 and Trp716. The interaction of the Aβ peptides with the H_4B co-factor of the active site during molecular docking was suggestive of the role this co-factor played in preventing the dimerization of the enzyme, thus leading to the inhibition of enzyme activity.

The mechanism of interaction between Aβ and nNOS was hydrophobically driven while the binding of nps and curcumin were driven by electrostatic and π–π stacking (aromatic) influences. Electrostatic interactions were most probably due to the charges on the nps and the aromatic interaction was due to the polyphenol rings of curcumin. Also while nNOS catalyzed the formation of fibrils from Aβ peptides, nps and curcumin reversed the formation of fibrils but did not stop the fibrils from forming completely. Also, although nps were not docked to nNOS, spectrofluorimetric and thermodynamic analysis have shown that these charged particles can interact with enzymes and induce structural changes within the enzyme, just like in the case of curcumin and Aβ binding to nNOS. In addition, curcumin unlike nanoparticles have the added

advantage of been non-toxic to the body due to it been a natural polyphenol and been biologically amenable to the blood system.

6.2 Future perspectives

Recently a novel approach in studying enzyme–inhibition kinetics is the use of biosensor analysis e.g. surface plasmon resonance (SPR). This technique is especially powerful in detecting the irreversible/slow dissociating nature of inhibitors (Gossas *et al*., 2013). Conventional enzyme kinetics confuse the slow binding of an inhibitor with slow association while in biosensor analysis, the slow binding of the inhibitor will be clearly observed as slow dissociation (Gossas *et al*., 2013). In view of the accuracy of data obtained from biosensor technologies, in future, it is essential to optimize the solubility of the Aβ pentapeptide and glycine zipper fragments in order to yield a favourable response on SPR. No doubt, a variety of protocols to aid the solubilization of Aβ are available in the literature. However, these procedures involve the use of extremely alkaline or acidic conditions or rely on organic solvents (Broersen *et al*., 2011). In view of this, solubility protocols, exclusive in the use of organic solvents with SPR should be further explored. One such protocol (Brännström *et al*., 2011) involved solubilizing peptides in 10 mM NaOH, followed by sonication in a water bath and centrifugation at 20 000 x g to remove residual oligomeric species. This treatment efficiently monomerised a peptide which was further diluted in phosphate buffered saline (PBS). Another robust and reproducible preparation protocol is based on the sequential solubilization procedure with organic solvents, followed by complete removal of these solvents by evaporation using a gentle stream of oxygen-free nitrogen or argon. In addition the Aβ dissolved in DMSO could be separated by means of a desalting column (Broersen *et al*., 2011).

Once the solubility of Aβ peptides has been optimized, SPR can be used further to confirm the association-dissociation principle which characterizes Aβ-nNOS interaction. This includes confirming the molecular features and the 'lock and dock' concept of fibril formation (Straub and Thirumalai, 2011). Moreover, a curcuminoid mixture was used in SPR experiments. Hence, in future, in order to utilize SPR in monitoring the interaction of curcumin with nNOS, the curcumin mixture should be separated into its three major curcuminoids: curcumin I, II, III, and

cyclocurcumin. The binding mechanisms and the effect of each separate curcuminoid on the formation of fibrils can thus be studied in a time-resolved manner. Also, since $A\beta_{1-40}$ was the only fragment shown to elicit an SPR response when interacting with immobilized nNOS, a kinetic, spectrofluorimetric, thermodynamic and docking analysis of this peptide will provide a suitable extension to the current studies performed on $A\beta_{1-40}$ (Padayachee *et al*., 2011; Padayachee and Whiteley, 2011; 2013).

As an alternative to the Stern Volmer model, the Tachiya model merits re-evaluation into the technical and mathematical basis of its derivations and formulae in order to validate binding constants and parameters associated with Aβ, np and curcumin interaction with nNOS (Xiao *et al*., 2008; Qin *et al*., 2010). Moreover time-resolved fluorescence measurements can be a future tool used in combination with the Stern Volmer model to confirm the dynamic quenching mechanism of ligand binding with nNOS (Jameson *et al*., 2013). It has also been reported that high amounts of the inducible form of NOS (iNOS) are found in the brains of AD patients (Barone *et al*., 2011). In view of this recent finding, mechanisms of Aβ interaction with iNOS will be a most interesting area of research since iNOS, like nNOS could play a potential role in fibril formation and could be a potential biomarker in the etiology of AD. Apart from the traditional ThT fibrillogenesis assays, novel techniques such as x-ray fiber diffraction, SPR and high-throughput screens can be used as screening tools for fibrillogenetic inhibitors (DaSilva *et al*., 2010).

Furthermore, electron micrographs before and after the addition of curcumin and metal nanoparticles in the presence of nNOS would be important to convincingly demonstrate the presence of fibrils followed by their disappearance. Finally, the electron micrographs would show whether fibril formation was reversed (i.e. Aβ peptides reverted to monomer), or if the nanoparticles and/or curcumin initiated precipitation of fibrils or other amorphous aggregates. Moreover the mechanisms proposed in Chapter 3 (Fig.3.14 and Fig.3.15) by which nanoparticles or curcumin reverse Aβ fibril formation could be easily tested with simple mathematical analysis in the future.

The rapid equilibrium between nNOS and substrate suggests that stopped-flow spectroscopy would be an ideal approach for the further characterization of enzyme kinetics and will the subject of future work.

To enhance the solubility of amyloid peptides for SPR experiments, in the future, the design of Aβ peptide 'analogues' that don't aggregate can be considered. Also the methodological approach of isothermal titration calorimetry can be employed in future experiments in order to obtain positive results from SPR and circumvent issues of amyloid peptide solubility.

In future, docking should be performed on possible allosteric or 'exosites' on the enzyme in order to confirm the mixed inhibition described in Chapter 2.

The dynamics of Trp 678 and Tyr 706 on the binding of Aβ and curcumin suggested that they play an essential role in the binding of ligands to the active site". In order to confirm the significance of their role in binding, the mutagenesis of these two residues can be carried out as future work.

Discrepancies in experimental vs. calculated data was due to not isolating individual curcuminoids. Therefore the isolation of each individual curcuminoid and its effect on fibrillogenesis will be conducted in the future.

No doubt, this research can be considered the beginning of many future studies to come in the field of AD. The findings regarding nps and curcumin have lead to knowledge gaps that if investigated and improved upon will spearhead the design of therapeutic targets against the disease. The current knowledge gaps gleaned from the current research are as follows:

1. Curcumin has been shown to display anti-Aβ aggregation potential. However, its poor absorption and low bioavailability make the development of curcumin-related drugs very challenging. To enhance the suppression or reversal effect, the selective targeting of nanoparticle-encapsulated curcumin to sites of aggregation on the neuron can be employed. These include encapsulation in polymeric micelles, liposomes, polymeric nanoparticles, lipid-based nanoparticles and hydrogels (Belkacemi *et al*., 2011).

2. Moreover the functionalizing of nanoparticles could be considered by the use of dendrimers. Nanoparticles can be conjugated to dendrimers to improve selectivity and targeting of drug molecules to the affected site without potential side effects. Dendrimers are polymeric structures that have branched units, capable of trapping peptides and proteins, protecting them against enzymatic and hydrolytic degradation and making them safe for oral delivery (Oliveira *et al*., 2010; Mohanraj and Chen, 2006).
3. Due to the inherent complexity of the CNS and the safety concerns of nanoparticle-mediated technologies, deeper studies into the toxicity of nanoparticles need to be undertaken. PEGylation which involves the covalent attachment of polyethylene glycol (PEG) to the particle has been commonly employed to reduce nanoparticle toxicity (Jokerst *et al*., 2011). A recent study has discovered that the sulfide anion significantly reduces the toxicity of the Ag nps in comparison to other anions (Hou *et al*., 2013). Also enzymatic digestions of the nanocarriers have been employed in selective delivery of the np to the target tissue. The biological recognition of the substrate by the enzyme can be utilized as a specific triggering event to release the cargo, which reduces toxicological issues related to hazardous drugs (Yang *et al.*, 2010, De La Rica *et al*., 2012). This strategy will create significant breakthroughs in AD drug treatment.

References

Abedini A., Raleigh D.P. (2009) A critical assessment of the role of helical intermediates in amyloid formation by natively unfolded proteins and polypeptides. *Protein Eng Des Sel* **22**:453-459

Agudelo D., Bourassa P., Bruneau J., Be´rube G., Asselin E´., Tajmir-Riahi H-A. (2012) Probing the binding sites of antibiotic drugs Doxorubicin and N-(trifluoroacetyl) Doxorubicin with Human and Bovine Serum Albumins. *PloS OnE* **7**:1-13

Ahmed M., Davis J., Aucoin D., Sato T., Ahuja S, Aimoto S., Elliot J.I.,Van Nostrand W.E., Smith S.O. (2010) Structural conversion of neurotoxic amyloid-β_{1-42} oligomers to fibrils. *Nature structural & molecular biology* **17**:561-567

Aitken R.J., Creely K.S. and Tran C.L. (2004). Nanoparticles: An occupational hygiene review.824-828. (Available online at: www.hse.gov.uk/research/rrpdf/rr274.pdf) Accessed on 06/02/2013

Akkermans C.,Venema P., Rogers S.S., Van der Goot A.J., Boom R.M., Van de Linden E. (2006) Shear pulses nucleate fibril aggregation. *Food Biophysics* **1**:144-150

Albanese A., Tang P.S., Chan W.C.W., (2012) The effect of nanoparticle size, shape and surface chemistry on biological systems. *Annual Review for Biomedical Engineering***14**:1-16

Alderton W.K., Cooper C.E., Knowles R.G. (2001) Nitric oxide synthases: structure, function and inhibition. *Biochemical Journal* **357**:593–615

Alvarez A., Alarco´n R., Opazo C., Campos E.O., Mun˜oz F.J., Caldero´n F.H., Dajas F., Gentry M.K., Doctor B.P., De Mello F.G., Inestrosa N.C. (1998) Stable complexes involving acetylcholinesterase and amyloid-beta peptide change the biochemical properties of the enzyme and increase the neurotoxicity of Alzheimer's fibrils. *Journal of Neuroscience* **18**:3213–3223

Alvarez A., Opazo C., Alarco´n R., Garrido J., Inesterosa N.C. (1997) Acetylcholinesterase promotes the aggregation of amyloid-beta-peptide fragments by forming a complex with the growing fibrils. *Journal of Molecular Biology* **272**:348-361

Alm E. and Baker D. (1999) Matching theory and experiment in protein folding. *Current Opinion in Structural Biology* **9**:189-196

Alzheimer's Association. (2012) Alzheimer's disease Facts and Figures. *Alzheimer's & Dementia* **8**: 1-72

Alzheimer A (1907) Uber eine eigenartige Erkrankung der Hirnrinde. Allgemeine Zeitschrift fur Psychiatrie und phychish-Gerichtliche Medizin, (Berlin) **64**: 146-148

American Health Assistance Foundation (2012) Alzheimer's Medical Illustrations, (available online at http://www.ahaf.org/alzheimers/about/understanding/medical_illustrations.html.) Accessed on 22/01/2013.

Anderson H.S. (2013) Alzheimer disease: pathophysiology, (available online at: http://emedicine.medscape.com/article/1134817-overview) Accessed on 24/01/2013.

Anderson A.M., Mitchell M.S., Mohan R.S. (2000) Isolation of Curcumin from Turmeric. *Journal of Chemical Education* **77**:359-360

Aggarwal B.B. and Sung B. (2008) Pharmacological basis for the role of curcumin in chronic diseases: an age-old spice with modern targets. *Trends in Pharmacological Sciences* **30**:85-94

Aggarwal B.B., Bhatt I.D., Ichikawa H., Ahn K-S., Sethi G., Sandur S.K., Natarajan C., Seeram N., Shishodia S. (2006) Chapter 10: Curcumin-Biological and Medicinal Properties (available online at: http://www.charakinternational.com/pdfs/article13.pdf) Accessed on 06/02/2013.

Aguilar M., Small D.H. (2005) Surface Plasmon Resonance for the analysis of β-amyloid interactions and fibril formation in Alzheimer's disease Research. *Neurotoxicity Research* **7**:17-27

Atamna H. and Boyle K., (2006) Amyloid-beta peptide binds with heme to form a peroxidase: relationship to the cytopathologies of Alzheimer's disease. *Proc Natl Acad Sci USA* **103**:3381-6

Auer S., Trovato A., Vendruscolo M. (2009) A condensation-ordering mechanism in nanoparticle-catalyzed peptide aggregation. *PloS Computational Biology* **5**:1-7

Babakhani A., Talley T.T., Taylor P., McCammon J.A. (2009) A virtual screening study of the acetylcholine binding protein using a relaxed-complex approach. *Computational Biological Chemistry* **33**:160–170

Baker D. (2000) A surprising simplicity to protein folding. *Nature* **405**:39-42

Ban T., Hoshino M., Takahashi S., Hamada D., Hasegawa K., Naiki H., Goto Y. (2004). Direct observation of Aβ amyloid fibril growth and inhibition. *Journal of Molecular Biology* **344**: 757-767

Barone E., Di Domenico F., Cenini G., Sultana R., Coccia R., Preziosi P., Perluigi M., Mancuso C., Butterfield D.A. (2011) Oxidative and nitrosative modifications of biliverdin reductase-A in the brain of subjects with Alzheimer's disease and amnestic mild cognitive impairment *Journal of Alzheimer's Disease* **25**:623-33

Bartolini M., Andrisano V., Cavrini V., Bertucci C. (2003).β-amyloid aggregation induced by human acetylcholinesterase:inhibition studies. *Biochemical Pharmacology* **65**:407-416

Belkacemi A., Doggui S., Dao L., Ramassamy C. (2011) Challenges associated with curcumin therapy in Alzheimer's disease. *Expert Reviews in Molecular Medicine* **13**:e34

Behlke M.A., Huang L., Bogh L., Rose S., Devor E.J. (2005) Fluorescence and Fluorescence Applications. Integrated DNA Technologies.

Bhattacharya R. and Mukherjee P. (2008) Biological properties of "naked nanoparticles". *Advanced Drug Delivery reviews* **60**:1289-1306

Bohacek R.S. and McMartin C. (1997) Modern computational chemistry and drug discovery: structure generating programs. *Current Opinion in Chemical Biology* **1**:157-61

Bokvist M., Lindstrom F., Watts A., Grobner.G. (2003) Two types of Alzheimer's β-amyloid (1-40) peptide membrane interactions: Aggregation preventing transmembrane anchoring versus accelerated surface fibril formation. *Journal of Molecular Biology* **335**:1039-1049

Boller F. and Forbes M.M. (1998) History of dementia and dementia in history: An overview *Journal of the Neurological Sciences* **158:**125-33

Boyde T.R.C. and Rahmatullah M. (1980) Optimization of conditions for the colorimetric determination of citrulline using diacetyl monoxime. *Analytical Biochemistry* **107**:424-431

Bradford M.M. (1976) A rapid and sensitive method for quantitation of microgram quantities of protein utilizing the principle of protein-dye-binding. *Analytical Biochemistry* **72**:248-254

Brännström K., Ohman A., Olofsson A. (2011) Aβ peptide fibrillar architectures controlled by conformational constraints of the monomer. *PLoS ONE* **6:**25157

Breydo L., Bocharova O.V., Baskakov I.V. (2005) Semi-automated cell-free conversion of prion protein: applications for high-throughput screening of potential anti-prion drugs. *Analytical Biochemistry* **339**:165-73

Broersen K., Jonckheere W., Rozenski J., Vandersteen A., Pauwels K., Pastore A., Rousseau F., Schymkowitz J. (2011) A standardized and biocompatible preparation of aggregate-free amyloid beta peptide for biophysical and biological studies of Alzheimer's disease. *Protein Engineering, Design & Selection* **2011**:1 -8

Bronner V., Bravman T., Notcovich A., Reichmann D., Schreiber G., Lavie K. (2006) Rapid optimization of immobilization and binding conditions for kinetic analysis of protein-protein interactions using the ProteOn XPR36 protein interaction array system. *Bio-Rad bulletin* **5367**

Bruckdorfer R. (2005) The basics about nitric oxide. *Molecular Aspects of Medicine* **26**: 3-31

Bryngelson J.D., Onuchic J.N., Socci N.D., Wolynes P.G. (1995) Funnels, pathways and the energy landscape of protein folding: A synthesis. *Proteins* **21**:167-195

Cabaleiro-Lago C., Quinlan-Pluck F., Lynch I., Dawson K. A., Linse S. (2010) Dual effect of amino modified polystyrene nanoparticles on amyloid *β* protein fibrillation. *ACS Chemical Neuroscience* **1**:279–287

Cabaleiro-Lago C., Quinlan-Pluck F., Lynch I., Lindman S., Minogue A.M., Thulin E., Walsh D,M., Dawson K.A., Linse S. (2008) inhibition of amyloid β protein fibrillation by polymeric nanoparticles. *Journal of American Chemical Society* **130**:15437-15443

Caffrey D.R., Somaroo S., Hughes J.D., Mintseris J., Huang E.S.(2004) Are protein-protein interfaces more conserved in sequence than the rest of the protein surface? *Protein Science* **13:**190-202

Caflisch A. and Pellarin R. (2006). Interpreting the aggregation kinetics of amyloid peptides. *Journal of Molecular Biology* **360**:882-892

Cairo C.W., Strzelec A., Murphy R.M., Kiessling L.L (2002) Affinity-based inhibition of β-amyloid toxicity. *Biochemistry* **41**:8620-8629

Campos K.L., Giovanelli J., Kaufman S. (1995) Characteristics of the nitric oxide synthase-catalyzed conversion of arginine to *N*-hydroxyarginine, the first oxygenation step in the enzymatic synthesis of nitric oxide. *Journal of Biological Chemistry* **270**:1721-1728

Cannon M.J., Williams A.D., Wetzel R., Myszka D.G. (2004) Kinetic analysis of beta-amyloid fibril elongation. *Analytical Biochemistry* **328**:67-75

Cantoni O., Palomba L., Musci G., Ascenzi P., Fioravanti E., Persichini T., Colasanti M., Venturini G.(2002). β–amyloid inhibits NOS activity by subtracting NADPH availability. *FASEB Journal* **10**:1096

Carlo M. (2010). Beta-amyloid peptide: from different aggregation forms to the activation of different biochemical pathways. *European Biophysics Journal* **39**:877-888

Castellani R.J., Shah R.S., Lee H.G., Xiongwei Z., Perry G., Smith M.A. (2008). Current approaches in the treatment of Alzheimer's disease. *Biomedicine and Pharmacotherapy* **62**:199-207

Chen Z., Krause G., Reif B. (2005) Structure and orientation of peptide inhibitors bound to beta-amyloid fibrils. *Journal of Molecular Biology* **354**:760-76

Chen Y., Mills J.D., Periasamy A. (2003) Protein localization in living cells and tissues using FRET and FLIM. *Differentiation* **71**: 528-54

Chi Z., Liu R., Yang H., Shen H and Wang J. (2011) Binding of Tetracycline and Chlortetracycline to the enzyme Trypsin: Spectroscopic and Molecular modeling investigations. *PLoS ONE* **6**:1-9

Citron M. (2002) Alzheimer's disease: treatments in discovery and development. *Nature neuroscience supplement* **5**:1055-1057

Clegg R. M (1996) Fluorescence resonance energy transfer. *Chemical Analysis Series* **137**:179-251, John Wiley & Sons, New York

Clegg R.M. (1995) Fluorescence resonance energy transfer. *Current opinion in Biotechnology* **6**:103-110.

Colvin V.L. and Kulinowski K.M. (2007) Nanoparticles as catalysts for protein fibrillation. *Proc Natl Acad Sci* **104**:8679-80

Cole G.M.,Yang F., Lim G.P., Cummings J.L., Masterman D.L., Frautschy S.A.(2003) A rationale for curcuminoids for the prevention or treatment of Alzheimer's disease. *Current Medicinal Chemistry* **3**:15-25

Cooper M.A. (2002) Optical biosensors in drug discovery. *Nature Reviews Drug Discovery* **1**:515-528

Cozzini P., Kellogg G.E., Spyrakis F., Abraham D.J., Costantino G., Emerson A., Fanelli F., Gohlke H. (2008) Target flexibility: an emerging consideration in drug discovery and design. *Journal of Medicinal Chemistry* **51**:6237–6255

Cramer P.E., Cirrito J.R., Wesson D.W., Daniel Lee C.Y., Colleen K. J., Zinn A.E., Casali B.T., Restivo J.L., Goebel W.D., James M.J., Brunden K.R., Wilson D.A, Landreth G.E. (2012) ApoE directed therapeutics rapidly clear β-amyloid and reverse deficits in AD mouse models. *Science* **335**:1503-1506

Crouse H.F., Petrunak E.M., Donovan A.M., Merkle A.C., Swartz B.L., Basu S. (2011) Static and Dynamic quenching of tryptophan fluorescence in various proteins by a chromium (III) complex. *Spectroscopy Letters* **44**:369-374

Cruz.S. (2012) New test that predicts Alzheimer's disease, (available online at: http://wonderfulword0.blogspot.com/2012/04/new-test-that-predict-alzheimers.html#!/2012/04/new-test-that-predict-alzheimers.html) Accessed on 06/02/2013.

Cummings J.L. (2003) The neuropsychiatry of Alzheimer's disease and related dementias. Taylor and Francis. London and New York.

DaSilva K.A., Shaw J.E., McLaurin J. (2010) Amyloid-β fibrillogenesis: Structural insight and therapeutic intervention. *Experimental Neurology* **223**:311-321

De La Rica R., Aili D., Stevens M.M. (2012) Enzyme-responsive nanoparticles for drug release and diagnostics. *Advanced Drug Delivery Reviews* **64**:967-978

De Meyer G.R.Y., Martinet W., Van De Parre T.J.L., Herman A.G., Bult H., Kockx M.M., Jans D.M. (2006) Processing of amyloid precursor protein as a biochemical link between Atherosclerosis and Alzheimer disease. *Cardiovascular & Haematological Disorders-Drug Targets* **6**:21-34

De Felice F.G. and Ferreira S.T. (2002) β-amyloid production, aggregation, and clearance as targets in Alzheimer's disease. *Cellular and Molecular Neurobiology* **22**:125-130

De Ferrari G. V., Mallender W. D., Inestrosa N. C., Rosenberry T. L. (2001) Thioflavin T is a fluorescent probe of the acetylcholinesterase peripheral site that reveals conformational interactions between the peripheral and acylation sites. *Journal of Biological Chemistry* **276**:23282-23287

Deremble C., and Lavery R. (2005) Macromolecular recognition. *Current Opinion in Structural Biology* **15**:171-175

Dong S., Duan Y., Hu Y., Zhao Z. (2012) Advances in the pathogenesis of Alzheimer's disease: a re-evaluation of amyloid cascade hypothesis. *Translational Neurodegeneration* **1**:18

Drouet B., Pincon-Raymond M., Chambaz J., Pillot T. (2000) Molecular basis of Alzheimer's disease. *Cellular and Molecular Life Sciences* **57**:705-715

Eftink M.R. (1991) Fluorescence techniques for studying protein structure. *Methods of Biochemical Analysis* **35**:127-205

Eftink M.R. and Ghiron C.A. (1981) Fluorescence quenching studies with proteins. *Analytical Biochemistry* **114:**199-227

Evans K.C., Berger E.P.,Cho C.,Weisgraber K.H., Lansbury P.T. (1995) Apolipoprotein E is a kinetic but not a thermodynamic inhibitor of amyloid formation: Implications for the pathogenesis and treatment of Alzheimer's disease. *Proc.Natl.Acad.Sci.USA* **92**:763-767

Fanelli F. and Ferrari S. (2006) Prediction of MEF2A-DNA interface by rigid body docking: a tool for fast estimation of protein mutational effects on DNA binding. *Journal of Structural Biology* **153**:278-283

Fang J., Ji H., Lawton G.R., Xue F., Roman L.J. (2009) L337H Mutant of Rat Neuronal Nitric Oxide Synthase Resembles Human Neuronal Nitric Oxide Synthase Toward Inhibitors. *Journal of Medicinal Chemistry* **52**:4533-4537

Farrow C.L., Ruan C-Y., Billinge S.J.L. (2010) Quantitative nanoparticle structures from electron crystallography data. *Physical Reviews B* **81**:1-8

Fei L. and Perrett S. (2009) Effect of nanoparticles on protein folding and fibrillogenesis. *International Journal of Molecular Science* **10**:646-655

Ferrari A.M., Wei B.Q., Costantino L., Shoichet B.K. (2004) Soft docking and Multiple Receptor conformations in virtual screening. *Journal of Medicinal Chemistry* **47**:5076-5084

Ferreira S.T. and De Felice F. G.(2001) Protein dynamics, folding and misfolding: from basic physical chemistry to human conformational diseases. *FEBS Letters* **498**:129-134

Fersht A (1999). Structure and mechanism in protein science: a guide to enzyme catalysis and protein folding. San Francisco: W.H. Freeman.

Fersht A.R. (1997) Nucleation mechanisms in protein folding. *Current Opinion in Structural Biology* **7**:3–9

Fersht A.R. (1995) Optimization of rates of protein folding: the nucleation-condensation mechanism and its implications. *Proc. Natl. Acad. Sci. U.S.A* **92**:10869–10873

Fersht A.R. and Requena Y. (1971a) Mechanism of the α-chymotrypsin hydrolysis of amides. pH dependence of k_c and K_m. Kinetic detection of an intermediate. *Journal of American Chemical Society* **93**:7079

Fersht A.R. and Requena Y. (1971b) Equilibrium and rate constants for the interconversion of two conformations of α-chymotrypsin. *Journal of Molecular Biology* **60**:279

Findeis M.A and Molineaux S.M. (1999) Amyloid, prions and other protein aggregates, design and testing of inhibitors of fibril formation. *Methods in Enzymology* **309**:476

Fink A.L. and Munishkina L.A. (2007) Fluorescence as a method to reveal structures and membrane-interactions of amyloidogenic proteins. *Biochimica et Biophysica Acta* **1768**:1862-1885

Fischer N.O., Verma A., Goodman C.M., Simard J.M., Rotello V.M.(2003) Reversible "irreversible" inhibition of chymotrypsin using nanoparticle receptors. *Journal of American Chemical Society* **125**:1338

Fischer O. (1907) Monatsschr Psychiatr *Neurol* **361**:72

Fischer E. (1894) Einfluss der Configuration auf die Wirkung der Enzyme. *Ber. Dt. Chem. Ges* **27**: 2985–93

Foloppe N. and Hubbard R. (2006) Towards predictive ligand design with free-energy computational methods. *Current Medicinal Chemistry* **13**:3583-3608

Fonte V., Dostal V., Roberts C.M., Gonzales P., Lacor P., Magrane J., Dingwell N., Fan E.Y., Silverman M.A., Stein G .H., Link C.D. (2011) A glycine zipper motif mediates the formation of toxic β-amyloid oligomers *in vitro and in vivo*. *Molecular Neurodegeneration* **6**:61

Fraser P.E., Levesque L., McLachlan D.R. (1993) Biochemistry of Alzheimer's disease plaques. *Clinical Biochemistry* **26**: 339-349

Freifelder D. (1976) Physical Biochemistry: applications to Biochemistry and Molecular biology. W.H. Freeman and Company, United States of America.

Gálvez N., Fernandez B., Valero E., Sánchez P., Cuesta R. and Domínguez-Vera J. (2008) Apoferritin as a nanoreactor for preparing metallic nanoparticles. *C.R. Chimie* **11**:1207-1212

Galdiero S., Falanga A., Vitiello M., Cantisani M., Marra V., Galdiero M. (2011) Silver nanoparticles as potential antiviral agents. *Molecules* **16**:8894-8918

Gawrisch K., Han K.H., Yang J.S., Bergelson L.D., Ferretti J.A. (1993) Interaction of peptide fragment 828-848 of the envelope glycoprotein of human immunodeficiency virus type I with lipid bilayers. *Biochemistry* **32**:3112-8

Gazit E (2007) Self assembly of short aromatic peptides into amyloid fibrils and related nanostructures. *Prion* **1**:32-35

Gazit E. (2005) Mechanisms of amyloid fibril self-assembly and inhibition: model short peptides as a key research tool. *FEBS Journal* **272**:5971-5978

Gazit E. (2002) A possible role for pi-stacking in the self-assembly of amyloid fibrils. *Faseb Journal* **16**:77-83

Gianni S., Guydosh N.R., Khan F., Caldas T.D., Mayor U., White W.N.G., DeMarco M.L., Daggett V., Fersht A.R. (2003) Unifying features in protein-folding mechanisms. *Proceedings of the National Academy of Sciences* **100**:13286-13291

Giordano C., Masi A., Pizzini A., Sansone A., Consalvi V., Chiaraluce R., Lucente G. (2009) Synthesis and activity of fibrillogenesis peptide inhibitors related to 17-21 β-amyloid fibrillogenesis. *European Journal of Medicinal Chemistry* **44**:179-189

Glabe C.G. (2006). Review: common mechanisms of amyloid oligomer pathogenesis in degenerative disease. *Neurobiology of Aging* **27**:570-575

Glibert H.F. (2000). Basic concepts in Biochemistry: a student's survival guide, 2nd Edition, McGraw-Hill Companies, United States of America.

Goel A., Kunnumakkara A.B., Aggarwal B.B. (2008) Curcumin as "Curecumin": from kitchen to clinic. *Biochemical Pharmacology* **75**:787-809

Goldschmidt L., Teng P.K., Riek R., Eisenberg D. (2010) Identifying the amylome, proteins capable of forming amyloid-like fibrils. *Proc.Natl.Acad.USA* **107**:3487-3492

Gohlke H. and Klebe G. (2002) Approaches to the description and prediction of the binding affinity of small-molecule ligands to macromolecular receptors. *Angewandte Chemie International Edition English* **41**:2644–2676

Gossas T., Nordström H., Xu M-H., Sun Z-H., Lin G-Q., Wallberg H., Danielson H. (2013) The advantage of biosensor analysis over enzyme inhibition studies for slow dissociating inhibitors – characterization of hydroxamate-based matrix metalloproteinase-12 inhibitors. *Med.Chem.Commun* **4**:432-442

Gromihar M. (2011) Protein Bioinformatics: from sequence to function. Academic Press, India, 339.

Groves J.T. and Wang C.C.Y. (2000) Nitric oxide synthase: models and mechanisms.*Current Opinion in Chemical Biology* **4**:687–695

Gschwend D.A., Good A.C., Kuntz I.D. (1996) Molecular docking towards drug discovery. *Journal of Molecular Recognition* **8**:175-186

Guex N., Peitsch M.C., Schwede T. and Diemand A. (2012) Swiss Institute of Bioinformatics Deepview/Swiss –Pdb viewer [V.3.7], (Available online at http://www.expasy.org/spdbv/) Accessed on 16/02/2013

Guex N. and Peitsch M.C. (1997) Swiss-Model and Swiss-PDB viewer: an environment for comparative protein modeling. *Electrophoresis* **18**:2714-2723

Gummadi N.S. (2003) What is the role of thermodynamics on protein stability? *Biotechnology and Bioprocess Engineering* **8**:9-18

Gursky O. and Aleshkov S. (2000) Temperature-dependent β-sheet conformation in β-amyloid Aβ1-40 peptide in water: uncoupling β-structure folding from aggregation. *Biochimica et Biophysica Acta* **1476**:93-102

Groves J.T and Wang C.C-Y. (2000) Nitric oxide synthase: models and mechanisms. *Current Opinion in Chemical Biology* **4**:687-695

Haass C. and Selkoe D.J. (2007) Soluble protein oligomers in neurodegeneration: lessons from Alzheimer's amyloid β-peptide. *Nature Reviews* **8**:101-112

Hamada D., Tanaka T., Tartaglia G.G., Pawar A.,Vendruscolo M., Kawamura M., Tamura A., Tanaka N., Dobson C.M.(2009) Competition between folding, native-state dimerisation and amyloid aggregation in β-lactoglobulin. *Journal of Molecular Biology* **386**: 878-890

Hampel H. (2013) Amyloid-β and Cognition in Aging and Alzheimer's disease: Molecular and Neurophysiological Mechanisms. *Journal of Alzheimer's Disease* **33**

Hang S., Rich A. (1997) Direct conversion of an oligopeptide from a β-sheet to an α-helix: a model for amyloid formation. *Proc Natl Acad Sci USA* **94**:23-28

Härd T and Lendel C. (2012) Inhibition of amyloid formation. *Journal of Molecular Biology* **421**:441-65

Hardy J.A. and Higgins G.A. (1992) Alzheimer's disease: the amyloid cascade hypothesis. *Science* **256:**184-185

Harmeier A., Wozny C., Rost B.R., Munter L.M., Hua H., Georgiev O., Beyermann M., Hildebrand P.W.,Weise C., Schaffner W., Schmitz D., Multhaup G. (2009) Role of amyloid-beta glycine 33 in oligomerization,toxicity and neuronal plasticity. *Journal of Neuroscience* **29**:7582-7590

Hasegawa K., Ono K., Yamada M., Naiki H. (2002) Kinetic modeling and determination of reaction constants of Alzheimer's beta-amyloid fibril extension and dissociation using surface plasmon resonance. *Biochemistry* **41**:13489-98

Herbstein F.H. (1993) Structural principles in the classification of crystalline binary adduct (molecular-compounds and complexes). *Acta Chimica Hungarica* **130**:377-387

He Y., Wang Y., Tang L., Liu H., Chen W., Zheng Z., Zou G.(2008) Binding of puerarin to human serum albumin: A spectroscopic analysis and molecular docking. *Journal of Fluorescence* **18**:433-442

Hilbich C., Kisters-Woike B., Reed J., Masters C.L., Beyreuther K. (1992) Substitutions of hydrophobic amino acids reduces the amyloidogenicity of Alzheimer's disease beta A40 peptides. *Journal of Molecular Biology* **228**:460-473

Hink M.A., Visser N.V., Borst J.W., Van Hoek A., Visser A.J.W. (2003) Practical use of corrected fluorescence excitation and emission spectra of fluorescent proteins in Förster Resonance Energy Transfer (FRET) studies. *Journal of Fluorescence* **13**:185-188

Hou J-L., Shuo G., Grozova L. (2013) Reduction of silver nanoparticle toxicity by sulfide. *Advanced Material Letters* **4**:131-133

Huang Y. and Mucke L. (2012) Alzheimer mechanisms and therapeutic strategies. *Cell* **148**:1204-1222

Huang T-C., Lu K-T., Wo Y-YP., Wu Y-J., Yang Y-L.(2011) Resveratrol Protects Rats from Aβ-induced Neurotoxicity by the Reduction of iNOS Expression and Lipid Peroxidation. *PLoS ONE* **6**:e29102

Huang S-Y., Grinter S.Z., Zou X. (2010) Scoring functions and their evaluation methods for protein–ligand docking: recent advances and future directions. *Physical Chemistry Chemical Physics* **12:**12899-12908

Huang H.C. and Jiang Z.F. (2009) Accumulated amyloid-beta peptide and hyperphosphorylated tau protein: relationship and links in Alzheimer's disease. *Journal Alzheimer's disease* **16**:15-27

Huang S-Y. and Zou X. (2010) Advances and challenges in protein-ligand docking. International Journal of Molecular Science **11**:3016-3034

Huey R., Morris G. M., Olson A. J., Goodsell D. S. (2007) A semi-empirical free energy force field with charge-based desolvation. *Journal of Computational Chemistry* **28**:1145-1152

Hu Y-J., Ou-Yang Y., Dai C.M., Liu Y., Xiao X-H. (2010) Binding of berberine to bovine serum albumin: spectroscopic approach. *Molecular Biology Reports* **37**:3827-32

Ikeda K., Galzitskaya O.V., Nakamura H., Hig O.J. (2003) β-Hairpins, α-helices, and the Intermediates among the Secondary structures in the energy landscape of a peptide from a distal β-pin of the SH3 domain. *Journal of Computational Chemistry* **24**:310-318

Ishii D., Kinbara K., Ishida Y., Ishii N., Okochi M., Yohda M. and Aida T. (2003) Chaperonin-mediated stabilization and ATP-triggered release of semiconductor nanoparticles. *Nature* **423**:628-632

Ishii Y., Yoshida T., Funatsu T., Wazawa T., Yanagida T. (1999) Fluorescence resonance energy transfer between single fluorophores attached to a coiled-coil protein in aqueous solution. *Chemical Physics* **247**: 163-173

Ishrat T., Hoda M.N., Khan M.B., Yousuf S., Ahamd M., Khan M.M., Ahmad A., Islam F.(2009) Amelioration of cognitive deficits and neurodegeneration by curcumin in rat model of sporadic dementia of Alzheimer's type (SDAT). *European Neuropsychopharmacology* **19**: 636-647

Iwunze M.O. (2004) Fluorescence quenching studies of curcumin by hydrogen peroxide in acetonitrile solution. *Monatshefte für Chemie* **135**:231-240

Jarrett J. T. and Lansbury P. T. Jr. (1993) Seeding “one-dimensional crystallization" of amyloid: a pathogenic mechanism in Alzheimer's disease and scrapie? *Cell* **763**:1055-1058.

Jarrett J.T., Berger E.P., Lansbury P.T. Jr. (1993) The carboxy terminus of the beta amyloid protein is critical for the seeding of amyloid formation: implications for the pathogenesis of Alzheimer's disease. *Biochemistry* **32**: 4693-7

Jackson M. and Mantsch H.H (1991) Beware of proteins in DMSO. *Biochim Biophys Acta* **1078**:231–235

Jain A.N. (2006) Scoring functions for protein-ligand docking. *Current Protein and Peptide Science* **7**:407-420

Jameson D.M.,Vetromile C.M., James N.G. (2013) Investigations of protein-protein interactions using time-resolved fluorescence and phasors. *Methods* doi: 10.1016/j.ymeth.2013.01.004

Ji H., Stanton B.Z., Igarashi J., Li H., Martasek P., Roman L.J., Poulos T.L., Silverman R.B. (2008) Minimal pharmacophoric elements and fragment hopping, an approach directed at molecular

diversity and isozyme selectivity. Design of selective neuronal nitric oxide synthase inhibitors. *Journal of American Chemical Society* **130**:3900–3914

Jochim A.L., Miller S.E., Angelo N.G., Arora P.S. (2009) Evaluation of triazolamers as active site inhibitors of HIV-1 protease. *Bioorganic & Medicinal Chemistry Letters* **19**:6023-6026

Jokerst J.V.,Lobovkina T., Zare R.N., Gambhir S.S. (2011) Nanoparticle PEGylation for imaging and therapy. *Nanomedicine* **6**:715-728

Jones O.G. and Mezzenga R. (2012) Inhibiting, promoting and preserving stability of functional protein fibrils. *Soft Matter* **8**:876

Jones S and Thornton J.M. (1996) Principles of protein-protein interactions. *Proc.Natl.Acad.Sci USA* **93**:13-20

Kallberg Y., Gustafsson M., Persson B, Thyberg J and Johansson J (2001) Prediction of amyloid fibril-forming proteins. *Journal of Biological Chemistry* **276**:12945-12950

Kammerer R.A., Kostrewa D., Zurdo J., Detken A., Garcia-Echeverria C.,Green J.D, Muller S.A., Meier B.H.,Winkler F.K., Dobson C.M., Steinmetz M.O.(2004) Exploring amyloid formation by a de novo design. *Proc.Natl.Acad.Sci.USA* **101**:4435-4440

Kang K.A., Wang J., Jasinski J.B., Achilefu S. (2011) Fluorescence manipulation by Gold nanoparticles: From complete quenching to extensive enhancement. *Journal of Nanobiotechnology* **9**:16

Kanski J.,Varadarajan S., Aksenova M., Butterfield D.A.(2001) Role of glycine-33 and methionine-35 in Alzheimer's amyloid β-peptide 1-42 associated oxidative stress and neurotoxicity. *Biochimica et Biophysica Acta* **1586**:190-198

Karplus M. and Weaver D.L. (1976) Protein-folding dynamics. *Nature* **260**:404-406

Kavraki L.E. (2006) Protein folding (available online at http://cnx.org/content/m11467/1.7/) Accessed on 14/02/2013

Kelly J.W. (1998) The alternative conformations of amyloidogenic proteins and their multi-step assembly pathways. *Current Opinion in Structural Biology* **8**:101–106

Kiefhaber T., Bachmann A., Jensen K.S.(2011) Dynamics and mechanisms of coupled protein folding and binding reactions. *Current Opinion in Structural Biology* **22**:1-9

Kim J (2009) Review: The roles of GxxxG motif and γ-secretase components in APP processing. *Interdisciplinary Biocentral* **15**:1-8

Kim S., Jeon T.J., Oberai A.,Yang D., Schimdt J.J., Bowie J.U.(2005) Transmembrane glycine zippers: physiological and pathological roles in membrane proteins. *Proc.Natl Acad Sci USA* **102**:14278-14283

Kolinski A., Ilkowski B., Skolnick J. (1999) Dynamics and thermodynamics of beta-hairpin assembly: insights from various simulation techniques. *Biophysics Journal* **77**:2942-52

Kontush A. (2001) Alzheimer's amyloid-β as a preventive antioxidant for brain lipoproteins. *Cellular and Molecular Neurobiology* **21**:299-315

Knowles R.G., Alderton W.K. and Cooper C.E. (2001) Nitric oxide synthases: structure, function and inhibition. *Journal of Biochemistry* **357**:593-615

Koshland D. E. (1958) Application of a Theory of Enzyme Specificity to Protein Synthesis. *Proc. Natl. Acad. Sci* **44**:98–104

Kotov N.A., Yoo S.I., Yang M., Brender J.R., Subramanian V., Sun K., Joo N.E., Jeong S., Ramamoorthy A. (2011). Inhibition of amyloid peptide fibrillation by inorganic nanoparticles: functional similarities with proteins. *Angew.Chemistry.International.Edition* **50**:5110-5115

Kraepelin, E. (1910) II. Band, Klinische Psychiatrie. Leipzig: Verlag Johann Ambrosius Barth.

Kumar S., Okello E.J., Harris J.R. (2012) Experimental inhibition of fibrillogenesis and neurotoxicity by amyloid-beta (Aβ) and other disease-related peptides/proteins by plant extracts and herbal compounds. *Subcellular Biochemistry* **65**:295-326

Kuntz I. D., Blaney J. M., Oatley S. J., Langridge R., Ferrin T. E. (1982) A geometric approach to macromolecule-ligand interactions. *Journal of Molecular Biology* **161**:269 – 288.

Lahiri D.K., Rogers J.T., Greig N.H., Sambamurti K. (2004) Rationale for the development of cholinesterase inhibitors as anti-Alzheimer agents. *Current Pharmaceutical Design* **10**: 3111-3119

Lakowicz J.R. (2009) Principles of Fluorescence Spectroscopy-3rd Edition. Springer Science and Business Media, Baltimore, United States of America.

Lakowicz J.R., Malicka J., Auria S.D., Gryczynski I. (2003) Release of the self-quenching of fluorescence near silver metallic surfaces. *Analytical Biochemistry* **320**:13–20

Lansbury P. Jnr and Rochet J. (2000) Amyloid fibrillogenesis: themes and variations. *Current Opinion in Structural Biology* **10**:60-68.

Lesk A. (2001). Introduction to Protein Architecture. University of Cambridge, Oxford university press, New York.

LeVine H.III and Scholten J.D. (1999) Screening for pharmacologic inhibitors of amyloid fibril formation. *Methods in Enzymology* **309**:467-476

Litzinger E.A, Martasek P., Roman L.J., Silverman R.B. (2006) Design, synthesis and biological testing of potential heme-coordinating nitric oxide synthase inhibitors. *Bioorganic and Medicinal Chemistry* **14**:3185-3198.

Liu B.,Yang C., Xiaona Y., Wang J., Lv Yunkai (2012) Interaction of Avelox with Bovine Serum Albumin and the effect of coexistent drugs on the reaction. *International Journal of Analytical Chemistry* **2012**: 1-8.

Liu T. and Altman R.B. (2011) Using Multiple Microenvironments to Find Similar Ligand-Binding Sites: Application to Kinase Inhibitor Binding. *PLoS Computational Biology* **7**: e1002326.

Liu E.H., Qi L.W., Li P. (2010) Structural relationship and binding mechanisms of five flavonoids with bovine serum albumin., *Molecules* **15**:9092-103

Liu K., Cho H.S., Lashuel H.A., Kelly J.W., Wemmer D.E (2000) A glimpse of a possible amyloidogenic intermediate of transthyretin. *Nature Structural and Molecular Biology* **7**: 754-757

Lomakin A., Teplow D.B., Kirschner D.A. and Benedek G.B. (1997). Kinetic theory of fibrillogenesis of amyloid β–protein (Alzheimer disease/light scattering). *Proceedings of the National Academy of Sciences* **94**:7942-7947

Loura L.M.S. and Prieto M. (2011) FRET in membrane biophysics: an overview. *Frontiers in physiology* **2**:82

Lynch I. and Dawson K.A. (2008) Protein-nanoparticle interactions. *Nanotoday* **3**:40-47

Mangialasche F., Solomon A., Winblad B., Mecocci P., and Kivipelto M. (2011) Alzheimer's disease: clinical trials and drug development. *Lancet Neurology* **9:**702-716

Mankar S., Anoop A., Sen S. and Maji S.K. (2011) Nanomaterials: amyloids reflect their brighter side. *Nano Reviews* **2**:6032

Marletta M.A., Hurshmen A.R. and Kristin M.R. (1998) Catalysis by Nitric oxide synthase. *Current opinion in Chemical Biology* **2**:656-663

Marlow M.S., Dogan J., Frederick K.K., Valentine K.G., Wand A.J. (2010) The role of conformational entropy in molecular recognition by calmodulin. *Nature Chemical Biology* **6**: 352-358

Masterton W.L. and Hurley N.C. (2009) Chemistry: principles and Reactions -6th Edition, Chapter 17: Spontaneity of Reactions, Thomson Brooks & Cole, United States of America

Mathew A., Fukuda T., Nagaoka Y., Hasumura T., Morimoto H., Yoshida Y., Venugopal K., Kumar D.S. (2012) Curcumin Loaded-PLGA Nanoparticles Conjugated with Tet-1 Peptide for Potential Use in Alzheimer's Disease. *PLoS ONE* **7**: e32616

Mathis C.A., Lopresti B.J., Klunk W.E. (2007) Impact of amyloid imaging on drug development in Alzheimer's disease. *Nuclear Medicine and Biology* **34**: 809-822

Maynard C.J., Bush A.I., Masters C.L., Cappai R., Li Q. (2005) Metals and amyloid-β in Alzheimer's disease. *International Journal of Experimental Pathology* **86**:147-159

Mebane-Sims I. (2009) 2009 Alzheimer's disease facts and figures. *Alzheimer's & Dementia* **5**:234-270.

Meiler J. and Baker D. (2006) ROSETTALIGAND: protein-small molecule docking with full side-chain flexibility. *Proteins* **65**:538–548

Mihasan M. (2012) What in silico molecular docking can do for the 'bench-working biologists'? *Journal of Bioscience* **37**:1089-95

Mimeault M. and Batra S.K. (2011) Review: Potential applications of curcumin and its novel synthetic analogs and nanotechnology-based formulations in cancer prevention and therapy. *Chinese Medicine* **6**:1-19

Mohanraj V.J. and Chen Y. (2006). Nanoparticles- A Review. *Tropical Journal of Pharmaceutical Research* **5**: 561-573

Morris G. M., Huey R., Lindstrom W., Sanner M.F., Belew R. K., Goodsell D. S. and Olson A. J. (2009) Autodock4 and AutoDockTools4: automated docking with selective receptor flexibility. *Journal of Computational Chemistry* **30**:2785-91

Morris G.M., Goodsell D.S., Halliday R.S., Huey R., Hart W.E., Belew R.K., Olson A.J. (1998) Automated docking using a Lamarckian genetic algorithm and an empirical binding free energy function. *Journal of Computational Chemistry* **19**:1639–1662

Miki M., Kobayashi T., Kimura H., Hagiwara A., Hai H., Maéda Y. (1998) Ca^{2+-} induced distance change between points on actin and troponin in skeletal muscle thin filaments estimated by fluorescence energy transfer spectroscopy. *Journal of Biochemistry* **123**:324-331

Muralidhara B.K., Negi S., Halpert J.R. (2007) Dissecting the thermodynamics and cooperativity of ligand binding in cytochrome P450eryF. *Journal of American Chemical Society* **129:** 2015–2024.

Murphy K. P., Privalov P.L., Gill S.J. (1990) Common features of protein unfolding and dissolution of hydrophobic compounds. *Science* **247**:559-561

Myszka D.G., Wood S.J., Biere A.L. (1999) Analysis of fibril elongation using surface plasmon resonance biosensors. *Methods in Enzymology* **309**:386-402

Myszka D.G. (1997) Kinetic analysis of macromolecular interactions using surface plasmon resonance biosensors. *Current Opinion in Biotechnology* **8**:50-57

Nabuurs S.B., Wagener M., De Vlieg J. (2007) A flexible approach to induced fit docking. *Journal of Medicinal Chemistry* **50**: 6507-18

Nazem A. and Mansoori G.A. (2011). Nanotechnology for Alzheimer's disease detection and treatment. *Insciences Journal* **1**:169-193

Neuvirth H., Raz R., Schreiber G. (2004) ProMate: a structure based prediction program to identify the location of protein protein binding sites. *Journal of Molecular Biology* **338:**181–199

Nichols M.R., Moss M.A., Reed D.K., Lin W.L., Mukhopadhyay R., Hoh J.H., Rosenberry T.L.(2002) Growth of beta-amyloid (1-40) protofibrils by monomer elongation and lateral association., characterization of distinct products by light scattering and atomic force microscopy. *Biochemistry* **41**: 6115-6127

Nilsson M.R. (2004). Techniques to study amyloid fibril formation *in vitro*. *Methods* **34**:151-160.

Nussinov R. and Ma B. (2012) Protein dynamics and conformational selection in bidirectional signal transduction. *Biomed Central Biology* **10**:2

Oliveira J.M., Salgado A-J., Sousa N., Mano J-F., Reis R.L. (2010) Dendrimers and derivatives as a potential therapeutic tool in regenerative medicine strategies-a review. *Progress in Polymer Science* **35**: 1163-1194

O'Mahony S., Harkany T., Rensink., A. A. M., Abrahám I., De Jong G.I.,Varga J.L., Zarándi M., Penke B., Nyakas C., Luiten P.G., Leonard B.E. (1998) β-amyloid induced cholinergic denervation correlates with enhanced nitric oxide synthase activity in rat cerebral cortex: Reversal by NMDA receptor blockade. *Brain Research Bulletin* **45**: 405–411

Ono K., Hasegawa K., Naiki H., Yamada M. (2004). Curcumin has potent anti-amyloidogenic effects for Alzheimer's beta-amyloid fibrils *in vitro*. *Journal of Neuroscience Research* **75**: 742-750.

Orynbayeva Z., Kolusheva S., Groysman N., Gavrielov N., Lobel L., Jelinek R. (2007) Vaccinia virus interactions with cell membrane studied by new chromatic vesicle and cell sensor assays. *Journal of Virology* **81**:1140-1147

Padayachee E.R. and Whiteley C.G. (2013) Interaction of glycine zipper fragments of Aβ-peptides with neuronal nitric oxide synthase: Kinetic, thermodynamic and spectrofluorimetric analysis. *Neuropeptides* http://dx.doi.org/10.1016/j.npep.2012.12.006

Padayachee E.R. and Whiteley C.G. (2011) Spectrofluorimetric analysis of amyloid peptides with neuronal nitric oxide synthase: Implications in Alzheimer's disease. *Biochimica et Biophysica Acta* **1810**: 1136-1140

Padayachee E.R., Ngqwala N., Whiteley C.G. (2011) Association of β-amyloid peptide fragments with neuronal nitric oxide synthase: Implications in the etiology of Alzheimer's disease. *Journal of Enzyme Inhibition and Medicinal Chemistry* **27**:356-64

Palmer T. (1995) Understanding enzymes, 4th Edition. Ellis Horwood, Great Britain.

Palop J.J. and Mucke L. (2010) Amyloid-β Induced Neuronal Dysfunction in Alzheimer's disease: From Synapses toward Neural Networks, *Nature Neuroscience* **13**: 812-818

Parihar M.S. and Hemnani T. (2004) Alzheimer's disease pathogenesis and therapeutic interventions. *Journal of Clinical Neuroscience* **11**: 456-467

Perry G., Moreira P.I., Oliveira C.R., Santos M.S., Nunomura A., Honda K., Zhu X., Smith M.A. (2005) A second look in to the oxidant mechanisms in Alzheimer's disease. *Current Neurovascular research* **2**:179-184

Porat Y, Abramowitz A., Gazit E (2006) Inhibition of amyloid fibril formation by polyphenols: structural similarity and aromatic interactions as a common inhibition mechanism. *Chemical Biology and Drug Design* **67**: 27-37

Poulos T.L., Li H., Shimizu H., Flinspach M., Jamal J., Yang W., Xian M., Cai T., Zhong W.E., Jia Q., Wang P.G. (2002) The novel binding mode of *N*-Alkyl-*N'*-hydroxyguanidine to neuronal nitric oxide synthase provides mechanistic insights into NO biosynthesis. *Biochemistry* **41**:13868-13875.

Prostak L., Barnea E., Yaish P. and Zharhary D. (2005). The Sigma-Aldrich BACE1 activity assay kit- a FRET based assay designed for BACE1 inhibitor screening. Sigma-Aldrich Inc, USA.

Qin Y., Zhang Y., Yan S and Ye.L (2010) A comparison study on the interaction of hyperoside and bovine serum albumin with Tachiya model and Stern–Volmer equation. *Spectrochimica Acta* **75**: 1506-1510

Rajamani D., Thiel S., Vajda S., Camacho C. J. (2004). Anchor residues in protein-protein interactions. *Proceeding of the National Academy of Sciences* **101**: 11287

Reinke A.A. and Gestwicki J.E. (2011) Insight into amyloid structure using chemical probes. *Chemical Biology and Drug Design* **77**:399-411.

Ribeiro C., Togawa R.C., Neshich I.A.P., Mazoni I., Mancini A.L., Minardi R.C.D.M., Da Silveira C.H., Jardine J.G. (2010) Analysis of binding properties and specificity through identification of the interface forming residues (IFR) for serine proteases in silico docked to different inhibitors. *Biomed Central Structural Biology* **10**:36

Ringman J.M., Frautschy S.A., Teng E., Begum A.N., Bardens.J., Beigi.M., Gylys K.H., Badmaev V., Heath D.D., Apostolova L.G., Porter V., Vanek Z., Marshall G.A., Hellemann G., Sugar.C., Masterman D.L., Montine T.J., Cummings J.L., Cole G.M., (2012) Oral curcumin for Alzheimer's disease: tolerability and efficacy in a 24-week randomized, double blind, placebo-controlled study. *Alzheimer's Research & Therapy* **4**:43.

Rochet J.C. and Lansbury P.T. Jr (2000) Amyloid fibrillogenesis: themes and variations. *Current Opinion in Structural Biology* **10**:60-68

Rosenfeld R.J., Goodsell D.S., Musah R.A., Morris G.M., Goodin D.B. (2003) Automated docking of ligands to an artificial active site: augmenting crystallographic analysis with computer modeling. *Journal of Computer Aided Molecular Design* **17**: 525–536

Ross D. and Subramanian S. (1981) Thermodynamics of protein association forces contributing to stability. *Biochemistry* **20**: 3096-3102

Sakakibara Y. and Yanagisawa H. (2003) Agmatine deiminase from cucumber seedlings is a mono-specific enzyme: purification and characteristics. *Protein Expression and Purification* **30**: 88-93

Sanchez P.E., Zhu L., Verret L., Vossel K.A., Cirrito J.R., Devidze N., Ho K., Yu G., Palop J.J., Mucke L. (2012) Levetiracetam suppresses neuronal network dysfunction and reverses synaptic and cognitive deficits in an Alzheimer's disease model., *PNAS* **109**:2895-2903.

Sayle R. and Bernstein H. (1998-2001) Rasmol (Raswin molecular graphics) [V.2.7.2.1]. University of Edinburgh's Biocomputing research unit and the Biomolecular structure Department at Glaxo research and development, Greenford, UK.

Sargis D. (2010) How Autodock 4 converts binding energy (kcal/mol) into K_i. (available online at: http://autodock.scripps.edu/faqs-help/faq/how-autodock-4-converts-binding-energy-kcal-mol-into-ki) Accessed on 27/01/2013.

Schmidt Jr D.E. and Weistheimer F.H. (1971) PK of the lysine amino group at the active site of acetoacetate decarboxylase. *Biochemistry* **10**:1249

Scheurich A.G. (2012) Signal crosstalk of TRAIL receptors,(available online at: http://www.uni-stuttgart.de/izi/forschung/scheurich/index.html) Accessed on 27/01/2013

Schrand A.M., Rahman M.F., Hussain S.M., Schlager J.J., Smith D.A., Syed A.F. (2010) Metal-based nanoparticles and their toxicity assessment. *WIRES NanomedicineNanobiotechnology* **2**: 544-568

Selkoe D.J. (2004) Cell biology of protein misfolding: the examples of Alzheimer's and Parkinson's diseases. *Nature Cell Biology* **6**:1054-61

Selkoe D.J. (1998) The cell biology of β-amyloid precursor protein and presenilin in Alzheimer's disease. *Trends in Cell Biology* **8**:443-457

Serpell L.C. (2000) Alzheimer's amyloid fibrils: structure and assembly. *Biochimica et Biophysica Acta* **1502**: 16-30

Sennuga A., van Marwijk J. and Whiteley C.G. (2012a) Ferroxidase activity of apoferritin is increased in the presence of platinum nanoparticles. *Nanotechnology* **23**:035102

Sennuga A., van Marwijk J., Boshoff A. and Whiteley C.G. (2012b) Enhanced activity of chaperonin GroEL in the presence of platinum nanoparticles. *Journal of Nanoparticle Research* **14**:824

Siddhanta U., Wu C., Abu-Soud H.M., Zhang J., Ghosh D.K., Stuehr D.J. (1996) Heme Iron reduction and catalysis by a nitric oxide synthase heterodimer containing one reductase and two oxygenase domains. *The Journal of Biological Chemistry* **271**:7309-7312

Silverman R.B. (2000) Enzyme Kinetics: (available online at: http://www.chem.missouri.edu/GatesGroup/enzymekinet.pdf) Accessed on 14/02/2013.

Shammas S.L., Knowles T.P., Baldwin A.J., Macphee C.E., Welland M.E., Dobson C.M., Devlin G.L. (2011) Perturbation of the stability of amyloid fibrils through alteration of electrostatic interactions. *Biophysical Journal* **100**:2783-91

Shen C.L. and Murphy R.M. (1995) Solvent effects on self-assembly of beta-amyloid peptide. *Biophysical Journal* **69**:640-651

Sjoback R., Nygren J., Kubista M. (1995) Absorption and fluorescence properties of fluorescein. *Spectrochim. Acta Part A* **51**: L7–L21.

Smith D.G., Cappai R. and Barnham K.J. (2007) The redox chemistry of the Alzheimer's disease amyloid β peptide. *Biochimica et Biophysica Acta* **1768**: 1976-1990

Soto C. (2001) Protein misfolding and disease, protein refolding and therapy. *FEBS Letters* **498**: 204-207.

Soto, C. (1999) Plaque busters: strategies to inhibit amyloid formation in Alzheimer's disease. *Molecular Medicine Today* **5:** 343-350

Soto C., Sigurdsson E.M., Morelli L., Kumar R.A., Castaño E.M., Frangione B. (1998) Beta-sheet breaker peptides inhibit fibrillogenesis in a rat brain model of amyloidosis: implications for Alzheimer's therapy. *Nature Medicine* **4**: 822-6

Soto C., Castano E.M., Frangione B., Inestrosa N.C. (1995) The alpha-helical to beta-strand transition in the amino-terminal fragment of the amyloid beta-peptide modulates amyloid formation. *Journal of Biological Chemistry* **270**:3063-3067

Sousa S.F., Fernandes P.A., Ramos M.J. (2006) Protein-ligand docking: current status and future challenges. *Proteins* **65**:15–26

Stepanichev M.Y., Onufriev M.V., Mitrokhina O.S., Moiseeva Y.V., Lazareva N.A., Victorov I.V. (2000) Neurochemical, behavioural and neuromorphological effects of central administration of β-amyloid peptide (25-35) in rat. *Neurochemistry* **17**:291-306

Stern O. and Volmer M. (1919) Über die Abklingzeit der Fluoreszenz. *Physik. Zeitschr* **20:** 183–188

Stites W.E. (1997). Protein-protein interactions: interface structure, binding thermodynamics, and mutational analysis. *Chemical Reviews* **97**: 1233-1250

Strazza S., Hunter R., Walker E., Darnall D.W. (1985) The thermodynamics of bovine and porcine insulin determined by concentration difference spectroscopy. *Archives of Biochemistry and Biophysics* **238:**30-42

Straub J.E. and Thirumalai D. (2011) Toward a molecular theory of early and late events in monomer to amyloid fibril formation. *Annual Review of Physical Chemistry* **62**:437-463

Stuehr D.J., Tejero J., Haque M.M. (2009) Structural and mechanistic aspects of flavoproteins: electron transfer through the nitric oxide synthase flavoprotein domain. *FEBS Journal* **276**:3959-3974

Stuehr D.J. (1997) Structure-function aspects in the nitric oxide synthases. *Annual Review of Pharmacology and Toxicology* **37**: 339-59.

Sundberg E.J. and Mariuzza R.A. (2000) Luxury accommodations: The expanding role of structural plasticity in protein-protein interactions. *Structure with Folding and Design* **8**: R137-142.

Syed M.A., Bhatti A.S., Li C., Bokhari H. (2011) Use of SPR biosensor for the study of proteolytic action of a serine protease enzyme. *American Journal of Biomedical Sciences* **3:**253-257

Szegedi V., Fülöp L., Farkas T., Rozsa E., Robotka H., Kis Z., Penke Z., Horvath S., Molnar Z., Datki Z., Soos K., Toldi J., Budai D., Zarandi M., Penke B.(2005) Pentapeptides derived from $A\beta_{1-42}$ protect neurons from the modulatory effect of Aβ fibrils- an *in vitro* and *in vivo* electrophysiological study. *Neurobiology of Disease* **18**:499-508

Szymczyna B.R., Taurog R.E., Young M.J., Snyder J.C., Johnson J.E., Williamson J.R. (2009). Synergy of NMR, computation, and X-ray crystallography for structural biology. *Structure* **17**: 499–507

Takahashi A., Masuda A., Sun M., Centonze V.E., Herman B.(2004) Oxidative stress-induced apoptosis is associated with alterations in mitochondrial caspase activity and Bcl-2-dependent alterations in mitochondrial pH (pHm). *Brain Research Bulletin* **62**: 497-504

Takano K. (2008) Amyloid beta conformation in aqueous environment. *Current Alzheimer's Research* **5**: 540-7.

Takeda T. and Klimov D.K. (2007) Dissociation of Aβ (16-22) amyloid fibrils probed by molecular dynamics. *Journal of Molecular Biology* **368**: 1202-13

Tartaglia G.G., Cavalli A., Pellarin R., Caflisch A. (2004) The role of aromaticity, exposed surface, and dipole moment in determining protein aggregation rates. *Protein Science* **13:** 1939-41

Taylor M., Moore S., Mourtas S., Niarakis A., Re F., Zona C., La Ferla B., Nicotra F., Masserini M., Antimisiaris S.G., Gregori M., Allsop D. (2011) Effect of curcumin-associated and lipid ligand-functionalized nanoliposomes on aggregation of Alzheimer's Aβ peptide. *Nanomedicine* **7**:541-50

Tayeb H.O., Yang H.D., Price B.H., Tarazi F.I. (2012) Pharmacotherapies for Alzheimer's disease: beyond cholinesterase inhibitors. *Pharmacology and Therapeutics* **134**:8-25

Thakur G., Micic M., Yang Y., Li W., Movia D., Giordani S., Zhang H., Leblanc R.M. (2011) Conjugated quantum dots inhibit the amyloid β (1-42) fibrillation process. *International Journal of Alzheimer's disease* **2011**: 1-15

Totrov M. and Abagyan R. (2008) Flexible ligand docking to multiple receptor conformations: a practical alternative. *Current Opinion in Structural Biology* **18**: 178-184

Truong K. and Ikura M. (2001) The use of FRET imaging microscopy to detect protein–protein interactions and protein conformational changes *in vivo* . *Current Opinion in Structural Biology* **11**:573–578

Tjernberg L.O., Naslund J., Lindqvist F., Johansson J., Karlstrom A.R., Thyberg J., Terenius L., Nordstedt C. (1996) Arrest of β-amyloid fibril formation by a pentapeptide ligand. *Journal of Biological Chemistry* **271**: 8545-8548.

Vassar P.S. and Culling C.F. (1959) Fluorescent stains, with special reference to amyloid and connective tissue. *Archives of Pathology and Laboratory Medicine* **68**: 487-498

Veselovsky A.V., Ivanov Y.D., Ivanov A.S., Archakov A.I., Lewi P., Janssen P. (2002).Protein-protein interactions: mechanisms and modifications by drugs. *Journal of Molecular Recognition* **15**:405-422

Vinogradov S.V., Bronich T.K., Kabanov A.V. (2002). Nanosized cationic hydrogels for drug delivery: preparation, properties and interactions with cells. *Advanced Drug Delivery Reviews* **54**:135-147

Virchow R.Z. (1854) Weitere Mittheilungen uber das Vorkommen der pflanzlichen Cellulose beim Menschen. *Virchows Arch* **6**: 268-71.

Visser A.J.W. and Rolinski O.J. (2010) Basic Photophysics Sciences (available online at http://www.photobiology.info/)Accessed:14/02/2013

Voet D and Voet J.D. (2011) Biochemistry: 4th Edition. John Wiley and sons. United States of America.

Wang W., Nema S., Teagarden D. (2010) Protein aggregation-pathways and influencing factors. *International Journal of Pharmaceutics* **390:**89-99

Wang S.S.S., Liu K., Lee W.H. (2009) Effect of curcumin on the amyloid fibrillogenesis of hen egg-white lysozyme. *Biophysical Chemistry* **144**:78-87

Warren G.L., Andrews C.W., Capelli A.M., Clarke B., LaLonde J. (2006) A critical assessment of docking programs and scoring functions. *Journal of Medicinal Chemistry* **49**: 5912-5931

Wetzel R. (2006) Kinetics and thermodynamics of amyloid fibril assembly. *Accounts of Chemical Research* **39**: 671-679

Wolynes P.G., Onuchic J.N., Thirumalai D. (1995) Navigating the folding routes. *Science* **267**:1619-1620

Whitten K.W., Davis R.E., Stanley G.G., Peck L.M. (2007) General Chemistry-8th Edition, Chapter 15: Chemical Thermodynamics, Thomson Brooks & Cole, United States of America.

Woo H., Baik S., Park J.S., Gwon A., Yang S., Yun Y. (2011) Secretases as therapeutic targets for Alzheimer's disease, *Biochemical and Biophysical Research Communications* **404**: 10-15

Wimo A. and Prince M. (2010) The global economic impact of dementia. Alzheimer's disease: International World Alzheimer Report 2010, (available online at: http://www.alz.co.uk/research/files/WorldAlzheimerReport2010ExecutiveSummary.pdf) Accessed on 06/02/2013.

Wu P. and Brand L. (1994) Resonance energy transfer: methods and applications. *Analytical Biochemistry* **218:**1-13

Wu Z., Zhang B., Yan B. (2009) Regulation of enzyme activity through interactions of nanoparticles. *International Journal of Molecular Sciences* **10**: 4198-4209

Wu W. H., Sun X., Yu Y.P., Hu J., Zhao L., Liu Q., Zhao Y.F., Li Y.M. (2008) TiO_2 nanoparticles promote *β*-amyloid fibrillation *in vitro*. *Biochemical and Biophysical Research Communications* **373**:315–318

Xiao J.B., Chen X.Q., Jiang X.Y., Hilczer M., Tachiya M. (2008) Probing the Interaction of Trans-resveratrol with bovine serum albumin: a fluorescence quenching study with Tachiya model. *Journal of Fluorescence* **18:** 671-678

Xiao L., Zhao D., Chan W. H., Choi M. M. F., Li H. W. (2010) Inhibition of beta 1–40 amyloid fibrillation with N-acetyl-l-cysteine capped quantum dots. *Biomaterials* **31**: 91–98

Yagi Y., Terada K., Noma T., Ikebukuro K., Sode K. (2007) *In silico* panning for a non-competitive peptide inhibitor. *BMC Bioinformatics* **8**:11

Yan B., Wu Z., Zhang B. (2009). Regulation of enzyme activity through interactions with nanoparticles, *International Journal of Molecular Science* **10**: 4198-4209

Yang H. (2010) Nanoparticle-mediated brain-specific drug delivery, imaging and diagnosis. *Pharmaceutical Research* **27**:1759-1771

Yang J., Ji Y., Mehta P., Bates K.A., Sun Y., Wisniewski T. (2011) Blocking the apolipoprotein E/amyloid-β interaction reduces fibrillar vascular amyloid deposition and cerebral microhemorrhages in TgSwDI mice. *Journal of Alzheimer's Disease* **24**:269–285

Yang F., Lim G.P., Begum A.N., Ubeda O.J., Simmons M.R. (2005) Curcumin inhibits formation of amyloid beta oligomers and fibrils, binds plaques and reduces amyloid *in vivo*. *Journal of Biological Chemistry* **280**: 5892-5901

Yao F., Zhang R., Tian H., Li X. (2012) Studies on the interactions of copper and zinc ions with β-amyloid peptides by surface Plasmon resonance biosensor. *International Journal of Molecular Sciences* **13**: 11832-11843

Yao H., Kristensen D.M., Mihalek I., Sowa M.E., Shaw C., Kimmel M., Kavraki L., Lichtarge O.(2003) An accurate, sensitive, and scalable method to identify functional sites in protein structures. *Journal of Molecular Biology* **326**:255-61

Yi J., Horky L.L., Friedlich A.L., Shi Y., Rogers J.T., Huang X. (2009) L-Arginine and Alzheimer's disease. *International Journal of Clinical Pathology* **2**:211-238

Yon J.M. (1997) Protein folding: concepts and perspectives. *Cellular and Molecular Life Sciences* **53:**557-567

Yu X. and Zheng J. (2011) Polymorphic Structures of Alzheimer's β-Amyloid Globulomers. *PLoS ONE* **6**: e20575

Zacharias N. and Dougherty A. (2002) Cation-π interactions in ligand recognition and catalysis. *Trends in Pharmacological Sciences* **23**:281

Zhang Y. and Lee D.H. (2011) Sink hypothesis and therapeutic strategies for attenuating Aβ levels. *Neuroscientist* **17**:163-173

Zhang L.,Gu F.X.,Chan J.M., Wang A.Z., Langer R.S., Farokhzad O.C. (2007) Nanoparticles in medicine: Therapeutic applications and developments. *Clinical Pharmacology and Therapeutics* **83**:761-769

Zhang J., Snyder S.H. (1995) Nitric oxide in the nervous system. *Annual Review of Pharmacology and Toxicology* **35**: 213-233

Zhou L. and Zhu D.Y. (2009) Neuronal nitric oxide synthase: structure, subcellular localization, regulation and clinical implications. *Nitric Oxide* **20**:223-230

K_i statistical analysis.pzf:1way ANOVA of K_i: Tabular results

		A	B	C	D
	Parameter	Value	Data Set-B	Data Set-C	Data Set-D
		Y	Y	Y	Y
1	Table Analyzed				
2	Ki				
3	One-way analysis of variance				
4	P value	P<0.0001			
5	P value summary	***			
6	Are means signif. different? (P < 0.05)	Yes			
7	Number of groups	12			
8	F	22.39			
9	R squared	0.9112			
10					
11	ANOVA Table	SS	df	MS	
12	Treatment (between columns)	1557	11	141.5	
13	Residual (within columns)	151.7	24	6.321	
14	Total	1709	35		
15					
16	Tukey's Multiple Comparison Test	Mean Diff.	q	P value	95% CI of diff
17	17-21P vs 29-33P	-2.000	1.378	P > 0.05	-9.402 to 5.402
18	17-21P vs 17-21R	8.000	5.511	P < 0.05	0.5985 to 15.40
19	17-21P vs 29-33R	6.000	4.133	P > 0.05	-1.402 to 13.40
20	17-21P vs Au	18.85	12.99	P < 0.001	11.45 to 26.25
21	17-21P vs Ag	18.88	13.01	P < 0.001	11.48 to 26.28
22	17-21P vs curcumin	18.75	12.91	P < 0.001	11.34 to 26.15
23	17-21P vs 17-21	13.90	9.576	P < 0.001	6.498 to 21.30
24	17-21P vs 25-37	8.000	5.511	P < 0.05	0.5985 to 15.40
25	17-21P vs 25-29	9.900	6.820	P < 0.01	2.498 to 17.30
26	17-21P vs 29-33	11.50	7.922	P < 0.001	4.098 to 18.90
27	17-21P vs 33-37	10.60	7.302	P < 0.01	3.198 to 18.00
28	29-33P vs 17-21R	10.00	6.889	P < 0.01	2.598 to 17.40
29	29-33P vs 29-33R	8.000	5.511	P < 0.05	0.5985 to 15.40
30	29-33P vs Au	20.85	14.36	P < 0.001	13.45 to 28.25
31	29-33P vs Ag	20.88	14.38	P < 0.001	13.48 to 28.28
32	29-33P vs curcumin	20.75	14.29	P < 0.001	13.34 to 28.15
33	29-33P vs 17-21	15.90	10.95	P < 0.001	8.498 to 23.30
34	29-33P vs 25-37	10.00	6.889	P < 0.01	2.598 to 17.40
35	29-33P vs 25-29	11.90	8.198	P < 0.001	4.498 to 19.30
36	29-33P vs 29-33	13.50	9.300	P < 0.001	6.098 to 20.90

K_i statistical analysis.pzf:1way ANOVA of K_i: Tabular results

37	29-33P vs 33-37	12.60	8.680	P < 0.001	5.198 to 20.00
38	17-21R vs 29-33R	-2.000	1.378	P > 0.05	-9.402 to 5.402
39	17-21R vs Au	10.85	7.475	P < 0.001	3.448 to 18.25
40	17-21R vs Ag	10.88	7.495	P < 0.001	3.478 to 18.28
41	17-21R vs curcumin	10.75	7.402	P < 0.01	3.343 to 18.15
42	17-21R vs 17-21	5.900	4.065	P > 0.05	-1.502 to 13.30
43	17-21R vs 25-37	0.0000	0.0000	P > 0.05	-7.402 to 7.402
44	17-21R vs 25-29	1.900	1.309	P > 0.05	-5.502 to 9.302
45	17-21R vs 29-33	3.500	2.411	P > 0.05	-3.902 to 10.90
46	17-21R vs 33-37	2.600	1.791	P > 0.05	-4.802 to 10.00
47	29-33R vs Au	12.85	8.853	P < 0.001	5.448 to 20.25
48	29-33R vs Ag	12.88	8.873	P < 0.001	5.478 to 20.28
49	29-33R vs curcumin	12.75	8.780	P < 0.001	5.343 to 20.15
50	29-33R vs 17-21	7.900	5.442	P < 0.05	0.4985 to 15.30
51	29-33R vs 25-37	2.000	1.378	P > 0.05	-5.402 to 9.402
52	29-33R vs 25-29	3.900	2.687	P > 0.05	-3.502 to 11.30
53	29-33R vs 29-33	5.500	3.789	P > 0.05	-1.902 to 12.90
54	29-33R vs 33-37	4.600	3.169	P > 0.05	-2.802 to 12.00
55	Au vs Ag	0.03000	0.02067	P > 0.05	-7.372 to 7.432
56	Au vs curcumin	-0.1050	0.07234	P > 0.05	-7.507 to 7.297
57	Au vs 17-21	-4.950	3.410	P > 0.05	-12.35 to 2.452
58	Au vs 25-37	-10.85	7.475	P < 0.001	-18.25 to -3.448
59	Au vs 25-29	-8.950	6.166	P < 0.01	-16.35 to -1.548
60	Au vs 29-33	-7.350	5.063	P > 0.05	-14.75 to 0.05154
61	Au vs 33-37	-8.250	5.684	P < 0.05	-15.65 to -0.8485
62	Ag vs curcumin	-0.1350	0.09300	P > 0.05	-7.537 to 7.267
63	Ag vs 17-21	-4.980	3.431	P > 0.05	-12.38 to 2.422
64	Ag vs 25-37	-10.88	7.495	P < 0.001	-18.28 to -3.478
65	Ag vs 25-29	-8.980	6.186	P < 0.01	-16.38 to -1.578
66	Ag vs 29-33	-7.380	5.084	P > 0.05	-14.78 to 0.02154
67	Ag vs 33-37	-8.280	5.704	P < 0.05	-15.68 to -0.8785
68	curcumin vs 17-21	-4.845	3.338	P > 0.05	-12.25 to 2.557
69	curcumin vs 25-37	-10.75	7.402	P < 0.01	-18.15 to -3.343
70	curcumin vs 25-29	-8.845	6.093	P < 0.05	-16.25 to -1.443
71	curcumin vs 29-33	-7.245	4.991	P > 0.05	-14.65 to 0.1565
72	curcumin vs 33-37	-8.145	5.611	P < 0.05	-15.55 to -0.7435
73	17-21 vs 25-37	-5.900	4.065	P > 0.05	-13.30 to 1.502
74	17-21 vs 25-29	-4.000	2.756	P > 0.05	-11.40 to 3.402
75	17-21 vs 29-33	-2.400	1.653	P > 0.05	-9.802 to 5.002
76	17-21 vs 33-37	-3.300	2.273	P > 0.05	-10.70 to 4.102

K_i statistical analysis.pzf:1way ANOVA of K_i: Tabular results

77	25-37 vs 25-29	1.900	1.309	P > 0.05	-5.502 to 9.302
78	25-37 vs 29-33	3.500	2.411	P > 0.05	-3.902 to 10.90
79	25-37 vs 33-37	2.600	1.791	P > 0.05	-4.802 to 10.00
80	25-29 vs 29-33	1.600	1.102	P > 0.05	-5.802 to 9.002

K_{sv} statistical analysis.pzf:2way ANOVA of K_{sv}: Tabular results

1	Table Analyzed	Ksv			
2					
3	Two-way ANOVA				
4					
5	Source of Variation	% of total variation	P value		
6	Column Factor	19.61	P<0.0001		
7	Temp	74.11	P<0.0001		
8					
9	Source of Variation	P value summary	Significant?		
10	Column Factor	***	Yes		
11	Temp	***	Yes		
12					
13	Source of Variation	Df	Sum-of-squares	Mean square	F
14	Column Factor	11	0.001683	0.0001530	9.364
15	Temp	3	0.006359	0.002120	129.8
16	Residual	33	0.0005391	0.00001634	
17					
18	Number of missing values	0			
19					
20	Bonferroni posttests				
21					
22	17-21 vs. 25-29				
23	Temp	17-21	25-29	Difference	95% CI of diff.
24	298.0	0.0150	0.0180	0.0030	-0.02101 to 0.02701
25	303.0	0.0190	0.0230	0.004000	-0.02001 to 0.02801
26	308.0	0.0310	0.0280	-0.003000	-0.02701 to 0.02101
27	313.0	0.0510	0.0410	-0.01000	-0.03401 to 0.01401
28					
29	Temp	Difference	t	P value	Summary
30	298.0	0.0030	0.5249	P > 0.05	ns
31	303.0	0.004000	0.6998	P > 0.05	ns
32	308.0	-0.003000	0.5249	P > 0.05	ns
33	313.0	-0.01000	1.750	P > 0.05	ns
34					
35	17-21 vs. 29-33				
36	Temp	17-21	29-33	Difference	95% CI of diff.
37	298.0	0.0150	0.0090	-0.0060	-0.03001 to 0.01801
38	303.0	0.0190	0.0110	-0.008000	-0.03201 to 0.01601
39	308.0	0.0310	0.0180	-0.0130	-0.03701 to 0.01101

K_{sv} statistical analysis.pzf:2way ANOVA of K_{sv}: Tabular results

40	313.0	0.0510	0.0410	-0.01000	-0.03401 to 0.01401
41					
42	Temp	Difference	t	P value	Summary
43	298.0	-0.0060	1.050	P > 0.05	ns
44	303.0	-0.008000	1.400	P > 0.05	ns
45	308.0	-0.0130	2.274	P > 0.05	ns
46	313.0	-0.01000	1.750	P > 0.05	ns
47					
48	17-21 vs. 33-37				
49	Temp	17-21	33-37	Difference	95% CI of diff.
50	298.0	0.0150	0.0110	-0.0040	-0.02801 to 0.02001
51	303.0	0.0190	0.0150	-0.0040	-0.02801 to 0.02001
52	308.0	0.0310	0.0190	-0.0120	-0.03601 to 0.01201
53	313.0	0.0510	0.0360	-0.0150	-0.03901 to 0.009014
54					
55	Temp	Difference	t	P value	Summary
56	298.0	-0.0040	0.6998	P > 0.05	ns
57	303.0	-0.0040	0.6998	P > 0.05	ns
58	308.0	-0.0120	2.099	P > 0.05	ns
59	313.0	-0.0150	2.624	P > 0.05	ns
60					
61	17-21 vs. 25-37				
62	Temp	17-21	25-37	Difference	95% CI of diff.
63	298.0	0.0150	0.0140	-0.001000	-0.02501 to 0.02301
64	303.0	0.0190	0.0190	0.0000	-0.02401 to 0.02401
65	308.0	0.0310	0.0310	0.0000	-0.02401 to 0.02401
66	313.0	0.0510	0.0410	-0.01000	-0.03401 to 0.01401
67					
68	Temp	Difference	t	P value	Summary
69	298.0	-0.001000	0.1750	P > 0.05	ns
70	303.0	0.0000	0.0000	P > 0.05	ns
71	308.0	0.0000	0.0000	P > 0.05	ns
72	313.0	-0.01000	1.750	P > 0.05	ns
73					
74	17-21 vs. 17-21r				
75	Temp	17-21	17-21r	Difference	95% CI of diff.
76	298.0	0.0150	0.0150	0.0000	-0.02401 to 0.02401
77	303.0	0.0190	0.0250	0.006000	-0.01801 to 0.03001
78	308.0	0.0310	0.0350	0.004000	-0.02001 to 0.02801
79	313.0	0.0510	0.0520	0.001000	-0.02301 to 0.02501

K_{sv} statistical analysis.pzf:2way ANOVA of K_{sv}: Tabular results

80					
81	Temp	Difference	t	P value	Summary
82	298.0	0.0000	0.0000	P > 0.05	ns
83	303.0	0.006000	1.050	P > 0.05	ns
84	308.0	0.004000	0.6998	P > 0.05	ns
85	313.0	0.001000	0.1750	P > 0.05	ns
86					
87	17-21 vs. 17-21p				
88	Temp	17-21	17-21p	Difference	95% CI of diff.
89	298.0	0.0150	0.0072	-0.0078	-0.03181 to 0.01621
90	303.0	0.0190	0.0120	-0.007000	-0.03101 to 0.01701
91	308.0	0.0310	0.0250	-0.006000	-0.03001 to 0.01801
92	313.0	0.0510	0.0290	-0.0220	-0.04601 to 0.002014
93					
94	Temp	Difference	t	P value	Summary
95	298.0	-0.0078	1.365	P > 0.05	ns
96	303.0	-0.007000	1.225	P > 0.05	ns
97	308.0	-0.006000	1.050	P > 0.05	ns
98	313.0	-0.0220	3.849	P<0.01	**
99					
100	17-21 vs. 29-33r				
101	Temp	17-21	29-33r	Difference	95% CI of diff.
102	298.0	0.0150	0.0190	0.0040	-0.02001 to 0.02801
103	303.0	0.0190	0.0260	0.007000	-0.01701 to 0.03101
104	308.0	0.0310	0.0360	0.005000	-0.01901 to 0.02901
105	313.0	0.0510	0.0620	0.0110	-0.01301 to 0.03501
106					
107	Temp	Difference	t	P value	Summary
108	298.0	0.0040	0.6998	P > 0.05	ns
109	303.0	0.007000	1.225	P > 0.05	ns
110	308.0	0.005000	0.8748	P > 0.05	ns
111	313.0	0.0110	1.924	P > 0.05	ns
112					
113	17-21 vs. 29-33p				
114	Temp	17-21	29-33p	Difference	95% CI of diff.
115	298.0	0.0150	0.0061	-0.0089	-0.03291 to 0.01511
116	303.0	0.0190	0.0120	-0.007000	-0.03101 to 0.01701
117	308.0	0.0310	0.0160	-0.0150	-0.03901 to 0.009014
118	313.0	0.0510	0.0290	-0.0220	-0.04601 to 0.002014
119					

K_{sv} statistical analysis.pzf:2way ANOVA of K_{sv}: Tabular results

120	Temp	Difference	t	P value	Summary
121	298.0	-0.0089	1.557	P > 0.05	ns
122	303.0	-0.007000	1.225	P > 0.05	ns
123	308.0	-0.0150	2.624	P > 0.05	ns
124	313.0	-0.0220	3.849	P<0.01	**
125					
126	17-21 vs. Au				
127	Temp	17-21	Au	Difference	95% CI of diff.
128	298.0	0.0150	0.0092	-0.005800	-0.02981 to 0.01821
129	303.0	0.0190	0.0120	-0.007000	-0.03101 to 0.01701
130	308.0	0.0310	0.0180	-0.0130	-0.03701 to 0.01101
131	313.0	0.0510	0.0320	-0.0190	-0.04301 to 0.005014
132					
133	Temp	Difference	t	P value	Summary
134	298.0	-0.005800	1.015	P > 0.05	ns
135	303.0	-0.007000	1.225	P > 0.05	ns
136	308.0	-0.0130	2.274	P > 0.05	ns
137	313.0	-0.0190	3.324	P<0.01	**
138					
139	17-21 vs. Ag				
140	Temp	17-21	Ag	Difference	95% CI of diff.
141	298.0	0.0150	0.0077	-0.0073	-0.03131 to 0.01671
142	303.0	0.0190	0.0100	-0.0090	-0.03301 to 0.01501
143	308.0	0.0310	0.0270	-0.004000	-0.02801 to 0.02001
144	313.0	0.0510	0.0480	-0.003000	-0.02701 to 0.02101
145					
146	Temp	Difference	t	P value	Summary
147	298.0	-0.0073	1.277	P > 0.05	ns
148	303.0	-0.0090	1.575	P > 0.05	ns
149	308.0	-0.004000	0.6998	P > 0.05	ns
150	313.0	-0.003000	0.5249	P > 0.05	ns
151					
152	17-21 vs. curcumin				
153	Temp	17-21	curcumin	Difference	95% CI of diff.
154	298.0	0.0150	0.0120	-0.0030	-0.02701 to 0.02101
155	303.0	0.0190	0.0200	0.0010	-0.02301 to 0.02501
156	308.0	0.0310	0.0330	0.0020	-0.02201 to 0.02601
157	313.0	0.0510	0.0440	-0.007000	-0.03101 to 0.01701
158					
159	Temp	Difference	t	P value	Summary

K_{sv} statistical analysis.pzf:2way ANOVA of K_{sv}: Tabular results

160	298.0	-0.0030	0.5249	P > 0.05	ns
161	303.0	0.0010	0.1750	P > 0.05	ns
162	308.0	0.0020	0.3499	P > 0.05	ns
163	313.0	-0.007000	1.225	P > 0.05	ns
164					
165	25-29 vs. 29-33				
166	Temp	25-29	29-33	Difference	95% CI of diff.
167	298.0	0.0180	0.0090	-0.0090	-0.03301 to 0.01501
168	303.0	0.0230	0.0110	-0.0120	-0.03601 to 0.01201
169	308.0	0.0280	0.0180	-0.0100	-0.03401 to 0.01401
170	313.0	0.0410	0.0410	0.0000	-0.02401 to 0.02401
171					
172	Temp	Difference	t	P value	Summary
173	298.0	-0.0090	1.575	P > 0.05	ns
174	303.0	-0.0120	2.099	P > 0.05	ns
175	308.0	-0.0100	1.750	P > 0.05	ns
176	313.0	0.0000	0.0000	P > 0.05	ns
177					
178	25-29 vs. 33-37				
179	Temp	25-29	33-37	Difference	95% CI of diff.
180	298.0	0.0180	0.0110	-0.007000	-0.03101 to 0.01701
181	303.0	0.0230	0.0150	-0.0080	-0.03201 to 0.01601
182	308.0	0.0280	0.0190	-0.009000	-0.03301 to 0.01501
183	313.0	0.0410	0.0360	-0.005000	-0.02901 to 0.01901
185	Temp	Difference	t	P value	Summary
186	298.0	-0.007000	1.225	P > 0.05	ns
187	303.0	-0.0080	1.400	P > 0.05	ns
188	308.0	-0.009000	1.575	P > 0.05	ns
189	313.0	-0.005000	0.8748	P > 0.05	ns
190					
191	25-29 vs. 25-37				
192	Temp	25-29	25-37	Difference	95% CI of diff.
193	298.0	0.0180	0.0140	-0.004000	-0.02801 to 0.02001
194	303.0	0.0230	0.0190	-0.004000	-0.02801 to 0.02001
195	308.0	0.0280	0.0310	0.003000	-0.02101 to 0.02701
196	313.0	0.0410	0.0410	0.0000	-0.02401 to 0.02401
197					
198	Temp	Difference	t	P value	Summary
199	298.0	-0.004000	0.6998	P > 0.05	ns
200	303.0	-0.004000	0.6998	P > 0.05	ns
201	308.0	0.003000	0.5249	P > 0.05	ns

K_{sv} statistical analysis.pzf:2way ANOVA of K_{sv}: Tabular results

202	313.0	0.0000	0.0000	P > 0.05	ns
203					
204	25-29 vs. 17-21r				
205	Temp	25-29	17-21r	Difference	95% CI of diff.
206	298.0	0.0180	0.0150	-0.0030	-0.02701 to 0.02101
207	303.0	0.0230	0.0250	0.0020	-0.02201 to 0.02601
208	308.0	0.0280	0.0350	0.007000	-0.01701 to 0.03101
209	313.0	0.0410	0.0520	0.0110	-0.01301 to 0.03501
210					
211	Temp	Difference	t	P value	Summary
212	298.0	-0.0030	0.5249	P > 0.05	ns
213	303.0	0.0020	0.3499	P > 0.05	ns
214	308.0	0.007000	1.225	P > 0.05	ns
215	313.0	0.0110	1.924	P > 0.05	ns
216					
217	25-29 vs. 17-21p				
218	Temp	25-29	17-21p	Difference	95% CI of diff.
219	298.0	0.0180	0.0072	-0.0108	-0.03481 to 0.01321
220	303.0	0.0230	0.0120	-0.0110	-0.03501 to 0.01301
221	308.0	0.0280	0.0250	-0.0030	-0.02701 to 0.02101
222	313.0	0.0410	0.0290	-0.0120	-0.03601 to 0.01201
223					
224	Temp	Difference	t	P value	Summary
225	298.0	-0.0108	1.889	P > 0.05	ns
226	303.0	-0.0110	1.924	P > 0.05	ns
227	308.0	-0.0030	0.5249	P > 0.05	ns
228	313.0	-0.0120	2.099	P > 0.05	ns
229					
230	25-29 vs. 29-33r				
231	Temp	25-29	29-33r	Difference	95% CI of diff.
232	298.0	0.0180	0.0190	0.0010	-0.02301 to 0.02501
233	303.0	0.0230	0.0260	0.0030	-0.02101 to 0.02701
234	308.0	0.0280	0.0360	0.008000	-0.01601 to 0.03201
235	313.0	0.0410	0.0620	0.0210	-0.003014 to 0.04501
236					
237	Temp	Difference	t	P value	Summary
238	298.0	0.0010	0.1750	P > 0.05	ns
239	303.0	0.0030	0.5249	P > 0.05	ns
240	308.0	0.008000	1.400	P > 0.05	ns
241	313.0	0.0210	3.674	P<0.01	**
242					

K_{sv} statistical analysis.pzf:2way ANOVA of K_{sv}: Tabular results

243	25-29 vs. 29-33p				
244	Temp	25-29	29-33p	Difference	95% CI of diff.
245	298.0	0.0180	0.0061	-0.0119	-0.03591 to 0.01211
246	303.0	0.0230	0.0120	-0.0110	-0.03501 to 0.01301
247	308.0	0.0280	0.0160	-0.0120	-0.03601 to 0.01201
248	313.0	0.0410	0.0290	-0.0120	-0.03601 to 0.01201
249					
250	Temp	Difference	t	P value	Summary
251	298.0	-0.0119	2.082	P > 0.05	ns
252	303.0	-0.0110	1.924	P > 0.05	ns
253	308.0	-0.0120	2.099	P > 0.05	ns
254	313.0	-0.0120	2.099	P > 0.05	ns
255					
256	25-29 vs. Au				
257	Temp	25-29	Au	Difference	95% CI of diff.
258	298.0	0.0180	0.0092	-0.008800	-0.03281 to 0.01521
259	303.0	0.0230	0.0120	-0.0110	-0.03501 to 0.01301
260	308.0	0.0280	0.0180	-0.0100	-0.03401 to 0.01401
261	313.0	0.0410	0.0320	-0.0090	-0.03301 to 0.01501
262					
263	Temp	Difference	t	P value	Summary
264	298.0	-0.008800	1.540	P > 0.05	ns
265	303.0	-0.0110	1.924	P > 0.05	ns
266	308.0	-0.0100	1.750	P > 0.05	ns
267	313.0	-0.0090	1.575	P > 0.05	ns
268					
269	25-29 vs. Ag				
270	Temp	25-29	Ag	Difference	95% CI of diff.
271	298.0	0.0180	0.0077	-0.0103	-0.03431 to 0.01371
272	303.0	0.0230	0.0100	-0.0130	-0.03701 to 0.01101
273	308.0	0.0280	0.0270	-0.0010	-0.02501 to 0.02301
274	313.0	0.0410	0.0480	0.007000	-0.01701 to 0.03101
275					
276	Temp	Difference	t	P value	Summary
277	298.0	-0.0103	1.802	P > 0.05	ns
278	303.0	-0.0130	2.274	P > 0.05	ns
279	308.0	-0.0010	0.1750	P > 0.05	ns
280	313.0	0.007000	1.225	P > 0.05	ns
281					
282	25-29 vs. curcumin				

K_{sv} statistical analysis.pzf:2way ANOVA of K_{sv}: Tabular results

283	Temp	25-29	curcumin	Difference	95% CI of diff.
284	298.0	0.0180	0.0120	-0.006000	-0.03001 to 0.01801
285	303.0	0.0230	0.0200	-0.0030	-0.02701 to 0.02101
286	308.0	0.0280	0.0330	0.005000	-0.01901 to 0.02901
287	313.0	0.0410	0.0440	0.003000	-0.02101 to 0.02701
288					
289	Temp	Difference	t	P value	Summary
290	298.0	-0.006000	1.050	P > 0.05	ns
291	303.0	-0.0030	0.5249	P > 0.05	ns
292	308.0	0.005000	0.8748	P > 0.05	ns
293	313.0	0.003000	0.5249	P > 0.05	ns
294					
295	29-33 vs. 33-37				
296	Temp	29-33	33-37	Difference	95% CI of diff.
297	298.0	0.0090	0.0110	0.0020	-0.02201 to 0.02601
298	303.0	0.0110	0.0150	0.0040	-0.02001 to 0.02801
299	308.0	0.0180	0.0190	0.0010	-0.02301 to 0.02501
300	313.0	0.0410	0.0360	-0.005000	-0.02901 to 0.01901
301					
302	Temp	Difference	t	P value	Summary
303	298.0	0.0020	0.3499	P > 0.05	ns
304	303.0	0.0040	0.6998	P > 0.05	ns
305	308.0	0.0010	0.1750	P > 0.05	ns
306	313.0	-0.005000	0.8748	P > 0.05	ns
307					
308	29-33 vs. 25-37				
309	Temp	29-33	25-37	Difference	95% CI of diff.
310	298.0	0.0090	0.0140	0.005000	-0.01901 to 0.02901
311	303.0	0.0110	0.0190	0.008000	-0.01601 to 0.03201
312	308.0	0.0180	0.0310	0.0130	-0.01101 to 0.03701
313	313.0	0.0410	0.0410	0.0000	-0.02401 to 0.02401
314					
315	Temp	Difference	t	P value	Summary
316	298.0	0.005000	0.8748	P > 0.05	ns
317	303.0	0.008000	1.400	P > 0.05	ns
318	308.0	0.0130	2.274	P > 0.05	ns
319	313.0	0.0000	0.0000	P > 0.05	ns
320					
321	29-33 vs. 17-21r				
322	Temp	29-33	17-21r	Difference	95% CI of diff.
323	298.0	0.0090	0.0150	0.0060	-0.01801 to 0.03001

K_{sv} statistical analysis.pzf:2way ANOVA of K_{sv}: Tabular results

324	303.0	0.0110	0.0250	0.0140	-0.01001 to 0.03801
325	308.0	0.0180	0.0350	0.0170	-0.007014 to 0.04101
326	313.0	0.0410	0.0520	0.0110	-0.01301 to 0.03501
327					
328	Temp	Difference	t	P value	Summary
329	298.0	0.0060	1.050	P > 0.05	ns
330	303.0	0.0140	2.449	P > 0.05	ns
331	308.0	0.0170	2.974	P < 0.05	*
332	313.0	0.0110	1.924	P > 0.05	ns
333					
334	29-33 vs. 17-21p				
335	Temp	29-33	17-21p	Difference	95% CI of diff.
336	298.0	0.0090	0.0072	-0.0018	-0.02581 to 0.02221
337	303.0	0.0110	0.0120	0.0010	-0.02301 to 0.02501
338	308.0	0.0180	0.0250	0.007000	-0.01701 to 0.03101
339	313.0	0.0410	0.0290	-0.0120	-0.03601 to 0.01201
340					
341	Temp	Difference	t	P value	Summary
342	298.0	-0.0018	0.3149	P > 0.05	ns
343	303.0	0.0010	0.1750	P > 0.05	ns
344	308.0	0.007000	1.225	P > 0.05	ns
345	313.0	-0.0120	2.099	P > 0.05	ns
346					
347	29-33 vs. 29-33r				
348	Temp	29-33	29-33r	Difference	95% CI of diff.
349	298.0	0.0090	0.0190	0.0100	-0.01401 to 0.03401
350	303.0	0.0110	0.0260	0.0150	-0.009014 to 0.03901
351	308.0	0.0180	0.0360	0.0180	-0.006014 to 0.04201
352	313.0	0.0410	0.0620	0.0210	-0.003014 to 0.04501
353					
354	Temp	Difference	t	P value	Summary
355	298.0	0.0100	1.750	P > 0.05	ns
356	303.0	0.0150	2.624	P > 0.05	ns
357	308.0	0.0180	3.149	P < 0.05	*
358	313.0	0.0210	3.674	P<0.01	**
359					
360	29-33 vs. 29-33p				
361	Temp	29-33	29-33p	Difference	95% CI of diff.
362	298.0	0.0090	0.0061	-0.0029	-0.02691 to 0.02111
363	303.0	0.0110	0.0120	0.0010	-0.02301 to 0.02501

K_{sv} statistical analysis.pzf:2way ANOVA of K_{sv}: Tabular results

364	308.0	0.0180	0.0160	-0.002000	-0.02601 to 0.02201
365	313.0	0.0410	0.0290	-0.0120	-0.03601 to 0.01201
366					
367	Temp	Difference	t	P value	Summary
368	298.0	-0.0029	0.5074	P > 0.05	ns
369	303.0	0.0010	0.1750	P > 0.05	ns
370	308.0	-0.002000	0.3499	P > 0.05	ns
371	313.0	-0.0120	2.099	P > 0.05	ns
372					
373	29-33 vs. Au				
374	Temp	29-33	Au	Difference	95% CI of diff.
375	298.0	0.0090	0.0092	0.0002000	-0.02381 to 0.02421
376	303.0	0.0110	0.0120	0.0010	-0.02301 to 0.02501
377	308.0	0.0180	0.0180	0.0000	-0.02401 to 0.02401
378	313.0	0.0410	0.0320	-0.0090	-0.03301 to 0.01501
379					
380	Temp	Difference	t	P value	Summary
381	298.0	0.0002000	0.03499	P > 0.05	ns
382	303.0	0.0010	0.1750	P > 0.05	ns
383	308.0	0.0000	0.0000	P > 0.05	ns
384	313.0	-0.0090	1.575	P > 0.05	ns
385					
386	29-33 vs. Ag				
387	Temp	29-33	Ag	Difference	95% CI of diff.
388	298.0	0.0090	0.0077	-0.0013	-0.02531 to 0.02271
389	303.0	0.0110	0.0100	-0.0010	-0.02501 to 0.02301
390	308.0	0.0180	0.0270	0.009000	-0.01501 to 0.03301
391	313.0	0.0410	0.0480	0.007000	-0.01701 to 0.03101
392					
393	Temp	Difference	t	P value	Summary
394	298.0	-0.0013	0.2274	P > 0.05	ns
395	303.0	-0.0010	0.1750	P > 0.05	ns
396	308.0	0.009000	1.575	P > 0.05	ns
397	313.0	0.007000	1.225	P > 0.05	ns
398					
399	29-33 vs. curcumin				
400	Temp	29-33	curcumin	Difference	95% CI of diff.
401	298.0	0.0090	0.0120	0.0030	-0.02101 to 0.02701
402	303.0	0.0110	0.0200	0.0090	-0.01501 to 0.03301
403	308.0	0.0180	0.0330	0.0150	-0.009014 to 0.03901
404	313.0	0.0410	0.0440	0.003000	-0.02101 to 0.02701

K_{sv} statistical analysis.pzf:2way ANOVA of K_{sv}: Tabular results

405					
406	Temp	Difference	t	P value	Summary
407	298.0	0.0030	0.5249	P > 0.05	ns
408	303.0	0.0090	1.575	P > 0.05	ns
409	308.0	0.0150	2.624	P > 0.05	ns
410	313.0	0.003000	0.5249	P > 0.05	ns
411					
412	33-37 vs. 25-37				
413	Temp	33-37	25-37	Difference	95% CI of diff.
414	298.0	0.0110	0.0140	0.0030	-0.02101 to 0.02701
415	303.0	0.0150	0.0190	0.0040	-0.02001 to 0.02801
416	308.0	0.0190	0.0310	0.0120	-0.01201 to 0.03601
417	313.0	0.0360	0.0410	0.005000	-0.01901 to 0.02901
418					
419	Temp	Difference	t	P value	Summary
420	298.0	0.0030	0.5249	P > 0.05	ns
421	303.0	0.0040	0.6998	P > 0.05	ns
422	308.0	0.0120	2.099	P > 0.05	ns
423	313.0	0.005000	0.8748	P > 0.05	ns
425	33-37 vs. 17-21r				
426	Temp	33-37	17-21r	Difference	95% CI of diff.
427	298.0	0.0110	0.0150	0.0040	-0.02001 to 0.02801
428	303.0	0.0150	0.0250	0.0100	-0.01401 to 0.03401
429	308.0	0.0190	0.0350	0.0160	-0.008014 to 0.04001
430	313.0	0.0360	0.0520	0.0160	-0.008014 to 0.04001
431					
432	Temp	Difference	t	P value	Summary
433	298.0	0.0040	0.6998	P > 0.05	ns
434	303.0	0.0100	1.750	P > 0.05	ns
435	308.0	0.0160	2.799	P < 0.05	*
436	313.0	0.0160	2.799	P < 0.05	*
437					
438	33-37 vs. 17-21p				
439	Temp	33-37	17-21p	Difference	95% CI of diff.
440	298.0	0.0110	0.0072	-0.0038	-0.02781 to 0.02021
441	303.0	0.0150	0.0120	-0.0030	-0.02701 to 0.02101
442	308.0	0.0190	0.0250	0.006000	-0.01801 to 0.03001
443	313.0	0.0360	0.0290	-0.007000	-0.03101 to 0.01701
444					
445	Temp	Difference	t	P value	Summary
446	298.0	-0.0038	0.6648	P > 0.05	ns

K_{sv} statistical analysis.pzf:2way ANOVA of K_{sv}: Tabular results

447	303.0	-0.0030	0.5249	P > 0.05	ns
448	308.0	0.006000	1.050	P > 0.05	ns
449	313.0	-0.007000	1.225	P > 0.05	ns
450					
451	33-37 vs. 29-33r				
452	Temp	33-37	29-33r	Difference	95% CI of diff.
453	298.0	0.0110	0.0190	0.008000	-0.01601 to 0.03201
454	303.0	0.0150	0.0260	0.0110	-0.01301 to 0.03501
455	308.0	0.0190	0.0360	0.0170	-0.007014 to 0.04101
456	313.0	0.0360	0.0620	0.0260	0.001986 to 0.05001
457					
458	Temp	Difference	t	P value	Summary
459	298.0	0.008000	1.400	P > 0.05	ns
460	303.0	0.0110	1.924	P > 0.05	ns
461	308.0	0.0170	2.974	P < 0.05	*
462	313.0	0.0260	4.549	P<0.001	***
463					
464	33-37 vs. 29-33p				
465	Temp	33-37	29-33p	Difference	95% CI of diff.
466	298.0	0.0110	0.0061	-0.0049	-0.02891 to 0.01911
467	303.0	0.0150	0.0120	-0.0030	-0.02701 to 0.02101
468	308.0	0.0190	0.0160	-0.003000	-0.02701 to 0.02101
469	313.0	0.0360	0.0290	-0.007000	-0.03101 to 0.01701
470					
471	Temp	Difference	t	P value	Summary
472	298.0	-0.0049	0.8573	P > 0.05	ns
473	303.0	-0.0030	0.5249	P > 0.05	ns
474	308.0	-0.003000	0.5249	P > 0.05	ns
475	313.0	-0.007000	1.225	P > 0.05	ns
476					
477	33-37 vs. Au				
478	Temp	33-37	Au	Difference	95% CI of diff.
479	298.0	0.0110	0.0092	-0.0018	-0.02581 to 0.02221
480	303.0	0.0150	0.0120	-0.0030	-0.02701 to 0.02101
481	308.0	0.0190	0.0180	-0.0010	-0.02501 to 0.02301
482	313.0	0.0360	0.0320	-0.004000	-0.02801 to 0.02001
483					
484	Temp	Difference	t	P value	Summary
485	298.0	-0.0018	0.3149	P > 0.05	ns
486	303.0	-0.0030	0.5249	P > 0.05	ns

K_{sv} statistical analysis.pzf:2way ANOVA of K_{sv}: Tabular results

487	308.0	-0.0010	0.1750	P > 0.05	ns
488	313.0	-0.004000	0.6998	P > 0.05	ns
489					
490	33-37 vs. Ag				
491	Temp	33-37	Ag	Difference	95% CI of diff.
492	298.0	0.0110	0.0077	-0.0033	-0.02731 to 0.02071
493	303.0	0.0150	0.0100	-0.0050	-0.02901 to 0.01901
494	308.0	0.0190	0.0270	0.008000	-0.01601 to 0.03201
495	313.0	0.0360	0.0480	0.0120	-0.01201 to 0.03601
496					
497	Temp	Difference	t	P value	Summary
498	298.0	-0.0033	0.5773	P > 0.05	ns
499	303.0	-0.0050	0.8748	P > 0.05	ns
500	308.0	0.008000	1.400	P > 0.05	ns
501	313.0	0.0120	2.099	P > 0.05	ns
502					
503	33-37 vs. curcumin				
504	Temp	33-37	curcumin	Difference	95% CI of diff.
505	298.0	0.0110	0.0120	0.0010	-0.02301 to 0.02501
506	303.0	0.0150	0.0200	0.0050	-0.01901 to 0.02901
507	308.0	0.0190	0.0330	0.0140	-0.01001 to 0.03801
508	313.0	0.0360	0.0440	0.008000	-0.01601 to 0.03201
509					
510	Temp	Difference	t	P value	Summary
511	298.0	0.0010	0.1750	P > 0.05	ns
512	303.0	0.0050	0.8748	P > 0.05	ns
513	308.0	0.0140	2.449	P > 0.05	ns
514	313.0	0.008000	1.400	P > 0.05	ns
515					
516	25-37 vs. 17-21r				
517	Temp	25-37	17-21r	Difference	95% CI of diff.
518	298.0	0.0140	0.0150	0.001000	-0.02301 to 0.02501
519	303.0	0.0190	0.0250	0.006000	-0.01801 to 0.03001
520	308.0	0.0310	0.0350	0.004000	-0.02001 to 0.02801
521	313.0	0.0410	0.0520	0.0110	-0.01301 to 0.03501
522					
523	Temp	Difference	t	P value	Summary
524	298.0	0.001000	0.1750	P > 0.05	ns
525	303.0	0.006000	1.050	P > 0.05	ns
526	308.0	0.004000	0.6998	P > 0.05	ns
527	313.0	0.0110	1.924	P > 0.05	ns

K_{sv} statistical analysis.pzf:2way ANOVA of K_{sv}: Tabular results

528					
529	25-37 vs. 17-21p				
530	Temp	25-37	17-21p	Difference	95% CI of diff.
531	298.0	0.0140	0.0072	-0.006800	-0.03081 to 0.01721
532	303.0	0.0190	0.0120	-0.007000	-0.03101 to 0.01701
533	308.0	0.0310	0.0250	-0.006000	-0.03001 to 0.01801
534	313.0	0.0410	0.0290	-0.0120	-0.03601 to 0.01201
535					
536	Temp	Difference	t	P value	Summary
537	298.0	-0.006800	1.190	P > 0.05	ns
538	303.0	-0.007000	1.225	P > 0.05	ns
539	308.0	-0.006000	1.050	P > 0.05	ns
540	313.0	-0.0120	2.099	P > 0.05	ns
541					
542	25-37 vs. 29-33r				
543	Temp	25-37	29-33r	Difference	95% CI of diff.
544	298.0	0.0140	0.0190	0.005000	-0.01901 to 0.02901
545	303.0	0.0190	0.0260	0.007000	-0.01701 to 0.03101
546	308.0	0.0310	0.0360	0.005000	-0.01901 to 0.02901
547	313.0	0.0410	0.0620	0.0210	-0.003014 to 0.04501
548					
549	Temp	Difference	t	P value	Summary
550	298.0	0.005000	0.8748	P > 0.05	ns
551	303.0	0.007000	1.225	P > 0.05	ns
552	308.0	0.005000	0.8748	P > 0.05	ns
553	313.0	0.0210	3.674	P<0.01	**
554					
555	25-37 vs. 29-33p				
556	Temp	25-37	29-33p	Difference	95% CI of diff.
557	298.0	0.0140	0.0061	-0.007900	-0.03191 to 0.01611
558	303.0	0.0190	0.0120	-0.007000	-0.03101 to 0.01701
559	308.0	0.0310	0.0160	-0.0150	-0.03901 to 0.009014
560	313.0	0.0410	0.0290	-0.0120	-0.03601 to 0.01201
561					
562	Temp	Difference	t	P value	Summary
563	298.0	-0.007900	1.382	P > 0.05	ns
564	303.0	-0.007000	1.225	P > 0.05	ns
565	308.0	-0.0150	2.624	P > 0.05	ns
566	313.0	-0.0120	2.099	P > 0.05	ns
567					

K_{sv} statistical analysis.pzf:2way ANOVA of K_{sv}: Tabular results

568	25-37 vs. Au				
569	Temp	25-37	Au	Difference	95% CI of diff.
570	298.0	0.0140	0.0092	-0.0048	-0.02881 to 0.01921
571	303.0	0.0190	0.0120	-0.007000	-0.03101 to 0.01701
572	308.0	0.0310	0.0180	-0.0130	-0.03701 to 0.01101
573	313.0	0.0410	0.0320	-0.0090	-0.03301 to 0.01501
574					
575	Temp	Difference	t	P value	Summary
576	298.0	-0.0048	0.8398	P > 0.05	ns
577	303.0	-0.007000	1.225	P > 0.05	ns
578	308.0	-0.0130	2.274	P > 0.05	ns
579	313.0	-0.0090	1.575	P > 0.05	ns
580					
581	25-37 vs. Ag				
582	Temp	25-37	Ag	Difference	95% CI of diff.
583	298.0	0.0140	0.0077	-0.0063	-0.03031 to 0.01771
584	303.0	0.0190	0.0100	-0.0090	-0.03301 to 0.01501
585	308.0	0.0310	0.0270	-0.004000	-0.02801 to 0.02001
586	313.0	0.0410	0.0480	0.007000	-0.01701 to 0.03101
587					
588	Temp	Difference	t	P value	Summary
589	298.0	-0.0063	1.102	P > 0.05	ns
590	303.0	-0.0090	1.575	P > 0.05	ns
591	308.0	-0.004000	0.6998	P > 0.05	ns
592	313.0	0.007000	1.225	P > 0.05	ns
593					
594	25-37 vs. curcumin				
595	Temp	25-37	curcumin	Difference	95% CI of diff.
596	298.0	0.0140	0.0120	-0.0020	-0.02601 to 0.02201
597	303.0	0.0190	0.0200	0.0010	-0.02301 to 0.02501
598	308.0	0.0310	0.0330	0.0020	-0.02201 to 0.02601
599	313.0	0.0410	0.0440	0.003000	-0.02101 to 0.02701
600					
601	Temp	Difference	t	P value	Summary
602	298.0	-0.0020	0.3499	P > 0.05	ns
603	303.0	0.0010	0.1750	P > 0.05	ns
604	308.0	0.0020	0.3499	P > 0.05	ns
605	313.0	0.003000	0.5249	P > 0.05	ns
606					
607	17-21r vs. 17-21p				
608	Temp	17-21r	17-21p	Difference	95% CI of diff.

K_{sv} statistical analysis.pzf:2way ANOVA of K_{sv}: Tabular results

609	298.0	0.0150	0.0072	-0.0078	-0.03181 to 0.01621
610	303.0	0.0250	0.0120	-0.0130	-0.03701 to 0.01101
611	308.0	0.0350	0.0250	-0.0100	-0.03401 to 0.01401
612	313.0	0.0520	0.0290	-0.0230	-0.04701 to 0.001014
613					
614	Temp	Difference	t	P value	Summary
615	298.0	-0.0078	1.365	P > 0.05	ns
616	303.0	-0.0130	2.274	P > 0.05	ns
617	308.0	-0.0100	1.750	P > 0.05	ns
618	313.0	-0.0230	4.024	P<0.01	**
619					
620	17-21r vs. 29-33r				
621	Temp	17-21r	29-33r	Difference	95% CI of diff.
622	298.0	0.0150	0.0190	0.0040	-0.02001 to 0.02801
623	303.0	0.0250	0.0260	0.0010	-0.02301 to 0.02501
624	308.0	0.0350	0.0360	0.001000	-0.02301 to 0.02501
625	313.0	0.0520	0.0620	0.01000	-0.01401 to 0.03401
626					
627	Temp	Difference	t	P value	Summary
628	298.0	0.0040	0.6998	P > 0.05	ns
629	303.0	0.0010	0.1750	P > 0.05	ns
630	308.0	0.001000	0.1750	P > 0.05	ns
631	313.0	0.01000	1.750	P > 0.05	ns
632					
633	17-21r vs. 29-33p				
634	Temp	17-21r	29-33p	Difference	95% CI of diff.
635	298.0	0.0150	0.0061	-0.0089	-0.03291 to 0.01511
636	303.0	0.0250	0.0120	-0.0130	-0.03701 to 0.01101
637	308.0	0.0350	0.0160	-0.0190	-0.04301 to 0.005014
638	313.0	0.0520	0.0290	-0.0230	-0.04701 to 0.001014
639					
640	Temp	Difference	t	P value	Summary
641	298.0	-0.0089	1.557	P > 0.05	ns
642	303.0	-0.0130	2.274	P > 0.05	ns
643	308.0	-0.0190	3.324	P<0.01	**
644	313.0	-0.0230	4.024	P<0.01	**
645					
646	17-21r vs. Au				
647	Temp	17-21r	Au	Difference	95% CI of diff.
648	298.0	0.0150	0.0092	-0.005800	-0.02981 to 0.01821

K_{sv} statistical analysis.pzf:2way ANOVA of K_{sv}: Tabular results

649	303.0	0.0250	0.0120	-0.0130	-0.03701 to 0.01101
650	308.0	0.0350	0.0180	-0.0170	-0.04101 to 0.007014
651	313.0	0.0520	0.0320	-0.0200	-0.04401 to 0.004014
652					
653	Temp	Difference	t	P value	Summary
654	298.0	-0.005800	1.015	P > 0.05	ns
655	303.0	-0.0130	2.274	P > 0.05	ns
656	308.0	-0.0170	2.974	P < 0.05	*
657	313.0	-0.0200	3.499	P<0.01	**
658					
659	17-21r vs. Ag				
660	Temp	17-21r	Ag	Difference	95% CI of diff.
661	298.0	0.0150	0.0077	-0.0073	-0.03131 to 0.01671
662	303.0	0.0250	0.0100	-0.0150	-0.03901 to 0.009014
663	308.0	0.0350	0.0270	-0.008000	-0.03201 to 0.01601
664	313.0	0.0520	0.0480	-0.004000	-0.02801 to 0.02001
665					
666	Temp	Difference	t	P value	Summary
667	298.0	-0.0073	1.277	P > 0.05	ns
668	303.0	-0.0150	2.624	P > 0.05	ns
669	308.0	-0.008000	1.400	P > 0.05	ns
670	313.0	-0.004000	0.6998	P > 0.05	ns
671					
672	17-21r vs. curcumin				
673	Temp	17-21r	curcumin	Difference	95% CI of diff.
674	298.0	0.0150	0.0120	-0.0030	-0.02701 to 0.02101
675	303.0	0.0250	0.0200	-0.005000	-0.02901 to 0.01901
676	308.0	0.0350	0.0330	-0.0020	-0.02601 to 0.02201
677	313.0	0.0520	0.0440	-0.008000	-0.03201 to 0.01601
678					
679	Temp	Difference	t	P value	Summary
680	298.0	-0.0030	0.5249	P > 0.05	ns
681	303.0	-0.005000	0.8748	P > 0.05	ns
682	308.0	-0.0020	0.3499	P > 0.05	ns
683	313.0	-0.008000	1.400	P > 0.05	ns
684					
685	17-21p vs. 29-33r				
686	Temp	17-21p	29-33r	Difference	95% CI of diff.
687	298.0	0.0072	0.0190	0.0118	-0.01221 to 0.03581
688	303.0	0.0120	0.0260	0.0140	-0.01001 to 0.03801
689	308.0	0.0250	0.0360	0.0110	-0.01301 to 0.03501

K_{sv} statistical analysis.pzf:2way ANOVA of K_{sv}: Tabular results

690	313.0	0.0290	0.0620	0.0330	0.008986 to 0.05701
691					
692	Temp	Difference	t	P value	Summary
693	298.0	0.0118	2.064	P > 0.05	ns
694	303.0	0.0140	2.449	P > 0.05	ns
695	308.0	0.0110	1.924	P > 0.05	ns
696	313.0	0.0330	5.773	P<0.001	***
697					
698	17-21p vs. 29-33p				
699	Temp	17-21p	29-33p	Difference	95% CI of diff.
700	298.0	0.0072	0.0061	-0.0011	-0.02511 to 0.02291
701	303.0	0.0120	0.0120	0.0000	-0.02401 to 0.02401
702	308.0	0.0250	0.0160	-0.0090	-0.03301 to 0.01501
703	313.0	0.0290	0.0290	0.0000	-0.02401 to 0.02401
704					
705	Temp	Difference	t	P value	Summary
706	298.0	-0.0011	0.1924	P > 0.05	ns
707	303.0	0.0000	0.0000	P > 0.05	ns
708	308.0	-0.0090	1.575	P > 0.05	ns
709	313.0	0.0000	0.0000	P > 0.05	ns
710					
711	17-21p vs. Au				
712	Temp	17-21p	Au	Difference	95% CI of diff.
713	298.0	0.0072	0.0092	0.0020	-0.02201 to 0.02601
714	303.0	0.0120	0.0120	0.0000	-0.02401 to 0.02401
715	308.0	0.0250	0.0180	-0.007000	-0.03101 to 0.01701
716	313.0	0.0290	0.0320	0.003000	-0.02101 to 0.02701
717					
718	Temp	Difference	t	P value	Summary
719	298.0	0.0020	0.3499	P > 0.05	ns
720	303.0	0.0000	0.0000	P > 0.05	ns
721	308.0	-0.007000	1.225	P > 0.05	ns
722	313.0	0.003000	0.5249	P > 0.05	ns
723					
724	17-21p vs. Ag				
725	Temp	17-21p	Ag	Difference	95% CI of diff.
726	298.0	0.0072	0.0077	0.0005000	-0.02351 to 0.02451
727	303.0	0.0120	0.0100	-0.0020	-0.02601 to 0.02201
728	308.0	0.0250	0.0270	0.0020	-0.02201 to 0.02601
729	313.0	0.0290	0.0480	0.0190	-0.005014 to 0.04301
730					

K_{sv} statistical analysis.pzf:2way ANOVA of K_{sv}: Tabular results

731	Temp	Difference	t	P value	Summary
732	298.0	0.0005000	0.08748	P > 0.05	ns
733	303.0	-0.0020	0.3499	P > 0.05	ns
734	308.0	0.0020	0.3499	P > 0.05	ns
735	313.0	0.0190	3.324	P<0.01	**
736					
737	17-21p vs. curcumin				
738	Temp	17-21p	curcumin	Difference	95% CI of diff.
739	298.0	0.0072	0.0120	0.0048	-0.01921 to 0.02881
740	303.0	0.0120	0.0200	0.008000	-0.01601 to 0.03201
741	308.0	0.0250	0.0330	0.008000	-0.01601 to 0.03201
742	313.0	0.0290	0.0440	0.0150	-0.009014 to 0.03901
743					
744	Temp	Difference	t	P value	Summary
745	298.0	0.0048	0.8398	P > 0.05	ns
746	303.0	0.008000	1.400	P > 0.05	ns
747	308.0	0.008000	1.400	P > 0.05	ns
748	313.0	0.0150	2.624	P > 0.05	ns
749					
750	29-33r vs. 29-33p				
751	Temp	29-33r	29-33p	Difference	95% CI of diff.
752	298.0	0.0190	0.0061	-0.0129	-0.03691 to 0.01111
753	303.0	0.0260	0.0120	-0.0140	-0.03801 to 0.01001
754	308.0	0.0360	0.0160	-0.0200	-0.04401 to 0.004014
755	313.0	0.0620	0.0290	-0.0330	-0.05701 to -0.008986
756					
757	Temp	Difference	t	P value	Summary
758	298.0	-0.0129	2.257	P > 0.05	ns
759	303.0	-0.0140	2.449	P > 0.05	ns
760	308.0	-0.0200	3.499	P<0.01	**
761	313.0	-0.0330	5.773	P<0.001	***
762					
763	29-33r vs. Au				
764	Temp	29-33r	Au	Difference	95% CI of diff.
765	298.0	0.0190	0.0092	-0.009800	-0.03381 to 0.01421
766	303.0	0.0260	0.0120	-0.0140	-0.03801 to 0.01001
767	308.0	0.0360	0.0180	-0.0180	-0.04201 to 0.006014
768	313.0	0.0620	0.0320	-0.0300	-0.05401 to -0.005986
769					
770	Temp	Difference	t	P value	Summary

K_{sv} statistical analysis.pzf:2way ANOVA of K_{sv}: Tabular results

771	298.0	-0.009800	1.715	P > 0.05	ns
772	303.0	-0.0140	2.449	P > 0.05	ns
773	308.0	-0.0180	3.149	P < 0.05	*
774	313.0	-0.0300	5.249	P<0.001	***
775					
776	29-33r vs. Ag				
777	Temp	29-33r	Ag	Difference	95% CI of diff.
778	298.0	0.0190	0.0077	-0.0113	-0.03531 to 0.01271
779	303.0	0.0260	0.0100	-0.0160	-0.04001 to 0.008014
780	308.0	0.0360	0.0270	-0.009000	-0.03301 to 0.01501
781	313.0	0.0620	0.0480	-0.0140	-0.03801 to 0.01001
782					
783	Temp	Difference	t	P value	Summary
784	298.0	-0.0113	1.977	P > 0.05	ns
785	303.0	-0.0160	2.799	P < 0.05	*
786	308.0	-0.009000	1.575	P > 0.05	ns
787	313.0	-0.0140	2.449	P > 0.05	ns
788					
789	29-33r vs. curcumin				
790	Temp	29-33r	curcumin	Difference	95% CI of diff.
791	298.0	0.0190	0.0120	-0.007000	-0.03101 to 0.01701
792	303.0	0.0260	0.0200	-0.006000	-0.03001 to 0.01801
793	308.0	0.0360	0.0330	-0.003000	-0.02701 to 0.02101
794	313.0	0.0620	0.0440	-0.0180	-0.04201 to 0.006014
795					
796	Temp	Difference	t	P value	Summary
797	298.0	-0.007000	1.225	P > 0.05	ns
798	303.0	-0.006000	1.050	P > 0.05	ns
799	308.0	-0.003000	0.5249	P > 0.05	ns
800	313.0	-0.0180	3.149	P < 0.05	*
801					
802	29-33p vs. Au				
803	Temp	29-33p	Au	Difference	95% CI of diff.
804	298.0	0.0061	0.0092	0.0031	-0.02091 to 0.02711
805	303.0	0.0120	0.0120	0.0000	-0.02401 to 0.02401
806	308.0	0.0160	0.0180	0.002000	-0.02201 to 0.02601
807	313.0	0.0290	0.0320	0.003000	-0.02101 to 0.02701
808					
809	Temp	Difference	t	P value	Summary
810	298.0	0.0031	0.5424	P > 0.05	ns
811	303.0	0.0000	0.0000	P > 0.05	ns

K_{sv} statistical analysis.pzf:2way ANOVA of K_{sv}: Tabular results

812	308.0	0.002000	0.3499	P > 0.05	ns
813	313.0	0.003000	0.5249	P > 0.05	ns
814					
815	29-33p vs. Ag				
816	Temp	29-33p	Ag	Difference	95% CI of diff.
817	298.0	0.0061	0.0077	0.0016	-0.02241 to 0.02561
818	303.0	0.0120	0.0100	-0.0020	-0.02601 to 0.02201
819	308.0	0.0160	0.0270	0.0110	-0.01301 to 0.03501
820	313.0	0.0290	0.0480	0.0190	-0.005014 to 0.04301
821					
822	Temp	Difference	t	P value	Summary
823	298.0	0.0016	0.2799	P > 0.05	ns
824	303.0	-0.0020	0.3499	P > 0.05	ns
825	308.0	0.0110	1.924	P > 0.05	ns
826	313.0	0.0190	3.324	P<0.01	**
827					
828	29-33p vs. curcumin				
829	Temp	29-33p	curcumin	Difference	95% CI of diff.
830	298.0	0.0061	0.0120	0.0059	-0.01811 to 0.02991
831	303.0	0.0120	0.0200	0.008000	-0.01601 to 0.03201
832	308.0	0.0160	0.0330	0.0170	-0.007014 to 0.04101
833	313.0	0.0290	0.0440	0.0150	-0.009014 to 0.03901
834					
835	Temp	Difference	t	P value	Summary
836	298.0	0.0059	1.032	P > 0.05	ns
837	303.0	0.008000	1.400	P > 0.05	ns
838	308.0	0.0170	2.974	P < 0.05	*
839	313.0	0.0150	2.624	P > 0.05	ns
840					
841	Au vs. Ag				
842	Temp	Au	Ag	Difference	95% CI of diff.
843	298.0	0.0092	0.0077	-0.0015	-0.02551 to 0.02251
844	303.0	0.0120	0.0100	-0.0020	-0.02601 to 0.02201
845	308.0	0.0180	0.0270	0.009000	-0.01501 to 0.03301
846	313.0	0.0320	0.0480	0.0160	-0.008014 to 0.04001

848	Temp	Difference	t	P value	Summary
849	298.0	-0.0015	0.2624	P > 0.05	ns
850	303.0	-0.0020	0.3499	P > 0.05	ns
851	308.0	0.009000	1.575	P > 0.05	ns

K_{sv} statistical analysis.pzf:2way ANOVA of K_{sv}: Tabular results

852	313.0	0.0160	2.799	P < 0.05	*
853					
854	Au vs. curcumin				
855	Temp	Au	curcumin	Difference	95% CI of diff.
856	298.0	0.0092	0.0120	0.0028	-0.02121 to 0.02681
857	303.0	0.0120	0.0200	0.008000	-0.01601 to 0.03201
858	308.0	0.0180	0.0330	0.0150	-0.009014 to 0.03901
859	313.0	0.0320	0.0440	0.0120	-0.01201 to 0.03601
860					
861	Temp	Difference	t	P value	Summary
862	298.0	0.0028	0.4899	P > 0.05	ns
863	303.0	0.008000	1.400	P > 0.05	ns
864	308.0	0.0150	2.624	P > 0.05	ns
865	313.0	0.0120	2.099	P > 0.05	ns
866					
867	Ag vs. curcumin				
868	Temp	Ag	curcumin	Difference	95% CI of diff.
869	298.0	0.0077	0.0120	0.0043	-0.01971 to 0.02831
870	303.0	0.0100	0.0200	0.0100	-0.01401 to 0.03401
871	308.0	0.0270	0.0330	0.006000	-0.01801 to 0.03001
872	313.0	0.0480	0.0440	-0.004000	-0.02801 to 0.02001
873					
874	Temp	Difference	t	P value	Summary
875	298.0	0.0043	0.7523	P > 0.05	ns
876	303.0	0.0100	1.750	P > 0.05	ns
877	308.0	0.006000	1.050	P > 0.05	ns
878	313.0	-0.004000	0.6998	P > 0.05	ns

K_d statistical analysis.pzf:2way ANOVA of K_d: Tabular results

		A	B	C	D
	Parameter	Data Set-A	Data Set-B	Data Set-C	Data Set-D
		Y	Y	Y	Y
1	Table Analyzed	Kd			
2					
3	Two-way ANOVA				
4					
5	Source of Variation	% of total variation	P value		
6	Column Factor	94.66	P<0.0001		
7	Temp	2.42	0.0002		
8					
9	Source of Variation	P value summary	Significant?		
10	Column Factor	***	Yes		
11	Temp	***	Yes		
12					
13	Source of Variation	Df	Sum-of-squares	Mean square	F
14	Column Factor	11	119200	10830	97.36
15	Temp	3	3050	1017	9.138
16	Residual	33	3672	111.3	
17					
18	Number of missing values	0			
19					
20	Bonferroni posttests				
21					
22	17-21 vs. 25-29				
23	Temp	17-21	25-29	Difference	95% CI of diff.
24	298.0	6.000	6.900	0.9000	-61.77 to 63.57
25	303.0	6.200	7.800	1.600	-61.07 to 64.27
26	308.0	7.800	8.300	0.5000	-62.17 to 63.17
27	313.0	9.800	9.400	-0.4000	-63.07 to 62.27
28					
29	Temp	Difference	t	P value	Summary
30	298.0	0.9000	0.06033	P > 0.05	ns
31	303.0	1.600	0.1073	P > 0.05	ns
32	308.0	0.5000	0.03352	P > 0.05	ns
33	313.0	-0.4000	0.02681	P > 0.05	ns
34					
35	17-21 vs. 29-33				
36	Temp	17-21	29-33	Difference	95% CI of diff.
37	298.0	6.000	2.700	-3.300	-65.97 to 59.37
38	303.0	6.200	2.800	-3.400	-66.07 to 59.27
39	308.0	7.800	3.000	-4.800	-67.47 to 57.87

K_d statistical analysis.pzf:2way ANOVA of K_d: Tabular results

40	313.0	9.800	3.300	-6.500	-69.17 to 56.17
41					
42	Temp	Difference	t	P value	Summary
43	298.0	-3.300	0.2212	P > 0.05	ns
44	303.0	-3.400	0.2279	P > 0.05	ns
45	308.0	-4.800	0.3218	P > 0.05	ns
46	313.0	-6.500	0.4357	P > 0.05	ns
47					
48	17-21 vs. 33-37				
49	Temp	17-21	33-37	Difference	95% CI of diff.
50	298.0	6.000	5.400	-0.6000	-63.27 to 62.07
51	303.0	6.200	5.600	-0.6000	-63.27 to 62.07
52	308.0	7.800	6.100	-1.700	-64.37 to 60.97
53	313.0	9.800	7.700	-2.100	-64.77 to 60.57
54					
55	Temp	Difference	t	P value	Summary
56	298.0	-0.6000	0.04022	P > 0.05	ns
57	303.0	-0.6000	0.04022	P > 0.05	ns
58	308.0	-1.700	0.1140	P > 0.05	ns
59	313.0	-2.100	0.1408	P > 0.05	ns
60					
61	17-21 vs. 25-37				
62	Temp	17-21	25-37	Difference	95% CI of diff.
63	298.0	6.000	5.500	-0.5000	-63.17 to 62.17
64	303.0	6.200	6.200	0.0000	-62.67 to 62.67
65	308.0	7.800	7.400	-0.4000	-63.07 to 62.27
66	313.0	9.800	8.700	-1.100	-63.77 to 61.57
67					
68	Temp	Difference	t	P value	Summary
69	298.0	-0.5000	0.03352	P > 0.05	ns
70	303.0	0.0000	0.0000	P > 0.05	ns
71	308.0	-0.4000	0.02681	P > 0.05	ns
72	313.0	-1.100	0.07374	P > 0.05	ns
73					
74	17-21 vs. 17-21r				
75	Temp	17-21	17-21r	Difference	95% CI of diff.
76	298.0	6.000	15.00	9.000	-53.67 to 71.67
77	303.0	6.200	16.00	9.800	-52.87 to 72.47
78	308.0	7.800	17.00	9.200	-53.47 to 71.87
79	313.0	9.800	17.00	7.200	-55.47 to 69.87
80					
81	Temp	Difference	t	P value	Summary

K_d statistical analysis.pzf:2way ANOVA of K_d: Tabular results

82	298.0	9.000	0.6033	P > 0.05	ns
83	303.0	9.800	0.6570	P > 0.05	ns
84	308.0	9.200	0.6167	P > 0.05	ns
85	313.0	7.200	0.4827	P > 0.05	ns
86					
87	17-21 vs. 17-21p				
88	Temp	17-21	17-21p	Difference	95% CI of diff.
89	298.0	6.000	101.0	95.00	32.33 to 157.7
90	303.0	6.200	108.0	101.8	39.13 to 164.5
91	308.0	7.800	125.0	117.2	54.53 to 179.9
92	313.0	9.800	126.0	116.2	53.53 to 178.9
93					
94	Temp	Difference	t	P value	Summary
95	298.0	95.00	6.369	P<0.001	***
96	303.0	101.8	6.824	P<0.001	***
97	308.0	117.2	7.857	P<0.001	***
98	313.0	116.2	7.790	P<0.001	***
99					
100	17-21 vs. 29-33r				
101	Temp	17-21	29-33r	Difference	95% CI of diff.
102	298.0	6.000	52.00	46.00	-16.67 to 108.7
103	303.0	6.200	55.00	48.80	-13.87 to 111.5
104	308.0	7.800	56.00	48.20	-14.47 to 110.9
105	313.0	9.800	74.00	64.20	1.530 to 126.9
106					
107	Temp	Difference	t	P value	Summary
108	298.0	46.00	3.084	P < 0.05	*
109	303.0	48.80	3.271	P < 0.05	*
110	308.0	48.20	3.231	P < 0.05	*
111	313.0	64.20	4.304	P<0.001	***
112					
113	17-21 vs. 29-33p				
114	Temp	17-21	29-33p	Difference	95% CI of diff.
115	298.0	6.000	132.0	126.0	63.33 to 188.7
116	303.0	6.200	153.0	146.8	84.13 to 209.5
117	308.0	7.800	166.0	158.2	95.53 to 220.9
118	313.0	9.800	200.0	190.2	127.5 to 252.9
119					
120	Temp	Difference	t	P value	Summary
121	298.0	126.0	8.447	P<0.001	***
122	303.0	146.8	9.841	P<0.001	***
123	308.0	158.2	10.61	P<0.001	***

K_d statistical analysis.pzf:2way ANOVA of K_d: Tabular results

124	313.0	190.2	12.75	P<0.001	***
125					
126	17-21 vs. Au				
127	Temp	17-21	Au	Difference	95% CI of diff.
128	298.0	6.000	73.00	67.00	4.330 to 129.7
129	303.0	6.200	86.00	79.80	17.13 to 142.5
130	308.0	7.800	97.00	89.20	26.53 to 151.9
131	313.0	9.800	119.0	109.2	46.53 to 171.9
132					
133	Temp	Difference	t	P value	Summary
134	298.0	67.00	4.491	P<0.001	***
135	303.0	79.80	5.350	P<0.001	***
136	308.0	89.20	5.980	P<0.001	***
137	313.0	109.2	7.320	P<0.001	***
138					
139	17-21 vs. Ag				
140	Temp	17-21	Ag	Difference	95% CI of diff.
141	298.0	6.000	39.00	33.00	-29.67 to 95.67
142	303.0	6.200	40.00	33.80	-28.87 to 96.47
143	308.0	7.800	76.00	68.20	5.530 to 130.9
144	313.0	9.800	89.00	79.20	16.53 to 141.9
145					
146	Temp	Difference	t	P value	Summary
147	298.0	33.00	2.212	P > 0.05	ns
148	303.0	33.80	2.266	P > 0.05	ns
149	308.0	68.20	4.572	P<0.001	***
150	313.0	79.20	5.309	P<0.001	***
151					
152	17-21 vs. curcumin				
153	Temp	17-21	curcumin	Difference	95% CI of diff.
154	298.0	6.000	27.00	21.00	-41.67 to 83.67
155	303.0	6.200	38.00	31.80	-30.87 to 94.47
156	308.0	7.800	48.00	40.20	-22.47 to 102.9
157	313.0	9.800	54.00	44.20	-18.47 to 106.9
158					
159	Temp	Difference	t	P value	Summary
160	298.0	21.00	1.408	P > 0.05	ns
161	303.0	31.80	2.132	P > 0.05	ns
162	308.0	40.20	2.695	P < 0.05	*
163	313.0	44.20	2.963	P < 0.05	*
164					
165	25-29 vs. 29-33				

K_d statistical analysis.pzf:2way ANOVA of K_d: Tabular results

166	Temp	25-29	29-33	Difference	95% CI of diff.
167	298.0	6.900	2.700	-4.200	-66.87 to 58.47
168	303.0	7.800	2.800	-5.000	-67.67 to 57.67
169	308.0	8.300	3.000	-5.300	-67.97 to 57.37
170	313.0	9.400	3.300	-6.100	-68.77 to 56.57
171					
172	Temp	Difference	t	P value	Summary
173	298.0	-4.200	0.2816	P > 0.05	ns
174	303.0	-5.000	0.3352	P > 0.05	ns
175	308.0	-5.300	0.3553	P > 0.05	ns
176	313.0	-6.100	0.4089	P > 0.05	ns
177					
178	25-29 vs. 33-37				
179	Temp	25-29	33-37	Difference	95% CI of diff.
180	298.0	6.900	5.400	-1.500	-64.17 to 61.17
181	303.0	7.800	5.600	-2.200	-64.87 to 60.47
182	308.0	8.300	6.100	-2.200	-64.87 to 60.47
183	313.0	9.400	7.700	-1.700	-64.37 to 60.97
184					
185	Temp	Difference	t	P value	Summary
186	298.0	-1.500	0.1006	P > 0.05	ns
187	303.0	-2.200	0.1475	P > 0.05	ns
188	308.0	-2.200	0.1475	P > 0.05	ns
189	313.0	-1.700	0.1140	P > 0.05	ns
190					
191	25-29 vs. 25-37				
192	Temp	25-29	25-37	Difference	95% CI of diff.
193	298.0	6.900	5.500	-1.400	-64.07 to 61.27
194	303.0	7.800	6.200	-1.600	-64.27 to 61.07
195	308.0	8.300	7.400	-0.9000	-63.57 to 61.77
196	313.0	9.400	8.700	-0.7000	-63.37 to 61.97
197					
198	Temp	Difference	t	P value	Summary
199	298.0	-1.400	0.09385	P > 0.05	ns
200	303.0	-1.600	0.1073	P > 0.05	ns
201	308.0	-0.9000	0.06033	P > 0.05	ns
202	313.0	-0.7000	0.04693	P > 0.05	ns
203					
204	25-29 vs. 17-21r				
205	Temp	25-29	17-21r	Difference	95% CI of diff.
206	298.0	6.900	15.00	8.100	-54.57 to 70.77
207	303.0	7.800	16.00	8.200	-54.47 to 70.87

K_d statistical analysis.pzf:2way ANOVA of K_d: Tabular results

208	308.0	8.300	17.00	8.700	-53.97 to 71.37
209	313.0	9.400	17.00	7.600	-55.07 to 70.27
210					
211	Temp	Difference	t	P value	Summary
212	298.0	8.100	0.5430	P > 0.05	ns
213	303.0	8.200	0.5497	P > 0.05	ns
214	308.0	8.700	0.5832	P > 0.05	ns
215	313.0	7.600	0.5095	P > 0.05	ns
216					
217	25-29 vs. 17-21p				
218	Temp	25-29	17-21p	Difference	95% CI of diff.
219	298.0	6.900	101.0	94.10	31.43 to 156.8
220	303.0	7.800	108.0	100.2	37.53 to 162.9
221	308.0	8.300	125.0	116.7	54.03 to 179.4
222	313.0	9.400	126.0	116.6	53.93 to 179.3
223					
224	Temp	Difference	t	P value	Summary
225	298.0	94.10	6.308	P<0.001	***
226	303.0	100.2	6.717	P<0.001	***
227	308.0	116.7	7.823	P<0.001	***
228	313.0	116.6	7.817	P<0.001	***
229					
230	25-29 vs. 29-33r				
231	Temp	25-29	29-33r	Difference	95% CI of diff.
232	298.0	6.900	52.00	45.10	-17.57 to 107.8
233	303.0	7.800	55.00	47.20	-15.47 to 109.9
234	308.0	8.300	56.00	47.70	-14.97 to 110.4
235	313.0	9.400	74.00	64.60	1.930 to 127.3
236					
237	Temp	Difference	t	P value	Summary
238	298.0	45.10	3.023	P < 0.05	*
239	303.0	47.20	3.164	P < 0.05	*
240	308.0	47.70	3.198	P < 0.05	*
241	313.0	64.60	4.331	P<0.001	***
242					
243	25-29 vs. 29-33p				
244	Temp	25-29	29-33p	Difference	95% CI of diff.
245	298.0	6.900	132.0	125.1	62.43 to 187.8
246	303.0	7.800	153.0	145.2	82.53 to 207.9
247	308.0	8.300	166.0	157.7	95.03 to 220.4
248	313.0	9.400	200.0	190.6	127.9 to 253.3
249					

K_d statistical analysis.pzf:2way ANOVA of K_d: Tabular results

250	Temp	Difference	t	P value	Summary
251	298.0	125.1	8.386	P<0.001	***
252	303.0	145.2	9.734	P<0.001	***
253	308.0	157.7	10.57	P<0.001	***
254	313.0	190.6	12.78	P<0.001	***
255					
256	25-29 vs. Au				
257	Temp	25-29	Au	Difference	95% CI of diff.
258	298.0	6.900	73.00	66.10	3.430 to 128.8
259	303.0	7.800	86.00	78.20	15.53 to 140.9
260	308.0	8.300	97.00	88.70	26.03 to 151.4
261	313.0	9.400	119.0	109.6	46.93 to 172.3
262					
263	Temp	Difference	t	P value	Summary
264	298.0	66.10	4.431	P<0.001	***
265	303.0	78.20	5.242	P<0.001	***
266	308.0	88.70	5.946	P<0.001	***
267	313.0	109.6	7.347	P<0.001	***
268					
269	25-29 vs. Ag				
270	Temp	25-29	Ag	Difference	95% CI of diff.
271	298.0	6.900	39.00	32.10	-30.57 to 94.77
272	303.0	7.800	40.00	32.20	-30.47 to 94.87
273	308.0	8.300	76.00	67.70	5.030 to 130.4
274	313.0	9.400	89.00	79.60	16.93 to 142.3
275					
276	Temp	Difference	t	P value	Summary
277	298.0	32.10	2.152	P > 0.05	ns
278	303.0	32.20	2.159	P > 0.05	ns
279	308.0	67.70	4.538	P<0.001	***
280	313.0	79.60	5.336	P<0.001	***
281					
282	25-29 vs. curcumin				
283	Temp	25-29	curcumin	Difference	95% CI of diff.
284	298.0	6.900	27.00	20.10	-42.57 to 82.77
285	303.0	7.800	38.00	30.20	-32.47 to 92.87
286	308.0	8.300	48.00	39.70	-22.97 to 102.4
287	313.0	9.400	54.00	44.60	-18.07 to 107.3
288					
289	Temp	Difference	t	P value	Summary
290	298.0	20.10	1.347	P > 0.05	ns
291	303.0	30.20	2.025	P > 0.05	ns

K_d statistical analysis.pzf:2way ANOVA of K_d: Tabular results

292	308.0	39.70	2.661	P < 0.05	*
293	313.0	44.60	2.990	P < 0.05	*
294					
295	29-33 vs. 33-37				
296	Temp	29-33	33-37	Difference	95% CI of diff.
297	298.0	2.700	5.400	2.700	-59.97 to 65.37
298	303.0	2.800	5.600	2.800	-59.87 to 65.47
299	308.0	3.000	6.100	3.100	-59.57 to 65.77
300	313.0	3.300	7.700	4.400	-58.27 to 67.07
301					
302	Temp	Difference	t	P value	Summary
303	298.0	2.700	0.1810	P > 0.05	ns
304	303.0	2.800	0.1877	P > 0.05	ns
305	308.0	3.100	0.2078	P > 0.05	ns
306	313.0	4.400	0.2950	P > 0.05	ns
307					
308	29-33 vs. 25-37				
309	Temp	29-33	25-37	Difference	95% CI of diff.
310	298.0	2.700	5.500	2.800	-59.87 to 65.47
311	303.0	2.800	6.200	3.400	-59.27 to 66.07
312	308.0	3.000	7.400	4.400	-58.27 to 67.07
313	313.0	3.300	8.700	5.400	-57.27 to 68.07
314					
315	Temp	Difference	t	P value	Summary
316	298.0	2.800	0.1877	P > 0.05	ns
317	303.0	3.400	0.2279	P > 0.05	ns
318	308.0	4.400	0.2950	P > 0.05	ns
319	313.0	5.400	0.3620	P > 0.05	ns
320					
321	29-33 vs. 17-21r				
322	Temp	29-33	17-21r	Difference	95% CI of diff.
323	298.0	2.700	15.00	12.30	-50.37 to 74.97
324	303.0	2.800	16.00	13.20	-49.47 to 75.87
325	308.0	3.000	17.00	14.00	-48.67 to 76.67
326	313.0	3.300	17.00	13.70	-48.97 to 76.37
327					
328	Temp	Difference	t	P value	Summary
329	298.0	12.30	0.8246	P > 0.05	ns
330	303.0	13.20	0.8849	P > 0.05	ns
331	308.0	14.00	0.9385	P > 0.05	ns
332	313.0	13.70	0.9184	P > 0.05	ns
333					

K_d statistical analysis.pzf:2way ANOVA of K_d: Tabular results

334	29-33 vs. 17-21p				
335	Temp	29-33	17-21p	Difference	95% CI of diff.
336	298.0	2.700	101.0	98.30	35.63 to 161.0
337	303.0	2.800	108.0	105.2	42.53 to 167.9
338	308.0	3.000	125.0	122.0	59.33 to 184.7
339	313.0	3.300	126.0	122.7	60.03 to 185.4
340					
341	Temp	Difference	t	P value	Summary
342	298.0	98.30	6.590	P<0.001	***
343	303.0	105.2	7.052	P<0.001	***
344	308.0	122.0	8.179	P<0.001	***
345	313.0	122.7	8.225	P<0.001	***
346					
347	29-33 vs. 29-33r				
348	Temp	29-33	29-33r	Difference	95% CI of diff.
349	298.0	2.700	52.00	49.30	-13.37 to 112.0
350	303.0	2.800	55.00	52.20	-10.47 to 114.9
351	308.0	3.000	56.00	53.00	-9.670 to 115.7
352	313.0	3.300	74.00	70.70	8.030 to 133.4
353					
354	Temp	Difference	t	P value	Summary
355	298.0	49.30	3.305	P<0.01	**
356	303.0	52.20	3.499	P<0.01	**
357	308.0	53.00	3.553	P<0.01	**
358	313.0	70.70	4.740	P<0.001	***
359					
360	29-33 vs. 29-33p				
361	Temp	29-33	29-33p	Difference	95% CI of diff.
362	298.0	2.700	132.0	129.3	66.63 to 192.0
363	303.0	2.800	153.0	150.2	87.53 to 212.9
364	308.0	3.000	166.0	163.0	100.3 to 225.7
365	313.0	3.300	200.0	196.7	134.0 to 259.4
366					
367	Temp	Difference	t	P value	Summary
368	298.0	129.3	8.668	P<0.001	***
369	303.0	150.2	10.07	P<0.001	***
370	308.0	163.0	10.93	P<0.001	***
371	313.0	196.7	13.19	P<0.001	***
372					
373	29-33 vs. Au				
374	Temp	29-33	Au	Difference	95% CI of diff.
375	298.0	2.700	73.00	70.30	7.630 to 133.0

K_d statistical analysis.pzf:2way ANOVA of K_d: Tabular results

376	303.0	2.800	86.00	83.20	20.53 to 145.9
377	308.0	3.000	97.00	94.00	31.33 to 156.7
378	313.0	3.300	119.0	115.7	53.03 to 178.4
379					
380	Temp	Difference	t	P value	Summary
381	298.0	70.30	4.713	P<0.001	***
382	303.0	83.20	5.577	P<0.001	***
383	308.0	94.00	6.301	P<0.001	***
384	313.0	115.7	7.756	P<0.001	***
385					
386	29-33 vs. Ag				
387	Temp	29-33	Ag	Difference	95% CI of diff.
388	298.0	2.700	39.00	36.30	-26.37 to 98.97
389	303.0	2.800	40.00	37.20	-25.47 to 99.87
390	308.0	3.000	76.00	73.00	10.33 to 135.7
391	313.0	3.300	89.00	85.70	23.03 to 148.4
392					
393	Temp	Difference	t	P value	Summary
394	298.0	36.30	2.433	P > 0.05	ns
395	303.0	37.20	2.494	P > 0.05	ns
396	308.0	73.00	4.894	P<0.001	***
397	313.0	85.70	5.745	P<0.001	***
398					
399	29-33 vs. curcumin				
400	Temp	29-33	curcumin	Difference	95% CI of diff.
401	298.0	2.700	27.00	24.30	-38.37 to 86.97
402	303.0	2.800	38.00	35.20	-27.47 to 97.87
403	308.0	3.000	48.00	45.00	-17.67 to 107.7
404	313.0	3.300	54.00	50.70	-11.97 to 113.4
405					
406	Temp	Difference	t	P value	Summary
407	298.0	24.30	1.629	P > 0.05	ns
408	303.0	35.20	2.360	P > 0.05	ns
409	308.0	45.00	3.017	P < 0.05	*
410	313.0	50.70	3.399	P<0.01	**
411					
412	33-37 vs. 25-37				
413	Temp	33-37	25-37	Difference	95% CI of diff.
414	298.0	5.400	5.500	0.1000	-62.57 to 62.77
415	303.0	5.600	6.200	0.6000	-62.07 to 63.27
416	308.0	6.100	7.400	1.300	-61.37 to 63.97
417	313.0	7.700	8.700	1.000	-61.67 to 63.67

K_d statistical analysis.pzf:2way ANOVA of K_d: Tabular results

418					
419	Temp	Difference	t	P value	Summary
420	298.0	0.1000	0.006704	P > 0.05	ns
421	303.0	0.6000	0.04022	P > 0.05	ns
422	308.0	1.300	0.08715	P > 0.05	ns
423	313.0	1.000	0.06704	P > 0.05	ns
424					
425	33-37 vs. 17-21r				
426	Temp	33-37	17-21r	Difference	95% CI of diff.
427	298.0	5.400	15.00	9.600	-53.07 to 72.27
428	303.0	5.600	16.00	10.40	-52.27 to 73.07
429	308.0	6.100	17.00	10.90	-51.77 to 73.57
430	313.0	7.700	17.00	9.300	-53.37 to 71.97
431					
432	Temp	Difference	t	P value	Summary
433	298.0	9.600	0.6436	P > 0.05	ns
434	303.0	10.40	0.6972	P > 0.05	ns
435	308.0	10.90	0.7307	P > 0.05	ns
436	313.0	9.300	0.6234	P > 0.05	ns
437					
438	33-37 vs. 17-21p				
439	Temp	33-37	17-21p	Difference	95% CI of diff.
440	298.0	5.400	101.0	95.60	32.93 to 158.3
441	303.0	5.600	108.0	102.4	39.73 to 165.1
442	308.0	6.100	125.0	118.9	56.23 to 181.6
443	313.0	7.700	126.0	118.3	55.63 to 181.0
444					
445	Temp	Difference	t	P value	Summary
446	298.0	95.60	6.409	P<0.001	***
447	303.0	102.4	6.865	P<0.001	***
448	308.0	118.9	7.971	P<0.001	***
449	313.0	118.3	7.930	P<0.001	***
450					
451	33-37 vs. 29-33r				
452	Temp	33-37	29-33r	Difference	95% CI of diff.
453	298.0	5.400	52.00	46.60	-16.07 to 109.3
454	303.0	5.600	55.00	49.40	-13.27 to 112.1
455	308.0	6.100	56.00	49.90	-12.77 to 112.6
456	313.0	7.700	74.00	66.30	3.630 to 129.0
457					
458	Temp	Difference	t	P value	Summary
459	298.0	46.60	3.124	P < 0.05	*

K_d statistical analysis.pzf:2way ANOVA of K_d: Tabular results

460	303.0	49.40	3.312	P<0.01	**
461	308.0	49.90	3.345	P<0.01	**
462	313.0	66.30	4.445	P<0.001	***
463					
464	33-37 vs. 29-33p				
465	Temp	33-37	29-33p	Difference	95% CI of diff.
466	298.0	5.400	132.0	126.6	63.93 to 189.3
467	303.0	5.600	153.0	147.4	84.73 to 210.1
468	308.0	6.100	166.0	159.9	97.23 to 222.6
469	313.0	7.700	200.0	192.3	129.6 to 255.0
470					
471	Temp	Difference	t	P value	Summary
472	298.0	126.6	8.487	P<0.001	***
473	303.0	147.4	9.881	P<0.001	***
474	308.0	159.9	10.72	P<0.001	***
475	313.0	192.3	12.89	P<0.001	***
476					
477	33-37 vs. Au				
478	Temp	33-37	Au	Difference	95% CI of diff.
479	298.0	5.400	73.00	67.60	4.930 to 130.3
480	303.0	5.600	86.00	80.40	17.73 to 143.1
481	308.0	6.100	97.00	90.90	28.23 to 153.6
482	313.0	7.700	119.0	111.3	48.63 to 174.0
483					
484	Temp	Difference	t	P value	Summary
485	298.0	67.60	4.532	P<0.001	***
486	303.0	80.40	5.390	P<0.001	***
487	308.0	90.90	6.094	P<0.001	***
488	313.0	111.3	7.461	P<0.001	***
489					
490	33-37 vs. Ag				
491	Temp	33-37	Ag	Difference	95% CI of diff.
492	298.0	5.400	39.00	33.60	-29.07 to 96.27
493	303.0	5.600	40.00	34.40	-28.27 to 97.07
494	308.0	6.100	76.00	69.90	7.230 to 132.6
495	313.0	7.700	89.00	81.30	18.63 to 144.0
496					
497	Temp	Difference	t	P value	Summary
498	298.0	33.60	2.252	P > 0.05	ns
499	303.0	34.40	2.306	P > 0.05	ns
500	308.0	69.90	4.686	P<0.001	***
501	313.0	81.30	5.450	P<0.001	***

K_d statistical analysis.pzf:2way ANOVA of K_d: Tabular results

502					
503	33-37 vs. curcumin				
504	Temp	33-37	curcumin	Difference	95% CI of diff.
505	298.0	5.400	27.00	21.60	-41.07 to 84.27
506	303.0	5.600	38.00	32.40	-30.27 to 95.07
507	308.0	6.100	48.00	41.90	-20.77 to 104.6
508	313.0	7.700	54.00	46.30	-16.37 to 109.0
509					
510	Temp	Difference	t	P value	Summary
511	298.0	21.60	1.448	P > 0.05	ns
512	303.0	32.40	2.172	P > 0.05	ns
513	308.0	41.90	2.809	P < 0.05	*
514	313.0	46.30	3.104	P < 0.05	*
515					
516	25-37 vs. 17-21r				
517	Temp	25-37	17-21r	Difference	95% CI of diff.
518	298.0	5.500	15.00	9.500	-53.17 to 72.17
519	303.0	6.200	16.00	9.800	-52.87 to 72.47
520	308.0	7.400	17.00	9.600	-53.07 to 72.27
521	313.0	8.700	17.00	8.300	-54.37 to 70.97
522					
523	Temp	Difference	t	P value	Summary
524	298.0	9.500	0.6369	P > 0.05	ns
525	303.0	9.800	0.6570	P > 0.05	ns
526	308.0	9.600	0.6436	P > 0.05	ns
527	313.0	8.300	0.5564	P > 0.05	ns
528					
529	25-37 vs. 17-21p				
530	Temp	25-37	17-21p	Difference	95% CI of diff.
531	298.0	5.500	101.0	95.50	32.83 to 158.2
532	303.0	6.200	108.0	101.8	39.13 to 164.5
533	308.0	7.400	125.0	117.6	54.93 to 180.3
534	313.0	8.700	126.0	117.3	54.63 to 180.0
535					
536	Temp	Difference	t	P value	Summary
537	298.0	95.50	6.402	P<0.001	***
538	303.0	101.8	6.824	P<0.001	***
539	308.0	117.6	7.884	P<0.001	***
540	313.0	117.3	7.863	P<0.001	***
541					
542	25-37 vs. 29-33r				
543	Temp	25-37	29-33r	Difference	95% CI of diff.

544	298.0	5.500	52.00	46.50	-16.17 to 109.2
545	303.0	6.200	55.00	48.80	-13.87 to 111.5
546	308.0	7.400	56.00	48.60	-14.07 to 111.3
547	313.0	8.700	74.00	65.30	2.630 to 128.0
548					
549	Temp	Difference	t	P value	Summary
550	298.0	46.50	3.117	P < 0.05	*
551	303.0	48.80	3.271	P < 0.05	*
552	308.0	48.60	3.258	P < 0.05	*
553	313.0	65.30	4.378	P<0.001	***
554					
555	25-37 vs. 29-33p				
556	Temp	25-37	29-33p	Difference	95% CI of diff.
557	298.0	5.500	132.0	126.5	63.83 to 189.2
558	303.0	6.200	153.0	146.8	84.13 to 209.5
559	308.0	7.400	166.0	158.6	95.93 to 221.3
560	313.0	8.700	200.0	191.3	128.6 to 254.0
561					
562	Temp	Difference	t	P value	Summary
563	298.0	126.5	8.480	P<0.001	***
564	303.0	146.8	9.841	P<0.001	***
565	308.0	158.6	10.63	P<0.001	***
566	313.0	191.3	12.82	P<0.001	***
567					
568	25-37 vs. Au				
569	Temp	25-37	Au	Difference	95% CI of diff.
570	298.0	5.500	73.00	67.50	4.830 to 130.2
571	303.0	6.200	86.00	79.80	17.13 to 142.5
572	308.0	7.400	97.00	89.60	26.93 to 152.3
573	313.0	8.700	119.0	110.3	47.63 to 173.0
574					
575	Temp	Difference	t	P value	Summary
576	298.0	67.50	4.525	P<0.001	***
577	303.0	79.80	5.350	P<0.001	***
578	308.0	89.60	6.007	P<0.001	***
579	313.0	110.3	7.394	P<0.001	***
580					
581	25-37 vs. Ag				
582	Temp	25-37	Ag	Difference	95% CI of diff.
583	298.0	5.500	39.00	33.50	-29.17 to 96.17
584	303.0	6.200	40.00	33.80	-28.87 to 96.47
585	308.0	7.400	76.00	68.60	5.930 to 131.3

K_d statistical analysis.pzf:2way ANOVA of K_d: Tabular results

586	313.0	8.700	89.00	80.30	17.63 to 143.0
587					
588	Temp	Difference	t	P value	Summary
589	298.0	33.50	2.246	P > 0.05	ns
590	303.0	33.80	2.266	P > 0.05	ns
591	308.0	68.60	4.599	P<0.001	***
592	313.0	80.30	5.383	P<0.001	***
593					
594	25-37 vs. curcumin				
595	Temp	25-37	curcumin	Difference	95% CI of diff.
596	298.0	5.500	27.00	21.50	-41.17 to 84.17
597	303.0	6.200	38.00	31.80	-30.87 to 94.47
598	308.0	7.400	48.00	40.60	-22.07 to 103.3
599	313.0	8.700	54.00	45.30	-17.37 to 108.0
600					
601	Temp	Difference	t	P value	Summary
602	298.0	21.50	1.441	P > 0.05	ns
603	303.0	31.80	2.132	P > 0.05	ns
604	308.0	40.60	2.722	P < 0.05	*
605	313.0	45.30	3.037	P < 0.05	*
606					
607	17-21r vs. 17-21p				
608	Temp	17-21r	17-21p	Difference	95% CI of diff.
609	298.0	15.00	101.0	86.00	23.33 to 148.7
610	303.0	16.00	108.0	92.00	29.33 to 154.7
611	308.0	17.00	125.0	108.0	45.33 to 170.7
612	313.0	17.00	126.0	109.0	46.33 to 171.7
613					
614	Temp	Difference	t	P value	Summary
615	298.0	86.00	5.765	P<0.001	***
616	303.0	92.00	6.167	P<0.001	***
617	308.0	108.0	7.240	P<0.001	***
618	313.0	109.0	7.307	P<0.001	***
619					
620	17-21r vs. 29-33r				
621	Temp	17-21r	29-33r	Difference	95% CI of diff.
622	298.0	15.00	52.00	37.00	-25.67 to 99.67
623	303.0	16.00	55.00	39.00	-23.67 to 101.7
624	308.0	17.00	56.00	39.00	-23.67 to 101.7
625	313.0	17.00	74.00	57.00	-5.670 to 119.7
626					
627	Temp	Difference	t	P value	Summary

628	298.0	37.00	2.480	P > 0.05	ns
629	303.0	39.00	2.614	P > 0.05	ns
630	308.0	39.00	2.614	P > 0.05	ns
631	313.0	57.00	3.821	P<0.01	**
632					
633	17-21r vs. 29-33p				
634	Temp	17-21r	29-33p	Difference	95% CI of diff.
635	298.0	15.00	132.0	117.0	54.33 to 179.7
636	303.0	16.00	153.0	137.0	74.33 to 199.7
637	308.0	17.00	166.0	149.0	86.33 to 211.7
638	313.0	17.00	200.0	183.0	120.3 to 245.7
639					
640	Temp	Difference	t	P value	Summary
641	298.0	117.0	7.843	P<0.001	***
642	303.0	137.0	9.184	P<0.001	***
643	308.0	149.0	9.989	P<0.001	***
644	313.0	183.0	12.27	P<0.001	***
645					
646	17-21r vs. Au				
647	Temp	17-21r	Au	Difference	95% CI of diff.
648	298.0	15.00	73.00	58.00	-4.670 to 120.7
649	303.0	16.00	86.00	70.00	7.330 to 132.7
650	308.0	17.00	97.00	80.00	17.33 to 142.7
651	313.0	17.00	119.0	102.0	39.33 to 164.7
652					
653	Temp	Difference	t	P value	Summary
654	298.0	58.00	3.888	P<0.01	**
655	303.0	70.00	4.693	P<0.001	***
656	308.0	80.00	5.363	P<0.001	***
657	313.0	102.0	6.838	P<0.001	***
658					
659	17-21r vs. Ag				
660	Temp	17-21r	Ag	Difference	95% CI of diff.
661	298.0	15.00	39.00	24.00	-38.67 to 86.67
662	303.0	16.00	40.00	24.00	-38.67 to 86.67
663	308.0	17.00	76.00	59.00	-3.670 to 121.7
664	313.0	17.00	89.00	72.00	9.330 to 134.7
665					
666	Temp	Difference	t	P value	Summary
667	298.0	24.00	1.609	P > 0.05	ns
668	303.0	24.00	1.609	P > 0.05	ns
669	308.0	59.00	3.955	P<0.01	**

K_d statistical analysis.pzf:2way ANOVA of K_d: Tabular results

670	313.0	72.00	4.827	P<0.001	***
671					
672	17-21r vs. curcumin				
673	Temp	17-21r	curcumin	Difference	95% CI of diff.
674	298.0	15.00	27.00	12.00	-50.67 to 74.67
675	303.0	16.00	38.00	22.00	-40.67 to 84.67
676	308.0	17.00	48.00	31.00	-31.67 to 93.67
677	313.0	17.00	54.00	37.00	-25.67 to 99.67
678					
679	Temp	Difference	t	P value	Summary
680	298.0	12.00	0.8044	P > 0.05	ns
681	303.0	22.00	1.475	P > 0.05	ns
682	308.0	31.00	2.078	P > 0.05	ns
683	313.0	37.00	2.480	P > 0.05	ns
684					
685	17-21p vs. 29-33r				
686	Temp	17-21p	29-33r	Difference	95% CI of diff.
687	298.0	101.0	52.00	-49.00	-111.7 to 13.67
688	303.0	108.0	55.00	-53.00	-115.7 to 9.670
689	308.0	125.0	56.00	-69.00	-131.7 to -6.330
690	313.0	126.0	74.00	-52.00	-114.7 to 10.67
691					
692	Temp	Difference	t	P value	Summary
693	298.0	-49.00	3.285	P<0.01	**
694	303.0	-53.00	3.553	P<0.01	**
695	308.0	-69.00	4.626	P<0.001	***
696	313.0	-52.00	3.486	P<0.01	**
697					
698	17-21p vs. 29-33p				
699	Temp	17-21p	29-33p	Difference	95% CI of diff.
700	298.0	101.0	132.0	31.00	-31.67 to 93.67
701	303.0	108.0	153.0	45.00	-17.67 to 107.7
702	308.0	125.0	166.0	41.00	-21.67 to 103.7
703	313.0	126.0	200.0	74.00	11.33 to 136.7
704					
705	Temp	Difference	t	P value	Summary
706	298.0	31.00	2.078	P > 0.05	ns
707	303.0	45.00	3.017	P < 0.05	*
708	308.0	41.00	2.749	P < 0.05	*
709	313.0	74.00	4.961	P<0.001	***
710					
711	17-21p vs. Au				

K_d statistical analysis.pzf:2way ANOVA of K_d: Tabular results

712	Temp	17-21p	Au	Difference	95% CI of diff.
713	298.0	101.0	73.00	-28.00	-90.67 to 34.67
714	303.0	108.0	86.00	-22.00	-84.67 to 40.67
715	308.0	125.0	97.00	-28.00	-90.67 to 34.67
716	313.0	126.0	119.0	-7.000	-69.67 to 55.67
717					
718	Temp	Difference	t	P value	Summary
719	298.0	-28.00	1.877	P > 0.05	ns
720	303.0	-22.00	1.475	P > 0.05	ns
721	308.0	-28.00	1.877	P > 0.05	ns
722	313.0	-7.000	0.4693	P > 0.05	ns
723					
724	17-21p vs. Ag				
725	Temp	17-21p	Ag	Difference	95% CI of diff.
726	298.0	101.0	39.00	-62.00	-124.7 to 0.6703
727	303.0	108.0	40.00	-68.00	-130.7 to -5.330
728	308.0	125.0	76.00	-49.00	-111.7 to 13.67
729	313.0	126.0	89.00	-37.00	-99.67 to 25.67
730					
731	Temp	Difference	t	P value	Summary
732	298.0	-62.00	4.156	P<0.001	***
733	303.0	-68.00	4.559	P<0.001	***
734	308.0	-49.00	3.285	P<0.01	**
735	313.0	-37.00	2.480	P > 0.05	ns
736					
737	17-21p vs. curcumin				
738	Temp	17-21p	curcumin	Difference	95% CI of diff.
739	298.0	101.0	27.00	-74.00	-136.7 to -11.33
740	303.0	108.0	38.00	-70.00	-132.7 to -7.330
741	308.0	125.0	48.00	-77.00	-139.7 to -14.33
742	313.0	126.0	54.00	-72.00	-134.7 to -9.330
743					
744	Temp	Difference	t	P value	Summary
745	298.0	-74.00	4.961	P<0.001	***
746	303.0	-70.00	4.693	P<0.001	***
747	308.0	-77.00	5.162	P<0.001	***
748	313.0	-72.00	4.827	P<0.001	***
749					
750	29-33r vs. 29-33p				
751	Temp	29-33r	29-33p	Difference	95% CI of diff.
752	298.0	52.00	132.0	80.00	17.33 to 142.7
753	303.0	55.00	153.0	98.00	35.33 to 160.7

K_d statistical analysis.pzf:2way ANOVA of K_d: Tabular results

754	308.0	56.00	166.0	110.0	47.33 to 172.7
755	313.0	74.00	200.0	126.0	63.33 to 188.7
756					
757	Temp	Difference	t	P value	Summary
758	298.0	80.00	5.363	P<0.001	***
759	303.0	98.00	6.570	P<0.001	***
760	308.0	110.0	7.374	P<0.001	***
761	313.0	126.0	8.447	P<0.001	***
762					
763	29-33r vs. Au				
764	Temp	29-33r	Au	Difference	95% CI of diff.
765	298.0	52.00	73.00	21.00	-41.67 to 83.67
766	303.0	55.00	86.00	31.00	-31.67 to 93.67
767	308.0	56.00	97.00	41.00	-21.67 to 103.7
768	313.0	74.00	119.0	45.00	-17.67 to 107.7
769					
770	Temp	Difference	t	P value	Summary
771	298.0	21.00	1.408	P > 0.05	ns
772	303.0	31.00	2.078	P > 0.05	ns
773	308.0	41.00	2.749	P < 0.05	*
774	313.0	45.00	3.017	P < 0.05	*
775					
776	29-33r vs. Ag				
777	Temp	29-33r	Ag	Difference	95% CI of diff.
778	298.0	52.00	39.00	-13.00	-75.67 to 49.67
779	303.0	55.00	40.00	-15.00	-77.67 to 47.67
780	308.0	56.00	76.00	20.00	-42.67 to 82.67
781	313.0	74.00	89.00	15.00	-47.67 to 77.67
782					
783	Temp	Difference	t	P value	Summary
784	298.0	-13.00	0.8715	P > 0.05	ns
785	303.0	-15.00	1.006	P > 0.05	ns
786	308.0	20.00	1.341	P > 0.05	ns
787	313.0	15.00	1.006	P > 0.05	ns
788					
789	29-33r vs. curcumin				
790	Temp	29-33r	curcumin	Difference	95% CI of diff.
791	298.0	52.00	27.00	-25.00	-87.67 to 37.67
792	303.0	55.00	38.00	-17.00	-79.67 to 45.67
793	308.0	56.00	48.00	-8.000	-70.67 to 54.67
794	313.0	74.00	54.00	-20.00	-82.67 to 42.67
795					

K_d statistical analysis.pzf:2way ANOVA of K_d: Tabular results

796	Temp	Difference	t	P value	Summary
797	298.0	-25.00	1.676	P > 0.05	ns
798	303.0	-17.00	1.140	P > 0.05	ns
799	308.0	-8.000	0.5363	P > 0.05	ns
800	313.0	-20.00	1.341	P > 0.05	ns
801					
802	29-33p vs. Au				
803	Temp	29-33p	Au	Difference	95% CI of diff.
804	298.0	132.0	73.00	-59.00	-121.7 to 3.670
805	303.0	153.0	86.00	-67.00	-129.7 to -4.330
806	308.0	166.0	97.00	-69.00	-131.7 to -6.330
807	313.0	200.0	119.0	-81.00	-143.7 to -18.33
808					
809	Temp	Difference	t	P value	Summary
810	298.0	-59.00	3.955	P<0.01	**
811	303.0	-67.00	4.491	P<0.001	***
812	308.0	-69.00	4.626	P<0.001	***
813	313.0	-81.00	5.430	P<0.001	***
814					
815	29-33p vs. Ag				
816	Temp	29-33p	Ag	Difference	95% CI of diff.
817	298.0	132.0	39.00	-93.00	-155.7 to -30.33
818	303.0	153.0	40.00	-113.0	-175.7 to -50.33
819	308.0	166.0	76.00	-90.00	-152.7 to -27.33
820	313.0	200.0	89.00	-111.0	-173.7 to -48.33
821					
822	Temp	Difference	t	P value	Summary
823	298.0	-93.00	6.234	P<0.001	***
824	303.0	-113.0	7.575	P<0.001	***
825	308.0	-90.00	6.033	P<0.001	***
826	313.0	-111.0	7.441	P<0.001	***
827					
828	29-33p vs. curcumin				
829	Temp	29-33p	curcumin	Difference	95% CI of diff.
830	298.0	132.0	27.00	-105.0	-167.7 to -42.33
831	303.0	153.0	38.00	-115.0	-177.7 to -52.33
832	308.0	166.0	48.00	-118.0	-180.7 to -55.33
833	313.0	200.0	54.00	-146.0	-208.7 to -83.33
834					
835	Temp	Difference	t	P value	Summary
836	298.0	-105.0	7.039	P<0.001	***
837	303.0	-115.0	7.709	P<0.001	***

K_d statistical analysis.pzf:2way ANOVA of K_d: Tabular results

838	308.0	-118.0	7.910	P<0.001	***
839	313.0	-146.0	9.787	P<0.001	***
840					
841	Au vs. Ag				
842	Temp	Au	Ag	Difference	95% CI of diff.
843	298.0	73.00	39.00	-34.00	-96.67 to 28.67
844	303.0	86.00	40.00	-46.00	-108.7 to 16.67
845	308.0	97.00	76.00	-21.00	-83.67 to 41.67
846	313.0	119.0	89.00	-30.00	-92.67 to 32.67
847					
848	Temp	Difference	t	P value	Summary
849	298.0	-34.00	2.279	P > 0.05	ns
850	303.0	-46.00	3.084	P < 0.05	*
851	308.0	-21.00	1.408	P > 0.05	ns
852	313.0	-30.00	2.011	P > 0.05	ns
853					
854	Au vs. curcumin				
855	Temp	Au	curcumin	Difference	95% CI of diff.
856	298.0	73.00	27.00	-46.00	-108.7 to 16.67
857	303.0	86.00	38.00	-48.00	-110.7 to 14.67
858	308.0	97.00	48.00	-49.00	-111.7 to 13.67
859	313.0	119.0	54.00	-65.00	-127.7 to -2.330
860					
861	Temp	Difference	t	P value	Summary
862	298.0	-46.00	3.084	P < 0.05	*
863	303.0	-48.00	3.218	P < 0.05	*
864	308.0	-49.00	3.285	P<0.01	**
865	313.0	-65.00	4.357	P<0.001	***
866					
867	Ag vs. curcumin				
868	Temp	Ag	curcumin	Difference	95% CI of diff.
869	298.0	39.00	27.00	-12.00	-74.67 to 50.67
870	303.0	40.00	38.00	-2.000	-64.67 to 60.67
871	308.0	76.00	48.00	-28.00	-90.67 to 34.67
872	313.0	89.00	54.00	-35.00	-97.67 to 27.67
873					
874	Temp	Difference	t	P value	Summary
875	298.0	-12.00	0.8044	P > 0.05	ns
876	303.0	-2.000	0.1341	P > 0.05	ns
877	308.0	-28.00	1.877	P > 0.05	ns
878	313.0	-35.00	2.346	P > 0.05	ns

ΔG statistical analysis.pzf:2way ANOVA of Delta G: Tabular results

		A	B	C	D
	Parameter	Data Set-A	Data Set-B	Data Set-C	Data Set-D
		Y	Y	Y	Y
1	Table Analyzed	Delta G			
2					
3	Two-way ANOVA				
4					
5	Source of Variation	% of total variation	P value		
6	Column Factor	39.46	P<0.0001		
7	Temp	53.47	P<0.0001		
8					
9	Source of Variation	P value summary	Significant?		
10	Column Factor	***	Yes		
11	Temp	***	Yes		
12					
13	Source of Variation	Df	Sum-of-squares	Mean square	F
14	Column Factor	11	39.42	3.583	16.77
15	Temp	3	53.41	17.80	83.31
16	Residual	33	7.052	0.2137	
17					
18	Number of missing values	0			
19					
20	Bonferroni posttests				
21					
22	17-21 vs. 25-29				
23	Temp	17-21	25-29	Difference	95% CI of diff.
24	298.0	9.900	13.00	3.100	0.3534 to 5.847
25	303.0	9.500	12.00	2.500	-0.2466 to 5.247
26	308.0	9.100	11.00	1.900	-0.8466 to 4.647
27	313.0	8.700	9.500	0.8000	-1.947 to 3.547
28					
29	Temp	Difference	t	P value	Summary
30	298.0	3.100	4.742	P<0.001	***
31	303.0	2.500	3.824	P<0.01	**
32	308.0	1.900	2.906	P < 0.05	*
33	313.0	0.8000	1.224	P > 0.05	ns
34					
35	17-21 vs. 29-33				
36	Temp	17-21	29-33	Difference	95% CI of diff.
37	298.0	9.900	12.00	2.100	-0.6466 to 4.847
38	303.0	9.500	11.00	1.500	-1.247 to 4.247
39	308.0	9.100	10.00	0.9000	-1.847 to 3.647
40	313.0	8.700	9.500	0.8000	-1.947 to 3.547
41					

ΔG statistical analysis.pzf:2way ANOVA of Delta G: Tabular results

42	Temp	Difference	t	P value	Summary
43	298.0	2.100	3.212	P < 0.05	*
44	303.0	1.500	2.294	P > 0.05	ns
45	308.0	0.9000	1.377	P > 0.05	ns
46	313.0	0.8000	1.224	P > 0.05	ns
47					
48	17-21 vs. 33-37				
49	Temp	17-21	33-37	Difference	95% CI of diff.
50	298.0	9.900	11.00	1.100	-1.647 to 3.847
51	303.0	9.500	11.00	1.500	-1.247 to 4.247
52	308.0	9.100	10.00	0.9000	-1.847 to 3.647
53	313.0	8.700	9.900	1.200	-1.547 to 3.947
54					
55	Temp	Difference	t	P value	Summary
56	298.0	1.100	1.683	P > 0.05	ns
57	303.0	1.500	2.294	P > 0.05	ns
58	308.0	0.9000	1.377	P > 0.05	ns
59	313.0	1.200	1.836	P > 0.05	ns
60					
61	17-21 vs. 25-37				
62	Temp	17-21	25-37	Difference	95% CI of diff.
63	298.0	9.900	11.00	1.100	-1.647 to 3.847
64	303.0	9.500	9.900	0.4000	-2.347 to 3.147
65	308.0	9.100	9.100	0.0000	-2.747 to 2.747
66	313.0	8.700	8.400	-0.3000	-3.047 to 2.447
67					
68	Temp	Difference	t	P value	Summary
69	298.0	1.100	1.683	P > 0.05	ns
70	303.0	0.4000	0.6119	P > 0.05	ns
71	308.0	0.0000	0.0000	P > 0.05	ns
72	313.0	-0.3000	0.4589	P > 0.05	ns
73					
74	17-21 vs. 17-21r				
75	Temp	17-21	17-21r	Difference	95% CI of diff.
76	298.0	9.900	10.00	0.1000	-2.647 to 2.847
77	303.0	9.500	9.300	-0.2000	-2.947 to 2.547
78	308.0	9.100	8.400	-0.7000	-3.447 to 2.047
79	313.0	8.700	7.500	-1.200	-3.947 to 1.547
80					
81	Temp	Difference	t	P value	Summary
82	298.0	0.1000	0.1530	P > 0.05	ns
83	303.0	-0.2000	0.3059	P > 0.05	ns
84	308.0	-0.7000	1.071	P > 0.05	ns
85	313.0	-1.200	1.836	P > 0.05	ns

ΔG statistical analysis.pzf:2way ANOVA of Delta G: Tabular results

86					
87	17-21 vs. 17-21p				
88	Temp	17-21	17-21p	Difference	95% CI of diff.
89	298.0	9.900	12.00	2.100	-0.6466 to 4.847
90	303.0	9.500	11.00	1.500	-1.247 to 4.247
91	308.0	9.100	9.800	0.7000	-2.047 to 3.447
92	313.0	8.700	8.700	0.0000	-2.747 to 2.747
93					
94	Temp	Difference	t	P value	Summary
95	298.0	2.100	3.212	P < 0.05	*
96	303.0	1.500	2.294	P > 0.05	ns
97	308.0	0.7000	1.071	P > 0.05	ns
98	313.0	0.0000	0.0000	P > 0.05	ns
99					
100	17-21 vs. 29-33r				
101	Temp	17-21	29-33r	Difference	95% CI of diff.
102	298.0	9.900	10.00	0.1000	-2.647 to 2.847
103	303.0	9.500	9.100	-0.4000	-3.147 to 2.347
104	308.0	9.100	8.300	-0.8000	-3.547 to 1.947
105	313.0	8.700	7.500	-1.200	-3.947 to 1.547
106					
107	Temp	Difference	t	P value	Summary
108	298.0	0.1000	0.1530	P > 0.05	ns
109	303.0	-0.4000	0.6119	P > 0.05	ns
110	308.0	-0.8000	1.224	P > 0.05	ns
111	313.0	-1.200	1.836	P > 0.05	ns
112					
113	17-21 vs. 29-33p				
114	Temp	17-21	29-33p	Difference	95% CI of diff.
115	298.0	9.900	13.00	3.100	0.3534 to 5.847
116	303.0	9.500	12.00	2.500	-0.2466 to 5.247
117	308.0	9.100	11.00	1.900	-0.8466 to 4.647
118	313.0	8.700	10.00	1.300	-1.447 to 4.047
119					
120	Temp	Difference	t	P value	Summary
121	298.0	3.100	4.742	P<0.001	***
122	303.0	2.500	3.824	P<0.01	**
123	308.0	1.900	2.906	P < 0.05	*
124	313.0	1.300	1.989	P > 0.05	ns
125					
126	17-21 vs. Au				
127	Temp	17-21	Au	Difference	95% CI of diff.
128	298.0	9.900	12.00	2.100	-0.6466 to 4.847
129	303.0	9.500	11.00	1.500	-1.247 to 4.247

ΔG statistical analysis.pzf:2way ANOVA of Delta G: Tabular results

130	308.0	9.100	9.900	0.8000	-1.947 to 3.547
131	313.0	8.700	9.000	0.3000	-2.447 to 3.047
132					
133	Temp	Difference	t	P value	Summary
134	298.0	2.100	3.212	P < 0.05	*
135	303.0	1.500	2.294	P > 0.05	ns
136	308.0	0.8000	1.224	P > 0.05	ns
137	313.0	0.3000	0.4589	P > 0.05	ns
138					
139	17-21 vs. Ag				
140	Temp	17-21	Ag	Difference	95% CI of diff.
141	298.0	9.900	12.00	2.100	-0.6466 to 4.847
142	303.0	9.500	10.00	0.5000	-2.247 to 3.247
143	308.0	9.100	8.000	-1.100	-3.847 to 1.647
144	313.0	8.700	7.000	-1.700	-4.447 to 1.047
145					
146	Temp	Difference	t	P value	Summary
147	298.0	2.100	3.212	P < 0.05	*
148	303.0	0.5000	0.7648	P > 0.05	ns
149	308.0	-1.100	1.683	P > 0.05	ns
150	313.0	-1.700	2.600	P > 0.05	ns
151					
152	17-21 vs. curcumin				
153	Temp	17-21	curcumin	Difference	95% CI of diff.
154	298.0	9.900	11.00	1.100	-1.647 to 3.847
155	303.0	9.500	10.00	0.5000	-2.247 to 3.247
156	308.0	9.100	8.600	-0.5000	-3.247 to 2.247
157	313.0	8.700	7.700	-1.000	-3.747 to 1.747
158					
159	Temp	Difference	t	P value	Summary
160	298.0	1.100	1.683	P > 0.05	ns
161	303.0	0.5000	0.7648	P > 0.05	ns
162	308.0	-0.5000	0.7648	P > 0.05	ns
163	313.0	-1.000	1.530	P > 0.05	ns
164					
165	25-29 vs. 29-33				
166	Temp	25-29	29-33	Difference	95% CI of diff.
167	298.0	13.00	12.00	-1.000	-3.747 to 1.747
168	303.0	12.00	11.00	-1.000	-3.747 to 1.747
169	308.0	11.00	10.00	-1.000	-3.747 to 1.747
170	313.0	9.500	9.500	0.0000	-2.747 to 2.747
171					
172	Temp	Difference	t	P value	Summary
173	298.0	-1.000	1.530	P > 0.05	ns

ΔG statistical analysis.pzf:2way ANOVA of Delta G: Tabular results

174	303.0	-1.000	1.530	P > 0.05	ns
175	308.0	-1.000	1.530	P > 0.05	ns
176	313.0	0.0000	0.0000	P > 0.05	ns
177					
178	25-29 vs. 33-37				
179	Temp	25-29	33-37	Difference	95% CI of diff.
180	298.0	13.00	11.00	-2.000	-4.747 to 0.7466
181	303.0	12.00	11.00	-1.000	-3.747 to 1.747
182	308.0	11.00	10.00	-1.000	-3.747 to 1.747
183	313.0	9.500	9.900	0.4000	-2.347 to 3.147
184					
185	Temp	Difference	t	P value	Summary
186	298.0	-2.000	3.059	P < 0.05	*
187	303.0	-1.000	1.530	P > 0.05	ns
188	308.0	-1.000	1.530	P > 0.05	ns
189	313.0	0.4000	0.6119	P > 0.05	ns
190					
191	25-29 vs. 25-37				
192	Temp	25-29	25-37	Difference	95% CI of diff.
193	298.0	13.00	11.00	-2.000	-4.747 to 0.7466
194	303.0	12.00	9.900	-2.100	-4.847 to 0.6466
195	308.0	11.00	9.100	-1.900	-4.647 to 0.8466
196	313.0	9.500	8.400	-1.100	-3.847 to 1.647
197					
198	Temp	Difference	t	P value	Summary
199	298.0	-2.000	3.059	P < 0.05	*
200	303.0	-2.100	3.212	P < 0.05	*
201	308.0	-1.900	2.906	P < 0.05	*
202	313.0	-1.100	1.683	P > 0.05	ns
203					
204	25-29 vs. 17-21r				
205	Temp	25-29	17-21r	Difference	95% CI of diff.
206	298.0	13.00	10.00	-3.000	-5.747 to -0.2534
207	303.0	12.00	9.300	-2.700	-5.447 to 0.04655
208	308.0	11.00	8.400	-2.600	-5.347 to 0.1466
209	313.0	9.500	7.500	-2.000	-4.747 to 0.7466
210					
211	Temp	Difference	t	P value	Summary
212	298.0	-3.000	4.589	P<0.001	***
213	303.0	-2.700	4.130	P<0.001	***
214	308.0	-2.600	3.977	P<0.01	**
215	313.0	-2.000	3.059	P < 0.05	*
216					
217	25-29 vs. 17-21p				

ΔG statistical analysis.pzf:2way ANOVA of Delta G: Tabular results

218	Temp	25-29	17-21p	Difference	95% CI of diff.
219	298.0	13.00	12.00	-1.000	-3.747 to 1.747
220	303.0	12.00	11.00	-1.000	-3.747 to 1.747
221	308.0	11.00	9.800	-1.200	-3.947 to 1.547
222	313.0	9.500	8.700	-0.8000	-3.547 to 1.947
223					
224	Temp	Difference	t	P value	Summary
225	298.0	-1.000	1.530	P > 0.05	ns
226	303.0	-1.000	1.530	P > 0.05	ns
227	308.0	-1.200	1.836	P > 0.05	ns
228	313.0	-0.8000	1.224	P > 0.05	ns
229					
230	25-29 vs. 29-33r				
231	Temp	25-29	29-33r	Difference	95% CI of diff.
232	298.0	13.00	10.00	-3.000	-5.747 to -0.2534
233	303.0	12.00	9.100	-2.900	-5.647 to -0.1534
234	308.0	11.00	8.300	-2.700	-5.447 to 0.04655
235	313.0	9.500	7.500	-2.000	-4.747 to 0.7466
236					
237	Temp	Difference	t	P value	Summary
238	298.0	-3.000	4.589	P<0.001	***
239	303.0	-2.900	4.436	P<0.001	***
240	308.0	-2.700	4.130	P<0.001	***
241	313.0	-2.000	3.059	P < 0.05	*
242					
243	25-29 vs. 29-33p				
244	Temp	25-29	29-33p	Difference	95% CI of diff.
245	298.0	13.00	13.00	0.0000	-2.747 to 2.747
246	303.0	12.00	12.00	0.0000	-2.747 to 2.747
247	308.0	11.00	11.00	0.0000	-2.747 to 2.747
248	313.0	9.500	10.00	0.5000	-2.247 to 3.247
249					
250	Temp	Difference	t	P value	Summary
251	298.0	0.0000	0.0000	P > 0.05	ns
252	303.0	0.0000	0.0000	P > 0.05	ns
253	308.0	0.0000	0.0000	P > 0.05	ns
254	313.0	0.5000	0.7648	P > 0.05	ns
255					
256	25-29 vs. Au				
257	Temp	25-29	Au	Difference	95% CI of diff.
258	298.0	13.00	12.00	-1.000	-3.747 to 1.747
259	303.0	12.00	11.00	-1.000	-3.747 to 1.747
260	308.0	11.00	9.900	-1.100	-3.847 to 1.647
261	313.0	9.500	9.000	-0.5000	-3.247 to 2.247

ΔG statistical analysis.pzf:2way ANOVA of Delta G: Tabular results

262					
263	Temp	Difference	t	P value	Summary
264	298.0	-1.000	1.530	P > 0.05	ns
265	303.0	-1.000	1.530	P > 0.05	ns
266	308.0	-1.100	1.683	P > 0.05	ns
267	313.0	-0.5000	0.7648	P > 0.05	ns
268					
269	25-29 vs. Ag				
270	Temp	25-29	Ag	Difference	95% CI of diff.
271	298.0	13.00	12.00	-1.000	-3.747 to 1.747
272	303.0	12.00	10.00	-2.000	-4.747 to 0.7466
273	308.0	11.00	8.000	-3.000	-5.747 to -0.2534
274	313.0	9.500	7.000	-2.500	-5.247 to 0.2466
275					
276	Temp	Difference	t	P value	Summary
277	298.0	-1.000	1.530	P > 0.05	ns
278	303.0	-2.000	3.059	P < 0.05	*
279	308.0	-3.000	4.589	P<0.001	***
280	313.0	-2.500	3.824	P<0.01	**
281					
282	25-29 vs. curcumin				
283	Temp	25-29	curcumin	Difference	95% CI of diff.
284	298.0	13.00	11.00	-2.000	-4.747 to 0.7466
285	303.0	12.00	10.00	-2.000	-4.747 to 0.7466
286	308.0	11.00	8.600	-2.400	-5.147 to 0.3466
287	313.0	9.500	7.700	-1.800	-4.547 to 0.9466
288					
289	Temp	Difference	t	P value	Summary
290	298.0	-2.000	3.059	P < 0.05	*
291	303.0	-2.000	3.059	P < 0.05	*
292	308.0	-2.400	3.671	P<0.01	**
293	313.0	-1.800	2.753	P < 0.05	*
294					
295	29-33 vs. 33-37				
296	Temp	29-33	33-37	Difference	95% CI of diff.
297	298.0	12.00	11.00	-1.000	-3.747 to 1.747
298	303.0	11.00	11.00	0.0000	-2.747 to 2.747
299	308.0	10.00	10.00	0.0000	-2.747 to 2.747
300	313.0	9.500	9.900	0.4000	-2.347 to 3.147
301					
302	Temp	Difference	t	P value	Summary
303	298.0	-1.000	1.530	P > 0.05	ns
304	303.0	0.0000	0.0000	P > 0.05	ns
305	308.0	0.0000	0.0000	P > 0.05	ns

ΔG statistical analysis.pzf:2way ANOVA of Delta G: Tabular results

306	313.0	0.4000	0.6119	P > 0.05	ns
307					
308	29-33 vs. 25-37				
309	Temp	29-33	25-37	Difference	95% CI of diff.
310	298.0	12.00	11.00	-1.000	-3.747 to 1.747
311	303.0	11.00	9.900	-1.100	-3.847 to 1.647
312	308.0	10.00	9.100	-0.9000	-3.647 to 1.847
313	313.0	9.500	8.400	-1.100	-3.847 to 1.647
314					
315	Temp	Difference	t	P value	Summary
316	298.0	-1.000	1.530	P > 0.05	ns
317	303.0	-1.100	1.683	P > 0.05	ns
318	308.0	-0.9000	1.377	P > 0.05	ns
319	313.0	-1.100	1.683	P > 0.05	ns
320					
321	29-33 vs. 17-21r				
322	Temp	29-33	17-21r	Difference	95% CI of diff.
323	298.0	12.00	10.00	-2.000	-4.747 to 0.7466
324	303.0	11.00	9.300	-1.700	-4.447 to 1.047
325	308.0	10.00	8.400	-1.600	-4.347 to 1.147
326	313.0	9.500	7.500	-2.000	-4.747 to 0.7466
327					
328	Temp	Difference	t	P value	Summary
329	298.0	-2.000	3.059	P < 0.05	*
330	303.0	-1.700	2.600	P > 0.05	ns
331	308.0	-1.600	2.447	P > 0.05	ns
332	313.0	-2.000	3.059	P < 0.05	*
333					
334	29-33 vs. 17-21p				
335	Temp	29-33	17-21p	Difference	95% CI of diff.
336	298.0	12.00	12.00	0.0000	-2.747 to 2.747
337	303.0	11.00	11.00	0.0000	-2.747 to 2.747
338	308.0	10.00	9.800	-0.2000	-2.947 to 2.547
339	313.0	9.500	8.700	-0.8000	-3.547 to 1.947
340					
341	Temp	Difference	t	P value	Summary
342	298.0	0.0000	0.0000	P > 0.05	ns
343	303.0	0.0000	0.0000	P > 0.05	ns
344	308.0	-0.2000	0.3059	P > 0.05	ns
345	313.0	-0.8000	1.224	P > 0.05	ns
346					
347	29-33 vs. 29-33r				
348	Temp	29-33	29-33r	Difference	95% CI of diff.
349	298.0	12.00	10.00	-2.000	-4.747 to 0.7466

ΔG statistical analysis.pzf:2way ANOVA of Delta G: Tabular results

350	303.0	11.00	9.100	-1.900	-4.647 to 0.8466
351	308.0	10.00	8.300	-1.700	-4.447 to 1.047
352	313.0	9.500	7.500	-2.000	-4.747 to 0.7466
353					
354	Temp	Difference	t	P value	Summary
355	298.0	-2.000	3.059	P < 0.05	*
356	303.0	-1.900	2.906	P < 0.05	*
357	308.0	-1.700	2.600	P > 0.05	ns
358	313.0	-2.000	3.059	P < 0.05	*
359					
360	29-33 vs. 29-33p				
361	Temp	29-33	29-33p	Difference	95% CI of diff.
362	298.0	12.00	13.00	1.000	-1.747 to 3.747
363	303.0	11.00	12.00	1.000	-1.747 to 3.747
364	308.0	10.00	11.00	1.000	-1.747 to 3.747
365	313.0	9.500	10.00	0.5000	-2.247 to 3.247
366					
367	Temp	Difference	t	P value	Summary
368	298.0	1.000	1.530	P > 0.05	ns
369	303.0	1.000	1.530	P > 0.05	ns
370	308.0	1.000	1.530	P > 0.05	ns
371	313.0	0.5000	0.7648	P > 0.05	ns
372					
373	29-33 vs. Au				
374	Temp	29-33	Au	Difference	95% CI of diff.
375	298.0	12.00	12.00	0.0000	-2.747 to 2.747
376	303.0	11.00	11.00	0.0000	-2.747 to 2.747
377	308.0	10.00	9.900	-0.1000	-2.847 to 2.647
378	313.0	9.500	9.000	-0.5000	-3.247 to 2.247
379					
380	Temp	Difference	t	P value	Summary
381	298.0	0.0000	0.0000	P > 0.05	ns
382	303.0	0.0000	0.0000	P > 0.05	ns
383	308.0	-0.1000	0.1530	P > 0.05	ns
384	313.0	-0.5000	0.7648	P > 0.05	ns
385					
386	29-33 vs. Ag				
387	Temp	29-33	Ag	Difference	95% CI of diff.
388	298.0	12.00	12.00	0.0000	-2.747 to 2.747
389	303.0	11.00	10.00	-1.000	-3.747 to 1.747
390	308.0	10.00	8.000	-2.000	-4.747 to 0.7466
391	313.0	9.500	7.000	-2.500	-5.247 to 0.2466
392					
393	Temp	Difference	t	P value	Summary

ΔG statistical analysis.pzf:2way ANOVA of Delta G: Tabular results

394	298.0	0.0000	0.0000	P > 0.05	ns
395	303.0	-1.000	1.530	P > 0.05	ns
396	308.0	-2.000	3.059	P < 0.05	*
397	313.0	-2.500	3.824	P<0.01	**
398					
399	29-33 vs. curcumin				
400	Temp	29-33	curcumin	Difference	95% CI of diff.
401	298.0	12.00	11.00	-1.000	-3.747 to 1.747
402	303.0	11.00	10.00	-1.000	-3.747 to 1.747
403	308.0	10.00	8.600	-1.400	-4.147 to 1.347
404	313.0	9.500	7.700	-1.800	-4.547 to 0.9466
405					
406	Temp	Difference	t	P value	Summary
407	298.0	-1.000	1.530	P > 0.05	ns
408	303.0	-1.000	1.530	P > 0.05	ns
409	308.0	-1.400	2.141	P > 0.05	ns
410	313.0	-1.800	2.753	P < 0.05	*
411					
412	33-37 vs. 25-37				
413	Temp	33-37	25-37	Difference	95% CI of diff.
414	298.0	11.00	11.00	0.0000	-2.747 to 2.747
415	303.0	11.00	9.900	-1.100	-3.847 to 1.647
416	308.0	10.00	9.100	-0.9000	-3.647 to 1.847
417	313.0	9.900	8.400	-1.500	-4.247 to 1.247
418					
419	Temp	Difference	t	P value	Summary
420	298.0	0.0000	0.0000	P > 0.05	ns
421	303.0	-1.100	1.683	P > 0.05	ns
422	308.0	-0.9000	1.377	P > 0.05	ns
423	313.0	-1.500	2.294	P > 0.05	ns
424					
425	33-37 vs. 17-21r				
426	Temp	33-37	17-21r	Difference	95% CI of diff.
427	298.0	11.00	10.00	-1.000	-3.747 to 1.747
428	303.0	11.00	9.300	-1.700	-4.447 to 1.047
429	308.0	10.00	8.400	-1.600	-4.347 to 1.147
430	313.0	9.900	7.500	-2.400	-5.147 to 0.3466
431					
432	Temp	Difference	t	P value	Summary
433	298.0	-1.000	1.530	P > 0.05	ns
434	303.0	-1.700	2.600	P > 0.05	ns
435	308.0	-1.600	2.447	P > 0.05	ns
436	313.0	-2.400	3.671	P<0.01	**
437					

ΔG statistical analysis.pzf:2way ANOVA of Delta G: Tabular results

438	33-37 vs. 17-21p				
439	Temp	33-37	17-21p	Difference	95% CI of diff.
440	298.0	11.00	12.00	1.000	-1.747 to 3.747
441	303.0	11.00	11.00	0.0000	-2.747 to 2.747
442	308.0	10.00	9.800	-0.2000	-2.947 to 2.547
443	313.0	9.900	8.700	-1.200	-3.947 to 1.547
444					
445	Temp	Difference	t	P value	Summary
446	298.0	1.000	1.530	P > 0.05	ns
447	303.0	0.0000	0.0000	P > 0.05	ns
448	308.0	-0.2000	0.3059	P > 0.05	ns
449	313.0	-1.200	1.836	P > 0.05	ns
450					
451	33-37 vs. 29-33r				
452	Temp	33-37	29-33r	Difference	95% CI of diff.
453	298.0	11.00	10.00	-1.000	-3.747 to 1.747
454	303.0	11.00	9.100	-1.900	-4.647 to 0.8466
455	308.0	10.00	8.300	-1.700	-4.447 to 1.047
456	313.0	9.900	7.500	-2.400	-5.147 to 0.3466
457					
458	Temp	Difference	t	P value	Summary
459	298.0	-1.000	1.530	P > 0.05	ns
460	303.0	-1.900	2.906	P < 0.05	*
461	308.0	-1.700	2.600	P > 0.05	ns
462	313.0	-2.400	3.671	P<0.01	**
463					
464	33-37 vs. 29-33p				
465	Temp	33-37	29-33p	Difference	95% CI of diff.
466	298.0	11.00	13.00	2.000	-0.7466 to 4.747
467	303.0	11.00	12.00	1.000	-1.747 to 3.747
468	308.0	10.00	11.00	1.000	-1.747 to 3.747
469	313.0	9.900	10.00	0.1000	-2.647 to 2.847
470					
471	Temp	Difference	t	P value	Summary
472	298.0	2.000	3.059	P < 0.05	*
473	303.0	1.000	1.530	P > 0.05	ns
474	308.0	1.000	1.530	P > 0.05	ns
475	313.0	0.1000	0.1530	P > 0.05	ns
476					
477	33-37 vs. Au				
478	Temp	33-37	Au	Difference	95% CI of diff.
479	298.0	11.00	12.00	1.000	-1.747 to 3.747
480	303.0	11.00	11.00	0.0000	-2.747 to 2.747
481	308.0	10.00	9.900	-0.1000	-2.847 to 2.647

ΔG statistical analysis.pzf:2way ANOVA of Delta G: Tabular results

482	313.0	9.900	9.000	-0.9000	-3.647 to 1.847
483					
484	Temp	Difference	t	P value	Summary
485	298.0	1.000	1.530	P > 0.05	ns
486	303.0	0.0000	0.0000	P > 0.05	ns
487	308.0	-0.1000	0.1530	P > 0.05	ns
488	313.0	-0.9000	1.377	P > 0.05	ns
489					
490	33-37 vs. Ag				
491	Temp	33-37	Ag	Difference	95% CI of diff.
492	298.0	11.00	12.00	1.000	-1.747 to 3.747
493	303.0	11.00	10.00	-1.000	-3.747 to 1.747
494	308.0	10.00	8.000	-2.000	-4.747 to 0.7466
495	313.0	9.900	7.000	-2.900	-5.647 to -0.1534
496					
497	Temp	Difference	t	P value	Summary
498	298.0	1.000	1.530	P > 0.05	ns
499	303.0	-1.000	1.530	P > 0.05	ns
500	308.0	-2.000	3.059	P < 0.05	*
501	313.0	-2.900	4.436	P<0.001	***
502					
503	33-37 vs. curcumin				
504	Temp	33-37	curcumin	Difference	95% CI of diff.
505	298.0	11.00	11.00	0.0000	-2.747 to 2.747
506	303.0	11.00	10.00	-1.000	-3.747 to 1.747
507	308.0	10.00	8.600	-1.400	-4.147 to 1.347
508	313.0	9.900	7.700	-2.200	-4.947 to 0.5466
509					
510	Temp	Difference	t	P value	Summary
511	298.0	0.0000	0.0000	P > 0.05	ns
512	303.0	-1.000	1.530	P > 0.05	ns
513	308.0	-1.400	2.141	P > 0.05	ns
514	313.0	-2.200	3.365	P<0.01	**
515					
516	25-37 vs. 17-21r				
517	Temp	25-37	17-21r	Difference	95% CI of diff.
518	298.0	11.00	10.00	-1.000	-3.747 to 1.747
519	303.0	9.900	9.300	-0.6000	-3.347 to 2.147
520	308.0	9.100	8.400	-0.7000	-3.447 to 2.047
521	313.0	8.400	7.500	-0.9000	-3.647 to 1.847
522					
523	Temp	Difference	t	P value	Summary
524	298.0	-1.000	1.530	P > 0.05	ns
525	303.0	-0.6000	0.9178	P > 0.05	ns

ΔG statistical analysis.pzf:2way ANOVA of Delta G: Tabular results

526	308.0	-0.7000	1.071	P > 0.05	ns
527	313.0	-0.9000	1.377	P > 0.05	ns
528					
529	25-37 vs. 17-21p				
530	Temp	25-37	17-21p	Difference	95% CI of diff.
531	298.0	11.00	12.00	1.000	-1.747 to 3.747
532	303.0	9.900	11.00	1.100	-1.647 to 3.847
533	308.0	9.100	9.800	0.7000	-2.047 to 3.447
534	313.0	8.400	8.700	0.3000	-2.447 to 3.047
535					
536	Temp	Difference	t	P value	Summary
537	298.0	1.000	1.530	P > 0.05	ns
538	303.0	1.100	1.683	P > 0.05	ns
539	308.0	0.7000	1.071	P > 0.05	ns
540	313.0	0.3000	0.4589	P > 0.05	ns
541					
542	25-37 vs. 29-33r				
543	Temp	25-37	29-33r	Difference	95% CI of diff.
544	298.0	11.00	10.00	-1.000	-3.747 to 1.747
545	303.0	9.900	9.100	-0.8000	-3.547 to 1.947
546	308.0	9.100	8.300	-0.8000	-3.547 to 1.947
547	313.0	8.400	7.500	-0.9000	-3.647 to 1.847
548					
549	Temp	Difference	t	P value	Summary
550	298.0	-1.000	1.530	P > 0.05	ns
551	303.0	-0.8000	1.224	P > 0.05	ns
552	308.0	-0.8000	1.224	P > 0.05	ns
553	313.0	-0.9000	1.377	P > 0.05	ns
554					
555	25-37 vs. 29-33p				
556	Temp	25-37	29-33p	Difference	95% CI of diff.
557	298.0	11.00	13.00	2.000	-0.7466 to 4.747
558	303.0	9.900	12.00	2.100	-0.6466 to 4.847
559	308.0	9.100	11.00	1.900	-0.8466 to 4.647
560	313.0	8.400	10.00	1.600	-1.147 to 4.347
561					
562	Temp	Difference	t	P value	Summary
563	298.0	2.000	3.059	P < 0.05	*
564	303.0	2.100	3.212	P < 0.05	*
565	308.0	1.900	2.906	P < 0.05	*
566	313.0	1.600	2.447	P > 0.05	ns
567					
568	25-37 vs. Au				
569	Temp	25-37	Au	Difference	95% CI of diff.

ΔG statistical analysis.pzf:2way ANOVA of Delta G: Tabular results

570	298.0	11.00	12.00	1.000	-1.747 to 3.747
571	303.0	9.900	11.00	1.100	-1.647 to 3.847
572	308.0	9.100	9.900	0.8000	-1.947 to 3.547
573	313.0	8.400	9.000	0.6000	-2.147 to 3.347
574					
575	Temp	Difference	t	P value	Summary
576	298.0	1.000	1.530	P > 0.05	ns
577	303.0	1.100	1.683	P > 0.05	ns
578	308.0	0.8000	1.224	P > 0.05	ns
579	313.0	0.6000	0.9178	P > 0.05	ns
580					
581	25-37 vs. Ag				
582	Temp	25-37	Ag	Difference	95% CI of diff.
583	298.0	11.00	12.00	1.000	-1.747 to 3.747
584	303.0	9.900	10.00	0.1000	-2.647 to 2.847
585	308.0	9.100	8.000	-1.100	-3.847 to 1.647
586	313.0	8.400	7.000	-1.400	-4.147 to 1.347
587					
588	Temp	Difference	t	P value	Summary
589	298.0	1.000	1.530	P > 0.05	ns
590	303.0	0.1000	0.1530	P > 0.05	ns
591	308.0	-1.100	1.683	P > 0.05	ns
592	313.0	-1.400	2.141	P > 0.05	ns
593					
594	25-37 vs. curcumin				
595	Temp	25-37	curcumin	Difference	95% CI of diff.
596	298.0	11.00	11.00	0.0000	-2.747 to 2.747
597	303.0	9.900	10.00	0.1000	-2.647 to 2.847
598	308.0	9.100	8.600	-0.5000	-3.247 to 2.247
599	313.0	8.400	7.700	-0.7000	-3.447 to 2.047
600					
601	Temp	Difference	t	P value	Summary
602	298.0	0.0000	0.0000	P > 0.05	ns
603	303.0	0.1000	0.1530	P > 0.05	ns
604	308.0	-0.5000	0.7648	P > 0.05	ns
605	313.0	-0.7000	1.071	P > 0.05	ns
606					
607	17-21r vs. 17-21p				
608	Temp	17-21r	17-21p	Difference	95% CI of diff.
609	298.0	10.00	12.00	2.000	-0.7466 to 4.747
610	303.0	9.300	11.00	1.700	-1.047 to 4.447
611	308.0	8.400	9.800	1.400	-1.347 to 4.147
612	313.0	7.500	8.700	1.200	-1.547 to 3.947
613					

ΔG statistical analysis.pzf:2way ANOVA of Delta G: Tabular results

614	Temp	Difference	t	P value	Summary
615	298.0	2.000	3.059	P < 0.05	*
616	303.0	1.700	2.600	P > 0.05	ns
617	308.0	1.400	2.141	P > 0.05	ns
618	313.0	1.200	1.836	P > 0.05	ns
619					
620	17-21r vs. 29-33r				
621	Temp	17-21r	29-33r	Difference	95% CI of diff.
622	298.0	10.00	10.00	0.0000	-2.747 to 2.747
623	303.0	9.300	9.100	-0.2000	-2.947 to 2.547
624	308.0	8.400	8.300	-0.1000	-2.847 to 2.647
625	313.0	7.500	7.500	0.0000	-2.747 to 2.747
626					
627	Temp	Difference	t	P value	Summary
628	298.0	0.0000	0.0000	P > 0.05	ns
629	303.0	-0.2000	0.3059	P > 0.05	ns
630	308.0	-0.1000	0.1530	P > 0.05	ns
631	313.0	0.0000	0.0000	P > 0.05	ns
632					
633	17-21r vs. 29-33p				
634	Temp	17-21r	29-33p	Difference	95% CI of diff.
635	298.0	10.00	13.00	3.000	0.2534 to 5.747
636	303.0	9.300	12.00	2.700	-0.04655 to 5.447
637	308.0	8.400	11.00	2.600	-0.1466 to 5.347
638	313.0	7.500	10.00	2.500	-0.2466 to 5.247
639					
640	Temp	Difference	t	P value	Summary
641	298.0	3.000	4.589	P<0.001	***
642	303.0	2.700	4.130	P<0.001	***
643	308.0	2.600	3.977	P<0.01	**
644	313.0	2.500	3.824	P<0.01	**
645					
646	17-21r vs. Au				
647	Temp	17-21r	Au	Difference	95% CI of diff.
648	298.0	10.00	12.00	2.000	-0.7466 to 4.747
649	303.0	9.300	11.00	1.700	-1.047 to 4.447
650	308.0	8.400	9.900	1.500	-1.247 to 4.247
651	313.0	7.500	9.000	1.500	-1.247 to 4.247
652					
653	Temp	Difference	t	P value	Summary
654	298.0	2.000	3.059	P < 0.05	*
655	303.0	1.700	2.600	P > 0.05	ns
656	308.0	1.500	2.294	P > 0.05	ns
657	313.0	1.500	2.294	P > 0.05	ns

ΔG statistical analysis.pzf:2way ANOVA of Delta G: Tabular results

658					
659	17-21r vs. Ag				
660	Temp	17-21r	Ag	Difference	95% CI of diff.
661	298.0	10.00	12.00	2.000	-0.7466 to 4.747
662	303.0	9.300	10.00	0.7000	-2.047 to 3.447
663	308.0	8.400	8.000	-0.4000	-3.147 to 2.347
664	313.0	7.500	7.000	-0.5000	-3.247 to 2.247
665					
666	Temp	Difference	t	P value	Summary
667	298.0	2.000	3.059	P < 0.05	*
668	303.0	0.7000	1.071	P > 0.05	ns
669	308.0	-0.4000	0.6119	P > 0.05	ns
670	313.0	-0.5000	0.7648	P > 0.05	ns
671					
672	17-21r vs. curcumin				
673	Temp	17-21r	curcumin	Difference	95% CI of diff.
674	298.0	10.00	11.00	1.000	-1.747 to 3.747
675	303.0	9.300	10.00	0.7000	-2.047 to 3.447
676	308.0	8.400	8.600	0.2000	-2.547 to 2.947
677	313.0	7.500	7.700	0.2000	-2.547 to 2.947
678					
679	Temp	Difference	t	P value	Summary
680	298.0	1.000	1.530	P > 0.05	ns
681	303.0	0.7000	1.071	P > 0.05	ns
682	308.0	0.2000	0.3059	P > 0.05	ns
683	313.0	0.2000	0.3059	P > 0.05	ns
684					
685	17-21p vs. 29-33r				
686	Temp	17-21p	29-33r	Difference	95% CI of diff.
687	298.0	12.00	10.00	-2.000	-4.747 to 0.7466
688	303.0	11.00	9.100	-1.900	-4.647 to 0.8466
689	308.0	9.800	8.300	-1.500	-4.247 to 1.247
690	313.0	8.700	7.500	-1.200	-3.947 to 1.547
691					
692	Temp	Difference	t	P value	Summary
693	298.0	-2.000	3.059	P < 0.05	*
694	303.0	-1.900	2.906	P < 0.05	*
695	308.0	-1.500	2.294	P > 0.05	ns
696	313.0	-1.200	1.836	P > 0.05	ns
697					
698	17-21p vs. 29-33p				
699	Temp	17-21p	29-33p	Difference	95% CI of diff.
700	298.0	12.00	13.00	1.000	-1.747 to 3.747
701	303.0	11.00	12.00	1.000	-1.747 to 3.747

ΔG statistical analysis.pzf:2way ANOVA of Delta G: Tabular results

702	308.0	9.800	11.00	1.200	-1.547 to 3.947
703	313.0	8.700	10.00	1.300	-1.447 to 4.047
704					
705	Temp	Difference	t	P value	Summary
706	298.0	1.000	1.530	P > 0.05	ns
707	303.0	1.000	1.530	P > 0.05	ns
708	308.0	1.200	1.836	P > 0.05	ns
709	313.0	1.300	1.989	P > 0.05	ns
710					
711	17-21p vs. Au				
712	Temp	17-21p	Au	Difference	95% CI of diff.
713	298.0	12.00	12.00	0.0000	-2.747 to 2.747
714	303.0	11.00	11.00	0.0000	-2.747 to 2.747
715	308.0	9.800	9.900	0.1000	-2.647 to 2.847
716	313.0	8.700	9.000	0.3000	-2.447 to 3.047
717					
718	Temp	Difference	t	P value	Summary
719	298.0	0.0000	0.0000	P > 0.05	ns
720	303.0	0.0000	0.0000	P > 0.05	ns
721	308.0	0.1000	0.1530	P > 0.05	ns
722	313.0	0.3000	0.4589	P > 0.05	ns
723					
724	17-21p vs. Ag				
725	Temp	17-21p	Ag	Difference	95% CI of diff.
726	298.0	12.00	12.00	0.0000	-2.747 to 2.747
727	303.0	11.00	10.00	-1.000	-3.747 to 1.747
728	308.0	9.800	8.000	-1.800	-4.547 to 0.9466
729	313.0	8.700	7.000	-1.700	-4.447 to 1.047
730					
731	Temp	Difference	t	P value	Summary
732	298.0	0.0000	0.0000	P > 0.05	ns
733	303.0	-1.000	1.530	P > 0.05	ns
734	308.0	-1.800	2.753	P < 0.05	*
735	313.0	-1.700	2.600	P > 0.05	ns
736					
737	17-21p vs. curcumin				
738	Temp	17-21p	curcumin	Difference	95% CI of diff.
739	298.0	12.00	11.00	-1.000	-3.747 to 1.747
740	303.0	11.00	10.00	-1.000	-3.747 to 1.747
741	308.0	9.800	8.600	-1.200	-3.947 to 1.547
742	313.0	8.700	7.700	-1.000	-3.747 to 1.747
743					
744	Temp	Difference	t	P value	Summary
745	298.0	-1.000	1.530	P > 0.05	ns

ΔG statistical analysis.pzf:2way ANOVA of Delta G: Tabular results

746	303.0	-1.000	1.530	P > 0.05	ns
747	308.0	-1.200	1.836	P > 0.05	ns
748	313.0	-1.000	1.530	P > 0.05	ns
749					
750	29-33r vs. 29-33p				
751	Temp	29-33r	29-33p	Difference	95% CI of diff.
752	298.0	10.00	13.00	3.000	0.2534 to 5.747
753	303.0	9.100	12.00	2.900	0.1534 to 5.647
754	308.0	8.300	11.00	2.700	-0.04655 to 5.447
755	313.0	7.500	10.00	2.500	-0.2466 to 5.247
756					
757	Temp	Difference	t	P value	Summary
758	298.0	3.000	4.589	P<0.001	***
759	303.0	2.900	4.436	P<0.001	***
760	308.0	2.700	4.130	P<0.001	***
761	313.0	2.500	3.824	P<0.01	**
762					
763	29-33r vs. Au				
764	Temp	29-33r	Au	Difference	95% CI of diff.
765	298.0	10.00	12.00	2.000	-0.7466 to 4.747
766	303.0	9.100	11.00	1.900	-0.8466 to 4.647
767	308.0	8.300	9.900	1.600	-1.147 to 4.347
768	313.0	7.500	9.000	1.500	-1.247 to 4.247
769					
770	Temp	Difference	t	P value	Summary
771	298.0	2.000	3.059	P < 0.05	*
772	303.0	1.900	2.906	P < 0.05	*
773	308.0	1.600	2.447	P > 0.05	ns
774	313.0	1.500	2.294	P > 0.05	ns
775					
776	29-33r vs. Ag				
777	Temp	29-33r	Ag	Difference	95% CI of diff.
778	298.0	10.00	12.00	2.000	-0.7466 to 4.747
779	303.0	9.100	10.00	0.9000	-1.847 to 3.647
780	308.0	8.300	8.000	-0.3000	-3.047 to 2.447
781	313.0	7.500	7.000	-0.5000	-3.247 to 2.247
782					
783	Temp	Difference	t	P value	Summary
784	298.0	2.000	3.059	P < 0.05	*
785	303.0	0.9000	1.377	P > 0.05	ns
786	308.0	-0.3000	0.4589	P > 0.05	ns
787	313.0	-0.5000	0.7648	P > 0.05	ns
788					
789	29-33r vs. curcumin				

ΔG statistical analysis.pzf:2way ANOVA of Delta G: Tabular results

790	Temp	29-33r	curcumin	Difference	95% CI of diff.
791	298.0	10.00	11.00	1.000	-1.747 to 3.747
792	303.0	9.100	10.00	0.9000	-1.847 to 3.647
793	308.0	8.300	8.600	0.3000	-2.447 to 3.047
794	313.0	7.500	7.700	0.2000	-2.547 to 2.947
795					
796	Temp	Difference	t	P value	Summary
797	298.0	1.000	1.530	P > 0.05	ns
798	303.0	0.9000	1.377	P > 0.05	ns
799	308.0	0.3000	0.4589	P > 0.05	ns
800	313.0	0.2000	0.3059	P > 0.05	ns
801					
802	29-33p vs. Au				
803	Temp	29-33p	Au	Difference	95% CI of diff.
804	298.0	13.00	12.00	-1.000	-3.747 to 1.747
805	303.0	12.00	11.00	-1.000	-3.747 to 1.747
806	308.0	11.00	9.900	-1.100	-3.847 to 1.647
807	313.0	10.00	9.000	-1.000	-3.747 to 1.747
808					
809	Temp	Difference	t	P value	Summary
810	298.0	-1.000	1.530	P > 0.05	ns
811	303.0	-1.000	1.530	P > 0.05	ns
812	308.0	-1.100	1.683	P > 0.05	ns
813	313.0	-1.000	1.530	P > 0.05	ns
814					
815	29-33p vs. Ag				
816	Temp	29-33p	Ag	Difference	95% CI of diff.
817	298.0	13.00	12.00	-1.000	-3.747 to 1.747
818	303.0	12.00	10.00	-2.000	-4.747 to 0.7466
819	308.0	11.00	8.000	-3.000	-5.747 to -0.2534
820	313.0	10.00	7.000	-3.000	-5.747 to -0.2534
821					
822	Temp	Difference	t	P value	Summary
823	298.0	-1.000	1.530	P > 0.05	ns
824	303.0	-2.000	3.059	P < 0.05	*
825	308.0	-3.000	4.589	P<0.001	***
826	313.0	-3.000	4.589	P<0.001	***
827					
828	29-33p vs. curcumin				
829	Temp	29-33p	curcumin	Difference	95% CI of diff.
830	298.0	13.00	11.00	-2.000	-4.747 to 0.7466
831	303.0	12.00	10.00	-2.000	-4.747 to 0.7466
832	308.0	11.00	8.600	-2.400	-5.147 to 0.3466
833	313.0	10.00	7.700	-2.300	-5.047 to 0.4466

ΔG statistical analysis.pzf:2way ANOVA of Delta G: Tabular results

835	Temp	Difference	t	P value	Summary
836	298.0	-2.000	3.059	P < 0.05	*
837	303.0	-2.000	3.059	P < 0.05	*
838	308.0	-2.400	3.671	P<0.01	**
839	313.0	-2.300	3.518	P<0.01	**
840					
841	Au vs. Ag				
842	Temp	Au	Ag	Difference	95% CI of diff.
843	298.0	12.00	12.00	0.0000	-2.747 to 2.747
844	303.0	11.00	10.00	-1.000	-3.747 to 1.747
845	308.0	9.900	8.000	-1.900	-4.647 to 0.8466
846	313.0	9.000	7.000	-2.000	-4.747 to 0.7466
847					
848	Temp	Difference	t	P value	Summary
849	298.0	0.0000	0.0000	P > 0.05	ns
850	303.0	-1.000	1.530	P > 0.05	ns
851	308.0	-1.900	2.906	P < 0.05	*
852	313.0	-2.000	3.059	P < 0.05	*
853					
854	Au vs. curcumin				
855	Temp	Au	curcumin	Difference	95% CI of diff.
856	298.0	12.00	11.00	-1.000	-3.747 to 1.747
857	303.0	11.00	10.00	-1.000	-3.747 to 1.747
858	308.0	9.900	8.600	-1.300	-4.047 to 1.447
859	313.0	9.000	7.700	-1.300	-4.047 to 1.447
860					
861	Temp	Difference	t	P value	Summary
862	298.0	-1.000	1.530	P > 0.05	ns
863	303.0	-1.000	1.530	P > 0.05	ns
864	308.0	-1.300	1.989	P > 0.05	ns
865	313.0	-1.300	1.989	P > 0.05	ns
866					
867	Ag vs. curcumin				
868	Temp	Ag	curcumin	Difference	95% CI of diff.
869	298.0	12.00	11.00	-1.000	-3.747 to 1.747
870	303.0	10.00	10.00	0.0000	-2.747 to 2.747
871	308.0	8.000	8.600	0.6000	-2.147 to 3.347
872	313.0	7.000	7.700	0.7000	-2.047 to 3.447
873					
874	Temp	Difference	t	P value	Summary
875	298.0	-1.000	1.530	P > 0.05	ns
876	303.0	0.0000	0.0000	P > 0.05	ns
877	308.0	0.6000	0.9178	P > 0.05	ns

ΔG statistical analysis.pzf:2way ANOVA of Delta G: Tabular results